INTERNATIONAL DOCTORAL
SCHOOL OF THE USC

Claudia
Gioé

PhD Thesis

Discovery and optimization of selective CB_2 receptor agonists

Santiago de Compostela, 2023

Doctoral Programme in Drug Research and Development

USC
UNIVERSIDADE
DE SANTIAGO
DE COMPOSTELA

DOCTORAL THESIS

DISCOVERY AND OPTIMIZATION OF SELECTIVE CB_2 RECEPTOR AGONISTS

Claudia Gioé

INTERNATIONAL PHD SCHOOL OF THE UNIVERSITY OF SANTIAGO DE COMPOSTELA

PHD PROGRAMME IN DRUG RESEARCH AND DEVELOPMENT

SANTIAGO DE COMPOSTELA, 2023

USC
UNIVERSIDADE
DE SANTIAGO
DE COMPOSTELA

DECLARACIÓN DEL AUTOR/A DE LA TESIS

D./Dña. **Claudia Gioé**

Título de la tesis: **Discovery and optimization of selective CB2 receptor agonists**

Presento mi tesis, siguiendo el procedimiento adecuado al Reglamento y declaro que:

1) La tesis abarca los resultados de la elaboración de mi trabajo.
2) De ser el caso, en la tesis se hace referencia a las colaboraciones que tuvo este trabajo.
3) Confirmo que la tesis no incurre en ningún tipo de plagio de otros autores ni de trabajos presentados por mí para la obtención de otros títulos.
4) La tesis es la versión definitiva presentada para su defensa y coincide la versión impresa con la presentada en formato electrónico.

Y me comprometo a presentar el Compromiso Documental de Supervisión en el caso que el original no esté depositado en la Escuela.

En **Santiago de Compostela**, **25 de mayo de 2023**.

Firma electrónica

USC
UNIVERSIDADE
DE SANTIAGO
DE COMPOSTELA

AUTORIZACIÓN DEL DIRECTOR / TUTOR DE LA TESIS

Discovery and optimization of selective CB_2 receptor agonists

D. Eddy Sotelo Pérez

INFORMA:

Que la presente tesis, se corresponde con el trabajo realizado por D/Dª. Claudia Gioé, bajo mi dirección/tutorización, y autorizo su presentación, considerando que reúne los requisitos exigidos en el Reglamento de Estudios de Doctorado de la USC, y que como director de esta no incurre en las causas de abstención establecidas en la Ley 40/2015.

De acuerdo con lo indicado en el Reglamento de Estudios de Doctorado, declara también que la presente tesis doctoral es idónea para ser defendida en base a la modalidad de Monográfica con reproducción de publicaciones, en los que la participación del doctorando/a fue decisiva para su elaboración y las publicaciones se ajustan al Plan de Investigación.

En Santiago de Compostela, 25 de Mayo de 2023

USC
UNIVERSIDADE
DE SANTIAGO
DE COMPOSTELA

ACKNOWLEDGEMENT

In primo luogo, **Eddy Sotelo Pérez**, al quale desidero esprimere la mia gratitudine per il supporto, l'incoraggiamento, l'impegno e la sua competenza che mi ha offerto durante l'intero percorso della tesi. Grazie per avermi accolto nella famiglia ComBioMed.

A **Jhonny Azuaje** che sin dal primo momento, armato di pazienza e buona volontà, mi ha insegnato a lavorare in un laboratorio, continuando a offrirmi consigli ed esperienza. Grazie per il supporto, lavorativo e no, durante questi anni.

A **Maria Majellaro**, tutor e amica, per la costanza, la pazienza, l'esperienza e il sapere che mi ha trasmesso in questi anni insieme. Grazie per avermi aiutato a crescere.

Ad **Angela**, grazie per avermi aperto il cammino che mi ha portato ad essere la persona che sono oggi e per l'affetto di tutti questi anni.

Ai collaboratori che hanno partecipato ad aumentare il valore scientifico di questa Tesi di Dottorato: **Rita Paleo** e **Xerando García-Mera**, del Dipartimento di Chimica Organica dell'Università di Santiago de Compostela, **María Isabel Loza** e **José Brea**, del laboratorio di farmacologia dell'Università di Santiago de Compostela, **Gemma Navarro Brugal** and **Iu Raich** del laboratorio di farmacologia dell'Università di Barcellona, **Marialessandra Contino** e **Angela Stefanachi** del Dipartimento di Farmacia-Scienze del farmaco dell'Università di Bari, **Chiara Riganti** del Dipartimenti di Oncologia dell'Università di Torino, **Miguel Abal** e **Jorge Barbazán** dell'Instituto di Ricerca Sanitaria di Santiago de Compostela (IDIS), **Christian O. Salas**, Facoltà di Chimica e Farmacia dell'Università di Santiago del Cile, Cile.

A **Rubén Prieto**, **Martina Migliavacca**, **Sandra Ortigueira**, **Lucía Pico**, **Samuel Rey**, **Mateo Eiroa** e **Giovanni Graziano** per aver contributo, ognuno in modo diverso, al lavoro svolto durante questi anni. Senza il vostro apporto, non sarebbe stato lo stesso.

USC
UNIVERSIDADE DE SANTIAGO DE COMPOSTELA

Carlos Rodríguez, **Rodrigo Bernárdez**, **Hugo Fojo**, **Antonio Andújar**, **Lucía Campos**, **Darío Miranda**, **Aitor García**, **David Reza**, **Ivan Pampín** e tutti gli altri membri di **ComBioMed** per aver reso questi anni indimenticabili.

A **Silvia**, **Alessandro**, **Olga**, **Enzo**, **Julius**, **Giovanni**, **Alberto**, **Sara** e **Marti** per far parte della mia vita.

Un ringraziamento speciale va a **Eddy Sotelo** e al gruppo **ComBioMed** per aver finanziato la mia tesi di dottorato durante questi anni.

USC
UNIVERSIDADE DE SANTIAGO DE COMPOSTELA

Index

PHD PUBLICATIONS LIST ..... **III**
ABBREVIATIONS INDEX ..... **V**
SUMMARY ..... **VII**
RESUMEN ..... **XVII**
RESUMO ..... **XXVII**
1 INTRODUCTION **1**
1.1 ENDOCANNABINOID SYSTEM 3
1.1.1 Endocannabinoids and enzymes involved in their synthesis, transport, and degradation *5*
1.1.2 Cannabinoid Receptors *6*
1.2 CB_1 RECEPTOR: BRIEF DESCRIPTION OF ITS DISTRIBUTION AND THERAPEUTIC POTENTIAL 10
1.3 CB_2 RECEPTOR: DISTRIBUTION, FUNCTIONS AND THERAPEUTIC POTENTIAL 11
1.4 MEDICINAL CHEMISTRY OF CBRS: PHYTOCANNABINOIDS 15
1.5 MEDICINAL CHEMISTRY OF CB_1R 18
1.7 MEDICINAL CHEMISTRY OF CB_2R 20
1.8 CB_2R LIGANDS IN CLINICAL TRIALS 23
1.9 BIASED AGONISM 25
1.10 SCRAS: SYNTHETIC CANNABINOID RECEPTOR AGONISTS AS NEW PSYCHOACTIVE SUBSTANCES 27
1.10.1 New Psychoactive substances (NPS) *27*
1.10.2 SCRAs: an emergent and dangerous family of new illegal drugs *32*
1.10.3 SCRAs general structure *35*
1.10.4 Off-target interactions *36*
2 AIMS AND OUTLINE OF THIS THESIS **37**
3 RESULT AND DISCUSSION **43**
3.1 CHAPTER 1. SYNTHESIS AND CHARACTERIZATION OF A LARGE COLLECTION OF SYNTHETIC CANNABINOID RECEPTOR AGONISTS DESIGNER DRUGS 47
3.2 CHAPTER 2. PHARMACOMODULATION OF INDOLE-BASED SCRAS. UGI-ASSISTED DISCOVERY OF POTENT AND CB_2R SELECTIVE LIGANDS: THE PROOF OF CONCEPT 73
3.3 CHAPTER 3. EXPLORATION OF THE EFFECT OF THE GROUP AT R^3 ON THE AFFINITY AND SELECTIVITY 117
3.4 CHAPTER 4. EXPLORATION OF THE INFLUENCE OF THE TERMINAL AMIDE (R^4) ON THE CB_2R DATA. 139
3.5 CHAPTER 5: ADVANCED PHARMACOLOGICAL STUDIES OF SELECTED CB_2R LIGANDS 159
4 EXPERIMENTAL SECTION **183**

USC UNIVERSIDADE DE SANTIAGO DE COMPOSTELA

4.2 GENERAL INFORMATION 185
4.2.1 Chemistry 185
4.2.2 General considerations on the spectroscopic characterization of chemotheques 187
4.2.3 Biological assay 187
4.3 DOSE RESPONSE CURVES OBTAINED AT CB_1R AND CB_2R DURING FUNCTIONAL AND BINDING DATA (CHAPTER 1, CPDS 22, 23, 24, 25) 193
4.4 COMPARISON TABLES BETWEEN THE EXPERIMENTAL DATA AND THE REPORTED DATA OF CHAPTER 1 (CPDS 22, 23, 24, 25) 195
4.5 GENERAL PROCEDURES OF SYNTHESIS AND SPECTROSCOPIC DATA 199
4.5.1 General pathways for the synthesis of N-alkyl-1H-indole-3-carboxylic acid (26a-d) 199
4.5.2 General procedure for the synthesis of 1-alkyl-1H-indazole-3-carboxylic acid (26e-h) 201
4.5.3 General pathways for the synthesis methyl (1H-indole (or indazole)-3-carbonyl)glycinate polysubstituted (22a-p and 23a-p) 203
4.5.5 General pathways for the synthesis of N-(1-amino-3-methyl-1-oxobutan-2yl)-1H-indole (indazole)-3-carboxamide polysubstituted (24a-p and 25a-p) 213
4.5.7 General pathways for the synthesis of alkyl (1H-indole-3-carbonyl)glycinate polysubstituted (35a-r and 36a-r) 224
4.5.8 General pathways for the synthesis of N-(2-amino-2-oxoethyl)-1H-indole-3-carboxamide polysubstituted (37a-v, 38a-v) 234
4.5.9 General pathway for the synthesis of alkyl (1H-indole-3-carbonyl)glycinate polysubstituted (39a-x and 40a-x) 249
4.5.1 General pathway for the synthesis of N-(2-amino-2-oxoethyl)-1H-indole-3-carboxamide polysubstituted (41a-x, 42a-x, 43a-h) 255
4.5.2 General pathways for the synthesis of N-(2-amino-2-oxoethyl)-1H-indole-3-carboxamide polysubstituted (44a-r, 45a-r, 46a-l, 47a-r) 264
4.6 HPLC TRACES OF COMPOUNDS 22, 23, 24, 25, 35, 36, 37, 38 276
4.7 HIGH-RESOLUTION MASS SPECTROMETRY (HRMS) 276

5 CONCLUSIONS 277
6 REFERENCES 281

USC UNIVERSIDADE DE SANTIAGO DE COMPOSTELA

PHD PUBLICATIONS LIST

"Pharmacological Insights Emerging from the Characterization of a Large Collection of Synthetic Cannabinoid Receptor Agonists Designer Drugs". Claudia Gioé-Gallo, Sandra Ortigueira, José Brea, Iu Raïch, Jhonny Azuaje, M. Rita Paleo, Maria Majellaro, María Isabel Loza, Cristian O. Salas, Xerardo García-Mera, Gemma Navarro, Eddy Sotelo. *Biomedicine & Pharmacotherapy.* **2023**, *164*, in press.

USC
UNIVERSIDADE DE SANTIAGO DE COMPOSTELA

USC
UNIVERSIDADE
DE SANTIAGO
DE COMPOSTELA

ABBREVIATIONS INDEX

Δ^9-THC: Δ^9-tetrahydrocannabinol

2-AG: 2-arachidonoylglycerol

AA: Arachidonic acid

AC: Adenylate cyclase

AD: Alzheimer disease

AEA: Anandamide

ALS: Amyotrophic Lateral Sclerosis

AMP: adenosine monophosphate

APCI: Atmospheric-pressure chemical ionization

***c*-Bu**: Cyclobutane

***c*-Pr**: Cyclopropane

cAMP: Cyclic adenosine monophosphate

CBD: Cannabidiol

CBR: Cannabinoid receptor

CB_1R: Cannabinoid repeptor type 1

CB_2R: Cannabinoid repeptor type 2

CD: Circular dichroism

CI: Chemical ionization

CNS: Central Nervous System

Cpds: Compounds

Cy: Cyclohexyl

Cyp: Cyclopentane

DIPEA: *N*,*N*-Diisopropylethylamine

eCBs: endocannabinoids

EC_{50}: Half maximal effective concentration

ECS: Endocannabinoid system

E_{max}: Maximum effect

EMCDDA: European Monitoring Centre fro Drugs and Drug Addiction

FAAH: Fatty Acid amide hydrolase

GPCR: G protein coupled receptor

HATU: Hexafluorophosphate Azabenzotriazole Tetramethyl Uronium

HEK-293: Human embryonic kidney 293 cells

HD: Huntington disease

HPLC: High-performance liquid chromatography

HRMS: High resolution Mass Spectrometry

IL: Interleukin family

K_i: Inhibitor constant

LMRS: Low Resolution Mass Spectometry

MAPK: Mitogen-Activated Protein Kinases

MCR: Multicomponent reaction

$MgSO_4$: Magnesium sulphate

Mp: Melting Point

MS: Multiple Sclerosis

NAM: Negative allosteric modulator

NNCA: National Narcotics Control Commission of China

NPS: New Psychoactive Substances

PAM: Positive allosteric modulator

PD: Parkinson disease

SAR: Structure-Activity relationship

SCRAs: Synthetic Cannabinoid Receptor Agonists

SEM: Standard error of the mean

SI: Selectivity index

SSR: Structure-Selectivity relationship

TLC: Thin-layer chromatography

TM: transmembrane domain

TNFα: Tumor necrosis factor α

U4CR: Ugi four component reaction

UNODC: United Nations Office on Drugs and Crime

UV: Ultraviolet

USC UNIVERSIDADE DE SANTIAGO DE COMPOSTELA

SUMMARY

The endocannabinoid system (ECS) comprises cannabinoid receptors (CBRs), their ligands (endocannabinoids, eCBs), and the enzymes involved in the synthesis, metabolism, and transport of eCBs. Currently, two CBRs are known: Cannabinoid Receptor type 1 (CB_1R), primarily present in the central nervous system (CNS), and Cannabinoid Receptor type 2 (CB_2R), heavily expressed in the periphery.

CB_2R is an underexplored G-protein coupled receptor (GPCR), primarily expressed in the periphery, especially in immune cells. Several pieces of evidence have demonstrated that CB_2R is upregulated in microglia and brain cells in neurodegenerative diseases, while its expression in the healthy CNS is yet to be clarified. Activation of CB_2R in the CNS leads to microglia polarization from the M1 state (the pro-inflammatory phenotype characterized by pro-inflammatory cytokines production) to the M2 state (the anti-inflammatory phenotype characterized by anti-inflammatory cytokines production). This anti-inflammatory effect represents a potential therapeutic strategy in the treatment of various pathologies such as neurodegenerative diseases, pain control, autoimmune diseases, and cancer.

Recently, the role of the ECS in the context of cancer has been extensively investigated, and several studies have demonstrated the antitumor effect of CB_2R agonists in different types of cancer. By selectively activating CB_2R, the agonists have shown promising results in various aspects of cancer treatment. One significant effect is their ability to induce apoptosis in cancer cells. CB_2R agonists have been found to trigger signaling pathways that promote apoptosis specifically in tumor cells while sparing healthy cells, leading to tumor regression. This targeted approach minimizes the potential side effects associated with conventional chemotherapy, which often affects both cancerous and healthy cells. Furthermore, CB_2R agonists exhibit anti-proliferative effects by inhibiting the growth and division of cancer cells. They can disrupt the signaling pathways responsible for cell proliferation, ultimately reducing tumor growth and progression.

However, the limited availability of potent and highly selective CB_2R agonists poses a significant challenge in the field of cancer therapy, hindering the full exploration of CB_2R activation and therapeutic potential.

USC UNIVERSIDADE DE SANTIAGO DE COMPOSTELA

The present Doctoral Thesis describes the ***design, synthesis, binding and functional data, structure-activity relationship, and advanced pharmacological studies of a series of novel and potent CB_2R selective ligands***. The results described herein are part of a methodological project that demonstrates the competitive advantages of multicomponent reactions in Medicinal Chemistry.

The first Chapter of this Doctoral Thesis describes the synthesis and characterization of a large collection of Synthetic Cannabinoid Receptor Agonists (SCRAs). During the last decade, SCRAs have emerged as the largest and most defiant group of New Psychoactive Substances (NPS) controlled by the European Monitoring Centre for Drugs and Drug Addiction (EMCDDA). In the mid-2000s, SCRAs entered the illicit drug market in several forms, such as powder or herbal smoking, as a "legal" alternative to cannabis. SCRAs and tetrahydrocannabinol (Δ^9-THC) differ both in structure and in the pharmacological profile. While Δ^9-THC acts as a partial agonist at both cannabinoid receptors (CBRs), SCRAs are full agonists exerting their psychoactive effects through their agonism on CB_1R, although they often exhibit a more pronounced agonist effect on CB_2R.

One of the main issues with these agonists is their high potency and excellent efficacy, as lower doses are sufficient to achieve psychoactive effects. However, the unpredictable biological effects, unregulated dosage, and variable usage increase the probability of overdose, intoxication, and severe toxicity. The rapid increase in reports of intoxications and deaths related to SCRAs underscores the importance of toxicity studies in assessing health risks and proposing appropriate medical management for intoxication cases. Several clinical reports confirm severe effects associated with SCRAs, such as seizures, cardiovascular damage, kidney damage, stroke, psychosis, paranoia, and anxiety attacks. Currently, little is understood about the mechanisms underlying these toxic effects.

USC
UNIVERSIDADE DE SANTIAGO DE COMPOSTELA

The first Chapter focused on the synthesis and pharmacological evaluation of a large collection of SCRAs (64 ligands, Figure I), enabling the investigation of the most salient features emerging from the structure-activity relationship (SAR) and the identification of selective CB_2R ligands (Figure I).

We conceived a 64-members collection containing skeletal (indole and indazole), functional (esters and amides), alkyl (*i*-Pr and *t*-Bu), and stereochemical [*(S)* stereoisomers and *(R)* stereoisomers] diversities (Figure I). Notably, 32 of the 64 SCRAs herein documented had not been previously reported (derivatives featuring the *(R)* configuration within the pendant amino acid residue) (Figure I).

In general, in both ester and amide series, most derivatives are highly affine at CB_1R and CB_2R. Taken together, the affinity data suggest that the functional diversity (ester and amide) is a more important contributor than the skeletal diversity (heterocyclic core) in defining the potency and selectivity. In general, in both esters and amides, the *i*-Pr derivatives seem to be slightly less affine (at both CBRs) than the *t*-Bu analogues.

Accordingly to their *in vitro* cannabimimetic profiles, it has been confirmed that *(S)* stereoisomers are more potent than the corresponding *(R)* stereoisomers, with a ΔpK_i [pK_i *(S)* - pK_i *(R)*] > 2 in most cases at both receptor subtypes. Furthermore, binding data analysis evidence that the *(R)* stereoisomers are generally less affine (at both cannabinoid receptors) and slightly more affine towards CB_2R.

Although the majority of the herein described ligands reproduce the intrinsic non-subtype-selective profile of SCRAs, the examination of the binding data enabled the identification of novel derivatives that combine an attractive CB_2R compounds (**22i**, **22l**, **22o**, **23j**, **23m** and **23o**).

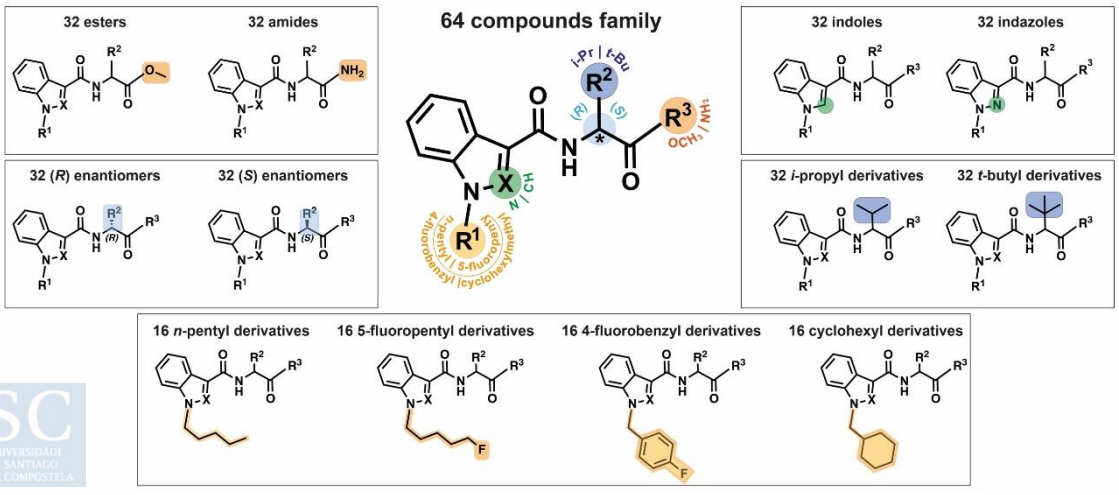


Figure I: General structure of the library and diversity elements included.

In the context of this study, we decided to preliminarily examine the neurotoxicity signatures of a subset of synthetic cannabinoid agonists prepared in this work, using primary mouse neuronal cells. The results suggest that all tested ligands significantly reduced cell viability, indicating a high level of neurotoxicity in this cell line. The reduction in cell viability appears to be both functional and scaffold-dependent, with amides derived from the indazole core exhibiting superior neurotoxicity.

In the second, third, and fourth Chapters of this Doctoral Thesis, the ***aim was to explore novel diversity spaces within the SCRA series to obtain new agonists that selectively target the CB_2R***. This study was inspired by the pharmacophoric model of the SCRA family (Figure IIA), and the SAR trends observed in Chapter 1. To avoid potential neurotoxic liabilities observed in the indazole series, we focused on the indole scaffold. The main purpose of these Chapters is to develop a proof of concept for the synthesis of novel, potent, and CB_2R selective agonists (amides and esters) using a previously unexplored Ugi-based approach (Figure IIC).

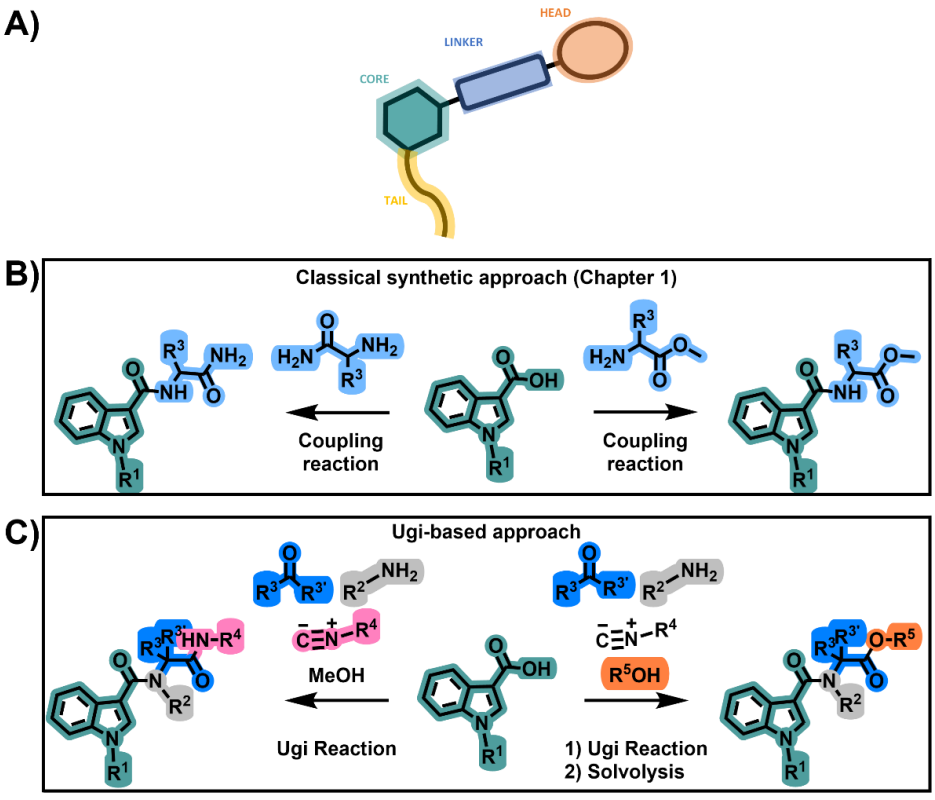


Figure II: A) Pharmacophoric model of SCRAs. B) Classical SCRAs synthesis. C) Proof of concept of U4CR (Ugi four component reaction) assembly of SCRA-like libraries.

USC UNIVERSIDADE DE SANTIAGO DE COMPOSTELA

This approach enables the convergent and high-throughput synthesis of both ester and amide series in a single-pot reaction, facilitating the efficient exploration of this pharmacophore for identifying CB_2R selective ligands. Additionally, we placed emphasis on exploring the most significant features of the structure-activity relationship (SAR) and structure-selectivity relationship (SSR) within these series.

This methodology enables not only the exploration of substituents at R^1, R^2, and R^3 but also the introduction of a second R^3 group, an alkyl residue at the terminal amide (R^4, amide series), or a different alkoxy group at the ester function (R^5, ester series) (Figure IIC). Within the amide series of SCRA, all described ligands are primary amides ($CONH_2$). Our study allows for the exploration of alkyl groups at the terminal amide (R^4, Figure IIC) that may alter the observed affinity and selectivity profiles.

For the design of the new series, we leverage the structural analogy between the SCRA pharmacophore and the chemical structure of Ugi adducts (acylamino amide) (Figure II). From a structural standpoint, the Ugi four-component reaction (U4CR) retains the pharmacophoric elements, including the linker between the central core and the head of the pharmacophoric model, thus enabling the modification and exploration at four different positions (Figure II). It was envisioned that the use of *N*-substituted-indole-3-carboxylic acids (R^1), appropriately substituted amines (R^2), aldehydes or ketones (R^3, $R^{3'}$), and isocyanides (R^4) would yield Ugi adducts that perfectly match the structure of the targeted compounds (Figure IIC). Exploiting the versatility of the Ugi reaction, we decided to introduce different moieties at R^3 (in addition to *i*-Pr and *t*-Bu from the SCRA collection in Chapter 1) and at R^4 to assess the impact of introducing groups at the terminal amide.

The multicomponent reaction (MCR)-based synthetic method proposed here allows for the rapid assembly of ester and amide libraries. We synthesized 168 new derivatives (esters and amides) with various unexplored substitution patterns in SCRA-like series. It is important to highlight that all the compounds obtained in these Chapters contain a stereocenter. Ligands were isolated and pharmacologically evaluated as racemic mixtures.

USC UNIVERSIDADE DE SANTIAGO DE COMPOSTELA

A comprehensive analysis of the binding data obtained for these series demonstrates the effectiveness of the pharmacomodulation process. Starting from a model dual CB_1R-CB_2R prototype, we completely dissociated the binding profile to these receptors and discovered novel and potent ligands that specifically recognize the CB_2R.

Forty-seven compounds (esters and amides) discovered in these Chapters stand out for their excellent affinity (K_i values between 34.8 - 307 nM) and selectivity profile (> 100-fold over CB_1R).

Finally, the most potent and CB_2R selective ligands were separated into their enantiomers through semi-preparative chiral HPLC, and they were pharmacologically evaluated at both cannabinoid receptors. The absolute configuration of the new CB_2R ligands was determined using circular dichroism (CD). The pharmacological data obtained confirmed that three of the new CB_2R selective ligands [(*S*)-**35m**, (*S*)-**37r**, (*S*)-**38n**] exhibited enantiospecific recognition towards CB_2R.

The main purpose of the fifth and last Chapter of this Doctoral Thesis was ***the advanced pharmacological evaluation and in vitro studies of selected CB_2R ligands***. This Chapter is dedicated to a deeper characterization of the pharmacology and preliminary evaluation of some of the therapeutic applications of the best compounds identified in this Thesis. In the first part, the agonist behavior of the selected compounds was corroborated through functional (cAMP) experiments, then a detailed study of their signaling pathways (biased or unbiased) was conducted. The selected ligands were grouped in two categories according to their functional (full or partial) behavior.

The phenomenon in which ligands of GPCRs selectively modulate the G protein and/or β-arrestin pathway to mediate specific signal transduction routes is referred to as "functional selectivity" or "biased agonism". The concept of biased agonism has significantly transformed our understanding of GPCR signaling and revolutionized the field of GPCR drug discovery. However, the molecular mechanisms underlying biased signaling are still largely unknown, and investigating the functional contributions of the G protein and β-arrestin signaling pathways for endogenous and exogenous ligands remains a challenging task.

USC UNIVERSIDADE DE SANTIAGO DE COMPOSTELA

Following membrane receptor (GPCR) activation, various signaling pathways and downstream effectors can coexist. In addition to G proteins, GPCRs can interact with multiple intracellular signaling molecules, including β-arrestins, scaffold proteins, and other signaling molecules. These molecules play a role in GPCR signaling by engaging alternative pathways, resulting in the activation of diverse downstream effectors and cellular responses. The intricate nature of GPCR signaling, with its involvement in multiple pathways, presents challenges in identifying ligands that exhibit selective biased signaling. Understanding the biased signaling profiles of novel selective CB_2R agonists is essential for the development of drugs with enhanced efficacy and safety profiles. This understanding can aid in the identification of compounds with favorable signaling profiles, selectively activating specific pathways while avoiding others. Such advancements can contribute to the development of drugs that more effectively target diseases with reduced side effects.

After the identification of a collection of CB_2R selective agonists in previous Chapters, it was deemed necessary to conduct a more comprehensive pharmacological characterization by investigating their functional selectivity profiles, specifically biased and unbiased signaling. The tested ligands can be classified into three distinct signaling profiles. First, the unbiased ligands (**38c** and **38n**) exhibit no preference between the G-protein and β-arrestin pathways. Second, the G-protein biased ligands (**37r**, **36r**, **38d**, **38f**, and **38q**) display high activity (EC_{50}) and excellent efficacy (E_{max} > 85%) in the cAMP pathway, along with moderate efficacy in β-arrestin recruitment. Lastly, the β-arrestin biased ligands (**35m**, **37f**, and **38r**) demonstrate superior performance in the non-canonical GPCR signaling pathway mediated by β-arrestin.

The second section of this Chapter is dedicated to the initial assessment of the therapeutic potential of the selected CB_2R agonists obtained in this Doctoral Thesis. For this purpose, four CB_2R agonists were chosen, and their effectiveness in reducing the proliferation of a highly aggressive cancer (glioblastoma) and their ability to modulate inflammation mediators (anti-inflammatory action) were evaluated.

The CB_2R, which is extensively expressed in immune cells and has been found to be involved in regulating inflammation and immune responses in the tumor microenvironment, holds great potential in cancer treatment. Selectively activating CB_2R with agonists has demonstrated promising effects across various aspects of cancer therapy. One significant effect is their ability to induce apoptosis in cancer cells. CB_2R

USC DE COMPOSTELA

agonists trigger signaling pathways that promote apoptosis specifically in tumor cells while sparing healthy cells, resulting in tumor regression. Additionally, CB_2R agonists exhibit anti-proliferative effects by inhibiting the growth and division of cancer cells. They disrupt the signaling pathways responsible for cell proliferation, ultimately reducing tumor growth and progression. The use of CB_2R agonists in cancer treatment offers significant advantages. Their targeted effects on tumor cells, ability to inhibit proliferation, anti-angiogenic properties, and immunomodulatory effects make them valuable candidates for combination therapies and personalized treatment approaches. However, the limited availability of potent and highly selective CB_2R agonists poses a significant challenge in the field of cancer therapy, impeding the full exploration of CB_2R activation's therapeutic potential. Further research and development of these agonists are essential to fully harness their therapeutic benefits and improve outcomes for cancer patients.

Given the potential role of CB_2R agonists in cancer treatment, our research aimed to investigate the proliferative activity of our most promising compounds in a tumor model cell line. Building upon previous studies that demonstrated the *in vitro* effectiveness of two phytocannabinoids, Δ^9-THC and CBD (a non-psychoactive phytocannabinoid), in a glioblastoma cell line (U87), we selected this particular cell line as our model. Glioblastoma is a highly aggressive tumor of the central nervous system characterized by reduced patient survival and an urgent demand for novel treatment options.

It has been observed that our compounds significantly reduced cell proliferation of the U87 glioblastoma cell line in a dose-dependent manner, with reductions ranging from approximately 15% to 40%. In particular, compound **37f** exhibited a remarkable 40% reduction in glioblastoma proliferation at a concentration of 10 μM. Although these findings are preliminary, the observed inhibition of cell proliferation *in vitro* highlights the potential of the selected CB_2R agonists as promising candidates for further exploration and inclusion in hit-to-lead programs. Furthermore, these results validate the role of CB_2R agonism in inhibiting cell proliferation in *in vitro* cancer models, underscoring the significance of the endocannabinoid system (ECS) in cancer treatment.

USC
UNIVERSIDADE DE SANTIAGO DE COMPOSTELA

The upregulation of CB_2R has been extensively demonstrated in various inflammatory processes, particularly in relation to neuroinflammation and neurodegeneration. Targeting CB_2R with selective agonists has shown potent anti-inflammatory effects. Studies have revealed that the administration of CB_2R agonists effectively reduces the activation of proinflammatory microglia, leading to a shift towards an anti-inflammatory phenotype. This modulation of microglial polarization plays a critical role in mitigating neuroinflammatory responses. Additionally, CB_2R agonists have been shown to inhibit the production and release of pro-inflammatory cytokines while promoting the secretion of anti-inflammatory cytokines. These combined actions contribute to the reduction of neuroinflammatory damage and provide neuroprotection in various central nervous system disorders characterized by inflammation and neurodegeneration.

It has been observed that our compounds showed a significant and dose-dependent reduction in the production of pro-inflammatory cytokines (such as TNF-α, IFN-γ, IL-1β, and IL-6) and a notable increase in the production of anti-inflammatory cytokines (including IL-4 and IL-10) in resting monocytes and macrophages. Interestingly, a more pronounced effect was observed in activated monocytes and macrophages. Importantly, the effect of the CB_2R agonists was completely reversed in the presence of JTE907 (a selective CB_2R antagonist), conclusively demonstrating the CB_2R-mediated nature of the observed effect. These findings provide compelling evidence for the anti-inflammatory properties of our CB_2R agonists in both resting and activated immune cells. The ability of our compounds to modulate cytokines production, reducing pro-inflammatory cytokines while promoting the release of anti-inflammatory cytokines, highlights their potential as therapeutic agents for inflammatory-based pathologies.

USC
UNIVERSIDADE DE SANTIAGO DE COMPOSTELA

USC
UNIVERSIDADE
DE SANTIAGO
DE COMPOSTELA

RESUMEN

El sistema endocannabinoide (ECS) comprende los receptores cannabinoides (CBRs), sus ligandos endógenos (endocannabinoides, eCBs) y las enzimas involucradas en la síntesis, metabolismo y transporte de los eCBs. Actualmente se conocen dos CBRs, ambos receptores de membrana (GPCRs): el Receptor Cannabinoide tipo 1 (CB_1R), presente principalmente en el sistema nervioso central (SNC), y el Receptor Cannabinoide tipo 2 (CB_2R), ampliamente expresado en la periferia.

CB_2R es un receptor muy poco explorado, expresado principalmente en la periferia, especialmente en las células del sistema inmunológico. Varias evidencias han demostrado que CB_2R se encuentra sobreexpresado en la microglia y en las células cerebrales en los enfermos de patologías neurodegenerativas, mientras que su expresión en el SNC saludable aún no ha sido aclarada. La activación de CB_2R en el SNC lleva a la polarización de la microglia del estado M1 (fenotipo pro-inflamatorio caracterizado por la producción de citoquinas pro-inflamatorias) al estado M2 (fenotipo anti-inflamatorio caracterizado por la producción de citoquinas anti-inflamatorias). Este efecto anti-inflamatorio representa una estrategia terapéutica potencial en el tratamiento de diversas patologías como las enfermedades neurodegenerativas, el control del dolor, las enfermedades autoinmunes y el cáncer.

El papel del ECS en el contexto del cáncer ha sido investigado exhaustivamente recientemente y varios estudios han demostrado los efectos antitumorales de los agonistas de CB_2R en diferentes tipos de cáncer. Al activar selectivamente CB_2R, los agonistas han mostrado efectos prometedores en diversos aspectos del tratamiento del cáncer. Un efecto significativo es su capacidad para inducir apoptosis en las células cancerosas. Se ha descubierto que los agonistas de CB_2R desencadenan vías de señalización que promueven específicamente la apoptosis en las células tumorales, mientras protegen las células sanas, lo que lleva a la regresión del tumor. Este enfoque dirigido minimiza los posibles efectos secundarios asociados a la quimioterapia convencional, que a menudo afecta tanto a células cancerosas como a células sanas. Además, los agonistas de CB_2R muestran efectos antiproliferativos al inhibir el crecimiento y división de las células cancerosas. Pueden interrumpir las vías de señalización responsables de la proliferación celular, reduciendo así el crecimiento y la progresión del tumor.

USC UNIVERSIDADE DE SANTIAGO DE COMPOSTELA

Sin embargo, la disponibilidad limitada de agonistas potentes y altamente selectivos de CB_2R plantea un desafío significativo en el campo de la terapia del cáncer, dificultando la exploración completa del potencial terapéutico de la activación de CB_2R.

La presente Tesis Doctoral describe el diseño, la síntesis, la evaluación farmacológica (datos de afinidad y funcionales), la relación estructura-actividad y los estudios farmacológicos avanzados de una serie de nuevos y potentes ligandos selectivos de CB_2R. Los resultados descritos aquí forman parte de un proyecto metodológico que demuestra las ventajas competitivas de las reacciones multicomponente en Química Médica.

El primer capítulo de esta Tesis Doctoral describe la síntesis y caracterización de una amplia colección de Agonistas Sintéticos de los Receptores Cannabinoides (SCRAs). Durante la última década, los SCRAs han surgido como el grupo más grande y desafiante de Nuevas Sustancias Psicoactivas (NPS) controladas por el Centro Europeo de Monitoreo de Drogas y Toxicomanías (EMCDDA). En la mitad de la década de 2000, los SCRAs entraron al mercado ilícito de drogas en varias formas, como polvos o integrados en materia vegetal que se fuma, como una alternativa "legal" al cannabis. Los SCRAs y el tetrahidrocannabinol (Δ^9-THC) difieren tanto en estructura como en perfil farmacológico. Mientras que el Δ^9-THC actúa como un agonista parcial en ambos receptores (CBRs), los SCRAs son agonistas completos (full agonists) que ejercen su efecto psicoactivo a través de su agonismo en CB_1R, aunque a menudo exhiben un efecto agonista más pronunciado en CB_2R.

Uno de los principales problemas con estos agonistas es su alta potencia y excelente eficacia, ya que dosis más bajas son suficientes para producir efectos psicoactivos. Sin embargo, los efectos biológicos impredecibles, la dosificación no regulada y el uso variable aumentan la probabilidad de sobredosis, intoxicación y toxicidad grave. El rápido aumento en casos de intoxicaciones y muertes relacionadas con los SCRAs subraya la importancia de los estudios de toxicidad para evaluar los riesgos para la salud y proponer un manejo médico adecuado para los casos de intoxicación. Varios informes clínicos confirman efectos graves asociados con los SCRAs, como convulsiones, daño cardiovascular, daño renal, accidente cerebrovascular, psicosis, paranoia y ataques de ansiedad. Actualmente, se sabe poco sobre los mecanismos subyacentes de estos efectos tóxicos.

USC DE COMPOSTELA

El primer capítulo se centró en la síntesis y evaluación farmacológica de una amplia colección de SCRAs (64 ligandos, Figura I). Esta colección exhibe diversidad esquelética, estereocémica y funcional, lo que permite investigar las características más destacadas que surgen de la relación estructura-actividad (SAR) y la identificación de ligandos selectivos de CB_2R (Figura I).

En general, tanto en la serie de los ésteres como en la serie de las amidas, la mayoría de los derivados tienen una afinidad alta hacia los receptores CB_1R y CB_2R. Tomados en conjunto, los datos de afinidad sugieren que la diversidad funcional (ésteres y amidas) es un factor más importante que la diversidad estructural (núcleo heterocíclico) para definir la potencia y selectividad. En general, tanto en los ésteres como en las amidas, los derivados con grupos *i*-Pr parecen tener una afinidad ligeramente menor (en ambos CBRs) que los análogos con grupos *t*-Bu.

De acuerdo con sus perfiles cannabimiméticos *in vitro*, se ha confirmado que los estereoisómeros *(S)* son más potentes que los estereoisómeros correspondientes *(R)*, con una diferencia de ΔpK_i [pK_i *(S)* - pK_i *(R)*] > 2 en la mayoría de los casos en ambos subtipos de receptores. Además, el análisis de los datos de unión evidencia que los estereoisómeros *(R)* tienen en general una afinidad menor (en ambos receptores cannabinoides) y cierta selectividad por CB_2R.

Aunque la mayoría de los ligandos descritos aquí reproducen el perfil intrínseco (no selectivo) de los agonistas de receptores cannabinoides (SCRAs), el examen de los datos de unión permitió identificar nuevos derivados que combinan elevadad afinidad e incipiente selectividad por CB_2R (**22i**, **22l**, **22o**, **23j**, **23m** y **23o**).

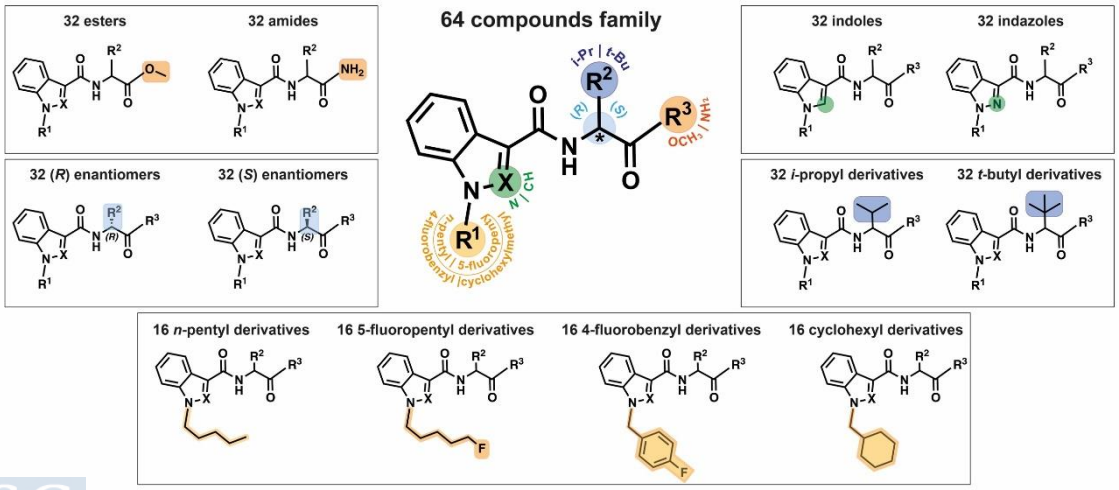


Figura I: Estructura general de la biblioteca y elementos de diversidad incluidos.

En el contexto de este estudio, decidimos examinar preliminarmente la neurotoxicidad de un conjunto de agonistas de cannabinoides sintéticos preparados en este trabajo, utilizando células neuronales primarias de ratón. Los resultados sugieren que todos los ligandos probados redujeron significativamente la viabilidad celular, lo que indica un alto nivel de neurotoxicidad en esta línea celular. La reducción en la viabilidad celular parece depender tanto del sistema heterocíclico como del grupo funcional pesente en el HEAD, siendo las amidas derivadas del núcleo de indazol las que presentaron mayor neurotoxicidad.

En los capítulos segundo, tercero y cuarto de esta Tesis Doctoral, el objetivo fue explorar nuevos espacios de diversidad dentro de la serie de SCRAs para obtener nuevos agonistas que se dirijan selectivamente al CB_2R. Este estudio se inspiró en el modelo farmacofórico de la familia de SCRAs (Figura IIA) y en las tendencias SAR observadas en el Capítulo 1. Para evitar posibles efectos neurotóxicos observados en la serie de indazol, nos centramos en el esqueleto de indol. El propósito principal de estos capítulos es desarrollar una prueba de concepto para la síntesis de nuevos agonistas selectivos del CB_2R (amidas y ésteres) que sean novedosos y potentes, utilizando un enfoque basado en la reacción de Ugi (previamente no explorado) (Figura IIC).

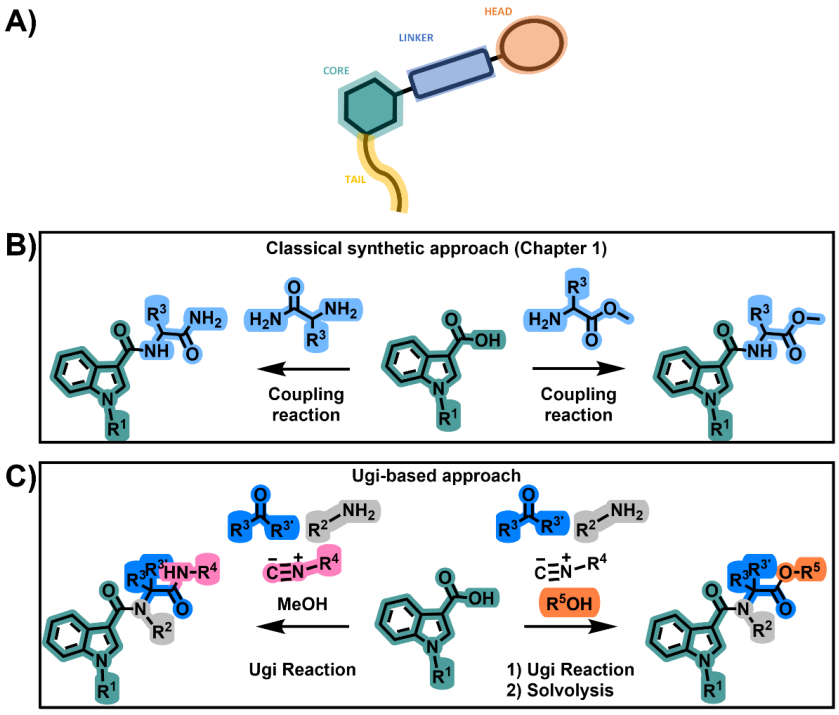


Figura II: A) Modelo farmacofórico de los agonistas de receptores cannabinoides (SCRAs). B) Síntesis clásica de SCRAs. C) Demostración del concepto de ensamblaje de quimiotecas análogos a SCRAs mediante la reacción de Ugi de cuatro componentes (U4CR).

USC UNIVERSIDADE DE SANTIAGO DE COMPOSTELA

Esta aproximación permite la síntesis convergente y de alto rendimiento de series de ésteres y amidas en una sola etapa, facilitando la exploración eficiente de este farmacóforo para identificar ligandos selectivos por el CB_2R. Además, hicimos hincapié en explorar las características más significativas de la relación estructura-actividad (SAR) y la relación estructura-selectividad (SSR) dentro de estas series.

Esta metodología permite explorar no solo los sustituyentes en R^1, R^2 y R^3, sino también la introducción de un segundo grupo R^3, un residuo alquilo en la amida terminal (R^4, serie de amidas) o un grupo alcoxi diferente en la función ester (R^5, serie de ésteres) (Figura IIC). Dentro de la serie de amidas SCRA, todos los ligandos descritos son amidas primarias ($CONH_2$). Nuestra aproximación permite explorar grupos alquilo en la amida terminal (R^4, Figura II), que pueden alterar el perfil de afinidad y selectividad observado.

Para el diseño de la nueva serie, aprovechamos la analogía estructural entre el farmacóforo de SCRA y la estructura química de los aductos de Ugi (acilamino amida) (Figura II). Desde un punto de vista estructural, la reacción de cuatro componentes de Ugi (U4CR) conserva los elementos farmacóforos, incluyendo el enlace entre el núcleo central y la cabeza del modelo farmacóforo, lo que permite la modificación y exploración en cuatro posiciones diferentes (Figura II). Se previó que el uso de ácidos N-substituidos-indol-3-carboxílicos (R^1), aminas apropiadamente sustituidas (R^2), aldehídos o cetonas (R^3, $R^{3'}$) e isonitrilos (R^4) generarían aductos de Ugi que se ajustan perfectamente a la estructura de los compuestos objetivo (Figura IIC). Explotando la versatilidad de la reacción de Ugi, decidimos introducir diferentes grupos en R^3 (además de *i*-Pr y *t*-Bu de la colección de SCRA en el Capítulo 1) y en R^4 para evaluar el impacto de la introducción de grupos en la amida terminal.

El método sintético basado en la química multicomponente propuesto aquí permite el rápido ensamblaje de quimiotecas de ésteres y amidas. Sintetizamos 168 nuevos derivados (ésteres y amidas) con diversos patrones de sustitución inexplorados en series similares a SCRA. Es importante destacar que todos los compuestos obtenidos en estos capítulos contienen un centro estereogénico. Los ligandos se aislaron y se evaluaron farmacológicamente como mezclas racémicas.

USC
UNIVERSIDADE DE SANTIAGO DE COMPOSTELA

Un análisis exhaustivo de los datos de afinidad obtenidos para estas series demuestra la efectividad del proceso de farmacomodulación. A partir de un prototipo dual CB_1R-CB_2R, hemos logrado disociar por completo el perfil de afinidad/selectividad de estos receptores y descubrir nuevos y potentes ligandos que reconocen específicamente el CB_2R. Cuarenta y siete compuestos (ésteres y amidas) descubiertos en estos capítulos destacan por su excelente afinidad (valores de K_i entre 34.8 - 307 nM) y perfil de selectividad (>100 veces sobre el CB_1R).

Finalmente, los ligandos más potentes y selectivos frente al CB_2R se separaron en sus enantiómeros, mediante cromatografía líquida de alta resolución (HPLC) quiral a escala semipreparativa, y se evaluaron farmacológicamente en ambos receptores cannabinoides. La configuración absoluta de los nuevos ligandos del CB_2R se determinó utilizando la técnica de dicroísmo circular (CD). Los datos farmacológicos obtenidos confirmaron que tres de los nuevos ligandos selectivos para el CB_2R [*(S)*-**35m**, *(S)*-**37r**, *(S)*-**38n**] mostraron reconocimiento enantioespecífico hacia el CB_2R.

El objetivo principal del quinto y último capítulo de esta Tesis Doctoral fue la evaluación farmacológica avanzada y los estudios *in vitro* de los ligandos seleccionados para el CB_2R. Este capítulo está dedicado a una caracterización más profunda de la farmacología y a la evaluación preliminar de algunas de las aplicaciones terapéuticas de los mejores compuestos identificados en esta Tesis. Inicialmente, se corroboró el comportamiento agonista de los compuestos seleccionados a través de experimentos funcionales de AMPc, luego se realizó un estudio detallado de sus vías de señalización (sesgadas o no sesgadas). Los ligandos seleccionados se agruparon en dos categorías según su comportamiento funcional (completo o parcial).

El fenómeno por el cual los ligandos de los GPCR modulan selectivamente la vía de la proteína G y/o de la β-arrestina para mediar rutas específicas de transducción de señales se conoce como "selectividad funcional" o "agonismo sesgado". El concepto de agonismo sesgado ha transformado significativamente nuestra comprensión de la señalización de los GPCR y ha revolucionado el campo del descubrimiento de fármacos. Sin embargo, los mecanismos moleculares que subyacen al sesgo en la señalización todavía son en gran medida desconocidos, e investigar las contribuciones funcionales de las vías de señalización de la proteína G y la β-arrestina para los ligandos endógenos y exógenos sigue siendo una tarea desafiante.

USC DE COMPOSTELA

Tras la activación de los receptores de membrana (GPCRs), pueden coexistir diversas vías de señalización y efectores celulares. Además de las proteínas G, los GPCR pueden interactuar con múltiples moléculas de señalización intracelular, incluyendo β-arrestinas, proteínas de andamiaje y otras moléculas de señalización. Estas moléculas desempeñan un papel en la señalización de los GPCR al involucrar vías alternativas, lo que resulta en la activación de diversos efectores celulares y respuestas. La naturaleza compleja de la señalización de los GPCRs, con la participación de múltiples vías, plantea desafíos para identificar ligandos que exhiban señalización sesgada. Comprender los perfiles de señalización sesgada de nuevos agonistas selectivos del CB_2R es esencial para el desarrollo de fármacos con una eficacia y perfiles de seguridad mejorados. Esta comprensión puede ayudar a identificar compuestos con perfiles de señalización favorables, activando selectivamente vías específicas mientras se evitan otras. Estos avances pueden contribuir al desarrollo de fármacos más selectivos y con menores efectos secundarios.

Una vez identificada una colección de agonistas selectivos del CB_2R en capítulos anteriores, consideramos interesante realizar una caracterización farmacológica más completa investigando sus perfiles de selectividad funcional, específicamente señalización sesgada y no sesgada. Esos experimentos permiten agrupar los ligandos estudiados en tres perfiles de señalización distintos. En primer lugar, los ligandos no sesgados (**38c** y **38n**), que no muestran preferencia entre las vías de la proteína G y las β-arrestinas. En segundo lugar, los ligandos sesgados hacia la proteína G (**37r**, **36r**, **38d**, **38f** y **38q**), que muestran alta actividad (EC_{50}) y excelente eficacia (Emax > 85%) en la vía del cAMP, junto con una eficacia moderada en el reclutamiento de las β-arrestinas. Por último, los ligandos sesgados hacia las β-arrestinas (**35m**, **37f** y **38r**), que demuestran una efficacia superior en la vía de señalización no canónica de los GPCR (mediada por las β-arrestinas.

USC
UNIVERSIDADE DE SANTIAGO DE COMPOSTELA

La segunda sección de este capítulo está dedicada a la evaluación inicial del potencial terapéutico de los agonistas selectivos del CB_2R seleccionados obtenidos en esta Tesis Doctoral. Con este propósito, se eligieron cuatro agonistas del CB_2R y se evaluó su eficacia en la reducción de la proliferación de un cáncer altamente agresivo (glioblastoma) y su capacidad para modular mediadores de la inflamación (acción antiinflamatoria).

El CB_2R, que se expresa ampliamente en células inmunes y que se ha encontrado que está involucrado en la regulación de la inflamación y las respuestas inmunes en el microambiente tumoral, tiene un gran potencial en el tratamiento del cáncer. La activación selectiva del CB_2R con agonistas ha demostrado efectos prometedores en diversos aspectos de la terapia contra el cáncer. Uno de los efectos más importantes es su capacidad para inducir apoptosis en las células cancerosas. Los agonistas del CB_2R activan vías de señalización que promueven la apoptosis especifica en las células tumorales, mientras protegen a las células sanas, lo que resulta en la regresión del tumor. Además, los agonistas del CB_2R muestran efectos antiproliferativos al inhibir el crecimiento y la división de las células cancerosas. Interfieren con las vías de señalización responsables de la proliferación celular, lo que finalmente reduce el crecimiento y la progresión del tumor. El uso de agonistas del CB_2R en el tratamiento del cáncer ofrece ventajas significativas. Sus efectos sobre las células tumorales: 1) capacidad para inhibir la proliferación, 2) propiedades antiangiogénicas y 3) efectos inmunomoduladores los convierten en candidatos valiosos para terapias combinadas y nuevas aproximaciones de la medicina personalizada. Sin embargo, la disponibilidad limitada de agonistas del CB_2R potente y altamente selectivos representa un desafío importante en el campo de la terapia contra el cáncer, lo que dificulta la exploración completa del potencial terapéutico de la activación del CB_2R. Se necesita una mayor investigación y desarrollo de estos agonistas para aprovechar plenamente sus beneficios terapéuticos y mejorar los resultados para los pacientes con cáncer.

Debido a la potencial aplicación de los agonistas del CB_2R en el tratamiento del cáncer, nuestro objetivo fue investigar la actividad proliferativa de nuestros compuestos más prometedores en una línea celular modelo. Basándonos en estudios previos que demostraron la efectividad *in vitro* de dos fitocannabinoides, el Δ^9-THC y el CBD (un fitocannabinoide no psicoactivo), en una línea celular de glioblastoma (U87),

USC DE COMPOSTELA

seleccionamos esta línea como nuestro modelo. El glioblastoma es un tumor altamente agresivo del sistema nervioso central caracterizado por una reducida supervivencia de los pacientes y una demanda urgente de nuevas opciones de tratamiento.

Observamos que los compuestos seleccionados redujeron significativamente la proliferación celular de la línea celular de glioblastoma U87 de manera dependiente de la dosis, con reducciones que oscilaron entre aproximadamente el 15% y el 40%. En particular, el compuesto **37f** mostró una notable reducción (40%) en la proliferación del glioblastoma a una concentración de 10 µM. Aunque estos hallazgos son preliminares, la inhibición observada de la proliferación celular *in vitro* resalta el potencial de los agonistas seleccionados del CB_2R como candidatos prometedores para una mayor exploración e inclusión en programas de desarrollo de fármacos. Además, estos resultados validan el papel del agonismo del CB_2R en la inhibición de la proliferación celular en modelos de cáncer *in vitro*, subrayando la importancia de la modulación del sistema endocannabinoide (ECS) en el tratamiento del cáncer.

La sobreexpresión del CB_2R es muy abundante durante los procesos inflamatorios, especialmente en los procesos de neuroinflamación y neurodegeneración. La inhibición selectiva del CB_2R mediante agonistas ha mostrado efectos anti-inflamatorios potentes. Estudios han revelado que la administración de agonistas del CB_2R reduce eficazmente la activación de la microglía pro-inflamatoria, promoviendo un cambio hacia un fenotipo anti-inflamatorio. Esta modulación de la polarización de la microglía juega un papel crucial en la mitigación de las respuestas neuroinflamatorias. Además, los agonistas CB_2R han demostrado inhibir la producción y liberación de citocinas pro-inflamatorias, al tiempo que promueven la secreción de citocinas anti-inflamatorias. Estas acciones combinadas contribuyen a la reducción del daño neuroinflamatorio y proporcionan neuroprotección en diversos trastornos del sistema nervioso central caracterizados por la inflamación y la neurodegeneración.

Nuestros compuestos mostraron una reducción significativa, y dependiente de la dosis, en la producción de citocinas pro-inflamatorias (como TNF-α, IFN-γ, IL-1β e IL-6) y un notable aumento en la producción de citocinas anti-inflamatorias (incluyendo IL-4 e IL-10) en monocitos y macrófagos en reposo. Interesantemente, se observó un efecto más pronunciado en monocitos y macrófagos activados. Es importante destacar que el efecto de los agonistas del CB_2R se revirtió por completo en presencia de JTE907

USC UNIVERSIDADE DE SANTIAGO

(un antagonista selectivo del CB_2R), lo que demuestra de manera concluyente que el efecto observado es mediado por el CB_2R. Estos hallazgos brindan evidencias contundente de las propiedades antiinflamatorias de nuestros agonistas CB_2R, tanto en células inmunológicas en reposo como activadas. La capacidad de nuestros compuestos para modular la producción de citocinas, reduciendo las citocinas pro-inflamatorias y promoviendo la liberación de citocinas anti-inflamatorias, resalta su potencial como agentes terapéuticos para patologías basadas en la inflamación.

USC
UNIVERSIDADE DE SANTIAGO DE COMPOSTELA

RESUMO

O sistema endocannabinoide (ECS) comprende os receptores cannabinoides (CBRs), os seus ligandos endóxenos (endocannabinoides, eCBs) e as enzimas involucradas na síntese, metabolismo e transporte dos eCBs. Actualmente coñécense dous CBRs, ámbolos dous receptores de membrana (GPCRs): o Receptor Cannabinoide tipo 1 (CB_1R), presente principalmente no sistema nervioso central (SNC), e o Receptor Cannabinoide tipo 2 (CB_2R), amplamente expresado na periferia.

CB_2R é un receptor moi pouco explorado, expresado principalmente na periferia, especialmente nas células do sistema inmunolóxico. Varias evidencias demostraron que CB_2R atópase sobreexpresado na microglia e nas células cerebrais nos enfermos de patoloxías neurodexenerativas, mentres que a súa expresión no SNC saudable aínda non foi aclarada. A activación de CB_2R no SNC leva á polarización da microglia do estado M1 (fenotipo proinflamatorio caracterizado pola produción de citoquinas proinflamatorias) ao estado M2 (fenotipo antiinflamatorio caracterizado pola produción de citoquinas antiinflamatorias). Este efecto antiinflamatorio representa unha estratexia terapéutica potencial no tratamento de diversas patoloxías como as enfermidades neurodexenerativas, o control da dor, as enfermidades autoinmunes e o cancro.

O papel do ECS no contexto do cancro foi investigado exhaustivamente nas últimas décadas e varios estudos demostraron os efectos antitumorais dos agonistas de CB_2R en diferentes tipos de cancro. Ao activar selectivamente CB_2R, os agonistas mostraron efectos prometedores en diversos aspectos do tratamento do cancro. Un efecto significativo é a súa capacidade para inducir apoptosis nas células cancerosas. Descubriuse que os agonistas de CB_2R desencadean vías de sinalización que promoven especificamente a apoptosis nas células tumorais, mentres protexen as células sas, o que leva á regresión do tumor. Este enfoque dirixido minimiza os posibles efectos secundarios asociados á quimioterapia convencional, que a miúdo afecta tanto a células cancerosas como a células sas. Ademais, os agonistas de CB_2R amosan efectos antiproliferativos ao inhibir o crecemento e división das células cancerosas. Poden interromper as vías de sinalización responsables da proliferación celular, reducindo así o crecemento e a progresión do tumor.

USC
UNIVERSIDADE DE SANTIAGO DE COMPOSTELA

Con todo, a dispoñibilidade limitada de agonistas potentes e altamente selectivos de CB_2R expón un desafío significativo no campo da terapia do cancro, dificultando a exploración completa do potencial terapéutico da activación de CB_2R.

A presente Tese Doutoral describe o deseño, a síntese, a avaliación farmacolóxica (datos de afinidade e funcionais), a relación estrutura-actividade e os estudos farmacolóxicos avanzados dunha serie de novos e potentes ligandos selectivos de CB_2R. Os resultados descritos aquí forman parte dun proxecto metodolóxico que demostra as vantaxes competitivas das reaccións multicompoñente en Química Médica.

O primeiro capítulo desta Tese Doutoral describe a síntese e caracterización dunha ampla colección de Agonistas Sintéticos dos Receptores Cannabinoides (SCRAs, polas súas siglas en inglés). Durante a última década, os SCRAs xurdiron como o grupo máis grande e desafiante de Novas Substancias Psicoactivas (NPS) controladas polo Centro Europeo de Vixilancia de Drogas e Toxicomanías (EMCDDA, polas súas siglas en inglés). Na metade da década de 2000, os SCRAs entraron ao mercado ilícito de drogas en varias formas, como pos ou integrados en materia vexetal que se fuma, como unha alternativa "legal" ao cánnabis. Os SCRAs e o tetrahidrocannabinol (Δ^9-THC) difiren tanto en estrutura como en perfil farmacolóxico. Mentres que o Δ^9-THC actúa como un agonista parcial en ambos receptores (CBRs), os SCRAs son agonistas completos (*full agonists*) que exercen o seu efecto psicoactivo a través do seu agonismo en CB_1R, aínda que a miúdo exhiben un efecto agonista máis pronunciado en CB_2R.

Un dos principais problemas con estes agonistas é a súa alta potencia e excelente eficacia, xa que doses máis baixas son suficientes para producir efectos psicoactivos. Non obstante, os efectos biolóxicos impredicibles, a dosaxe non regulada e o uso variable aumentan a probabilidade de sobredose, intoxicación e toxicidade grave. O rápido aumento en casos de intoxicacións e mortes relacionadas cos SCRAs subliña a importancia dos estudos de toxicidade para avaliar os riscos para a saúde e propoñer un manexo médico adecuado para os casos de intoxicación. Varios informes clínicos confirman efectos graves asociados cos SCRAs, como convulsións, dano cardiovascular, dano renal, accidente cerebrovascular, psicose, paranoia e ataques de ansiedade. Actualmente, sábese pouco sobre os mecanismos subxacentes destes efectos tóxicos.

USC
UNIVERSIDADE DE SANTIAGO DE COMPOSTELA

O primeiro capítulo centrouse na síntese e avaliación farmacolóxica dunha ampla colección de SCRAs (64 ligandos, Figura I). Esta colección exhibe diversidade esquelética, estereocémica e funcional, o que permite investigar as características máis destacadas que xorden da relación estrutura-actividade (SAR) e a identificación de ligandos selectivos de CB_2R (Figura I).

En xeral, tanto na serie dos ésteres como na serie das amidas, a maioría dos derivados teñen unha afinidade alta cara aos receptores CB_1R e CB_2R. Tomados en conxunto, os datos de afinidade suxiren que a diversidade funcional (ésteres e amidas) é un factor máis importante que a diversidade estrutural (núcleo heterocíclico) para definir a potencia e selectividade. En xeral, tanto nos ésteres como nas amidas, os derivados con grupos *i*-Pr parecen ter unha afinidade lixeiramente menor (en ambos CBRs) que os análogos con grupos *t*-Bu.

De acordo cos seus perfís cannabimiméticos *in vitro*, confirmouse que os estereoisómeros *(S)* son máis potentes que os estereoisómeros correspondentes *(R)*, cunha diferenza de ΔpK_i [pKi *(S)* - pK_i *(R)*] > 2 na maioría dos casos en ambos subtipos de receptores. Ademais, a análise dos datos de unión evidencia que os estereoisómeros *(R)* teñen en xeral unha afinidade menor (en ambos receptores cannabinoides) e certa selectividade por CB_2R.

Aínda que a maioría dos ligandos descritos aquí reproducen o perfil intrínseco (non selectivo) dos agonistas de receptores cannabinoides (SCRAs), o exame dos datos de unión permitiu identificar novos derivados que combinan elevada afinidade e incipiente selectividade por CB_2R (**22i**, **22l**, **22o**, **23j**, **23m** e **23o**).

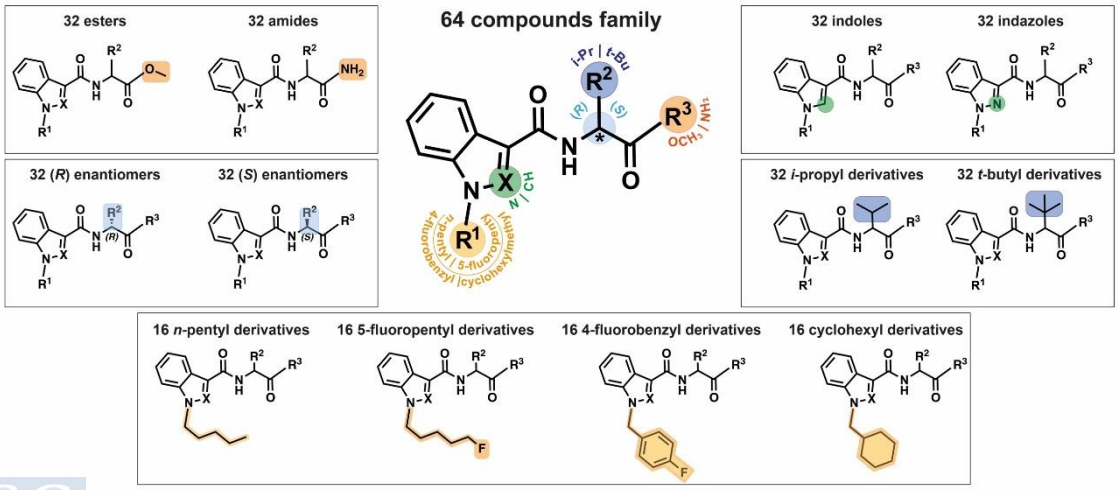


Figura I: Estrutura xeral da biblioteca e elementos de diversidade incluídos.

USC UNIVERSIDADE DE SANTIAGO DE COMPOSTELA

No contexto deste estudo, decidimos examinar preliminarmente a neurotoxicidade dun conxunto de agonistas de cannabinoides sintéticos preparados neste traballo, utilizando células neuronais primarias de rato. Os resultados suxiren que todos os ligandos probados reduciron significativamente a viabilidade celular, o que indica un alto nivel de neurotoxicidade nesta liña celular. A redución na viabilidade celular parece depender tanto do sistema heterocíclico como do grupo funcional presente na cabeza do modelo farmacóforo, sendo as amidas derivadas do núcleo de indazol as que presentaron maior neurotoxicidade.

Nos capítulos segundo, terceiro e cuarto desta Tese Doutoral, o obxectivo foi explorar novos espazos de diversidade dentro da serie dos SCRAs para obter novos agonistas que se dirixiran selectivamente ao CB_2R. Este estudo inspirouse no modelo farmacofórico da familia de SCRAs (Figura IIA) e nas tendencias SAR observadas no Capítulo 1. Para evitar posibles efectos neurotóxicos observados na serie de indazol, centrámonos no esqueleto de indol. O propósito principal destes capítulos é desenvolver unha proba de concepto para a síntese de novos agonistas selectivos do CB_2R (amidas e ésteres) que sexan novos e potentes, empregando un enfoque baseado na reacción de Ugi (previamente non explorado) (Figura IIC).

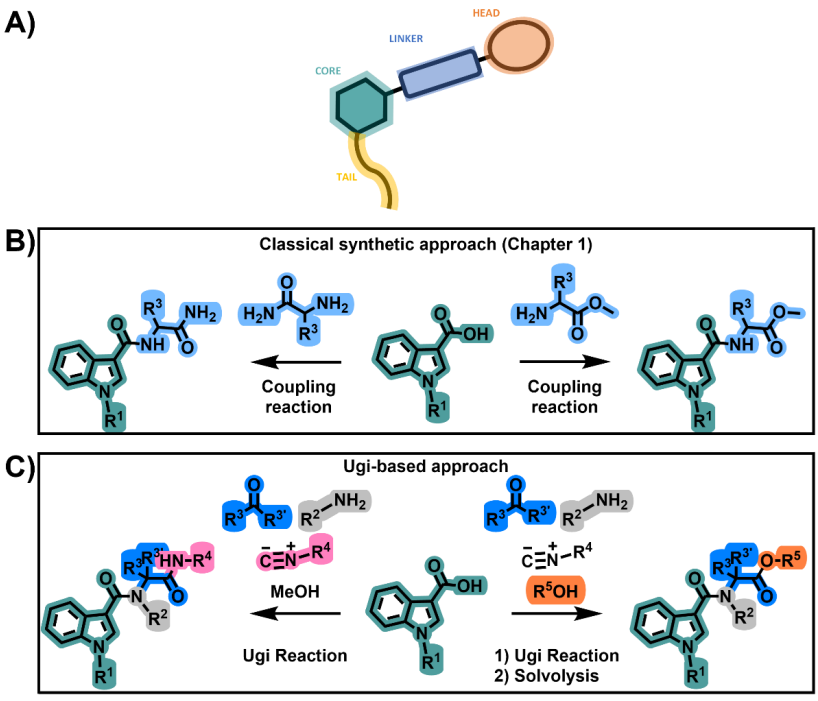


Figura II: A) Modelo farmacofórico dos agonistas de receptores cannabinoides (SCRAs). B) Síntese clásica de SCRAs. C) Demostración do concepto de ensamblaxe de quimiotecas análogas a SCRAs mediante a reacción de Ugi de catro compoñentes (U4CR).

USC UNIVERSIDADE DE SANTIAGO DE COMPOSTELA

Esta aproximación permite a síntese converxente e de alto rendemento de series de ésteres e amidas nunha soa etapa, facilitando a exploración eficiente deste farmacóforo para identificar ligandos selectivos polo CB_2R. Ademais, fixemos fincapé en explorar as características máis significativas da relación estrutura-actividade (SAR) e a relación estrutura-selectividade (SSR) dentro destas series.

Esta metodoloxía permite explorar non só os substituíntes en R^1, R^2 e R^3, senón tamén a introdución dun segundo grupo R^3, un residuo alquilo na amida terminal (R^4, serie de amidas) ou un grupo alcoxi diferente na función éster (R^5, serie de ésteres) (Figura IIC). Dentro da serie de amidas SCRA, todos os ligandos descritos son amidas primarias ($CONH_2$). A nosa aproximación permite explorar o efecto de grupos alquilo na amida terminal (R^4, Figura II), que poden alterar o perfil de afinidade e selectividade observado.

Para o deseño da nova serie, aproveitamos a analoxía estrutural entre o farmacóforo de SCRA e a estrutura química dos adutos de Ugi (acilamino amida) (Figura II). Dende un punto de vista estrutural, a reacción de catro compoñentes de Ugi (U4CR) conserva os elementos farmacóforos, incluíndo a ligazón entre o núcleo central e a cabeza do modelo farmacóforo, o que permite a modificación e exploración en catro posicións diferentes (Figura II). Previuse que o uso de ácidos *N*-substituidos-indol-3-carboxílicos (R^1), aminas apropiadamente substituídas (R^2), aldehídos ou cetonas (R^3, $R^{3'}$) e isonitrilos (R^4) xerarían adutos de Ugi que se axustan perfectamente á estrutura dos compostos obxectivo (Figura IIC). Explotando a versatilidade da reacción de Ugi, decidimos introducir diferentes grupos en R^3 (ademais de *i*-Pr e *t*-Bu da colección de SCRA no Capítulo 1) e en R^4 para avaliar o impacto da introdución de grupos na amida terminal.

O método sintético baseado na química multicompoñente proposto aquí permite a rápida ensamblaxe de quimiotecas de ésteres e amidas. Sintetizamos 168 novos derivados (ésteres e amidas) con diversos patróns de substitución inexplorados en series similares á SCRA. É importante destacar que todos os compostos obtidos nestes capítulos conteñen un centro estereoxénico. Os ligandos illáronse e avaliáronse farmacoloxicamente como mesturas racémicas.

USC
UNIVERSIDADE DE SANTIAGO DE COMPOSTELA

Unha análise exhaustiva dos datos de afinidade obtidos para estas series demostra a efectividade do proceso de farmacomodulación. A partir dun prototipo dual CB_1R-CB_2R, logramos disociar por completo o perfil de afinidade / selectividade a estes receptores e descubrir novos e potentes ligandos que recoñecen especificamente o CB_2R. Corenta e sete compostos (ésteres e amidas) descubertos nestes capítulos destacan pola súa excelente afinidade (valores de K_i entre 34.8 - 307 nM) e perfil de selectividade (>100 veces sobre o CB_1R).

Finalmente, os ligandos máis potentes e selectivos cara ao CB_2R separáronse nos seus enantiómeros mediante cromatografía líquida de alta resolución (HPLC) quiral a escala semipreparativa e avaliáronse farmacoloxicamente en ambos receptores cannabinoides. A configuración absoluta dos novos ligandos do CB_2R determinouse utilizando a técnica de dicroísmo circular (CD, polas súas siglas en inglés). Os datos farmacolóxicos obtidos confirmaron que tres dos novos ligandos selectivos para o CB_2R [*(S)*-**35m**, *(S)*-**37r**, *(S)*-**38n**] mostraron recoñecemento enantioespecífico cara ao CB_2R.

O obxectivo principal do quinto e último capítulo desta Tese Doutoral foi a avaliación farmacolóxica avanzada e os estudos *in vitro* dos ligandos seleccionados para o CB_2R. Este capítulo está dedicado a unha caracterización máis profunda da farmacoloxía e á avaliación preliminar dalgunhas das aplicacións terapéuticas dos mellores compostos identificados nesta Tese. Inicialmente, corroborouse o comportamento agonista dos compostos seleccionados a través de experimentos funcionais de AMPc, logo realizouse un estudo detallado das súas vías de sinalización (nesgadas ou non nesgadas). Os ligandos seleccionados agrupáronse en dúas categorías segundo o seu comportamento funcional (completo ou parcial).

O fenómeno polo cal os ligandos dos GPCR modulan selectivamente a vía da proteína $G_{i/o}$ da β-arrestina para mediar rutas específicas de transdución de sinais coñécese como "selectividade funcional" ou "agonismo nesgado". O concepto de agonismo nesgado transformou significativamente a nosa comprensión da sinalización dos GPCR e revolucionou o campo do descubrimento de fármacos. Con todo, os mecanismos moleculares que subxacen ao nesgo na sinalización aínda son en gran medida descoñecidos e investigar as contribucións funcionais das vías de sinalización da proteína G e a β-arrestina para os ligandos endóxenos e exóxenos segue sendo unha tarefa desafiante.

USC UNIVERSIDADE DE SANTIAGO DE COMPOSTELA

Trala activación dos receptores de membrana (GPCRs), poden coexistir diversas vías de sinalización e efectores celulares. Ademais das proteínas G, os GPCR poden interactuar con múltiples moléculas de sinalización intracelular, incluíndo β-arrestinas, proteínas de estadas e outras moléculas de sinalización. Estas moléculas desempeñan un papel na sinalización dos GPCR ao involucrar vías alternativas, o que resulta na activación de diversos efectores celulares e respostas. A natureza complexa da sinalización dos GPCRs, coa participación de múltiples vías, expón desafíos para identificar ligandos que exhiban sinalización nesgada. Comprender os perfís de sinalización nesgada de novos agonistas selectivos do CB_2R é esencial para o desenvolvemento de fármacos cunha eficacia e perfís de seguridade mellorados. Esta comprensión pode axudar a identificar compostos con perfís de sinalización favorables, activando selectivamente vías específicas mentres que se evitan outras. Estes avances poden contribuír ao desenvolvemento de fármacos máis selectivos e con menores efectos secundarios.

Unha vez identificada unha colección de agonistas selectivos do CB_2R en capítulos anteriores, consideramos interesante realizar unha caracterización farmacolóxica máis completa, investigando os seus perfís de selectividade funcional, especificamente sinalización nesgada e non nesgada. Eses experimentos permiten agrupar os ligandos estudados en tres perfís de sinalización distintos. En primeiro lugar, os ligandos non nesgados (**38c** e **38n**), que non amosan preferencia entre as vías da proteína G e as β-arrestinas. En segundo lugar, os ligandos nesgados cara á proteína G (**37r**, **36r**, **38d**, **38f** e **38q**), que mostran alta actividade (EC_{50}) e excelente eficacia (Emax > 85%) na vía do cAMP, xunto cunha eficacia moderada no recrutamento das β-arrestinas. Por último, os ligandos nesgados cara ás β-arrestinas (**35m**, **37f** e **38r**), que demostran unha eficacia superior na vía de sinalización non canónica dos GPCR (mediada polas β-arrestinas).

A segunda sección deste capítulo está dedicada á avaliación inicial do potencial terapéutico dos agonistas selectivos do CB_2R seleccionados obtidos nesta Tese Doutoral. Con este propósito, elixíronse catro agonistas do CB_2R e avaliouse a súa eficacia na redución da proliferación dun cancro altamente agresivo (glioblastoma) e a súa capacidade para modular mediadores da inflamación (acción antiinflamatoria).

USC
UNIVERSIDADE DE SANTIAGO DE COMPOSTELA

O CB_2R, que se expresa amplamente en células inmunes e que se atopou que está involucrado na regulación da inflamación e as respostas inmunes no microambiente tumoral, ten un gran potencial no tratamento do cancro. A activación selectiva do CB_2R con agonistas demostrou efectos prometedores en diversos aspectos da terapia contra o cancro. Un dos efectos máis importantes é a súa capacidade para inducir apoptosis nas células cancerosas. Os agonistas do CB_2R activan vías de sinalización que promoven a apoptosis específica nas células tumorais, mentres protexen ás células sas, o que resulta na regresión do tumor. Ademais, os agonistas do CB_2R amosan efectos antiproliferativos ao inhibir o crecemento e a división das células cancerosas. Interfiren coas vías de sinalización responsables da proliferación celular, o que finalmente reduce o crecemento e a progresión do tumor. O uso de agonistas do CB_2R no tratamento do cancro ofrece vantaxes significativas. Os seus efectos sobre as células tumorais: 1) capacidade para inhibir a proliferación, 2) propiedades antianxioxénicas e 3) efectos inmunomoduladores, convértenos en valiosos candidatos para terapias combinadas e para novas aproximacións da medicina personalizada. Non obstante, a limitada dispoñibilidade de agonistas do CB_2R potentes e altamente selectivos representa un desafío importante no campo da terapia contra o cancro, o que dificulta a exploración completa do potencial terapéutico da activación do CB_2R. Necesítase unha maior investigación e desenvolvemento destes agonistas para aproveitar plenamente os seus beneficios terapéuticos e mellorar os resultados para os pacientes con cancro.

Debido á potencial aplicación dos agonistas do CB_2R no tratamento do cancro, o noso obxectivo foi investigar a actividade proliferativa dos nosos compostos máis prometedores nunha liña celular modelo. Baseándonos en estudos previos, que demostraron a efectividade *in vitro* de dous fitocannabinoides, o Δ^9-THC e o CBD (un fitocannabinoide non psicoactivo), nunha liña celular de glioblastoma (U87), seleccionamos esta liña como o noso modelo. O glioblastoma é un tumor altamente agresivo do sistema nervioso central, caracterizado por unha reducida supervivencia dos pacientes e unha demanda urxente de novas opcións de tratamento.

Observamos que os compostos seleccionados reduciron significativamente a proliferación da liña celular de glioblastoma U87 de forma dependente da dose, con reducións que oscilaron entre o 15% e o 40% aproximadamente. En particular, o composto **37f** mostrou unha notable redución (40%) na proliferación do glioblastoma a unha concentración de 10 µM. Aínda que estes achados son preliminares, a inhibición observada da proliferación celular *in vitro* resalta o potencial dos agonistas

USC DE COMPOSTELA

seleccionados do CB_2R como candidatos prometedores para unha maior exploración e inclusión en programas de desenvolvemento de fármacos. Ademais, estes resultados validan o papel do agonismo do CB_2R na inhibición da proliferación celular en modelos de cancro *in vitro*, subliñando a importancia da modulación do sistema endocannabinoide (ECS) no tratamento do cancro.

A sobreexpresión do CB_2R é moi abundante durante os procesos inflamatorios, especialmente nos procesos de neuroinflamación e neurodexeneración. A inhibición selectiva do CB_2R mediante agonistas mostrou efectos antiinflamatorios potentes. Estudos revelaron que a administración de agonistas do CB_2R reduce eficazmente a activación da microglía proinflamatoria, promovendo un cambio cara a un fenotipo antiinflamatorio. Esta modulación da polarización da microglía xoga un papel crucial na mitigación das respostas neuroinflamatorias. Ademais, os agonistas CB_2R demostraron inhibir a produción e liberación de citocinas proinflamatorias, á vez que promoven a secreción de citocinas antiinflamatorias. Estas accións combinadas contribúen á redución do dano neuroinflamatorio e proporcionan neuroprotección en diversos trastornos do sistema nervioso central caracterizados pola inflamación e a neurodexeneración.

Os nosos compostos mostraron unha redución significativa, e dependente da dose, na produción de citocinas proinflamatorias (como TNF-α, IFN-γ, IL-1β e IL-6) e un notable aumento na produción de citocinas antiinflamatorias (incluíndo IL-4 e IL-10) en monocitos e macrófagos en repouso. Do mesmo xeito, tamén se observou un efecto máis pronunciado en monocitos e macrófagos activados. É importante destacar que o efecto dos agonistas do CB_2R reverteuse por completo en presenza de JTE907 (un antagonista selectivo do CB_2R), o que demostra de maneira concluínte que o efecto observado é mediado polo CB_2R. Estes achados brindan evidencias contundentes das propiedades antiinflamatorias dos nosos agonistas CB_2R, tanto en células inmunolóxicas en repouso como activadas. A capacidade dos nosos compostos para modular a produción de citocinas, reducindo as citocinas proinflamatorias e promovendo a liberación de citocinas antiinflamatorias, resalta o seu potencial como axentes terapéuticos para patoloxías baseadas na inflamación.

USC
UNIVERSIDADE DE SANTIAGO DE COMPOSTELA

USC
UNIVERSIDADE
DE SANTIAGO
DE COMPOSTELA

1 INTRODUCTION

USC
UNIVERSIDADE
DE SANTIAGO
DE COMPOSTELA

USC
UNIVERSIDADE
DE SANTIAGO
DE COMPOSTELA

1.1 ENDOCANNABINOID SYSTEM

The endocannabinoid system (ECS) consists of cannabinoid receptors (CBRs), their ligands (endocannabinoids, eCBs), and the enzymes involved in the synthesis, metabolism and transport of eCBs (Figure 1).[1] The ECS is present in the central and peripheral nervous system, but also in many other peripheral tissues, then regulating distinct functions. It regulates several physiological functions and mediates the crosstalk between different neurotransmitter systems, therefore exerting pivotal roles in the control of behavioural responses and being involved in the regulation of emotions, motivational behaviour, and cognitive functions.[2–4]

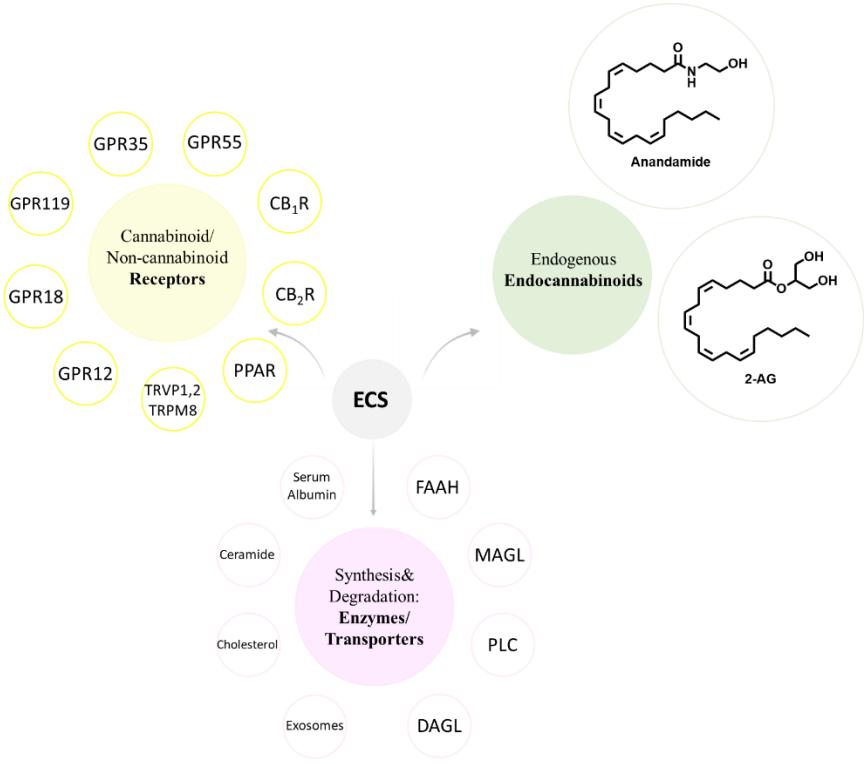


Figure 1: Representation of the endocannabinoid system.

Nowadays two CBRs are known: Cannabinoid Receptor type 1 (CB_1R), mostly present in the central nervous system (CNS), and Cannabinoid Receptor type 2 (CB_2R), heavily expressed in the periphery.[2,4] CB_2R is especially expressed in the cells of the immune system, and is a potential therapeutic target for the treatment of challenging autoimmune diseases, neuropathic pain and cancer.[5] Besides CB_1R and CB_2R, further CB-like receptors, including GPR18, GPR55 and GPR119, have been described to interact with endocannabinoids.[3,6]

A graphical representation of the distribution and functions of CB_1R and CB_2R all over the body is presented in Figure 2.

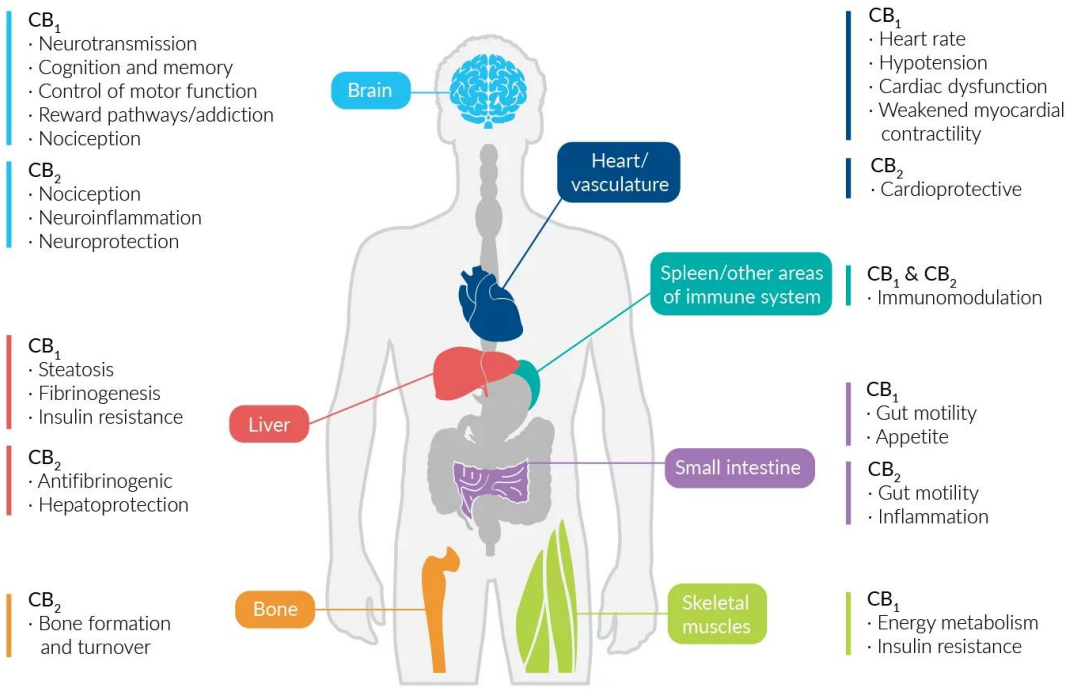


Figure 2: Functions and distribution of CB_1 and CB_2 receptors all over the body (Figure from caymanchem.com).[7]

USC UNIVERSIDADE DE SANTIAGO DE COMPOSTELA

1.1.1 Endocannabinoids and enzymes involved in their synthesis, transport, and degradation

The two main eCBs are derivatives of arachidonic acid (AA): *N*-arachidonoylethanolamine (anandamide, AEA) and 2-arachidonoylglycerol (2-AG), (Figure 3). Both act as endogenous agonists at cannabinoid receptor subtypes. In the brain, the 2-AG is much more abundant than the AEA.[8] Unlike other neurotransmitters, eCBs are produced on demand when and where needed, and have a relatively short action time. While the most studied eCBs are 2-AG and AEA, other frequent representative eCBs are *N*-eicosapentaenoylethanolamine (EPEA) and *N*-docosahexaenoyl-ethanolamine (DHEA) which are also agonists of CBRs (Figure 3).[5,8,9]

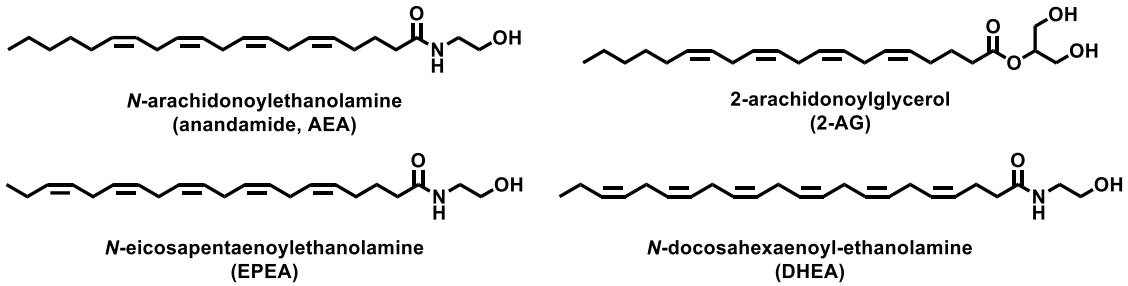


Figure 3: Structure of the most representative endocannabinoids (eCBs).

ECBs are biosynthesized from endogenous membrane components by different lipases and are rapidly degraded by enzymes. AEA is released from its membrane precursors via *N*-acylphosphatidyl-ethanolamine-specific phospholipase D (NAPE-PLD) while FAAH (fatty acid amide hydrolase) is responsible for its degradation into AA and ethanolamine. DAGLα and DAGLβ, two diacylglycerol lipases, are responsible for the formation of 2-AG and MGL (monoacyl glycerol lipase) for its degradation into AA and glycerol.[5] Both AEA and 2-AG can also be inactivated by cycloxygenase-2 (COX-2), cytochrome P450 and an endocannabinoid membrane transporter (EMT) which is responsible for their uptake.[9] ECBs activate CBRs, but they also interact with other receptors like transient receptor potential vanilloid 1 channel (TRPV1), expressed in peripheral sensory neurons, endothelial and immune cells and the peroxisome proliferator-activated receptors α and γ (PPARα and PPARγ), that are involved in lipid metabolism.[4,9] Recently, the eCBs role in several neurodegenerative diseases has been reported.[4]

USC UNIVERSIDADE DE SANTIAGO

1.1.2 Cannabinoid Receptors

Cannabinoid receptors (CBRs) are membrane proteins that belong to the G protein coupled receptors (GPCRs) family.[4] They are coupled primarily to $G_{i/o}$ proteins, which inhibit adenylate cyclase (AC) and cyclic AMP (cAMP) signaling. They also block certain voltage-sensitive calcium channels, stimulate MAPK (Mitogen-Activated Protein Kinases) and recruit β-arrestins.[4] Under specific circumstances, CB_1R also couples with $G\alpha_s$ increasing the cAMP production and with $G\alpha_q$ stimulating calcium release (Figure 4).[10] GPCRs are membrane receptors constituted by seven transmembrane domains (indeed they were recently named 7TMRs) that alternate between the intracellular and extracellular region.[11] G proteins are constituted by three subunits: α, β and γ. In resting conditions, the α subunit binds to a GDP molecule: when an agonist binds to the receptor, the receptor activation causes the replacement of GDP with GTP in the α subunit. Afterwards, this subunit dissociates from the β and γ subunits, which will now activate/inhibit enzymes or ion channels, called effectors. Thanks to its GTPase activity, the α subunit remains active until it hydrolyses the GTP to GDP; then the inactive α, β and γ complex is reformed (Figure 4).[11]

Recent studies demonstrate that following the binding of an agonist with a GPCR, two main signal transduction pathways can be activated. It is well documented that different ligands stabilize different conformations at the GPCR, which explains that GPCRs have different functional selectivity profiles, meaning they can signalize through different pathways and generate multiple downstream effects. This phenomenon is known as "biased agonism" or "biased signaling" and provides exciting opportunities for the development of novel, selective and safer drugs.[12,13] In Figure 4, the CBRs signal transduction pathways are briefly shown.

USC UNIVERSIDADE DE SANTIAGO DE COMPOSTELA

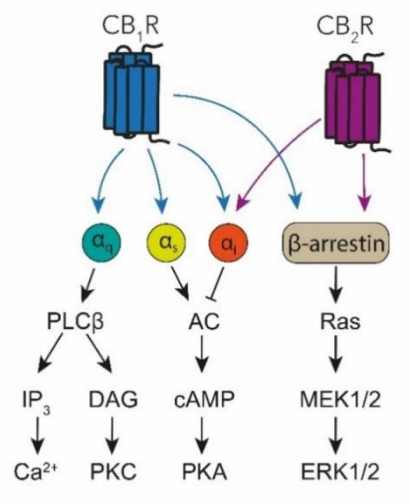


Figure 4: Representation of CBRs signal transduction pathways.[7]

Like other membrane receptors, CBRs can associate with other GPCRs forming oligomers, mostly homodimers or heterodimers.[14] The most studied dimers of CB_1R are those with dopamine D_2 receptors, adenosine A_2 receptors and δ opioid receptors. CB_1R may also interact with other types of proteins, for example with CRIP1a (Cannabinoid receptor interacting protein 1a) which can compete with β-arrestin for binding the C-terminus of CB_1R leading to a slower desensitization and internalization.[14]

CB_1R was the first cannabinoid receptor described (in 1990).[8] This receptor is encoded by the CNR1 gene and, as all GPCRs, is constituted by seven transmembrane domains connected by three extracellular and three intracellular loops, an extracellular N-terminal tail, and an intracellular C-terminal tail.[8] CB_1R structure is now well-known and has been crystallized with an antagonist, Taranabant (PDB: 5U09) (Figure 5).[15] It has been found that Taranabant interacts with TM1 and TM7 and fills into the CB_1R orthosteric pocket inside the opening between these transmembrane domains.[15] CB_1R orthosteric pocket is highly hydrophobic, indeed Taranabant makes several hydrophobic interactions but only three polar interactions with D104, S123 and S383 in the orthosteric binding site (Figure 5).[15] It has also been observed that the N-terminal region of CB_1R maintains a similar conformation to the structure in absence of the ligand.[15] Docking studies demonstrate that Rimobanant, another CB_1R antagonist, interacts in the same way and with the same residues as Tarabanant.[15] The same study has been carried out with (−)-*trans*-Δ^9-tetrahydrocannabinol (Δ^9-THC), a phytocannabinoid eliciting partial agonist behaviour. Δ^9-THC interacts with TM1 and TM7, as Taranabant and Rimonabant, but its alkyl chain also interacts with W356. The conformational change (to agonist) of this residue may be implicated in the CB_1R activation.[15]

USC UNIVERSIDADE DE SANTIAGO DE COMPOSTELA

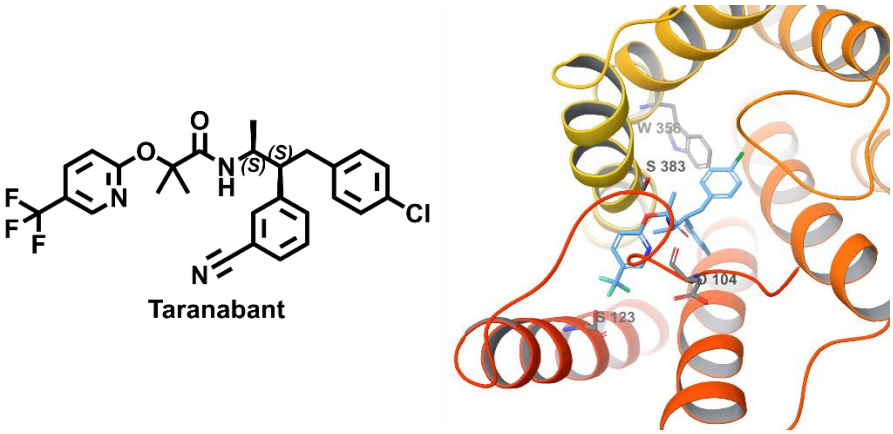


Figure 5: Structure of Taranabant and its binding to the orthosteric site of CB_1R.[15]

Recently, the drug-receptor complex structure of CB_1R with a potent and non-selective agonist [MDMB-FUBINACA (FUB)] (Figure 6) has been published (PDB: 6N4B)[16]. It has been shown that FUB binds CB_1R orthosteric pocket, making direct contact with residues F200 and W356. F200, which is stabilized by interactions with W356 in the inactive receptor state, rotates away to interact with the indazole ring of FUB.[16] The rotation of F200 allows W356 to rotate towards the outside, with a consequent outward movement of the cytoplasmic end of TM6 that serves to create a cavity for G protein binding.[16] This cavity is not present in the structure of CB_1R bound to antagonists reported to date, so it is possible that the movement of the N-terminal plays a role in the activation of the receptor.[15] It also shows that the alkyl chain in Δ^9-THC overlaps with the *p*-Fluorobenzyl group in FUB.[16]

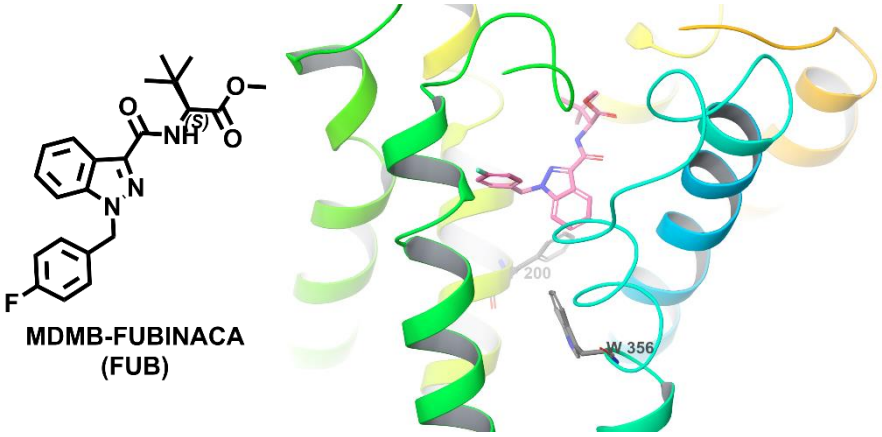


Figure 6: Structure of FUB and its interactions in the CB_1 binding site.[16]

In 1993, the CB_2R was isolated by a PCR-based strategy and studied for the first time.[17] The structure of CB_2R shares 44% sequence identity with CB_1R. The crystal structure of CB_2R has recently been obtained in a complex with the ligand AM10257 (PDB:5ZTY) (Figure 7).[18] This compound acts as a CB_2R antagonist and a CB_1R partial agonist. This dual profile is justified by a high comparability between CB_2R antagonists and CB_1R agonists binding pockets.[18] From a structural point of view AM10257 has a central pyrazole core and three-arms (Figure 7): compared to CB_1R, arm 3 (in green) assumes a vertical pose and interacts with F87 and F91, since AM10257 displays towards helices III and IV, so helices I and II move towards the ligand binding site. The adamantyl group within the arm 3 (in green) overlaps with the F102 and therefore, the N-terminal region does not actively contribute to the binding.[18] Arm 1 (in red) confines the side chain of W258 to a relatively rare rotamer and makes impossible to helix VI to rotate outward: this stabilizes the inactive state of the receptor.[15,18]

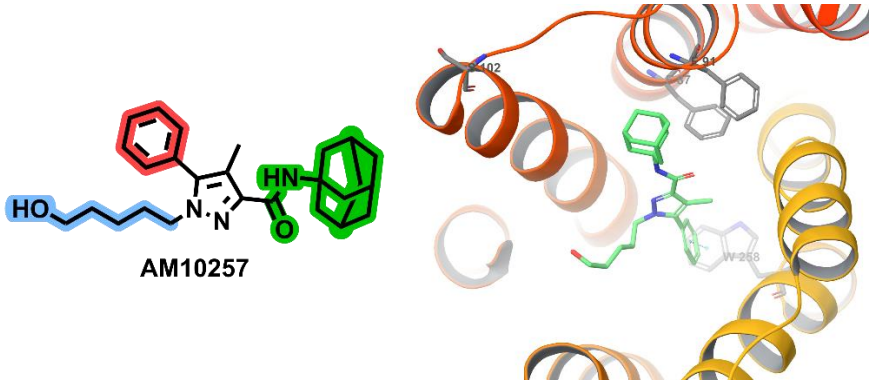


Figure 7: Structure of AM10257 and its binding to CB_2R.[18]

GPR18, GPR55 and GPR119 are orphan G-protein-coupled receptors, which can be modulated by various endogenous and synthetic cannabinoids; therefore they are classified as non-CB_1/CB_2 cannabinoid receptors.[19–21] GPR18 is expressed in the spleen, thymus, peripheral blood leukocytes, lymph nodes, cerebellum, lung, and testis; GPR55 is widely expressed in the brain, especially in the cerebellum; GPR119 is expressed predominantly in the pancreas and gastrointestinal tract.[19–21] GPR18 and GPR55 may be involved in pain, immunomodulation, intraocular pressure, metabolism, and cancer; while GPR119 is involved in the regulation of incretin and insulin hormone secretion: it might represent a potential therapeutic target for the treatment of obesity and diabetes.[19–21]

USC UNIVERSIDADE DE SANTIAGO DE COMPOSTELA

1.2 CB_1 RECEPTOR: BRIEF DESCRIPTION OF ITS DISTRIBUTION AND THERAPEUTIC POTENTIAL

The CB_1R is one of the most widely expressed membrane receptor in the central nervous system (CNS), mostly in neurons and glial cells.[4,8] At the peripheral level, CB_1R is expressed in the reproductive system (uterus, ovaries, testicles, prostate), heart, liver, kidney, lung, thymus and bone marrow. CB_1R mediates neurotransmitter release and controls different motor, emotional, cognitive, and sensory functions at both central and peripheral nervous systems, thus being involved in the regulation of feeding behaviour, metabolism, and energy balance.[4,8] CB_1R has been found in different neurons, including GABAergic, glutamatergic, cholinergic, glycinergic and serotonergic: they are particularly present on synaptic terminals, which explains their role in modulating synaptic transmission.[4,8] Recent studies demonstrated that the activation of CB_1R produces anxiolytic, analgesic, neuroprotective and anti-nausea effects. At the CNS, Δ^9-THC and the synthetic cannabinoid receptor agonists (SCRAs) induce several deleterious effects (such as agitation, psychosis, anxiety, tachycardia, and hypothermia).[3,5,8] The psychotropic effect derived by CB_1R modulation is one of its main limitations in drug development.[4,5,8,16] Different studies have pointed out that the use of Cannabis can be effective in the prevention and treatment of chemotherapy-induced nausea and vomiting in patients that do not respond to conventional antiemetic medicaments.[8] It has also been demonstrated that Δ^9-THC, through the activation of CB_1R, is able to lower the intraocular pressure making it potentially useful for the treatment of glaucoma.[22] In order to minimize psychoactive effects, it might be better to use a topical application.[22]

Moreover, it is now accepted that CB_1R activation at peripheral tissues contributes to energy balance and metabolic process. The role of eCBs as appetite promoters (acting via hypothalamic CB_1R) and the clinical observations of ECS (particularly CB_1R) overactivation play a critical role in regulating energy homeostasis in obese patients, with increased levels of eCBs in plasma at both central and peripheral tissues. This provided solid foundations for the pharmaceutical development of CB_1R antagonists for the treatment of obesity and its metabolic complications.[23,24] Studies have provided strong evidence for continued exploration of the therapeutic benefit derived from CB_1R in peripheral tissues, thus enabled to suppress food intake, increase energy expenditure and reduce lipogenesis.[23,24]

USC UNIVERSIDADE SANTIAGO

1.3 CB_2 RECEPTOR: DISTRIBUTION, FUNCTIONS AND THERAPEUTIC POTENTIAL

Unlike CB_1R, CB_2R is preferably expressed in the periphery, especially in immune cells.[2,4] It is mainly localized in macrophages, spleen, tonsils, thymus, leukocytes, lung, and testes.[2,4] It has been demonstrated that in neurodegenerative diseases (such as Alzheimer's disease and multiple sclerosis) CB_2R is upregulated in microglia and brain cells, while its expression in the healthy CNS is yet to be clarified.[12,17] CB_2R is coupled to G_I/G_O proteins and inhibits adenylyl cyclase, MAPK (mitogen-activated protein kinase) activation and increases intracellular calcium levels due to the modulation of PLC (phospholipase C). CB_2R also regulates ERK-MAPK pathways, involved in mitogenesis and in cancer cell proliferation.[25] Given its preferential expression in the peripheral nervous system and its upregulation in neuroinflammation and neurodegeneration, CB_2R is turning into an emerging target for the development of new drugs for the treatment of severe neuroinflammatory and neurodegenerative diseases.[2,9]

Recent studies demonstrated CB_2R upregulation during neurodegeneration and neuroinflammation. In microglial cells, the CB_2R activation promotes the release of anti-inflammatory cytokines and inhibits the release of proinflammatory cytokines. It has been observed that two microglial activation states can be involved in the neurodegeneration: M1, a proinflammatory state, and M2, an anti-inflammatory state.[2] Microglia plays an important role in chronic pain control. CB_2R agonists have been studied for their analgesic effect by inhibiting microglial activation and the subsequent inflammatory cascades.[26] In 2016, Bu et al. proposed the activation and modulation of microglia by CB_2R for the treatment of traumatic brain injury: a CB_2R inverse agonist (SMM-189) has been tested *in vitro* showing the capability to modulate the microglia from M1 to M2 state.[27] In the last decade, CB_2R has been considered as a promising target for the treatment of several neurodegenerative diseases such as Alzheimer's disease (AD), multiple sclerosis (MS), Parkinson's disease (PD) and Huntington's disease (HD).[2,9,28–30]

AD is a neurodegenerative disease that causes dementia: in 2020, AD affected more than 50 million people worldwide. The pathogenesis of this disease is poorly understood. Possible causes are the deposition of β-amyloid protein (Aβ), τ protein hyperphosphorylation and neuroinflammation.[2,28] In AD patients, CB_2R is overexpressed in microglia cells surrounding Aβ plaques. *In vitro* and *in vivo* studies

UFG UNIVERSIDADE DE GRANADA

have demonstrated that CB_2R agonists can reduce both neuroinflammation, promoting the M2 state in microglia, and β-amyloid protein levels, inhibiting the deposition of plaques.[2,28]

PD is a degenerative disease of the CNS that leads to shaking, stiffness, and difficulty in walking, balance, and coordination. PD is caused by a loss of nerve cells responsible for dopamine production in the substantia nigra compromising the dopaminergic neurotransmission in the basal ganglia. Recently, the role of ECS in this disease has been studied: via CB_2R on neurons, agonists exhibit neuroprotective effects by preventing the loss of nigral dopaminergic neurons.[9,29]

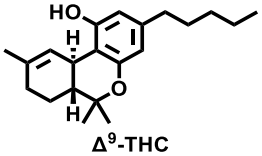
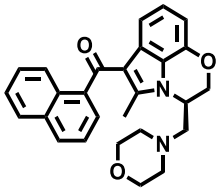
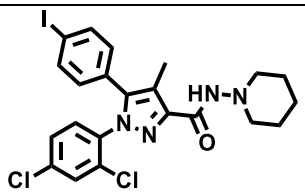
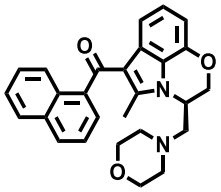
Amyotrophic lateral sclerosis (ALS) is a neurodegenerative disease that results in the progressive loss of motor neurons that control voluntary muscles. It can affect swallowing, talking and even breathing. Since neuroinflammation is a hallmark of ALS, modulators of ECS have been investigated. It has been proven that administration of agonist exerts neuroprotective effects through CB_2R.[9,30]

Multiple sclerosis (MS) is a neurodegenerative and autoimmune disease that affects more than two million people all over the world. The immune system attacks the protective sheath, the myelin that covers nerve fibres and causes communication problems between the brain and the rest of the body leading to a progressive neurodegeneration and disability.[9] Clinical evidence demonstrated that eCBs might exhibit neuroprotective and anti-inflammatory effects and slow down MS progression.[9] Lately, different Cannabis-based preparations have been approved for the treatment of MS-induced muscle spasticity and rigidity. *Ex vivo* assays demonstrated an alteration of CB_2R in MS patients, while *in vivo* experiments showed that the administration of agonists such as Δ^9-THC, methanandamide (more stable analogue of AEA) and JWH-133 improved tremor and spasticity, whereas using CB_2R selective antagonists (SR141716A and SR144528), made these effects disappear. This indicates that ECS is involved in the control of multiple sclerosis symptoms. It has also been found out that the selective activation of CB_2R on T-cell by eCBs might control autoimmune inflammation and delay disease progression.[2,9,31] Thus, it seems plausible that CBRs participate in the control of MS in two different ways: CB_2R might be involved in the modulation of the immune response, while CB_1R might participate in the control of symptoms like spasticity, rigidity and tremor.[9,31] Recent discoveries about the involvement of CB_2R in the pathogenesis of MS have opened new opportunities for the treatment of this condition.[2,9]

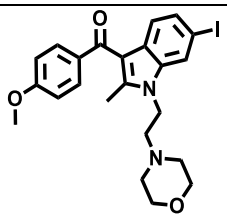
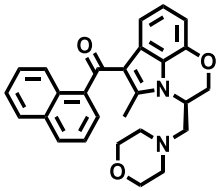
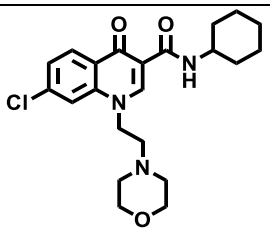
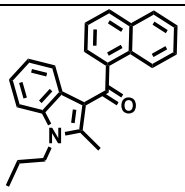
USC DE COMPOSTELA

Cell migration, invasion, and metastasis play an important role in cancer evolution, causing more than 67% of cancer-related deaths (rather than the primary tumor itself). The function of the ECS in the context of cancer has been extensively investigated, showing a critical role in cancer cell invasion and metastasis.[32–40] Table 1 shows a summary of the effects of representative CBR ligands on cell invasion and metastasis.

Table 1: Summary of the effects of representative cannabinoid ligands on cancer cell invasion and metastasis.[32]

RECEPTOR	CANCER TYPE	LIGAND	EFFECT
CB_1R	Endometrial cancer	 **Δ^9-THC (Partial agonist)**	Decreased invasion[34]
CB_1R and CB_2R	Chronic myelogenous leukemia	 **WIN 55,212-2 (Agonist)**	Decreased potential for invasion[35]
CB_1R and CB_2R	Chronic myelogenous leukemia	 **AM251 (CB_1 antagonist)**	Increased MMP2 and MMP9[35]
CB_1R and CB_2R	Gastric cancer	 **WIN 55,212-2 (Agonist)**	Decreased invasion[36]

USC UNIVERSIDADE DE SANTIAGO DE COMPOSTELA

CB_1R and CB_2R	Gastric cancer	 **AM630 (Antagonist)**	Reversal of decreased invasive effect[36]
CB_1R	Prostate cancer	 **WIN 55,212-2 (Agonist)**	Decreased migration[37]
CB_2R	Hepatocellular carcinoma	 **CB65 (Agonist)**	Decreased invasion[38]
CB_2R	Breast cancer	 **JWH-015 (Agonist)**	Decreased invasion[39]
CB_2R	Non-small cell lung cancer	None (Knockdown of CB_2R)	Decreased invasion with knockdown of CB_2R[40]

In 2012, the effect of CB65, a selective CB_2R agonist, in human hepatocellular carcinoma cells was investigated. This compound was able to reduce cell viability and cell invasion while also decreasing the concentration of matrix metalloproteinases (MMPs), especially MMP2 and MMP9.[32,38] In breast cancer cells, the activation of CB_2R by the agonist JWH-015 leads to decreased cell invasion, down-regulation of epidermal growth factor receptor (EGFR) and insulin-like growth factor-I receptor (IGF-IR).[32,39]

Although scarcely explored, available evidence supports a promising role for CB_2R agonists in the context of cancer therapy.[32–40] One of the main limitations in this regard is the availability of potent, selective, and bioavailable CB_2R agonists.

USC DE COMPOSTELA

1.4 MEDICINAL CHEMISTRY OF CBRS: PHYTOCANNABINOIDS

Phytocannabinoids are the bioactive constituents of Cannabis Sativa. At least 113 phytocannabinoids have been isolated from the plant.[41] They are classified into 13 structural families.[41] The most abundant and most studied are: Δ^9-THC [(-)-*trans*-Δ^9-tetrahydrocannabinol)], CBD (Cannabidiol), CBC (Cannabichromene) and CBG (Cannabigerol) along with their acid analogues (Δ^9-THCA, CBDA, CBCA and CBGA) (Figure 8).[41] Apart from plants, phytocannabinoids have been found in various fungi, such as Mycorrhizal fungi of the genus *Albatrellus* that produces grufolin and confluentin, and *Cylindrocarpon olidum* that produces CBCA.[41]

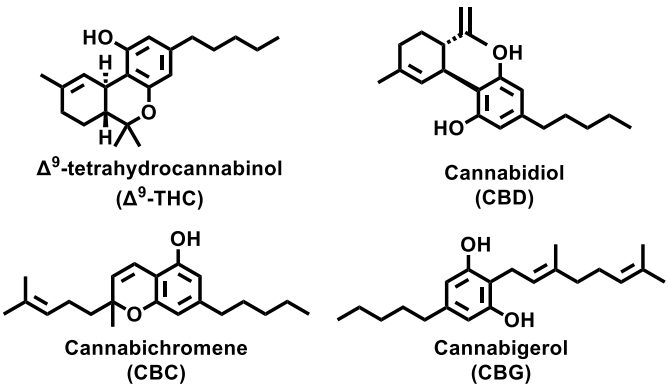


Figure 8: Structure of the most representative phytocannabinoids.

Δ^9-THC is a non-selective CBRs ligand with a partial agonist behaviour [CB_1R K_i = 80.3 nM; EC_{50} = 240 nM (E_{max} = 56%); CB_2R K_i = 75.3 nM; EC_{50} = 180 nM (E_{max}=76%)].[3] Besides its well-known interactions with CBRs, Δ^9-THC interacts with other intracellular targets, such as opioid receptors, prostaglandin synthetic pathway, proteins and nucleic acids metabolism. This behaviour and target unspecificity may explain the diverse *in vivo* effects of Δ^9-THC.[42] Most common effects derived from Cannabis use are: euphoria, relaxation, altered perception and lack of concentration. Its use can affect heart rate, increase appetite and vasodilatation, and decrease respiratory rate. The heavy and continued use of Cannabis may lead to psychosis disorders, while abstinence can cause anxiety and irritability.[42,43] Δ^9-THC can be smoked or mixed with food and taken orally. Due to its lipophilic structure, when consumed, it gets distributed in adipose tissue, liver, and lungs. When Δ^9-THC is smoked, at least 30% is destroyed by pyrolysis and more than two thousand compounds are produced.[42,43] This means that the systemic bioavailability is between 15-25% in this route. Δ^9-THC is rapidly absorbed through the body and is detectable in plasma within few seconds after

consuming.[42,43] Δ^9-THC is metabolized in the liver by cytochrome (CYP) P450 enzymes and is excreted in feces and in urine.[42] First, it is metabolized to 11-hydroxymethyl-Δ^9tetrahydrocannabinol (11-OH- Δ^9-THC) via hydroxylation and then to the inactive metabolite, 11-nor-9-carboxy-Δ 9-tetrahydrocannabinol (Δ^9-THC - COOH), via oxidation.[42] The metabolic pathway is showed in Figure 9.

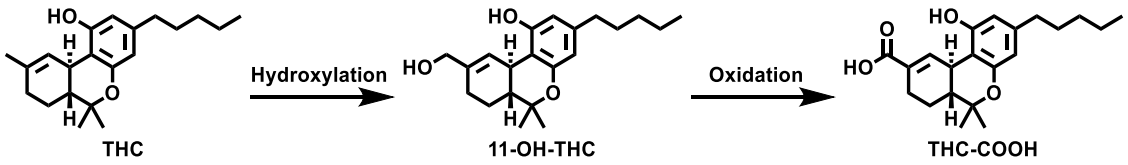


Figure 9: Most common products of the Δ^9-THC metabolic (oxidative) pathways.

CBD (Cannabidiol) is a potent and non-selective antagonist at both CBRs and an allosteric modulator of the μ opioid receptor.[44] It seems to act as an antiemetic, antipsychotic, and anticonvulsant. Importantly, CBD does not show psychotropic effects, in fact the administration of CBD reduces Δ^9-THC psychotic symptoms.[44]

CBC (Cannabichromene), another non-psychoactive substance of Cannabis Sativa, does not interact with CBRs but inhibits endocannabinoid inactivation and activates $TRPA_1$ (Transient receptor potential cation channel, subfamily A, member 1): *in vitro* assays have shown that it exerts protective effects during intestinal inflammation.[45]

Since time immemorial Cannabis has been used for medicinal and recreational purposes. Beyond the typical psychotropic effects, preparations made from Cannabis sativa have been used for the treatment of pain, anxiety, nausea, and vomit induced by chemotherapy. It has also been prescribed for the treatment of glaucoma, since Δ^9-THC decreases the intraocular pressure.[46] In the 80's, under the name of Marinol®, (Dronabinol, synthetic Δ^9-THC) was approved from FDA as an appetite stimulant for HIV/AIDS-induced anorexia, antiemetic for chemotherapy-induced collateral effects, and sleep apnea relief. Cesamet® (Nabilona, Figure 10) was approved in different countries for the treatment of glaucoma, spasticity in multiple sclerosis, wasting due to AIDS, and chronic pain, beyond chemotherapy-induced nausea. Sativex (Nabiximols, Figure 10) is a prescription-only medicine for the treatment of spasticity and muscle stiffness due to multiple sclerosis.[9]

USC UNIVERSIDADE DE SANTIAGO DE COMPOSTELA

In 2018 FDA approved Epidiolex® (cannabidiol [CBD], Figure 10) oral solution for the treatment of seizures associated with two rare and severe forms of epilepsy, Lennox-Gastaut syndrome and Dravet syndrome, in patients aged two years and older.[47]

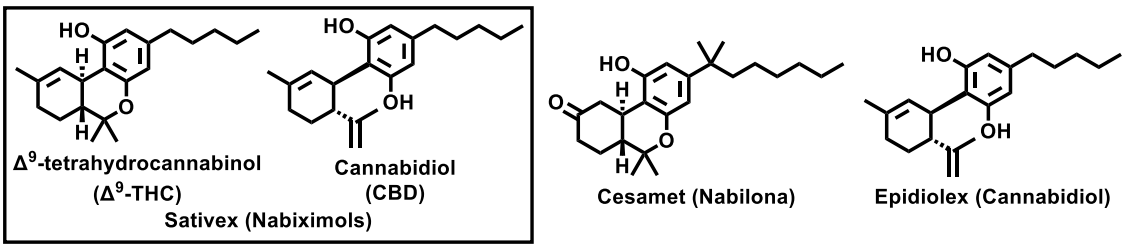


Figure 10: Structure of THC-based drugs.

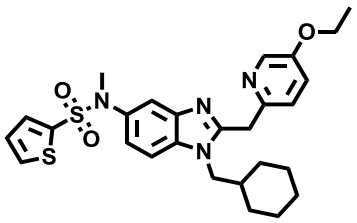
Phytocannabinoids have also been evaluated as potential antibiotics, since they show some antimicrobial activity against several Gram-positive (*Bacillus subtilis* and *Staphylococcus aureus*) and Gram-negative bacteria (*Escherichia Coli*).[41]

The use and beneficial effects of Δ^9-THC encouraged the study and exploration of the ECS in order to modulate CBRs for medical purposes and inspire the design and development of new synthetic molecules.[8,48,49] Starting with a Δ^9-THC-based scaffold, the structure of these compounds was modified to obtain new synthetic ligands to selectively target a specific cannabinoid receptor subtype. In 2008, non-selective synthetic cannabinoids saw a shift in their intended use, from research tools to drugs of abuse (designer drugs), as they started to appear in the illicit drug market.[8,48,49]

USC UNIVERSIDADE DE SANTIAGO DE COMPOSTELA

1.5 MEDICINAL CHEMISTRY OF CB_1R

From the structural point of view, CBRs agonists can be classified in two main categories: phytocannabinoids-based compounds and synthetic derivatives. AZ11713908 (Figure 11) is the prototype of non-phytocannabinoid-based CBR ligands. Synthetized by Astrazeneca, this ligand acts as a potent dual CB_1R and CB_2R agonist. *In vivo* this compound demonstrated analgesic effects.[50] While most of the known agonists show scarce (CB_1R or CB_2R) selectivity, the antagonists are usually highly selective.[12]



AZ11713908
CB_1R K_i = 3.0 nM
CB_2R K_i = 0.56 nM

Figure 11: Structure of AZ11713908.

The potent and CB_1 selective inverse agonist, Rimonabant (Acomplia®, Figure 12), was approved for the treatment of obesity with associated metabolic dysregulation, but a few years later it was withdrawn worldwide because of its collateral effects such as suicide ideation, depressive disorders, anxiety, irritability, and insomnia. A couple of years later, another inverse agonist/antagonist, Taranabant (Figure 12), had its clinical trials stopped for the same psychiatric adverse effects.[23]

Recently, the interest is focused on the discovery of CB_1R antagonists peripherally selective.[15,23,24] Preclinical studies confirmed that peripheral populations of CB_1R can be selectively targeted using compounds that have limited brain penetration, thus enabling to retain most of their benefits (e.g. treatment of type 2 diabetes, metabolic syndromes, and liver disease), while minimizing neuropsychiatric liabilities.[15,23,24] The main structural criteria guiding the development of emerging families is minimizing brain penetration and CNS activity (peripheral restriction).[15,24] JD5037 and AM6545, two drug candidates against obesity and its metabolic issues, are examples with limited brain penetration which do not cause behavioural side effects.[51,52]

USC UNIVERSIDADE DE SANTIAGO DE COMPOSTELA

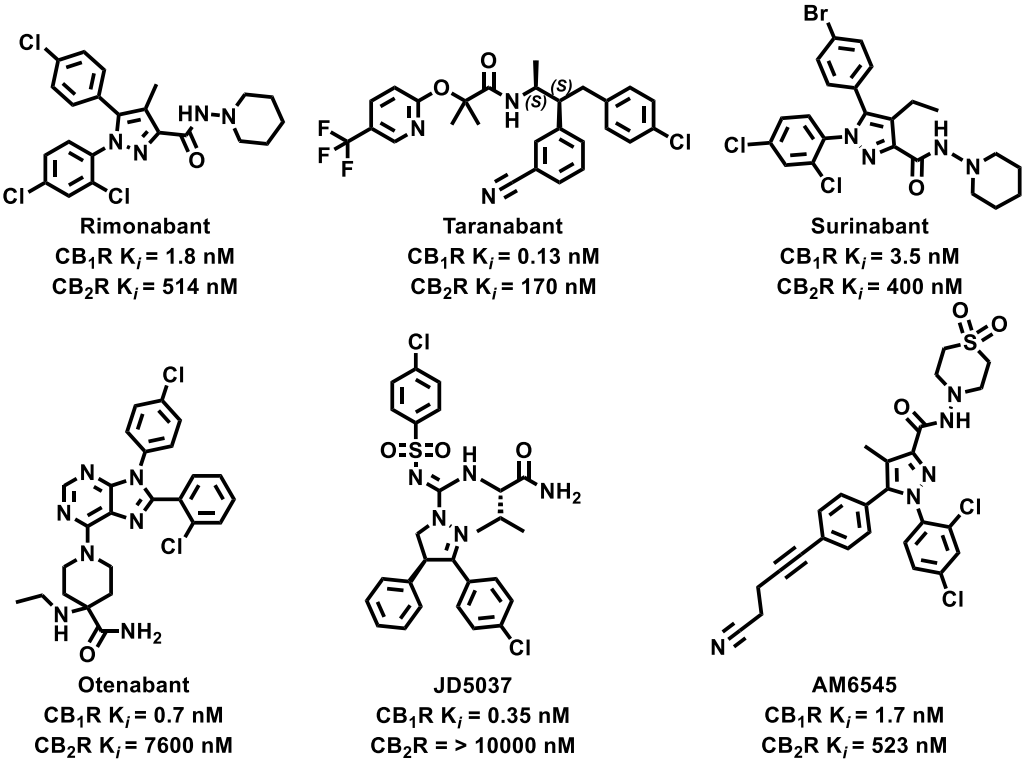


Figure 12: Structure of the most representative CB_1R antagonists.

Positive allosteric modulators (PAM) may constitute a valid alternative to CBR agonists in the treatment of neurodegenerative diseases, in order to avoid side stimulant effects and the selectivity issues of orthosteric ligands.[53] The (*S*) enantiomer of GAT229 (Figure 13) has been reported as a positive allosteric modulator of the CB_1R while the (*R*) enantiomer shows a weak PAM activity.[53] Pregnenolone (Figure 13), a steroid hormone, acts as a negative allosteric modulator (NAM) at the CB_1R, reducing the Δ^9-THC signalization. *In vitro*, CBD demonstrates the same behaviour at CB_1R.[4]

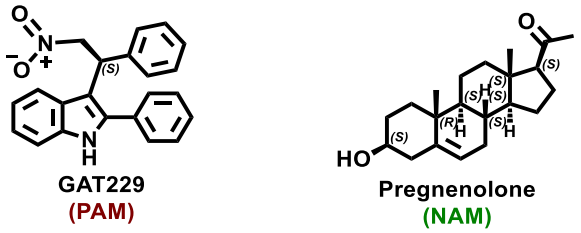


Figure 13: Structure of representative allosteric modulators of CB_1R.

USC UNIVERSIDADE DE SANTIAGO DE COMPOSTELA

1.7 MEDICINAL CHEMISTRY OF CB_2R

Like CB_1R ligands, compounds modulating CB_2R can be divided in two families: phytocannabinoids-like compounds and non-phytocannabinoids ligands. Selective CB_2R agonists represent potential drugs in the treatment of peripheral pain, without central and psychoactive effects. At the CNS level, the activation of CB_2R leads to microglia polarization to the M1-state (the microglia pro-inflammatory phenotype, characterized by pro-inflammatory cytokine production) to the M2-state (the microglia anti-inflammatory phenotype, characterized by anti-inflammatory cytokine production). CB_2R agonists inhibit pro-inflammatory cytokines, like IL-6, IL-1β (interleukin family), TNF-α (tumor necrosis factor-α) and can prevent cellular oxidative damage.[25,54,55] This anti-inflammatory effect represents a potential therapeutic strategy in the treatment of different pathologies such as neurodegenerative diseases, pain control, autoimmune diseases and cancer.[2,56]

The early discovery of selective CB_2R agonists was inspired by the structure of phytocannabinoids. In this context, HU-910 and JBT-101 (Figure 14) were discovered.[57,58] HU-910 is a potent and selective CB_2R agonist that exhibits protective effects in several inflammation-related diseases.[57] Lenabasum or JBT-101 (Figure 14) is a potent and selective CB_2R agonist that inhibits pro-inflammatory cytokine secretion and neutrophil migration *in vivo*.[58] JBT-101 is currently in Phase II clinical trials for the treatment of systemic lupus erythematosus.[58,59] A-796260 and AM1241 (Figure 14) are both CB_2R selective agonists that show potent analgesic and inflammatory effects, without psychotropic adverse effects.[60,61]

The most abundant family of CB_2R agonist are the non-phytocannabinoids. Diverse families of nitrogenated heterocyclic compounds have been designed and optimised to selectively activate CB_2R. Among these series, two main groups can be identified: mono-cyclic and bi-cyclic derivatives (Figure 14). More recently, structurally simple CB_2R ligands start to emerge (Figure 14). Among this mono-cyclic derivatives, we can highlight compound 4 in [54, Giovanni Graziano et al.][54] and compound 8 in [62, Sari Yrjölä et al.][62] (Figure 14), since they combine excellent affinity/selectivity and structural simplicity.[54,62]

USC UNIVERSIDADE DE SANTIAGO DE COMPOSTELA

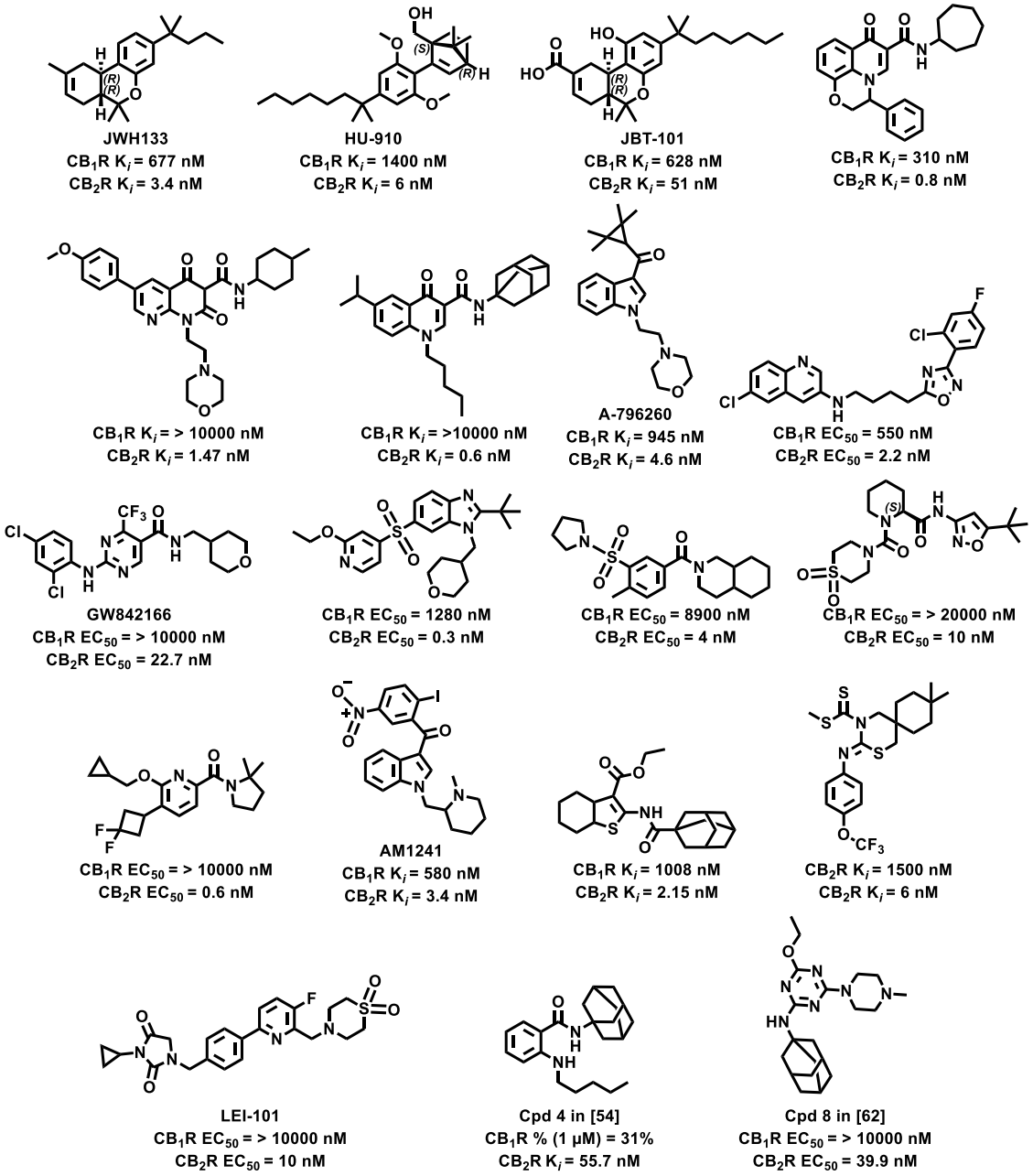


Figure 14: Structure of representative CB_2R agonists.[25,54,62,63]

Many studies evidence that CB_2R antagonists may be used in the treatment of inflammation associated with obesity, insulin resistance, and non-alcoholic fatty liver disease (NAFLD).[64] In 1998, the first potent and selective CB_2R antagonist was described: SR144528 (Figure 15). *In vitro* and *ex vivo* assays showed that this antagonist is capable of selectively blocking CB_2R mediated responses, showing no significant interaction with CB_1 receptor or other receptors. *In vitro*, SR144528 blocks both the inhibitory activity and the MAPK activity induced by the CB_2R agonist CP 55,940.[65] Only few selective CB_2R inverse agonists have been described in literature so far, and it has been demonstrated that they might serve as novel immunomodulators in

the treatment of inflammatory diseases.[27,66] *In vitro* assays show that SMM-189 (Figure 15) promotes the M2 anti-inflammatory state of microglia in the treatment of traumatic brain injury.[27,66] Another CB_2R inverse agonist, SCH.336 (Figure 15), has been demonstrated to modulate leukocyte recruitment *in vitro*.[67]

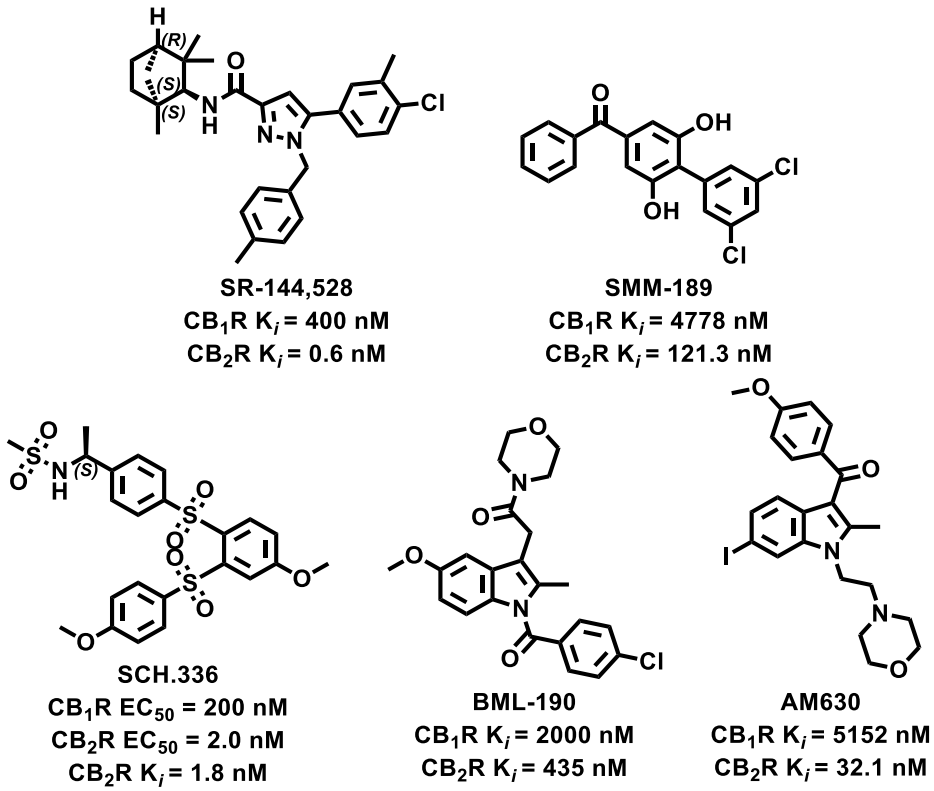


Figure 15: Most representative CB_2R antagonists/inverse agonists described in literature.

In 2018, a PAM of the CB_2R, EC21a (Figure 16), was described, which exhibited antinociceptive activity *in vivo*. This compound represents a promising ligand for clinical trials.[53,68]*In vitro* and *in vivo* experiments demonstrated that DHGA (Figure 16) may act as NAM of CB_2R. Their activity profile in *in vivo* models of CNS inflammation is yet to be published.[63]

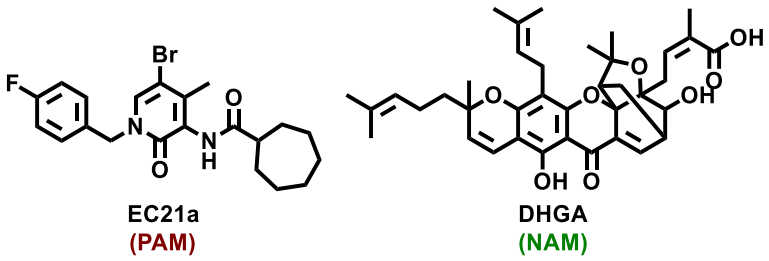


Figure 16: Chemical structure of CB_2R allosteric modulators.

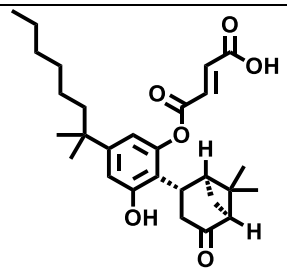
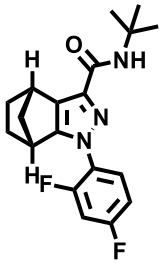
USC UNIVERSIDADE DE SANTIAGO DE COMPOSTELA

1.8 CB_2R LIGANDS IN CLINICAL TRIALS

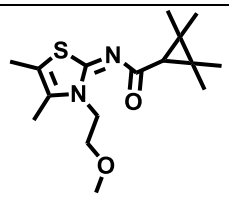
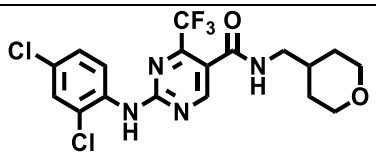
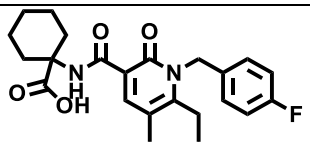
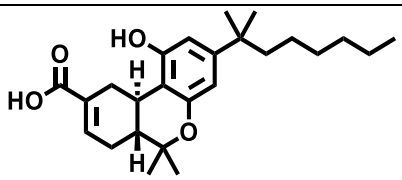
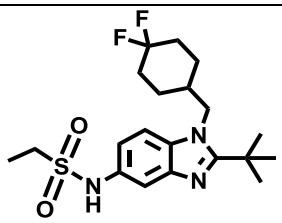
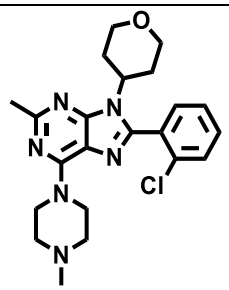
The difficulties associated with the discovery and optimization of selective CB_2R agonists are reflected in the few candidates that have reached clinical trials.[25,53]A compilation of CB_2R currently under study can be found in Table 2. The most studied indications for clinical studies are pain relief and osteoarthritis. Although recent preclinical and clinical studies are more focused on cancer treatment[25,32–40]

PRS-211375 (Cannabinor), from Pharmos Corp., was nominated as the first candidate of this target to enter in clinical trials, but it failed in Phase II.[25] GRC10693, (Tedalinab) is a CB_2R-selective agonist synthetized by Glenmark Pharmaceuticals currently in Phase I for the treatment of osteoarthritis and neuropathic pain.[25] Abbott Laboratories reported a CB_2R agonist for the treatment of pain: A-836339. At lower doses, A-836339 shows analgesic and anti-inflammatory effects, but at higher doses it shows to interact with CB_1R, exhibiting typical cannabis-like effects.[25]

Table 2: Structure and therapeutic indication of CB_2R agonists in clinical trials.

Name	Therapeutical indication	Clinical development status
 **PRS-211375 (Cannabinor) (Pharmos Corp.)**	Pain	Phase II[25]
 **GRC10693 (Tedalinab) (Glenmark Pharmaceuticals)**	Osteoarthritis, neuropathic pain	Phase I[25]

USC UNIVERSIDADE DE SANTIAGO DE COMPOSTELA

 **A-836339 (Abbott Laboratories)**	Pain	Phase I[25]
 **GW842166 (GlaxoSmithKlane)**	Osteoarthritis, Pain	Phase I[59]
 **S777469 (Shionogi&Co)**	Atopic dermatitis	Phase II[59]
 **JBT-101 (JB Therapautics)**	Systemic lupus erythematosus	Phase II[59]
 **AZD1940 (AstraZeneca)**	Pain	Phase II[59]
 **LY2828360 (Eli Lilli)**	Osteoarthritis	Phase II[59]

USC UNIVERSIDADE DE SANTIAGO DE COMPOSTELA

1.9 BIASED AGONISM

Most GPCRs show a functional selectivity profile, which means that they can adopt different conformations and then signalize through different pathways. It has been studied that following the binding of an agonist to a GPCR, two main transductional pathways can be activated: one through the G protein (canonical) and the other through the β-arrestin.[10,32,69] This phenomenon occurs due to the different conformational states that GPCRs can adopt: the binding of the ligand causes the receptor to stabilize into a characteristic conformational state activating different second messengers, therefore leading to a particular downstream signaling pathway.[32,69] CBRs are well-characterized in their signaling via G protein, but there is few information about the β-arrestin signaling pathway.[32,69] β-arrestins act as negative regulators of the G protein, blocking the G protein's signaling and inducing receptor endocytosis. They can also function as signaling scaffolds during the activation of downstream cascades, such as the MAPK (mitogen-activated protein kinase).[69] β-arrestin1 and β-arrestin2 are those involved in the CBR signaling. After binding to CB_1R and CB_2R, β-arrestin2 signaling promotes desensitization and internalization of the receptor. Concerning β-arrestin1, there are contradictious (or conflicting) opinions: some studies found little to no recruitment by CB_1R after receptor activation while other studies found β-arrestin1 recruitment, which leads to the activation of extracellular signal-regulated kinase pathway.[10]

Currently, we have few information about the correlation of the structure of the agonist with signaling pathway predilection (or profile) and the consequent pharmacological behavior.[10] For example, for the dopamine D_2 receptor, the β-arrestin-biased ligands may represent promising new drugs for schizophrenia; quite the opposite for the μ opioid receptor, since agonists that signal preferentially through the G protein pathway produce analgesia with reduced side effects.[10]

Regarding CBRs, the therapeutic advantage/disadvantage of specific signaling pathways for both receptors has yet to be elucidated.[10] Recent studies demonstrated that G protein-biased agonists may show reduced adverse effects, since, after CB_1 activation, β-arrestin negatively influences the acute responses and increases chronic responses.[10] Figure 17 shows some representative CBRs biased and unbiased ligands reported in literature.

USC UNIVERSIDADE DE SANTIAGO DE COMPOSTELA

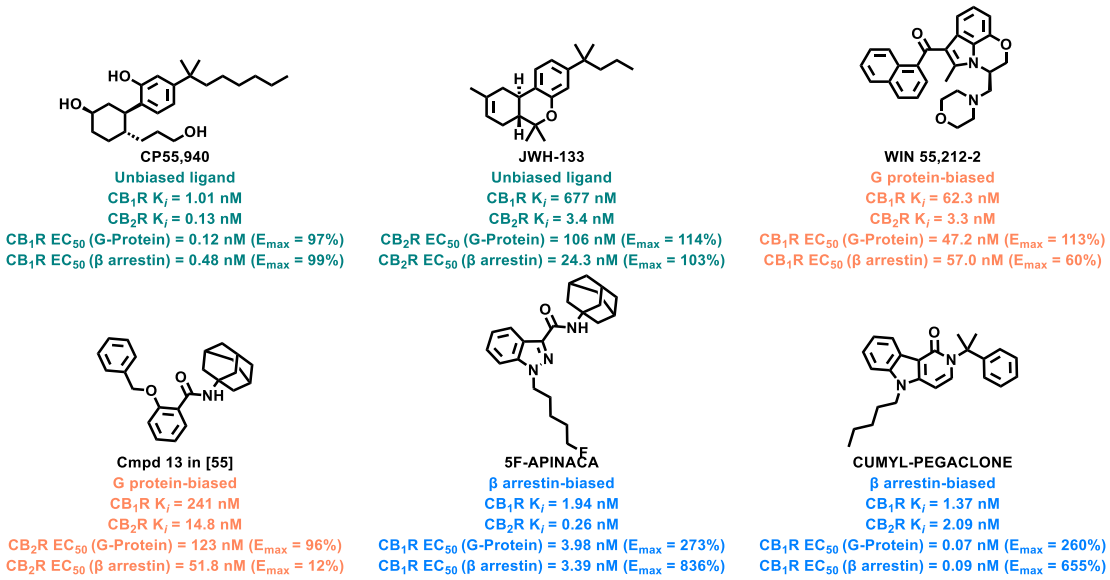


Figure 17: Structure and preferential signaling profile of representative CBR biased agonists.

CP 55,940, JWH-018 and JWH-133 (CBRs full agonists) have been described as unbiased ligands, which signalize equally through G protein or β-arrestin pathways.[70,71] It has been reported that Δ^9-THC, a phytocannabinoid partial agonist, signals preferentially through the G protein pathway.[70] WIN55,212-2 and compound 13 in [55, Francesca Intranuovo et al][55] (CB_2R agonists) has been reported as G protein-biased ligands.[70,71] To date, few β-arrestin-biased ligands have been described (5F-APINACA and CUMYL-PEGACLONE) (Figure 17).[10]

The discovery and optimization of subtype selective and biased CBR agonists remains an unsolved challenge. Biased ligands are highly demanded as pharmacological tools enabling to better understand cannabinoid signaling pathways and as tailored drugs to face challenging and unsolved pathologies.

An additional and important unsolved challenge during the discovery of biased ligands is the subtype selectivity. As observed (Figure 17), most known biased ligands are non-subtype selective, and this promiscuous profile prevents its use for advanced *in vitro* and *in vivo* studies.

USC UNIVERSIDADE DE SANTIAGO DE COMPOSTELA

1.10 SCRAs: SYNTHETIC CANNABINOID RECEPTOR AGONISTS AS NEW PSYCHOACTIVE SUBSTANCES

1.10.1 New Psychoactive substances (NPS)

New Psychoactive substances (NPS) are defined from the United Nations Office on Drugs and Crime (UNODC) as "substances of abuse, either in a pure form or a preparation, that are not controlled by the 1961 Single Convention on Narcotic Drugs or the 1971 Convention on Psychotropic Substances. These substances may pose a public health threat", specifying that "the term "new" does not necessarily refer to new inventions but to substances that have recently become available on the market; many of them were first synthesized decades ago".[72] Up to 2022, 1124 novel NPS drugs have been reported all over the world.[72] As showed in Figure 18, the United States of America and Sweden reported more than 500 NPS; while England and German more than 400 and Spain more than 300.[72]

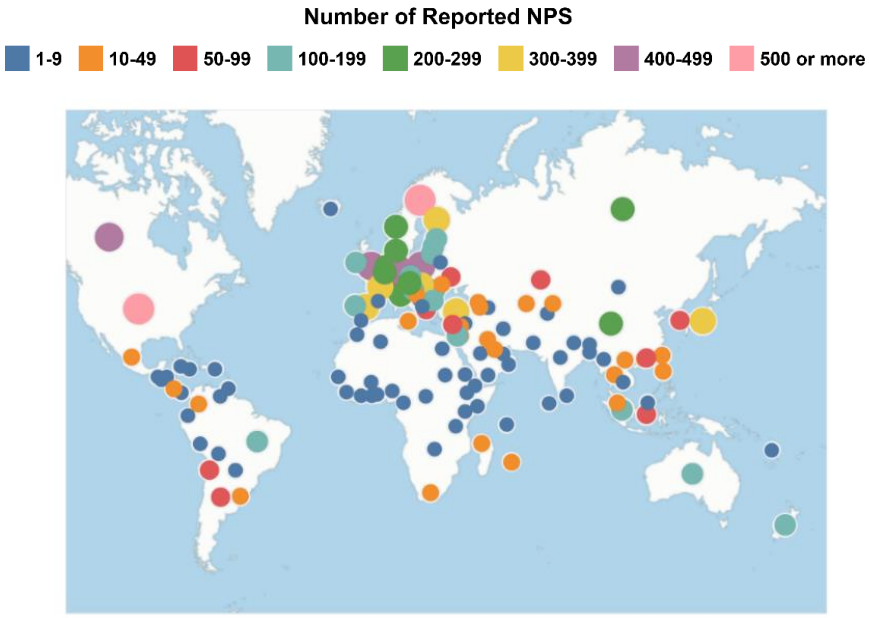


Figure 18: Global representation of NPS reported all over the world by country/territory.[72]

NPS represent a serious global public health threat. In the past years, severe intoxications due to NPS have been increasingly reported all over the world. However, the absence of detailed scientific information regarding their pharmacology, toxicology and abuse liability is critical. Up to 2022, more than 1000 NPS have been described in 136 countries, where stimulants represent the majority, followed by synthetic cannabinoid receptor agonists (Figure 19).

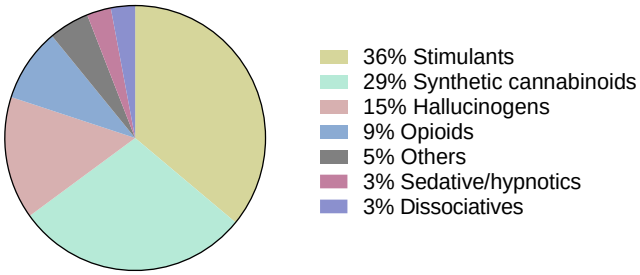


Figure 19: NPS reported in 2020 by UNODC.[72]

NPS are classified in four main groups: synthetic stimulants, synthetic hallucinogens, synthetic depressants (synthetic opioids and benzodiazepines) and synthetic cannabinoids.[73–75]

Synthetic Stimulants include traditional stimulants, which are classical controlled drugs, such as cocaine, MDMA and amphetamines. These substances stimulate the activity of the central nervous system, causing a euphoric and energetic state.[73,74] They mostly interact with dopamine (DA) and serotonin (5-TH) receptors and promote an increase in synaptic availability of neurotransmitters, (e.g., dopamine and serotonin). Their most common adverse effects are agitation, nausea, vomiting, headache, palpitations, tachycardia, hypertension, and hyperthermia, and less frequently paranoia, hallucinations, seizures, and collapse. In few cases, severe adverse effects such as significant peripheral organ damage and rhabdomyolysis have been reported. These drugs can be insufflated, swallowed, inhaled, smoked or injected; the most common preparation is in pill/table form.[73,74]

There are three main families of synthetic stimulants (Figure 20): phenethylamines, cathinones and piperazines. Synthetic cathinones represent the biggest and most monitored group of NPS. Most common cathinones are mephedrone, methylone, methcathinone, buphedrone, bupropion, pyrovalerone.[72,73]

USC UNIVERSIDADE DE SANTIAGO DE COMPOSTELA

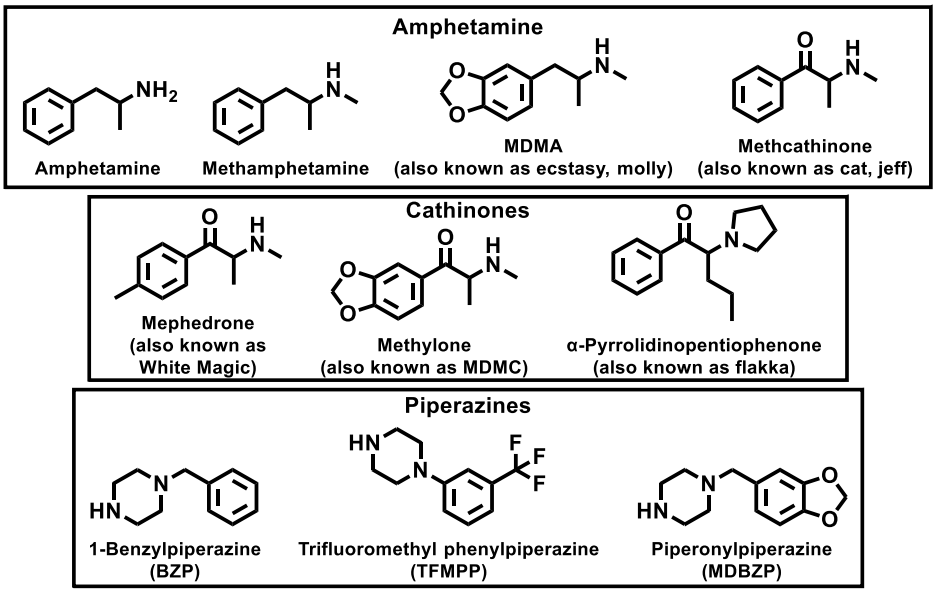


Figure 20: Most common synthetic stimulants.

Synthetic Hallucinogens can be divided into hallucinogens and dissociative drugs. Both classes can cause hallucinations, sensations and images that seem real even though they are not and can cause users to feel out of control or disconnected from their body and environment.[73,74] They can be defined as "Entheogens", which are psychoactive substances that induce alterations in perception, mood, consciousness, cognition, or behaviour causing a visionary and mystical experience.[76]

Hallucinogens interact with serotonin receptors involved in the control of mood, hunger, body temperature, sexual behaviour, muscle control and sensory perception. This kind of drugs provides psychedelic, mystical and spiritual experiences. Hallucinogens can be divided into three chemical classes: Phenethylamines (like 2C-D, 25B-NBOMe and mescaline), Tryptamines (like 5-MeO-DPT) and Lysergamines (like 1B-LSD and its analogues such as LSA/LAA, DAM-57 and MIPLA) (Figure 21).[73,74,77]

Dissociative drugs act as selective non-competitive antagonists at the ionotropic glutamatergic NMDAR. Dissociatives can cause numbness, disorientation, loss of coordination, hallucinations, increased blood pressure, heart rate and body temperature, memory loss, panic and anxiety, psychotic symptoms, amnesia, and breathing troubles. PCP and ketamine are the most known dissociative drugs (Figure 21).[73–75,77]

USC
UNIVERSIDADE DE SANTIAGO DE COMPOSTELA

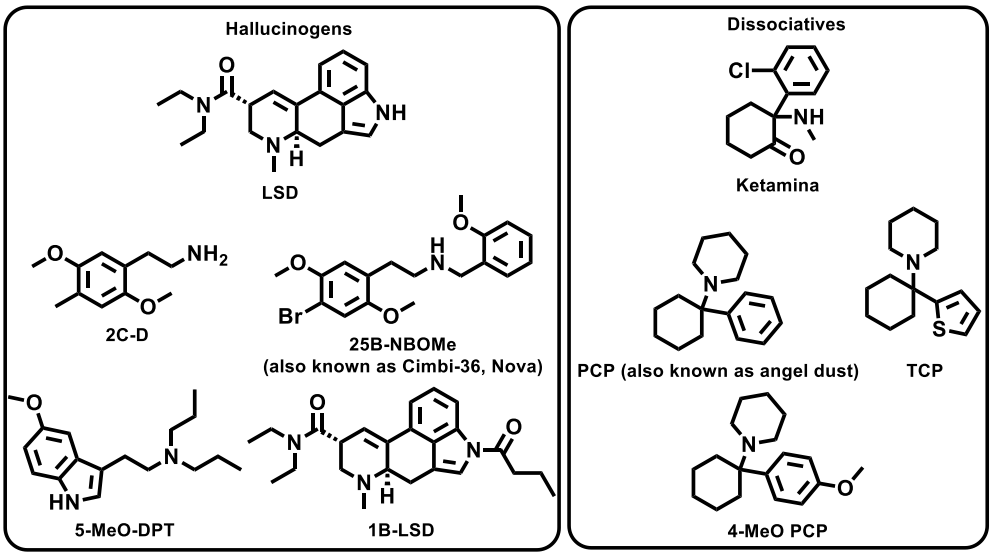


Figure 21: Structure of representative Synthetic Hallucinogens.

Synthetic depressants are broadly classified in two sub-families: benzodiazepines and synthetic opioids.

Designer benzodiazepines are consumed with non-medical prescription and, like prescribed benzodiazepines, mediate their effects through interactions at GABA-A receptors, causing a sedative, hypnotic, anxiolytic, and muscle relaxant effect. Most common adverse effects are confusion, dizziness, drowsiness fatigue, auditory and visual hallucinations, delirium, seizures, deep sleep, agitation, tachycardia, anxiety, panic attacks, and insomnia.[73,78,79] Flualprazolam, fluclotizolam and methylclonazepam are a few examples of this class of NPS (Figure 22).

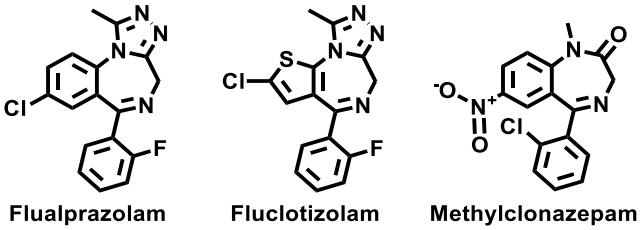


Figure 22: Structure of representative designer benzodiazepines.

Synthetic opioids are designed to bind to the same receptors as opiates and produce euphoria, anxiolysis, feeling of relaxation and drowsiness. Adverse effects include nausea, vomiting, constipation, tolerance, respiratory depression, apnea and central nervous system depression.[73,74] The most common synthetic opioids are methadone, meperidine, fentanyl and all the fentanyl analogues (alfentanil, carfentanil, remifentanil and so on) (Figure 23).

USC DE COMPOSTELA

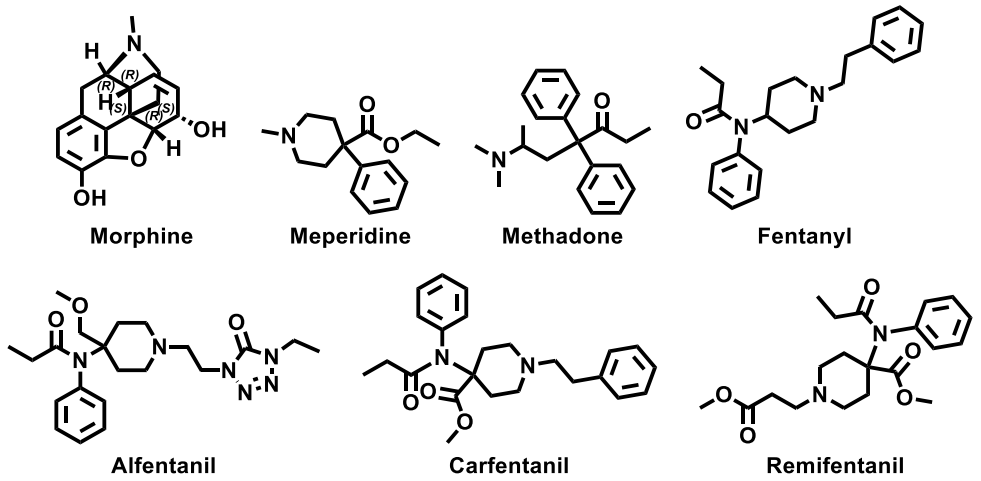


Figure 23: Representative structure of synthetic opioids classified as NPS.

Synthetic Cannabinoids: Because of their ability to mimic the psychotropic effects of Δ^9-THC, synthetic cannabinoids have been introduced within the illicit drug market to create pseudo-legal or unregulated alternatives to Cannabis.[3,73,74] They are usually misleadingly advertised as "synthetic marijuana". The variety of structures in this class and its growing importance makes them the largest class of NPS. SCs interact with both CBRs and induce euphoria and disinhibition, like Δ^9-THC. They can also cause nausea, agitation, confusion, tachycardia, chest pain, and other several adverse effects.[3,73,74] In Figure 24, the most representative SCRAs are showed.

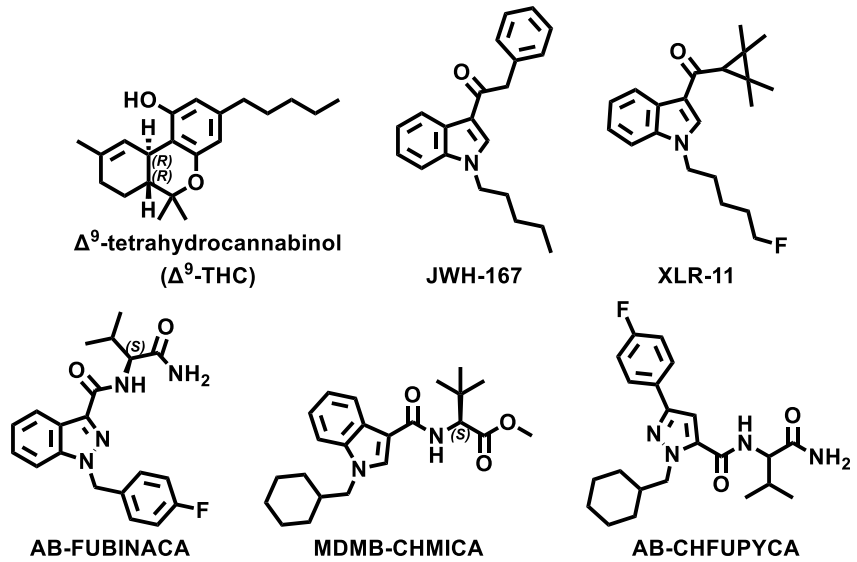


Figure 24: Structure of Δ^9-THC and representative Synthetic Cannabinoid Receptor Agonists (SCRAs).

USC UNIVERSIDADE DE SANTIAGO DE COMPOSTELA

1.10.2 SCRAs: an emergent and dangerous family of new illegal drugs

In the early 1960s, the chemical structure of Δ^9-THC, the principal psychoactive constituent of cannabis, was determined by Gaoni and Mechoulam.[80] This finding marked the beginning of the discovery and study of the endocannabinoid system. It has been proved that, after smoking Cannabis, Δ^9-THC travels through the blood to the brain where the CB receptors are expressed producing multiple central effects. Elation, relaxation, sedation, pain relief, energy, laughter, dry mouth, red/itchy eyes, anxiety or paranoia, "couch lock" or intense body heaviness, laziness, drowsiness, hunger and memory impairment are the most common effects.[8]

Although clinical evidence validated the beneficial effects of Cannabis and its components in the treatment of some health conditions (e.g. anorexia, side-effects of chemotherapy, neuropathic pain, or multiple sclerosis), their therapeutic effect is limited by its adverse psychotropic effects and potential abuse.[49,81] The therapeutic potential of Δ^9-THC, and its recreational uses, encouraged new medicinal chemistry programs aimed at the discovery of new non-THC-based structures able to mimic useful pharmacological effects. In this context, synthetic cannabinoid receptor agonists emerged, currently known as SCRAs.[3,8,82] In the last years, UNODC has detected more than one thousand NPS, including an important number of synthetic cannabinoids, as new designer drugs.[72] Unlike Δ^9-THC, this new designer drug family acts as full agonists at both CBRs, and shows a very high affinity (most of them exhibiting K_i value in the sub-nanomolar range).[3,8]

In a clear contrast to the other NPS families, the information about SCRAs' pharmacology, metabolism, toxicology, and abuse liability remains poorly reported.[8] Based on the increasing evidence of the therapeutic potential of ECS's modulation, in the 80's Pfizer started a program to synthesize the first synthetic phytocannabinoids analogues CP 47,497 and CP 55,940 (Figure 25). Later on, for research purposes, an American research group synthesized JWH-018 and Pfizer described AB-FUBINACA: two indole-based synthetic compounds exhibiting potent CB_1R and CB_2R agonist effects (Figure 25).[83] In 2008, for the first time in Europe, JWH-018 was detected in the illicit drug market under the name of "Spice". This finding marked the beginning of the SCRA family, its inclusion as NPS and its massive arrival on the illicit drug market. An enormous number of different and highly potent SCRAs appear continuously all over the world. Their chemical diversity and the pace at which they hit the market make them

USC UNIVERSIDADE SANTIAGO

difficult to control. When a compound is regulated and prohibited, new similar substitutes rapidly appear on the market. The name of these substances is often changed to facilitate their entry on the market: APINACA has been sold as AKB-48, a Japanese musical group; APICA as 2NE1, a Korean musical group; XLR-11 owes its name to the first liquid fuel rocket developed in the USA.[48,49,83] SCRAs are usually sold through the internet in different preparations, such as powder, herbal smoking, or e-liquid for electronic cigarettes. These substances are synthesized wholesale in China and then transported to Europe. The solid powder SCRAs are dissolved in acetone or methanol and then pulverized (sprayed) into a matrix of plant matter (e.g., cannabis, lemon balm, mint, and thyme). Thus, they are commercialized in the internet in sachets.[49] The use of these illegal substances poses new and serious risks to public health. In addition to its intrinsic pharmacological effect and toxicity, one of the main problems related to these substances is the manufacturing process, considering that different distributions of substances have been found within the herb mixture: therefore, some doses may contain a higher concentration of cannabinoids than others. Mixtures of synthetic cannabinoids with other substances such as stimulants, hallucinogens, hypnotic-sedatives, and ecstasy have also been identified on the market.[48,49]

Like Δ^9-THC, SCRAs are non-selective agonists of both cannabinoid receptors (CB_1R and CB_2R), although they usually exhibit higher efficacies and potencies at CB_1R when compared to the partial agonist Δ^9-THC: they are 10-200 times more potent that Δ^9-THC. Hitherto, little is known about the side effects: tachycardia, agitation, nausea, vomiting, convulsions, hypertension, heart attacks, trembling and dizziness, psychosis, hallucination, organ toxicity, and even death. There are also substances that cause addiction and withdrawal symptons.[3,81,83,84]

In 2014, more than 600 people poisoned with SCRAs were registered in Russia, 15 of whom died due to the use of the MDMB-FUBINACA.[48] In 2016, 25 acute poisonings and 28 deaths associated with the MDMB-CHMICA were recorded in Europe.[48] In 2016, 33 people were intoxicated in New York as a result of the use of AMB-FUBINACA: an event defined by the press as a "zombie outbreak" due to the condition of the intoxicated individuals.[48] AMB-FUBINACA was discovered to be 85 times more potent than Δ^9-THC and 50 times more powerful than JHW-018 (Spice); it is sold on the market at a price ranging from 1.95 to 3.8 $ per gram.[48,49]

USC UNIVERSIDADE DE SANTIAGO DE COMPOSTELA

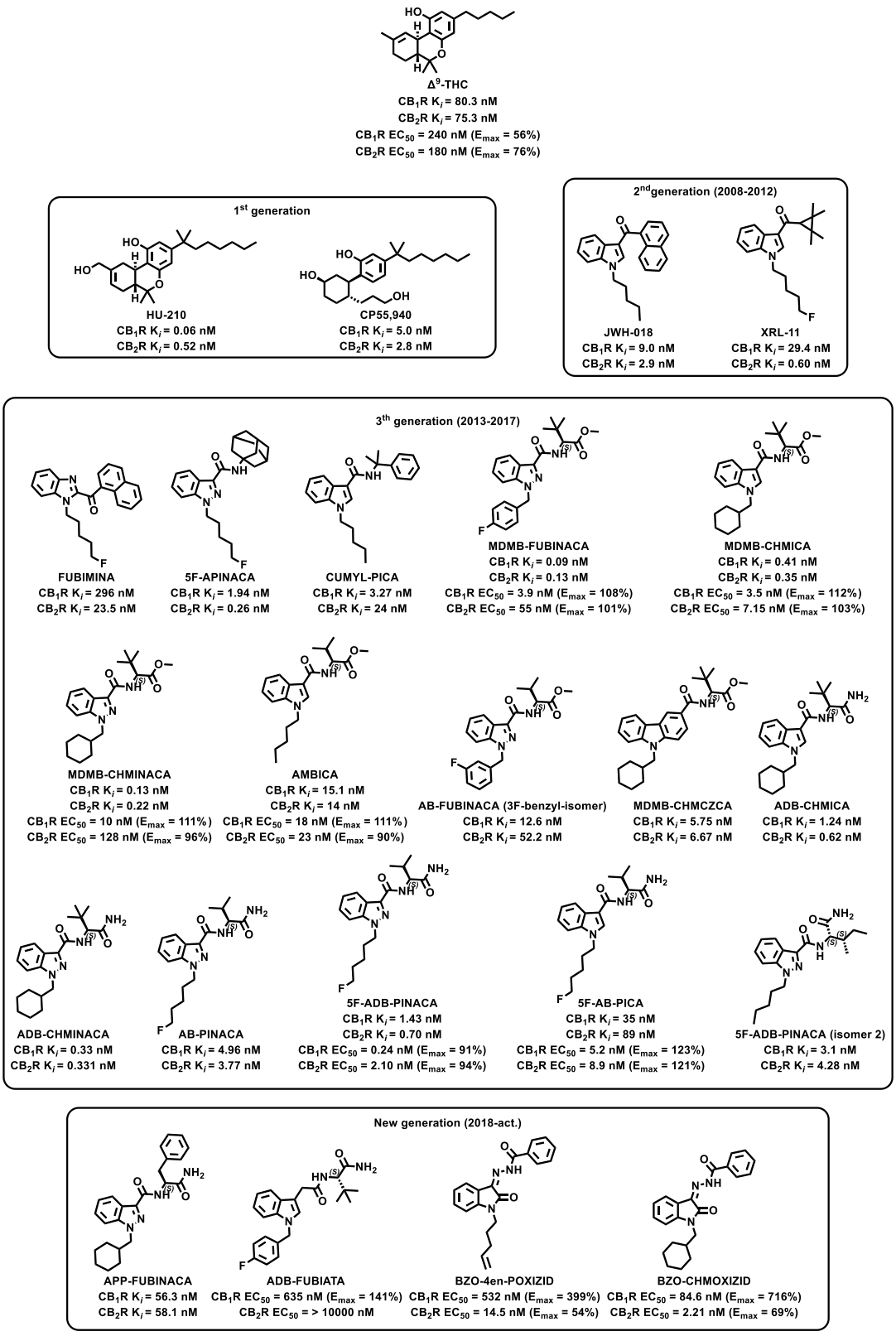


Figure 25: Representative SCRAs and their pharmacological data.[3,7,85]

USC UNIVERSIDADE DE SANTIAGO DE COMPOSTELA

1.10.3 SCRAs general structure

In 2021, the National Narcotics Control Commission of China (NNCA) announced that SCRAs will be included into national control using a generic class definition approach.[86] To circumvent the governmental regulations, the structure of cannabinoid designer drugs is constantly modified by illegal producers, which poses a challenge for treating SCRAs intoxications and for drug regulatory authorities.[72,86]

The pharmacophoric model of SCRAs consists of four structural elements (Figure 25): the central core, the linker, the tail, and the ring/substituent. Indole and indazole heterocycles constitute the most representative core structures. The linker has seen a change in recent incorporations, as substances now bear an ester or amide group instead of a ring. The tail generally is a pentyl, 5-F-pentyl chain or lipophilic cyclic moieties like 4-F-benzyl or methyl-cyclohexyl ring.[3,49,83] In Figure 26, the general structure of SCRA family is shown: the core in green, the tail in yellow, the linker in blue and the substituent in orange. The structure and binding data of representative indole and indazole-based SCRAs are presented in Figure 25.

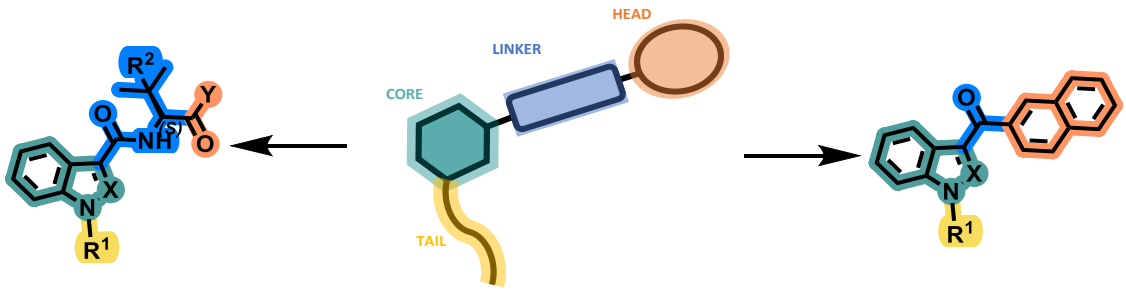


Figure 26: Common structural features of SCRAs.[3]

The most abundant and recent SCRAs contain a stereocenter in their structure.[82] The stereo disposition within the group in the linker remains an intriguing characteristic feature of SCRAs, with reported data so far being somewhat underexplored and contradictory.[87,88] Pfizer compound AB-FUBINACA and all the SCRAs within the illicit market are *(S)* enantiomers; the (*R*) enantiomer of these compounds has not been evaluated in the literature so far.[3,83]

USC UNIVERSIDADE DE SANTIAGO DE COMPOSTELA

1.10.4 Off-target interactions

The uncontrolled and recreative uses of SCRAs have evidenced their dangerous nature and toxicity associated with their uses. Recent studies have pointed out off-target effects of SCRAs as key contributors to some of its most dangerous pharmacological effects. Because of their implication in psychosis, hypothermia and cardiovascular effects, dopamine, adrenergic, serotonin and *N*-methyl-*D*-aspartate receptors have been pointed out as the off-targets.[89–93]

CBRs activation by selective or non-selective agonists does not modulate the dopamine transporter (DAT), but SCRAs are capable of increasing the dopamine (DA) levels via inhibition of GABAergic and glutamatergic neurotransmissions.[91,93] An increase in DA levels produced by Δ^9-THC, APINACA and JWH-018 has been observed *in vivo*.[93] CB_1R agonists have been demonstrated to induce alterations in *N*-methyl-D-aspartate receptor (NMDAR) activity *in vitro* and *in vivo*, probably interfering with the release of glutamate.[91,93] Moreover, it has been demonstrated that the indole/indazole-core interacts with serotonin receptors.[91,93] The upregulation of 5-$HT_{2A}R$ in the brain induced by SCRAs has been suggested as the mechanism that may initiate psychosis.[93] They also show a considerable antagonism of 5-HT_{2B} receptors, although it does not explain the cardiovascular effects of SCRAs, since the antagonist activity is more cardioprotective than cardiotoxic.[92] It has also been found that compounds JWH-018 and AM2201 act as positive allosteric modulators (PAM) of 5-HT_{1A} receptors, that are responsible for the hypothermia.[92]

It should be pointed out that, since SCRAs' structures were never submitted to clinical development, most of their physiological, toxicological and pharmacokinetic profile remains unknown.[49,94] Accordingly, these substances constitute a serious global health threat that demand collaborative investigation of scientific community and regulatory authorities.

USC UNIVERSIDADE DE SANTIAGO DE COMPOSTELA

2 AIMS AND OUTLINE OF THIS THESIS

USC
UNIVERSIDADE
DE SANTIAGO
DE COMPOSTELA

USC
UNIVERSIDADE
DE SANTIAGO
DE COMPOSTELA

The cannabinoid system plays crucial roles in both physiological and pathological conditions, exerting widespread effects throughout the body. It consists of endocannabinoids, cannabinoid receptors, and enzymes involved in their synthesis and degradation. In physiology, the endocannabinoid system helps regulate various processes such as pain sensation, appetite, mood, immune function, and neuroprotection. However, dysregulation of this system has been implicated in several pathological conditions, including chronic pain, inflammation, cancer, neurodegenerative disorders, and psychiatric disorders. The potential of the endocannabinoid system in tackling challenging diseases stems from its ability to modulate these processes. Cannabinoid-based therapies, such as cannabis-derived compounds or synthetic cannabinoids, show promise in alleviating symptoms and even modifying disease progression in conditions such as epilepsy, multiple sclerosis, and chemotherapy-induced nausea. Furthermore, ongoing research explores the therapeutic potential of drugs modulating cannabinoid receptors (CBRs) in areas such as anxiety and neurodegenerative diseases, pain, cancer, post-traumatic stress disorder, and substance abuse disorders. Understanding and harnessing the cannabinoid system's intricate mechanisms may offer innovative avenues for treating challenging diseases and improving patients' quality of life.

The last discovered, and less studied, cannabinoid receptor is CB_2R. CB_2R is predominantly found in the immune system, with lesser expression in the central nervous system. It plays a vital role in regulating immune responses, inflammation, and cell survival. Activation of CB_2R has been shown to modulate the immune system, reducing inflammatory responses, and promoting immune homeostasis. This receptor has emerged as an attractive therapeutic target for a range of conditions, including autoimmune diseases, neuroinflammatory disorders, cancer, and chronic pain. Modulating CB_2R activity holds great therapeutic potential, as it can help restore immune balance, attenuate inflammation, and alleviate pain without the psychotropic effects associated with CB_1R activation. Recent studies have highlighted the promise of CB_2R modulation in treating conditions such as rheumatoid arthritis, inflammatory bowel disease, neuropathic pain, several cancer types, and neurodegenerative disorders like Alzheimer's disease.

USC UNIVERSIDADE DE SANTIAGO DE COMPOSTELA

In this context, our group recently initiated a collaborative project aimed at improving scientific knowledge regarding the pharmacological actions, toxicology, and signaling pathways of chemical entities capable of modulating the endocannabinoid system. Moreover, the research described herein is part of a long-term project that utilizes the multicomponent reactions as a tailored exploratory tool in Medicinal Chemistry.

The present Doctoral Thesis ***focuses on the discovery, SAR exploration and optimization of novel series of potent and CB_2R selective agonists***. Additionally, it aims at the exploration of the therapeutic applications of these agents in the context of inflammatory-based diseases and cancer. This general goal was implemented through specific aims groups into five Chapters, each with its own specific context and objectives. A summary of the main goals for each Chapter is provided below.

The first Chapter of the Thesis (**3.1**) focuses on the preparation and detailed pharmacological characterization (binding and functional) of a collection of 64 indole and indazole derivatives, which are Synthetic Cannabinoid Receptor Agonists (SCRAs). These substances are extensively and illegally used as substitutes for marijuana. These designer drugs are dual agonists of the CB_1R and CB_2R receptors, and their structure rapidly changes. However, there is a lack of samples and pharmacological and toxicological data for these compounds, posing a significant risk to society. The objective was to synthesize and characterize a wide collection of SCRAs and make the library and their pharmacological data available to the scientific community and drug enforcement agencies. Another specific objective of this Chapter was to identify the main structure-activity relationship trends in these series to guide the design of selective CB_2R agonists developed in Chapters 2-4.

The following three Chapters of the Thesis (**3.2**, **3.3** and **3.4**) were dedicated to the discovery and optimization of new selective agonists for CB_2R. Building upon the knowledge gained in Chapter 1, we decided to approach a pharmacomodulation process that would allow us to transform the promiscuous profile (CB_1R and CB_2R) of the SCRAs into selective CB_2R drugs. To achieve this, we selected the indole core as the model scaffold and retained two of the frequently encountered groups at position 1 of the SCRAs.

USC UNIVERSIDADE DE SANTIAGO DE COMPOSTELA

In Chapter 2, our aim was to develop a multicomponent synthetic method that would enable efficient, versatile, and rapid access to diverse libraries of indole-based ligands structurally related to SCRAs, which could be characterized for their interaction with CB_1R and CB_2R. The ultimate goal was to investigate the structure-activity relationship within these series, discover new selective CB_2R agonists, and evaluate the influence of stereochemistry on the interaction with CB_2R.

The availability of an efficient method, based on the Ugi reaction, allowed us to expand the SAR study of these series in Chapters 3 and 4. Specifically, we aimed to extensively explore the effect of groups at R^3 and R^4 and their roles in achieving potent and selective CB_2R ligands.

The last Chapter was conceived with a more pharmacological and translational focus, aiming to provide a more in-depth pharmacological characterization of representative ligands and the preliminary exploration of their therapeutic applications. We firstly focused on evaluating the functional activity profile (agonist or antagonist) of selected CB_2R agonists. Additionally, it includes a detailed study of the signaling pathways these compounds affect (biased or unbiased). Then, we decided to the preliminary assessment of the ability of four representative ligands to modulate inflammation mediators (anti-inflammatory action) and their effectiveness in reducing the proliferation of a highly aggressive central nervous system cancer (glioblastoma).

USC
UNIVERSIDADE DE SANTIAGO DE COMPOSTELA

USC
UNIVERSIDADE
DE SANTIAGO
DE COMPOSTELA

3 RESULT AND DISCUSSION

USC
UNIVERSIDADE
DE SANTIAGO
DE COMPOSTELA

USC
UNIVERSIDADE
DE SANTIAGO
DE COMPOSTELA

CHAPTER 1: SYNTHESIS AND CHARACTERIZATION OF A LARGE COLLECTION OF SYNTHETIC CANNABINOID RECEPTOR AGONISTS DESIGNER DRUGS.

The results of this chapter have been published in:

"Pharmacological insights emerging from the characterization of a large collection of synthetic cannabinoid receptor agonists designer drugs. *Biomedine & Pharmacotherapy*, **2023**, *164*, in press**.** DOI: 10.1016/j.biopha.2023.114934

Impact Factor: 7.419. D1 in Pharmacology & Pharmacy. No written permission from *Elsevier* is necessary. Copyright 2023

Claudia Gioé-Gallo[a, b], Sandra Ortigueira[a, b], José Brea[c, *,] Iu Raïch[d, e], Jhonny Azuaje[a, b], M. Rita Paleo[a], Maria Majellaro[a, b], María Isabel Loza[c], Cristian O. Salas[f], Xerardo García-Mera[b], Gemma Navarro[d, e, **,] Eddy Sotelo[a, b, ***]

[a] *Centro Singular de Investigación en Química Biolóxica e Materiais Moleculares (CiQUS), Universidade de Santiago de Compostela, Santiago de Compostela 15782, Spain.* [b] *Departamento de Química Orgánica, Facultad de Farmacia, Universidade de Santiago de Compostela, Santiago de Compostela 15782, Spain.*[c] *Centro Singular de Investigación en Medicina Molecular y Enfermedades Crónicas (CiMUS), Universidade de Santiago de Compostela, Santiago de Compostela 15782, Spain.* [d] *Department of Biochemistry and Physiology, School of Pharmacy and Food Science, Universitat de Barcelona, Barcelona 08028, Spain.* [e] *Institute of Neurosciences (NeuroUB), Campus Mundet, University of Barcelona, Barcelona 08035, Spain.* [f] *Department of Organic Chemistry, Faculty of Chemistry and Pharmacy, Pontificia Universidad Católica de Chile, Vicuña Mackenna 4860, Macul, Santiago 7820436, Chile.*

Contributions: Investigation, Validation, Writing – original draft.

USC UNIVERSIDADE DE SANTIAGO DE COMPOSTELA

USC
UNIVERSIDADE
DE SANTIAGO
DE COMPOSTELA

3.1 CHAPTER 1. SYNTHESIS AND CHARACTERIZATION OF A LARGE COLLECTION OF SYNTHETIC CANNABINOID RECEPTOR AGONISTS DESIGNER DRUGS

New psychoactive substances (NPS), also known as “designer drugs” or “legal highs” are a broad class of abuse drugs that have emerged on the illicit drug market.[72,73] They are usually conceived by performing structural modifications of existing controlled substances, thereby mimicking their pharmacological effects, and circumventing governmental legislation.[72–74] NPS are generally grouped into four somewhat overlapping functional categories (according to their chemical structure and pharmacological effects): stimulants, hallucinogens, depressants, and cannabinoids.[8,72,74] NPS provide users with novel alternatives to traditional and well-characterized drugs of abuse (e.g. amphetamines, heroin, cocaine, and cannabis).[8] They are undergoing a period of proliferation and diversification, with a significant increase in the challenges faced by emergency and critical care physicians, toxicologists, and regulatory governmental authorities.[89,94]

Synthetic cannabinoid receptor agonists (SCRAs) have proliferated during the last decade, emerging as the largest and most defiant group of NPS controlled by the European Monitoring Centre for Drugs and Drug Addiction (EMCDDA).[3,8,72] Initially conceived for therapeutic purposes, SCRAs have become a major public health concern due to their adverse effects, limited safety profile, evolving structure and diversity (Figure 1).[3,82,94] In the middle of the 2000s, SCRAs entered the abuse drug market in the form of herbal mixtures (e.g. “Spice”, “K2”, “AK-47 24 Karat Gold”). Their use was popularized thanks to their image as a "legal" inexpensive alternative to cannabis (e.g., psychoactive and analgesic effects), which, at the time, was undetectable to routine drug testing.[3,48,94]

SCRAs and the main psychoactive component of cannabis [Δ^9-tetrahydrocannabinol (Δ^9-THC)] do not differ only in their structure, but also qualitatively and quantitatively in their pharmacological profile[95,96] [(the former usually being more potent and efficacious as cannabinoid receptor agonists than Δ^9-THC which is a partial agonist of both Cannabinoid receptors (CBRs)]. However, *in vivo* studies have evidenced that SCRAs produce most of the characteristic effects of cannabis consumption in rodents (e.g., hypothermia, bradycardia, catalepsy, hypo-locomotion and antinociception).[8] It is well documented that SCRAs exert their psychoactive effects through their agonism on the central cannabinoid receptor 1 (CB_1R)[8,82,89], although they

often exhibit a more pronounced agonist effect on cannabinoid receptor 2 (CB_2R).[8,82,89] The exception to this trend is a newly emerged SCRA that has been reported to have CB_1R but not CB_2R activation potential.[97] CBRs are classical G-protein-coupled receptors (GPCRs), that belong to the large rhodopsin-like class A family.[98] Both CBRs are coupled to G_i proteins, inhibiting adenylate cyclase and inducing a reduction in the intracellular cyclic adenosine monophosphate (cAMP) levels.[99] CB_1Rs are one of the most abundant GPCRs in the brain,[99,100] also being highly expressed in the peripheral nervous system and other peripheral tissues. In contrast, CB_2Rs are poorly expressed in brain tissue, being mainly restricted to microglial cells.[101] CB_2Rs are predominantly expressed in immune cells,[102] and are actively implicated in inflammation.[103]

The paucity of thorough studies delineating the pharmacology, toxicity, and abuse liability of new SCRAs poses a threat to public health.[94,104] SCRAs consumption has been unequivocally associated with severe adverse effects (e.g. psychosis, delirium, cardiotoxicity, seizures, acute kidney injury, hypothermia), being implicated in numerous deaths in several countries.[8,48,81,89,105] Because many abused SCRAs (Figure 27) are unknown before they are detected by forensic scientists, their effects on humans are poorly or not known at all.[73,104] Likewise, clinical and forensic toxicology laboratories are confronted by analytical challenges when dealing with this family of abuse substances. The huge number and diversity of compounds, their evolving structure and the limited availability of SCRA standards, metabolites and analytical methods complicate these tasks.[75,91,104]

USC UNIVERSIDADE DE SANTIAGO DE COMPOSTELA

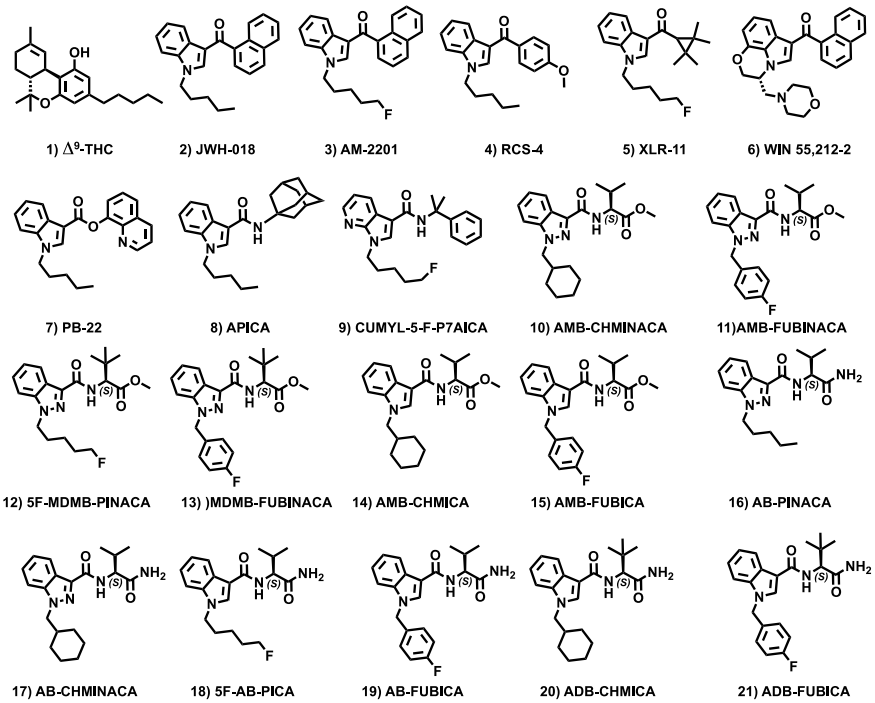


Figure 27: Structure of Δ^9-THC and representative SCRAs.[3,83,84,105]

Since their early detection on the illicit drug market,[1] SCRAs have undergone continuous structural evolution and diversification. Representative structures can be found in Figure 27. Structural modifications not only affect the central heterobicyclic core, but also involve functional group replacements (ketones, esters, and amides) and diversification of the alkyl chains.[3,81,82,89] The most prevalent chemotypes in SCRAs are indole-3-carboxamides and indazole-3-carboxamides featuring pendant amino acid derivatives.[3,82,89] Inspired by earlier Pfizer patents,[106] which claimed synthetic CBR agonists as analgesics, the stereocenter within the pendant amino acid in these compounds is always in the (*S*) configuration.[8,16,29,81,83,107] Although a recent study explored the role of the stereodisposition of the *iso*-propyl and *tert*-butyl side chains of representative SCRAs (Figure 27),[83] this issue remains unresolved.[108] The evolving structure and limited availability of large SCRAs collections by the scientific community has impeded their in-depth characterization from a pharmacological, pharmacokinetic, and toxicological point of view.[75] Several academic groups have generated valuable structural and pharmacological data that sheds light on the complex physiological actions elicited by the SCRAs.[10,88] These studies generally focus on the most frequently abused compounds (and their analogues) and usually exclusively evaluate the (*S*) enantiomers, while the corresponding (*R*) stereoisomers remain almost unexplored.[3,81–83,88] Moreover, published available pharmacological data of SCRAs are

USC UNIVERSIDADE DE SANTIAGO DE COMPOSTELA

usually incomplete. It is well accepted that both the affinity of a drug for its receptor and its ability to produce an effect are important features during ligand characterization and should be determined. Accordingly, there is a demand for large and stereochemically diverse collections of SCRAs for detailed characterization to be shared within the scientific community, in a collaborative manner, to unravel the molecular basis of the SCRAs physio/toxicological actions. Furthermore, these libraries provide reference standards to forensic laboratories and regulatory authorities[75], thus enabling the fight against abusive substances by anticipating drugs that might enter the illegal market. In addition, comprehensive SAR data would allow a better understanding of the structural features that govern CBRs activation and their translation into new therapeutic opportunities.

Herein we report the synthesis and pharmacological characterization (at CB_1R and CB_2R) of the largest published collection of SCRAs (Figure 28, 64 ligands). The library, which exhibits skeletal, stereochemical and functional diversity, as well as the most frequent alkyl groups at positions R^1 and R^2, was conceived as a collaborative resource to foster the investigation of the physiological effects of SCRAs. The pharmacological profiling (binding affinities and functional data) enabled both the analysis of the most salient features emerging from the structure-activity relationship (SAR) and structure-selectivity relationship (SSR) in these series, and the identification of some CB_2R selective ligands. We also examined the neurotoxicity of representative SCRAs on mouse primary neuronal cells, preliminarily demonstrating a significant neurotoxic effect for some of the frequently abused ligands.

Chemistry. A mixture of the 1-alkyl-1*H*-indole (or indazole)-3-carboxylic acid (1 mmol), the corresponding amino acid derivative (**30** or **31**) (1,5 mmol), HATU (1,5 mmol) and DIPEA (4 mmol) in CH_2Cl_2 (2 mL) was stirred with orbital stirring at room temperature for 24 h. After completion of the reaction, water was added, and the mixture was extracted with CH_2Cl_2. The organic phase was dried over $MgSO_4$, filtered, and concentrated. The resulting product was purified by column chromatography on silica gel. The purity of all prepared compounds was established by high-performance liquid chromatography (HPLC) and showed to be >95%. A detailed description of the experimental protocols, equipment and techniques used in the synthesis of targeted ligands, as well as the structural and spectroscopic data obtained for all the compounds described is given in the Experimental Section.

USC DE SANTIAGO

Design. The obtained library (Figure 28), which contains five diversity points (R^1, R^2, R^3, X, and the stereodisposition of R^2), was designed to systematically explore the structural determinants governing the SCRAs' bioactivity profile. We conceived a 64 members collection (Figure 28) containing skeletal (indole and indazole), functional (esters and amides), alkyl (*iso*-propyl and *tert*-butyl) and stereochemical [(*S*) stereoisomers and (*R*) stereoisomers] diversities. The obtained library also features the four most frequent residues present at R^1 (*n*-pentyl, 5-fluoropentyl, 4-fluorobenzyl and cyclohexylmethyl) of the SCRA's heterocyclic cores (Figure 28). To properly compile and evaluate SAR trends, the library contains 32 representative known SCRAs. Notably, 32 of the 64 cannabinoid receptor agonists herein documented had not been previously reported (e.g. derivatives featuring the (*R*) configuration within the pendant aminoacid residue). Therefore, to our knowledge, this is the largest SCRA library ever published to date. For the sake of simplicity, and to allow a more direct appreciation of emerging SAR trends, the 64-membered collection was divided into four subsets, representing functional (esters or amides) and skeletal (indoles or indazoles) diversities (Scheme 1).

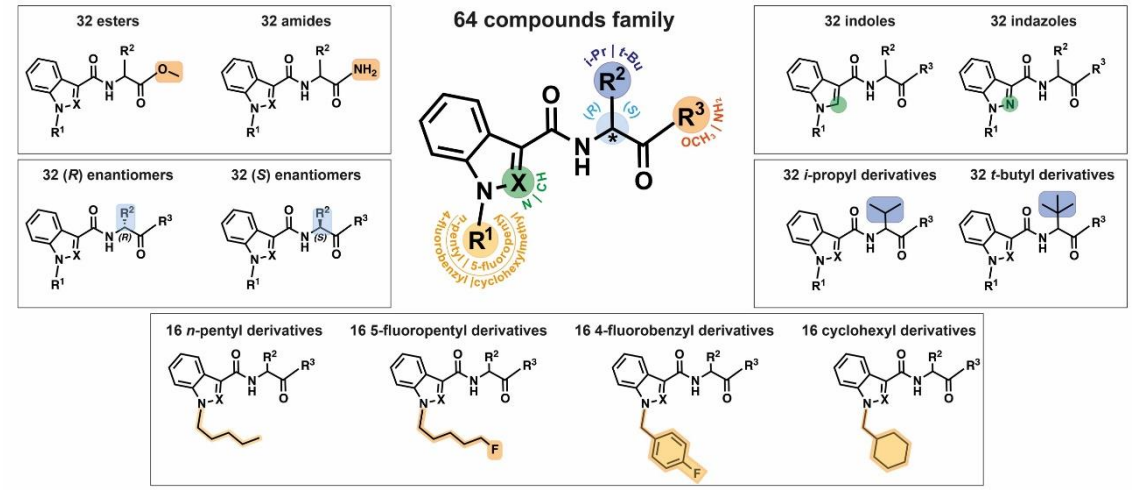


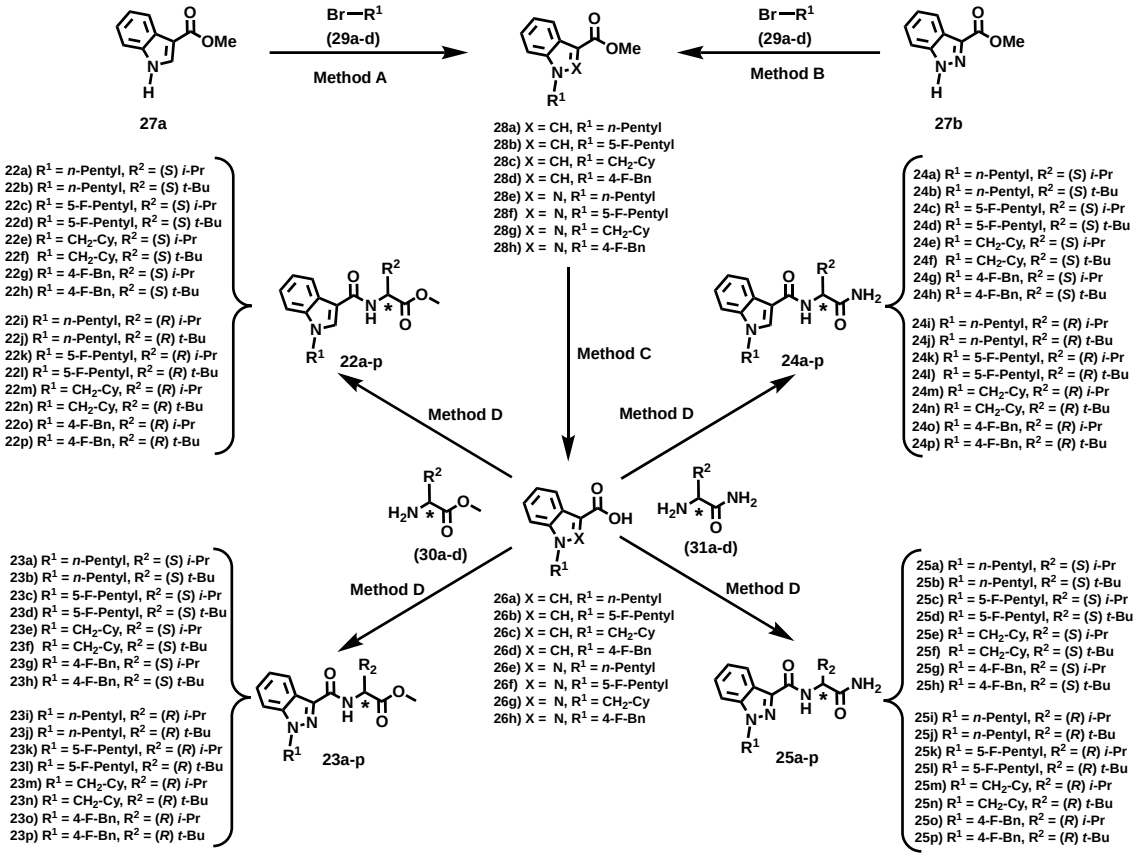
Figure 28: General structure of the library, including elements diversities.

USC UNIVERSIDADE DE SANTIAGO DE COMPOSTELA

The targeted SCRAs collection (Scheme 1, compounds **22a**-**p**, **23a**-**p**, **24a**-**p**, and **25a**-**p**) was assembled following robust and well-established amide synthesis protocols (Scheme 1). The required carboxylic acids (**26a**-**h**) were prepared (Scheme 1, Method C), by saponification of the *N*-alkylated esters **28a**-**h**. Esters **28** were obtained by alkylation of precursors **27** [methyl 3-indolecarboxylate (**27a**) and methyl 3-indazolecarboxylate (**27b**)] with four alkyl halides (**29a**-**d**) under basic conditions (Scheme 1, Methods A or B). The two regioisomers obtained during the alkylation of methyl 3-indazolecarboxylate (**27b**) were separated by chromatographic techniques (Scheme 1, Method B). The unambiguous identity of the major N^1-alkylated compound (3:1 ratio) (**28e**-**h**) was confirmed by NMR experiments. Commercially available (Sigma Aldrich) enantiopure (ee ≥ 99%) amino acid derivatives [methyl glycinate derivatives (**30a**-**d**) and glycinamide derivatives (**31a**-**d**)] of both the (*R*) and (*S*) series, bearing either *iso*-propyl or *tert*-butyl groups at R_1, were used for the synthesis of targeted compounds (Scheme 1, Method D). The amide coupling protocol (HATU) afforded the targeted derivatives (**22ap**−**25ap**) in moderate (47%) to excellent yields (96%) ensuring retention of the enantiomeric fidelity.[109]

All reactions were monitored by thin-layer chromatography (TLC) employing UV light, iodine, or a dissolution of phosphomolybdic acid for the compound's detection. After completion of the reaction, the solvent was evaporated to dryness and the isolated solid was purified by column chromatography on silica gel. A detailed description of the synthetic methods and the complete structural, spectroscopic, and analytical data for all compounds is provided in the Experimental Section.

USC UNIVERSIDADE DE SANTIAGO DE COMPOSTELA



Scheme 1: Synthesis of the SCRAs 22-25. Method A) NaH, DMF, rt, 24 h. Method B) NaH, DMF, rt, 24 h and then chromatographic separation to isolate the regioisomers. Method C) NaOH, dioxane, 120 ºC, 12 h. Method D) HATU, DIPEA, CH_2Cl_2, rt, 24 h.

Although the carboxylic acids **26** are non-chiral, and racemization is mechanistically unlikely under the employed amide coupling conditions,[109,110] all members of the library were routinely controlled by analytical chiral HPLC to confirm that the stereocenter remained intact in the final compounds (see Experimental Section). A selection of the HPLC traces obtained for representative enantiomeric pairs is presented in Figure 29. Circular dichroism (CD) spectroscopy[111,112] is an orthogonal and versatile biophysical technique that provides valuable structural information[113,114] of proteins, peptides, small molecules, and functional macromolecules. As part of the characterization of herein described SCRAs, it was envisioned that they contain the two structural requirements to interact with circularly polarized light used in CD spectroscopy: a chromophore (indole or indazole cores) and an enantiopure aminoacidic residue (chirality). Accordingly, it was decided to study the circular dichroism (CD) spectra of representative SCRAs pairs, all experiments were performed employing enantiopure derivatives eliciting ee ≥ 98%.

USC UNIVERSIDADE DE SANTIAGO DE COMPOSTELA

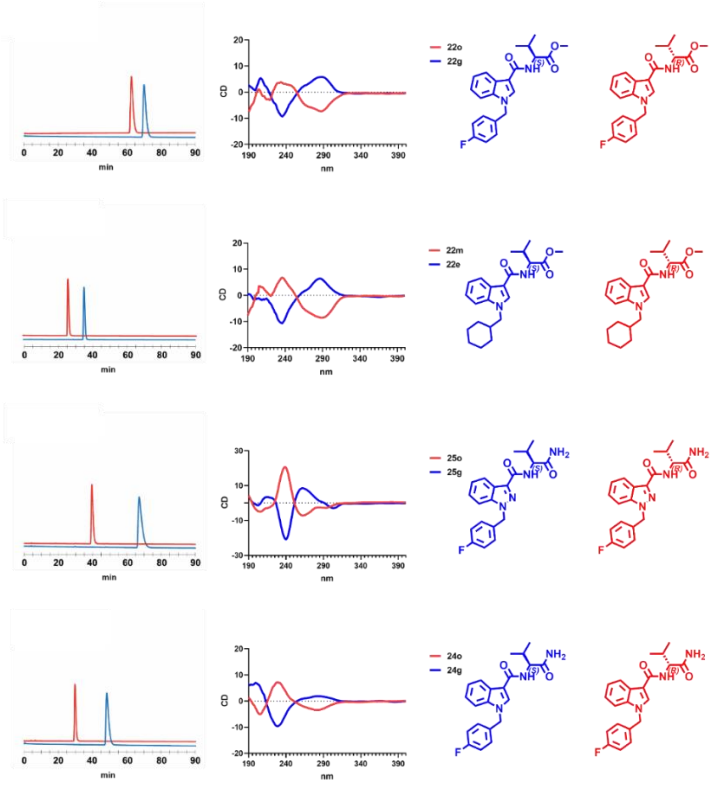


Figure 29: HPLC traces of representative enantiopure esters and amides SCRAs (left) and circular dichroism spectra of enantiomer pairs (right). At 240 nm the (S) enantiomer showed a negative Cotton effect (blue line), while the (R) stereoisomer gave a positive Cotton effect (red line).

As observed (Figure 29), regardless of the functional group within the amino acid residue (ester or amide), each single stereoisomer of the enantiomer pairs elicited symmetrical CD spectra, mirrored at the x-axis and with opposite sign. The absorbance of circularly polarized light by the chiral center in the SCRAs gives rise to a characteristic CD signal at low wavelength (far-UV: 240 nm) that provides information about the secondary structure (stereochemistry). On the other hand, the heterocyclic chromophore, despite being non-chiral, gives rise to CD signals in the near-UV (250-330 nm), because they are affected by the adjacent chiral environment. The characteristic CD signal around 240 nm allowed the unambiguous assignment of the absolute configuration of each enantiomer (Figure 29). At this wavelength, the (*S*) enantiomer showed a negative Cotton effect (blue line), while the (*R*) stereoisomer gave a positive Cotton effect (red line). These additional experiments confirmed that all the obtained ligands contained a stereo-defined configuration and were pharmacologically evaluated as enantiopure compounds (ee >98%). In view of its robustness, performance and minimal sample preparation requirements, circular dichroism spectroscopy offers unique insights to rapidly assess the configuration of SCRA enantiopure samples.

Biological Evaluation. One of the aims of this study was to address the limited availability of large SCRA collections and, consequently, the lack of homogeneous and reliable pharmacological data of these drugs of abuse. Thus, the cannabimimetic profile of the 64 SCRAs was studied *in vitro* by evaluating its functional activity (EC_{50} and E_{max}) and binding affinity (K_i) for human CB_1Rs and CB_2Rs according to established experimental protocols. All the studied indole and indazole derivatives bind and activated both CB_1R and CB_2R. The pharmacological data (Tables 3-6) are expressed as pEC_{50} ± SEM or pK_i ± SEM [and EC_{50} and K_i (nM)]. The data obtained for Δ^9-THC, Surinabant, CP 55,940 and GW405833, using described experimental protocols, were reported in Tables 3-6 for the sake of comparison. The *in vitro* affinity data was acquired via competitive radioligand binding assays using membrane preparations of human CB_1Rs and CB_2Rs transfected in CHO-CB1 C3 cells and HEK-293T cells respectively and a well-characterized tritiated ligand ([^{3}H]-CP 55,940). As cannabinoid receptors are GPCRs coupled to the G_i protein, the functional activity of synthesized SCRAs at CB_1Rs and CB_2Rs was assessed by determining the decreases in cAMP levels induced by forskolin treatment. During functional experiments, the maximum effects of ligands **22-25** and Δ^9-THC were normalized to a maximal efficacious concentration of CP 55,940. Data for each experiment were normalized to the change in fluorescence intensity produced by a maximally effective concentration of CP 55,940.

Representative dose-response curves obtained for selected ligands during the functional studies and binding affinity determinations at CB_1R and CB_2R, are presented in Figure 30. A detailed description of the protocols is reported in the Experimental Section. The dose-response curves obtained for all the ligands documented here are given in the Experimental Section.

USC
UNIVERSIDADE DE SANTIAGO DE COMPOSTELA

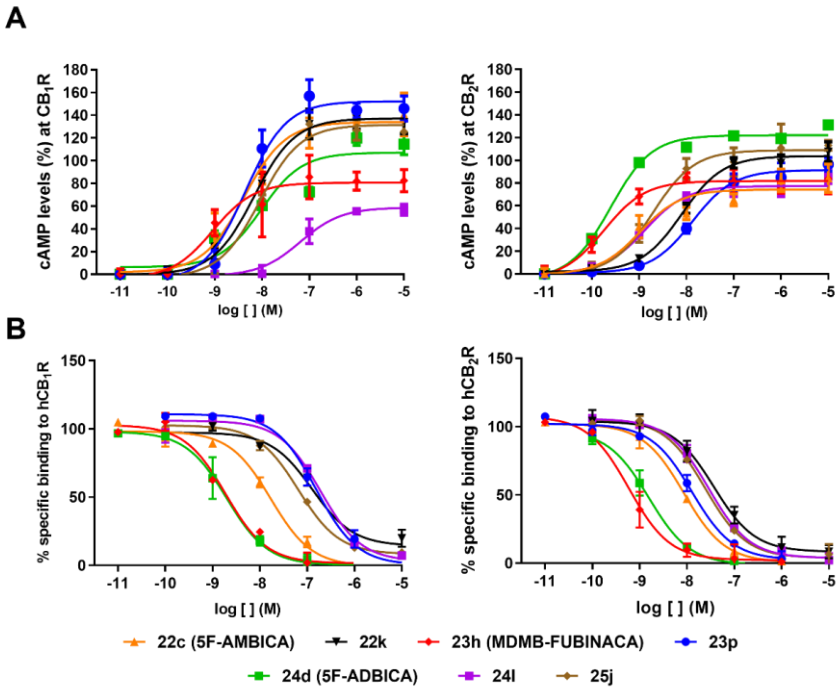
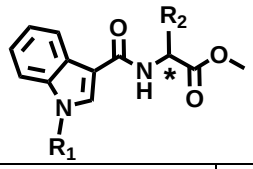


Figure 30: Representative dose-response curves obtained for selected ligands at CB_1R and CB_2R during functional (A) and binding studies (B).

The pharmacological data obtained for the 64-membered collection are presented in Table 3-6, each one containing 16 derivatives [the first 8 bearing the *(S)* configuration at the pendant amino acid residue and the other 8 the *(R)* configuration]. Tables 3-4 present the pharmacological data of esters (indole and indazoles, respectively) while Tables 5-6 report the data obtained for amides (indole and indazoles respectively). Novel compounds are indicated with an asterisk (Tables 3-6) and already described SCRAs with their common acronym in the illicit drug market (Tables 3-6). The original articles describing the known compounds are also listed in the Tables 3-6.[3,81,83] To facilitate the identification of the most salient features of the structure-selectivity relationship throughout the series, the selectivity index (SI), calculated using the affinity data (K_i CB_2R/K_i CB_1R), is also reported in Tables 3-6.

USC UNIVERSIDADE DE SANTIAGO DE COMPOSTELA

Table 3: Structure, affinity, and functional data obtained for the indole esters **22a-p**.

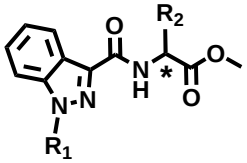


Compound	R^1	R^2	CB_1R			CB_2R			SI
			pEC_{50} ± SEM[a] [EC_{50} nM)]	E_{max}[b]	pK_i ± SEM[c] [K_i nM)]	pEC_{50} ± SEM[a] [EC_{50} nM)]	E_{max}[b]	pK_i ± SEM[d] [K_i nM)]	K_iCB_1R/K_iCB_2R
22a (AMBICA)[81]	Pentyl	(*S*) *i*-Pr	7.27 ± 0.05 [53.7]	80%	7.58 ± 0.07 [26.6]	7.34 ± 0.05 [45.2]	77%	7.79 ± 0.09 [16.4]	1.62
22b (MDMB-PICA)[81]	Pentyl	(*S*) *t*-Bu	7.55 ± 0.03 [28.4]	74%	8.14 ± 0.05 [7.20]	8.94 ± 0.07 [1.14]	95%	8.54 ± 0.03 [2.90]	2.48
22c (5F-AMBICA)[81]	5-F-Pentyl	(*S*) *i*-Pr	8.34 ± 0.06 [4.62]	134%	8.09 ± 0.08 [8.10]	8.98 ± 0.06 [1.05]	74%	8.38 ± 0.07 [4.23]	1.91
22d (5F-MDMB-PICA)[81]	5-F-Pentyl	(*S*) *t*-Bu	9.15 ± 0.08 [0.70]	88%	8.59 ± 0.09 [2.61]	9.29 ± 0.07 [0.51]	103%	9.15 ± 0.05 [0.70]	3.73
22e (MMB-CHMICA)[81]	CH_2-Cy	(*S*) *i*-Pr	7.74 ± 0.09 [18.1]	79%	7.98 ± 0.06 [10.5]	8.64 ± 0.08 [2.27]	68%	8.47 ± 0.07 [3.44]	3.05
22f (MDBM-CHMICA)[81]	CH_2-Cy	(*S*) *t*-Bu	8.82 ± 0.07 [1.50]	58%	10.05± 0.12 [0.09]	9.22 ± 0.09 [0.60]	61%	9.74 ± 0.08 [0.18]	0.50
22g (MMB-FUBICA)[81]	4-F-Bn	(*S*) *i*-Pr	7.94 ± 0.05 [11.4]	88%	7.32 ± 0.03 [47.8]	7.32 ± 0.03 [48.2]	101%	7.70 ± 0.05 [20.0]	2.39
22h (MDMB-FUBICA)[81]	4-F-Bn	(*S*) *t*-Bu	8.16 ± 0.07 [6.99]	75%	8.42 ± 0.08 [3.83]	8.67 ± 0.06 [2.12]	82%	8.95 ± 0.07 [1.12]	3.42
22i*	Pentyl	(*R*) *i*-Pr	7.14 ± 0.06 [72.3]	66%	6.20 ± 0.04 [632]	8.34 ± 0.07 [4.60]	94%	7.43 ± 0.09 [37.1]	17.1
22j*	Pentyl	(*R*) *t*-Bu	7.72 ± 0.08 [19.0]	126%	6.60 ± 0.02 [251]	7.24 ± 0.04 [57.0]	66%	6.69 ± 0.03 [110]	2.28
22k*	5-F-Pentyl	(*R*) *i*-Pr	8.16 ± 0.09 [6.92]	137%	7.22 ± 0.05 [60.2]	8.11 ± 0.07 [7.79]	104%	7.72 ± 0.05 [19.2]	3.14
22l*	5-F-Pentyl	(*R*) *t*-Bu	7.83 ± 0.05 [14.9]	137%	6.89 ± 0.09 [127]	9.60 ± 0.06 [0.25]	126%	8.21 ± 0.04 [6.11]	20.8
22m*	CH_2-Cy	(*R*) *i*-Pr	7.86 ± 0.06 [13.9]	87%	7.12 ± 0.06 [76.4]	7.21 ± 0.08 [61.6]	107%	7.92 ± 0.08 [12.1]	6.31
22n*	CH_2-Cy	(*R*) *t*-Bu	7.75 ± 0.04 [17.6]	89%	6.82 ± 0.07 [151]	7.64 ± 0.03 [22.8]	64%	7.27 ± 0.03 [53.5]	2.82
22o*	4-F-Bn	(*R*) *i*-Pr	7.71 ± 0.06 [19.7]	109%	6.84 ± 0.04 [145]	8.30 ± 0.07 [5.01]	91%	8.10 ± 0.07 [8.21]	17.6
22p*	4-F-Bn	(*R*) *t*-Bu	7.88 ± 0.07 [13.2]	120%	6.75 ± 0.06 [179]	8.03 ± 0.06 [9.43]	49%	7.64 ± 0.05 [22.8]	7.85
Δ^9-THC	-	-	7.47 ± 0.16 [33.8]	51%	-	6.62 ± 0.25 [238]	21%	-	-
Surinaban t	-	-	-	-	8.52 ± 0.08 [3.00]	-	-	6.39 ± 0.06 [400]	0.0075
GW405833	-	-	-	-	5.32 ± 0.05 [4772]	-	-	8.23 ± 0.07 [5.80]	822
CP 55,940	-	-	-	-	8.99±0.11 [1.01]	-	-	10.21±0.32 [0.13]	7.76

[a] Functional activity assessed in transfected HEK-293T cells by determining cAMP levels after forskolin stimulation. [b] E_{max} values were normalized to a maximal efficacious concentration of CP 55,940. [c] Displacement of specific [^{3}H]-CP 55,940 binding in membrane preparations of human CB_1Rs transfected in CHO-CB1 C3 cell line expressed as K_i in nM (n = 3) or percentage displacement of specific binding at a concentration of 1 μM (n = 2). [d] Displacement of specific [^{3}H]-CP 55,940 binding in membrane preparations of human CB_2Rs transfected in HEK-293T cells expressed as K_i in nM (n = 3) or percentage displacement of specific binding at a concentration of 1 μM (n = 2). * These SCRAs have not been previously described.

USC UNIVERSIDADE DE SANTIAGO DE COMPOSTELA

Table 4: Structure, affinity, and functional data obtained for the indazole esters **23a**-**p**.

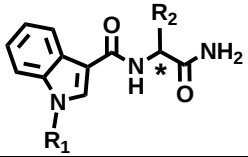


Compound	R^1	R^2	CB_1R			CB_2R			SI
			pEC_{50} ± SEM[a] [EC_{50} nM)]	E_{max}[b]	pK_i ± SEM[c] [K_i nM)]	pEC_{50} ± SEM[a] [EC_{50} nM)]	E_{max}[b]	pK_i ± SEM[d] [K_i nM)]	K_iCB_1R/ K_iCB_2R
23a (AMB)[81]	Pentyl	(*S*) *i*-Pr	8.56 ± 0.08 [2.73]	72%	8.39 ± 0.09 [4.17]	8.79 ± 0.08 [1.61]	62%	8.89 ± 0.06 [1.30]	3.21
23b (MDMB-PINACA)[81]	Pentyl	(*S*) *t*-Bu	8.59 ± 0.07 [2.60]	66%	8.68 ± 0.09 [2.10]	9.89 ± 0.09 [0.13]	68%	9.70 ± 0.04 [0.26]	8.08
23c (5F-AMB)[81]	5-F-Pentyl	(*S*) *i*-Pr	8.90 ± 0.04 [1.27]	90%	8.77 ± 0.06 [1.74]	9.24 ± 0.06 [0.58]	81%	9.30 ± 0.07 [0.52]	3.35
23d (5F-MDMB-PINACA)[81]	5-F-Pentyl	(*S*) *t*-Bu	9.24 ± 0.06 [0.58]	75%	9.10 ± 0.09 [0.80]	10.0 ± 0.09 [0.10]	88%	10.0 ± 0.08 [0.10]	8.00
23e (AMB-CHMINACA)[81]	CH_2-Cy	(*S*) *i*-Pr	8.69 ± 0.07 [2.02]	104%	8.72 ± 0.05 [1.90]	8.05 ± 0.05 [8.82]	83%	9.30 ± 0.07 [0.51]	3.73
23f (MDMB-CHMINACA)[81]	CH_2-Cy	(*S*) *t*-Bu	9.12 ± 0.05 [0.76]	84%	9.00 ± 0.07 [1.08]	8.72 ± 0.06 [1.92]	76%	9.52 ± 0.08 [0.33]	3.27
23g (AMB-FUBINACA)[81]	4-F-Bn	(*S*) *i*-Pr	8.64 ± 0.09 [2.29]	115%	8.14 ± 0.03 [3.90]	9.92 ± 0.08 [0.12]	80%	9.22 ± 0.05 [0.62]	6.29
23h (MDMB-FUBINACA)[81]	4-F-Bn	(*S*) *t*-Bu	9.04 ± 0.07 [0.92]	81%	9.10 ± 0.02 [0.83]	9.77 ± 0.06 [0.17]	82%	9.52 ± 0.07 [0.30]	2.77
23i*	Pentyl	(*R*) *i*-Pr	8.04 ± 0.06 [9.02]	58%	7.04 ± 0.04 [91.6]	8.59 ± 0.09 [2.6]	98%	8.18 ± 0.06 [6.61]	13.8
23j*	Pentyl	(*R*) *t*-Bu	7.67 ± 0.04 [21.6]	100%	6.36 ± 0.07 [435]	8.38 ± 0.07 [4.2]	104%	7.85 ± 0.04 [14.7]	29.6
23k*	5-F-Pentyl	(*R*) *i*-Pr	8.10 ± 0.06 [7.91]	67%	7.63 ± 0.08 [23.5]	8.94 ± 0.05 [1.14]	70%	8.59 ± 0.09 [2.60]	9.04
23l*	5-F-Pentyl	(*R*) *t*-Bu	7.29 ± 0.03 [51.3]	66%	7.09 ± 0.08 [81.1]	9.27 ± 0.07 [0.54]	87%	7.86 ± 0.05 [13.3]	6.10
23m*	CH_2-Cy	(*R*) *i*-Pr	8.18 ± 0.05 [6.59]	130%	7.61 ± 0.05 [24.4]	8.66 ± 0.06 [2.17]	92%	8.85 ± 0.07 [1.40]	17.4
23n*	CH_2-Cy	(*R*) *t*-Bu	8.28 ± 0.07 [5.26]	138%	7.42 ± 0.03 [38.4]	8.75 ± 0.06 [1.79]	106%	8.10 ± 0.06 [8.05]	4.77
23o*	4-F-Bn	(*R*) *i*-Pr	8.28 ± 0.04 [5.22]	134%	7.56 ± 0.07 [29.7]	8.83 ± 0.08 [1.49]	118%	9.00 ± 0.07 [1.20]	24.7
23p*	4-F-Bn	(*R*) *t*-Bu	8.36 ± 0.09 [4.35]	152%	7.16 ± 0.03 [68.4]	7.88 ± 0.04 [13.2]	91%	8.17 ± 0.09 [6.70]	10.2
Δ⁹-THC	-	-	7.47 ± 0.16 [33.8]	51%	-	6.62 ± 0.25 [238]	21%	-	-
Surinabant	-	-	-	-	8.52 ± 0.08 [3.00]	-	-	6.39 ± 0.06 [400]	0.0075
GW405833	-	-	-	-	5.32 ± 0.05 [4772]	-	-	8.23 ± 0.07 [5.80]	822
CP 55,940	-	-	-	-	8.99±0.11 [1.01]	-	-	10.21±0.32 [0.13]	7.76

[a] Functional activity assessed in transfected HEK-293T cells by determining cAMP levels after forskolin stimulation. [b] E_{max} values were normalized to a maximal efficacious concentration of CP 55,940. [c] Displacement of specific [^{3}H]-CP 55,940 binding in membrane preparations of human CB_1Rs transfected in CHO-CB1 C3 cell line expressed as K_i in nM (n = 3) or percentage displacement of specific binding at a concentration of 1 μM (n = 2). [d] Displacement of specific [^{3}H]-CP 55,940 binding in membrane preparations of human CB_2Rs transfected in HEK-293T cells expressed as K_i in nM (n = 3) or percentage displacement of specific binding at a concentration of 1 μM (n = 2). * These SCRAs have not been previously described.

USC UNIVERSIDADE DE SANTIAGO DE COMPOSTELA

Table 5: Structure, affinity, and functional data obtained for the indole amides **24a-p.**

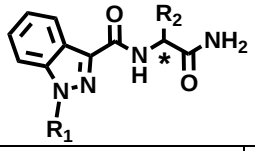


Compound	R^1	R^2	CB_1R			CB_2R			SI
			pEC_{50} ± SEM[a] [EC_{50} nM)]	E_{max}[b]	pK_i ± SEM[c] [K_i nM)]	pEC_{50} ± SEM[a] [EC_{50} nM)]	E_{max}[b]	pK_i ± SEM[d] [K_i nM)]	K_iCB_1R/K_iCB_2R
24a (AB-PICA)[83]	Pentyl	(*S*) *i*-Pr	6.92 ± 0.02 [120]	85%	7.76 ± 0.03 [17.5]	8.36 ± 0.07 [4.32]	120%	7.95 ± 0.04 [11.2]	1.56
24b (AD-BICA)[83]	Pentyl	(*S*) *t*-Bu	8.79 ± 0.07 [1.64]	76%	9.10 ± 0.08 [0.80]	9.00 ± 0.09 [1.00]	105%	9.30 ± 0.09 [0.52]	1.54
24c (5F-AB-PICA)[83]	5-F-Pentyl	(*S*) *i*-Pr	8.31 ± 0.07 [4.95]	109%	7.83 ± 0.07 [14.8]	8.67 ± 0.09 [2.15]	123%	8.07 ± 0.05 [8.60]	1.72
24d (5F-AD-BICA)[83]	5-F-Pentyl	(*S*) *t*-Bu	7.88 ± 0.03 [13.1]	109%	9.05 ± 0.09 [0.91]	9.62 ± 0.05 [0.24]	122%	9.15 ± 0.09 [0.74]	1.23
24e (AB-CHMICA)[3]	CH_2-Cy	(*S*) *i*-Pr	9.60 ± 0.07 [0.25]	95%	8.62 ± 0.09 [2.43]	8.70 ± 0.07 [1.98]	86%	7.45 ± 0.04 [35.3]	0.07
24f (ADB-CHMICA)[3]	CH_2-Cy	(*S*) *t*-Bu	6.66 ± 0.05 [221]	70%	8.96 ± 0.07 [1.10]	8.09 ± 0.03 [8.20]	73%	9.12 ± 0.06 [0.76]	1.45
24g (AB-FUBICA)[83]	4-F-Bn	(*S*) *i*-Pr	7.94 ± 0.04 [11.5]	89%	7.45 ± 0.04 [35.2]	8.04 ± 0.07 [9.15]	86%	6.22 ± 0.06 [83.2]	0.42
24h (ADB-FUBICA)[83]	4-F-Bn	(*S*) *t*-Bu	7.19 ± 0.06 [64.1]	69%	7.27 ± 0.04 [53.8]	8.95 ± 0.09 [1.11]	77%	8.29 ± 0.07 [5.15]	10.4
24i*	Pentyl	(*R*) *i*-Pr	8.30 ± 0.09 [4.96]	95%	6.17 ± 0.03 [672]	7.52 ± 0.04 [29.9]	117%	6.48 ± 0.05 [328]	2.05
24j*	Pentyl	(*R*) *t*-Bu	8.60 ± 0.08 [2.54]	92%	7.19 ± 0.07 [65]	8.88 ± 0.09 [1.32]	102%	7.69 ± 0.04 [20.3]	3.20
24k*	5-F-Pentyl	(*R*) *i*-Pr	6.59 ± 0.04 [258]	72%	6.14 ± 0.08 [720]	6.15 ± 0.08 [703]	42%	6.37 ± 0.07 [425]	1.69
24l*	5-F-Pentyl	(*R*) *t*-Bu	7.20 ± 0.06 [62.7]	59%	7.04 ± 0.06 [90.6]	8.88 ± 0.07 [1.33]	77%	7.82 ± 0.09 [15.1]	6.00
24m*	CH_2-Cy	(*R*) *i*-Pr	7.08 ± 0.04 [82.5]	47%	6.51 ± 0.03 [311]	6.65 ± 0.05 [225]	48%	6.96 ± 0.05 [109]	2.85
24n*	CH_2-Cy	(*R*) *t*-Bu	8.31 ± 0.07 [4.90]	81%	7.18 ± 0.05 [66.1]	8.60 ± 0.05 [2.49]	54%	7.66 ± 0.06 [21.8]	3.03
24o*	4-F-Bn	(*R*) *i*-Pr	7.41 ± 0.03 [39.1]	85%	6.00 ± 0.07 [588]	8.08 ± 0.08 [8.38]	82%	6.78 ± 0.08 [167]	3.52
24p*	4-F-Bn	(*R*) *t*-Bu	7.83 ± 0.04 [14.8]	127%	7.14 ± 0.06 [72.8]	8.49 ± 0.07 [3.24]	79%	7.63 ± 0.03 [23.3]	3.12
Δ^9-THC	-	-	7.47 ± 0.16 [33.8]	51%	-	6.62 ± 0.25 [238]	21%	-	-
Surinabant	-	-	-	-	8.52 ± 0.08 [3.00]	-	-	6.39 ± 0.06 [400]	0.0075
GW405833	-	-	-	-	5.32 ± 0.05 [4772]	-	-	8.23 ± 0.07 [5.80]	822
CP 55,940	-	-	-	-	8.99±0.11 [1.01]	-	-	10.21±0.32 [0.13]	7.76

[a] Functional activity assessed in transfected HEK-293T cells by determining cAMP levels after forskolin stimulation. [b] E_{max} values were normalized to a maximal efficacious concentration of CP 55,940. [c] Displacement of specific [^{3}H]-CP 55,940 binding in membrane preparations of human CB_1Rs transfected in CHO-CB1 C3 cell line expressed as K_i in nM (n = 3) or percentage displacement of specific binding at a concentration of 1 μM (n = 2). [d] Displacement of specific [^{3}H]-CP 55,940 binding in membrane preparations of human CB_2Rs transfected in HEK-293T cells expressed as K_i in nM (n = 3) or percentage displacement of specific binding at a concentration of 1 μM (n = 2). * These SCRAs have not been previously described.

USC UNIVERSIDADE DE SANTIAGO DE COMPOSTELA

Table 6: Structure, affinity, and functional data obtained for the indazole amides **25a-p**.



Compound	R^1	R^2	CB_1R			CB_2R			SI
			pEC_{50} ± SEM[a] [EC_{50} nM)]	E_{max}[b]	pK_i ± SEM[c] [K_i nM)]	pEC_{50} ± SEM[a] [EC_{50} nM)]	E_{max}[b]	pK_i ± SEM[d] [K_i nM)]	K_iCB_1R/K_iCB_2R
25a (AB-PINACA)[83]	Pentyl	(*S*) *i*-Pr	8.83 ± 0.07 [1.49]	94%	8.96 ± 0.08 [1.16]	9.68 ± 0.09 [0.21]	128%	9.05 ± 0.08 [0.94]	1.23
25b (ADB-PINACA)[83]	Pentyl	(*S*) *t*-Bu	11.0 ± 0.09 [0.01]	138%	9.40 ± 0.08 [0.40]	9.89 ± 0.08 [0.13]	129%	9.52 ± 0.08 [0.30]	1.33
25c (5F-AB-PINACA)[83]	5-F-Pentyl	(*S*) *i*-Pr	8.87 ± 0.09 [1.36]	164%	7.75 ± 0.07 [17.9]	9.17 ± 0.06 [0.67]	127%	7.84 ± 0.05 [14.3]	1.25
25d (5F-ADB-PINACA)[83]	5-F-Pentyl	(*S*) *t*-Bu	8.91 ± 0.08 [1.22]	134%	8.57 ± 0.05 [2.73]	9.44 ± 0.07 [0.36]	135%	9.52 ± 0.03 [0.31]	8.81
25e (AB-CHMINACA)[3]	CH_2-Cy	(*S*) *i*-Pr	8.89 ± 0.06 [1.04]	78%	9.05 ± 0.09 [0.90]	8.12 ± 0.08 [7.67]	63%	8.96 ± 0.06 [1.10]	0.82
25f (ABD-CHMINACA)[3]	CH_2-Cy	(*S*) *t*-Bu	7.34 ± 0.04 [46.2]	80%	9.05 ± 0.09 [0.98]	8.46 ± 0.04 [3.49]	53%	9.22 ± 0.09 [0.60]	1.63
25g (AB-FUBINACA)[83]	4-F-Bn	(*S*) *i*-Pr	8.41 ± 0.08 [3.86]	95%	8.64 ± 0.06 [2.31]	8.24 ± 0.06 [5.77]	86%	8.96 ± 0.08 [1.17]	1.97
25h (ADB-FUBINACA)[83]	4-F-Bn	(*S*) *t*-Bu	7.67 ± 0.03 [21.3]	104%	9.10 ± 0.04 [0.83]	8.40 ± 0.08 [3.96]	84%	10.0 ± 0.07 [0.14]	5.93
25i*	Pentyl	(*R*) *i*-Pr	7.99 ± 0.02 [10.3]	137%	6.98 ± 0.06 [105]	8.95 ± 0.06 [1.12]	113%	7.43 ± 0.05 [37.3]	2.82
25j*	Pentyl	(*R*) *t*-Bu	8.05 ± 0.03 [8.82]	131%	7.51 ± 0.05 [30.8]	8.71 ± 0.03 [1.97]	109%	7.92 ± 0.03 [12.1]	2.55
25k*	5-F-Pentyl	(*R*) *i*-Pr	7.32 ± 0.06 [48.2]	97%	6.79 ± 0.07 [160]	7.43 ± 0.07 [36.9]	65%	6.87 ± 0.02 [133]	1.20
25l*	5-F-Pentyl	(*R*) *t*-Bu	7.02 ± 0.04 [95.7]	96%	6.28 ± 0.04 [520]	7.71 ± 0.06 [19.4]	54%	6.66 ± 0.08 [221]	2.35
25m*	CH_2-Cy	(*R*) *i*-Pr	7.75 ± 0.03 [17.7]	100%	7.75 ± 0.08 [17.9]	7.57 ± 0.04 [26.9]	43%	7.61 ± 0.07 [24.5]	0.73
25n*	CH_2-Cy	(*R*) *t*-Bu	8.60 ± 0.05 [2.50]	130%	7.71 ± 0.07 [19.4]	7.24 ± 0.06 [57.2]	52%	7.77 ± 0.05 [17.2]	1.13
25o*	4-F-Bn	(*R*) *i*-Pr	8.65 ± 0.05 [2.25]	126%	6.85 ± 0.06 [139]	5.89 ± 0.03 [1301]	93%	7.07 ± 0.09 [84.3]	1.65
25p*	4-F-Bn	(*R*) *t*-Bu	7.70 ± 0.07 [19.8]	106%	7.85 ± 0.03 [26.2]	7.44 ± 0.07 [36.4]	89%	7.95 ± 0.06 [11.2]	2.34
Δ^9-THC	-	-	7.47 ± 0.16 [33.8]	51%	-	6.62 ± 0.25 [238]	21%	-	-
Surinabant	-	-	-	-	8.52 ± 0.08 [3.00]	-	-	6.39 ± 0.06 [400]	0.0075
GW405833	-	-	-	-	5.32 ± 0.05 [4772]	-	-	8.23 ± 0.07 [5.80]	822
CP 55,940	-	-	-	-	8.99±0.11 [1.01]	-	-	10.21±0.32 [0.13]	7.76

[a] Functional activity assessed in transfected HEK-293T cells by determining cAMP levels after forskolin stimulation. [b] E_{max} values were normalized to a maximal efficacious concentration of CP 55,940. [c] Displacement of specific [^{3}H]-CP 55,940 binding in membrane preparations of human CB_1Rs transfected in CHO-CB1 C3 cell line expressed as K_i in nM (n = 3) or percentage displacement of specific binding at a concentration of 1 μM (n = 2). [d] Displacement of specific [^{3}H]-CP 55,940 binding in membrane preparations of human CB_2Rs transfected in HEK-293T cells expressed as K_i in nM (n = 3) or percentage displacement of specific binding at a concentration of 1 μM (n = 2). * These SCRAs have not been previously described.

USC UNIVERSIDADE DE SANTIAGO DE COMPOSTELA

Structure-Activity Relationship analysis. The binding affinities (pK_i), potencies (pEC_{50}) and efficacies (E_{max}) obtained during the pharmacological evaluation of the library (**22ap**−**25ap**) at CB_1R and CB_2R are presented in Tables 3-6. The affinity and functional data herein determined for known SCRAs (**22-25a-h**) are in the same range as reported (see Tables S1-S4, Experimental section).[5,7,8,10,20] For comparative purposes the phytocannabinoid Δ^9-THC and three synthetic CBR ligands (surinabant, GW405833 and CP 55,940) were evaluated with the same experimental protocols and their functional (Δ^9-THC) or affinity (surinabant, GW405833 and CP 55,940) data were also included in Tables 3-6. The functional data obtained unequivocally confirm that derivatives **22-25** activate both CB_1Rs and CB_2Rs. In contrast with Δ^9-THC (a partial agonist with moderate activity at both receptors), all members of the library (**22ap**−**25ap**) exhibited excellent activity and greater potency than Δ^9-THC at both CB_1Rs and CB_2Rs. Comparisons of the affinity (pK_i) and functional (pEC_{50}) values obtained for the members of the library (Tables 3-6) with published data reveal that there are no significant differences (Tables S1-S4, Experimental section). As a general trend, the functional data (especially in CB_2R) are slightly higher than reported. It is however well documented[115] that functional data (EC_{50}) and efficacy (E_{max}) are highly dependent on the expression level of the receptors or "receptor reserve", while K_i values obtained in binding studies are largely independent on the employed cellular background. For these reasons, affinity data (pK_i) will be used for subtype selectivity analysis and to establish the most of salient SAR and SSR features within the collection.

As stated in the introduction, the herein obtained comprehensive library is intended to be used (in a collaborative manner) with academics and law enforcement to address and control the threat to human health of this family of NPS. In addition, SAR observations from this large subset inspired our ongoing research project aimed at developing CB_2R agonists as candidates for autoimmune and inflammatory diseases.

A first inspection of the data included in Tables 3-6 reveals that most of the ligands studied show a very consistent profile, generally behaving as highly potent, non-selective, full agonists at both receptors, regardless of their functional (ester or amide), skeletal (indole or indazole), stereochemical (*S* or *R*) or alkyl (R^1 and R^2) diversities. According to their *in vitro* cannabimimetic profiles (Tables 3-6), of the novel 32 ligands herein reported [bearing the (*R*) configuration at the pendant amino acid chain], fourteen derivatives (ligands **22k**, **22p**, **23m**, **23n**, **23o**, **23p**, **24i**, **24j**, **24n**, **24p, 25i**, **25j**, **25n**,

25o) present the prototypical profile of SCRAs (e.g., low nanomolar affinity and activity, generally combined with high efficacy) and therefore could be (or may currently be) used as illegal psychoactive substances (prophetic SCRAs).

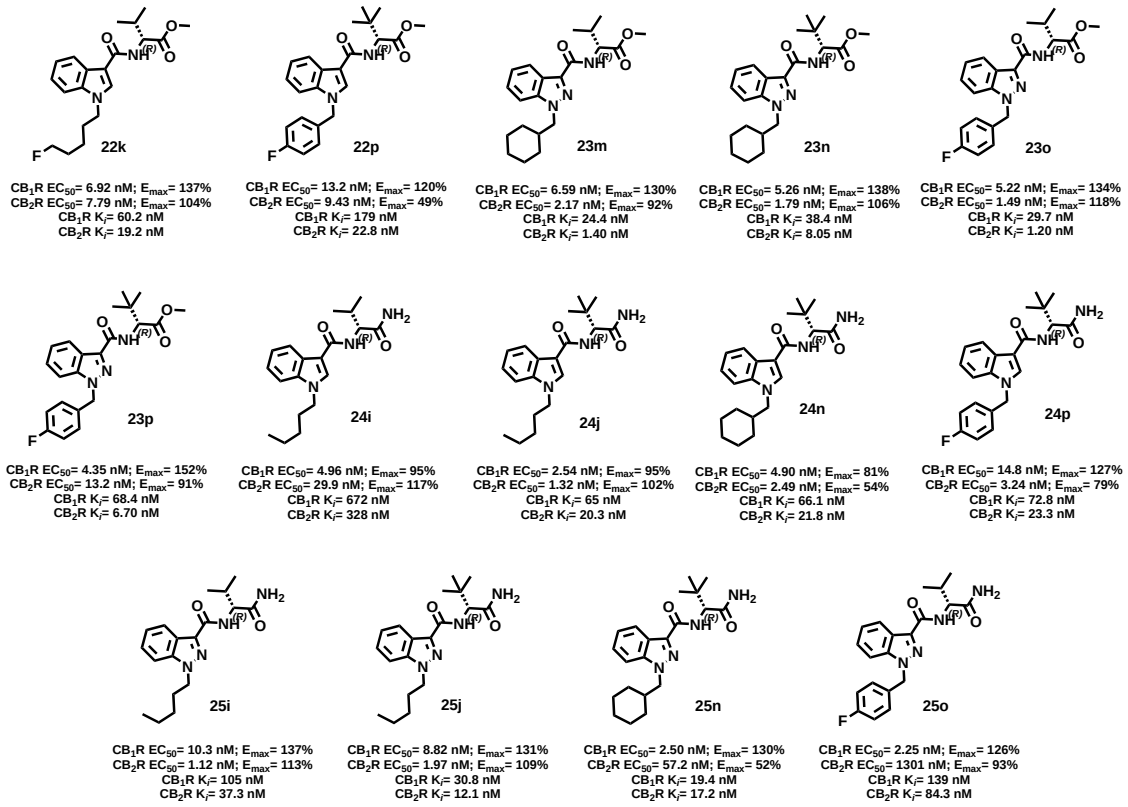


Figure 31: Structure and cannabimimetic data of the 14 previously unexplored *(R)* derivatives that show a pharmacological profile similar to the one of commonly abused SCRAs.

As observed (Figure 31), functional data reveal that most of these potential SCRAs are significantly more efficacious at the CB_1R. Thus, these derivatives (Figure 31) deserve attention/monitoring by regulatory authorities [e.g., European Monitoring Centre for Drugs and Drug Addiction (EMCDDA) and United Nations Office on Drugs and Crime (UNODC)] and the scientific community. Further studies are now in progress in our laboratories to complete the pharmacological, functional selectivity and toxicological characterization of these 14 novel derivatives and commonly abused SCRAs. However, it is worth noting that recent legislation in some countries has shifted towards a more comprehensive approach to control the emergence of SCRAs, thus one might expect typical structure would be less likely to emerge on the recreational drug market.

USC UNIVERSIDADE DE SANTIAGO DE COMPOSTELA

For the sake of clarity, the discussion of the structure-activity relationship (SAR) trends, and to a lesser extent of the structure-selectivity relationship (SSR), is made here in an integrated fashion, according to the structural classifications reported in Scheme 1 and Tables 3-6. The affinity data were employed to rapidly evaluate trends and compare profiles, and then the analysis complemented with the functional information. For a more immediate and efficient analysis of the variation of both affinity and selectivity, the binding data (pK_i) are presented graphically as a plot of pK_i CB_1R (*Y* axis) versus pK_i CB_2R (*X* axis) using the same scale and range for both axes (square plot) in Figure 32-34. On the diagonal of this plot (*Y* = *X*) compounds with equal affinities at both receptors will be found, whereas CB_1R or CB_2R selective compounds will be seen below or above the diagonal, respectively. The distance of their pK_i values from the diagonal is a direct measure of their degree of selectivity.

We first focused on the analysis of the two main functional series herein described (esters and amides). pK_i values ranging from 6.20 to 10.05 and from 6.22 to 10.00 were measured for the CB_1R and the CB_2R respectively. Their relationship and distribution are represented as a plot of pK_i CB_1R vs pK_i CB_2R in Figure 32 for esters (Figure 32A) and amides (Figure 32B). The skeletal diversity (scaffold) in each subset is represented in colors (red: indoles, blue: indazoles). A simple visual inspection of the plots (Figure 32) for both functional series (plot A: esters, plot B: amides) revealed that CB_1R and CB_2R binding affinities are highly correlated [non-selective (dual) CB_1R - CB_2R profile]. In the ester series most of the examined ligands are slightly more affine toward the CB_2R subtype [particularly indazole-based derivatives (blue circles)]. The exception to this trend is the indole derivative **22f**, lying slightly above the diagonal of the plot, its dual profile is observed also comparing its functional data. Seven ester derivatives (**22i**, **22l**, **22o**, **23i**, **23j**, **23m**, **23o**) fall below the second dashed diagonal line on the graph (Figure 32), showing some selectivity (13–29 fold) towards CB_2R. Analysis of the functional data (EC_{50}) obtained for these ligands confirmed the incipient selectivity toward CB_2R. A superior correlation among CB_1R and CB_2R binding affinities (evidencing highly dual CB_1R - CB_2R profile) is appreciated within the amide subset (Figure 32B), with most of the amides standing near the diagonal of the square plot. Anyhow, most of them are somewhat more affine towards the CB_2R subtype. Two amide derivatives [one indazole (**25d**) and one indole (**24h**)] elicit an incipient selectivity (≈ 10-fold) towards CB_2R (Figure 32B). In clear contrast to this trend,

USC UNIVERSIDADE DE SANTIAGO

ligands **24g** and **24e** exhibit some CB_1R selectivity. The incipient selectivities observed for **25d**, **24h**, **24g** and **24e** are generally corroborated when comparing their functional data.

Taken together, the affinity data suggest that the functional diversity (ester or amide) is a more important contributor than the skeletal diversity (heterocyclic core) in defining the potency and selectivity profile in this series. The large set of ligands and the comprehensive pharmacological data documented here (Figure 32) reveal new features of the SCRAs' behavior, while providing additional validation to the reported observations.[116]

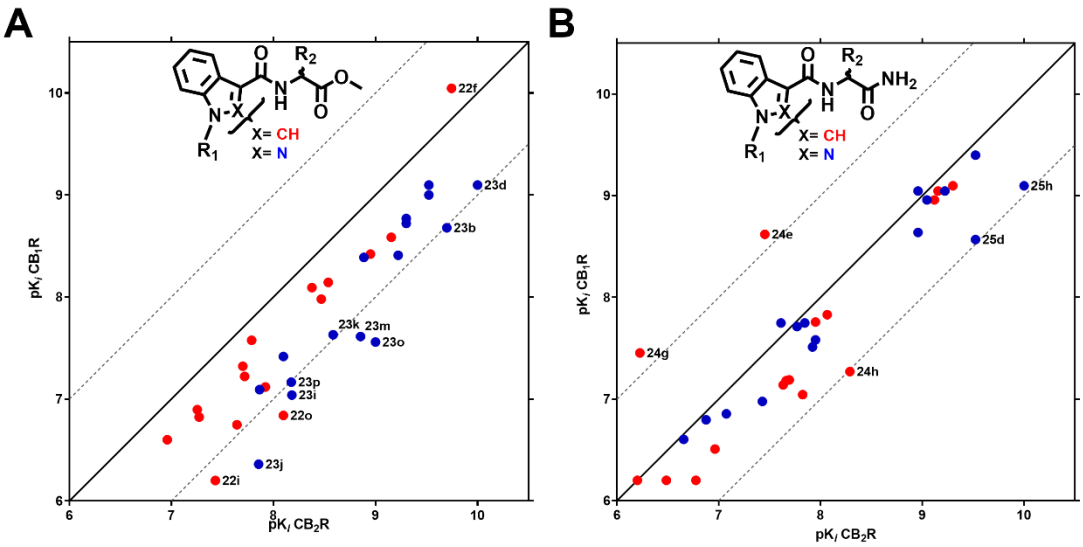


Figure 32: Affinity-selectivity plot for 32 esters (6A) and 32 amides (6B) obtained.

Figure 33 was designed to gain insight into the contribution of the stereodisposition (*R* or *S*) of the R^2 group in the cannabimimetic profile (potency and selectivity) of the ligands herein documented. For the analysis, the collection was divided into two subsets, esters (Figure 33A) and amides (Figure 33B), with the binding affinity presented graphically as a plot of pK_i CB_1R (*Y* axis) vs pK_i CB_2R (*X* axis) using the same scale and range for both axes (square plot). For each subset, the stereochemistry at the pendant amino acid residue is denoted in green (*R*) or orange (*S*). The plot also addresses the influence of the skeletal diversity (indoles or indazoles), represented as a circle or triangle (Figure 33).

USC UNIVERSIDADE DE SANTIAGO DE COMPOSTELA

The presented data unequivocally confirmed that the (*S*) stereoisomers (green) are consistently more potent than the corresponding (*R*) stereoisomers (orange), with ΔpK_i [pK_i (*S*) - pK_i (*R*)] > 2 in most cases at both receptor subtypes. The difference in affinity between the (*S*) and (*R*) enantiomers seems to be more pronounced for indazole derivatives (when compared to their corresponding indole congeners).

Figure 33A evidences that (*R*) stereoisomers (orange triangles) are generally less affine (at both receptors) and slightly more affine towards CB_2R (below the diagonal). Thus, some (*R*) stereoisomers of the ester series (**22i**, **23j**, **22o**, **23o**, **23m**) combine excellent affinity (K_i = 37.1, 14.7, 8.21, 1.20, 1.40 nM) and an attractive selectivity (6–29 fold) towards CB_2R. On the other hand, derivatives **23b** and **23d**, bearing (*S*) stereochemistry at R^2, showed high CB_2R affinity and somewhat subtype selectivity (8–fold). The selectivity trends noticed for the listed ligands can be also corroborated when comparing their functional data in CB_1R and CB_2R (Tables 3-6). The general SAR trends identified for ester derivatives are reproduced within the amide subset (Figure 33B), with most derivatives being highly affine at CB_1R and CB_2R and the (*S*) enantiomers (green) being systematically more affine than their correspondent (*R*) stereoisomers (orange). However, some amides show a slight preference for CB_2R (**25d** and **24h**), while derivatives **24g** and **24e** exhibit the opposite behavior, eliciting high affinity and superior selectivity towards CB_1R. Like in the previous cases, the above-mentioned trends can also be verified if we compare the functional data obtained for the listed ligands.

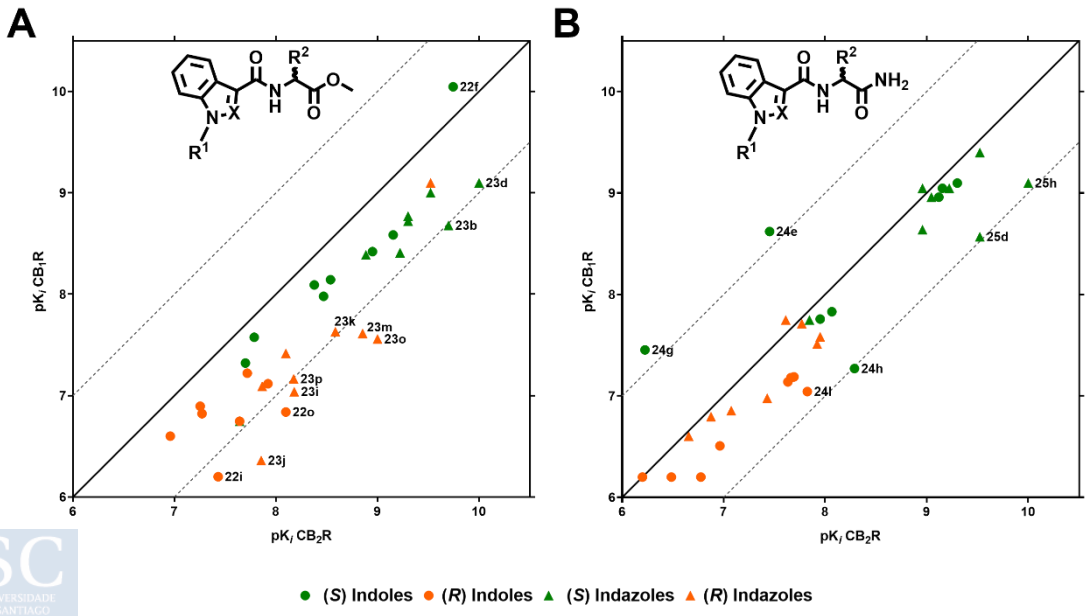


Figure 33: Influence of the stereochemistry in the cannabimimetic profile.

Figure 34 was designed to evaluate the influence of the R^2 group (*iso*-propyl or *tert*-butyl) on the binding affinity at CB_1R and CB_2R for esters or amides, and to calibrate the contribution of the scaffold (indole or indazole) and the stereodisposition (*S* or *R*). As in previous figures, the data are represented as a plot of pK_i CB_1R vs pK_i CB_2R, with the stereochemistry at the pendant amino acid residue denoted in green (*R*) or orange (*S*) and the heterocyclic core represented as a circle (indole) or triangle (indazole) (Figure 34).

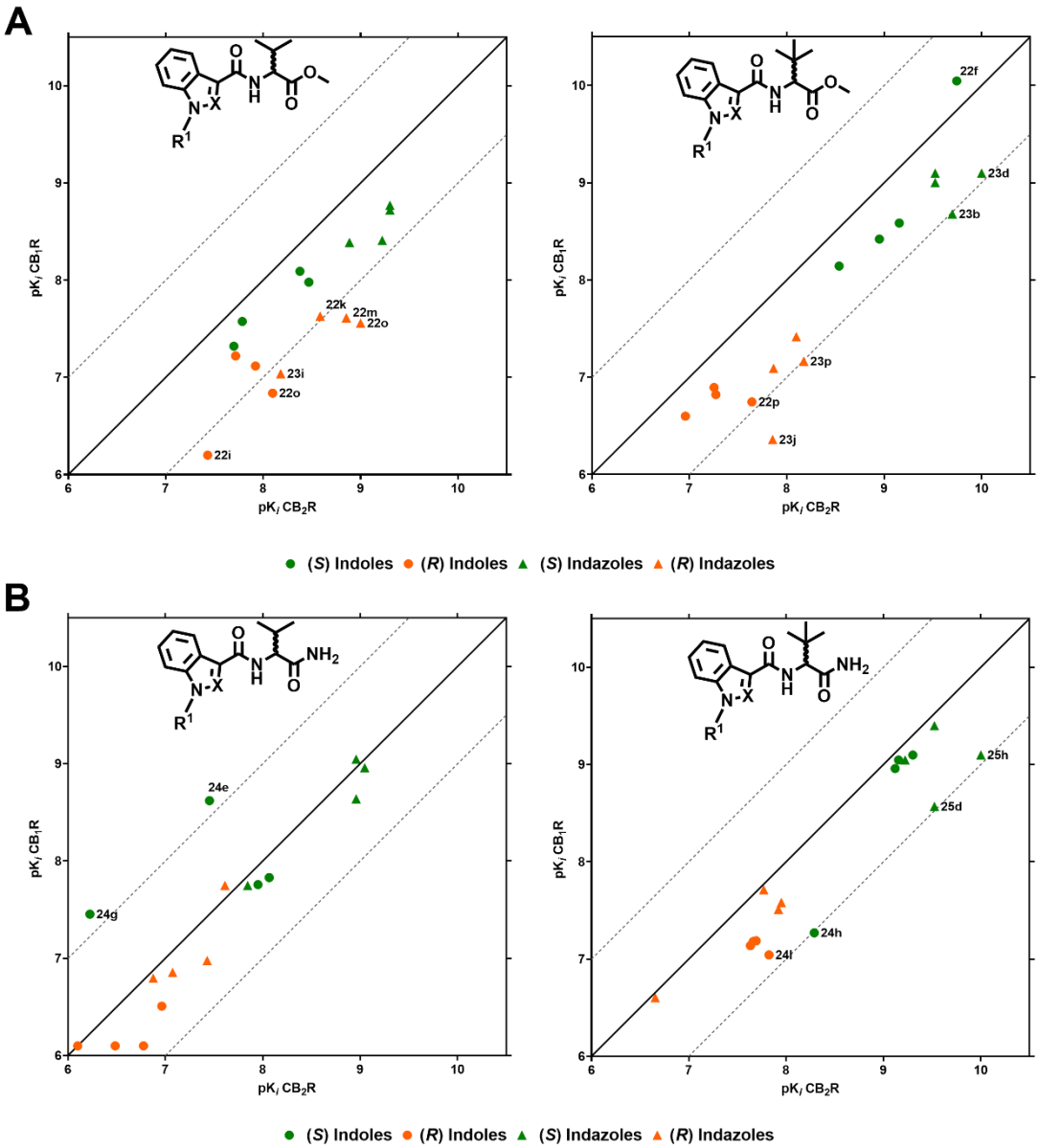


Figure 34: Influence of the group at R^2 on the cannabimimetic profile. Affinity-selectivity plot for *(S)*(green) and *(R)* (orange) in the esters (A) and amides (B).

USC UNIVERSIDADE DE SANTIAGO DE COMPOSTELA

As observed, within the ester series (Figure 34A), in general, *iso*-propyl derivatives seem to be slightly less affine (at both receptors) than *tert*-butyl analogues, particularly in the indole series. Within the indazole series the differences between *iso*-propyl or *tert*-butyl seem to be attenuated. A similar, but more accentuated, trend is observed when analyzing the influence of *iso*-propyl or *tert*-butyl groups in amide derivatives (Figure 34B). Here, ligands bearing a *tert*-butyl group are consistently more affine that their *iso*-propyl analogues and this effect is more pronounced for the indazole series. Interestingly, within the amides of the (*S*) series carrying an indole core, a significant increase in affinity at both receptors can be observed when comparing a *tert*-butyl group with an *iso*-propyl group.

A bar plot was used to graphically evaluate the impact of R^1 (the tail of the SCRA structure) on the measured cannabimimetic effect. In sharp contrast to the previous discussion (Figures 32-34), attempts to generalize the influence of the group at R^1, with the affinity measured in CB_1R and CB_2R, did not provide a clear trend (Figure 35). As observed, most of the four derivatives in each subset (R^1 = pentyl, 5-F-pentyl, cyclohexylmethyl and 4-F-benzyl) elicited similar affinities. A possible explanation may lie in the fact that according to the proposed binding modes[4,5,7,19,22,23] for this class of ligands, at their respective orthosteric sites, this portion of the ligand allows for the greatest variation due to the large size of the hydrophobic pocket.[16,18]

USC
UNIVERSIDADE DE SANTIAGO DE COMPOSTELA

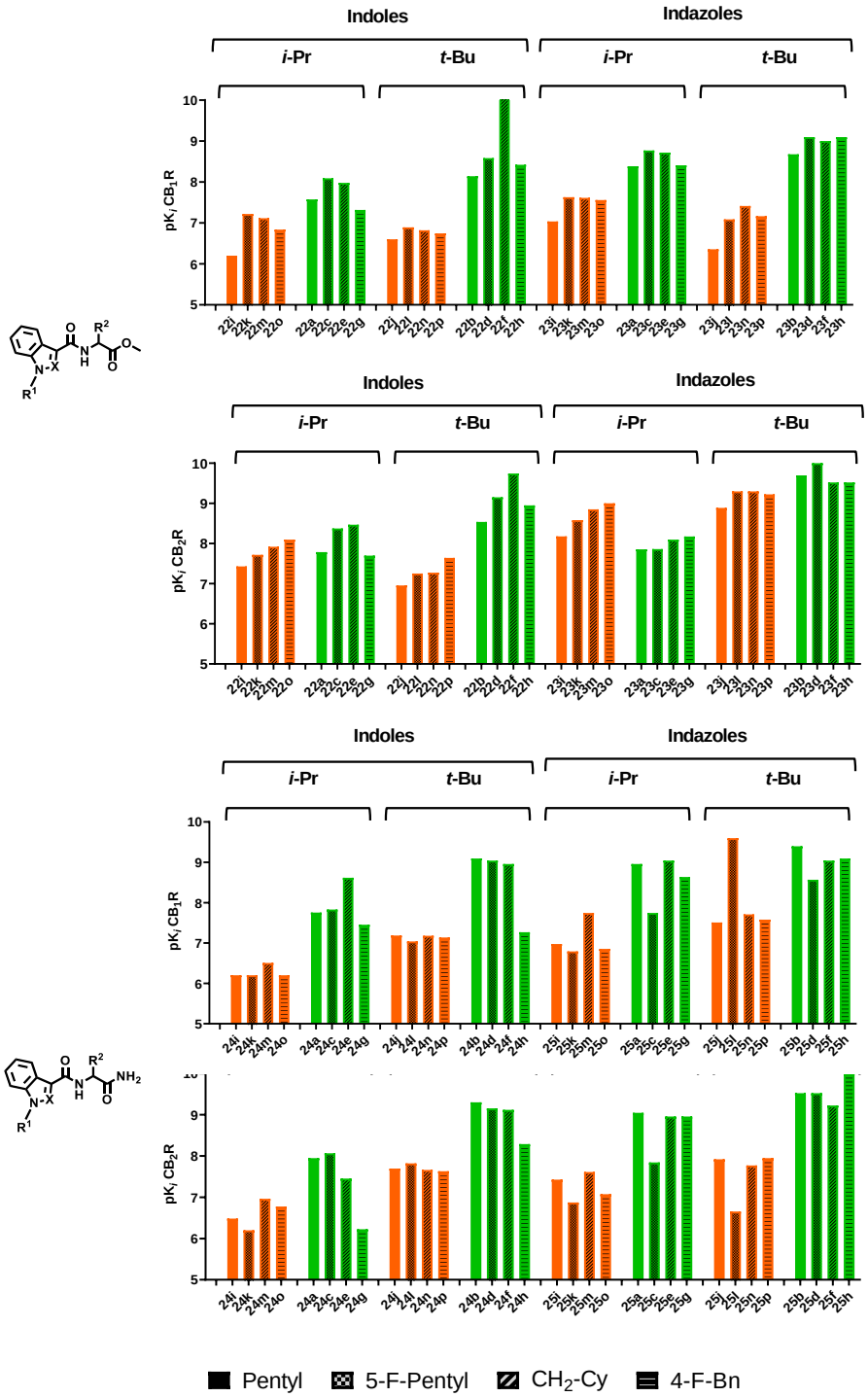


Figure 35: Bar diagram evaluating the influence of the group at R^1 on the cannabimimetic profile in esters (above) and amides (bottom). Green bars correspond to *(S)* enantiomers and orange bars to *(R)* enantiomers.

USC UNIVERSIDADE DE SANTIAGO DE COMPOSTELA

Although the vast majority of the herein described ligands reproduce the intrinsic non-subtype-selective profile of SCRAs, examination of the large binding (pK_i) data (Tables 3-6) enabled the identification of novel derivatives that combine an attractive CB_2R affinity (K_i ranging 1.20 – 37.1 nM) and incipient selectivity towards CB_2Rs [e.g., compounds **22i**, **22l** and **22o** (Table 3), **23j**, **23m** and **23o** (Table 4)]. Representative ligands exhibiting this profile are presented in Figure 36. As observed, they contain an amino acid pendant residue bearing an ester group, either *iso*-propyl or *tert*-butyl residues group at R^2 and feature the (*R*) configuration within the stereocenter. As indicated above, the observed selectivity is modest, being more pronounced when comparing binding data (>10-fold) than functional data (>4-fold), and most derivatives in Figure 36 retaining high affinity and potency at CB_1R.

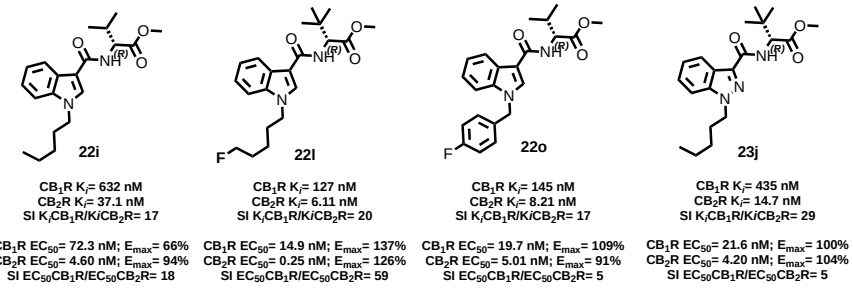


Figure 36: Novel synthetic cannabinoid agonists eliciting incipient CB_2R selective profile.

Among these derivatives, **22l** and **22i** emerge as model ligands that show excellent efficacy, moderate and consistent subtype selectivity towards CB_2R in functional and affinity experiments. These ligands are currently being used in our programs to explore the significant, yet unrealized, therapeutic potential of CB_2R activation. In contrast to previous studies, usually focusing on the characterization of drugs of abuse and small subsets, the library approach herein adopted has been instrumental in discovering CB_2R agonists with incipient selectivity and identifying SAR trends that will inspire our ongoing program to develop CB_2R agonists as anti-inflammatory, analgesic, and immunomodulatory therapeutics.[2,25] It must be noted that although the ligands shown in Figure 36 have modest selectivity and reveal structural features (*R* configuration) that inspire the design of new CB_2R ligands, the inherent metabolic instability of SCRA esters and suboptimal physicochemical properties preclude their direct exploitation in drug discovery programs. Accordingly, functional derivatization using different pharmacomodulation strategies and physicochemical parameters optimization are currently being pursued in our laboratories.

USC
COMPOSTELA

Preliminary neurotoxicity study. The ever-changing structure of ligands in the illegal market makes it challenging to monitor abused SCRAs as well as to undertake systematic studies on their toxicological effects. Their high potency and excellent efficacy lead to lower doses being sufficient to obtain psychoactive effects. However, due to their unpredictable biological effects and unregulated and variable dosage and uses, overdose, intoxication and severe toxicity are more likely to occur.[117] With reports of intoxications and deaths following SCRAs use rapidly increasing,[118,119] toxicity studies are not only helpful in assessing the health threats associated with SCRAs abuse, but also in proposing appropriate medical management for cases of intoxication arising from SCRA consumption.[120–122] Although case reports and retrospective studies of acute intoxication by SCRAs confirm that they cause severe effects (e.g. seizures, cardiovascular damage, kidney damage, stroke, psychosis, paranoia, anxiety attacks),[117,120,122,123] little is currently known about the mechanisms by which these structures exert toxic effects.[123] Several reports have assessed the toxicity of commonly abused SCRAs evidencing remarkable harmful effects. Noteworthily, growing scientific evidence highlights that SCRAs consume alters psychoactive and cognitive responses.[96,124] However, the cytotoxicity of known SCRAs (and emerging derivatives) in mammalian neuronal cells remains scarcely explored.[125]

In the context of this study, we decided to preliminarily examine the neurotoxicity signatures of a subset of herein prepared synthetic cannabinoid agonists in primary mouse neuronal cells. The selected ligands included well-known SCRAs [**22c** (5F-MDMB-PICA), **22e** (MMB-CHMICA), **22f** (MDBM-CHMICA), **22h** (MDMB-FUBICA), **23e** (AMB-CHMINACA), **23f** (MDMB-CHMINACA), **23h** (MDMB-FUBINACA), **24d** (5-F-AD-BICA), **24e** (AB-CHMICA), **24f** (ADB-CHMICA), **24g** (AB-FUBICA), **25d** (5-FADB-PINACA), **25e** (AD-CHMINACA), **25f** (ABD-CHMINACA), **25h** (ADB-FUBINACA)] as well as four hitherto untapped derivatives [(*R*) stereoisomers, **22m**, **23m**, **24n**, **25n**], all of them being representatives of the structural diversity explored within the study. As the enantiomers (*R*) showed generally lower potency and efficacy compared to their congeners (*S*), for this preliminary exploration it was decided to prioritize the latter subset (S). Figure 37 represents the results of the neuronal toxicity of selected ligands, evaluated at 100 nM in mouse primary neuronal cells.

USC UNIVERSIDADE DE SANTIAGO DE COMPOSTELA

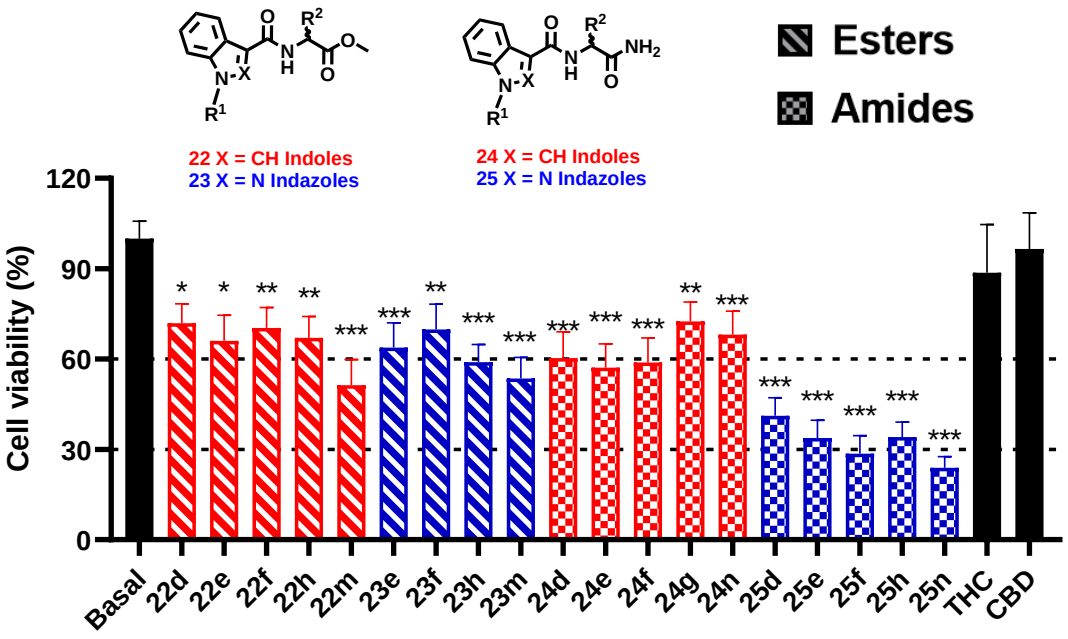


Figure 37: Neuronal toxicity of representative SCRAs (100 nM) in mouse primary neuronal cells.

A first inspection of the generated data (Figure 37) reveals that, in a clear contrast to the effect measured for Δ^9-THC and CBD, all ligands significantly reduced cell viability (typically from 30 to 70%). The reduction in cell viability seems to be functional and scaffold dependent, with amides derived of the indazole core (Figure 37, compounds **25**) eliciting superior neurotoxicity. Whereas the observed toxicity profiles could be a consequence of different features (e.g. pharmacological and pharmacokinetic), a first analysis of the structural relationship among the selected ligands enables the ascertaining of similarities and/or differences that could be potentially affecting the observed neurotoxicity signatures. Thus, indole ester derivatives seem to be slightly less cytotoxic than their indazole analogues (Figure 37, comparing **22e** and **23e**, **22f** and **23f**, **22h** and **23h**). Such a trend is considerably more pronounced in the amide series, with indole amides being clearly less cytotoxic than their corresponding analogues in the indazole series (Figure 37, compare **24d** and **25d**, **24e** and **25e**, **24f** and **25f**). Although the limited number of derivatives with stereochemistry (*R*) in the pendant amino acid chain studied precludes reaching definitive conclusions, the obtained data suggest that, except for **24n**, these derivatives generally exhibit superior neurotoxicity. Indeed, the ligand exhibiting superior neuronal toxicity (**25n**) is an indazole amide bearing a *tert*-butyl group with (*R*) configuration on the pendant aminoacid chain. These preliminary results suggest that special attention

USC UNIVERSIDADE DE SANTIAGO DE COMPOSTELA

and control should be paid to the possible emergence on the illicit market of SCRAs based on an indazole core and containing an amide group. Further studies are currently being conducted in our laboratories to complete the pharmacological characterization and broaden the toxicity analysis of this large collection of SCRAs.

Finally, it should be mentioned that the herein obtained library is a research resource that we are sharing with other academic groups and regulatory authorities, in a collaborative manner.

The aim of this initiative is contributed to make available to researchers samples of known and new potential SCRAs and to shed light on the complex pharmacology, toxicology and medicinal chemistry of these abuse drugs.

USC
UNIVERSIDADE DE SANTIAGO DE COMPOSTELA

3.2 CHAPTER 2. PHARMACOMODULATION OF INDOLE-BASED SCRAS. UGI-ASSISTED DISCOVERY OF POTENT AND CB2R SELECTIVE LIGANDS: THE PROOF OF CONCEPT

SCRAs (Synthetic Cannabinoid Receptor Agonists) constitute the largest class of New Psychoactive Substances (NPS),[72,74] being sold on the internet in different preparations as a pseudo-legal or unregulated alternative to cannabis.[94] While Δ^9-THC acts as a partial agonist with micromolar activity towards both CBRs, SCRAs are highly potent non-selective (dual) full agonists of CBRs, exhibiting K_i values in the low nanomolar, or even picomolar, range at both receptor subtypes (Figure 38).[3,81,83] However, knowledge of the pharmacology, pharmacokinetics and toxicology of these abuse substances is rather scarce, with common adverse effects including agitation, psychosis, anxiety, tachycardia, hypothermia, and even death.[49] As discussed in the previous Chapter, we have contributed to facing this challenge by obtaining the largest library of SCRAs synthesised to date. The CB_1R agonism exerted by SCRAs is responsible for their psychoactive effects.[3,49,93] Moreover, the off-target interactions with other receptors (e.g., serotonin or dopamine) represent one of the biggest issues of these abuse substances, since non-selective behaviour might lead to worse adverse effects.[89–93] The constant growth and abuse of this class of designer drugs represent a serious threat to public health.

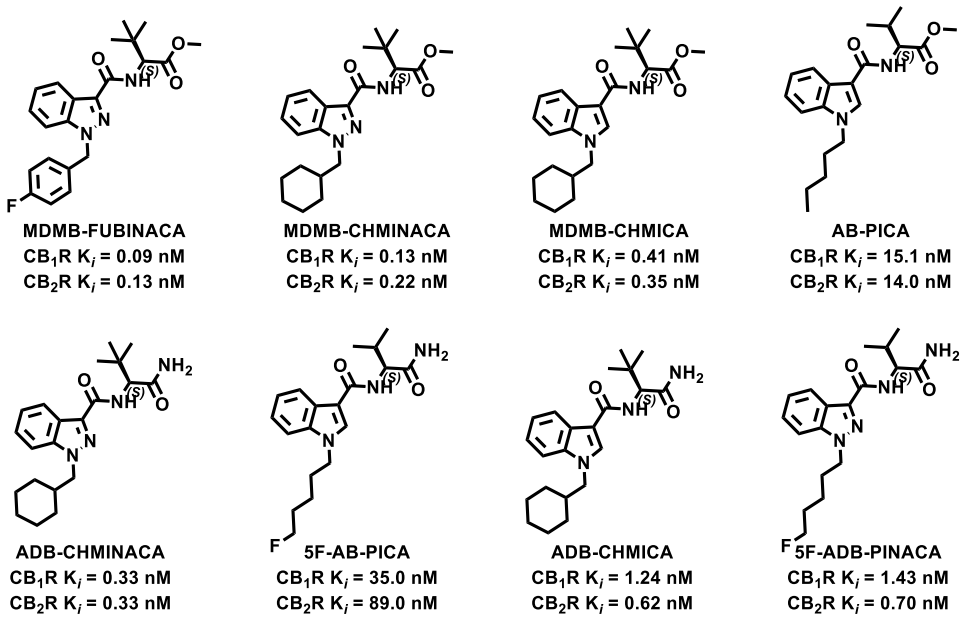


Figure 38: Representative Synthetic Cannabinoid Receptor Agonists (SCRAs).

USC UNIVERSIDADE DE SANTIAGO DE COMPOSTELA

In Chapter 1, a collection of 64 SCRAs has been synthesised and studied in detail, with a full primary pharmacological evaluation at CBRs (affinity, activity, and efficacy), leading to the identification of never seen before SAR trends (Figure 39). Even though, in general, SCRAs show a promiscuous (dual) profile (CB_1R and CB_2R), we have identified certain structural modifications inducing incipient selectivity towards the CB_2R, as well as some ligands that combine attractive CB_2R affinity and selectivity (Figure 39).

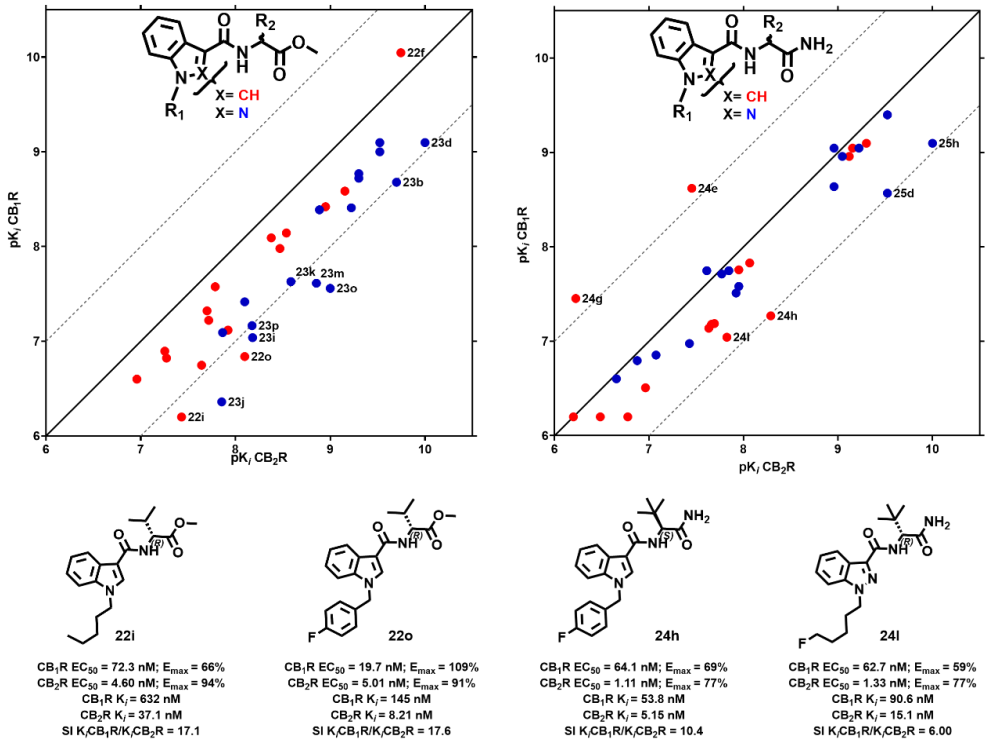


Figure 39: Graphical representation of the affinity-selectivity profile observed for the SCRAs collection obtained in Chapter 1 and structure and data of selected SCRAs exhibiting selectivity toward CB_2R.

As discussed in the introduction, CB_2R is a highly attractive and underexplored receptor that could further lead to the development of new therapeutic approaches to challenging diseases. As part of our new project to develop novel CB_2R selective agonists, it was conceived a program inspired by the excellent affinity, activity, and efficacy of SCRAs. ***The aim was to explore novel diversity spaces across the SCRA series to obtain new agonists selectively targeting the CB_2R***. To the best of our knowledge, no previous systematic programs documenting the pharmacomodulation of SCRA series have been described so far.

USC UNIVERSIDADE DE SANTIAGO DE COMPOSTELA

The project was inspired by the pharmacophoric model of these ligands and the SAR trends observed within the series disclosed in the Chapter 1. To avoid potential neurotoxic liabilities observed in the indazole subset (see Chapter 1), we decided to focus our efforts on the indole scaffold.

In order to rapidly obtain the targeted molecules, the program will rely on the efficient and high-throughput generation of indole-based libraries via a multicomponent-assisted synthetic strategy employing the robust Ugi reaction. The designed approach allows the convergent and throughput synthesis of both ester and amide series (Figure 40) in one pot reaction, as well as the effective exploration of this pharmacophore to identify CB_2R selective ligands (Figure 40C). Despite their expected limited metabolic stability, a small subset of esters (**35** and **36**) has been synthetized for comparative purposes and to study the influence of the alkoxy residue of the ester function on binding affinity. Accordingly, ***the main purpose of this Chapter is to develop a proof of concept for the synthesis of novel potent and selective CB_2R agonists (amides and esters) using a previously unexplored Ugi-based approach***. In addition, we focused on the exploration of the most salient features of the SAR and SSR in these series. The general structure of the new ligands obtained is presented in Figure 40C. In clear contrast with previous studies, our approach enables not only the exploration of the substituents at R^1, R^2 and R^3, but also the evaluation of the effect derived from the introduction of a second R^3 group and alkyl residues at the terminal amide group (R^4) during their interaction with the CBRs (Figure 40C).

USC UNIVERSIDADE DE SANTIAGO DE COMPOSTELA

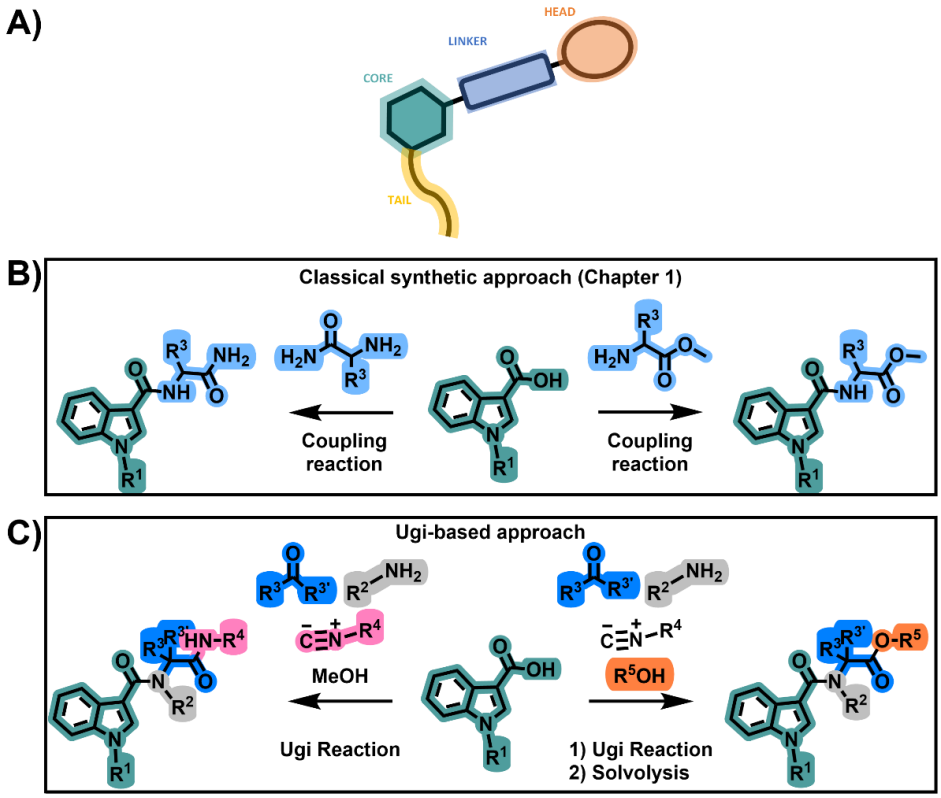


Figure 40: Classical SCRAs synthesis and proof of concept of U4CR (Ugi four component reaction) assembly of SCRAs like libraries.

The pharmacophoric model of SCRAs (Figure 40A) consists of four structural elements: the heterocyclic core (indole or indazole) (in green), the linker (in blue), the tail (in yellow) and the head (in orange). SCRAs are traditionally synthetized by a coupling reaction that involves a carboxylic acid and an amine to form an amide bond (classical amide coupling, Figure 40B).[126] Despite its efficiency, this synthetic method shows some intrinsic limitations: repetitive and stepwise sequences are required to obtain large and diverse collections exploring the influence of different groups.[126] Moreover, the limited commercial availability of non-naturally occurring amino acid derivatives (esters or amides) precludes the extensive exploration of diversities at the linker (R^3) (Figure 40C). Finally, the exploration of the effect of R^4 would require the synthesis of *N*-substituted amino amide precursors.

The pharmacophoric model presented in Figure 40A has proven to be particularly versatile for scaffolding strategies.[116] Accordingly, we envisioned the development of a general, robust, efficient, and versatile synthetic MCR-based pathway to prepare new synthetic cannabinoid agonists in a time and cost-effective manner (Figure 40C). As indicated, SCRAs have not been studied systematically and there are no examples of comprehensive pharmacomodulation programs within these families.

Within the amide SCRAs subset, all described ligands are primary amides ($CONH_2$). Our exploratory computational studies suggested that the introduction of alternative groups at R^3 and particularly the introduction of alkyl groups at the terminal amide (R^4) may change the observed affinity and selectivity profiles.

Chemistry. The Ugi four component reaction (U4CR) is an efficient and highly convergent isocyanide-based multicomponent transformation.[127] The reaction is characterized by its excellent atomic and bond economy. Moreover, the U4CR is highly robust and exploratory, thus being optimal for medicinal chemistry programs.[128–131] MCRs are transformations in which three or more precursors are combined, in a single step, to generate a new chemical entity that incorporates structural elements of all the starting materials involved in the reaction. The various types of reactions differ in the number of reagents participating, functional precursors, and the number of new bonds that are formed.[127]

The U4CR is one of the most studied and versatile multi-component reaction. In 1959, Ivar Ugi synthesized an α-acyl-amino acid (Figure 41) by reacting four components: an acid, a carbonyl component (aldehyde or ketone), an amine and an isonitrile.[127,132] A plethora of modifications and applications have been published since its discovery, thus the U4CR is becoming increasingly popular in medicinal chemistry projects.[128–131]

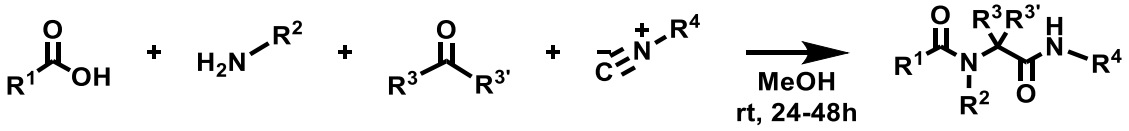


Figure 41: The Ugi reaction.

The most accepted mechanism of the U4CR is represented in Figure 42.[131] The first step of the transformation (Figure 42) involves the condensation of the carbonyl component (aldehyde or ketone) and the amine to generate an imine intermediate (a). Then, the dissociated carboxylic acid protonates the nitrogen of the imine to generate an iminium ion (b). Protonation of the imine increases the electrophilic character of the bond C=N. The iminium ion is then attacked by the isocyanide, generating an α-adduct (c) containing a highly electrophilic center (nitrile ion) which is simultaneously attacked by the carboxylate ion. The structural analogy between the α-adduct (d) and the acid

USC UNIVERSIDADE DE SANTIAGO

anhydrides (one of the oxygen atoms has been replaced by an N-R group), explains their behavior in the reaction medium. The anhydrides are acylating agents, as are their nitrogenous analogs (Figure 5, intermediate d), while the closest atom that can be acylated being the nitrogen of the amine. Finally, an intramolecular acylation and tautomerization generates the Ugi adduct.

The intramolecular acylation, which constitutes the last step of the reaction, is the Mumm rearrangement. All steps of this sequence are in equilibrium, except the Mumm rearrangement. This last irreversible stage gives rise to a very stable acyl-amino-amide (e), which shifts the equilibrium of the reaction irreversibly toward its formation.

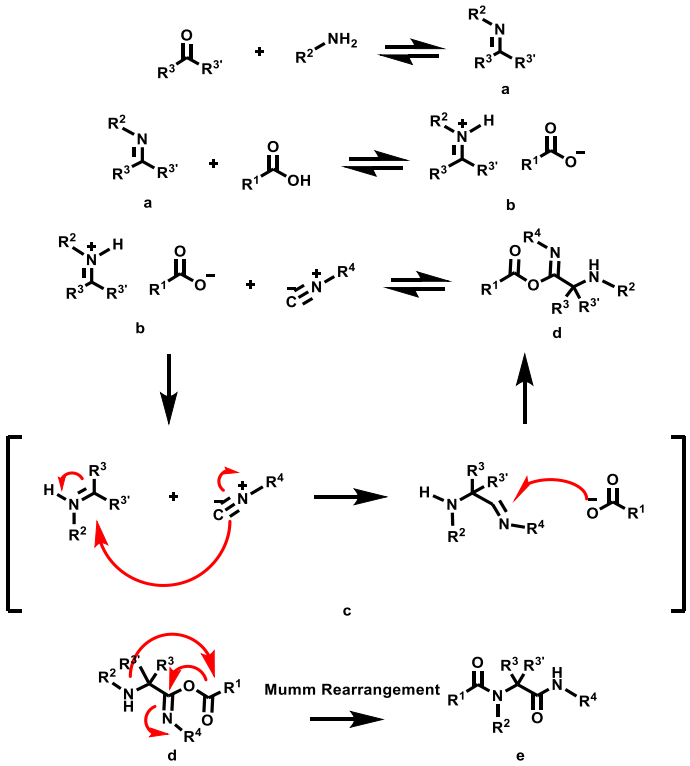


Figure 42: Most accepted mechanism of the Ugi Reaction.

The experimental protocol of the U4CR is generally simple, with starting materials dissolved in MeOH, and submitted to stirring at room temperature (24–48 hours). The transformation can be performed in one pot (4 component) or step-wise fashion (by early condensation of amide and carbonyl compound and then the addiction of the acid component and the isocyanide).

USC UNIVERSIDADE DE SANTIAGO DE COMPOSTELA

Methanol is the most used solvent for U4CR,[129,130] whose polarity can stabilize the reaction intermediates. In addition, the limited solubility of the Ugi adduct in methanol usually facilitates its precipitation and isolation.[130,132,133] The U4CR usually takes place under atmospheric pressure and without the need for anhydrous conditions (solvent or atmosphere) or catalysts. Using collections of the four functional precursors, it is possible to obtain practically infinite structures. Since aldehydes (except formaldehyde) and asymmetrically substituted ketones during the U4CR produce Ugi adducts that contain a stereogenic center, these products are generally isolated as racemates.

The key component of the U4CR is the isocyanide, whose employment in organic synthesis has been considerably limited by its intense and repulsive odor[134]. To overcome this, the ComBioMed group has developed a new method in which a solid phase extraction approach enables the capture of the unreacted isocyanide.[130] To achieve this, the p-toluenesulfonic resin is used to capture the excess of isocyanide in the reaction and transforms it into the corresponding amine. The resin also enables the extraction to solid phase of compounds containing a basic moiety following a catch and release sequence that usually accelerates and simplifies the isolation and purification of the Ugi adducts bearing basic groups.[130,135]

Design and synthesis of the novel ligands. The MCR-based strategy herein documented was conceived to rapidly assemble large libraries of SCRA analogues, thus enabling the exhaustive exploration of the SAR in these series and the identification of novel CB_2R selective agonists. As shown in Scheme 2, Scheme 3 and Figure 43, for the design of the new series (Cpds **35 - 38**) we took advantage of the structural analogy of the SCRAs pharmacophore and the chemical architecture characteristic of the Ugi adducts (acylamino amide). It was envisioned that the use of *N*-substituted indole-3-carboxylic acids **26** (R^1), appropriated substituted amines **32** (R^2), aldehydes or ketones **34** (R^3) and isocyanides **33** (R^4) would provide Ugi adducts that perfectly match with the structure of targeted compounds (Figure 40C).

From a structural point of view, the U4CR maintains the pharmacophoric elements, with the linker between the central core and the head of the pharmacophoric model, thus allowing the modification and the exploration at four different positions (Figure 40A and Figure 40C). One of the structural signature elements of the Ugi's adduct is the presence of a stereocenter, thus producing racemic mixtures.

USC DE COMPOSTELA

As we were interested in rapidly exploring as much diversity as possible, we focused on the synthesis of racemic mixtures. Further studies of our group will also pursue enantioselective versions of the reaction with optimized substrates.

Because of the huge number of possible combinations that the Ugi reaction allows to synthetize, and the neurotoxicity observed for indazole derivatives, for the proof of concept and for this Doctoral Thesis, the *N*-alkyl-1*H*-indole-3-carboxylic acid has been maintained as central core with two different substitutions at R^1 (4-F-Bn and CH_2-Cy). At R^2, we decided to examine not only the classical substituents (H), but also the effect of a methyl group at this position, that has not been previously investigated in the SCRAs collection (Scheme 2, Scheme 3, Figure 43).

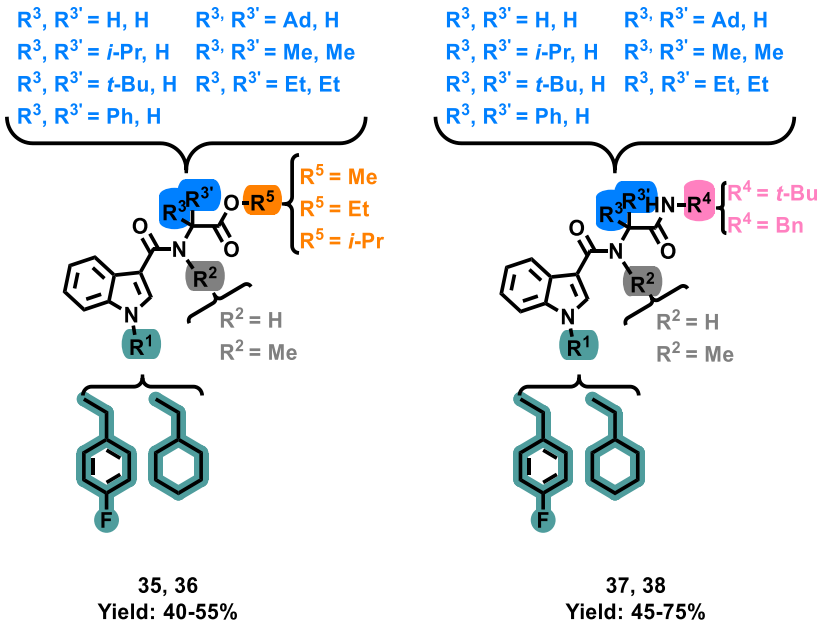


Figure 43: General structure and diversity space explored for esters (**35a-r**,**36a-r**) and amides (**37a-v**,**38a-v**).

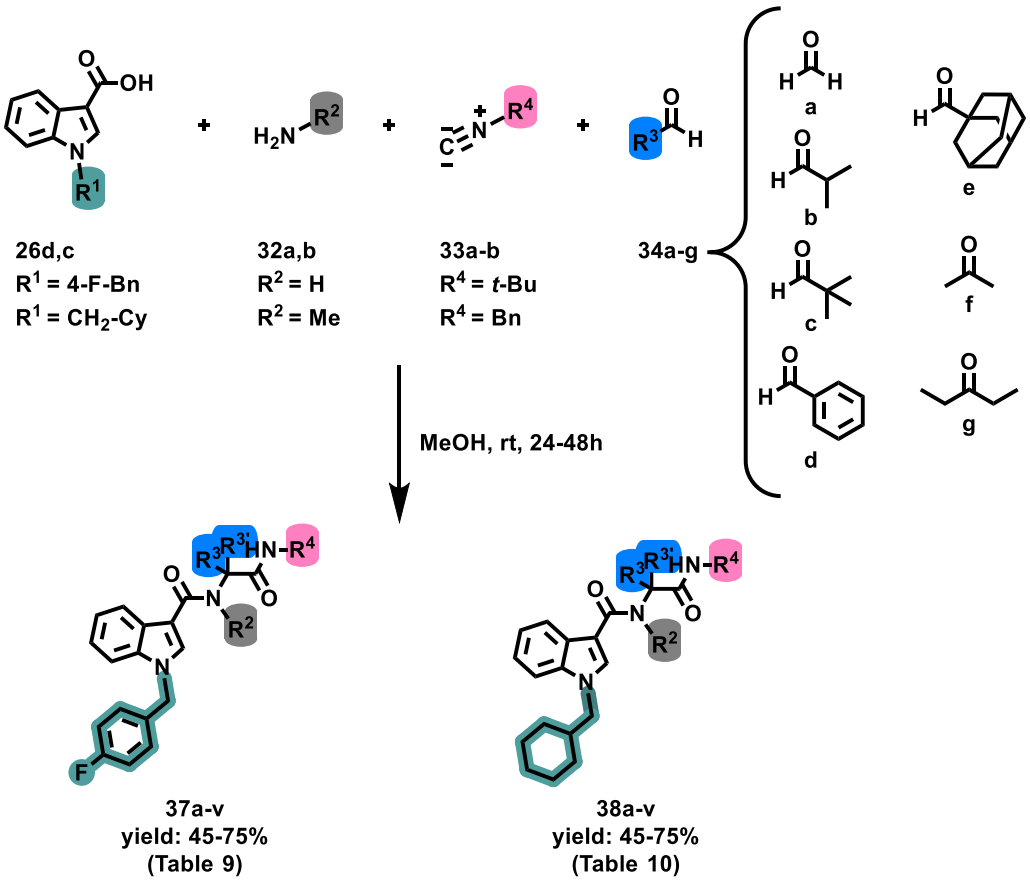
At R^3, the *i*-Pr and *t*-Bu moieties have been initially maintained, considering that they represent the most common substituents at this position in the model series of SCRAs. Exploiting the versatility of the Ugi reaction, we decided to introduce different moieties at R^3. Thus, in addition to *i*-Pr and *t*-Bu, H, phenyl, and adamantyl groups were introduced, as well as two model ketones [which were employed to investigate the effect of introducing smaller or bigger groups, respectively (Figure 43)]. Two model isocyanides (*t*-Bu and Bn) were selected to preliminarily assess the impact of the introduction of groups on the terminal amide (Scheme 2, R^4). As shown in Scheme 2, the Ugi adducts (Cpds **37** and **38**) were obtained in moderate to satisfactory yields (40-

USC DE SANTIAGO DE COMPOSTELA

75%). The reactions were performed in sealed Kimble vials using methanol as solvent and, once finished, quenched, and elaborated to isolate and purify the corresponding Ugi adducts as described in the Experimental Section.

As depicted in Figure 43, the herein proposed MCR-based synthetic method permits the rapid assembly of ester (Cpds **35** and **36**) and amide (Cpds **37** and **38**) libraries. The obtained collection contains 80 new derivatives (36 esters and 44 amides) bearing several previously unexplored substitution patterns in SCRA-like series. The diversity space explored (R^1, R^2, R^3, $R^{3'}$, R^4 and R^5) during this proof of concept is presented in Figure 43. As observed, the direct and efficient assembly facilitates the exhaustive exploration of the SAR in these series.

Figure 44 shows the ^{1}H-NMR spectra obtained during the spectroscopic characterization of a representative compound of this series.



Scheme 2: Ugi-based assembly of amides **37a-v** and **38a-v**.

USC UNIVERSIDADE DE SANTIAGO DE COMPOSTELA

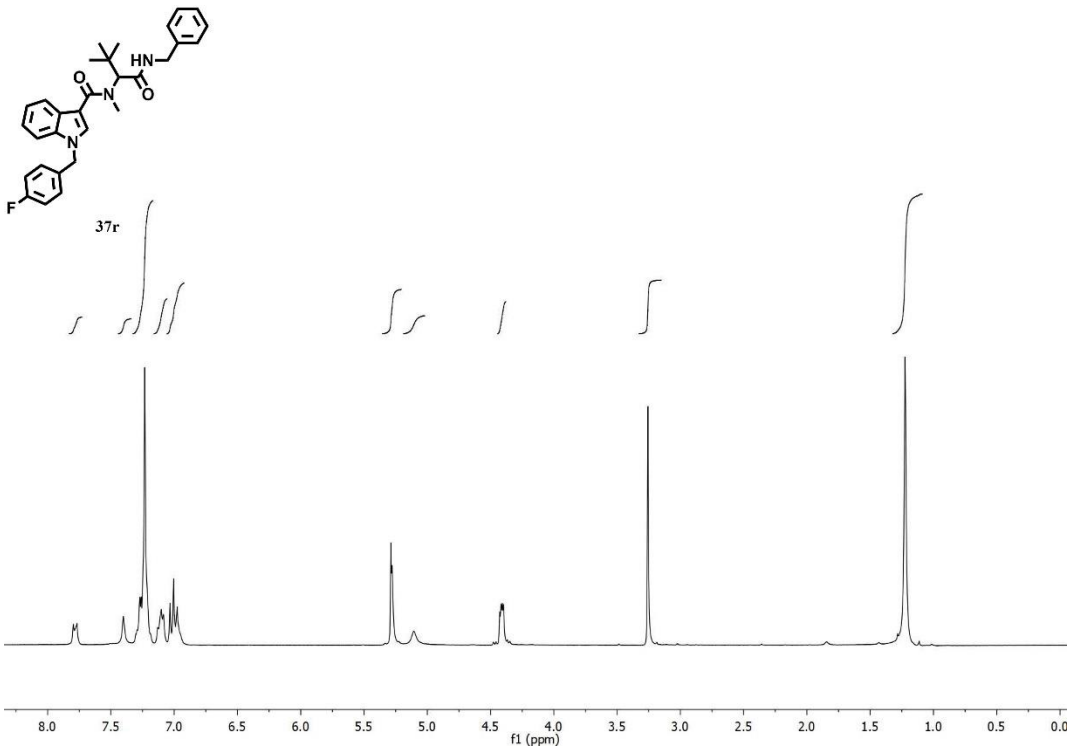
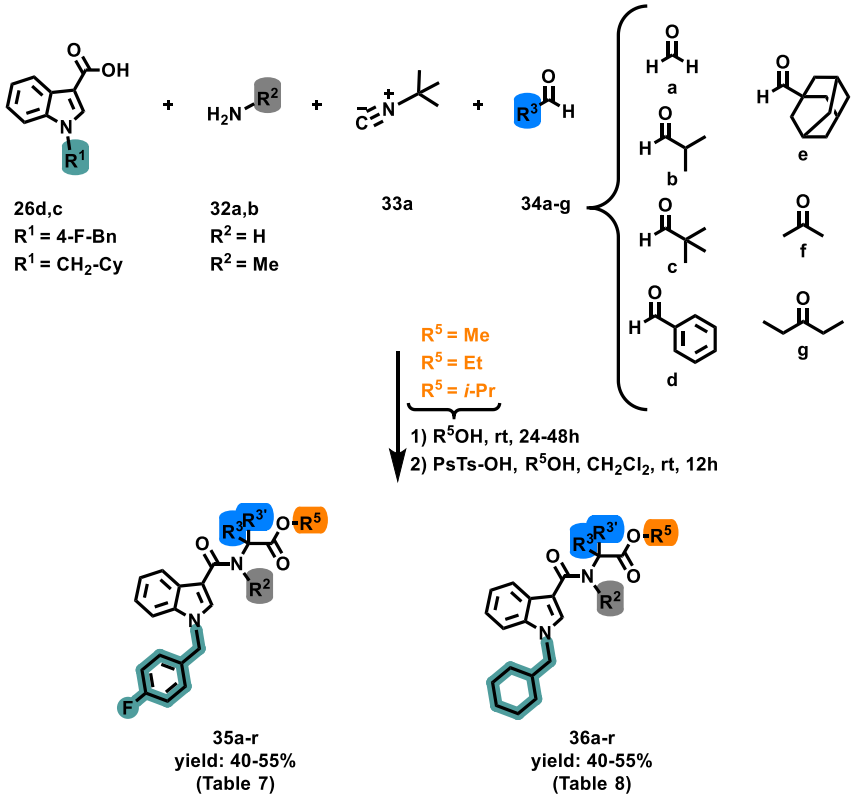


Figure 44: ^{1}H-NMR spectra of compound **37r**.

Following earlier observations of several authors,[131,136,137] and our own experience with Ugi reaction,[138] we designed a direct and efficient assembly of targeted esters (Cpds **35** and **36**) by promoting the acid-mediated solvolysis (alcoholysis) of the terminal amide group within the Ugi adducts (Scheme 3). This transformation, that takes place by treating the corresponding Ugi adduct with supported p-toluene sulfonic acid in a mixture of dichloromethane and the corresponding alcohol, provides the desired ligands in moderate to satisfactory yields (40-55%). Even though the transformation is feasible and described with different amides, we systematically used *tert*-butyl isocyanide (**33a**) to promote solvolysis, as it is a commercially available and robust isocyanide that undergoes the desired alcoholysis in a particularly efficient manner. Three alcoholic solvents (methanol, ethanol, and isopropanol) were used to briefly explore the influence of the alkoxy residue (R^5) present in the ester group on the cannabimimetic profile of these series. The reactions were performed in sealed Kimble vials using the corresponding alcohol as solvent and, once finished, quenched, and elaborated to isolate and purify the corresponding Ugi adduct (Scheme 3).

Figure 45 shows the ^{1}H-NMR spectra obtained during the spectroscopic characterization of a representative compound of this series.

USC UNIVERSIDADE DE SANTIAGO DE COMPOSTELA



Scheme 3: Ugi-based assembly of esters **35a-r** and **36a-r**.

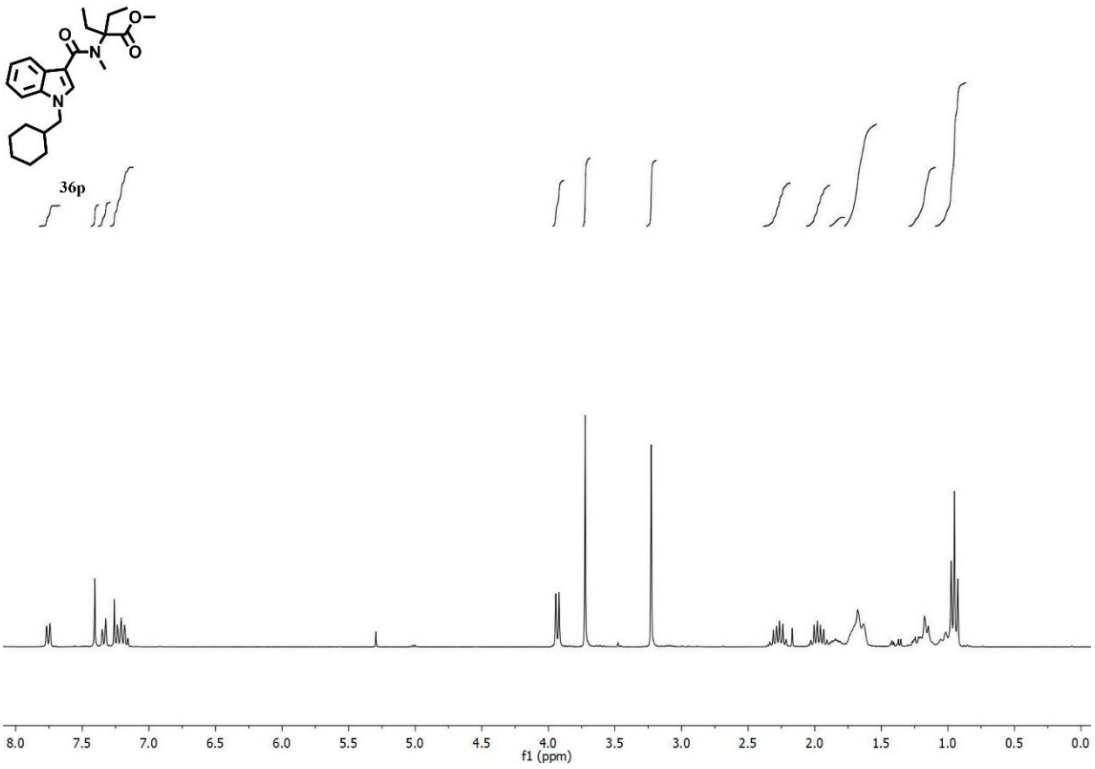


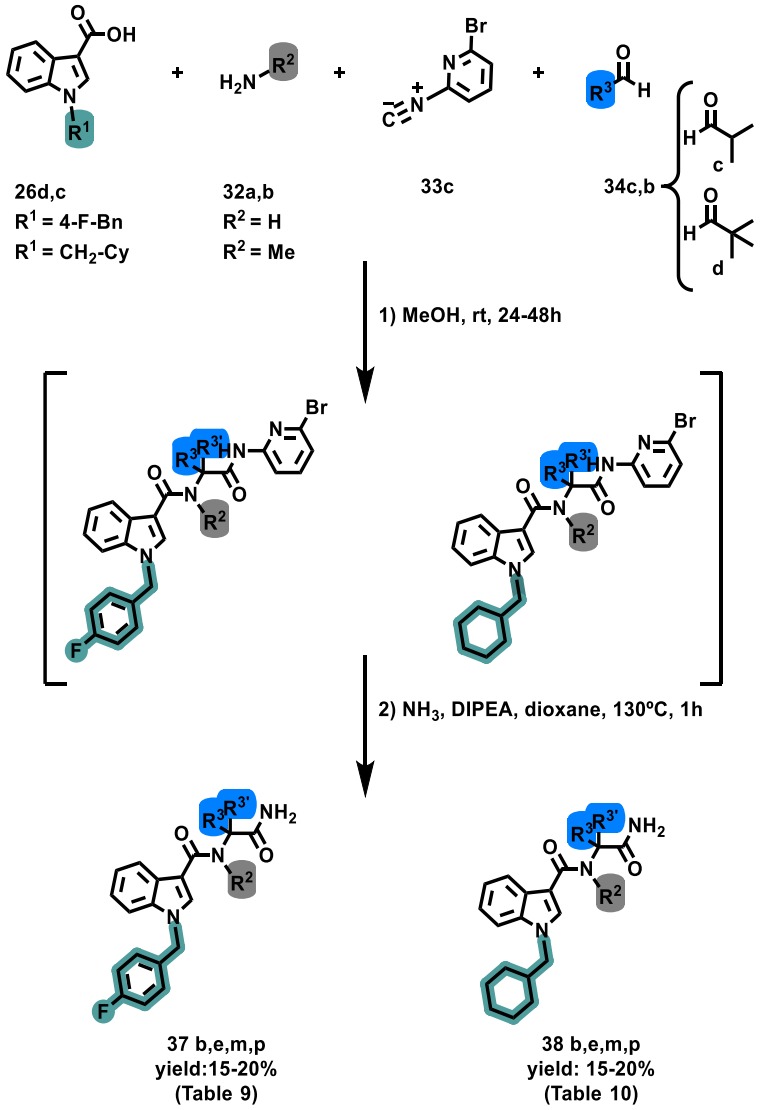
Figure 45: ^{1}H-NMR spectra of compound **36p**.

USC UNIVERSIDADE DE SANTIAGO DE COMPOSTELA

With the aim to provide a more comprehensive picture of the SAR studies in these series, we also decided to prepare ligands **37b**, **37e**, **37m**, **37p** and **38b**, **38e**, **38m**, **38p** (Scheme 4). These eight derivatives contain unsubstituted terminal amides (R^4 = H), isolated as racemates, and bear a *tert*-butyl group or *iso*-propyl at R^3, thus enabling direct affinity comparisons with other members of the library and being key to unequivocally evaluate the impact of R^4 on the affinity and selectivity of the series.

It was envisioned that the synthesis of **37b**, **37e**, **37m**, **37p** and **38b**, **38e**, **38m**, **38p** (Scheme 4) could be feasible by modifying the previous approach (Scheme 4). The proposed synthesis involves a U4CR, like the one performed previously, but employing the convertible isocyanide concept.[139] Among the different convertible isocyanides available, the use of 6-bromopyridine-2-isocyanide (**33c**) seemed to be particularly appealing. The synthesis of the required isocyanide was accomplished following the experimental protocol described by Van der Heijden.[139] Once the multicomponent reaction finished, ammonolysis of the Ugi adduct afforded the targeted derivatives with low yields (15-20%). The reaction was performed in a one-pot (two stages) fashion, so the 6-bromo-pyridin-carboxamide Ugi adducts were not isolated/purified and used in the next step.

USC UNIVERSIDADE DE SANTIAGO DE COMPOSTELA



Scheme 4: U4CR-ammonolysis sequence for the synthesis of amides **37b,e,m,p** and **38b,e,m,p**.

As in the previous Chapter, all reactions were monitored by thin-layer chromatography (TLC). After completion of the reaction, the catch procedure (or acid-catalyzed solvolysis) was performed as indicated in the Experimental Section. Then, the solvent was evaporated to dryness and the isolated solid/oil was purified by column chromatography on silica gel or preparative chromatography. A detailed description of the synthetic methods and the complete structural, spectroscopic, and analytical data for all compounds are provided in the Experimental Section.

USC UNIVERSIDADE DE SANTIAGO DE COMPOSTELA

Enantiomers Separation and Circular Dichroism. As described in literature,[3,81–83] and evidenced in Chapter 1, the stereocenter within the linker is a signature element of SCRAs that seems to have a relevant role during the interaction with CBRs. Most of the ligands obtained in this Chapter contain a stereogenic center and were tested as racemates (Tables 7-10). To further elucidate the importance of the enantioselective recognition in these novel series, the enantiomeric separation, assignment, and biological evaluation (Table 11) for some representative ligands has been performed. A validated approach, using chiral HPLC and circular dichroism (CD) spectroscopy, was employed to separate and assign the configuration of the enantiomers of six representative ligands exhibiting a CB_2R selective profile. Semipreparative HPLC separation of these racemic ligands, on a chiral stationary phase [250 mm x 20 mm Chiralpak® 5µm IE-3 (DAICEL)], afforded the corresponding enantiomers with excellent stereochemical purity (e.e. > 99%).

To assign the absolute configuration of the ligands we used the characteristic pattern observed within the CD spectra of structurally related enantiopure SCRAs studied in Chapter 1 (Figure 46). Although in Chapter 1 we studied the CD spectra of more than eight pairs of SCRAs agonists (both esters and amides), for this study we selected four representative derivatives for comparative purposes and to verify the predictability and reproducibility of the proposed method (Figure 46). As documented in literature,[140] the CD spectra of these series contain a characteristic intense peak around 240 nm. This peak can be assigned to the chiral information present at the aminoacid residue that influences the push pull system within the heterocycle and the ester or amide group. As experimentally validated in Chapter 1 (with enantiopure ligands), SCRAs derivatives exhibiting negative cotton effect at 240 nm correspond to the (*S*) enantiomer, while the (*R*) enantiomers exhibit a CD spectrum with positive cotton effect at 240 nm. These observations enabled the unequivocal assignment of the absolute configuration of each enantiomer (Figure 46) and will be used in this Chapter with this aim (Figure 48).[140]

The analysis of the HPLC traces obtained for selected racemic mixtures (Figure 48) enabled to verify that the *(R)* enantiomer is systematically more abundant (5-10%) in the Ugi adduct racemates (Figure 48, left).

USC UNIVERSIDADE DE SANTIAGO DE COMPOSTELA

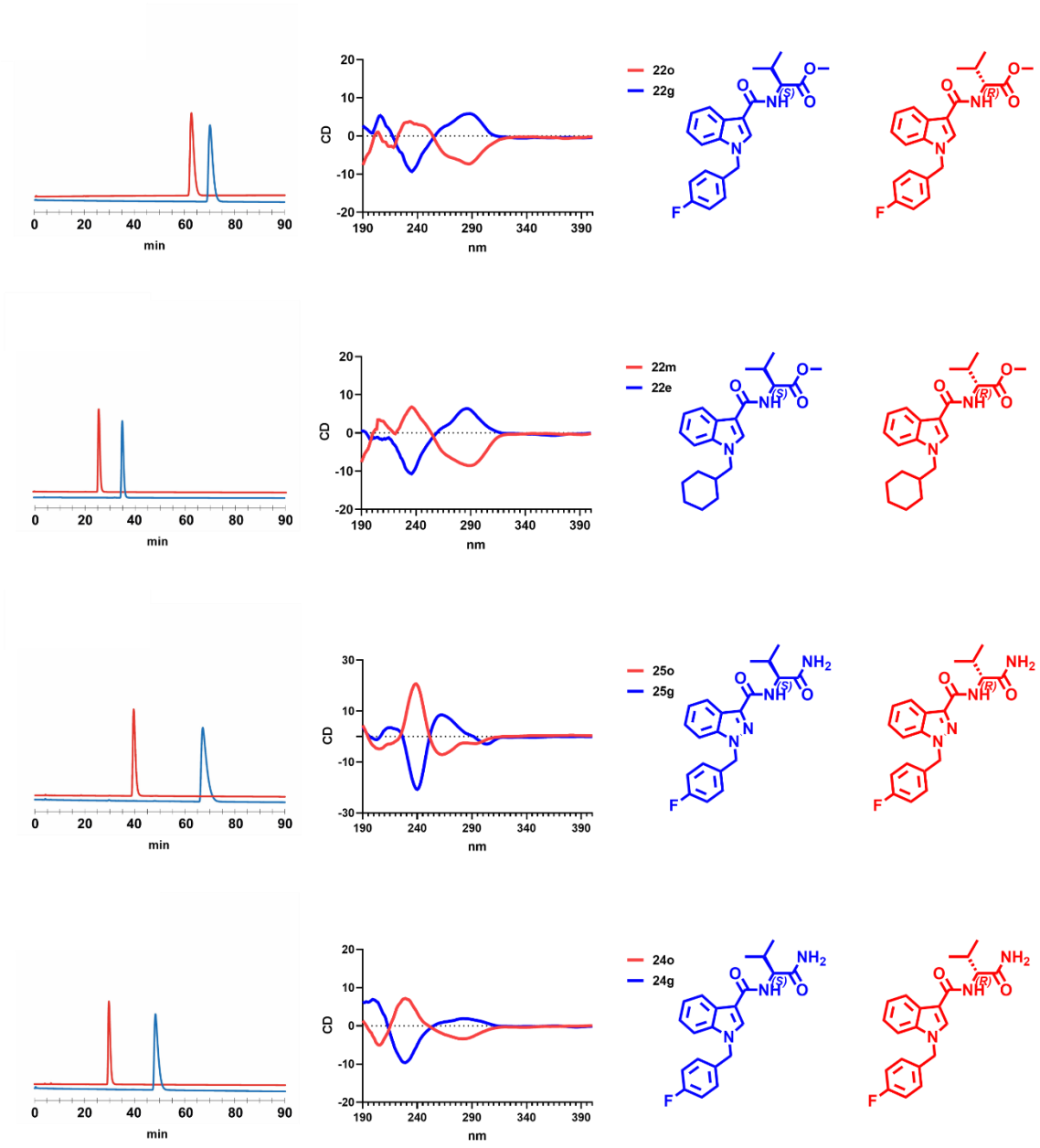


Figure 46: HPLC traces and circular dichroism spectra of 4 representative SCRAs obtained in Chapter 1: the *(R)* enantiomers are in red; the *(S)* enantiomers are in blue.

USC
UNIVERSIDADE DE SANTIAGO DE COMPOSTELA

To evaluate the importance of the configuration at the stereogenic center on the CBR affinity, we used six ligands (Figure 47). The selected ligands exhibit potent and CB_2R selective effect and are representative of the functionality (esters and amides), and substitutions at R^1, R^2, R^3, R^4 and R^5. Once the HPLC separation of the six racemates was optimized (and enantiomeric excess >99% were obtained), we recorded the CD spectra of the twelve obtained enantiomers. The obtained chromatograms and CD spectrum are presented in Figure 48. The absolute configuration of the new CB_2R enantiomers has been assigned (Figure 48): the *(S)* enantiomers are represented in blue, while the *(R)* enantiomers are presented in red. As for early series (Chapter 1, Figure 46) the most characteristic peak of CD spectra is at 240 nm, and these ligands reproduce the early observed behavior. The enantiopure ligands were then tested *in vitro* at CBRs (Table 11). For comparative purposes Table 11 also contains the data of the corresponding racemic ligands.

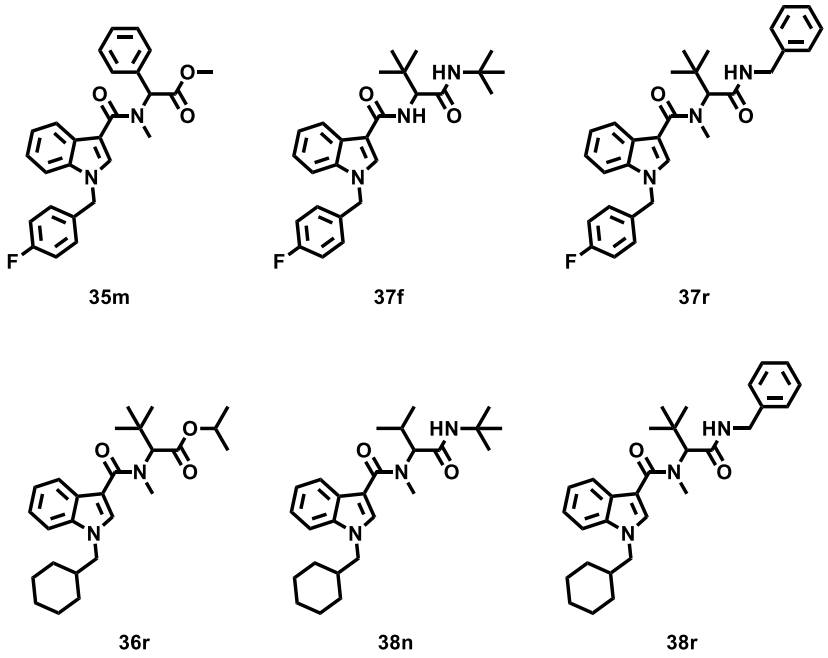


Figure 47: Structure of selected racemic ligands.

USC UNIVERSIDADE DE SANTIAGO DE COMPOSTELA

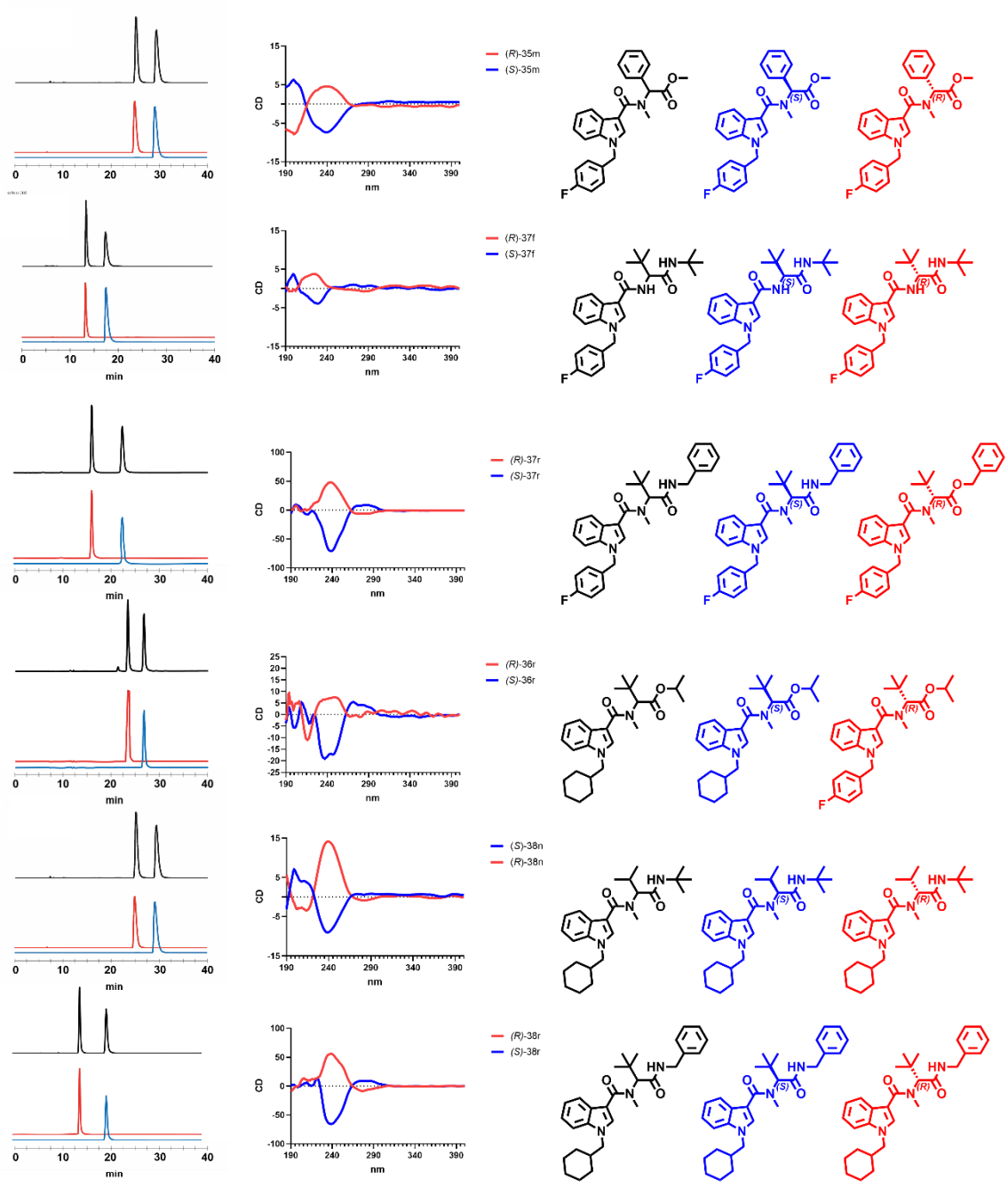


Figure 48: HPLC traces obtained during the enantiomeric separation of representative ligands and the assignment of their configuration using CD. The *(S)* configuration correspond to enantiomers eliciting negative cotton effect at 240 nm, while the *(R)* enantiomers show positive cotton effect at 240 nm.

USC UNIVERSIDADE DE SANTIAGO DE COMPOSTELA

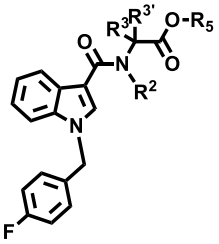
Biological Evaluation. The affinity and selectivity profiles of the novel indole-based compounds were evaluated *in vitro* using radioligand binding assay at the two human CBR subtypes. Tables 7-11 contain the binding data obtained. Except for the enantiopure compounds described in Table 11, all ligands reported were obtained and tested as racemic mixtures. All experiments were performed *in vitro* in transfected HEK-293T cells and [^{3}H]-CP 55,940 was employed as radioligand.

The binding data (Tables 7-11) is presented as K_i ± SEM (nM, n = 3) or as specific binding inhibition percentage at 1 μM (n = 2, mean) for those compounds which do not reach a minimum of 60% of radioligand displacement at such concentration. Prism 5.0 software (GraphPad, San Diego, CA) was employed for data analysis. K_i values were acquired by fitting the data by non-linear regression. Results are the average of three experiments, each performed in duplicate. Two well-known CBR ligands [Surinabant (CB_1R antagonist) and GW405833 (CB_2R agonist)] were also assessed using our experimental protocols, their binding data is reported in Tables 7-11 for comparison purposes.

In order to facilitate the analysis of the obtained data, those ligands eliciting high CB_2R selectivity are highlighted across the tables (bold).

USC UNIVERSIDADE DE SANTIAGO DE COMPOSTELA

Table 7: Affinity and selectivity data obtained for esters **35a-r**.

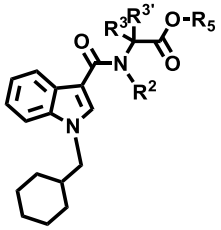


CODE	R^2	R^3	$R^{3'}$	R^5	CB_1R	CB_2R	SI[b]
					K_i (nM) or % at 1 μM[a]	K_i (nM) or % at 1 μM[a]	K_i CB_1R/ K_i CB_2R
35a	H	H	H	Me	181 nM	125 nM	1.4
35b	H	*i*-Pr	H	Me	81.6 nM	43.4 nM	1.9
35c	H	*t*-Bu	H	Me	2.70 nM	2.09 nM	1.3
35d	H	Ph	H	Me	61.5 nM	68.0 nM	0.9
35e	H	Ad	H	Me	29%	**188 nM**	**>100**
35f	H	Me	Me	Me	29.0 nM	17.0 nM	1.7
35g	H	Et	Et	Me	2.33 nM	0.88 nM	2.6
35h	H	*t*-Bu	H	Et	8.30 nM	4.00 nM	2.1
35i	H	*t*-Bu	H	*i*-Pr	31.5 nM	17.2 nM	1.8
35j	Me	H	H	Me	33%	28%	-
35k	Me	*i*-Pr	H	Me	14%	**731 nM**	**>100**
35l	Me	*t*-Bu	H	Me	119 nM	7.26 nM	16
35m	Me	Ph	H	Me	28%	**216 nM**	**>100**
35n	Me	Ad	H	Me	9%	37%	-
35o	Me	Me	Me	Me	95.9 nM	14.5 nM	6.6
35p	Me	Et	Et	Me	11%	**607 nM**	**>100**
35q	Me	*t*-Bu	H	Et	260 nM	52.9 nM	4.9
35r	Me	*t*-Bu	H	*i*-Pr	14%	**583 nM**	**>100**
Surinabant	-	-	-	-	3.00 nM	400 nM	-
GW405833	-	-	-	-	4772 nM	5.80 nM	-

[a] Displacement of specific [^{3}H]-CP 55,940 binding in human HEK cells expressed as K_i in nM (n = 3) or percentage displacement of specific binding at a concentration of 1 μM (n = 2). [b] Selectivity index is the ratio between K_i CB_1R and K_i CB_2R.

USC UNIVERSIDADE DE SANTIAGO DE COMPOSTELA

Table 8: Affinity and selectivity data obtained for esters **36a-r**.

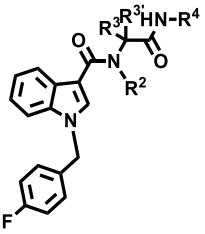


CODE	R^2	R^3	$R^{3'}$	R^5	CB_1R	CB_2R	SI[b] K_i CB_1R/ K_i CB_2R
					K_i (nM) or % at 1 μM[a]	K_i (nM) or % at 1 μM[a]	
36a	H	H	H	Me	68.2 nM	71.7 nM	1.0
36b	H	*i*-Pr	H	Me	32.4 nM	7.50 nM	4.3
36c	H	*t*-Bu	H	Me	1.40 nM	0.35 nM	4.0
36d	H	Ph	H	Me	25.1 nM	43.2 nM	0.6
36e	H	Ad	H	Me	22%	**688 nM**	**>100**
36f	H	Me	Me	Me	22.3 nM	6.70 nM	3.3
36g	H	Et	Et	Me	13.2 nM	1.40 nM	9.4
36h	H	*t*-Bu	H	Et	5.40 nM	2.70 nM	2.0
36i	H	*t*-Bu	H	*i*-Pr	11.6 nM	6.00 nM	1.9
36j	Me	H	H	Me	33%	28%	
36k	Me	*i*-Pr	H	Me	92.4 nM	51.4 nM	1.8
36l	Me	*t*-Bu	H	Me	46.8 nM	25.9 nM	1.8
36m	Me	Ph	H	Me	167 nM	89.9 nM	1.9
36n	Me	Ad	H	Me	2%	39%	-
36o	Me	Me	Me	Me	47.0 nM	31.2 nM	1.5
36p	Me	Et	Et	Me	22%	**301 nM**	**>100**
36q	Me	*t*-Bu	H	Et	71.3 nM	101 nM	0.7
36r	Me	*t*-Bu	H	*i*-Pr	30%	**114 nM**	**>100**
Surinabant	-	-	-	-	3.00 nM	400 nM	-
GW405833	-	-	-	-	4772 nM	5.80 nM	-

[a] Displacement of specific [^{3}H]-CP 55,940 binding in human HEK cells expressed as K_i in nM (n = 3) or percentage displacement of specific binding at a concentration of 1 μM (n = 2). [b] Selectivity index is the ratio between K_i CB_1R and K_i CB_2R.

USC UNIVERSIDADE DE SANTIAGO DE COMPOSTELA

Table 9: Affinity and selectivity data obtained for amides **37a-v**.

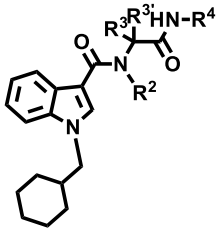


CODE	R^2	R^3	$R^{3'}$	R^4	CB_1R	CB_2R	SI[b]
					K_i (nM) or % at 1 μM[a]	K_i (nM) or % at 1 μM[a]	K_i CB_1R/ K_i CB_2R
37a	H	H	H	*t*-Bu	281 nM	93.8 nM	3.0
37b	H	*i*-Pr	H	H	80.6 nM	71.5 nM	1.1
37c	H	*i*-Pr	H	*t*-Bu	16%	**276 nM**	**>100**
37d	H	*i*-Pr	H	Bn	10%	**571 nM**	**>100**
37e	H	*t*-Bu	H	H	9.60 nM	2.20 nM	4.3
37f	H	*t*-Bu	H	*t*-Bu	36%	**98.7 nM**	**>100**
37g	H	*t*-Bu	H	Bn	123 nM	35.8 nM	3.4
37h	H	Ph	H	*t*-Bu	17%	23%	-
37i	H	Ad	H	*t*-Bu	1%	37%	-
37j	H	Me	Me	*t*-Bu	31%	29%	-
37k	H	Et	*Et*	*t*-Bu	1%	34%	-
37l	Me	H	H	*t*-Bu	17%	23%	-
37m	Me	*i*-Pr	H	H	192 nM	132 nM	1.4
37n	Me	*i*-Pr	H	*t*-Bu	3%	**483 nM**	**>100**
37o	Me	*i*-Pr	H	Bn	9%	**237 nM**	**>100**
37p	Me	*t*-Bu	H	H	59.3 nM	8.20 nM	7.2
37q	Me	*t*-Bu	H	*t*-Bu	3%	32%	-
37r	Me	*t*-Bu	H	Bn	27%	**204 nM**	**>100**
37s	Me	Ph	H	*t*-Bu	3%	16%	-
37t	Me	Ad	H	*t*-Bu	5%	14%	-
37u	Me	Me	Me	*t*-Bu	15%	22%	-
37v	Me	Et	*Et*	*t*-Bu	4%	24%	-
Surinabant	-	-	-	-	3.00 nM	400 nM	-
GW405833	-	-	-	-	4772 nM	5.80 nM	-

[a] Displacement of specific [^{3}H]-CP 55,940 binding in human HEK cells expressed as K_i in nM (n = 3) or percentage displacement of specific binding at a concentration of 1 μM (n = 2). [b] Selectivity index is the ratio between K_i CB_1R and K_i CB_2R.

USC UNIVERSIDADE DE SANTIAGO DE COMPOSTELA

Table 10: Affinity and selectivity data obtained for amides **38a-v**.

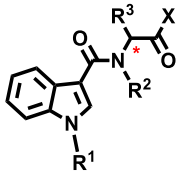


CODE	R^2	R^3	$R^{3'}$	R^4	CB_1R	CB_2R	SI[b]
					K_i (nM) or % at 1 μM[a]	K_i (nM) or % at 1 μM[a]	K_i CB_1R/ K_i CB_2R
38a	H	H	H	*t*-Bu	99.5 nM	51.2 nM	1.9
38b	H	*i*-Pr	H	H	5.00 nM	4.30 nM	1.1
38c	H	*i*-Pr	H	*t*-Bu	28%	**50.2 nM**	**>100**
38d	H	*i*-Pr	H	Bn	37%	**109 nM**	**>100**
38e	H	*t*-Bu	H	H	2.40 nM	0.44 nM	5.4
38f	H	*t*-Bu	H	*t*-Bu	35%	**34.8 nM**	**>100**
38g	H	*t*-Bu	H	Bn	28.4 nM	7.60 nM	3.7
38h	H	Ph	H	*t*-Bu	28%	31%	-
38i	H	Ad	H	*t*-Bu	1%	1%	-
38j	H	Me	Me	*t*-Bu	170 nM	176 nM	1.0
38k	H	Et	Et	*t*-Bu	25%	**128 nM**	**>100**
38l	Me	H	H	*t*-Bu	44%	36%	-
38m	Me	*i*-Pr	H	H	58.1 nM	14.0 nM	4.1
38n	Me	*i*-Pr	H	*t*-Bu	30%	**40.9 nM**	**>100**
38o	Me	*i*-Pr	H	Bn	1%	**672 nM**	**>100**
38p	Me	*t*-Bu	H	H	16.8 nM	2.4 nM	7.0
38q	Me	*t*-Bu	H	*t*-Bu	5%	**237 nM**	**>100**
38r	Me	*t*-Bu	H	Bn	26%	**108 nM**	**>100**
38s	Me	Ph	H	*t*-Bu	4%	28%	-
38t	Me	Ad	H	*t*-Bu	6%	4%	-
38u	Me	Me	Me	*t*-Bu	3%	28%	-
38v	Me	Et	Et	*t*-Bu	8%	35%	-
Surinabant	-	-	-	-	3.00 nM	400 nM	-
GW405833	-	-	-	-	4772 nM	5.80 nM	-

[a] Displacement of specific [^{3}H]-CP 55,940 binding in human HEK cells expressed as K_i in nM (n = 3) or percentage displacement of specific binding at a concentration of 1 μM (n = 2). [b] Selectivity index is the ratio between K_i CB_1R and K_i CB_2R.

USC UNIVERSIDADE DE SANTIAGO DE COMPOSTELA

Table 11: Affinity and selectivity data obtained for racemates and their corresponding enantiomers.



CODE	R^1	R^2	R^3	X	CB_1R K_i (nM) or % at 1 μM[a)]	CB_2R K_i (nM) or % at 1 μM[a)]	SI[b)] K_i CB_1R/ K_i CB_2R
(±)-35m	4-F-Bn	Me	Ph	OMe	28%	**216 nM**	**>100**
(*S*)-35m	4-F-Bn	Me	Ph	OMe	40%	**121 nM**	**>100**
(*R*)-35m	4-F-Bn	Me	Ph	OMe	11%	**652 nM**	**>100**
(±)-37f	4-F-Bn	H	*t*-Bu	NH-*t*-Bu	36%	**98.7 nM**	**>100**
(*S*)-37f	4-F-Bn	H	*t*-Bu	NH-*t*-Bu	39%	**60.1 nM**	**>100**
(*R*)-37f	4-F-Bn	H	*t*-Bu	NH-*t*-Bu	15%	**343 nM**	**>100**
(±)-37r	4-F-Bn	Me	*t*-Bu	NH-Bn	27%	**204 nM**	**>100**
(*S*)-37r	4-F-Bn	Me	*t*-Bu	NH-Bn	22%	**113 nM**	**>100**
(*R*)-37r	4-F-Bn	Me	*t*-Bu	NH-Bn	19%	23%	**-**
(±)-36r	CH_2-Cy	Me	*t*-Bu	O-*i*-Pr	30%	**114 nM**	**>100**
(*S*)-36r	CH_2-Cy	Me	*t*-Bu	O-*i*-Pr	34%	**109 nM**	**>100**
(*R*)-36r	CH_2-Cy	Me	*t*-Bu	O-*i*-Pr	26%	**156 nM**	**>100**
(±)-38n	CH_2-Cy	Me	*i*-Pr	NH-*t*-Bu	30%	**40.9 nM**	**>100**
(*S*)-38n	CH_2-Cy	Me	*i*-Pr	NH-*t*-Bu	13%	**18.4 nM**	**>100**
(*R*)-38n	CH_2-Cy	Me	*i*-Pr	NH-*t*-Bu	18%	18%	-
(±)-38r	CH_2-Cy	Me	*t*-Bu	NH-Bn	26%	**108 nM**	**>100**
(*S*)-38r	CH_2-Cy	Me	*t*-Bu	NH-Bn	47%	**21.8 nM**	**>100**
(*R*)-38r	CH_2-Cy	Me	*t*-Bu	NH-Bn	23%	**324 nM**	**>100**
Surinabant	-	-	-	-	3.00 nM	400 nM	-
GW405833	-	-	-	-	4772 nM	5.80 nM	-

[a)] Displacement of specific [^{3}H]-CP 55,940 binding in human HEK cells expressed as K_i in nM (n = 3) or percentage displacement of specific binding at a concentration of 1 μM (n = 2). [b)] Selectivity index is the ratio between K_i CB_1R and K_i CB_2R.

USC UNIVERSIDADE DE SANTIAGO DE COMPOSTELA

Structure-Activity Relationship Analyses. In this Chapter, exploratory series of esters (**35** and **36**) and amides (**37** and **38**) have been obtained, using efficient and experimentally simple variants of the versatile Ugi reaction, to discover novel indole-based CB_2R selective agonists. A first analysis of the binding data obtained (Tables 7-10) reveals the identification of several potent and highly CB_2R selective (> 100-fold) ligands (Figure 49). These results evidence the effectiveness of the pharmacomodulation process, which, starting from model dual CB_1-CB_2 prototypes, enabled us to dissociate completely the binding profile to these receptors and to discover novel and potent ligands that specifically recognize the CB_2R. As observed in Figure 49, eight derivatives belong to the ester series (**35e**, **35k**, **35m**, **35p**, **35r**, **36e**, **36p**, **36r**) and ten ligands to the amide series (**37c**, **37f**, **37n**, **37r**, **38c**, **38f**, **38k**, **38n**, **38q**, **38r**). Ligands **38c**, **38f** and **38n** stand out for their excellent potency (K_i < 55 nM) and selectivity profile (> 100-fold).

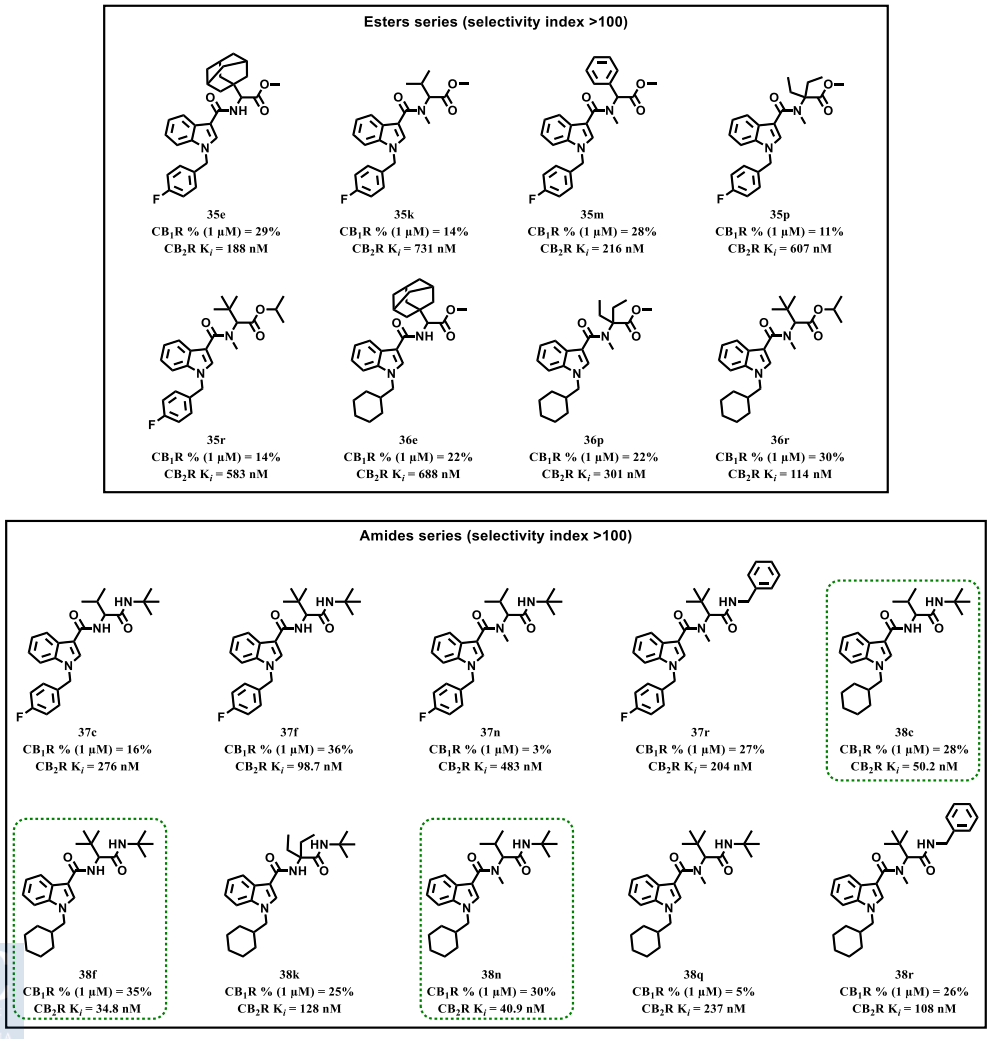


Figure 49: Structure and cannabimimetic data of selective CB_2R ligands identified during this study.

During our study, groups frequently encountered in SCRAs, but also previously unexplored substituents, have been introduced to evaluate the emerging SAR trends. In both series, esters and amides, ligands bearing the CH_2-Cy group (at R^1 of the indole core) showed higher affinity at CBRs (when compared to the 4-F-Bn moiety). As for Chapter 1, for a more immediate and efficient analysis of the variation of both affinity and selectivity, the binding data (pK_i) are presented graphically as a plot of pK_i *h*CB_1R (*Y* axis) versus pK_i *h*CB_2R (*X* axis) using the same scale and range for both axes (square plot). Therefore, compounds with equal affinities at both receptors will lie on the diagonal of this plot ($Y = X$) , whereas *h*CB_1R or *h*CB_2R selective compounds will be seen above or below the diagonal, respectively. The distance of their pK_i values from the diagonal is a direct measure of their degree of selectivity. The graphic comparation between the two series is shown in Figure 50. As observed, ester series (red) show higher affinity at both CBR, showing a K_i values in the low to medium nanomolar range, but in general most of the ester derivatives reproduce the dual CB_1R/CB_2R (non-selective) profile. In clear contrast, some ligands of the amide series (blue), although with clearly inferior affinity, show noticeable selectivity towards CB_2R.

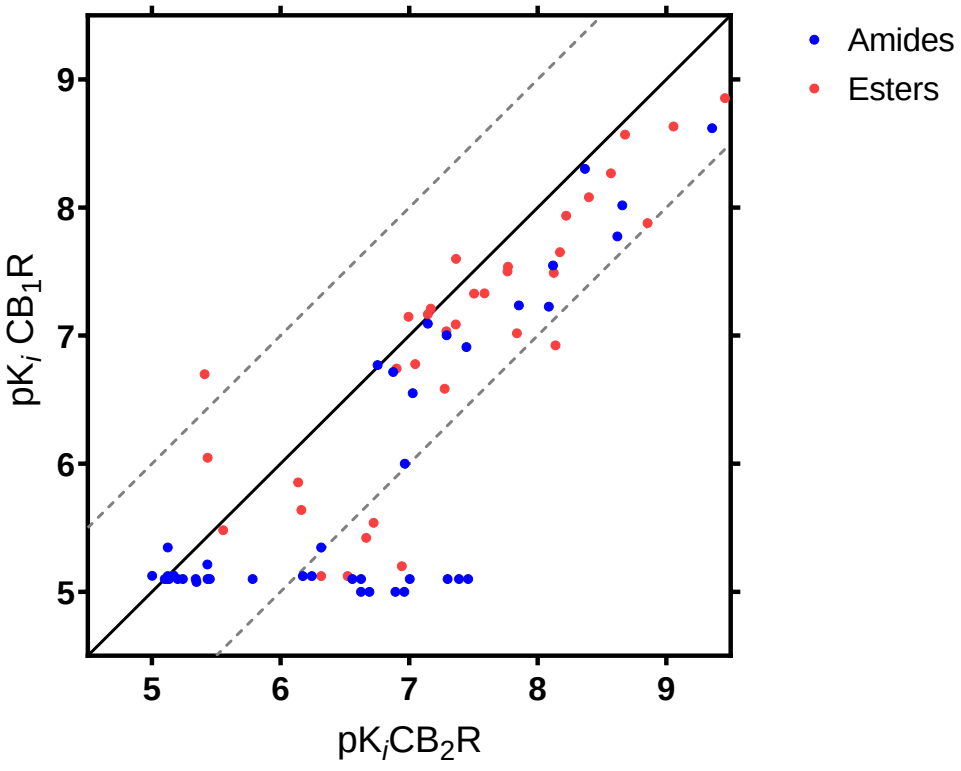


Figure 50: Graphical representation of the binding data obtained for the esters (red) and amides (blue).

Although not directly comparable, the esters obtained throughout this project (racemates) generally retain the potent and non-selective profile observed in the corresponding SCRA analogues (enantiopure) obtained in Chapter 1. As the new series herein described were obtained and tested as racemates, a logical (and expected) reduction in affinity is observed.

Despite their usual promiscuous (CB_1R/CB_2R) profile, certain CB_2R selectivity is observed for some compounds (ligands below the lower dashed line in Figure 51). Due to their suboptimal selectivity, and expected reduced metabolic stability, the ester series will not be discussed in detail, and we will only explore briefly the most salient features of the SAR in this family.

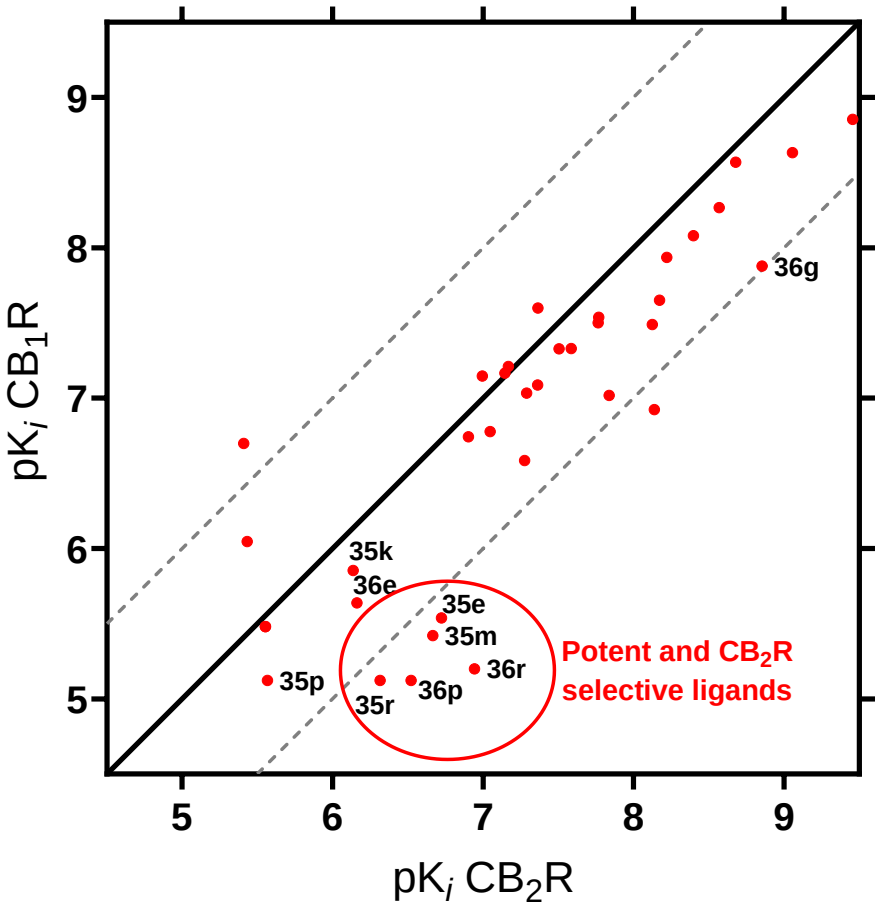


Figure 51: Graphical representation of the binding data obtained for the ester series.

USC
UNIVERSIDADE DE SANTIAGO DE COMPOSTELA

As previously observed in the SCRA series, R^3 plays a critical role in the affinity at both CBRs. In addition to *i*-Pr and *t*-Bu, the introduction of H, *i*-Pr, *t*-Bu, Ph and Adamantyl has been studied in these series (Tables 7-8). The peak effect is observed in each subset (4-F-Bn or CH_2-Cy), reaching the maximum affinity when R^3 = *t*-Bu (Figure 52). This trend is observed at both receptors, regardless of the substitution at R^1 or R^2. The importance of R^3 can be measured when comparing the CB_1R and CB_2R affinity of **35a** and **36a** (R^3 = H) with the other ligands in the series. In general, a phenyl group is tolerated, giving compounds with moderate affinity for both CB_1R and CB_2R. The introduction of the adamantyl group at R^3 produces ligands with moderate (**35e**, K_i = 188 nM) or low affinity (**36e**, K_i = 688 nM) only if R^2 = H. The introduction of two alkyl groups at R^3 and $R^{3'}$ (Me, Me / Et, Et) produces potent and non-selective compounds when R^2 = H. Interestingly, in this subset, the methyl group at R^2 led to an improved of CB_2R selectivity, and this effect is more pronounced (complete loss of affinity at CB_1R) for derivatives bearing R^3, $R^{3'}$ = Et, Et (**35p** and **36p**, Tables 7-8). This modification allowed the identification of compound **36p** that shows a moderate affinity (K_i = 301 nM) and high selectivity (> 100-fold) for CB_2R.

Although the substituent that contributes the most to the potency and selectivity in the series is R^3, the H/Me change at R^2 also produces interesting and previously unexplored binding data. Its contribution to selectivity/potency can be also appreciated in Figure 49, with eleven of eighteen compounds highlighted bearing a methyl group at R^2. It should be noticed the complete loss of affinity (at both CB_1R and CB_2R) when R^2 = Me for compounds in which R^3 = H (compounds **35j**, **36j**). In general, the methylation at R^2 decreases the affinity at CB_1R and CB_2R (Figure 52), with the drop in affinity at CB_1R being more pronounced. This trend favors the identification of selective CB_2R ligands (compounds **36r** and **35m**), although with moderate affinity (K_i value of 114 and 216 nM, respectively). As in SCRA series, the R^1 group has a mild affinity modulating function against CB_1R and CB_2R. Overall, ligands containing the CH_2-Cy group are (slightly) more potent (at both receptor subtypes) than those containing 4-F-Bn.

The effect of the methylation at R^2 can be exhaustively evaluated by comparing the binding data of selected compounds in Tables 7-8.

USC UNIVERSIDADE DE SANTIAGO DE COMPOSTELA

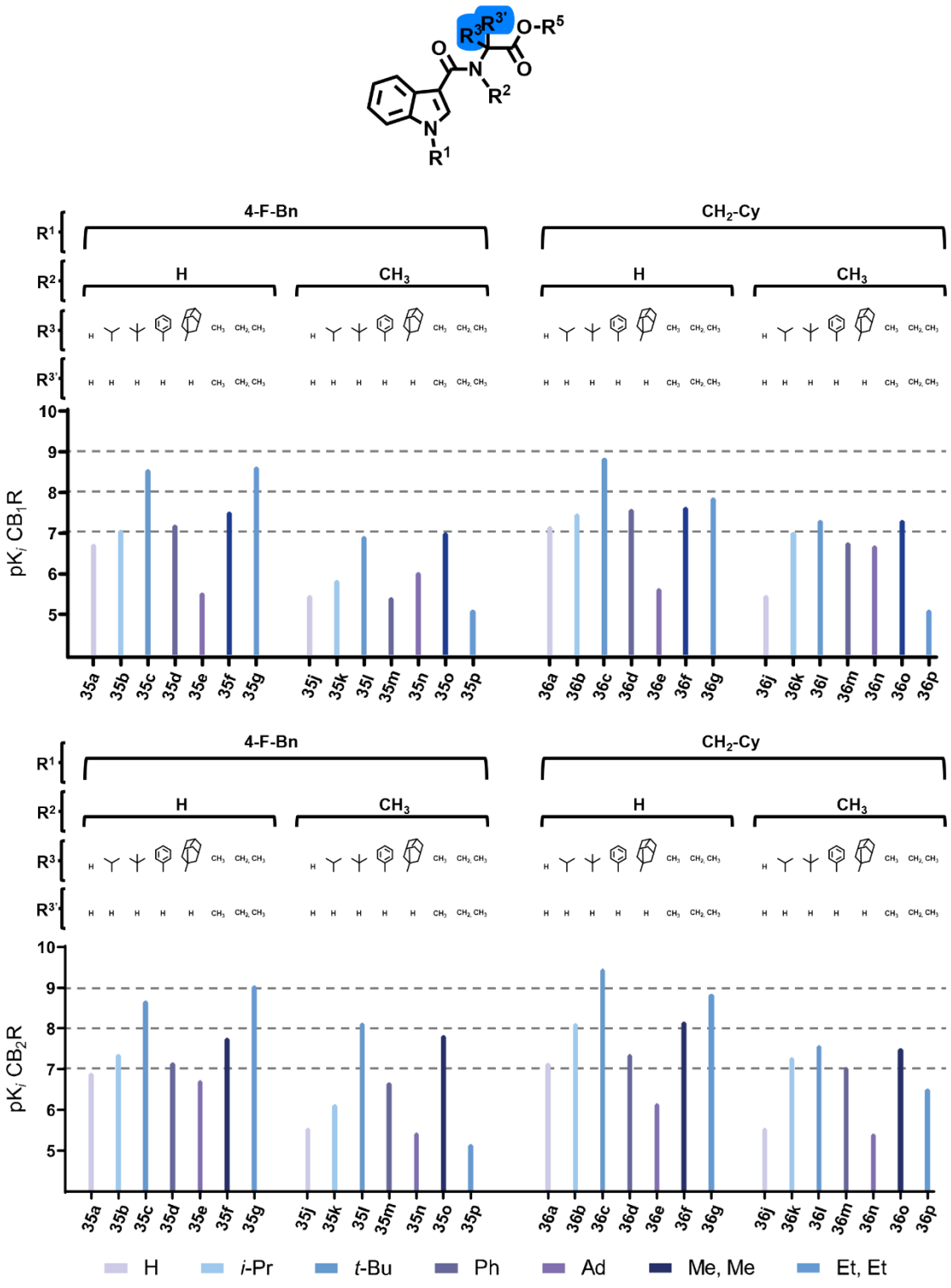


Figure 52: Bar chart representation of the SAR trends related to R^3 and $R^{3'}$ groups in the ester series. CB_1R affinity data (above) and CB_2R affinity data (bottom) are reported.

USC UNIVERSIDADE DE SANTIAGO DE COMPOSTELA

The substitution of Me by Et or *i*-Pr at R^5 leads to ligands with lower affinity at CB_1R and CB_2R (Figure 53). As observed (Figure 53), the drop in affinity is correlated with the steric volume of the alkoxy residue (R^5). As in previous cases (R^2), the affinity decrease in CB_1R is higher, which led to the identification of isopropyl derivatives combing CB_2R selective profile (e.g. compounds **36r** and **35r**) with moderate affinity of 114 nM and 483 nM, respectively.

Figure 52 and Figure 53 graphically represent the above indicated SAR trends in bar representations.

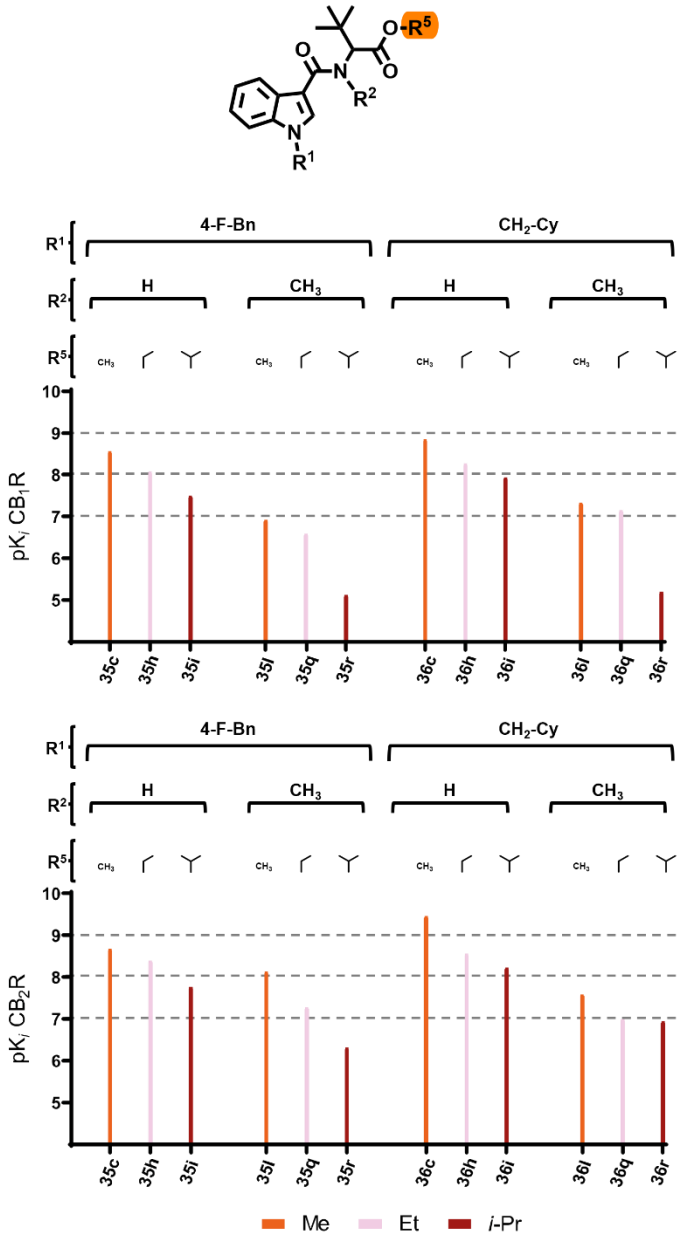


Figure 53: Bar chart representation of the SAR trends related to R^5 groups in the ester series. CB_1R affinity data (above) and CB_2R affinity data (bottom) are reported.

In a clear contrast to the ester series (which are mostly dual CB_1R and CB_2R agonists), the amide series (compounds **37a-v**, **38a-v**) in general show a decrease in potency but superior CB_2R selectivity profile (Figure 54). Within this series, we can identify the most attractive CB_2R ligands found in this Chapter (**37c**, **37f**, **37n**, **37r**, **38c**, **38f**, **38k**, **38m**, **38q**, **38r**). In order to evaluate the effect of groups at R^4, we have also obtained several compounds with R^4 = H. The design of the series allows the exhaustive comparisons of the influence of groups at R^1, R^2, R^3 and R^4.

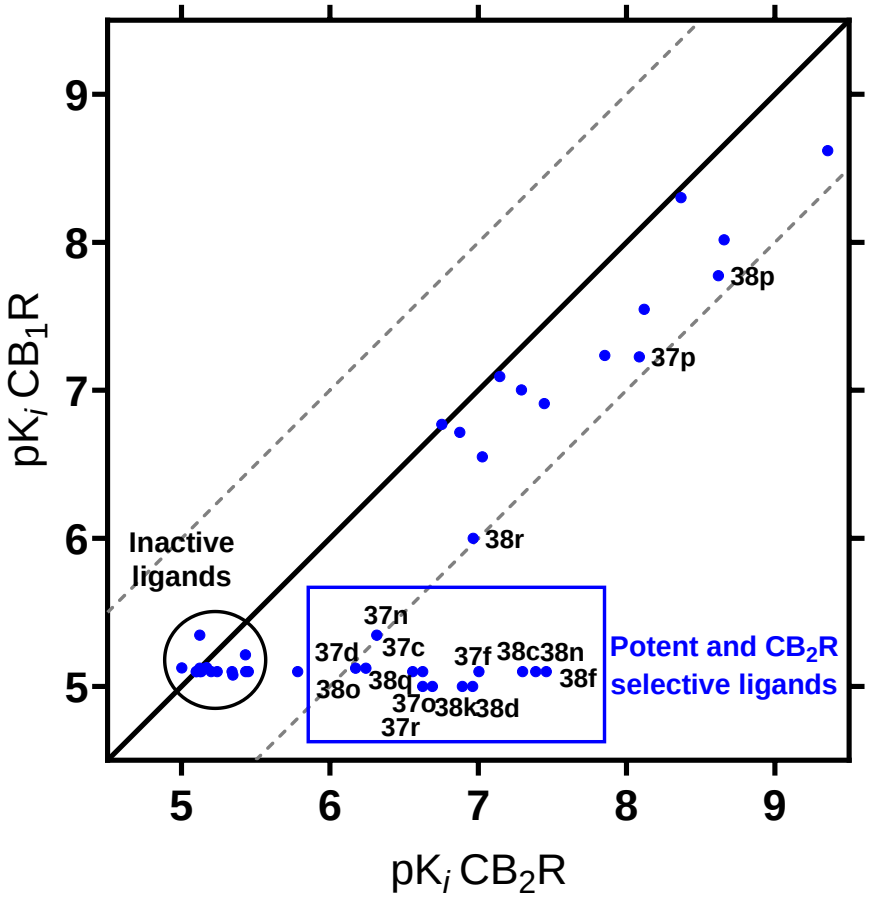


Figure 54: Graphical representation of the binding data obtained for the amide series.

USC UNIVERSIDADE DE SANTIAGO DE COMPOSTELA

As observed in the ester series, the R^3 group plays a key role in the potency and selectivity profiles at both CBRs (Tables 9-10). Using the compounds with R^3 = H as reference, two profiles were observed depending on the substituent at R^2. Thus, when R^2 = H (cpds **37a** and **38a**) relatively potent (with a K_i value of 99.5 and 281 nM at CB_1R and 51.2 and 93.8 nM at CB_2R, respectively), but no selective ligands have been found. On the other hand, when R^2 = Me the compounds are completely inactive.

Independently from R^2 and with the exception of **37g** and **38g** (R^4 = Bn), the introduction of *i*-Pr or *t*-Bu group at R^3 led to potent and CB_2R selective compounds. The use of bulkier groups, such as phenyl or adamantyl, leads to inactive compounds (cpds **37h**, **37i**, **37s**, **37t**, **38h**, **38i**, **38s**, **38t,** Tables 9-10). The excellent affinity and CB_2R selectivity of the ligands **38c** (CB_2R K_i = 50.2 nM), **38f** (CB_2R K_i = 34.8 nM) and **38n** (CB_2R K_i = 40.9 nM) are noteworthy (Table 10, Figure 55).

The introduction of two groups (Me/Me, Et/Et) at the R^3 leads to inactive compounds, except for compounds **38j** and **38k** (R^1 = CH_2-Cy, R^2 = H). Among these derivatives, **38j** shows moderate affinity but no selectivity; however, **38k** shows higher affinity and selectivity for CB_2R (K_i = 128 nM).

The comparison of the pharmacological data obtained for the two sub-series (4-F-Bn and CH_2-Cy) leads to the conclusion that in all cases the CH_2-Cy group provides more potent compounds.

The effect of the substituent at R^2 was evaluated by exchanging H for Me. Taking as reference compounds where R^2 = H and R^3 = H (which are relatively potent, but not selective) it is observed that the introduction of a methyl at R^2 leads to inactive ligands. The effect of methylation at R^2 is also apparent when comparing compounds **37b**, **37e**, **38b** y **38e** (R^2 = H, R^3 = H, R^4 = H) with their *N*-methyl analogues (cpds **37m**, **37p**, **38m** and **38p**). In general, as can be seen in Figure 55, the methylation at R^2 leads to slightly more potent compounds than when R^2 = H, while maintaining selectivity for CB_2R (Figure 55).

USC UNIVERSIDADE DE SANTIAGO DE COMPOSTELA

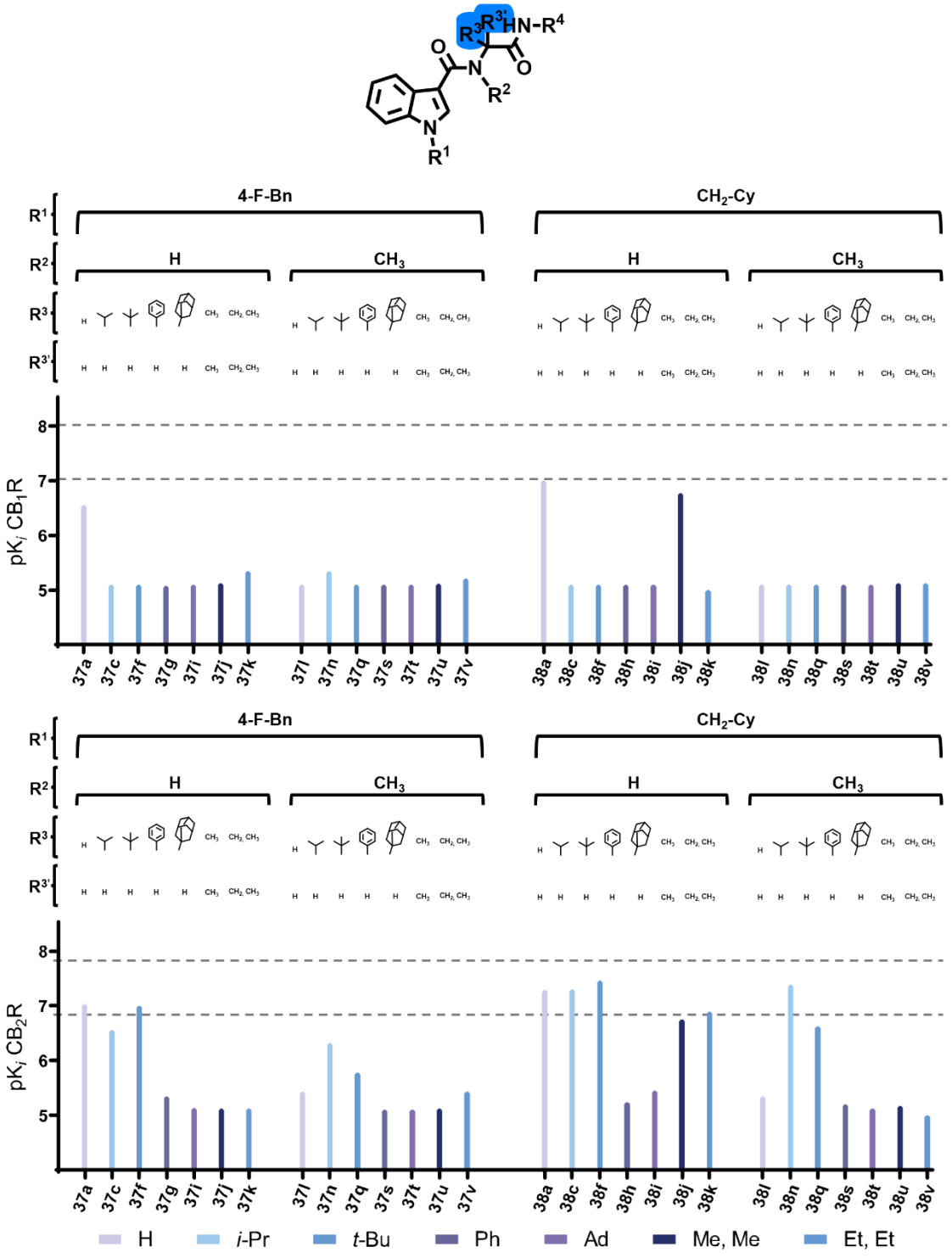


Figure 55: Bar chart representation of the SAR trends related to R^3 and $R^{3'}$ groups in the amide series. CB_1R affinity data (above) and CB_2R affinity data (bottom) are reported.

USC UNIVERSIDADE DE SANTIAGO DE COMPOSTELA

To analyze the effect of the substituent at R^4, the compounds with R^4 = H have been used as reference and compared with the corresponding analogues where R^4 = *t*-Bu or Bn in each sub-series. As shown in Figure 56, the introduction of a *t*-Bu group at R^4 removed the affinity for CB_1R, but not towards CB_2R, thus identifying CB_2R selective compounds with excellent to moderate affinity. On the other hand, the introduction of a Bn group produces CB_2R selective compounds if R^3 = *i*-Pr (compounds **37d**, **37o**, **38d**, **38o**). When R^3 = *t*-Bu and R^2 = Me, selective ligands (compounds **37r**, **38r**) are obtained (K_i = 204 nM and 108 nM, respectively); but the methylation at R^2 leads to a loss of selectivity (compounds **37g** and **38g**) (Tables 9-10, Figure 56).

The observed effect for R^4 is similar to the trend experienced for R^2, thus the substitution of hydrogen atoms by other groups at R^4 (*t*-Bu or Bn) and R^2 (Me) produced a significant reduction in CBR binding affinity. Since the CB_2R seems to be most tolerant to this substitution, we have identified relatively potent and highly CB_2R selective ligands.

USC UNIVERSIDADE DE SANTIAGO DE COMPOSTELA

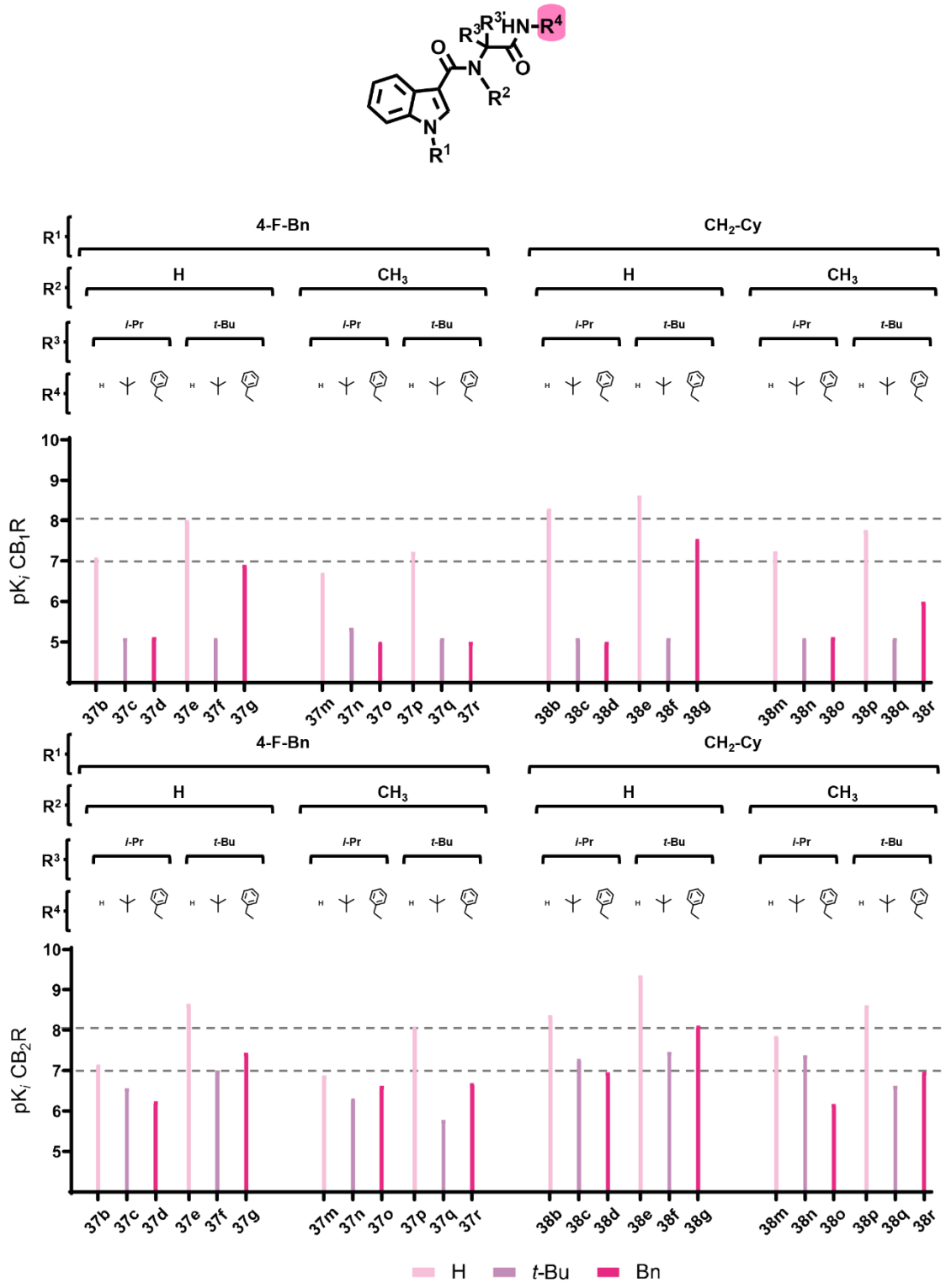


Figure 56: Bar chart representation of the SAR trends related to R^4 groups in the amide series. CB_1R affinity data (above) and CB_2R affinity data (bottom) are reported.

USC UNIVERSIDADE DE SANTIAGO DE COMPOSTELA

In Chapter 1, enantiopure series of SCRAs (derived from the functionalized ester and amides) have been synthesized and evaluated. It has been demonstrated that both the (*S*) and (*R*) stereoisomers are generally able to bind with excellent affinity to both CBRs (Figure 57). Moreover, we observed a certain CB_2R selectivity profile for selected *(R)* enantiomers.

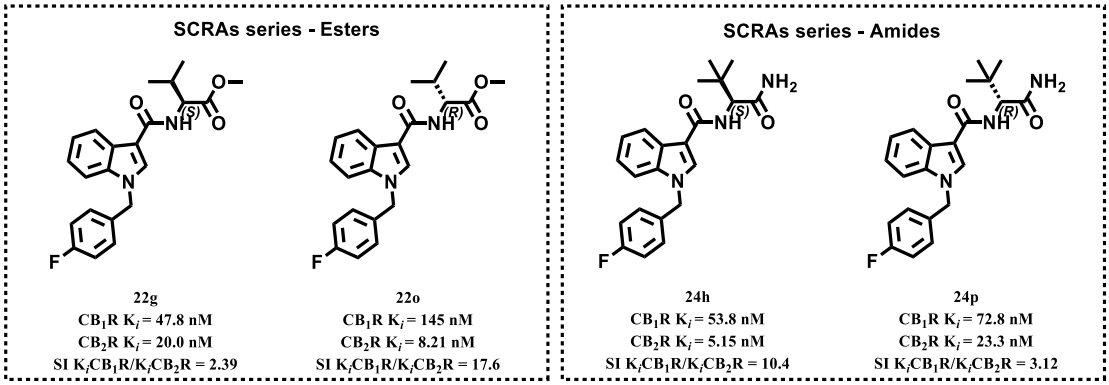


Figure 57: (*S*) and (*R*) stereoisomers of the SCRA series (Chapter 1).

As part of this project, six selective CB_2R ligands (ester and amide) identified in this Chapter were selected, separated, and their corresponding enantiomers evaluated *in vitro* at CBRs (Table 11, Figure 58).

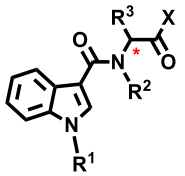
The SAR trends observed after analyzing the binding data reported in Table 11 are summarized here. The stereoisomers of the racemic ester **36r** are able to bind the CB_2R, so no enantioselective recognition is observed for this ligand. Although both enantiomers [*(S)* and *(R)*] bind CB_2R, the affinity of the *(S)* enantiomers is clearly superior. Therefore, the *(S)* enantiomer of ester **35m** exhibits enantiospecific recognition at CB_2R (K_i = 121 nM) and no affinity towards CB_1R. All the esters tested are *N*-methyl derivatives (R^2 = Me), while differ in the group at R^3 (*t*-Bu or Ph), R^1 (4-F-Bn or CH_2Cy) and the alkoxy residue in the ester function (R^5 = Me or *i*-Pr).

The SAR data emerging from stereoisomers of the analyzed amide subset seem to be more complex than the ones observed for esters. Thus, the *(S)* stereoisomers of the amides **37r** and **37n** exhibit enantiospecific recognition at CB_2R (K_i = 113 nM and 18.4 nM, respectively, > 100-fold selectivity over CB_1R). On the other hand, both stereoisomers of **37f** and **38r** (although differing in R^1, R^2 and R^4) reproduced the same behavior observed for the ester **36r**. Thus, both enantiomers are able to bind CB_2R and the *(S)* stereoisomer eliciting superior affinity (K_i = 60.1 nM and 21.8 nM, respectively) towards CB_2R.

USC UNIVERSIDADE DE SANTIAGO DE COMPOSTELA

The pharmacological data obtained allows us to confirm that three [***(S)*-35m**, ***(S)*-37r** and ***(S)*-38n**] of the new CB_2R-selective agonists discovered in this Chapter show enantiospecific recognition towards the CB_2R. As shown in Figure 58 (and in Table 11) in all cases the most affine stereoisomer (eutomer) corresponds to the (*S*) configuration. The eutomer of **38n,** which exhibits an excellent binding affinity (K_i = 18.4 nM) and complete selectivity at CB_2R, is particularly noteworthy.

Table 11: Affinity and selectivity data obtained for racemates and their corresponding enantiomers.



CODE	R^1	R^2	R^3	X	CB_1R K_i (nM) or % at 1 μM[a)]	CB_2R K_i (nM) or % at 1 μM[a)]	SI[b)] K_i CB_1R/ K_i CB_2R
(±)-35m	4-F-Bn	Me	Ph	OMe	28%	**216 nM**	**>100**
(*S*)-35m	4-F-Bn	Me	Ph	OMe	40%	**121 nM**	**>100**
(*R*)-35m	4-F-Bn	Me	Ph	OMe	11%	**652 nM**	**>100**
(±)-37f	4-F-Bn	H	*t*-Bu	NH-*t*-Bu	36%	**98.7 nM**	**>100**
(*S*)-37f	4-F-Bn	H	*t*-Bu	NH-*t*-Bu	39%	**60.1 nM**	**>100**
(*R*)-37f	4-F-Bn	H	*t*-Bu	NH-*t*-Bu	15%	**343 nM**	**>100**
(±)-37r	4-F-Bn	Me	*t*-Bu	NH-Bn	27%	**204 nM**	**>100**
***(S)*-37r**	4-F-Bn	Me	*t*-Bu	NH-Bn	22%	**113 nM**	**>100**
***(R)*-37r**	4-F-Bn	Me	*t*-Bu	NH-Bn	19%	23%	**-**
(±)-36r	CH_2-Cy	Me	*t*-Bu	O-*i*-Pr	30%	**114 nM**	**>100**
***(S)*-36r**	CH_2-Cy	Me	*t*-Bu	O-*i*-Pr	34%	**109 nM**	**>100**
***(R)*-36r**	CH_2-Cy	Me	*t*-Bu	O-*i*-Pr	26%	**156 nM**	**>100**
(±)-38n	CH_2-Cy	Me	*i*-Pr	NH-*t*-Bu	30%	**40.9 nM**	**>100**
(*S*)-38n	CH_2-Cy	Me	*i*-Pr	NH-*t*-Bu	13%	**18.4 nM**	**>100**
(*R*)-38n	CH_2-Cy	Me	*i*-Pr	NH-*t*-Bu	18%	18%	-
(±)-38r	CH_2-Cy	Me	*t*-Bu	NH-Bn	26%	**108 nM**	**>100**
***(S)*-38r**	CH_2-Cy	Me	*t*-Bu	NH-Bn	47%	**21.8 nM**	**>100**
***(R)*-38r**	CH_2-Cy	Me	*t*-Bu	NH-Bn	23%	**324 nM**	**>100**
Surinabant	-	-	-	-	3.00 nM	400 nM	-
GW405833	-	-	-	-	4772 nM	5.80 nM	-

[a)] Displacement of specific [^{3}H]-CP 55,940 binding in human HEK cells expressed as K_i in nM (n = 3) or percentage displacement of specific binding at a concentration of 1 μM (n = 2). [b)] Selectivity index is the ratio between K_i CB_1R and K_i CB_2R.

USC UNIVERSIDADE DE SANTIAGO DE COMPOSTELA

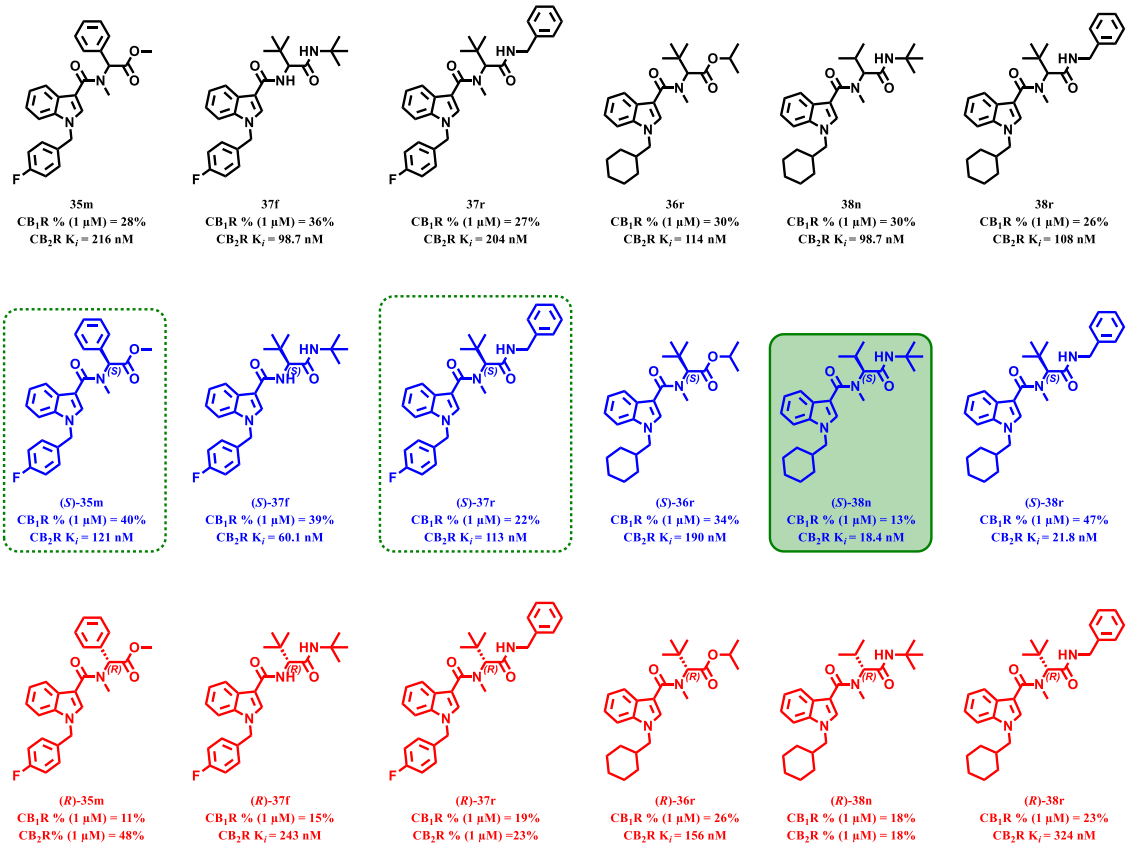


Figure 58: Racemic and enantiomer affinity data of the selected CB_2R-selective ligands.

The comparison with their closest analogues in the SCRA series allows us to verify that the structural modifications we have performed enabled us not only to obtain CB_2R selective ligands, but also to identify novel compounds with enantiospecific recognition at the CB_2R.

USC UNIVERSIDADE DE SANTIAGO DE COMPOSTELA

Preliminary docking simulation studies.

During the development of this Chapter, we have discovered potent and selective CB_2R ligands, observed structure-activity relationship trends in these series, and identified the most decisive groups for inducing selectivity against CB_2R. As we have mentioned, the structural modifications that have the greatest effect on potency and selectivity are the introduction of a carbonated group in the terminal amide (R^4), particularly a *t*-Bu group, and the methylation of the nitrogen of the amide function (R^2) attached to the heterocyclic ring. These modifications have consistently shown to decrease affinity for CB_1R and CB_2R, with the negative effect being much more significant on CB_1R, thereby generating selective compounds. In order to verify these trends at different levels, we have selected model compounds and compared their affinity, either as racemic mixtures or as enantiopure compounds. These comparisons are shown in Figure 59 and Figure 60, respectively.

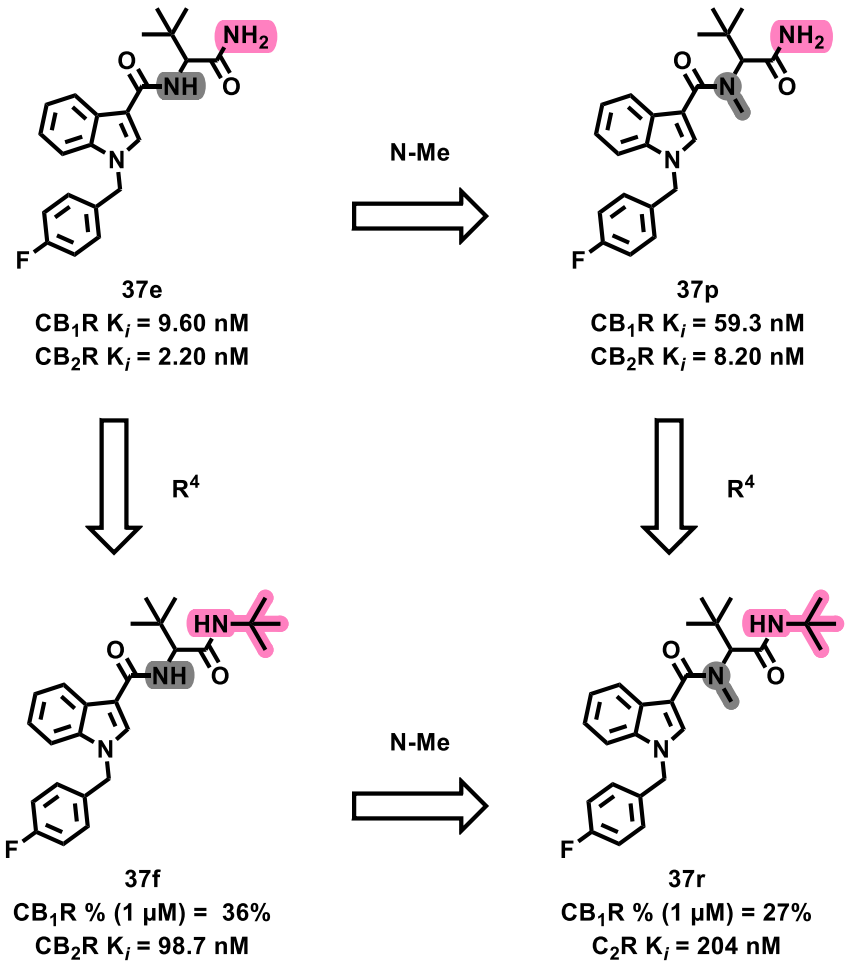


Figure 59: Structure and binding data of compounds **37e**, **37p**, **37f** and **37r**.

USC UNIVERSIDADE DE SANTIAGO DE COMPOSTELA

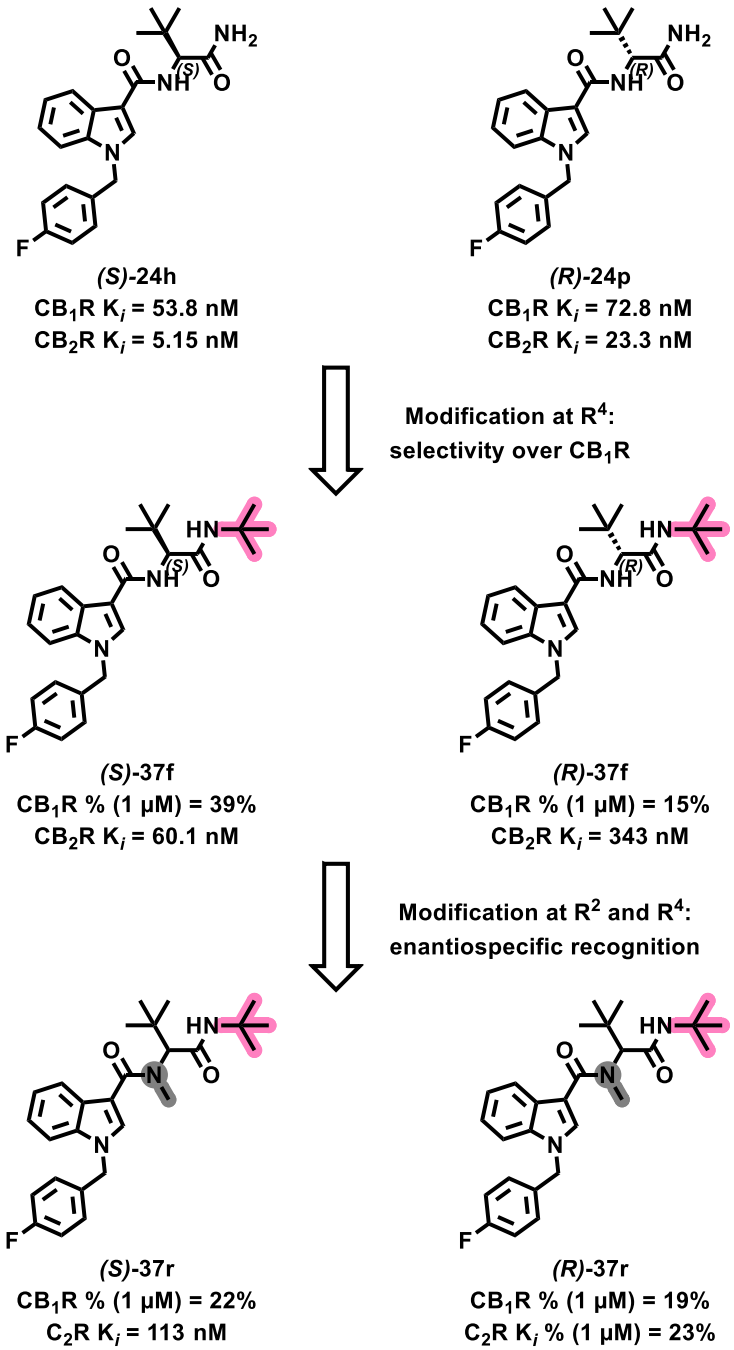


Figure 60: Structure and binding data of compounds **24h**, **24p**, **(S)-37f**, **(R)-37f**, **(S)-37r** and **(R)-37r.**

The selected compounds (Figure 59 and Figure 60) allow for both a general (racemic) and a more specific (enantiomers) evaluation of the impact of variations in R^2 and R^4 on affinity. To obtain preliminary information on the molecular basis underlying the pharmacological data and SAR trends obtained, we decided to perform simple docking studies using the enantiomers from Figure 60.

It should be pointed out that the study and the detailed interpretation of the obtained SAR trends employing computational methods go beyond the scope of this

USC UNIVERSIDADE DE SANTIAGO

Doctoral Thesis. These studies are currently in progress in collaboration with the group of Dr. Giuseppe Mangiatordi from CNR - Institute of Crystallography (Bari, Italy). The docking simulation studies were performed on representative indole derivatives (Cpds: **24h**, **24p**, *(S)*-**37f**, *(R)*-**37f**, *(S)*-**37f**, *(R)*-**37f**, *(S)*-**37r**, *(R)*-**37r**, *(S)*-**37r** and *(R)*-**37r**, Figure 60).

For the *in silico* experiments we used the reported models of the crystal structures for CB_1R (PDB: 5TGZ) and CB_2R (PDB: 5ZTY). The proposed binding mode of each compound was explored through iterative optimizations using the Schrödinger Maestro program until the most favorable binding pose was identified (Figure 61 and Figure 62).

Figure 61 and Figure 62 display the proposed binding modes of the six ligands studied in CB_1R and CB_2R, respectively. In these figures, favorable interactions are represented by blue dashed lines, while repulsive or non-favored interactions are indicated by orange dashed lines. Specific repulsive interactions resulting from significant steric clashes, which are responsible for the poor binding data, are denoted by a black dashed circle. As observed, the obtained binding modes agree with the obtained pharmacological data and SAR observations. As shown in Figure 61 and Figure 62, small but important differences exist in the orthosteric binding site of CB_1R and CB_2R that constitute the structural basis for the identification of selective ligands. However, in both receptors, towards the inner side, there are aromatic amino acids (e.g., phenylalanine and tryptophan) able to stabilize in both cases the aromatic rings of the explored compounds.

To perform a preliminary comparative exploration of the binding mode, three pairs of enantiomers were selected: **24h**/**24p**, (*S*)-**37f**/(*R*)-**37f**, and (*S*)-**37r**/(*R*)-**37r**. These pairs allow us to investigate three different points of diversity: the stereochemistry, the terminal amide substitution (R^4), and methylation at R^2 (Figure 60). Focusing on the **24h** and **24p** pair (R^2 = H, R^4 = H, Figure 61A-B and Figure 62A-B), we observed a distinct behavior: the (*S*) enantiomer (**24h**, CB_1R K_i = 53.8 nM, CB_2R K_i = 5.15 nM) displayed better affinity values compared to the (*R*) enantiomer (**24p**, CB_1R K_i = 72.8 nM, CB_2R K_i = 23.3 nM). At CB_1R, both enantiomers formed a hydrogen bond with $Met^{N\text{-}term}$, along with two π-π interactions with Phe^{ECL2} and $Trp^{5.43}$ (Figure 61A-B). However, the spatial conformation of **24p** caused collisions within the binding site ($Trp^{6.48}$, Figure 61B). At CB_2R, the same π-π interactions were conserved, but both enantiomers were able to form two different hydrogen bonds, one with Leu^{ECL2} (e.g.,

24h, Figure 62A) and one with $Ser^{2.60}$ (e.g., **24p**, Figure 62B). As mentioned earlier, the introduction of a substituent in the terminal amide (R^4) caused a change in selectivity, completely eliminating the affinity for CB_1R and slightly decreasing the affinity for CB_2R (Figure 59 and Figure 60).

A good example illustrating this behavior is compound **37f** and its enantiomers (Figure 59 and Figure 60, Figure 61C-D and Figure 62C-D). Both enantiomers show no affinity for CB_1R (39% and 15% radioligand displacement at 1 μM) while retaining good to moderate affinity for CB_2R [(*S*)-**37f** K_i = 60.1 nM and (*R*)-**37f** K_i = 343 nM]. The introduction of a *t*-Bu group at R^4 hinders binding to CB_2R by significantly increasing clashes with the orthosteric binding site (Figure 62C-D, highlighted in orange). In this case, the difference between the two enantiomers becomes more pronounced due to the increased steric hindrance with the amide substitution. The (*S*) enantiomer fits well, while clashes occur with $Ser^{2.60}$ in the case of the (*R*) enantiomer. When a methyl group is introduced at R^2 in addition to the substitution at R^4 (compound **37r**, Figure 59 and Figure 60), the selectivity profile is maintained, but only the (*S*) enantiomer retains affinity. As shown in Figure 62E-F, clashes with CB_1R are still present, and in the case of the (*R*) enantiomer, collisions with the receptor are further increased. This may be attributed to the stabilization of a specific structural conformation (Figure 62E-F), favoring clashes between *t*-Bu groups and amino acids such as $Phe^{7.35}$ and $Phe^{N\text{-}term}$.

The preliminary docking studies provide a first approach to the rationale understanding of the experienced binding data and SAR trends within the series. These observations allow us to draw the following conclusions: stereochemistry plays a significant role in the affinity of the enantiomers. The (*S*) enantiomer generally displayed better affinity values compared to the (*R*) enantiomer. At CB_1R, both enantiomers formed a hydrogen bond with $Met^{N\text{-}term}$, along with π-π interactions with Phe^{ECL2} and $Trp^{5.43}$. However, the spatial conformation of the (*R*) enantiomer caused collisions within the binding site, potentially affecting its binding affinity. At CB_2R, both enantiomers maintained the π-π interactions, but they formed different hydrogen bonds. The (*S*) enantiomer interacted with Leu^{ECL2}, while the (*R*) enantiomer formed a hydrogen bond with $Ser^{2.60}$. The introduction of a substituent in the terminal amide (R^4) led to a change in selectivity, eliminating the affinity for CB_1R and slightly decreasing the affinity for CB_2R. These conclusions highlight the importance of stereochemistry, specific interactions, and the impact of structural modifications on the affinity and

USC UNIVERSIDADE DE SANTIAGO DE COMPOSTELA

selectivity of the ligands towards CB_1R and CB_2R. Further studies (computational and experimental) and new collaborations are now in progress to unequivocally validate these data by using advanced biophysical mapping studies and obtaining a co-crystal of our ligands with the CB_2R (X-ray crystallography or CryoEM).

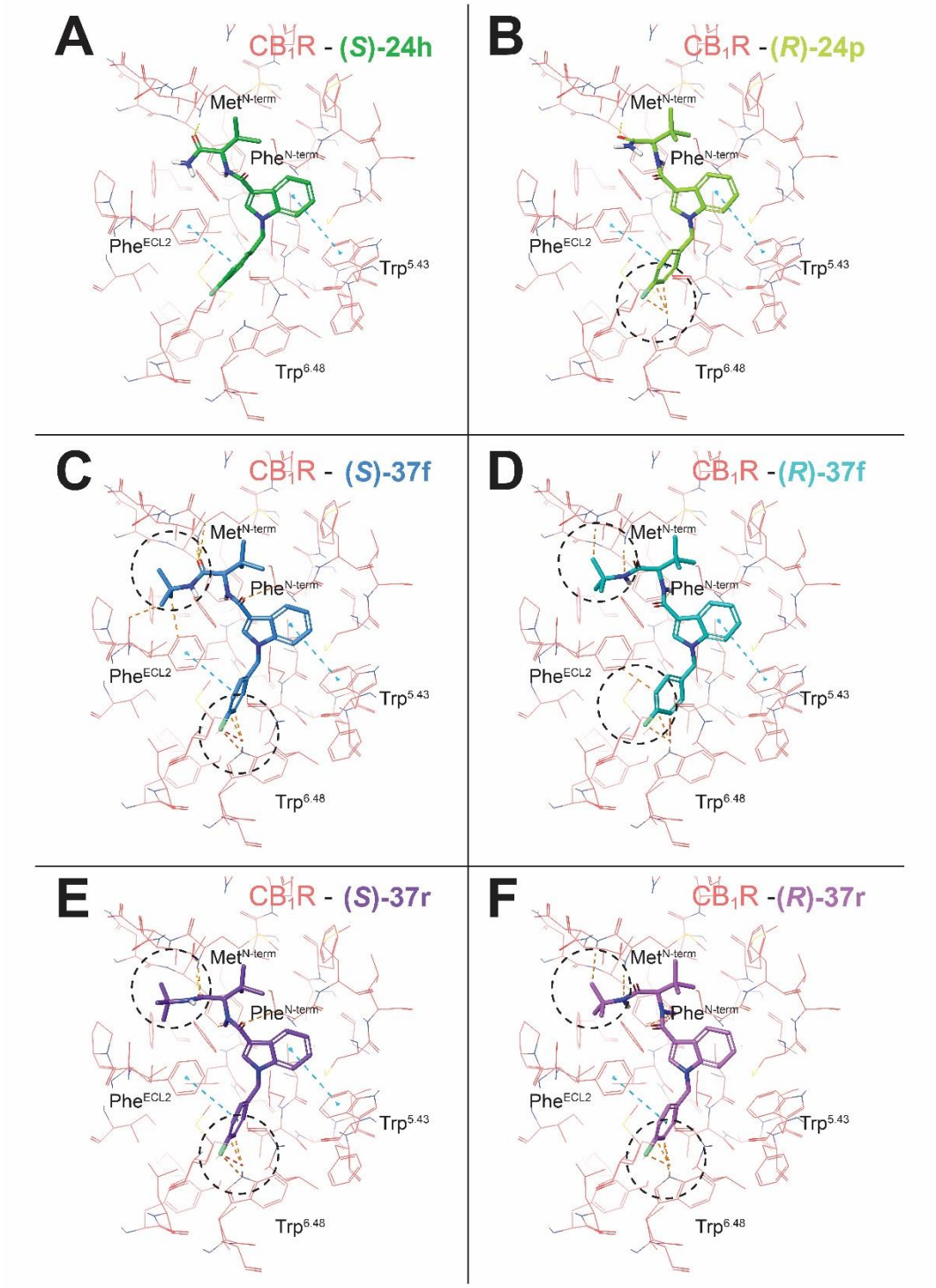


Figure 61: Docking-predicted binding mode of A) **24h** at CB_1R, B) **24p** at CB_1R, *C*) (*S*)-**37f** at CB_1R, *D*) (*R*)-**37f** at CB_1R, *E*) (*S*)-**37*r*** at CB_1R, *F*) (*R*)-**37*r*** at CB_1R. CB_1R and CB_2R 3D structures are PDB: 5TGZ and 5ZTY respectively. Yellow dashed lines: hydrogen bonds, blue dashed lines: π-π interactions, orange and red dashed lines: bad contacts (highlighted in orange).

USC UNIVERSIDADE DE SANTIAGO DE COMPOSTELA

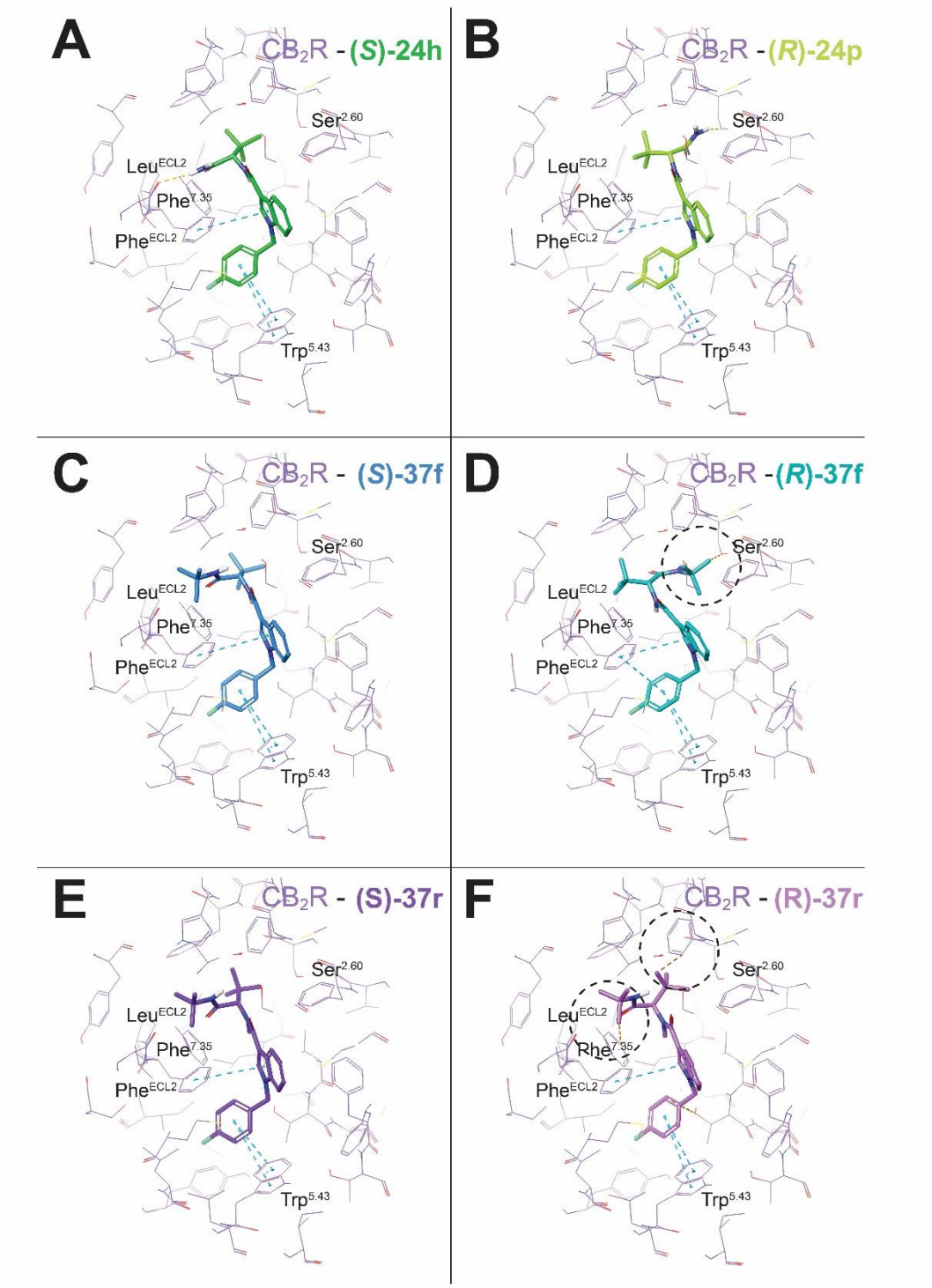


Figure 62: Docking-predicted binding mode of A) **24h** at CB_2R, B) **24p** at CB_2R, *C*) (*S*)-**37f** at CB_2R, *D*) (*R*)-**37f** at CB_2R, *E*) (*S*)-**37*r*** at CB_2R, *F*) (*R*)-**37*r*** at CB_2R. CB_1R and CB_2R 3D structures are PDB: 5TGZ and 5ZTY respectively. Yellow dashed lines: hydrogen bonds, blue dashed lines: π-π interactions, orange and red dashed lines: bad contacts (highlighted in orange).

USC UNIVERSIDADE DE SANTIAGO DE COMPOSTELA

USC
UNIVERSIDADE
DE SANTIAGO
DE COMPOSTELA

3.3 CHAPTER 3. EXPLORATION OF THE EFFECT OF THE GROUP AT R^3 ON THE AFFINITY AND SELECTIVITY

The Ugi-based approach developed in Chapter 2 has demonstrated the capability and versatility of the Ugi reaction for the design and the synthesis of a SCRA-like library, thus enabling the identification of novel, potent and CB_2R selective ligands. The aim of this Chapter is to investigate unexplored moieties at R^3, since the influence of this group for the affinity at CB_2R has been demonstrated (see Chapter 2).

The general structure of the new series obtained is presented in Figure 63. This approach enables to investigate not only the position R^3, but also the positions R^1 and R^2 at both esters and amides. For the sake of simplicity, during this study, the groups at R^4 (amides) and at R^5 (esters) have not been modified. The position R^5 has been briefly investigated in Chapter 2, while a more exhaustive study of the position R^4 will be explored within Chapter 4. We have then selected a subset of twelve carbonyl compounds (nine aldehyde and three ketones) to accomplish the indicated aim (Scheme 5-6).

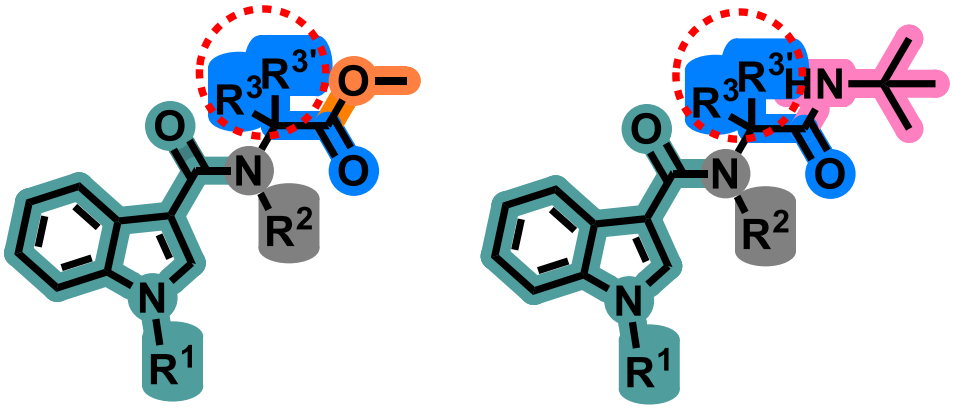


Figure 63: General structure and diversity explored at esters and amides obtained in this Chapter.

USC
UNIVERSIDADE DE SANTIAGO DE COMPOSTELA

Chemistry. These series of novel ligands herein described have been synthetized employing the Ugi reaction. The Ugi four component reaction (U4CR) is a multicomponent reaction that involves an acid, a carbonyl component (aldehyde or ketone), an amine and an isonitrile to form a bis-amide in one single reaction step (Figure 64).[127,132]

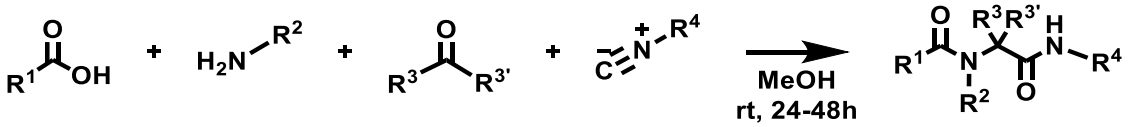


Figure 64: The Ugi reaction.

A brief description of the mechanism of the Ugi reaction and the modification that enable the synthesis of the ester analogues have been documented in Chapter 2. A detailed description of the synthetic methods and the complete structural, spectroscopic, and analytical data for all compounds are provided in the Experimental Section.

Design and synthesis of amides and esters. In this Chapter, the exploration of the effect of the R^3 group has been further investigated in both ester (**39** and **40**) and amide (**41** and **42**) series. Twelve carbonyl compounds (Scheme 5, Scheme 6), nine aldehydes and three ketones, were selected for this study. Unexplored groups [*i*-Bu, 4,4-DMPN (4,4-dimethylaminopentanitrile), *c*-Pr, *c*-Bu, Cyp (Cyclopentyl), together with the groups investigated in Chapter 2] were proposed to examine the effect of these structural modifications on the CBR affinity and selectivity profile. At R^2, the H and Me substitutions have been maintained in order to comparatively study the influence of this substitution. With the aim of simplicity, we decided to fix at the terminal amide (R^4) a *t*-Bu group that produced better CB_2R selectivity profile in the previous Chapter.

As depicted in Figure 65, the herein proposed synthetic method permits the rapid assembly of ester (Cpds **39** and **40**) and amide (Cpds **41**, **42** and **43**) libraries. The obtained collection contains 48 new derivatives (20 esters and 28 amides) bearing several previously unexplored substitution patterns in the SCRA-like series. The diversity space explored (R^1, R^2, R^3 and $R^{3'}$) during this study is presented in Figure 65.

USC UNIVERSIDADE DE SANTIAGO DE COMPOSTELA

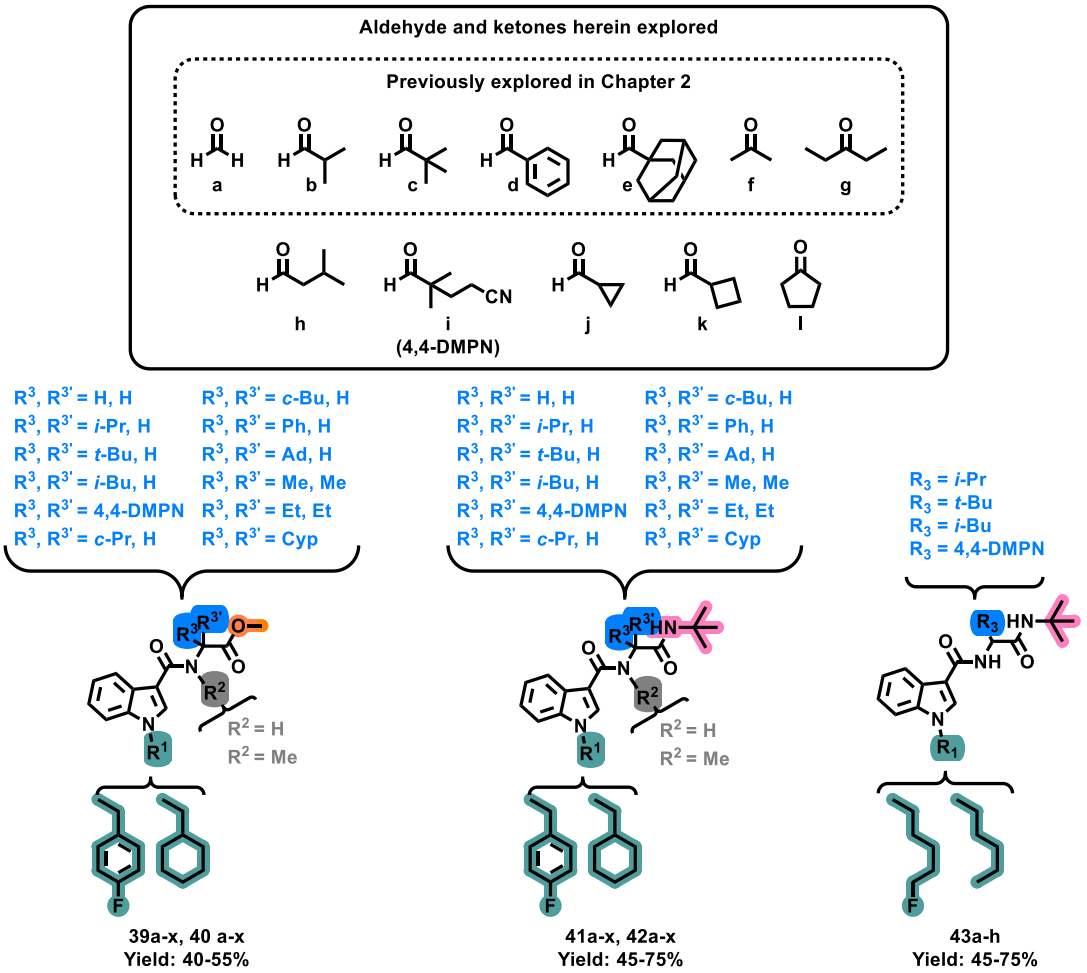
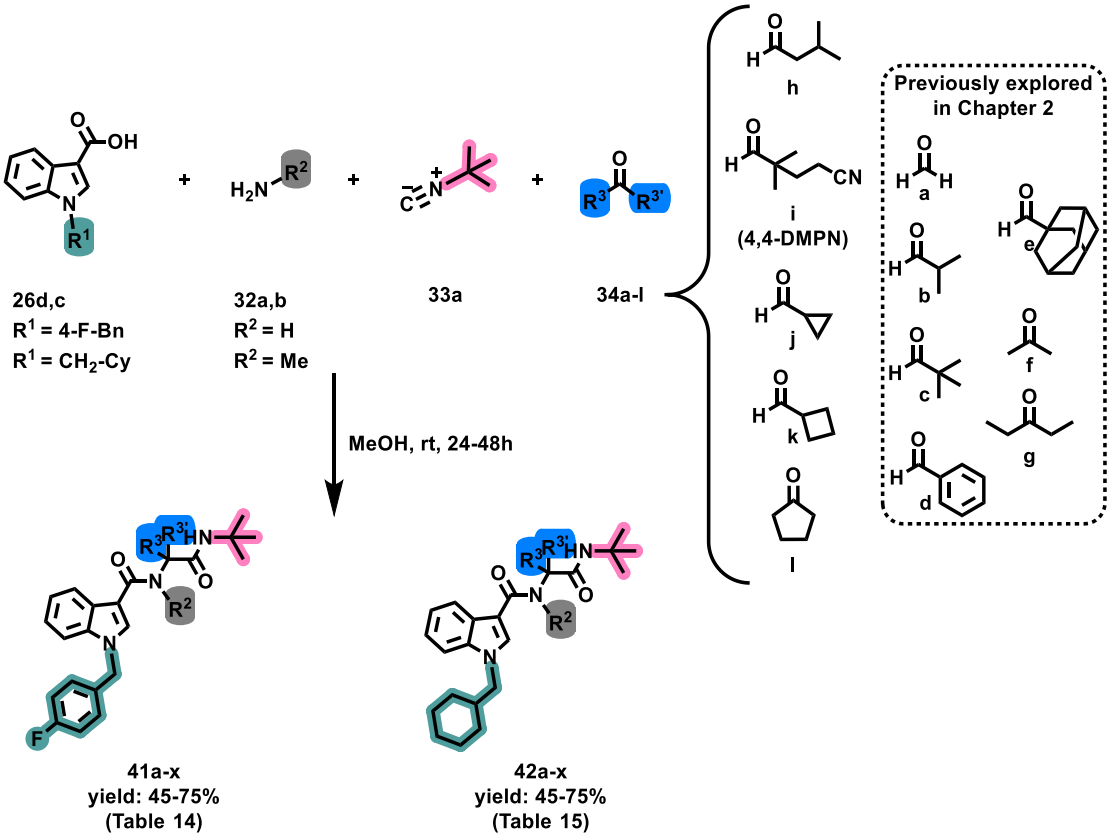


Figure 65: General structure and diversity space explored in this Chapter for ester (**39** and **40**) and amide (**41, 42** and **43**) series.

As shown in Scheme 5, the Ugi adducts (Cpds **41** and **42**) were obtained in moderate to satisfactory yields (45-75%) as racemic mixtures. The reactions were performed in sealed Kimble vials using methanol as solvent and, once finished, quenched, and elaborated to isolate and purify the corresponding Ugi adducts as described in the Experimental Section.

Figure 66 shows the ^{1}H-NMR spectra obtained during the spectroscopic characterization of a representative compound of this series.

USC UNIVERSIDADE DE SANTIAGO DE COMPOSTELA



Scheme 5: Ugi-based assembly of targeted amides **41a-x** and **42a-x**.

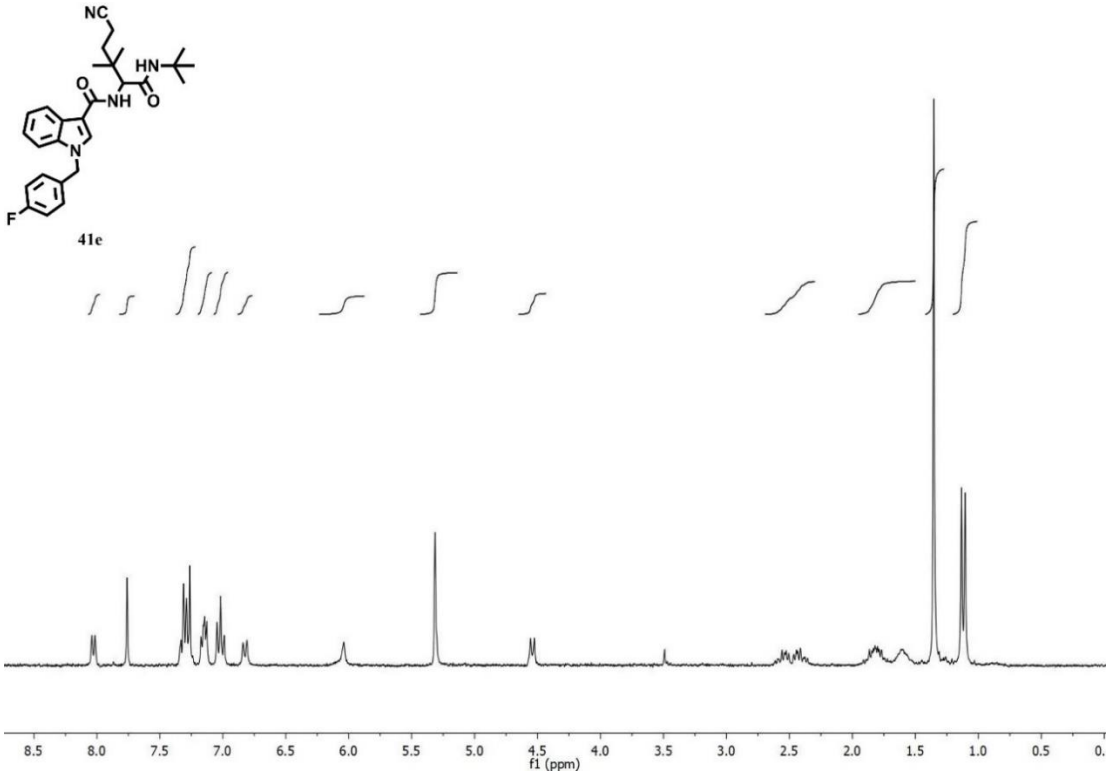
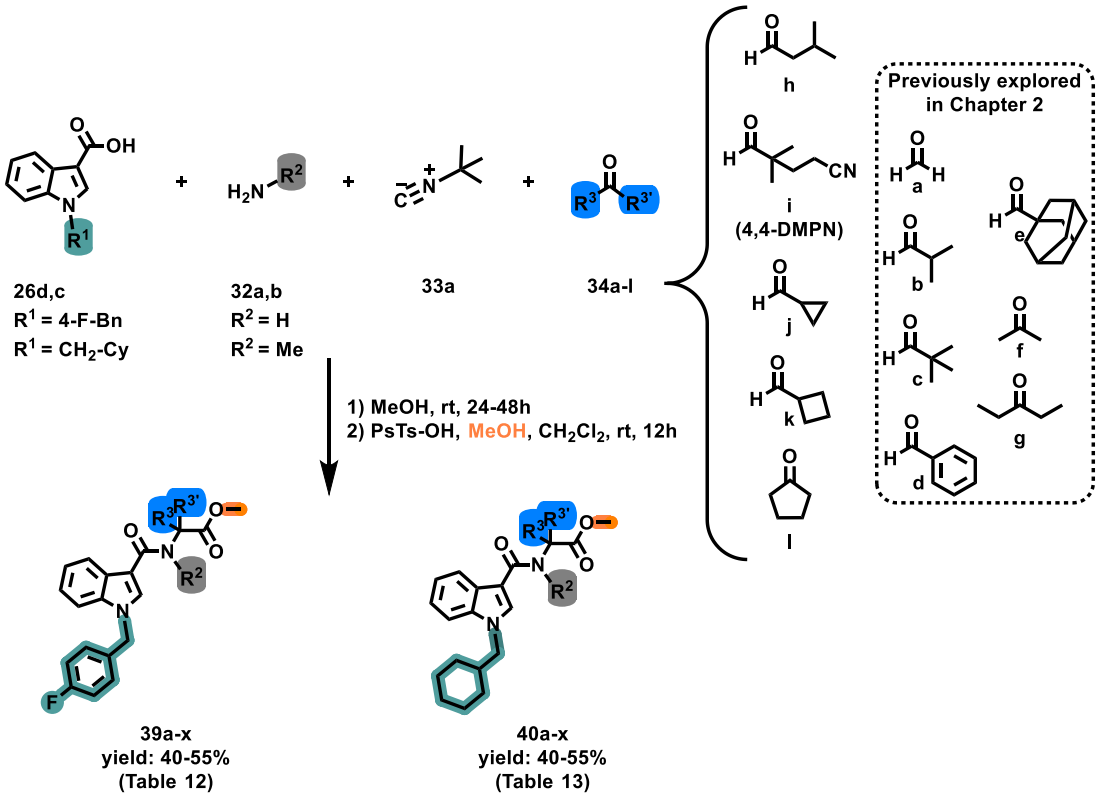


Figure 66: ^{1}H-NMR spectra of compound **41e**.

In the ester series, the same approach employed in Chapter 2 has been used. As observed (Scheme 6) the methyl group at R^5 has been mainteined during the study. The previously unexplored moieties have been investigated at R^3 and $R^{3'}$, within the modification at R^1 and R^2.

As shown in Scheme 6, the Ugi adducts (Cpds **39** and **40**) were obtained in moderate to satisfactory yields (40-55%). The mechanism operating during the solvolysis (alcoholysis) reaction has been described in literature and pointed out in Chapter 2. The reactions were performed in sealed Kimble vials using methanol as solvent and, once finished, quenched, and elaborated to isolate and purify the corresponding ligands **39** and **40** as described in the Experimental Section.

Figure 67 shows the ^{1}H-NMR spectra obtained during the spectroscopic characterization of a representative compound of this series.



Scheme 6: Ugi-based assembly of amides **39a-x** and **40a-x**.

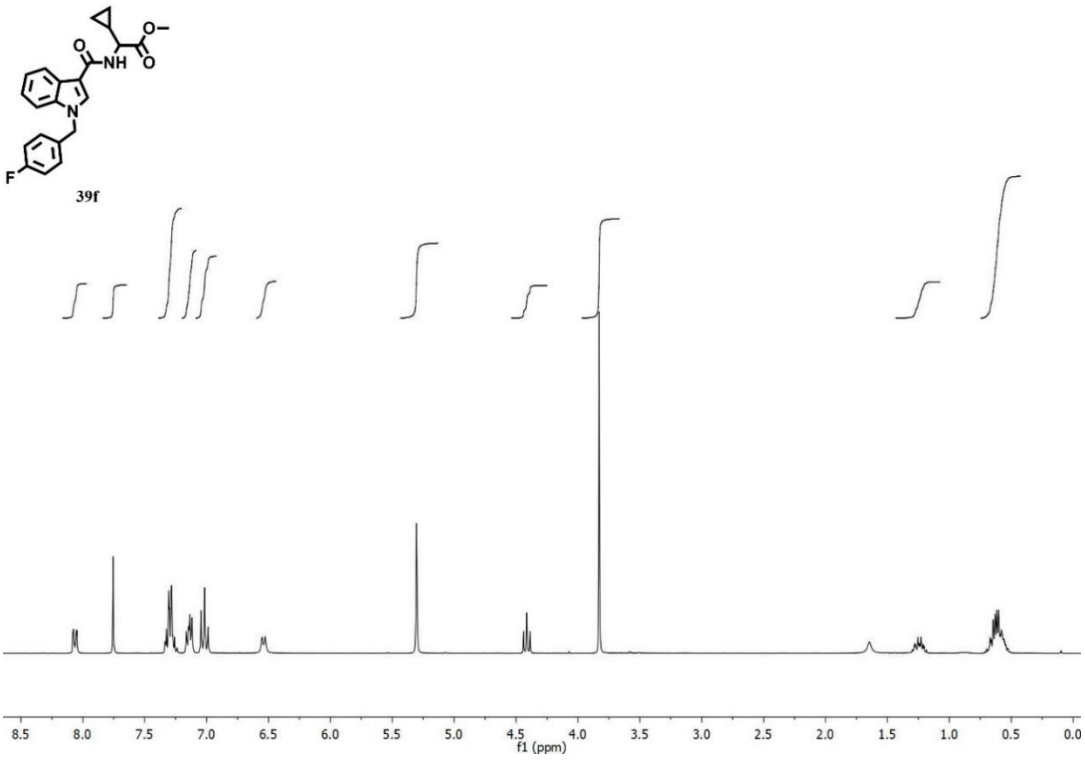
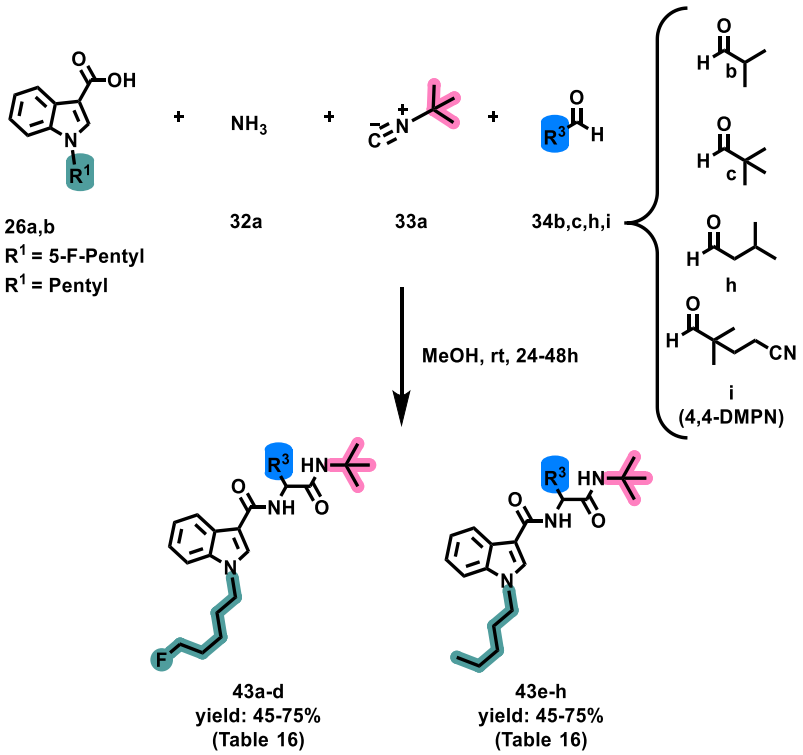


Figure 67: ^{1}H-NMR spectra of compound **39f**.

To better understand the influence of R^1 in the amide series, an exploratory subset of ligands has been designed and synthetized (Scheme 7, cpds **43a-d** and **43e-h**), these derivatives bear two different R^1 group: 5-F-pentyl and pentyl. Capitalizing the information learned in previous series, the best groups at R^3 (*i*-Pr, *t*-Bu, *i*-Bu, 4,4-DMPN) have been introduced to improve CB_2R selectivity, while at R^2 the hydrogen atom has been maintained. As shown in Scheme 7, the Ugi adducts were obtained in moderate to satisfactory yield (45-75%). As in the previous Chapter, the reactions were performed in sealed Kimble vials using methanol as solvent and were monitored by thin-layer chromatography (TLC). After completion of the reaction, catch procedure (or acid-catalyzed solvolysis) was performed as indicated in the Experimental Section. Then, the solvent was evaporated to dryness and the isolated solid/oil was purified by column chromatography on silica gel or preparative chromatography. A detailed description of the synthetic methods and the complete structural, spectroscopic, and analytical data for all compounds are provided in the Experimental Section.

Figure 68 shows the ^{1}H-NMR spectra obtained during the spectroscopic characterization of a representative compound of this series.

USC UNIVERSIDADE DE SANTIAGO DE COMPOSTELA



Scheme 7: Ugi-based assembly of amides **43a-h.**

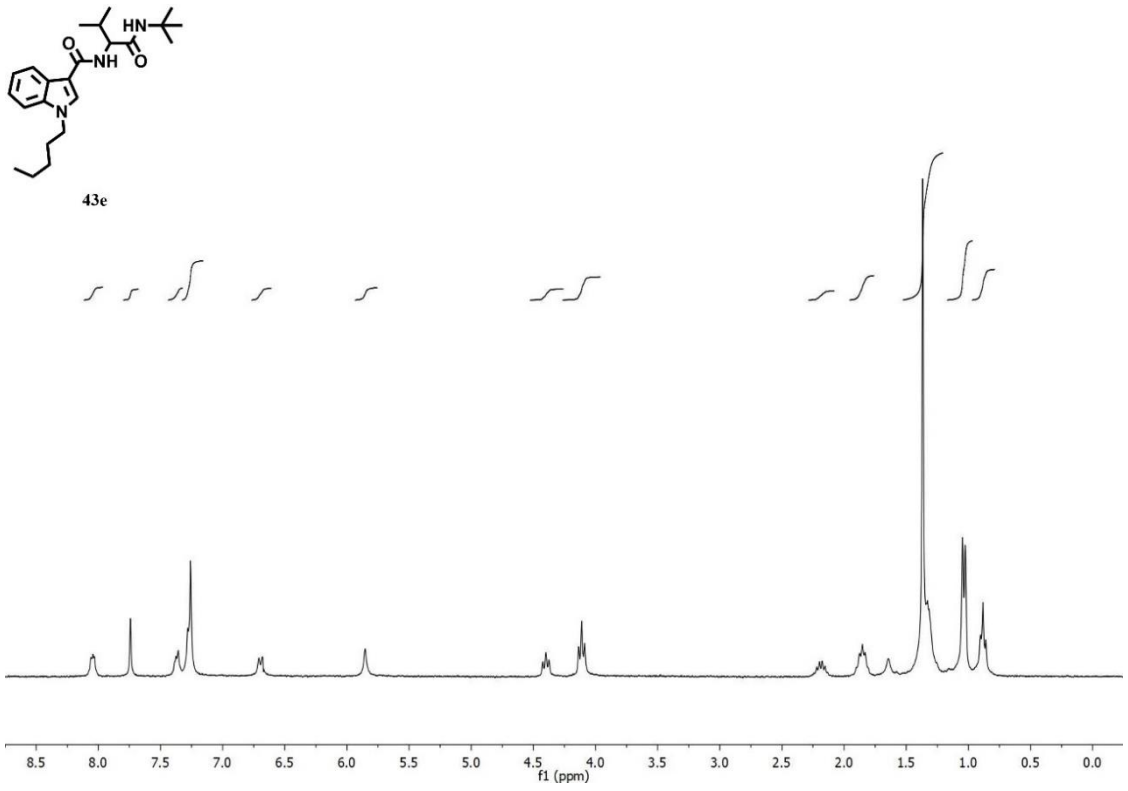


Figure 68: ^{1}H-NMR spectra of compound **43e.**

USC UNIVERSIDADE DE SANTIAGO DE COMPOSTELA

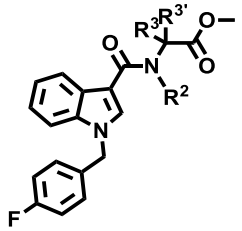
Biological Evaluation. The affinity and selectivity of the novel indole-based compounds were evaluated *in vitro* using radioligand binding assays at the two human CBR subtypes. Tables 12-16 contain the binding data obtained. All ligands reported in Tables 12-16 were obtained and tested as racemic mixtures. The experiments were performed *in vitro* on transfected HEK-293T cells and [^{3}H]-CP 55,940 was employed as radioligand. The binding data is presented as K_i ± SEM (nM, n = 3) or as specific binding inhibition percentage at 1 μM (n = 2, mean) for those compounds which do not reach a minimum of 60% of radioligand displacement at such concentration. Prism 5.0 software (GraphPad, San Diego, CA) was employed for data analysis. The K_i values were acquired by fitting the data by non-linear regression.

Results are the average of three experiments, each performed in duplicate. Two of well-known CBR ligands [Surinabant (CB_1R antagonist) and GW405833(CB_2R agonist)] were assessed using our experimental protocols, their binding data is reported in Tables 12-16 for comparative purposes. With the aim of facilitating the comparison of the effect of R^1, R^3 and R^4 on binding affinity, we decided to include in Tables 12-16 the data obtained for some derivatives described in Chapter 2 (indicated in tables with an asterisk).

In order to facilitate the analysis of the obtained data, those ligands eliciting high CB_2R selectivity are highlighted across the tables (bold).

USC UNIVERSIDADE DE SANTIAGO DE COMPOSTELA

Table 12: Affinity and selectivity data obtained for esters **39a-x**.

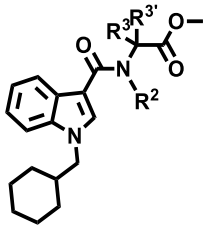


CODE	R^2	R^3	$R^{3'}$	CB_1R	CB_2R	SI[b] K_i CB_1R/ K_i CB_2R
				K_i (nM) or % (1 μM)[a]	K_i (nM) or % (1 μM)[a]	
39a*	H	H	H	181 nM	125 nM	1.4
39b*	H	*i*-Pr	H	81.6 nM	43.4 nM	1.9
39c*	H	*t*-Bu	H	2.70 nM	2.09 nM	1.3
39d	H	*i*-Bu	H	144 nM	98.6 nM	1.5
39e	H	4,4-DMPN	H	62.4 nM	31.3 nM	2.0
39f	H	*c*-Pr	H	46.6 nM	31.5 nM	1.5
39g	H	*c*-Bu	H	53.4 nM	17.4 nM	3.1
39h*	H	Ph	H	61.5 nM	68 nM	0.9
39i*	H	Ad	H	29%	**188 nM**	**>100**
39j*	H	Me	Me	29 nM	17.2 nM	1.7
39k*	H	Et	Et	2.33 nM	0.88 nM	2.6
39l	H	Cyp		19.5 nM	7.10 nM	2.7
39m*	Me	H	H	33%	28%	-
39n*	Me	*i*-Pr	H	14%	48%	-
39o*	Me	*t*-Bu	H	119 nM	7.26 nM	16.4
39p	Me	*i*-Bu	H	23%	16%	-
39q	Me	4,4-DMPN	H	37%	**243 nM**	**>100**
39r	Me	*c*-Pr	H	213 nM	101 nM	2.1
39s	Me	*c*-Bu	H	29%	47%	-
39t*	Me	Ph	H	28%	**216 nM**	**>100**
39u*	Me	Ad	H	9%	37%	-
39v*	Me	Me	Me	95.9 nM	14.5 nM	6.6
39w*	Me	Et	Et	11%	21%	-
39x	Me	Cyp		803 nM	471 nM	1.7
Surinabant	-	-	-	3.00 nM	400 nM	-
GW405833	-	-	-	4772 nM	5.80 nM	-

[a] Displacement of specific [^{3}H]-CP 55,940 binding in human HEK cells expressed as K_i in nM (n = 3) or percentage displacement of specific binding at a concentration of 1 μM (n = 2). [b] Selectivity index is the ratio between K_i CB_1R and K_i CB_2R. *These compounds were described in Chapter 2.

USC UNIVERSIDADE DE SANTIAGO DE COMPOSTELA

Table 13: Affinity and selectivity data obtained for esters **40a-x**.

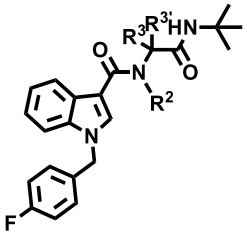


CODE	R^2	R^3	$R^{3'}$	CB_1R	CB_2R	SI[b] K_i CB_1R/ K_i CB_2R
				K_i (nM) or % (1 μM)[a]	K_i (nM) or % (1 μM)[a]	
40a*	H	H	H	68.2 nM	71.7 nM	1.0
40b*	H	*i*-Pr	H	32.4 nM	7.5 nM	4.3
40c*	H	*t*-Bu	H	1.40 nM	0.35 nM	4.0
40d	H	*i*-Bu	H	15.7 nM	8 nM	2.0
40e	H	4,4-DMPN	H	56.0 nM	5.5 nM	10.2
40f	H	*c*-Pr	H	7.4 nM	25.4 nM	0.3
40g	H	*c*-Bu	H	12.6 nM	4.70 nM	2.7
40h*	H	Ph	H	25.1 nM	43.2 nM	0.6
40i*	H	Ad	H	23%	29%	-
40j*	H	Me	Me	22.3 nM	6.70 nM	3.3
40k*	H	Et	Et	13.2 nM	1.40 nM	9.4
40l	H	Cyp		8.30 nM	3.70 nM	2.2
40m*	Me	H	H	33%	28%	-
40n*	Me	*i*-Pr	H	92.4 nM	51.4 nM	1.8
40o*	Me	*t*-Bu	H	46.8 nM	25.9 nM	1.8
40p	Me	*i*-Bu	H	26%	**98.1 nM**	**>100**
40q	Me	4,4-DMPN	H	30%	**143 nM**	**>100**
40r	Me	*c*-Pr	H	90.6 nM	65.8 nM	1.4
40s	Me	*c*-Bu	H	44%	55%	-
40t*	Me	Ph	H	167 nM	89.9 nM	1.9
40u*	Me	Ad	H	2%	39%	-
40v*	H	Me	Me	47.0 nM	31.2 nM	1.5
40w*	H	Et	Et	22%	**301 nM**	**>100**
40x	H	Cyp		121 nM	164 nM	0.7
Surinabant	-	-	-	3.00 nM	400 nM	-
GW405833	-	-	-	4772 nM	5.80 nM	-

[a] Displacement of specific [^{3}H]-CP 55,940 binding in human HEK cells expressed as K_i in nM (n = 3) or percentage displacement of specific binding at a concentration of 1 μM (n = 2). [b] Selectivity index is the ratio between K_i CB_1R and K_i CB_2R. *These compounds were described in Chapter 2.

USC UNIVERSIDADE DE SANTIAGO DE COMPOSTELA

Table 14: Affinity and selectivity data obtained for amides **41a-x**.

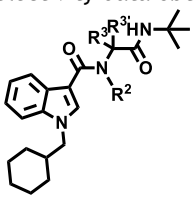


CODE	R^2	R^3	$R^{3'}$	CB_1R	CB_2R	SI[b]
				K_i (nM) or % (1 μM)[a]	K_i (nM) or % (1 μM)[a]	K_i CB_1R/ K_i CB_2R
41a*	H	H	H	281 nM	93.8 nM	3.0
41b*	H	*i*-Pr	H	16%	**276 nM**	**>100**
41c*	H	*t*-Bu	H	36%	**98.7 nM**	**>100**
41d	H	*i*-Bu	H	12%	40%	-
41e	H	4,4-DMPN	H	30%	**191 nM**	**>100**
41f	H	*c*-Pr	H	27%	**1800 nM**	**>100**
41g	H	*c*-Bu	H	3%	10%	-
41h*	H	Ph	H	17%	23%	-
41i*	H	Ad	H	1%	37%	-
41j*	H	Me	Me	31%	29%	-
41k*	H	Et	Et	1%	34%	-
41l	H	Cyp		1%	2%	-
41m*	Me	H	H	1%	19%	-
41n*	Me	*i*-Pr	H	3%	**952 nM**	**>100**
41o*	Me	*t*-Bu	H	3%	32%	-
41p	Me	*i*-Bu	H	2%	33%	-
41q	Me	4,4-DMPN	H	31%	**248 nM**	**>100**
41r	Me	*c*-Pr	H	5%	30%	-
41s	Me	*c*-Bu	H	1%	25%	-
41t*	Me	Ph	H	3%	16%	-
41u*	Me	Ad	H	5%	14%	-
41v*	Me	Me	Me	15%	22%	-
41w*	Me	Et	Et	4%	24%	-
41x	Me	Cyp		5%	3%	-
Surinabant	-	-	-	3 nM	400 nM	-
GW405833	-	-	-	4772 nM	5.8 nM	-

[a] Displacement of specific [^{3}H]-CP 55,940 binding in human HEK cells expressed as K_i in nM (n = 3) or percentage displacement of specific binding at a concentration of 1 μM (n = 2). [b] Selectivity index is the ratio between K_i CB_1R and K_i CB_2R. *These compounds were described in Chapter 2.

USC UNIVERSIDADE DE SANTIAGO DE COMPOSTELA

Table 15: Affinity and selectivity data obtained for amides **42a-x**.

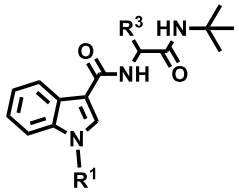


CODE	R^2	R^3	$R^{3'}$	CB_1R K_i (nM) or % (1 μM)[a)]	CB_2R K_i (nM) or % (1 μM)[a)]	SI[b)] K_i CB_1R/ K_i CB_2R
42a*	H	H	H	99.5 nM	51.2 nM	1.9
42b*	H	*i*-Pr	H	28%	**50.2 nM**	**>100**
42c*	H	*t*-Bu	H	35%	**34.8 nM**	**>100**
42d	H	*i*-Bu	H	41%	32%	-
42e	H	4,4-DMPN	H	32%	**100 nM**	**>100**
42f	H	*c*-Pr	H	27%	23%	-
42g	H	*c*-Bu	H	11%	13%	-
42h*	H	Ph	H	28%	31%	-
42i*	H	Ad	H	1%	1%	-
42j*	H	Me	Me	170 nM	176 nM	1.0
42k*	H	Et	Et	25%	**128 nM**	**>100**
42l	H	Cyp		9%	46%	-
42m*	Me	H	H	44%	36%	-
42n*	Me	*i*-Pr	H	30%	**40.9 nM**	**>100**
42o*	Me	*t*-Bu	H	5%	**237 nM**	**>100**
42p	Me	*i*-Bu	H	1%	20%	-
42q	Me	4,4-DMPN	H	3%	**720 nM**	**>100**
42r	Me	*c*-Pr	H	228 nM	653 nM	0.3
42s	Me	*c*-Bu	H	4%	**691 nM**	**>100**
42t*	Me	Ph	H	4%	28%	-
42u*	Me	Ad	H	6%	4%	-
42v*	Me	Me	Me	3%	28%	-
42w*	Me	Et	Et	8%	35%	-
42x	Me	Cyp		35%	43%	-
Surinabant	-	-	-	3 nM	400 nM	-
GW405833	-	-	-	4772 nM	5.8 nM	-

[a)] Displacement of specific [^{3}H]-CP 55,940 binding in human HEK cells expressed as K_i in nM (n = 3) or percentage displacement of specific binding at a concentration of 1 μM (n = 2). [b)] Selectivity index is the ratio between K_i CB_1R and K_i CB_2R. *These compounds were described in Chapter 2.

USC UNIVERSIDADE DE SANTIAGO DE COMPOSTELA

Table 16: Affinity and selectivity data obtained for amides **43a-h**.



CODE	R^1	R^3	CB_1R	CB_2R	SI[b] K_i CB_1R/ K_i CB_2R
			K_i (nM) or % (1 μM)[a]	K_i (nM) or % (1 μM)[a]	
43a	5-F-Pentyl	*i*-Pr	19%	**191 nM**	**>100**
43b	5-F-Pentyl	*t*-Bu	26%	**104 nM**	**>100**
43c	5-F-Pentyl	*i*-Bu	40%	47%	-
43d	5-F-Pentyl	4,4-DMPN	35%	**207 nM**	**>100**
43e	Pentyl	*i*-Pr	1%	32%	-
43f	Pentyl	*t*-Bu	22%	**99.2 nM**	**>100**
43g	Pentyl	*i*-Bu	27%	1%	-
43h	Pentyl	4,4-DMPN	29%	**192 nM**	**>100**
Surinabant	-	-	3 nM	400 nM	-
GW405833	-	-	4772 nM	5.8 nM	-

[a] Displacement of specific [^{3}H]-CP 55,940 binding in human HEK cells expressed as K_i in nM (n = 3) or percentage displacement of specific binding at a concentration of 1 μM (n = 2). [b] Selectivity index is the ratio between K_i CB_1R and K_i CB_2R.

USC UNIVERSIDADE DE SANTIAGO DE COMPOSTELA

Structure-Activity Relationship Analyses. In this Chapter, a more exhaustive exploration of the effect derived from the introduction of different groups at R^3 has been investigated for both ester (**39** and **40**) and amide (**41** and **42**) series. The introduction of unexplored diversities (*i*-Bu, 4,4-DMPN, *c*-Pr and *c*-Bu) has been studied, together with the groups introducted in Chapter 2 (H, *i*-Pr, *t*-Bu, Ph, Ad) that lead to the discovery of novel CB_2R selective ligands. In addiction, in this Chapter, a few derivatives bearing the 5-F-pentyl and pentyl group at R^1 have been also synthetized in order to study the influence and the relationship between the R^3 and R^1 groups. As observed in Figure 69, three derivatives (**39q**, **40p**, **40q**) belonging to the ester series and eight amide derivatives (**41e**, **41q**, **42e**, **43a**, **43b**, **43d**, **43f**, **43h**) exhibit potent-to-moderate CB_2R affinity and excellent selectivity (> 100-fold). To better understand the modification of the affinity and selectivity profiles of these new derivatives, some compounds early described in Chapter 2 have been also reported in the Tables 12-16 and in the graphical representation of this Chapter as refence compounds. The ligands already described in Chapter 2 (Tables 12-16) were herein differently numbered.

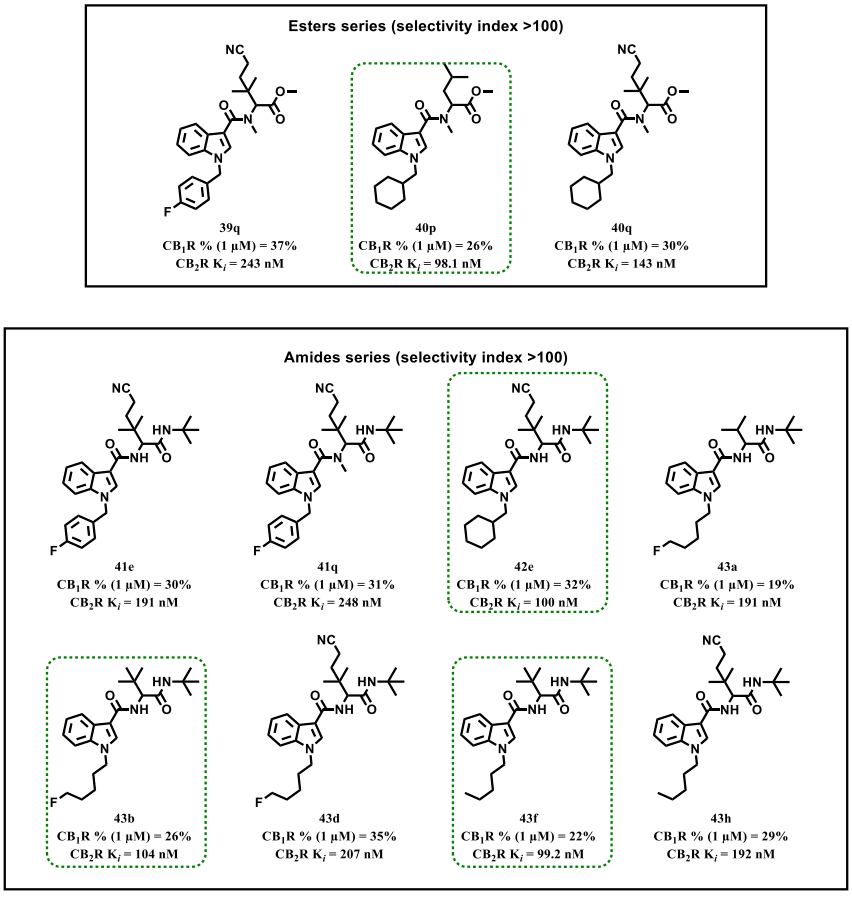


Figure 69: Structure and cannabimimetic data of selective CB_2R ligands identified during this study.

As for Chapter 1 and Chapter 2, for a more immediate and efficient analysis of the variation of both affinity and selectivity, the binding data (pK_i) are presented graphically as a plot of pK_i *h*CB_1R (*Y* axis) versus pK_i *h*CB_2R (*X* axis) using the same scale and range for both axes (square plot). Therefore, compounds with equal affinities at both receptors will lie on the diagonal of this plot (*Y* = *X*), whereas *h*CB_1R or *h*CB_2R selective compounds will be seen above or below the diagonal, respectively. The distance of their pK_i values from the diagonal is a direct measure of their degree of selectivity. The graphical representation of the ester and amide series is shown in Figure 70. Like in Chapter 2, the esters (red) show a more dual (promiscuous) profile with pK_i values in the low nanomolar range, while the amides (blue) are generally inactive (at both receptors) or exhibit excellent affinity and selectivity towards CB_2R.

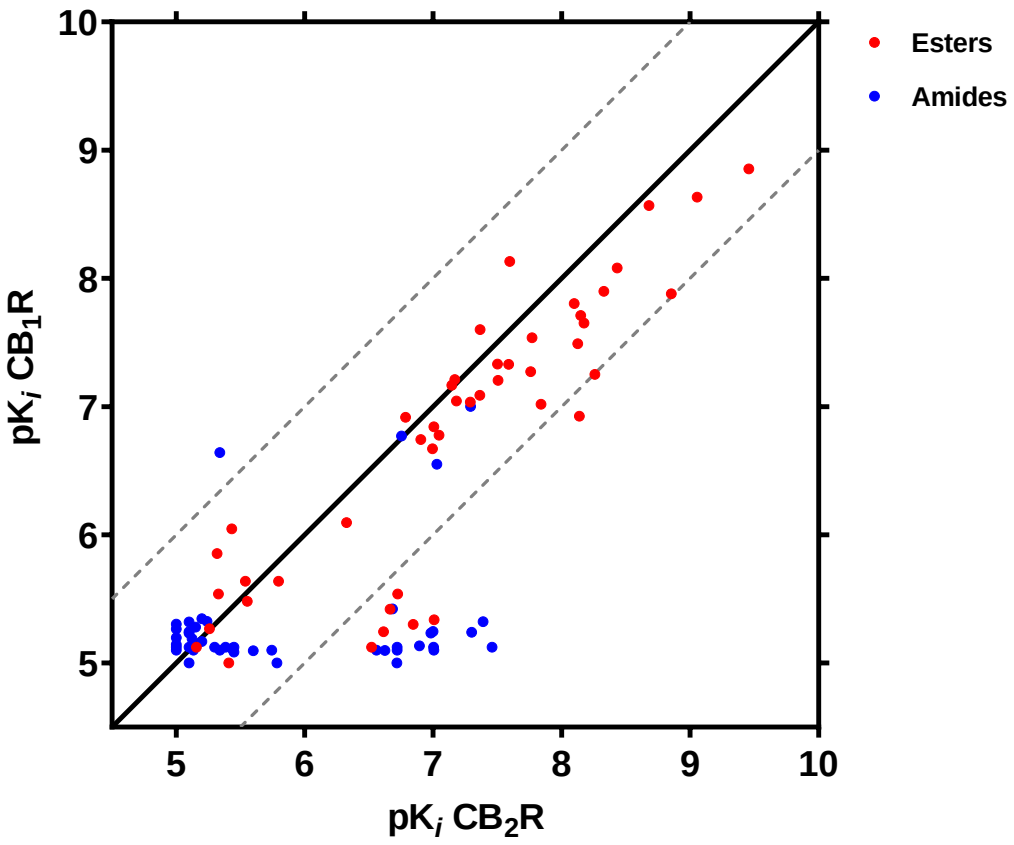


Figure 70: Graphical representation of the binding data obtained for the esters (red) and amides (blue).

USC
UNIVERSIDADE DE SANTIAGO DE COMPOSTELA

Notwithstanding the generally dual (promiscuous) profile of ester series, a SAR and SSR trends can be extrapolate from the graphical representation in Figure 71. Compounds **39q**, **40p** and **40q** are the most potent and CB_2R selective ligands of the ester series (ligands below the lower dashed line in Figure 71).

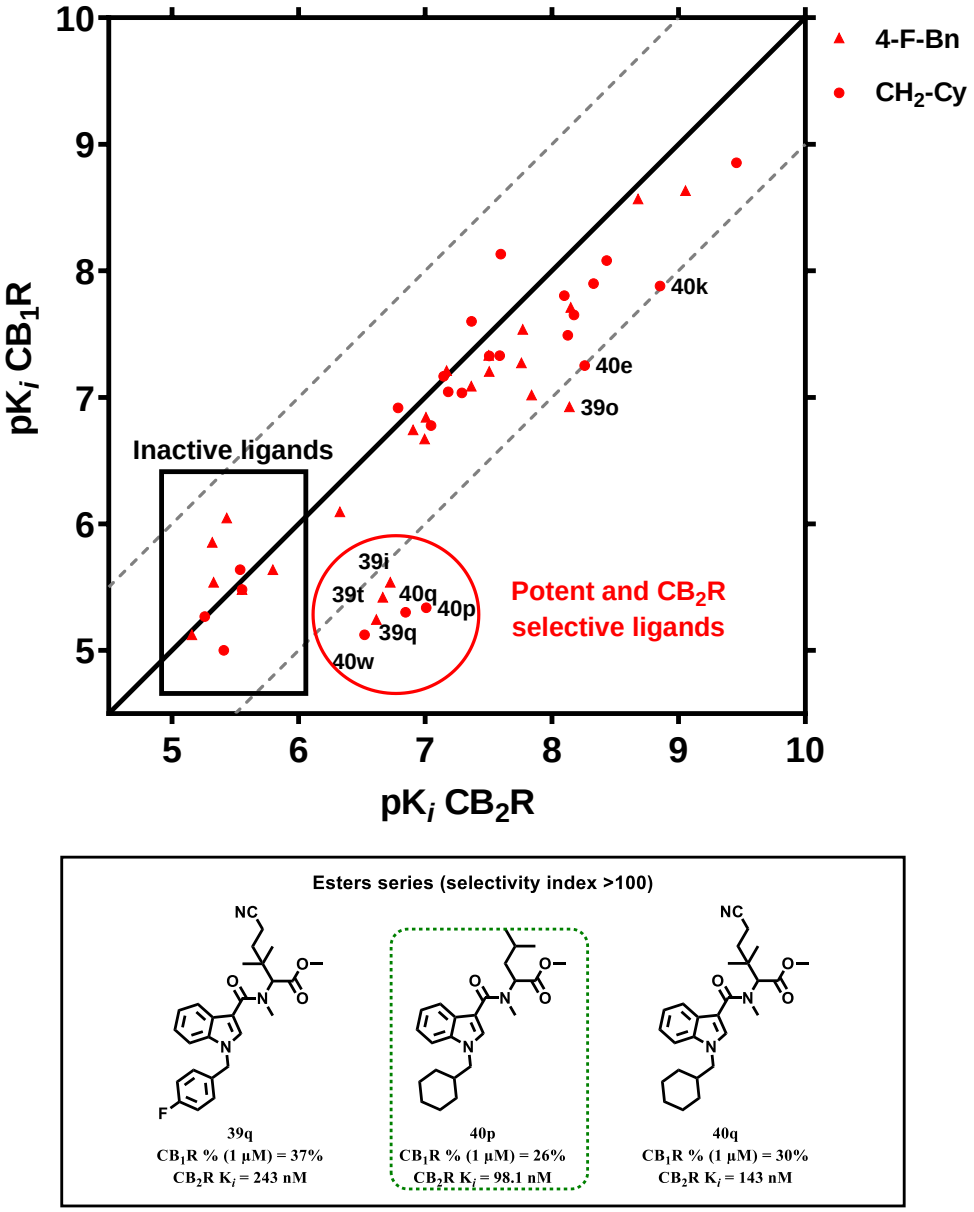


Figure 71: Graphical representation of the binding data obtained for the esters and the structure of the best CB_2R ligands of ester series.

As already observed in Chapter 2, the maximum CB_2R effect is reached when R^3 = *t*-Bu. When R^2 = H, *i*-Bu and 4,4-DMPN moieties at R^3 are well tollerated leading to potent but not selective compounds (**39d**, **39e**, **40d** and **40e**). The introduction of small cyclic groups (*c*-Pr and *c*-Bu) led to no selective ligands, with high-to-moderate affinity at both CBRs. The introduction of two substituent at R^3 and $R^{3'}$ (Me, Me; Et, Et) in Chapter 2 inspired the introduction of a cyclopentyl group within the linker, which led to potent but no selective compounds (cpds **39l**, **39x**, **40l** and **40x**, Tables 12-13) (Figure 72).

For those derivatives bearing a methyl group at R^2, the introduction of *i*-Bu and 4,4-DMPN at R^3 leads to potent and highly CB_2R selective ligands: compounds **39q**, **40p** and **40q** with a K_i values of 243 nM, 98.1 nM and 143 nM, respectively. These results are in agreement with findings observed in Chapter 2, and support the beneficial effect of methylation to obtain CB_2R selective ligands. A bar chart representation of the SAR trends effect of the ester series is presented in Figure 72.

As shown in Chapter 1 and Chapter 2, both groups introduced at R^1 (4-F-Bn and CH_2-Cy) generally produce potent compounds at CB_1R and CB_2R. In general, the CH_2-Cy moiety provides ligands with higher affinity at both receptor subtypes [compared to 4-F-Bn (Figure 72)].

Figure 72 enables to rapidly visualize the effect of the variation at R^3 within each subset, but also to observe the effect of the introduction of a methyl group at R^2.

As observed, methylation strongly decrease the affinity towards CB_1R and CB_2R, except for the ligands bearing a *t*-Bu group at R^3 (**39o** and **40o**).

USC UNIVERSIDADE DE SANTIAGO DE COMPOSTELA

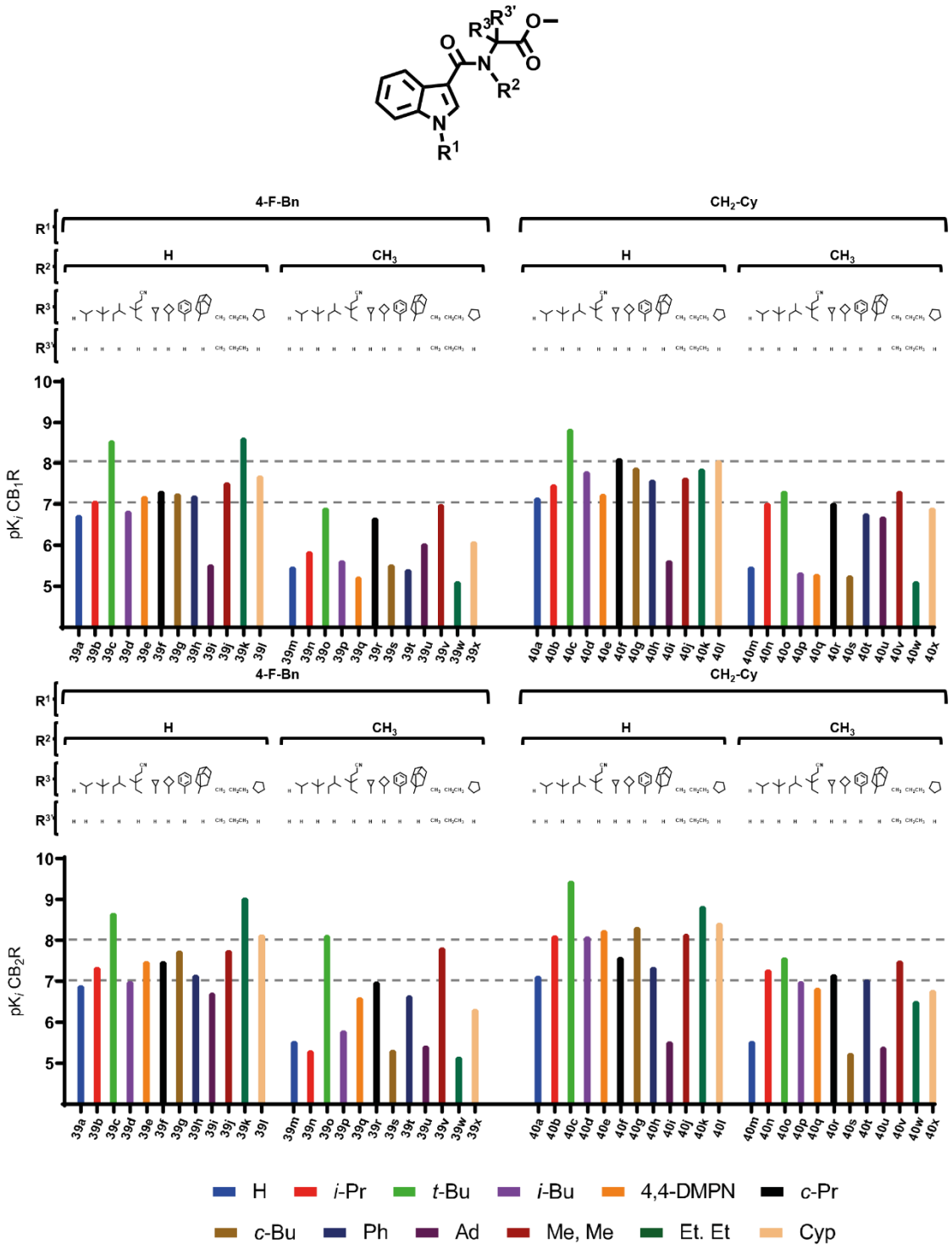


Figure 72: Bar chart representation of the SAR trends related to R^3 and $R^{3'}$ groups in the ester series. CB_1R affinity data (above) and CB_2R affinity data (bottom) are reported.

USC UNIVERSIDADE DE SANTIAGO DE COMPOSTELA

As observed in Figure 73, most of the evaluated amides fall into two cathegories: 1) inactive compounds (black circle) at both CBR, or 2) potent and highly selective CB_2R ligands (blue rectangle). Within these series, cpds **41e**, **42e**, **43a**, **43b**, **43f**, and **43h** are new compounds exhibiting the highest CB_2R affinity and selectivity (ligands below the lower dashed line in Figure 73).

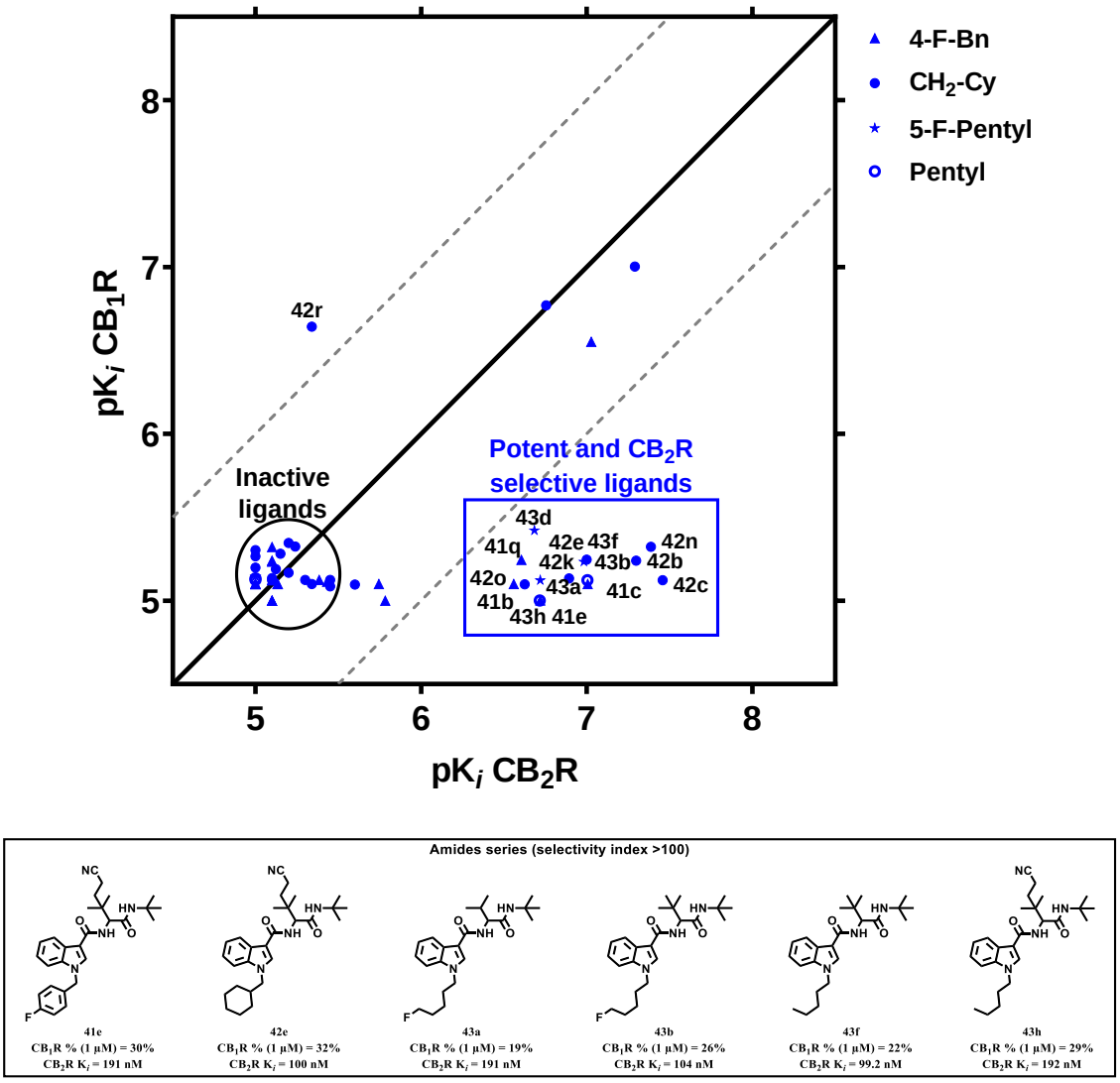


Figure 73: Graphical representation of the binding data obtained for the amides and the structure of the best CB_2R ligands of amide series.

USC UNIVERSIDADE DE SANTIAGO DE COMPOSTELA

As previusoly demonstrated in Chapter 2, amides are generally more affine to CB_2R [when compared to the esters (Figure 74)]. The introduction of *i*-Bu, *c*-Pr and *c*-Bu are not well tolerated, leading to inactive compounds. The introduction of the 4,4-DMPN group enabled the indentification of two of the best compounds of the series: compounds **41e** (K_i = 191 nM at CB_2R) and **42e** (K_i = 100 nM at CB_2R). The introduction of a substituent at $R^{3'}$ leads to ligands with no affinity (CB_1R and CB_2R), especially with the new introduction of the cyclopentyl within the linker. As in the esters series, the methylated analogues show a drop in the affinity at both CBRs (Figure 74). The methyl analogue of 4-F-Bn (**41q**) maintains the selectivity towards CB_2R with a K_i of 248 nM, while the CH_2-Cy analogue (**42q**) shows a decreased affinity (with a K_i of 720 nM). The 4,4-DMPN moiety has proved to be the most effective group of the new substitutions (Figure 74).

As observed in Chapter 1 and Chapter 2 (and for the ester series of this Chapter), both groups introduced at R^1 (4-F-Bn and CH_2-Cy) are generally well tolerated and produced ligands with excellent affinity and in some cases outstanding CB_2R selectivity. In general, ligands bearing a CH_2-Cy group are more potent and CB_2R selectives (Figure 74).

A bar chart representation summarizing the main SAR trends observed is presented in Figure 74.

USC
UNIVERSIDADE DE SANTIAGO DE COMPOSTELA

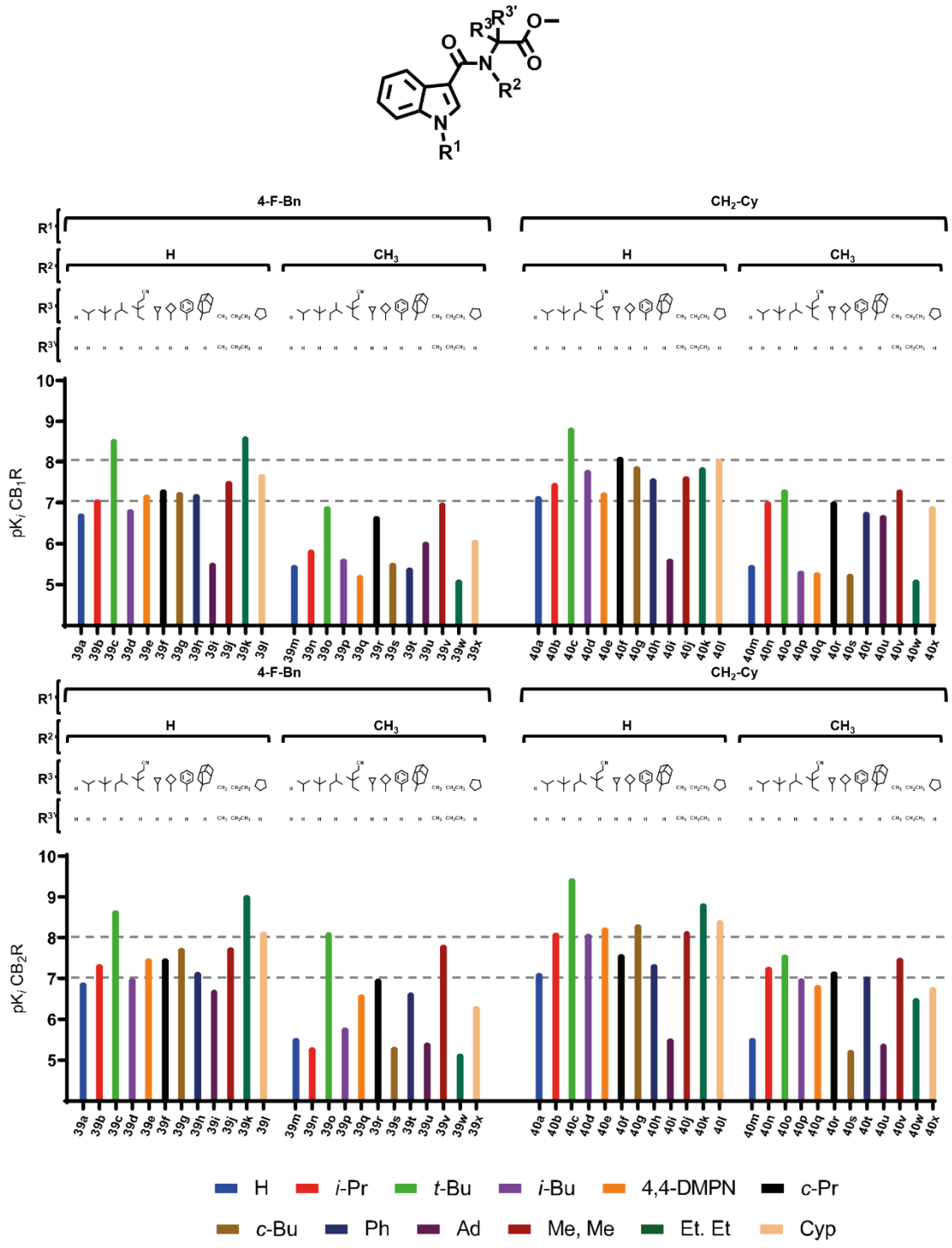


Figure 74: Bar chart representation of the SAR trends related to R^3 and $R^{3'}$ groups in the amide series. CB_1R affinity data (above) and CB_2R affinity data (bottom) are reported.

USC UNIVERSIDADE DE SANTIAGO DE COMPOSTELA

Analysis of the data obtained for the small sub-set exploring the introduction of 5-F-pentyl and pentyl at R^1 (cpds **43**) and effective R^3 groups (*i*-Pr, *t*-Bu, *i*-Bu and 4,4-DMPN) revealed complete abolition of CB_1R affinity (Table 16, Figure 75).

The measured CB_2R confirmed the best tolerated groups at R^3 are *t*-Bu and 4,4-DMPN (Figure 75), with no significative differences observed for the residue at R^1. Among these derivatives, we should highlight cpds **43b**, **43d**, **43f** and **43h** (K_i = 100 – 200 nM). The introduction of a *i*-Bu group produced inactive compounds (Table 16, cpds **43c** and **43g**). Finally, the introduction of *i*-Pr is well tolerated only when R^1 = 5-F-pnetyl (Figure 75).

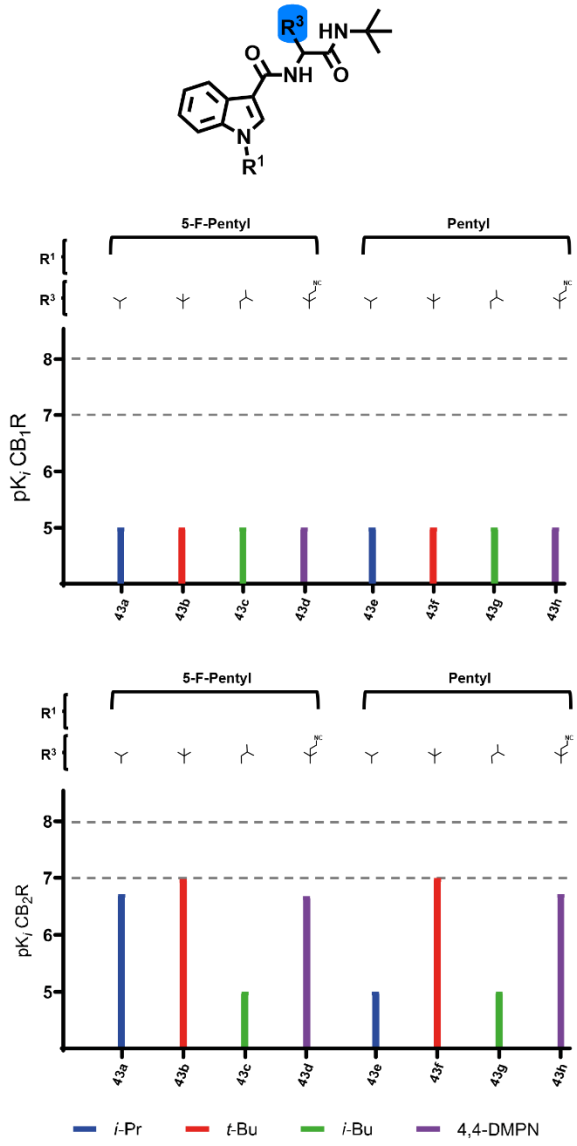


Figure 75: Bar chart representation of the SAR trends related to R^1 and R^3 groups in the amide series. CB_1R affinity data (above) and CB_2R affinity data (bottom) are reported.

USC UNIVERSIDADE DE SANTIAGO DE COMPOSTELA

3.4 CHAPTER 4. EXPLORATION OF THE INFLUENCE OF THE TERMINAL AMIDE (R^4) ON THE CB_2R DATA.

Because of the metabolic instability of esters and the promising selective profile observed for some compounds in previous Chapters, the focus of this Chapter has been centered in the amide series R^4. The versatility of the Ugi reaction allows to rapidly investigate the effect of R^4 by changing the isocyanide precursors (Figure 76). It should be pointed that, to the best of our knowledge, the exploration of the effect of substituents at the terminal amides of SCRAs has not been previously described in literature. As early described, the amide series of the SCRA libraries (Chapter 1) always contain a primary amide ($CONH_2$). In Chapter 2, we have briefly explored the substitution at R^4 (with *t*-Bu and Bn groups) leading to compounds with high selectivity and moderate-to-high affinity towards CB_2R.

In this Chapter we propose the exploration of R^4, together with modifications at R^1, R^2 and R^3, thus enabling the discovery of potent and CB_2R selective ligands.

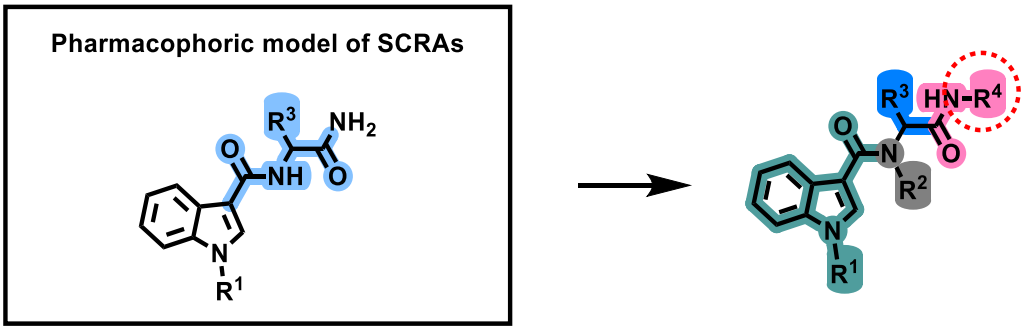


Figure 76: Ugi-based approach of SCRA-like libraries: focus on the terminal amide.

Chemistry. As in previous Chapters, the Ugi four component reaction (U4CR) has been employed for the synthesis of these novel ligands (Figure 77).

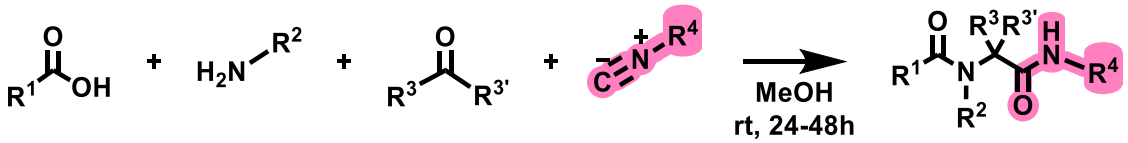


Figure 77: The Ugi reaction.

USC
UNIVERSIDADE DE SANTIAGO DE COMPOSTELA

The description of the mechanism of the Ugi reaction and the design criteria behind the series were briefly explained in Chapter 2. A detailed description of the synthetic methods and the complete structural, spectroscopic, and analytical data for all compounds are provided in the Experimental Section.

Design and synthesis of amides. In this Chapter, we explored the effect of introducing different groups on the terminal amide (R^4). This study can be divided into three levels of molecular exploration (Figure 78).

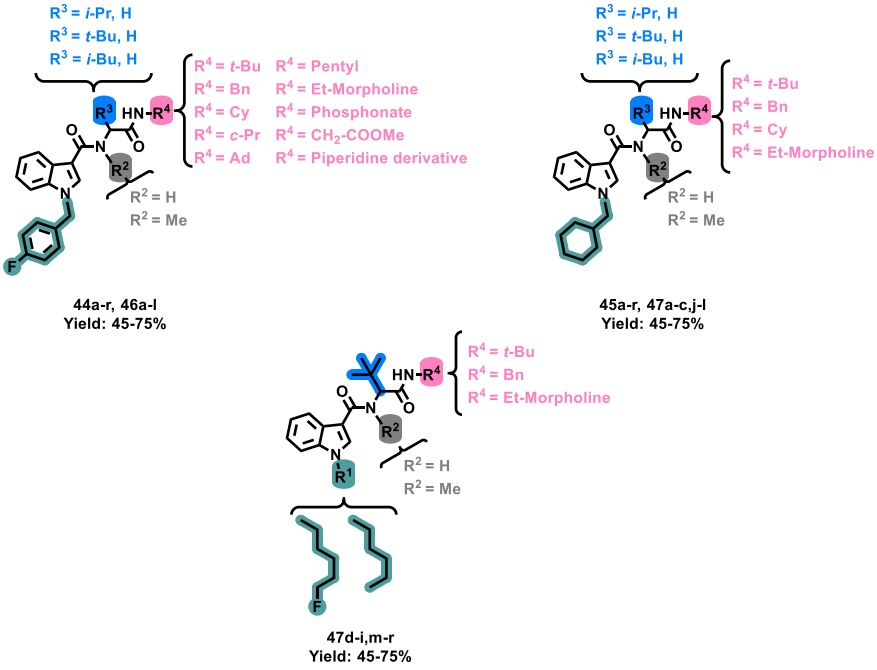


Figure 78: General structure and diversity space explored for amide **44a-r, 46a-l, 45a-r** and **47a-r**.

First, in order to complete the exploration of Chapter 2, [where *t*-Bu and Bn groups have earlier been introduced leading to ligands with moderate-to-high affinity and CB_2R selectivity (e.g, **44a**, **44b**, **44d**, **44k**, **44n**, **45a**, **45b**, **45d**, **45h**, **45j**, **45m**, **45n**)], the Cy has been introduced at R^4. Systematically, in Chapter 2, we also explored *t*-Bu and *i*-Pr at R^3; so herein at R^3 we maintained these groups and included *i*-Bu moiety. Ammonia or methylamine were employed during the Ugi reaction to study the influence of R^2 in these subsets.

USC UNIVERSIDADE DE SANTIAGO DE COMPOSTELA

Then, maintaining the 4-F-Bn at R^1, the *t*-Bu at R^3 and by changing H/Me at R^2, we focused on the influence of R^4 groups at both CBRs. Accordingly, a set of diverse and unexplored groups (*c*-Pr, Ad, Pentyl, Et-Morpholine, Phosphonate, CH_2-COOMe, piperidine derivative) have been proposed to evaluate their contribution to the affinity and selectivity towards CBRs.

Finally, a set of derivatives (**47**) bearing CH_2-Cy, 5-F-pentyl and pentyl have also been designed and synthetized in order to study the effect of R^1 in these series. It should be noticed that subset **47** was conceived by the incorporation of the best groups previously identified.

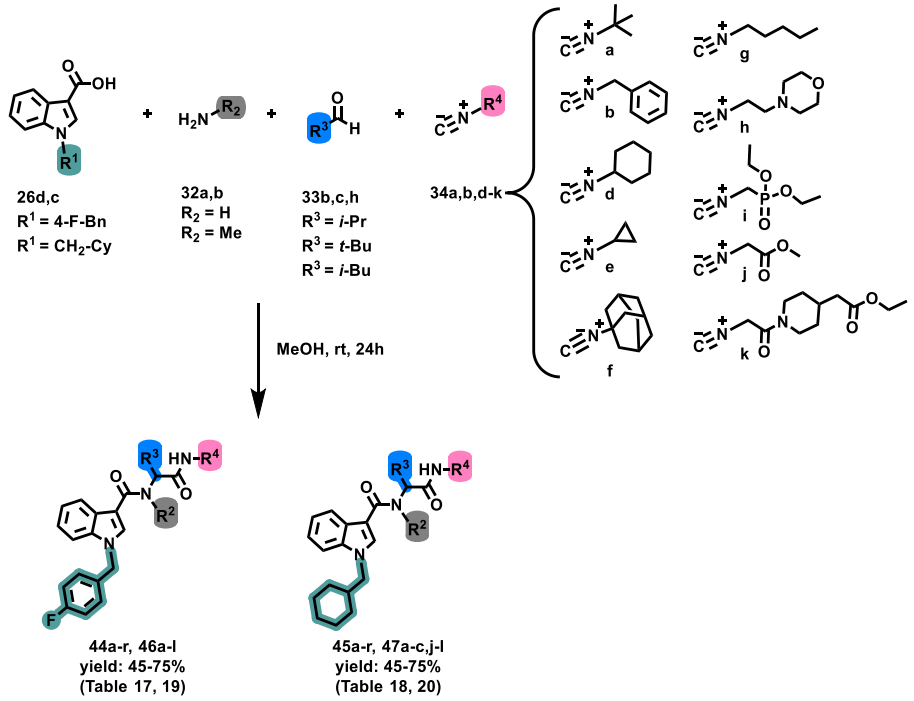
As depicted in Figure 78, the herein proposed synthetic method permits the rapid assembly of amide libraries (Cpds **44, 45, 46** and **47**). The obtained collection contains 40 new amide derivatives bearing several previously unexplored substitution patterns in SCRA-like series. The diversity space explored (R^1, R^2, R^3, and R^4) during this study is presented in Figure 78. As observed, the direct and efficient assembly facilitates the exhaustive exploration of the SAR trends in these series.

The compounds already described in Chapter 2 and Chapter 3 (Tables 17-20) were herein differently numbered.

As shown in Scheme 8 and Scheme 9, the Ugi adducts (Cpds **44**, **45**, **46** and **47**) were obtained in moderate to satisfactory yields (45-75%) as racemic mixtures. As in the previous Chapters, the reactions were performed in sealed Kimble vials using methanol as solvent and were monitored by thin-layer chromatography (TLC). After completion of the reaction, the catch and the release protocol were performed as indicated in the Experimental Section. Then, the solvent was evaporated to dryness and the isolated solid/oil was purified by column chromatography on silica gel or preparative chromatography. A detailed description of the synthetic methods and the complete structural, spectroscopic, and analytical data for all compounds are provided in the Experimental Section.

Figure 79 and Figure 80 show the ^{1}H-NMR spectra obtained during the spectroscopic characterization of a representative compound of these series.

USC UNIVERSIDADE DE SANTIAGO DE COMPOSTELA



Scheme 8: Ugi-based assembly of amide **44a-r, 46a-l**, **45a-r** and **47a-c,j-l**.

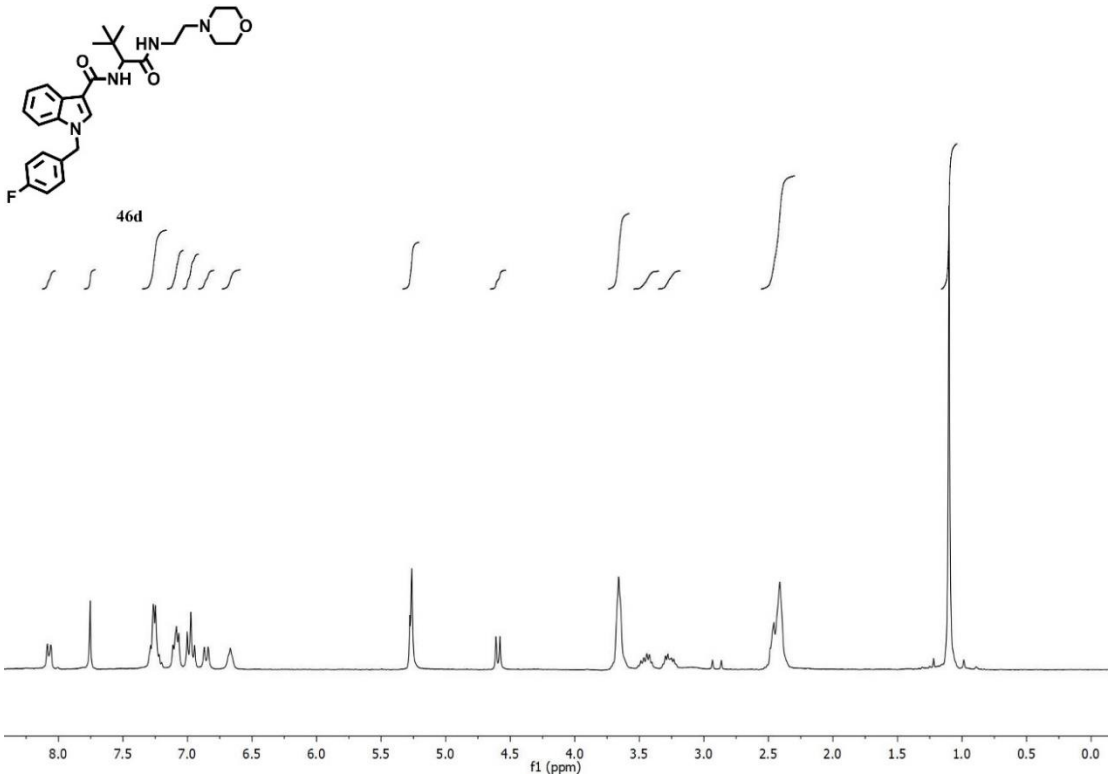
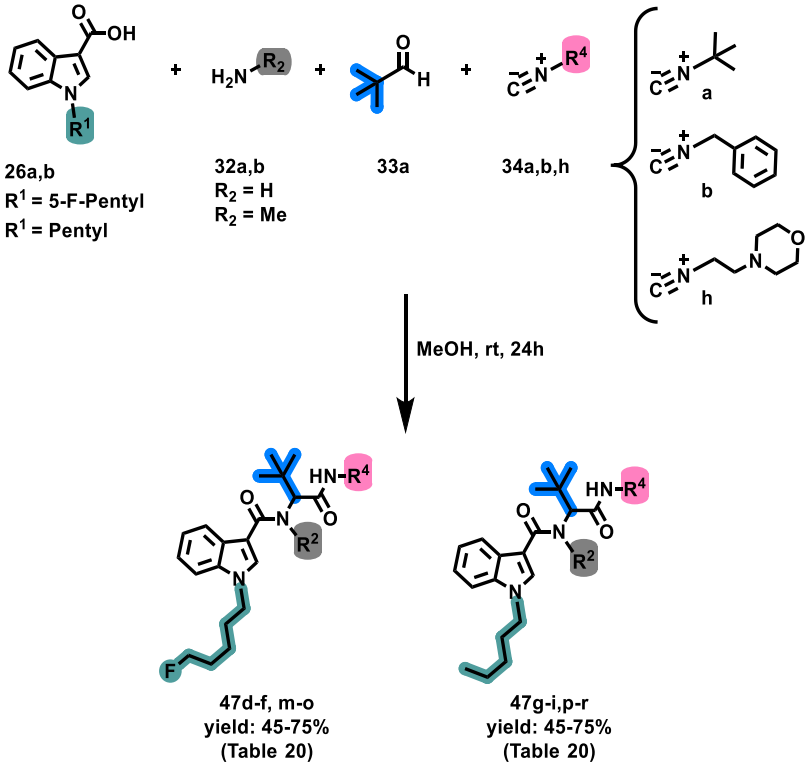


Figure 79: ^{1}H-NMR spectra of compound **46d**.



Scheme 9:Ugi-based assembly of amides **47d-i,l-o.**

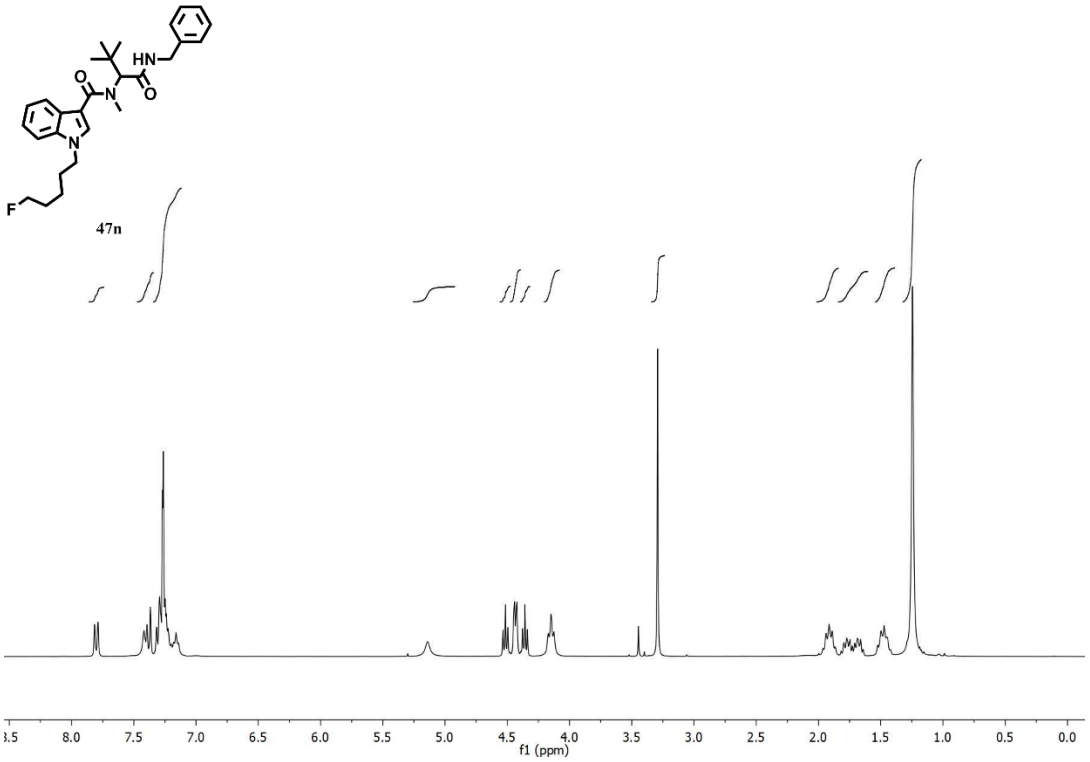


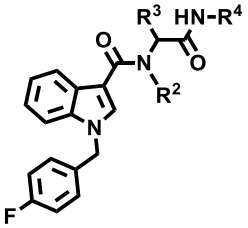
Figure 80: ^{1}H-NMR spectra of compound **47n.**

Biological evaluation. The affinity and selectivity of the novel indole-based compounds was evaluated *in vitro* using radioligand binding assays at the two human CBR subtypes. Tables 17-20 contain the binding data obtained. All ligands reported in Tables 17-20 were obtained and tested as racemic mixtures. The experiments were performed *in vitro* on transfected HEK-293T cells and [^{3}H]-CP 55,940 was employed as radioligand. The binding data is presented as K_i ± SEM (nM, n = 3) or as specific binding inhibition percentage at 1 μM (n = 2, mean) for those compounds which do not reach a minimum of 60% of radioligand displacement at such concentration. Prism 5.0 software (GraphPad, San Diego, CA) was employed for data analysis. The K_i values were acquired by fitting the data by non-linear regression.

Results are the average of three experiments, each performed in duplicate. Two of well-known CBR ligands [Surinabant (CB_1R antagonist) and GW405833(CB_2R agonist)] were assessed using our experimental protocols, their binding data is reported in Tables 17-20 for comparative purposes. With the aim of facilitating the comparison of the effect of R^1, R^3 and R^4 on binding affinity, we decided to include in Tables 17-20 the data obtained for some derivatives described in Chapter 2 and in Chapter 3 (indicated in tables with an asterisk).

USC UNIVERSIDADE DE SANTIAGO DE COMPOSTELA

Table 17: Affinity and selectivity data obtained for amides **44a-r**.

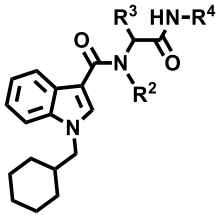


CODE	R^2	R^3	R^4	CB_1R	CB_2R	SI[b] K_i CB_1R/ K_i CB_2R
				K_i (nM) or % at 1 μM[a]	K_i (nM) or % at 1 μM[a]	
44a*	H	*i*-Pr	*t*-Bu	16%	**276 nM**	**>100**
44b*	H	*i*-Pr	Bn	10%	**571 nM**	**>100**
44c	H	*i*-Pr	Cy	4%	33%	-
44d*	H	*t*-Bu	*t*-Bu	36%	**98.7 nM**	
44e*	H	*t*-Bu	Bn	123 nM	35.8 nM	3.4
44f	H	*t*-Bu	Cy	28%	**724 nM**	**>100**
44g*	H	*i*-Bu	*t*-Bu	12%	40%	-
44h	H	*i*-Bu	Bn	9%	**603 nM**	**>100**
44i	H	*i*-Bu	Cy	10%	15%	-
44j*	Me	*i*-Pr	*t*-Bu	3%	44%	-
44k*	Me	*i*-Pr	Bn	9%	**237 nM**	**>100**
44l	Me	*i*-Pr	Cy	18%	37%	-
44m*	Me	*t*-Bu	*t*-Bu	3%	32%	-
44n*	Me	*t*-Bu	Bn	27%	**204 nM**	**>100**
44o	Me	*t*-Bu	Cy	5%	45%	-
44p*	Me	*i*-Bu	*t*-Bu	2%	33%	-
44q	Me	*i*-Bu	Bn	1%	37%	-
44r	Me	*i*-Bu	Cy	3%	14%	-
Surinabant	-	-	-	3 nM	400 nM	-
GW405833	-	-	-	4772 nM	5.8 nM	-

[a] Displacement of specific [^{3}H]-CP 55,940 binding in human HEK cells expressed as K_i in nM (n = 3) or percentage displacement of specific binding at a concentration of 1 μM (n = 2). [b] Selectivity index is the ratio between K_i CB_1R and K_i CB_2R. *These compounds were described in Chapter 2 and Chapter 3.

USC UNIVERSIDADE DE SANTIAGO DE COMPOSTELA

Table 18: Affinity and selectivity data obtained for amides **45a-r**.

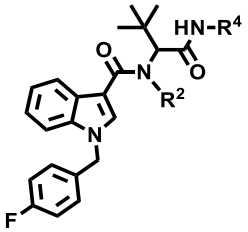


CODE	R^2	R^3	R^4	CB_1R	CB_2R	SI[b] K_i CB_1R/ K_i CB_2R
				K_i (nM) or % at 1 μM[a]	K_i (nM) or % at 1 μM[a]	
45a*	H	*i*-Pr	*t*-Bu	28%	**50.2 nM**	**>100**
45b*	H	*i*-Pr	Bn	37%	**109 nM**	**>100**
45c	H	*i*-Pr	Cy	7%	**581 nM**	**>100**
45d*	H	*t*-Bu	*t*-Bu	35%	**34.8 nM**	**>100**
45e*	H	*t*-Bu	Bn	28.4 nM	7.60 nM	3.7
45f	H	*t*-Bu	Cy	30%	**613 nM**	**>100**
45g*	H	*i*-Bu	*t*-Bu	41%	32%	-
45h	H	*i*-Bu	Bn	31%	**106 nM**	**>100**
45i	H	*i*-Bu	Cy	30%	**590 nM**	**>100**
45j*	Me	*i*-Pr	*t*-Bu	31%	**40.9 nM**	**>100**
45k*	Me	*i*-Pr	Bn	1%	41%	-
45l	Me	*i*-Pr	Cy	2%	**668 nM**	**>100**
45m*	Me	*t*-Bu	*t*-Bu	5%	**237 nM**	**>100**
45n*	Me	*t*-Bu	Bn	26%	**108 nM**	**>100**
45o	Me	*t*-Bu	Cy	14%	**711 nM**	**>100**
45p*	Me	*i*-Bu	*t*-Bu	1%	20%	-
45q	Me	*i*-Bu	Bn	28%	**141 nM**	**>100**
45r	Me	*i*-Bu	Cy	39%	**348 nM**	**>100**
Surinabant	-	-	-	3 nM	400 nM	-
GW405833	-	-	-	4772 nM	5.8 nM	-

[a] Displacement of specific [^{3}H]-CP 55,940 binding in human HEK cells expressed as K_i in nM (n = 3) or percentage displacement of specific binding at a concentration of 1 μM (n = 2). [b] Selectivity index is the ratio between K_i CB_1R and K_i CB_2R. *These compounds were described in Chapter 2 and Chapter 3.

USC UNIVERSIDADE DE SANTIAGO DE COMPOSTELA

Table 19: Affinity and selectivity data obtained for amides **46a-l**.

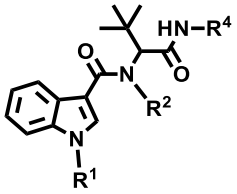


CODE	R^2	R^4	CB_1R	CB_2R	SI[b] K_i CB_1R/ K_i CB_2R
			K_i (nM) or % at 1 μM[a]	K_i (nM) or % at 1 μM[a]	
46a	H	*c*-Pr	41.4 nM	9.2 nM	4.5
46b	H	Ad	19%	10%	-
46c	H	Pentyl	34%	**85.0 nM**	**>100**
46d	H	Et-Morpholine	31%	**42.7 nM**	**>100**
46e	H	CH_2-P(O)-$(OEt)_2$	36%	**307 nM**	**>100**
46f	H	CH_2-COOMe	80.6 nM	15.3 nM	5.2
46g	H	Piperidine der.	24.6 nM	10.6 nM	2.3
46h	Me	*c*-Pr	35%	**59.3 nM**	**>100**
46i	Me	Pentyl	27%	**273 nM**	**>100**
46j	Me	Et-Morpholine	29%	**71.2 nM**	**>100**
46k	Me	CH_2-COOMe	36%	**90.3 nM**	**>100**
46l	Me	Piperidine der.	34%	**78.5 nM**	**>100**
Surinabant	-	-	3 nM	400 nM	-
GW405833	-	-	4772 nM	5.8 nM	-

[a] Displacement of specific [^{3}H]-CP 55,940 binding in human HEK cells expressed as K_i in nM (n = 3) or percentage displacement of specific binding at a concentration of 1 μM (n = 2). [b] Selectivity index is the ratio between K_i CB_1R and K_i CB_2R.

USC UNIVERSIDADE DE SANTIAGO DE COMPOSTELA

Table 20: Affinity and selectivity data obtained for amides **47a-r**.



CODE	R^1	R^2	R^4	CB_1R K_i (nM) or % at 1 μM[a)]	CB_2R K_i (nM) or % at 1 μM[a)]	SI[b)] K_i CB_1R/ K_i CB_2R
47a*	CH_2-Cy	H	*t*-Bu	35%	**34.8 nM**	**>100**
47b*	CH_2-Cy	H	Bn	28.4 nM	7.60 nM	3.7
47c	CH_2-Cy	H	Et-Morpholine	108 nM	13.8 nM	7.8
47d*	5-F-Pentyl	H	*t*-Bu	26%	**104 nM**	**>100**
47e	5-F-Pentyl	H	Bn	115 nM	11.5 nM	10
47f	5-F-Pentyl	H	Et-Morpholine	172 nM	42.4 nM	4.1
47g*	Pentyl	H	*t*-Bu	22%	**99.2 nM**	**>100**
47h	Pentyl	H	Bn	269 nM	30.5 nM	8.8
47i	Pentyl	H	Et-Morpholine	34%	**98.2 nM**	**>100**
47j*	CH_2-Cy	Me	*t*-Bu	5%	**237 nM**	**>100**
47k*	CH_2-Cy	Me	Bn	26%	**108 nM**	**>100**
47l	CH_2-Cy	Me	Et-Morpholine	36%	**97.3 nM**	**>100**
47m	5-F-Pentyl	Me	*t*-Bu	12%	**260 nM**	**>100**
47n	5-F-Pentyl	Me	Bn	32%	**125 nM**	**>100**
47o	5-F-Pentyl	Me	Et-Morpholine	28%	**112 nM**	**>100**
47p	Pentyl	Me	*t*-Bu	15%	**396 nM**	**>100**
47q	Pentyl	Me	Bn	30%	**128 nM**	**>100**
47r	Pentyl	Me	Et-Morpholine	33%	**104 nM**	**>100**
Surinabant	-	-	-	3 nM	400 nM	-
GW405833	-	-	-	4772 nM	5.8 nM	-

[a)] Displacement of specific [^{3}H]-CP 55,940 binding in human HEK cells expressed as K_i in nM (n = 3) or percentage displacement of specific binding at a concentration of 1 μM (n = 2). [b)] Selectivity index is the ratio between K_i CB_1R and K_i CB_2R. *These compounds were described in Chapter 4.

USC UNIVERSIDADE DE SANTIAGO DE COMPOSTELA

Structure-Activity Relationship Analyses. The Ugi-based approach allows the full exploration of R^4, enabling the rapid introduction of small or bulky, polar, or non-polar groups, thus facilitating the identification of novel CB_2R ligands (Figure 81). During this study, the exploration of R^4 leads to the discovery of new compounds showing a remarkable affinity and selectivity towards CB_2R. Ligands **45h**, **45q**, **46c**, **46d**, **46e**, **46h**, **46i**, **46j**, **46k**, **46l**, **47i**, **47l**, **47m**, **47n**, **47o**, **47p**, **47q**, and **47r** represent the best compounds of the series with K_i values in the range from 42.7 nM to 307 nM (> 100-fold selectivity over CB_1R) (Figure 81). It should be noticed that thirteen of the eighteen ligands reported in Figure 81 are *N*-methyl derivatives (R^2 = Me).

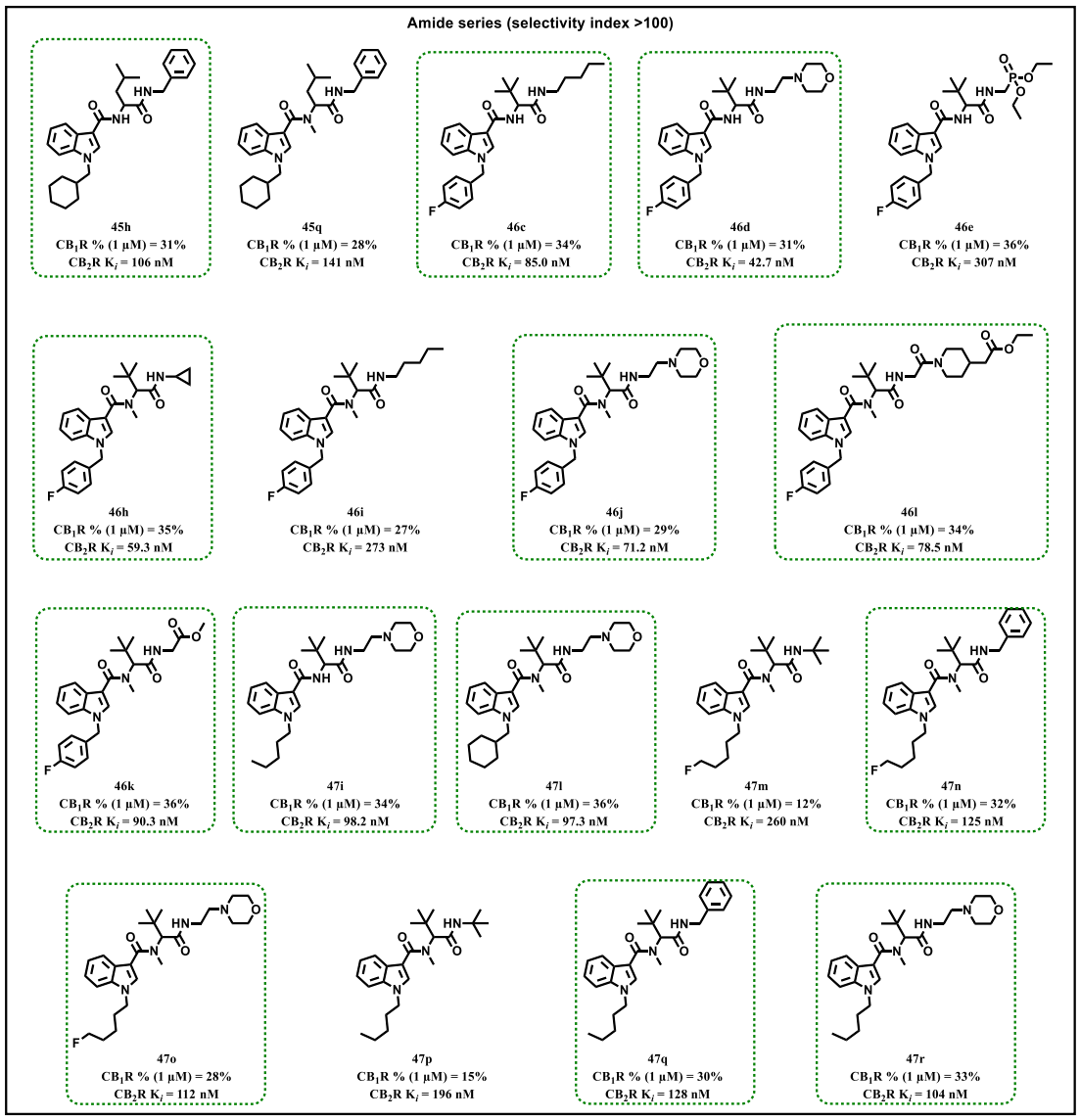


Figure 81: Structure and cannabimimetic data of selective CB_2R ligands identified in this Chapter.

USC UNIVERSIDADE DE SANTIAGO DE COMPOSTELA

As for previous Chapters, for a more immediate and efficient analysis of the variation of both affinity and selectivity, the binding data (pK_i) are presented graphically as a plot of pK_i *h*CB_1R (*Y* axis) versus pK_i *h*CB_2R (*X* axis) using the same scale and range for both axes (square plot). Therefore, compounds with equal affinities at both receptors will lie on the diagonal of this plot (*Y* = *X*), whereas *h*CB_1R or *h*CB_2R selective compounds will be seen above or below the diagonal, respectively. The distance of their pK_i values from the diagonal is a direct measure of their degree of selectivity. The graphical representation of the binding data of the amide series is shown in Figure 82.

Observation of the data presented in Figure 82 confirms that most of the ligands exhibit excellent CB_2R affinity and selectivity.

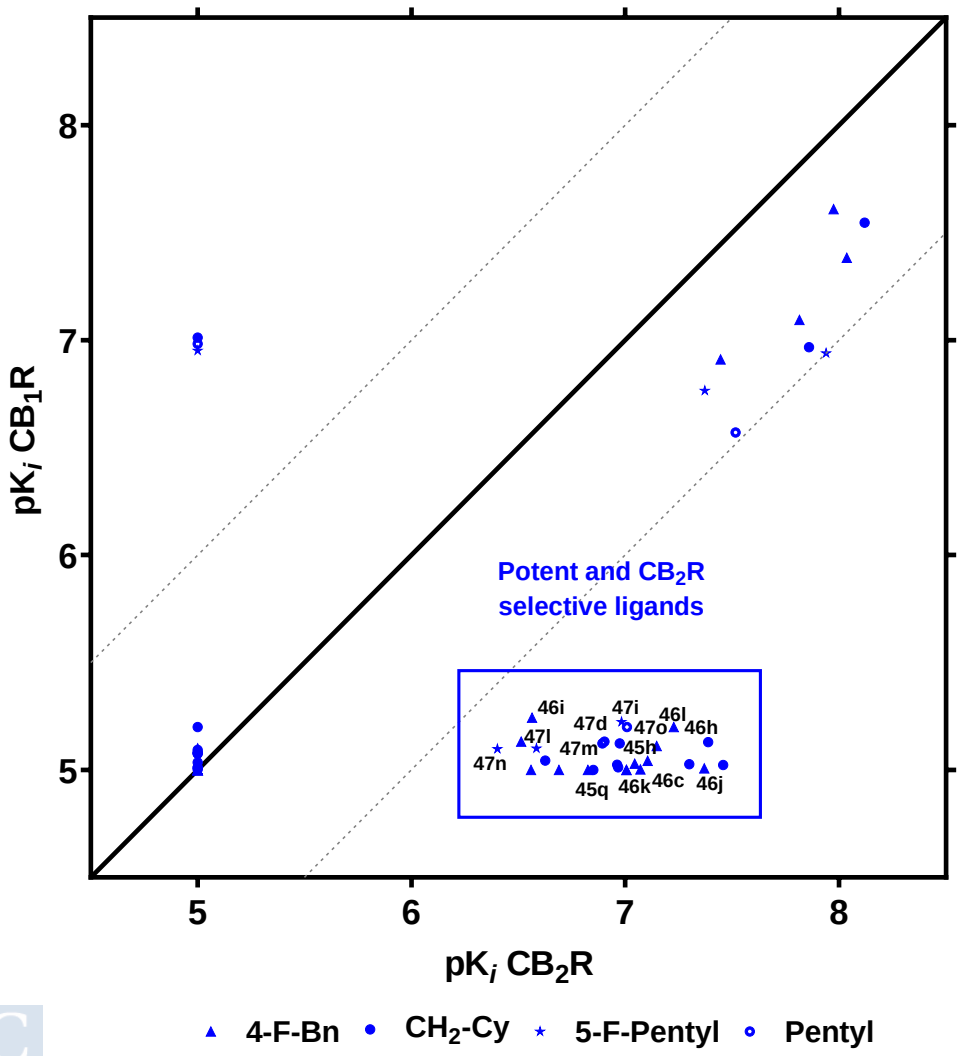


Figure 82: Graphical representation of the binding data obtained for the amides.

Series **44** and **45** were conceived to complete the analysis of the impact caused by the introduction of three groups at R^4 (*t*-Bu, Bn, Cy). For comparative purposes, representative diversities at R^1 (4-F-Bn, CH_2-Cy), R^2 (H, Me) and R^3 (*i*-Pr, *t*-Bu, *i*-Bu) were introduced.

Additionally, with the aim of better evaluating the impact of R^4, several earlier obtained ligands with no substituent at the terminal amide (R^4 = H) were considered here (Figure 83).

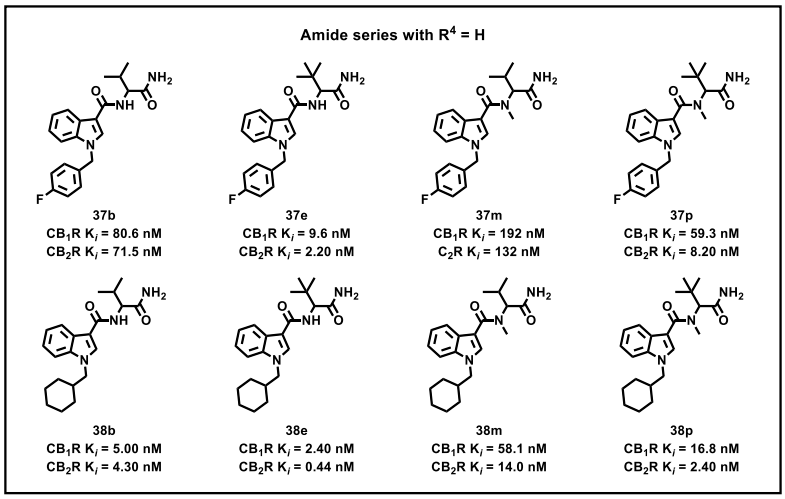


Figure 83: Structure and binding data of the amide series with R^4 = H.

To better and rapidly understand the SAR trends operating in these series, Figure 85 presents a bar charts representation of the obtained affinity data (CB_1R and CB_2R).

The first conclusion emerging from the available data (Figure 85) is the negligible CB_1R affinity observed for most compounds of this subset. The only exceptions to this trend are the *N*-benzyl carboxamides (**44e** and **45e**) when R^2 = H.

Focusing now on the SAR analysis of the obtained CB_2R data, it seems that the affinity is highly affected by steric factors. Thus, a *t*-Bu group is well tolerated only if $R^3 \neq$ *t*-Bu. On the other hand, a cyclohexyl group at R^4 systematically produced inactive compounds (regardless of the substitution pattern at R^1, R^2 or R^3).

Finally, the effect of introducing a benzyl group at R^4 is generally positive (in terms of CB_2R affinity). This modification does not seem to be dependent on the groups at R^1 and R^2 but showed to be affected by the substituent at R^3. Thus, the introduction of a benzyl group at R^4 when R^3 = *i*-Pr generally produced inactive or comparatively less potent compounds.

USC
UNIVERSIDADE DE SANTIAGO DE COMPOSTELA

Among new compounds in this subset, we would like to highlight ligands **45h** and **45q**. They show remarkable selectivity and K_i values of 106 nM and 141 nM, respectively.

The net impact of introducing R^4 on the cannabimimetic profile of these series can be evaluated by comparing the obtained data for ligands showed in Figure 84.

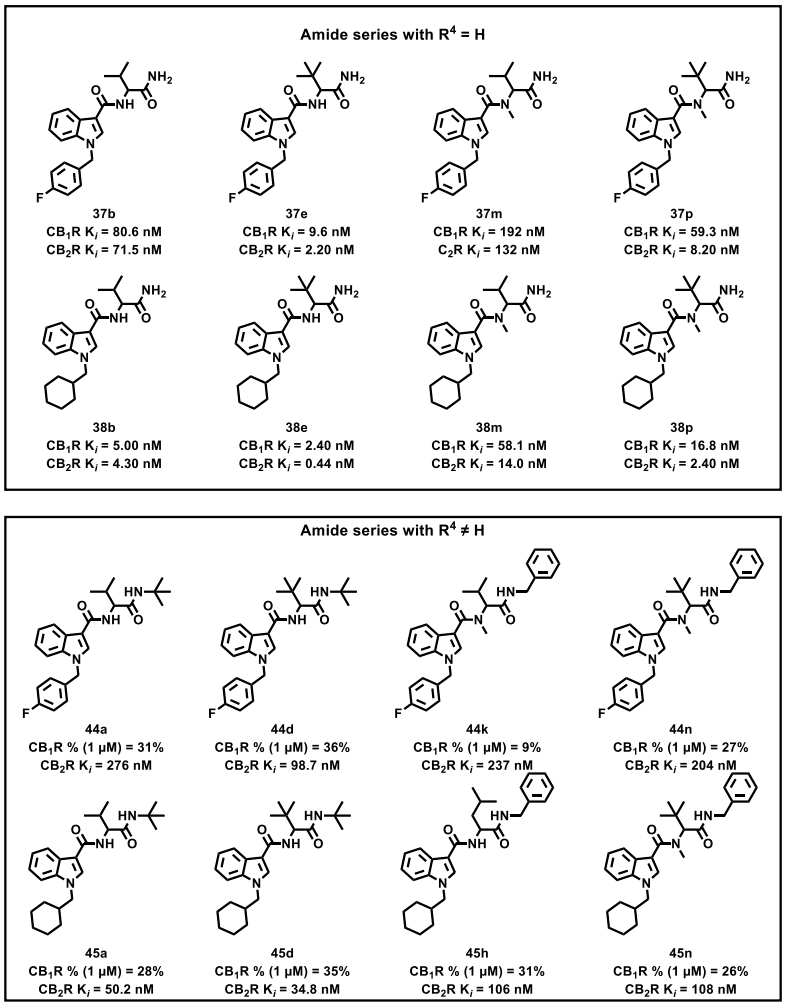


Figure 84: Comparison between the obtained data for the amide series with R^4 = H and the amide series with $R^4 \neq$ H.

USC UNIVERSIDADE DE SANTIAGO DE COMPOSTELA

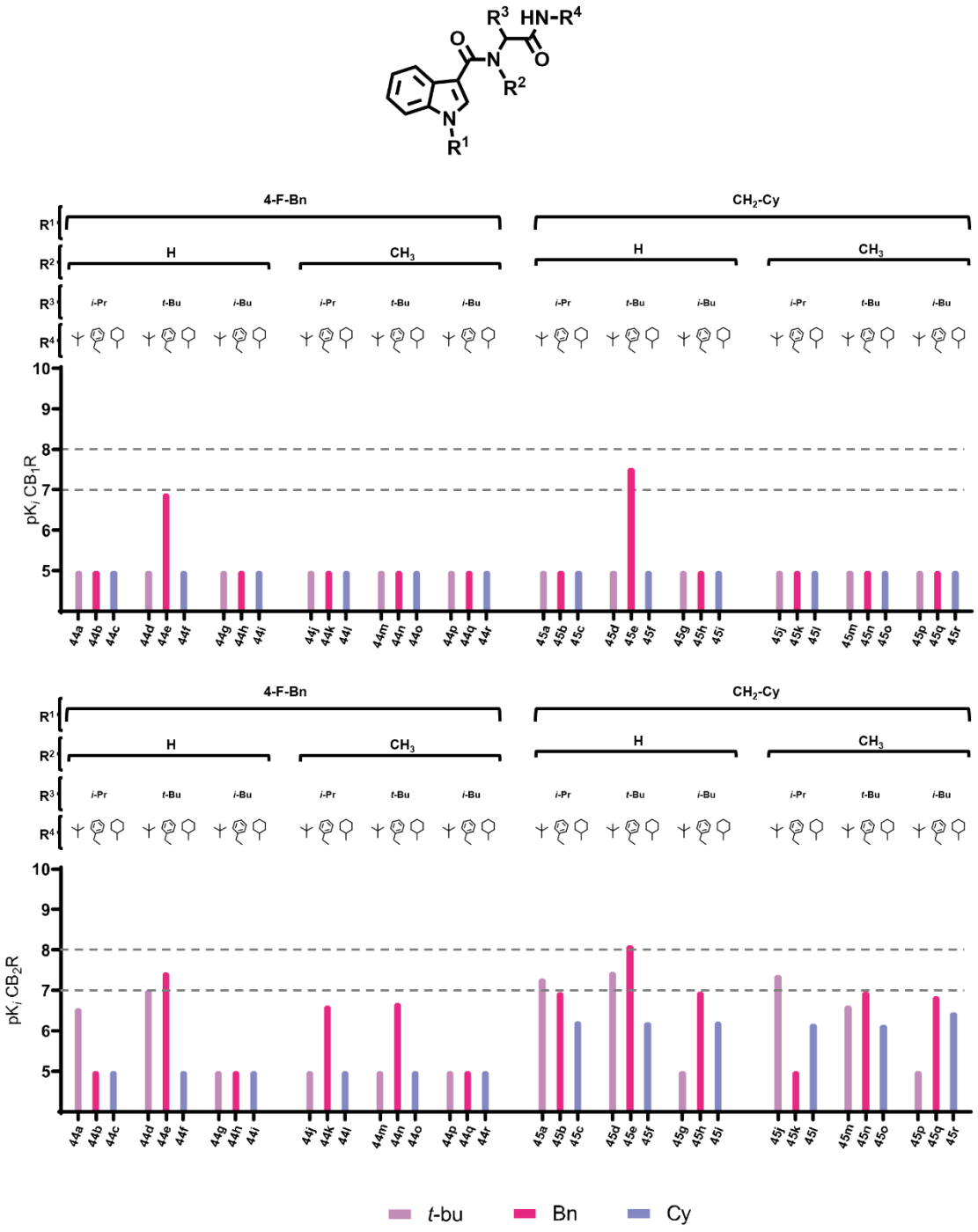


Figure 85: Bar chart representation of the SAR trends related to R^3 and R^4 groups in the amide series. CB_1R affinity data (above) and CB_2R affinity data (bottom) are reported.

USC
UNIVERSIDADE DE SANTIAGO DE COMPOSTELA

As indicated in the introduction of this Chapter, a collection of structurally diverse isocyanide was selected to explore the effect of other R^4 groups on the cannabimimetic profile of the series. Seven highly diverse isocyanides that differ in polarity, complexity and steric hindrance were employed.

For the sake of brevity, this study was performed on a model series (R^1 = 4-F-Bn, R^3 = *t*-Bu). Further studies are now in progress in our group to expand the analysis to other series.

As observed, most derivatives in this subset elicit negligible CB_1R affinity. The exceptions to this trend are three ligands bearing R^2 = H [the cyclopropyl (**46a**), the methyl ester (**46e**) the piperidine derivatives (**46g**)] (Figure 86). The Ad group produces a total loss of affinity (**46b**) (Figure 86). The methyl phosphonate group is well tolerated, leading to the compound **46e** with a K_i value of 307 nM. The introduction of pentyl group produces an improvement in both affinity and selectivity: compound **46c** shows a K_i value of 85.0 nM (> 100-fold selectivity over CB_1R). The best R^4 group is the Et-Morpholine leading to the most affine and CB_2R selective compound of the series: **46d** with a K_i value of 42.7 nM at CB_2R (Table 19, Figure 86). The further introduction of a methyl group at R^2 leads to the discovery of potent and CB_2R selective ligands: compounds **46h**, **46i**, **46j**, **46k** and **46l** show a remarkable selectivity towards CB_2R with a K_i values between 59.3 and 273 nM at CB_2R (> 100-fold selectivity over CB_1R) (Table 19, Figure 86).

USC UNIVERSIDADE DE SANTIAGO DE COMPOSTELA

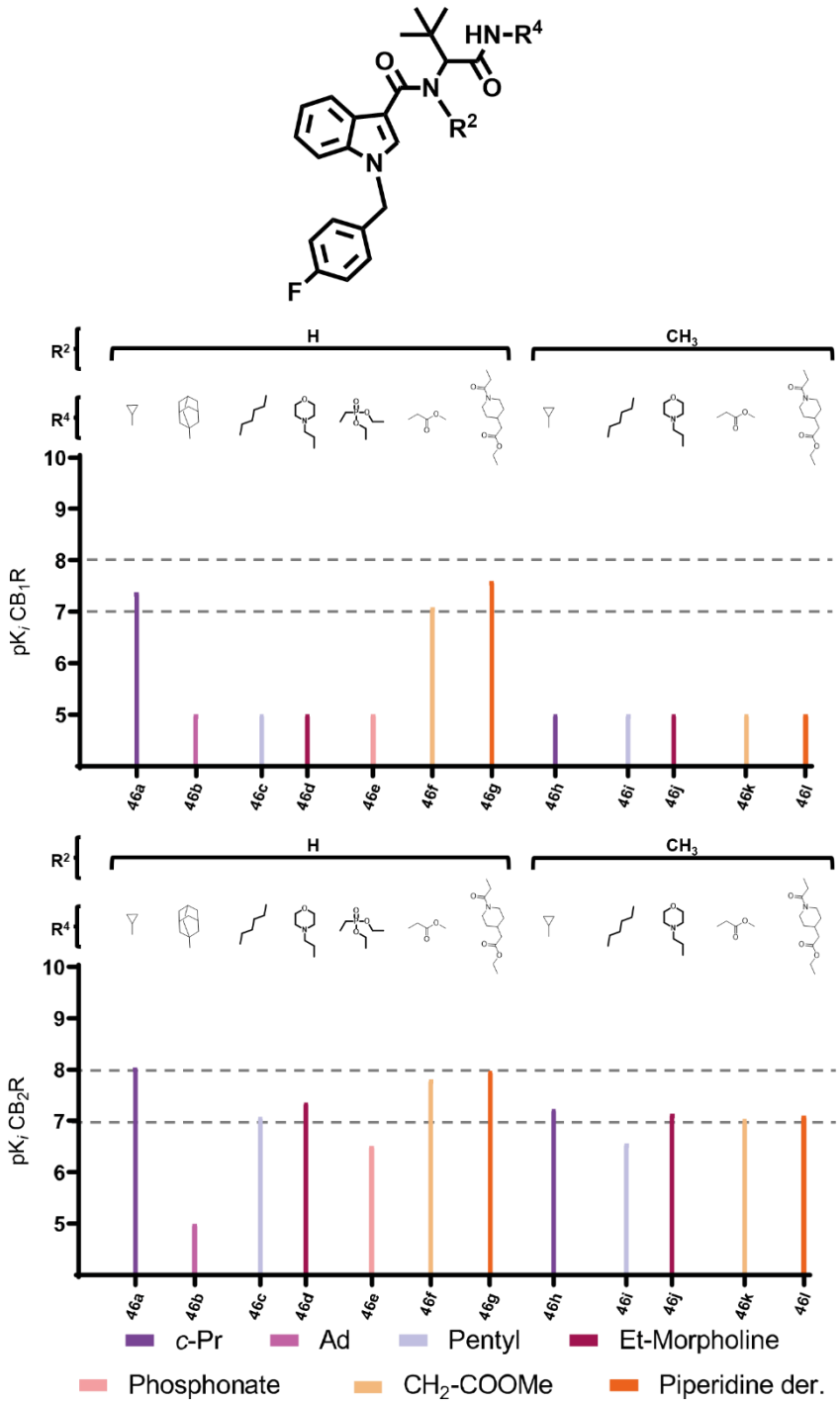


Figure 86: Bar chart representation of the SAR trends related to R^4 groups in the amide series (II subset). CB_1R affinity data (above) and CB_2R affinity data (bottom) are reported.

USC
UNIVERSIDADE DE SANTIAGO DE COMPOSTELA

In order to investigate the effect of R^1 in this series, together with the *t*-Bu and Bn group at R^4, the analogues of the most affine and selective compound of this Chapter (**46d**) have been synthetized. The Bn group at R^4 produces potent but not selective compounds (**47e** and **47h**, Table 20, Figure 87). When R^4 = Et-Morpholine, the introduction of CH_2-Cy and 5-F-Pentyl at R^1 leads to highly affine but not selective compounds (**47c** and **47f**), while the Pentyl derivative (**47i**) shows a remarkable selectivity towards CB_2R (K_i = 98.2 nM, > 100-fold selectivity over CB_1R) (Table 20, Figure 87).

Then, we investigated the influence of R^2: independently of R^1, in the *t*-Bu derivatives, when R^2 = Me, we observed a decrease in affinity but not in selectivity towards CB_2R (cpds **47m** and **47q**) compared to the NH compounds (**47d** and **47g**). In the Bn and Et-Morpholine derivatives, with the introduction of a methyl at R^2, an improvement in selectivity has been observed: cpds **47n**, **47o**, **47o**, **47q** and **47r** show a K_i value between 97.3 and 386 nM at CB_2R (> 100-fold selectivity over CB_1R) (Table 20, Figure 87).

USC UNIVERSIDADE DE SANTIAGO DE COMPOSTELA

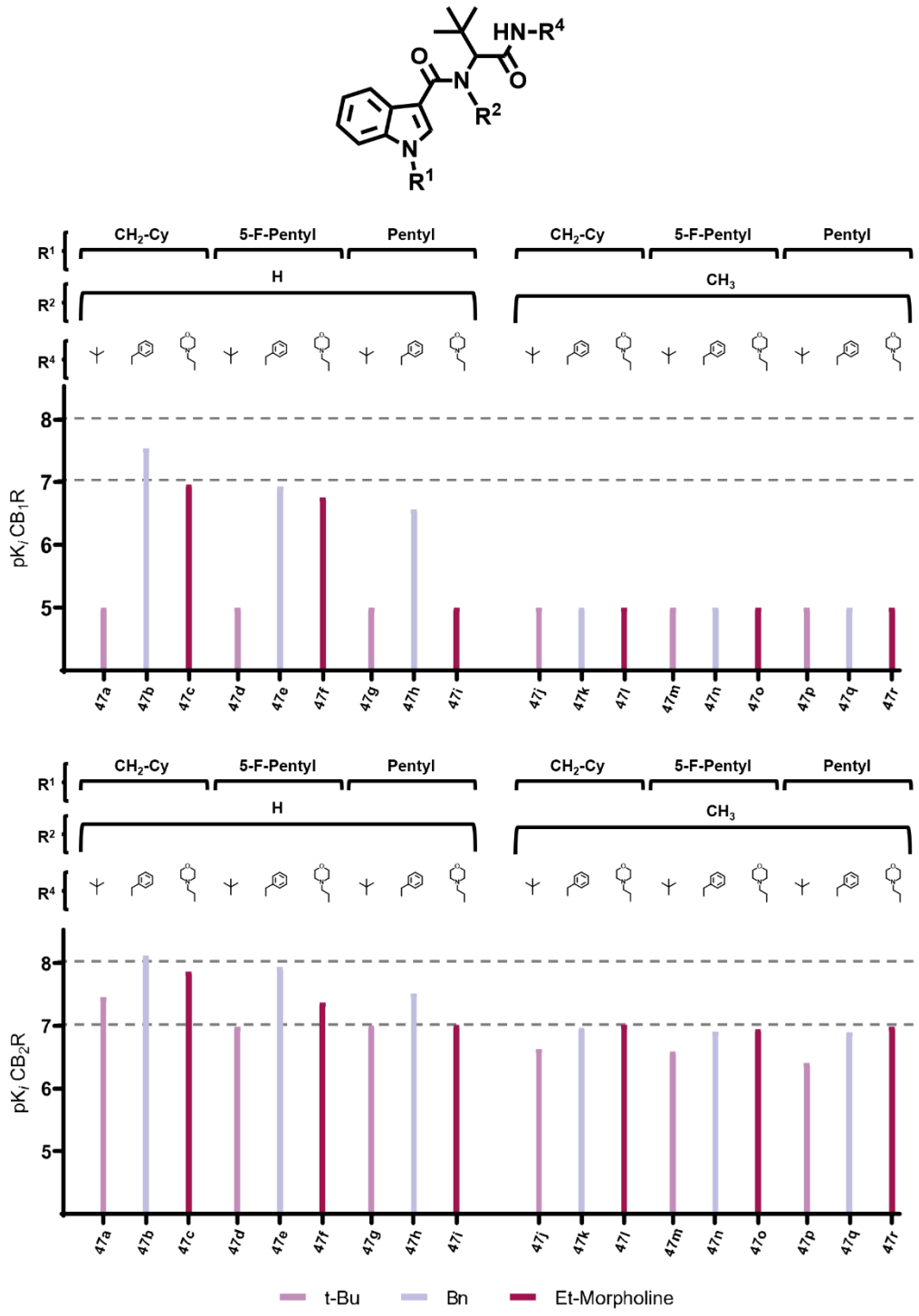


Figure 87: Bar chart representation of the SAR trends related to R^1 and R^4 groups in the amide series. CB_1R affinity data (above) and CB_2R affinity data (bottom) are reported.

USC
UNIVERSIDADE DE SANTIAGO DE COMPOSTELA

USC
UNIVERSIDADE
DE SANTIAGO
DE COMPOSTELA

3.5 CHAPTER 5: ADVANCED PHARMACOLOGICAL STUDIES OF SELECTED CB_2R LIGANDS

Diverse studies have demonstrated the favorable therapeutic effects derived from the CB_2R activation for the treatment of neuroinflammatory and neurodegenerative diseases.[2,9,12,17,26,54] More recently, the breathtaking and synergistic facets of CB_2R agonists in the context of cancer (immune) therapy started to be unveiled.[2,9,12,17,26,54] The scarce availability of high affine pharmacological tools and drugs that selectively target the CB_2R (agonists, antagonists or allosteric modulators), and the limited scientific understanding of the intricate signaling pathways involving the endocannabinoid system (in both physiological and pathological conditions) represent a significant obstacle in the development of innovative cannabinergic-based therapies for these pathologies.[2,9,12,17,26,54]

Within the context of this Thesis, we conducted a multicomponent-assisted pharmacomodulation process that led to the discovery of several ligands that exhibit high affinity and exceptional selectivity towards CB_2R. This last Chapter, which has a more pharmacological and translational focus, is dedicated to a deeper characterization of the pharmacology and preliminary evaluation of some of the therapeutic applications of the best compounds identified in this work. Thus, in the first part of this Chapter, we describe the evaluation of the functional activity profile (agonist or antagonist) of a selection of the best compounds herein identified in terms of affinity and selectivity (but also using the structural diversity criteria) and the detailed study of their signaling pathways (biased or unbiased). The second part of this Chapter is focused on the preliminary evaluation of the therapeutic potential of representative compounds. For this aim we selected four CB_2R agonists and evaluated both their effectiveness to reduce the proliferation of a highly aggressive central nervous system cancer (glioblastoma) and their ability to modulate inflammation mediators (anti-inflammatory action).

USC UNIVERSIDADE DE SANTIAGO DE COMPOSTELA

Evaluation of the functional behavior of selected CB_2R agonists. Ten CB_2R selective ligands identified during this project (Figure 88), that are representatives of the two functional series (esters and amides) and diversities explored (R^1, R^2, R^3, R^4 and R^5), were submitted to functional studies to evaluate their functional (agonist or antagonist) behavior.

Radioligand binding assays provide valuable information about receptor binding and ligand affinity (K_i), but not about the ligand's ability to activate or inhibit receptor signaling pathways. To address the ligand's functional profile, it is required to measure the downstream response of CB_2R activation, e.g., measuring intracellular calcium release, cAMP levels, or phosphorylation of specific signaling proteins.

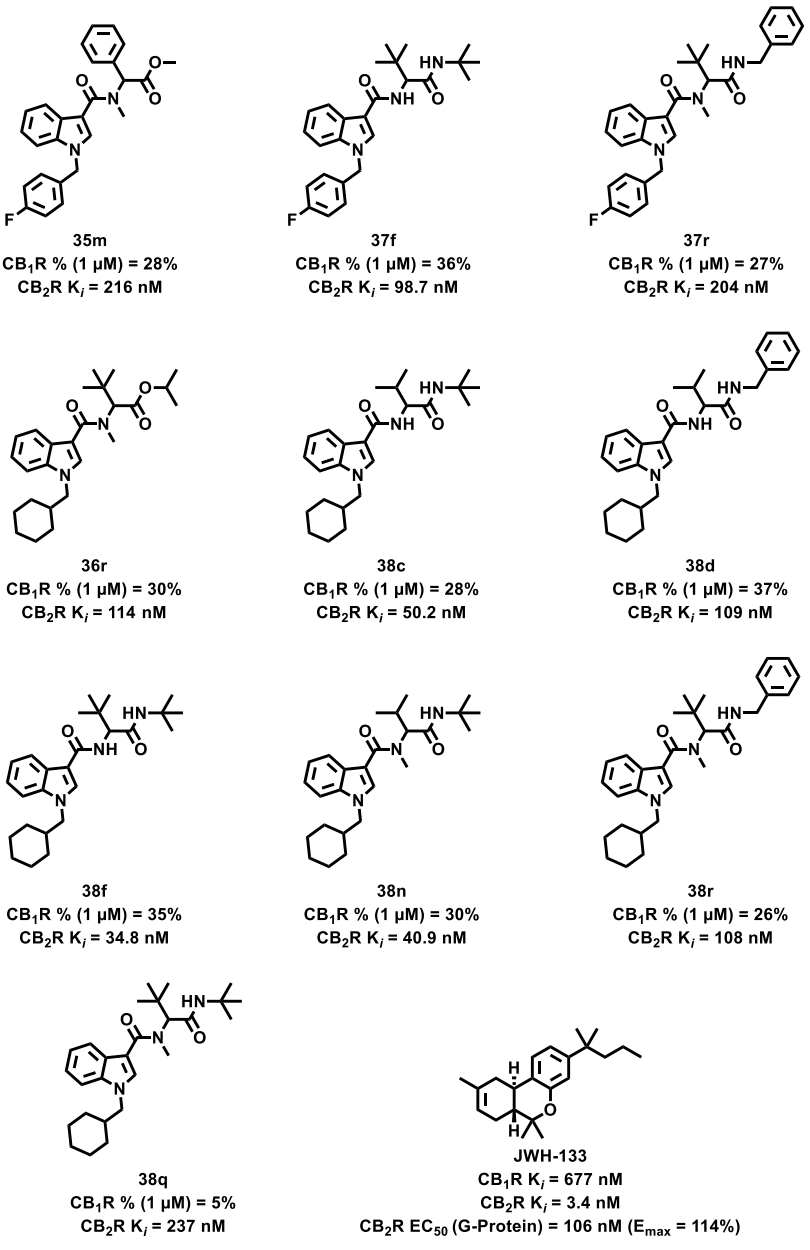


Figure 88: Structure of the CB_2R ligands selected for functional studies and JWH-133.

The functional experiments were performed by the group of the Professor Gemma Navarro (University of Barcelona), following established protocols evaluating cAMP levels.[141] For comparative reasons, JWH-133 (Figure 88), a potent and CB_2R selective agonist (structurally related to Δ^9-THC, Figure 88) was employed as reference compound and submitted to the same experimental conditions.

The results obtained during these experiments are shown in Table 21, for comparative purposes the affinity data of selected ligands was also incorporated. As observed, all compounds were able to increase cAMP concentrations in a dose-dependent manner and exhibit EC_{50} values ranging 19 - 903 nM (Table 21). These results unequivocally validated their agonist behavior. Analysis of the E_{max} data reported in Table 21 enabled to confirm that the new compounds herein identified behave as full (E_{max} > 85%) or partial (E_{max} = 40-85%) agonists of CB_2R (Table 21). The dose-response curves obtained during this study are presented in Figure 89.

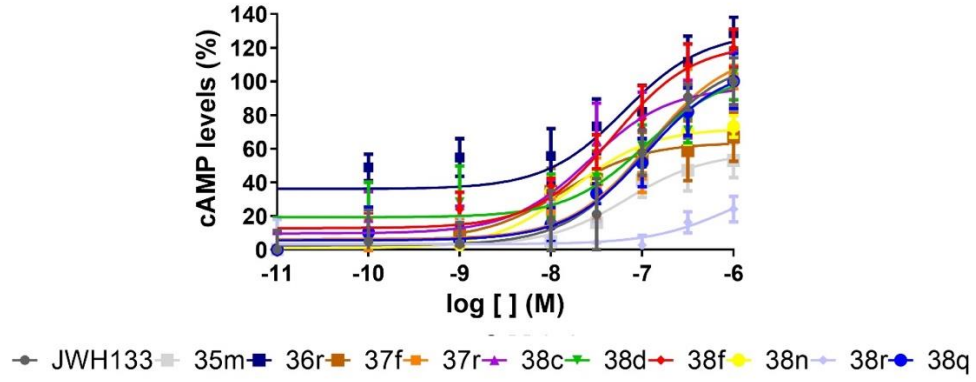
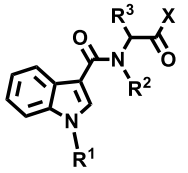


Figure 89: Dose-response curves obtained for reference ligand (JWH133) and selected ligands at CB_2R during cAMP functional assay.

USC UNIVERSIDADE DE SANTIAGO DE COMPOSTELA

Table 21: Structure, affinity, and CB_2R functional data obtained for representative CB_2R selective ligands.



Compound numbers and diversity explored					Binding data		CB_2R Functional cAMP Data	
					CB_1R	CB_2R		
Code	**R^1**	**R^2**	**R^3**	**X**	**% at 1 μM[a)]**	**K_i[b)]**	**EC_{50}[c)]**	**E_{max}[d)]**
35m	4-F-Bn	Me	Ph	OMe	28%	216 nM	82.5 nM	62%
37f	4-F-Bn	H	*t*-Bu	NH-*t*-Bu	36%	98.7 nM	19.3 nM	68%
37r	4-F-Bn	Me	*t*-Bu	NH-Bn	27%	204 nM	119 nM	118%
36r	CH_2-Cy	Me	*t*-Bu	O-*i*-Pr	30%	114 nM	63.8 nM	129%
38c	CH_2-Cy	H	*i*-Pr	NH-*t*-Bu	28%	50.2 nM	26.4 nM	96%
38d	CH_2-Cy	H	*i*-Pr	NH-Bn	37%	109 nM	110 nM	105%
38f	CH_2-Cy	H	*t*-Bu	NH-*t*-Bu	35%	34.8 nM	48.9 nM	122%
38n	CH_2-Cy	Me	*i*-Pr	NH-*t*-Bu	30%	40.9 nM	19.9 nM	74%
38q	CH_2-Cy	Me	*t*-Bu	NH-*t*-Bu	5%	237 nM	110 nM	109%
38r	CH_2-Cy	Me	*t*-Bu	NH-Bn	25%	108 nM	903 nM	44%
JWH133	-	-	-	-	-	-	106 nM	114%

[a)] Displacement of specific [^{3}H]-CP 55,940 binding in membrane preparations of human CB_1Rs transfected in CHO-CB1 C3 cell line expressed as K_i in nM (n = 3) or percentage displacement of specific binding at a concentration of 1 μM (n = 2). [b)] Displacement of specific [^{3}H]-CP 55,940 binding in membrane preparations of human CB_2Rs transfected in HEK-293T cells expressed as K_i in nM (n = 3) or percentage displacement of specific binding at a concentration of 1 μM (n = 2). [c)] Functional activity assessed in transfected HEK-293T cells by determining cAMP levels after forskolin stimulation. [d)] E_{max} values were normalized to a maximal efficacious concentration of CP 55,940.

USC UNIVERSIDADE DE SANTIAGO DE COMPOSTELA

As observed in Table 21, the studied ligands differ in efficacy (E_{max}) and, according to this parameter, can be classified in two groups. Thus, six of the ten evaluated CB_2R selective agonists (**37r**, **36r**, **38c**, **38d**, **38f** and **38q**) behave as full agonists (E_{max} = 96 - 129%), while the other four ligands (**35m**, **37f**, **38n** and **38r**) behave as partial agonists (E_{max} = 44 - 74%). Figure 90 depicts the structure of the ligands and the functional data, grouping them according to their functional profile (full agonists or partial agonists).

The structural analysis of the selected CB_2R ligands allows to verify the reason for their inclusion in this study, as they perfectly represent the diversity space (substitution patterns and diversity elements) that was explored in the context of this study (R^1 = 4-F-Bn or CH_2-Cy, R^2 = H or Me, R^3 = *t*-Bu or *i*-Pr, or X = OMe, NH-*t*-Bu or NH-Bn). Upon conducting a substructural analysis of common substitution patterns at the six full agonists (Figure 90), five of the six compounds behaving as full agonists have been revealed to contain a common structural element: the cyclohexyl methyl (CH_2-Cy) group at R^1. This observation suggests that the group at R^1 could be the most influential structural parameter when defining the efficacy profile (full or partial agonist) of these ligands. Interestingly, the ligand with the lowest efficacy in this series (**38r**) also contains a cyclohexyl methyl at R^1 (Figure 90). Moreover, ligand **37r**, the only full agonist that does not contain cyclohexyl methyl residue at R^1, exhibits excellent efficacy (E_{max} = 118%).

Although more experimental data should be required to stablish definitive conclusion, the obtained results suggest that the presence of the cyclohexyl methyl group may be a necessary, but not sufficient requirement to provide high efficacy and the other structural elements (R^2, R^3 and X) seem to have a role in the definition of the full/partial agonist profile in these series.

USC
UNIVERSIDADE DE SANTIAGO DE COMPOSTELA

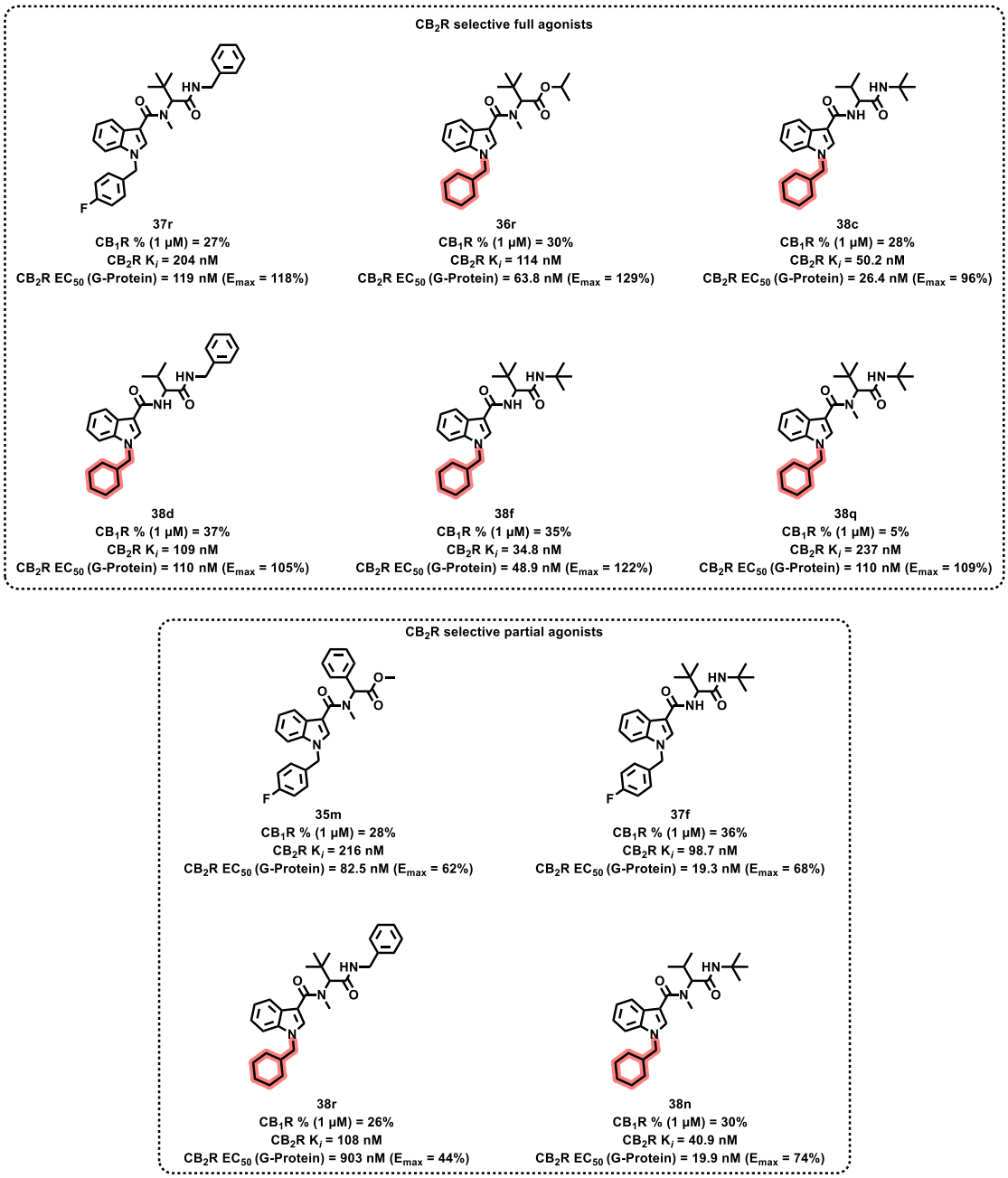


Figure 90: Structure and functional data of selected CB_2R agonists grouped according to their functional behavior.

USC UNIVERSIDADE DE SANTIAGO DE COMPOSTELA

Functional selectivity studies. The concept of biased agonism has changed our understanding of GPCR signaling and has modified the paradigm of GPCR signaling in different contexts, particularly in drug discovery.[142,143] Functional selectivity can be defined as the ability of a ligand to preferentially signaling through a precise pathway among other possible routes.[32,69,144] As briefly explained in the introduction of the Thesis, the signaling phenomenon has a crucial role in drug development and is being instrumental to understand and dissociate the adverse effects of many drugs.[32,69,142–144] The biased agonism of a ligand cannot be considered as an absolute description of its action, since it also heavily depends on the receptor, reference ligand, and the involved pathways[145] (Figure 91).

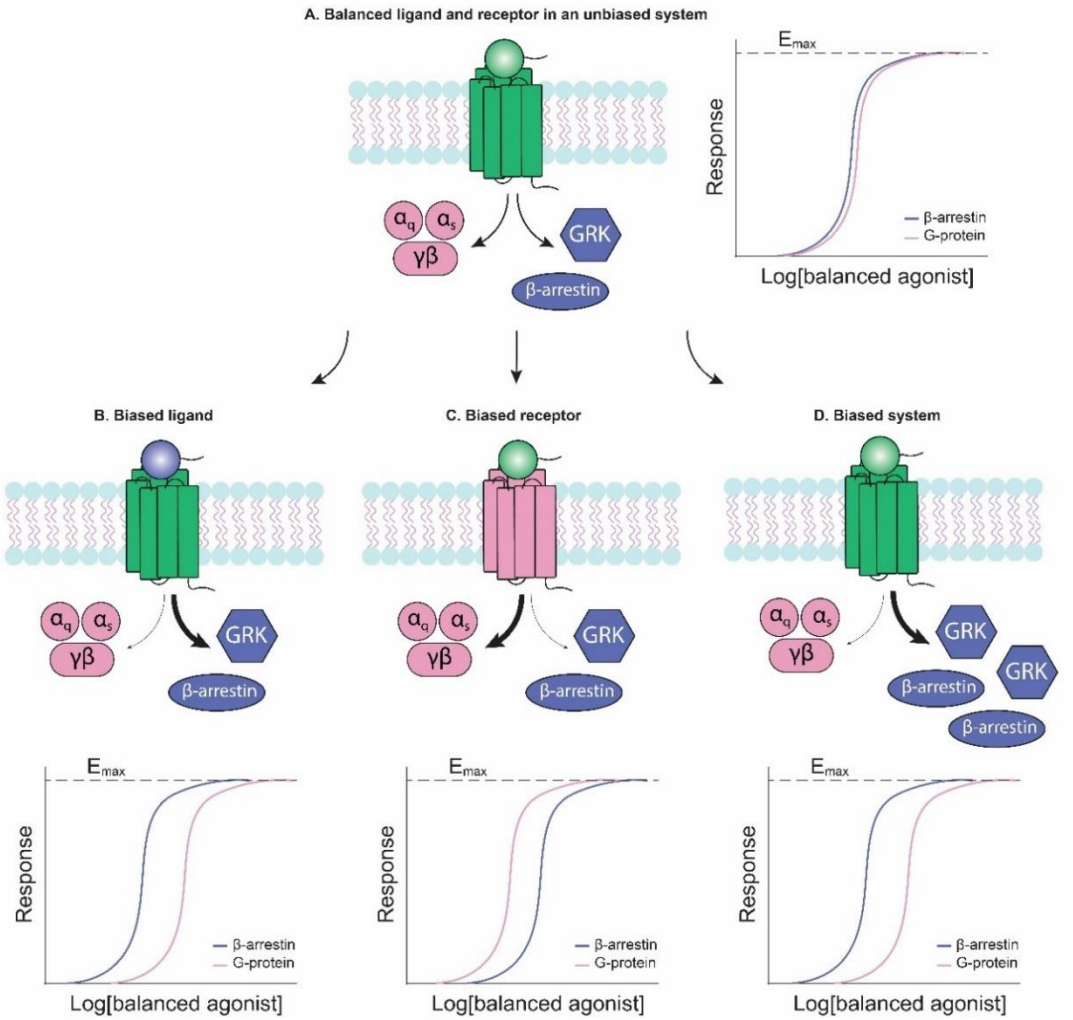


Figure 91: Graphical representation of the different facets of the biased signaling phenomena.

USC UNIVERSIDADE DE SANTIAGO DE COMPOSTELA

In the case of the GPCRs concerned within this Thesis (CBRs), the therapeutic profile (advantages/disadvantages) derived from CB_2R-biased signaling has not yet been thoroughly investigated. Indeed, only a few truly CB_2Rs biased ligands have been described to date.[10,69–71] The main problem with known biased ligands, both for cannabinoid receptors and other GPCRs, is their lack of selectivity (promiscuity) against other receptor subtypes within the family.[70,71] Many ligands that exhibit a biased signaling profile at a particular receptor (e.g., CB_2R) are not selective against their congeners (e.g., CB_1R). Although these compounds may be useful for studying processes in transfected cells (that express only the receptor of interest), their promiscuity against other subtypes limits their usefulness and the correct interpretation of their effects when used in more complex systems (e.g., cell models, *in vivo* studies, or drug uses).

This data is indicative of the enormous scientific challenge posed by the development of ligands that simultaneously show receptor subtype selectivity and biased signaling. The challenge of identifying new biased ligands is on a par with the intricacy of GPCR signaling. After G protein-coupled receptor (GPCR) activation, different signaling pathways and downstream effectors can coexist. GPCRs can interact with multiple intracellular signaling molecules beyond G proteins, such as β-arrestins, scaffold proteins, and other signaling molecules.[10,69–71] These molecules can mediate GPCR signaling through alternative pathways, leading to the activation of different downstream effectors and cellular responses. For example, β-arrestins can interact with GPCRs and initiate alternative signaling pathways, such as the mitogen-activated protein kinase (MAPK) pathway, independently of G protein activation.[10,69–71,145,146] In summary, multiple signaling pathways can coexist after GPCR activation due to the complex interactions between GPCRs and intracellular signaling molecules.

The G protein-cAMP (cyclic adenosine monophosphate) pathway is the most common and well-characterized signaling pathway of GPCRs, being considered the "canonical" signaling form of membrane receptors.[10,69] GPCRs are typically coupled to heterotrimeric G proteins that can activate intracellular signaling cascades. When a ligand binds to a GPCR, it can activate the associated G protein, which then stimulates the production of cAMP by adenylate cyclase. cAMP can then activate downstream effector proteins such as protein kinase A (PKA) to regulate cellular processes such as gene expression and metabolism. The G protein-cAMP pathway has been extensively

USC DE COMPOSTELA

studied for its roles in a wide range of physiological and pathological processes.[10,69–71,146]

β-arrestins are proteins that bind to G protein-coupled receptors (GPCRs) after they are activated by a ligand (endogenous or exogenous). β-arrestins act as negative regulators of GPCR signaling, meaning that after they bind to an activated receptor, they interrupt the signaling activated by the receptor and can induce its desensitization (loss of response) and endocytosis.[10,69–71,146] In addition to their role in regulating GPCRs, β-arrestins have been found to have functions in other cellular processes, such as cell proliferation and cell migration, and can act as modulators of signaling in other cellular pathways. Moreover, β-arrestins have been implicated in the pathogenesis of various diseases, including cancer, inflammation, and cardiovascular disorders.[10,69–71,146]

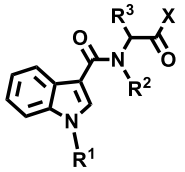
The complexity of GPCR signaling, and the multiple pathways involved, make it challenging to identify ligands that exhibit selective biased signaling. Shedding light on the biased signaling profile of new selective CB_2R agonists is crucial for the development of drugs with improved efficacy and safety profiles. This knowledge can help to identify compounds with desirable signaling profiles, which can selectively activate specific pathways while avoiding the activation of others. This can lead to the development of drugs that target diseases more effectively and with fewer side effects. Therefore, investigating the biased signaling profiles of new CB_2R agonists is an important step towards the development of more effective and safer drugs.

After identifying a collection of CB_2R-selective ligands in earlier Chapters, it was decided to complete their pharmacological characterization by investigating their functional selectivity profile (biased/unbiased signaling). To accomplish this, ten ligands (Figure 88) that were previously used to validate the functional (agonist) behavior of the series were employed, as they effectively represent the diversity space explored during this project. To fully characterize the signaling (biased/unbiased) profile of the selected ligands, we evaluated their ability to recruit β-arrestin, that complements the previously evaluated canonical G protein signaling (cAMP).

The results of these investigations are presented in Table 22 and provide a more complete picture of the signaling landscape of these ligands. The dose-response curves for all studied ligands at each signaling pathway are presented in Figure 92.

USC UNIVERSIDADE DE SANTIAGO DE COMPOSTELA

Table 22: Binding and functional data of the best CB_2R selective ligands.



					Binding data		Functional data at CB_2R in different signaling pathways		Biased profile
					CB_1R	CB_2R			
Code	R^1	R^2	R^3	X	% at 1μM[a]	K_i[b]	cAMP EC_{50}(nM)[c] [E_{max}][d]	β-arrestin EC_{50}(nM)[c] [E_{max}][d]	
35m	4-F-Bn	Me	Ph	OMe	28%	216 nM	82.5 [62%]	29.1 [86%]	**β-arrestin**
37f	4-F-Bn	H	*t*-Bu	NH-*t*-Bu	36%	98.7 nM	19.3 [68%]	17.8 [86%]	**β-arrestin**
37r	4-F-Bn	Me	*t*-Bu	NH-Bn	27%	204 nM	119 [118%]	1.52 [62%]	**G-protein**
36r	CH_2-Cy	Me	*t*-Bu	O-*i*-Pr	30%	114 nM	63.8 [129%]	11.2 [78%]	**G-protein**
38c	CH_2-Cy	H	*i*-Pr	NH-*t*-Bu	28%	50.2 nM	26.4 [96%]	11.7 [86%]	**Unbiased**
38d	CH_2-Cy	H	*i*-Pr	NH-Bn	37%	109 nM	110 [105%]	2.25 [37%]	**G-protein**
38f	CH_2-Cy	H	*t*-Bu	NH-*t*-Bu	35%	34.8 nM	48.9 [122%]	7.20 [36%]	**G-protein**
38n	CH_2-Cy	Me	*i*-Pr	NH-*t*-Bu	30%	40.9 nM	19.9 [74%]	9.39 [64%]	**Unbiased**
38q	CH_2-Cy	Me	*t*-Bu	NH-*t*-Bu	5%	237 nM	110 [109%]	12.5 [43%]	**G-protein**
38r	CH_2-Cy	Me	*t*-Bu	NH-Bn	25%	108 nM	903 [44%]	35.8 [64%]	**β-arrestin**
JWH133	-	-	-	-	-	-	106 [114%]	24.3 [103%]	**Unbiased**

[a] Displacement of specific [^{3}H]-CP 55,940 binding in membrane preparations of human CB_1Rs transfected in CHO-CB1 C3 cell line expressed as K_i in nM (n = 3) or percentage displacement of specific binding at a concentration of 1 μM (n = 2). [b] Displacement of specific [^{3}H]-CP 55,940 binding in membrane preparations of human CB_2Rs transfected in HEK-293T cells expressed as K_i in nM (n = 3) or percentage displacement of specific binding at a concentration of 1 μM (n = 2). [c] EC_{50} and E_{max} values are the average of five experiments, each performed in duplicate. [d] E_{max} relative to the effect of the reference agonist JWH-133.

USC UNIVERSIDADE DE SANTIAGO DE COMPOSTELA

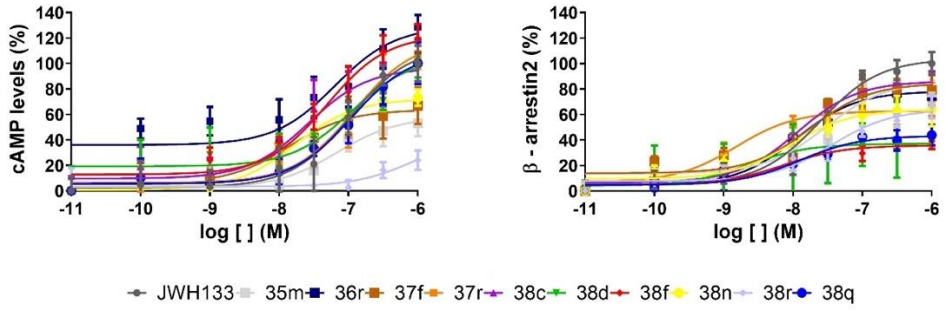


Figure 92: Dose-response curves obtained for reference ligand (JWH133) and selected ligands at CB_2R during functional assays.

In this study, the CB_2R selective ligand JWH133 (Figure 88) has been employed as reference ligand due to the widespread consensus in the scientific community regarding its classification as an unbiased agonist.[70,144] The aim of the study was to explore the signalling profile (biased/unbiased) of selected ligands and, if possible, to identify general trends evidencing direct relationships between the structure of the agonists and their preferred signalling pathway.

The analysis of the data obtained (Table 22) leads us to conclude that the ten tested ligands can be classified into three signaling profiles. Firstly, there are two unbiased ligands (**38c** and **38n**) that do not exhibit a preference between the G-protein or β-arrestin pathway. Secondly, there are five G-protein biased ligands (**37r**, **36r**, **38d**, **38f**, and **38q**) that display high activity (EC_{50}) and excellent efficacy (Emax >85%) in the cAMP pathway, along with low-to-moderate efficacy in β-arrestin recruitment. Lastly, there are three β-arrestin biased ligands (**35m**, **37f**, and **38r**) that demonstrate superior performance in the non-canonical GPCR signaling pathway (β-arrestin).

An integrated analysis of these findings confirms the identification of novel CB_2R selective agonists, both unbiased and biased. It is noteworthy that these closely related structural analogues exhibit distinct signaling profiles, underscoring the substantial impact of minor structural modifications on functional signaling. The newly identified ligands, which selectively target the CB_2R and exhibit distinct intracellular signaling profiles, represent excellent pharmacological tools for studying the complex and intricate intracellular signaling pathways of CB_2R in the context of challenging pathologies (neuroinflammation, pain or cancer).

USC UNIVERSIDADE DE SANTIAGO DE COMPOSTELA

Figure 93 shows the whole ligands collection studied with the ligands grouped according to the signaling profiles observed [unbiased or biased (G-protein or β-arrestin)].

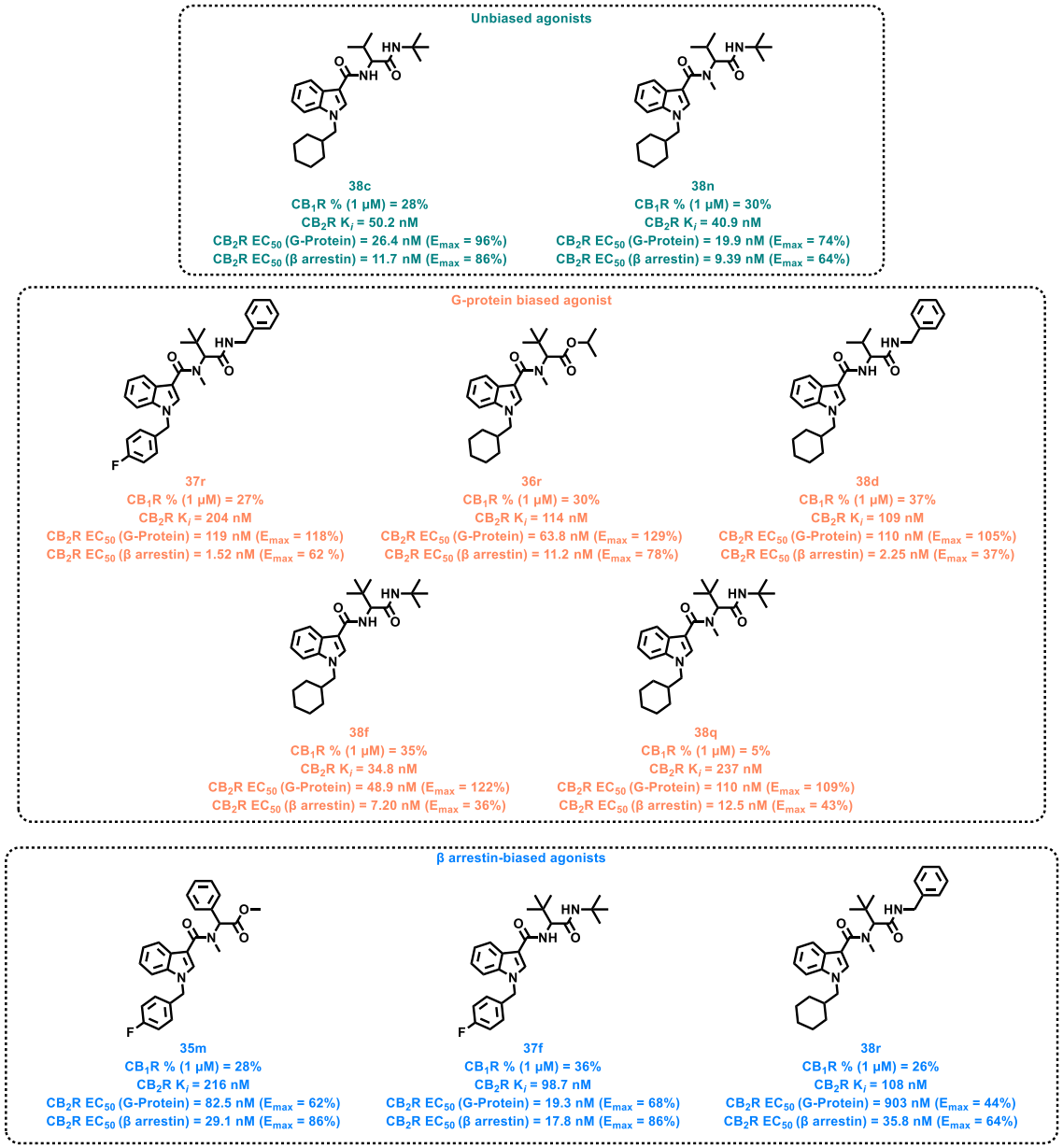


Figure 93: Structure of the ligands grouped according to their signaling profiles.

USC UNIVERSIDADE DE SANTIAGO DE COMPOSTELA

It is important to note that the exploration of the therapeutic applications of biased CB_2R agonists (e.g., G-protein biased and β-arrestin biased) is still under investigation, and more research is needed to fully understand their efficacy, safety, and clinical potential in these and other disease conditions.[10,69–71,146] A key factor in addressing the unequivocal validation of the role of biased CB_2R agonists, which would represent an unexplored approach for the treatment of serious pathologies, is the availability of truly selective and biased ligands. The comparative evaluation of the efficacy of the ligands discovered here, specifically the G-protein biased and β-arrestin biased ligands, in advanced pharmacological studies would greatly contribute to a deeper understanding of the true impact of CB_2R biased signaling in various pathologies. Therefore, we firmly believe that the discovery of the compounds identified in this section holds significant value and utility within the drug discovery context. Some of the potential therapeutic applications of these agonists include:

G-protein biased CB_2R agonists: Pain management: G-protein biased CB_2R agonists can be used as analgesics for the treatment of chronic pain, including neuropathic pain and inflammatory pain. By selectively activating G-protein signaling pathways, these agonists can modulate pain perception and provide analgesic effects.[10,69–71,146] Inflammation and autoimmune diseases: CB_2Rs are predominantly expressed in immune cells, and G-protein biased agonists can target these receptors to modulate immune responses. They may have therapeutic applications in inflammatory conditions (e.g., rheumatoid arthritis, inflammatory bowel disease, multiple sclerosis), and other autoimmune diseases by reducing inflammation and immune cell activation.[10,69–71,146] Neurological disorders: G-protein biased CB_2R agonists have shown promise in preclinical studies for the treatment of neurodegenerative disorders (e.g., Alzheimer's, Parkinson's and Huntington's diseases). These agonists can modulate neuroinflammation and provide neuroprotective effects.[10,69–71,146] Cancer therapy: CB_2Rs are expressed in certain cancer cells, and G-protein biased agonists can target these receptors to modulate tumor growth and progression. They may have potential applications in cancer therapy by inhibiting cell proliferation, inducing apoptosis, and reducing tumor angiogenesis.[2,9,36–40,54,69–71,146,10,147,12,17,26,32–35]

USC UNIVERSIDADE DE SANTIAGO DE COMPOSTELA

β-arrestin biased CB_2R agonists: Neuroprotection and neuroinflammation: β-arrestin biased CB_2R agonists have shown promise in preclinical studies as neuroprotective agents. They may have applications in the treatment of neurodegenerative disorders, such as multiple sclerosis, by modulating neuroinflammation and promoting neuronal survival.[10,69–71,146] Anti-inflammatory effects: β-arrestin biased CB_2R agonists may have therapeutic potential in various inflammatory conditions, including autoimmune diseases and chronic inflammatory disorders. By selectively activating the β-arrestin pathway, they can modulate immune responses and reduce inflammation.[10,69–71,146] Cardiovascular disorders: β-arrestin biased CB_2R agonists have been investigated for their potential cardioprotective effects. They may offer benefits in conditions such as myocardial ischemia-reperfusion injury, heart failure, and atherosclerosis by modulating inflammatory responses, improving cardiac function, and reducing tissue damage.[10,69–71,146] Metabolic disorders: β-arrestin biased CB_2R agonists are being explored for their potential applications in metabolic disorders, including obesity and type 2 diabetes. They may modulate adipose tissue function, improve insulin sensitivity, and regulate energy metabolism.[10,69–71,146]

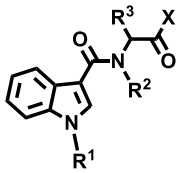
To further complement the signaling characterization study and gather additional evidence for upcoming pharmacological evaluations, we also assessed the selected ligands' performance within the MAPK/ERK downstream pathway.

The MAPK (mitogen-activated protein kinases), also referred to as MAPK/ERK (MAPK: mitogen-activated protein kinases, ERK: signaling regulated kinases), is a vital cellular signaling pathway responsible for regulating a multitude of cellular processes, including cell growth, proliferation, differentiation, and survival.[25,148] The pathway can be activated either by G-protein or β-arrestin signaling and in response to various extracellular signals, such as growth factors and cytokines, and leads to the activation of a cascade of kinases that ultimately phosphorylate and activate the extracellular signal-regulated kinases (ERKs). ERKs then translocate to the nucleus and modulate the expression of genes involved in various cellular processes.[25,148] The pathway is responsible for transmitting signals from the cell surface to the nucleus, ultimately influencing multiple cellular functions and contributing to various physiological and pathological processes including inflammation, neurodegeneration, and cancer cell proliferation.[25,148]

USC COMPOSTELA

The results of these experiments are documented in Table 23, and the corresponding dose-response curves are illustrated in Figure 94. As observed, the majority of the tested CB_2R selective agonists activate the MAPK signaling pathway, revealing potent activity, and predominantly acting as full agonists (E_{max} 62 – 120%). Notably, compounds **37r**, **36r**, and **38r** are particularly noteworthy as they exhibit sub-nanomolar EC_{50} values (0.44, 0.04, and 0.21 nM, respectively).

Table 23: Binding and functional data of the best CB_2R selective ligands.



					Binding data		MAPK/ERK pathway	
					CB_1R	CB_2R		
Code	**R^1**	**R^2**	**R^3**	**X**	**% at 1μM[a)]**	**K_i[b)]**	**EC_{50}(nM)[c)]**	**[E_{max}][d)]**
35m	4-F-Bn	Me	Ph	Ome	28%	216 nM	2.01	120%
37f	4-F-Bn	H	*t*-Bu	NH-*t*-Bu	36%	98.7 nM	3.9	78%
37r	4-F-Bn	Me	*t*-Bu	NH-Bn	27%	204 nM	0.44	105%
36r	CH_2-Cy	Me	*t*-Bu	O-*i*-Pr	30%	114 nM	0.04	98%
38c	CH_2-Cy	H	*i*-Pr	NH-*t*-Bu	28%	50.2 nM	3.35	107%
38d	CH_2-Cy	H	*i*-Pr	NH-Bn	37%	109 nM	1.82	95%
38f	CH_2-Cy	H	*t*-Bu	NH-*t*-Bu	35%	34.8 nM	1.83	97%
38n	CH_2-Cy	Me	*i*-Pr	NH-*t*-Bu	30%	40.9 nM	36.6	111%
38q	CH_2-Cy	Me	*t*-Bu	NH-*t*-Bu	5%	237 nM	3.02	76%
38r	CH_2-Cy	Me	*t*-Bu	NH-Bn	25%	108 nM	0.21	62%
JWH133	-	-	-	-	-	-	4.27	100%

[a)] Displacement of specific [^{3}H]-CP 55,940 binding in membrane preparations of human CB_1Rs transfected in CHO-CB1 C3 cell line expressed as K_i in nM (n = 3) or percentage displacement of specific binding at a concentration of 1 μM (n = 2). [b)] Displacement of specific [^{3}H]-CP 55,940 binding in membrane preparations of human CB_2Rs transfected in HEK-293T cells expressed as K_i in nM (n = 3) or percentage displacement of specific binding at a concentration of 1 μM (n = 2). [c)] EC_{50} and E_{max} values are the average of five experiments, each performed in duplicate. [d)] E_{max} relative to the effect of the reference agonist JWH-133.

USC UNIVERSIDADE DE SANTIAGO DE COMPOSTELA

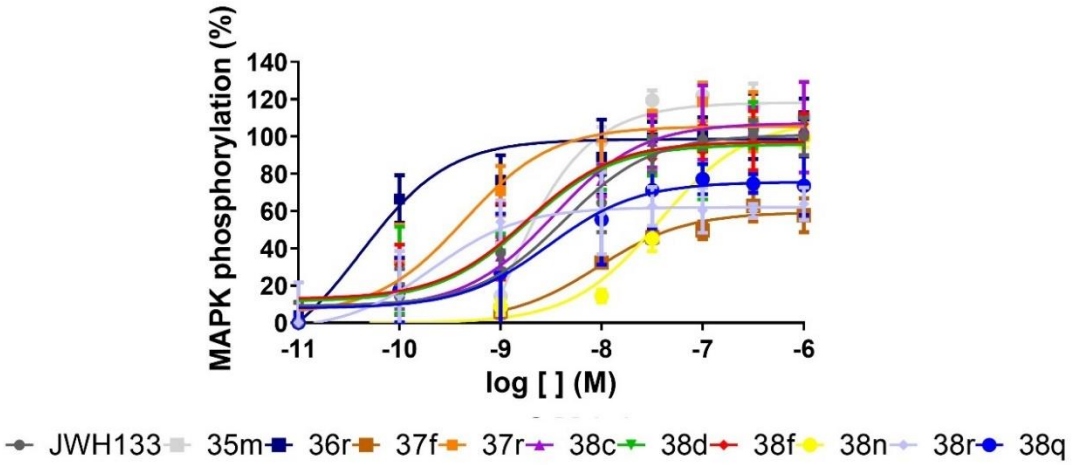
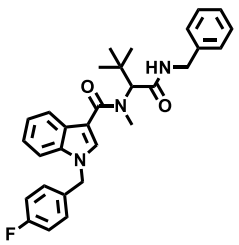
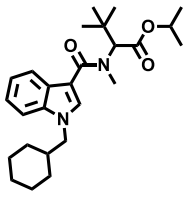


Figure 94: Dose-response curves obtained for reference ligand (JWH133) and selected ligands at CB_2R during MAPK/ERK functional assay.

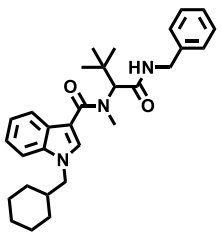
The compounds exhibiting superior performance (sub-nanomolar EC_{50}) at the MAPK/ERK pathway are depicted in Figure 95. As observed, two of them (amides) contain identical groups at R^2 (Me), R^3 (*t*-Bu), and X (NH-Bn), differing only in the substituent at R^1 (4-F-Bn and CH_2-Cy). While further experiments are needed to draw definitive conclusions, these data suggest that the activity of these compounds in the MAPK/ERK pathway is more reliant on the substituents at R^2 and R^3, and it is enhanced in compounds containing bulky groups at X. Interestingly, the most potent ligand in this pathway is an ester that also features a bulky group (*i*-Pr) in the alkyl residue of the ester group.



37r
CB_1R % (1 μM) = 27%
CB_2R K_i = 204 nM
CB_2R EC_{50} (MAPK/ERK) = 0.44 nM
E_{max} = 105%



36r
CB_1R % (1 μM) = 30%
CB_2R K_i = 114 nM
CB_2R EC_{50} (MAPK/ERK) = 0.04 nM
E_{max} = 98%



38r
CB_1R % (1 μM) = 26%
CB_2R K_i = 108 nM
CB_2R EC_{50} (MAPK/ERK) = 0.21 nM
E_{max} = 62%

Figure 95: Structure of the ligands exhibiting sub-nanomolar EC_{50} at the MAPK/ERK pathway.

The EC_{50} obtained for these ligands (Figure 95) and the significant role of the MAPK/ERK signaling pathway in inflammatory processes and different type of cancer, inspired us to preliminary evaluate **37r**, **36r** and **38r** in other biological assays.

USC UNIVERSIDADE DE SANTIAGO DE COMPOSTELA

***In vitro* studies encompassing CB_2R agonists in cancer models.** As described in the introduction of this Doctoral Thesis, the CB_2R is upregulated in diverse pathological conditions,[2,9,12,17,26,54] with the most recognized therapeutic applications of CB_2R agonists being pain relief, neurological disorders treatment, and cancer therapy.[2,9,12,17,26,54] The role of ECS in the context of cancer has been broadly investigated during the last years[32–40,147] and several studies have demonstrated the antitumoral effects of CB_2R agonists in different types of cancer (see Introduction for more details).[2,9,37–40,54,147,12,17,26,32–36]

The CB_2R, which is extensively expressed in immune cells, has been found to be involved in regulating inflammation and immune responses in the tumor microenvironment. By selectively activating CB_2R, agonists have shown promising effects in various aspects of cancer treatment. One significant effect is their ability to induce apoptosis in cancer cells. CB_2R agonists have been found to trigger signaling pathways that promote apoptosis specifically in tumor cells while sparing healthy cells, leading to tumor regression.[2,9,37–40,54,147,12,17,26,32–36] This targeted approach minimizes the potential side effects associated with conventional chemotherapy, which often affects both cancerous and healthy cells. Furthermore, CB_2R agonists exhibit anti-proliferative effects by inhibiting the growth and division of cancer cells.[2,9,37–40,54,147,12,17,26,32–36] They can disrupt the signaling pathways responsible for cell proliferation, ultimately reducing tumor growth and progression. Additionally, CB_2R agonists have demonstrated the ability to inhibit angiogenesis, the formation of new blood vessels that supply nutrients to tumors. By disrupting this process, they effectively cut off the blood supply to tumors, starving them of vital resources and impeding their growth.[2,9,37–40,54,147,12,17,26,32–36] Moreover, CB_2R agonists have shown immunomodulatory effects by enhancing the anti-tumor immune response. Thus, they can stimulate immune cells, such as T cells and natural killer (NK) cells, to target and eliminate cancer cells more effectively. This immune-boosting property can enhance the body's natural defenses against cancer and complement other immunotherapeutic approaches. Overall, the use of CB_2R agonists in the context of cancer treatment holds immense potential. Their targeted effects on tumor cells, ability to inhibit proliferation, anti-angiogenic properties, and immunomodulatory effects make them valuable candidates for combination therapies and personalized treatment approaches. However, the limited availability of potent and highly selective CB_2R agonists poses a significant

USC DE COMPOSTELA

challenge in the field of cancer therapy, hindering the full exploration of CB_2R activation's therapeutic potential.

Further research and development of these agonists are essential to fully exploit their therapeutic benefits and improve outcomes for cancer patients.

Cytotoxicity assays in SH-SY5Y, HGC-27, MCF-7 and CACO-2 cell lines. As indicated in the objectives, one of the aims of our project was to evaluate the involvement of the CB_2R in the landscape of inflammatory diseases and cancer treatment and study the performance of our series within the context of cellular *in vitro* studies.

In Chapter 1 (SCRA libraries), we observed highly relevant neurotoxicity of representative designer drugs in primary mouse neuronal cells. The neurotoxicity data obtained for reference compounds we included in the study, but also some bibliographic findings, suggest that the neurotoxicity was directly linked to the high CB_1R affinity (agonism) mostly circumscribed to indazole derivatives (see Chapter 1).[117–120,122,123] Upon these findings, during this Doctoral Thesis we focused on the synthesis and the optimization of novel CB_2R selective agonists, dissociating the CB_1R affinity for this indole-based derivatives.

In this part of the Thesis, we decided to evaluate some representative CB_2R agonists in different cancer cell lines to preliminarily assess their potential as anticancer agents. To purse this objective, we selected four of our CB_2R selective agonists (Figure 96), chosen according to the CB_2R affinity criteria, to preliminary evaluate their effect in representative cancer cell lines.

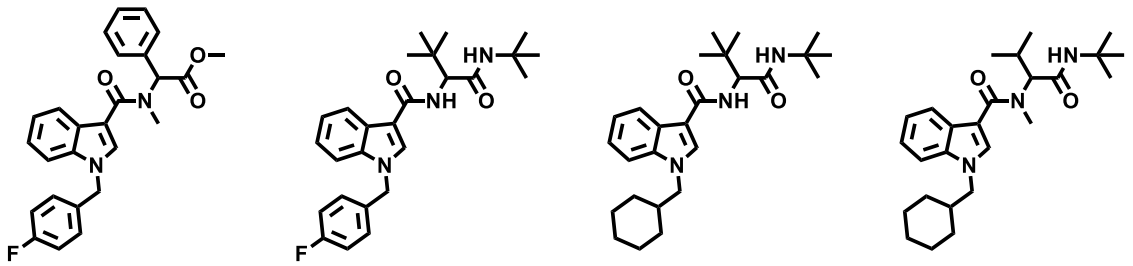


Figure 96: Selected CB_2R agonists for the *in vitro* studies in cancer models.

USC UNIVERSIDADE DE SANTIAGO DE COMPOSTELA

Several cancer cell lines were chosen for these studies: SH-SY5Y (human neuroblastoma), HGC-27 (human gastric carcinoma, both resistant and sensitive), MCF-7 (human breast adenocarcinoma), and CACO-2 (human colorectal adenocarcinoma). The experiments were conducted under the supervision of Prof. Marialessandra Contino at University of Bari, following established experimental protocols.[149] All assays were performed in duplicate and repeated at least three times. Cytotoxicity was initially assessed at 48 hours, with additional measurements conducted after 72 hours depending on the initial results.

The results of these studies are presented in Table 24. As observed, regardless of the diversity of the chosen cell lines, all evaluated compounds (**35m**, **37f**, **38f**, and **38n**) exhibit either no or very low cytotoxicity. Compound **38f** stands out as the most promising within the group, being the least toxic of all. It is worth noting that, although an IC_{50} value has been determined for some compounds (Table 24), these values are all in the micromolar range, approximately a thousand times higher than the affinity values described for these molecules (Table 24). Therefore, it is possible to conclude that the four studied ligands can be considered non-cytotoxic against the evaluated cell lines.

Table 24: Preliminary cytotoxicity data of selected ligands in different cell lines.

Code	CB_2R Binding data K_i	Cell line							
		IC_{50} (μM) or % cytotoxicity at 10 μM							
		SH-SY5Y	HGC-27 (RESISTANT)		HGC-27 (SENSITIVE)		MCF-7		CACO-2
		48h	48h	72h	48h	72h	48h	72h	72h
35m	216 nM	No toxic	62 μM	31 μM	20 μM	36.2 μM	No toxic	No toxic	50.8 μM
37f	98.7 nM	No toxic	12 μM	45.2 μM	14 μM	93 μM	No toxic	50%	31.7 μM
38f	34.8 nM	No toxic	No toxic	No toxic	No toxic	No toxic	No toxic	No toxic	No toxic
38n	40.9 nM	No toxic	13 μM	34.6 μM	16.5 μM	32 μM	No toxic	0.70 μM	42.2 μM

USC UNIVERSIDADE DE SANTIAGO DE COMPOSTELA

Assessment of the antiproliferative efficacy of selected CB_2R agonists in the U87 glioblastoma cell line. Once the low cytotoxicity of the compounds was validated, and with the aim of obtaining evidence of the potential of the four selected CB_2R agonists in the context of cancer treatment, we decided to study their proliferative activity in a model cell line. Inspired by previous studies that demonstrated the *in vitro*[150–153] effectiveness of two phytocannabinoids [Δ^9-THC and CBD (a non-psychoactive phytocannabinoid)] in a glioblastoma cell line, we chose to employ this cell line as a model. Glioblastoma is a tumor of the central nervous system known for its aggressiveness, reduced patient survival, and urgent need for new treatments. The studies were performed in collaboration with the laboratory of Dr. Miguel Abal and Dr. Jorge Barbazán, from the Institute of Health Research of Santiago (IDIS). The antiproliferative activity of the compounds was evaluated in the U87 glioblastoma cell line at three different concentrations (5, 10 and 20 µM). All assays were performed in duplicate and repeated at least three times. In these studies, the drug Temozolomide (TMZ)[154,155] has been used as a reference, which is an orally administered chemotherapeutic agent with moderate efficacy that is routinely used in clinical practice.[154,155]

As observed in Figure 97, compounds **35m**, **37f**, **38f**, and **38n** significatively reduced (≅ 15-40%) the cell proliferation of the U87 glioblastoma cell line in a dose-dependent manner, particularly at 20 µM. Amongst these compounds, ligand **37f** emerges as the most promising. As observed, **37f** reduces glioblastoma proliferation by 40% at a concentration of 10 µM (Figure 97), outperforming the measured effect of Temozolomide.

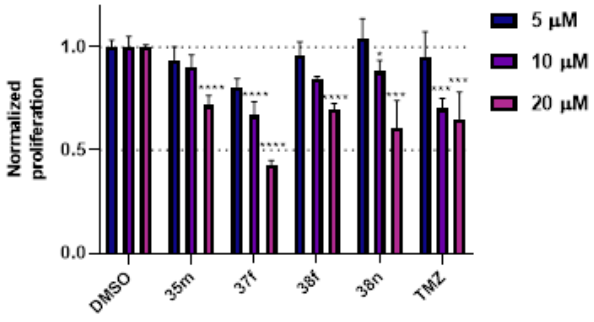


Figure 97: Bar chart representation of proliferation assay in U87 cell line. Cells were exposed to compounds for 48 h. Each bar represents the mean ± SEM of three experiments performed in duplicate. Two-Way ANOVA followed by Tukey post-hoc test was applied. Significance of symbols as follows: 1 symbol = $p < 0.05$; 2 symbols = $p < 0.01$; 3 symbols = $p < 0.001$; 4 symbols = $p < 0.0001$. Legend for symbols as follows: * indicates *vs* CTRL.

USC UNIVERSIDADE DE SANTIAGO DE COMPOSTELA

Although very preliminary, the observed inhibition (*in vitro* cell proliferation) demonstrated that the selected CB_2R agonists can be promising candidates for in deep exploration and hit to lead programs. Moreover, these results validated not only the important role of CB_2R agonism in the inhibition of cell proliferation in *in vitro* cancer models, but also the importance of the ECS in the treatment of cancer.

Anti-Inflammatory and Pro-Inflammatory Cytokines Production. The upregulation of CB_2R has been extensively demonstrated during different inflammatory processes, especially in relation to neuroinflammation and neurodegeneration.[25,54,55] By specifically targeting CB_2R, selective agonists exert potent anti-inflammatory effects.[25,54,55] For instance, studies have shown that the administration of CB_2R agonists can effectively attenuate the activation of pro-inflammatory microglia, resulting in a shift towards an anti-inflammatory phenotype. This modulation of microglial polarization plays a crucial role in dampening neuroinflammatory responses. Furthermore, CB_2R agonists have been demonstrated to inhibit the production and release of pro-inflammatory cytokines while promoting the secretion of anti-inflammatory cytokines.[25,54,55] These actions collectively contribute to the reduction of neuroinflammatory damage and provide neuroprotection in various CNS disorders characterized by inflammation and neurodegeneration. In addition, CB_2R agonists have shown promising results in preclinical models of neuroinflammatory diseases, such as multiple sclerosis and Alzheimer's disease. The ability of CB_2R agonists to selectively target neuroinflammation without producing psychoactive effects, as observed with CB_1R activation, further enhances their potential as tailored CNS anti-inflammatory agents. Consequently, CB_2R agonists represent a compelling therapeutic strategy for combating neuroinflammation and mitigating associated neurodegenerative processes in the CNS.

With the aim of investigating the potential of our ligands for treating inflammatory-based pathologies, considering the established role of CB_2R activation in modulating the release of anti-inflammatory cytokines and inhibiting pro-inflammatory cytokines, we conducted experiments to test four of our most promising ligands (Figure 96) in this context. These experiments were carried out by the research groups led by Prof. Chiara Riganti (University of Turin) and Prof. Marialessandra Contino (University of Bari), following well-established experimental protocols.[54,55] Throughout the study,

USC DE COMPOSTELA

the impact of our CB_2R agonists on the production of both anti-inflammatory (IL-4 and IL-10) and pro-inflammatory (TNF-α, IFN-γ, IL-1β, and IL-6) cytokines in human monocytes and macrophages was quantified. To induce the inflammatory condition, both monocytes and macrophages were treated with LPS (Lipopolysaccharide). This allowed us to assess the anti-inflammatory effects of our ligands on both resting and activated monocytes and macrophages.

For comparative purposes, we utilized CB65, a selective CB_2R agonist, as a reference compound.[54,55] To unequivocally establish that the observed effect is mediated through CB_2R activation, the CB_2R agonist was incubated both alone and in the presence of JTE907, a CB_2R selective antagonist.[54,55] Detailed descriptions of the experimental protocols can be found in the Experimental Section. The results obtained from the various conducted experiments are presented in Figure 98 and Figure 99.

Based on preliminary studies (data not shown), we determined that a concentration of 10 μM for each reference compound was suitable for testing, as it resulted in the maximal effect of CB65 on cytokine production, while JTE907 remained inactive at this dose. The CB_2R agonists (**35m**, **37f**, **38f**, **38n**) were then tested at concentrations of 5 and 20 μM, both alone and in the presence of JTE907, as depicted in Figure 98 and Figure 99. As illustrated in Figure 98 and Figure 99, our compounds exhibited a significant dose-dependent decrease in the production of pro-inflammatory cytokines (TNF-α, IFN-γ, IL-1β, and IL-6) and a notable increase in the production of anti-inflammatory cytokines (IL-4 and IL-10) in resting monocytes and macrophages. As observed, in all cases the effect is more pronounced at superior concentration (20 μM). Remarkably, a more pronounced effect was observed in activated monocytes and macrophages (Figure 98 and Figure 99). Importantly, the effect of the CB_2R agonists was completely reversed by the presence of JTE907, thereby conclusively demonstrating the CB_2R-mediated nature of the observed effect.

These findings provide compelling evidence for the anti-inflammatory properties of our CB_2R agonists, both in resting and activated immune cells. The ability of our compounds to modulate cytokine production, reducing pro-inflammatory cytokines while promoting the release of anti-inflammatory cytokines, highlights their potential as therapeutic agents for inflammatory-based pathologies. Furthermore, the dependence of these effects on CB_2R activation further supports the notion that targeting CB_2R is a viable approach for modulating immune responses and potentially ameliorating inflammatory conditions.

USC DE COMPOSTELA

Further investigation and optimization of these compounds are warranted to fully explore their therapeutic potential and evaluate their efficacy in relevant disease models.

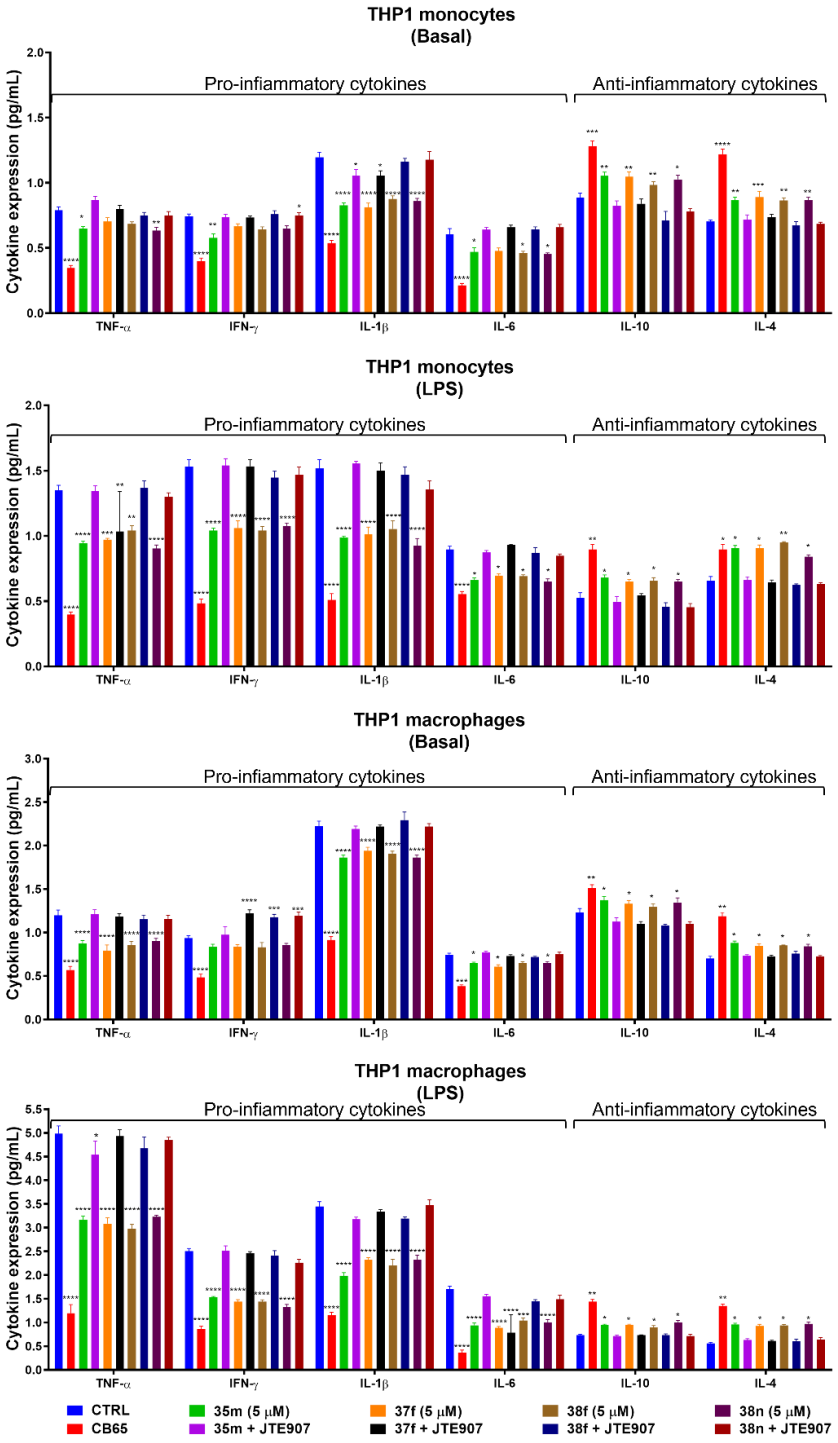


Figure 98: Cytokine levels in human monocytes and macrophages in resting (basal) and activated (LPS) conditions by treatment with the CB_2R agonist reference compound CB65 (10 μM) and the CB_2R agonist compounds **35m**, **37f**, **38f** and **38n** (at 5 μM), alone and in the presence of the CB_2R antagonist JTE907 (10 μM). Each bar represents the mean ± SEM of two experiments performed in triplicate. Two-Way ANOVA followed by Tukey post-hoc test was applied. Significance of symbols as follows: 1 symbol = $p < 0.05$; 2 symbols = $p < 0.01$; 3 symbols = $p < 0.001$; 4 symbols = $p < 0.0001$. Legend for symbols as follows: * indicates *vs* CTRL.

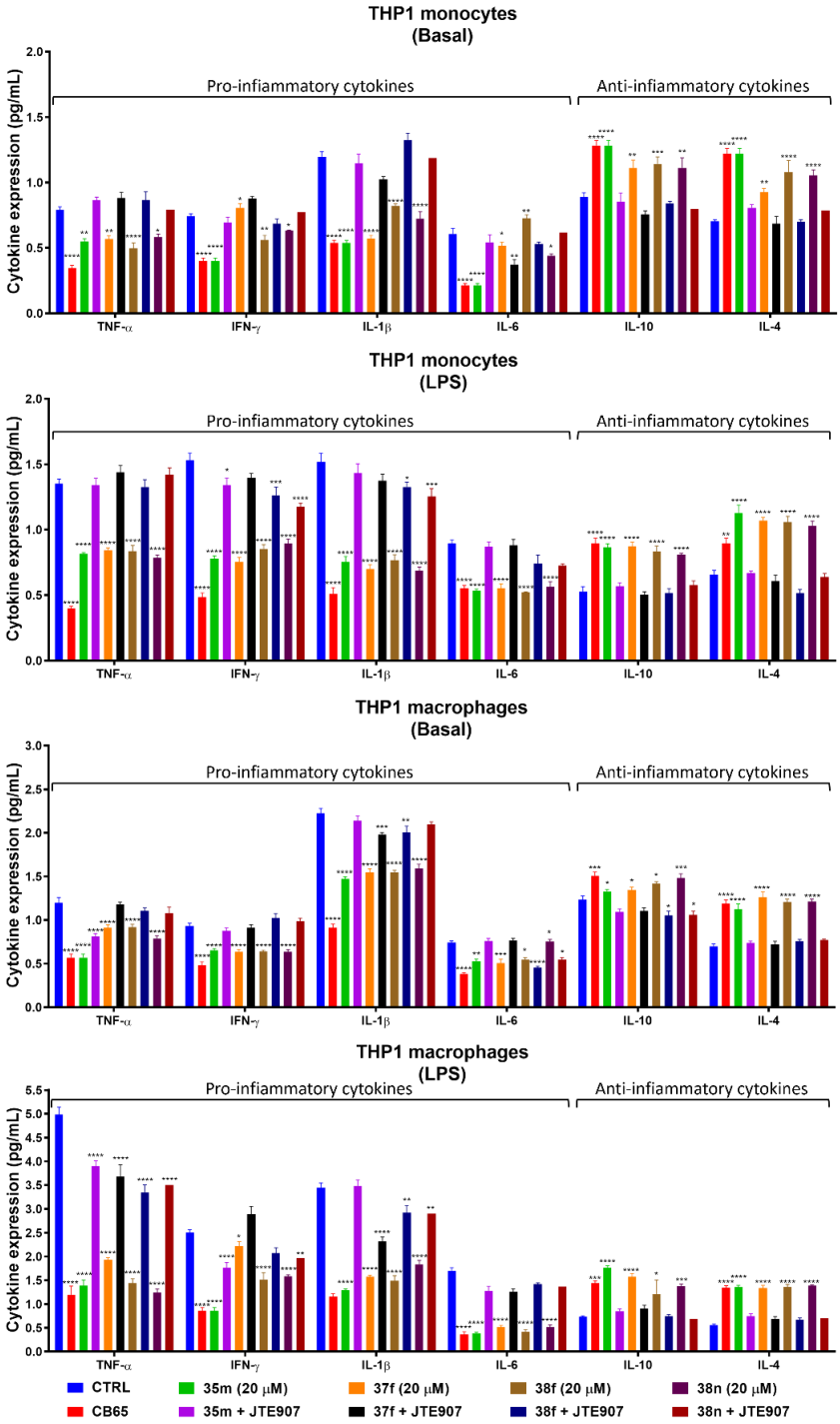


Figure 99: Cytokine levels in human monocytes and macrophages in resting (basal) and activated (LPS) conditions by treatment with the CB_2R agonist reference compound CB65 (10 μM) and the CB_2R agonist compounds **35m**, **37f**, **38f** and **38n** (at 20 μM), alone and in the presence of the CB_2R antagonist JTE907 (10 μM). Each bar represents the mean ± SEM of two experiments performed in triplicate. Two-Way ANOVA followed by Tukey post-hoc test was applied. Significance of symbols as follows: 1 symbol = $p < 0.05$; 2 symbols = $p < 0.01$; 3 symbols = $p < 0.001$; 4 symbols = $p < 0.0001$. Legend for symbols as follows: * indicates *vs* CTRL.

USC
UNIVERSIDADE DE SANTIAGO DE COMPOSTELA

4 EXPERIMENTAL SECTION

USC
UNIVERSIDADE
DE SANTIAGO
DE COMPOSTELA

USC
UNIVERSIDADE
DE SANTIAGO
DE COMPOSTELA

4.2 GENERAL INFORMATION

4.2.1 Chemistry

Unless otherwise indicated, all starting materials, reagents and solvents were purchased and used without further purification.

The Ugi reactions were performed in coated Kimble vials on a PLS (6×4) Organic Synthesizer with orbital stirring. The reactions were monitored by thin-layer chromatography (TLC) on 2.5 mm Merck silica gel GF 254 strips, and each purified compound showed a single spot; unless stated otherwise, UV light and/or iodine vapor were used to detect compounds. After extraction from aqueous phases, the organic solvents were dried over anhydrous magnesium sulfate. The purity and identity of all tested compounds were established by a combination of HPLC, mass spectrometry and NMR spectroscopy. Purification of isolated products was carried out by one of the following methods: a) column flash chromatography (Kieselgel 0.040-0.063 mm, E. Merck), or b) preparative chromatography (Uniplate^{TM} Techware 20x20 cm Silica G 1000 mm Thick 15 μm).

Melting points were determined on a Stuart Scientific melting point apparatus SMP3 and are uncorrected. Samples were dissolved in deuterated solvent ($CDCl_3$, DMSO-d_6 or MeOD) and the NMR spectra were recorded on Bruker AM300 and XM500 spectrometers. Chemical shifts are given as δ values against tetramethylsilane as internal standard and J values are given in Hz. The signal multiplicity shown with the abbreviatures s, singlet; d, doublet; t, triplet; q, quartet; quin, quintet; hept, heptet; dd, doublet of doublets; dt, doublet of triplets; dq, doublet of quartet; td, triplet of doublets; brs, broad singlet; and m, multiplet, followed by number of protons (deduced by integration). The coupling constants (*J*) are deduced in Hertz (Hz).

Low-resolution mass spectra (LRMS) were obtained on an Agilent 8890 GC coupled to 5977B GC/MSD system (CI). High-resolution mass spectra (HRMS) were obtained on an Autospec Micromass spectrometer. Analytical HPLC was performed on a Water Breeze™ 2 system (binary pump 1525, detector UV/Visible 2489, 7725i Manual Injector Kit 1500 Series) using a Luna 5 μm Silica (2) 100 Å, LC Column 150 x 4.6 mm column with gradient elution using the mobile phases dichloromethane, isopropanol, and a flow rate of 1 mL/min. The purity of all tested compounds was determined to be >95%. The structural and spectroscopic data obtained for all

USC DE COMPOSTELA

compounds described are provided and they can be found in General Procedures of Synthesis and Spectroscopic Data, in the paragraph corresponding to each Chapter.

The chiral analysis was performed using a Water Breeze™ 2 (binary pump 1525, detector UV/Visible 2489, 7725i Manual Injector Kit 1500 Series). Enantiomers were evaluated with 250 mm x 20 mm Chiralpak® 5μm IE-3 (DAICEL). All the separations were performed at 25 ºC with hexane (or dichloromethane)/*i*-propanol mixture in different percentages as mobile phase (see Spectroscopic Data for all compounds described and their enantiomers below). The enantiomers *(R)*-**35m** (0.5 mg, tR = 25.0 min), *(S)*-**35m** (0.5 mg, tR = 29.1 min), *(R)*-**37f** (0.5 mg, tR = 13.2 min), *(S)*-**37f** (0.5 mg, tR = 17.4 min), *(R)*-**37r** (0.5 mg, tR = 16.0 min), *(S)*-**37r** (0.5 mg, tR = 22.9 min), *(R)*-**36r** (0.5 mg, tR = 22.4 min), *(S)*-**36r** (0.5 mg, tR = 27.1 min), *(R)*-**38n** (0.5 mg, tR = 21.6 min), *(S)*-**38n** (0.5 mg, tR = 23.5 min), *(R)*-**38r** (0.5 mg, tR = 14.5 min), *(S)*-**38r** (0.5 mg, tR = 20.0 min) were isolated, their stereochemical purity analyzed by chiral HPLC (e.g.: 97-99% for each enantiomer, reports showed below, chromatogram at 254 nm) and then characterized by ^{1}H NMR and Circular dichroism (CD).

CD spectra were recorded on a Jasco-815 system equipped with a Peltier-type thermostatic accessory (CDF-426S, Jasco). Measurements were carried out at 20 °C using a 1 mm quartz cell in a volume of 600 μL. Compounds (0.5 mg) were dissolved in MeOH (1.0 mL) and then diluted 10-fold in MeOH. The instrument settings were bandwidth, 1.0 nm; data pitch, 1.0 nm; speed, 500 nm/min; accumulation, 10; wavelengths, 400-190 nm.

USC UNIVERSIDADE DE SANTIAGO DE COMPOSTELA

4.2.2 General considerations on the spectroscopic characterization of chemotheques

Taking into consideration the quantity of compounds obtained within the framework of this Doctoral Thesis and following the general criteria accepted by the scientific community for the characterization of chemotheques, the general guidelines indicated below have been followed in the structural characterization of the compounds:

1 All the described compounds have been routinely characterized including:
   a. ^{1}H-NMR.
   b. Low Resolution Mass Spectrometry (LRMS).
   c. Melting point (Mp).
2 In each series, representative compounds have been chosen for determination of (in addition to the characterization indicated in the previous section):
   a. ^{13}C NMR.
   b. High Resolution Mass Spectrometry (HRMS).

4.2.3 Biological assay

Binding assays. Radioligand binding competition assays of CB_1 receptors were carried out in polypropylene 96-well plates by incubating 5 µg of membranes from Chinese hamster ovary (CHO)-CB1 C3 cell line (PerkinElmer) with 1 nM [^{3}H]-CP 55,940 (Perkin Elmer) and test compounds in binding buffer (50 mM Tris-HCl, 5 mM $MgCl_2$, 1 mM EDTA, 0.5% BSA, pH 7.4). Non-specific binding was determined in the presence of 10 µM Surinabant. The reaction mixture was incubated at 30 °C for 60 min, then 200 µL were transferred to GF/C 96-well plate (Millipore, Madrid, Spain) and washed four times with 250 µL of washing buffer (50 mM Tris-HCl, 5 mM $MgCl_2$, 1 mM EDTA, 0.5% BSA, pH 7.4). Radioactivity was detected in a microplate beta scintillation counter (Microbeta Trilux, PerkinElmer, Madrid, Spain). Radioligand binding competition assays of CB_2 receptors were carried out in polypropylene 96-well plates by incubating 5 µg of membranes from Human embryonic kidney 293 cells (HEK)-CB2 cell line with 0.2 nM [^{3}H]-CP 55,940 (Perkin Elmer) and test compounds in binding buffer (50 mM Tris-HCl, 5 mM $MgCl_2$, 2.5 mM EGTA, 0.1% BSA, pH 7.4). Non-specific binding was determined in the presence of 10 µM GW405833. The reaction mixture was incubated at 30 °C for 90 min, then 200 µL were transferred to GF/C 96-well plate (Millipore, Madrid, Spain) and washed four times with 250 µL washing buffer (50 mM Tris-HCl, 5 mM $MgCl_2$, 2.5 mM EGTA, 1% BSA, pH 7.4).

Data were fitted to 4-parameter logistic equation by employing GraphPad Prism software (V7.0) and K_i data was calculated with the equation:

$$K_i = IC_{50} / [1 + (F/K_D)];$$

where IC_{50} was the concentration of the ligand that displaced the specific binding of the radioligand in a 50%; K_D is the dissociation constant of the radioligand, and F is the concentration of the radioligand employed in the assay.

Functional experiments. **Cell Culture and Transient Transfection**. HEK-293T cells were grown in Dulbecco's Modified Eagle's Medium (DMEM) medium (Gibco, Paisley, Scotland, United Kingdom) supplemented with 2 mM L-glutamine, 100 U/mL penicillin/streptomycin, MEM Non-Essential Amino Acids Solution (1/100) and 5% (v/v) heat inactivated Fetal Bovine Serum (FBS) (Invitrogen, Paisley, Scotland, United Kingdom). Cells were maintained in a humid atmosphere of 5% CO_2 at 37 ºC. Cells were transiently transfected with the PEI (Polyethyleneimine, Sigma, St. Louis, MO, United States) method as previously described[156] and used for functional assays 48 h later.

cAMP Determination. Signaling experiments have been performed as previously described.[157] Two hours before initiating the experiment, HEK-293T cell-culture medium was replaced by serum-starved DMEM medium. Then, cells were detached, resuspended in growing medium containing 50 mM zardaverine (Tocris, Bristol, UK) and placed in 384-well microplates (2,500 cells/well). Cells were pretreated (15 min) with cannabinoid compounds (1 nM to 100 µM) -or vehicle- before adding 0.5 mM forskolin (Tocris, Bristol, UK) to induce cAMP accumulation. Readings were performed after 15 min incubation at 25 ºC. Homogeneous Time Resolved Fluorescence (HTRF) energy transfer measures were performed using the Lance Ultra cAMP kit (PerkinElmer, Waltham, MA, United States). Fluorescence at 665 nm was analyzed in a PHERA star Flagship microplate reader equipped with an HTRF optical module (BMG Lab Technologies, Offenburg, Germany).

β-Arrestin 2 Recruitment. Arrestin recruitment was determined as previously described.[146,158] Briefly, BRET experiments were performed in HEK-293T cells 48 h after transfection with the cDNA corresponding to the CB_2R-YFP or CB_1R-YFP and 1 mg cDNA corresponding to β-arrestin 2-Rluc. Cells (20 mg protein) were distributed in 96-well microplates (Corning 3600, white plates with white bottom) and were incubated

USC DE COMPOSTELA

with CBG for 15 min and stimulated with the agonist for 10 min prior the addition of 5 mM coelenterazine H (Molecular Probes, Eugene, OR, United States). After 1 min of adding coelenterazine H, BRET between β-arrestin 2-Rluc and receptor-YFP was determined and quantified. The readings were collected using a Mithras LB940 (Berthold Technologies, Bad Wildbad, Germany) that allows the integration of the signals detected in the short-wavelength filter at 485 nm and the long-wavelength filter at 530 nm. To quantify protein-RLuc expression luminescence readings were also performed 10 min of adding 5 mM coelenterazine H.

ERK Phosphorylation Assays. To determine ERK1/2 phosphorylation, 50,000 HEK-293T cells/well were plated in transparent Deltalab 96-well microplates and kept in the incubator for 24 h. 2 to 4 h before the experiment, the medium was substituted by serum-starved DMEM medium. Then, cells were treated at 25 ºC for 7 min with vehicle or cannabinoid compounds in serum-starved DMEM medium. Cells were then washed twice with cold PBS before addition of lysis buffer (20 min treatment). 10 mL of each supernatant were placed in white ProxiPlate 384-well microplates and ERK1/2 phosphorylation was determined using AlphaScreen SureFire kit (Perkin Elmer) following the instructions of the supplier and using an EnSpire Multimode Plate Reader (PerkinElmer, Waltham, MA, United States).

Cytotoxicity assays on neurons.

Neuronal primary cultures. To prepare primary neurons, brains from fetuses of pregnant CD1 mice were removed (gestational age: 19 days). Neurons were isolated as described in Hradsky et al.[159] Briefly, after removal of the meninges, samples were dissected and digested with 0.25% trypsin (20 min at 37 ºC). The effect of trypsin was stopped by adding an equal volume of culture medium (supplemented DMEM). A single-cell suspension was obtained by repeated pipetting followed by passage through a 100 μm-pore mesh. Pelleted (7 min, 200×g) cells were resuspended in 2 mL of supplemented DMEM and seeded at a density of 3.5×10^5 cells/mL in 6-well plates. After 24 h, the medium was replaced by neurobasal medium supplemented with 2 mM L-glutamine, 100 U/mL penicillin/streptomycin and 2% (v/v) B27 medium (GIBCO, Waltham, MA, USA). Primary neurons were assayed after 14 days in culture. Using NeuN as a marker, the percentage of neurons in the culture was >90%.

USC DE COMPOSTELA

Viability assay. Primary cultures of striatal neurons were treated for 24 h with 19 representative SCRAs (100 nM). Afterwards, cells were scrapped from the plate and resuspended in neurobasal medium supplemented with 2 mM L-glutamine, 100 U/mL penicillin/streptomycin and 2% (v/v) B27 (GIBCO). Trypan blue staining was performed mixing 1 part of 0.4% trypan blue and 1 part of cell suspension in a plastic tube. After ~3 min of incubation at room temperature, 10 µL of the mixture were sampled in a Neubauer chamber and counted with a Countess II FL (Life Technologies, California, CA, USA). The unstained (viable) and stained (nonviable) cells were counted separately, and the percentage of viability was calculated as: total number of viable cells/total number of cells x 100.

Cytotoxicity assays on cancer cells.

Cell cultures. Human gastric cancer sensitive and resistant to paclitaxel cell lines (HGC), breast cancer cell line (MCF-7) and colorectal cancer adenocarcinoma cell line (CACO-2) were grown in DMEM high glucose supplemented with 10% Fetal Bovine Serum (FBS), 2 mM glutamine, 100 U/mL penicillin, 100 mg/mL streptomycin, in an humidified incubator at 37 °C with a 5% CO_2 atmosphere. Human neuroblastoma (SH-SY5Y) cancer cell line was grown in DMEM/HAMSF12 (1:1) supplemented with 10% FBS, 2 mM glutamine, 100 U/mL penicillin, 100 mg/mL streptomycin, in a humidified incubator at 37 °C with a 5% CO_2 atmosphere.

Viability assay. Determination of cell growth was performed using the MTT assay at 24 h, 48 h and 72 h. On day 1, 5,000-10,000 cells/well were seeded into 96-well plates in a volume of 100 µL/well. On day 2, the test compound was added at different concentrations. In all the experiments, the various drug-solvents (ethanol, DMSO) were added in each control to evaluate a possible solvent cytotoxicity. After the established incubation time with drugs, MTT (0.5 mg/mL) was added to each well, and after 3 h incubation at 37 °C, the supernatant was removed. The formazan crystals were solubilized using 100 µL/well of DMSO and the absorbance values at 570 and 630 nm were determined with the microplate reader Victor 3 (PerkinElmer).

Proliferation assay. U87-MG cell line was purchased from the American Type Culture Collection (ATCC) and cultured in DMEM GlutaMAX (ThermoFisher Scientific), supplemented with 10% Fetal Bovine Serum (FBS) (ThermoFisher Scientific). Cell cultures were regularly tested for the presence of mycoplasma. The

USC DE COMPOSTELA

effect of CB_2R agonists on the proliferation of U87-MG cells was tested by plating 2,000 cells/well on a 96-well plate overnight in complete medium. Cells were then incubated for another 24 h with solutions containing CB_2R agonists at 2 μM in complete medium. Controls with the equivalent amount of DMSO, used as the solvent for the indicated agonists, were as well performed. After incubations, the number of viable cells was determined by using AlamarBlue (ThermoFisher Scientific) following manufacturer's recommendations. Proliferation rates for each condition were represented as % proliferation respect to the appropriate DMSO controls.

Anti-Inflammatory and Pro-Inflammatory Cytokines Detection. The amount of cytokines was measured in 5 μL of supernatants, derived from 1×10^4 cells, using the ProQuantum immunoassays kits for TNF-α, IFN-γ, IL-1β, IL-6, IL-10, IL-4, and IL-17A [all from ThermoFisher Scientific (Waltham, MA)] according to the manufacturer's instructions. The results were expressed as pg/mL based on the titration curved of each kit. In order to allow the differentiation into macrophages, THP-1 cells were treated with 0.01 μM PMA for 48 hours. Both THP-1 (monocytes) and differentiated THP-1 (macrophages) were incubated for additional 24 hours in the presence of 10 μg/mL lipopolysaccharide (LPS) to induce the inflammatory state. CB_2R ligands were incubated during these 24 hours with or without the CB_2R antagonist JTE907. Cytokines levels were measured with an ELISA coupled with qRT-PCR.

Data and statistical analysis. K_i and EC_{50} values were obtained by fitting the data with nonlinear regression using Prism 9 software (GraphPad, San Diego, CA). Results are the mean of four experiments (n = 4), each performed in duplicate. Data are represented as mean ± standard error of mean (SEM) with statistical significance set at $P < 0.05$. The number of samples (n) in each experimental condition is indicated in the corresponding figure legend. Outliers were assessed by the ROUT method, thus any sample was excluded assuming a Q value of 1% in GraphPad Prism 9. Comparisons among experimental groups were performed by Student's t test or one-way analysis of variance (ANOVA) followed by Tukey's multiple comparisons post-hoc test using GraphPad Prism 9, as indicated.

USC UNIVERSIDADE DE SANTIAGO DE COMPOSTELA

System preparation and MD/FEP simulations.

CB_1R and CB_2R 3D structures are PDB: 5TGZ[160] and 5ZTY[18], respectively, and here processed using the Protein Preparation Wizard pipeline in Maestro (Schrodinger ver. 2023-1). Subsequently, possible 3D tautomer and protomers at pH 7 ± 2 were generated for each compound using OPLS4 force field and Epik, the lowest energy conformer was chosen for molecular docking. A receptor grid was generated with the default Van der Waals radius scaling settings, and it was positioned in the center of geometry of the binding site. Thereafter, Glide XP docking was performed, selecting the best poses in basis of docking score.

USC UNIVERSIDADE DE SANTIAGO DE COMPOSTELA

4.3 DOSE RESPONSE CURVES OBTAINED AT CB_1R AND CB_2R DURING FUNCTIONAL AND BINDING DATA (CHAPTER 1, CPDS 22, 23, 24, 25)

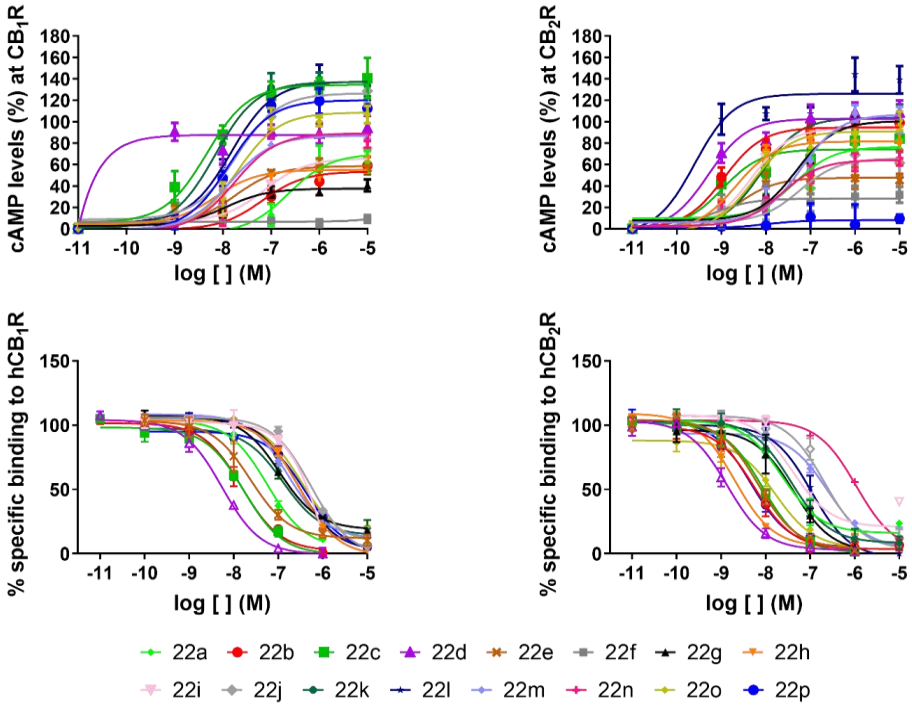


Figure S1. Dose-response curves obtained for ligands in Table 3 at CB_1R and CB_2R during functional and binding studies.

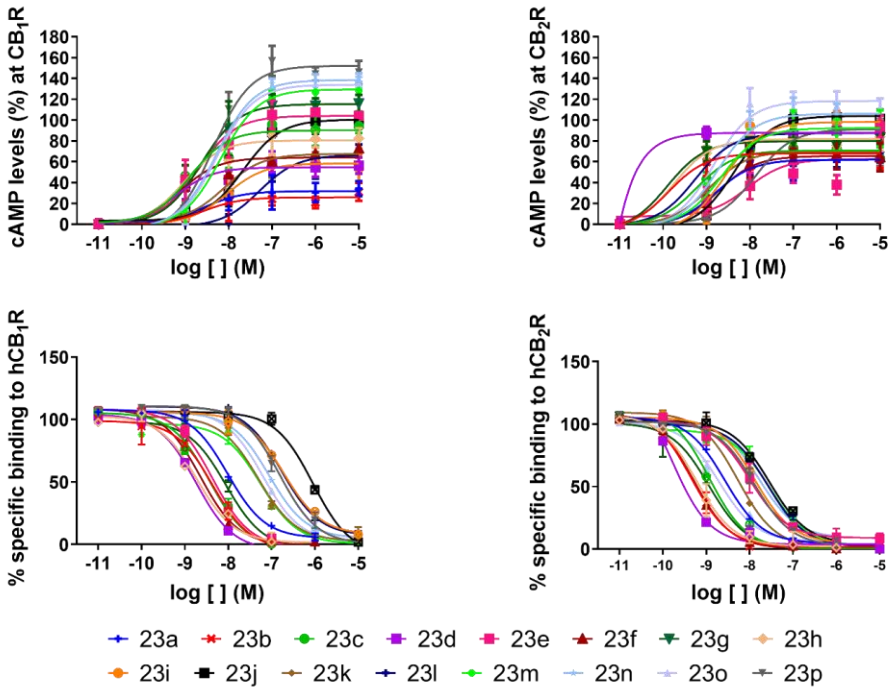


Figure S2. Dose-response curves obtained for ligands in Table 4 at CB_1R and CB_2R during functional and binding studies.

USC UNIVERSIDADE DE SANTIAGO DE COMPOSTELA

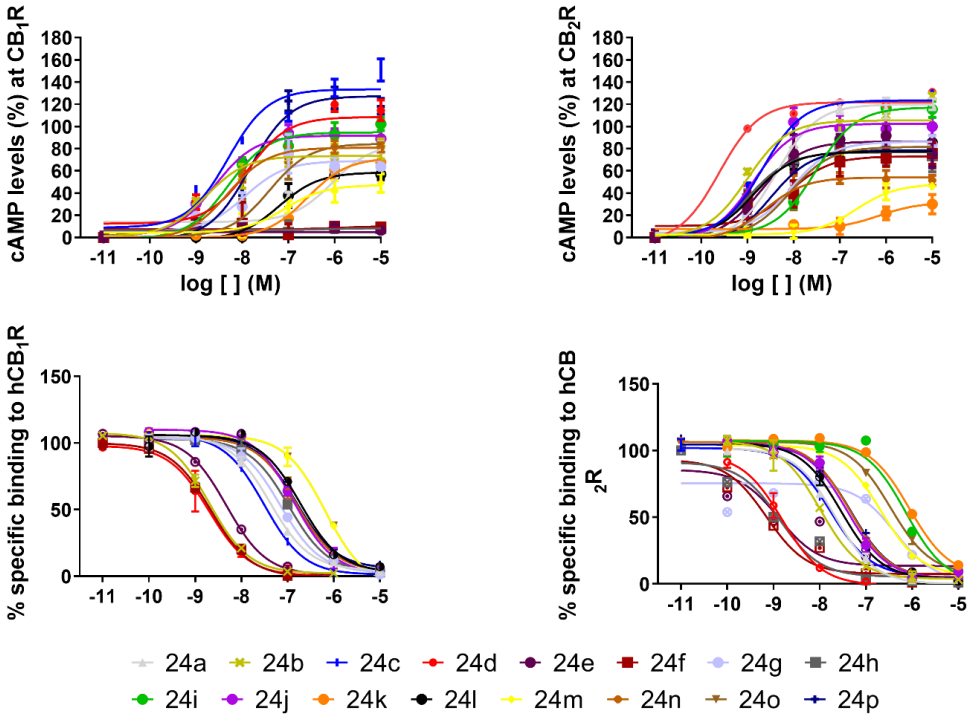


Figure S3. Dose-response curves obtained for ligands in Table 5 at CB_1R and CB_2R during functional and binding studies.

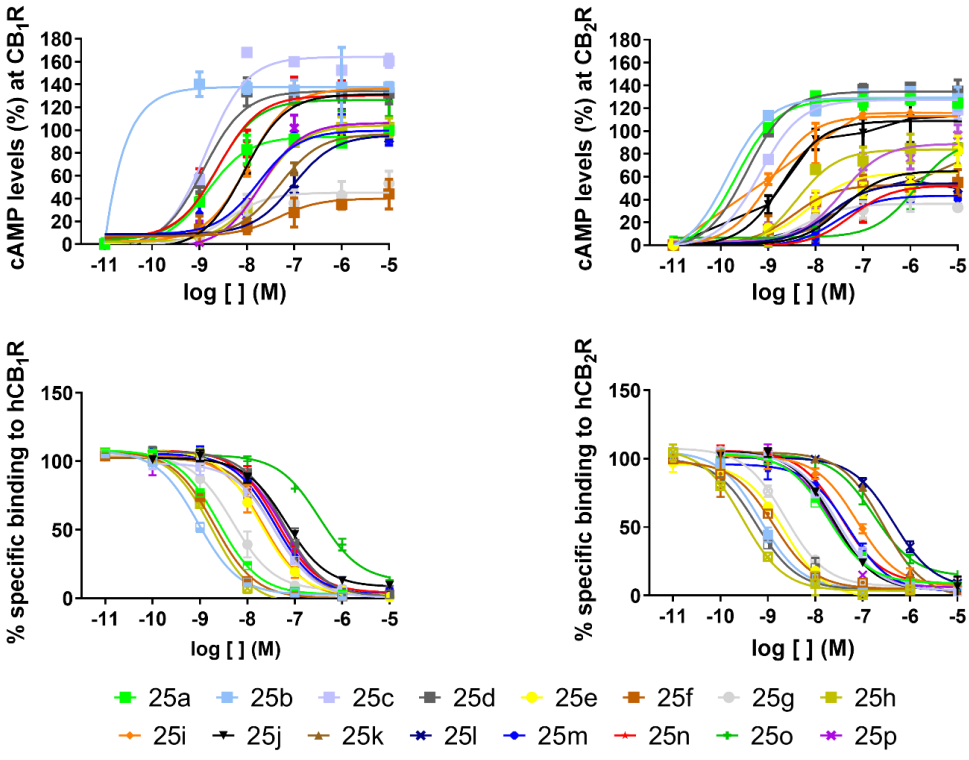
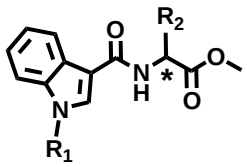


Figure S4. Dose-response curves obtained for ligands in Table 6 at CB_1R and CB_2R during functional and binding studies.

USC UNIVERSIDADE DE SANTIAGO DE COMPOSTELA

4.4 COMPARISON TABLES BETWEEN THE EXPERIMENTAL DATA AND THE REPORTED DATA OF CHAPTER 1 (CPDS 22, 23, 24, 25)

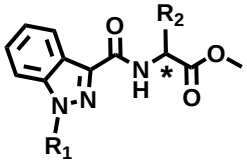
Table S1: Comparison table between the experimental and the reported data for the indole esters **22a-p**.



Compound	Experimental data vs Reported data	CB_1R			CB_2R		
		pEC_{50}±SEM[a) [EC_{50} nM)]	E_{max}[b)	pK_i±SEM[c) [K_i nM)]	pEC_{50}±SEM[a) [EC_{50} nM)]	E_{max}[b)	pK_i±SEM[d) [K_i nM)]
22a (AMBICA)[81]	Experimental data	7.27 ± 0.05 [53.7]	80%	7.58 ± 0.07 [26.6]	7.34 ± 0.05 [45.2]	77%	7.79 ± 0.09 [16.4]
	Reported data	7.74 ± 0.10 [18]	111%		7.63 ± 0.08 [23]	90%	
22b (MDMB-PICA)[81]	Experimental data	7.55 ± 0.03 [28.4]	74%	8.14 ± 0.05 [7.20]	8.94 ± 0.07 [1.14]	95%	8.54 ± 0.03 [2.90]
	Reported data	8.77 ± 0.06 [1.7]	109%		7.78 ± 0.13 [17]	90%	
22c (5F-AMBICA)[81]	Experimental data	8.34 ± 0.06 [4.62]	134%	8.09 ± 0.08 [8.10]	8.98 ± 0.06 [1.05]	74%	8.38 ± 0.07 [4.23]
	Reported data	8.62 ± 0.06 [2.4]	107%		8.34 ± 0.07 [4.6]	94%	
22d (5F-MDMB-PICA)[81]	Experimental data	9.15 ± 0.08 [0.70]	88%	8.59 ± 0.09 [2.61]	9.29 ± 0.07 [0.51]	103%	9.15 ± 0.05 [0.70]
	Reported data	9.35 ± 0.07 [0.45]	110%		8.13 ± 0.05 [7.4]	94%	
22e (MMB-CHMICA)[81]	Experimental data	7.74 ± 0.09 [18.1]	79%	7.98 ± 0.06 [10.5]	8.64 ± 0.08 [2.27]	68%	8.47 ± 0.07 [3.44]
	Reported data	8.45 ± 0.08 [3.5]	114%	9.38± 0.05 [0.41]	7.93 ± 0.07 [12]	88%	9.45 ± 0.05 [0.35]
22f (MDBM-CHMICA)[81]	Experimental data	8.82 ± 0.07 [1.50]	58%	10.05± 0.12 [0.09]	9.22 ± 0.09 [0.60]	61%	9.74 ± 0.08 [0.18]
	Reported data	8.45 ± 0.08 [3.5]	112%		7.15 ± 0.05 [71]	103%	
22g (MMB-FUBICA)[81]	Experimental data	7.94 ± 0.05 [11.4]	88%	7.32 ± 0.03 [47.8]	7.32 ± 0.03 [48.2]	101%	7.70 ± 0.05 [20.0]
	Reported data	7.45 ± 0.05 [36]	106%		7.85 ± 0.09 [14]	86%	
22h (MDMB-FUBICA)[81]	Experimental data	8.16 ± 0.07 [6.99]	75%	8.42 ± 0.08 [3.83]	8.67 ± 0.06 [2.12]	82%	8.95 ± 0.07 [1.12]
	Reported data	8.57 ± 0.05 [2.7]	109%		7.60 ± 0.12 [25]	92%	

USC UNIVERSIDADE DE SANTIAGO DE COMPOSTELA

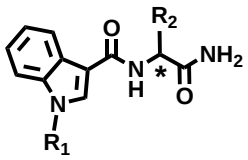
Table S2. Comparison table between the experimental and the reported data for the indazole esters **23a-p.**



Compound	Experimental data vs Reported data	CB_1R			CB_2R		
		pEC_{50}±SEM[a] [EC_{50} nM)]	E_{max} ±SEM[b]	pK_i±SEM[c] [K_i nM)]	pEC_{50}±SEM[a] [EC_{50} nM)]	E_{max} ±SEM[b]	pK_i±SEM[d] [K_i nM)]
23a (AMB)[81]	Experimental data	8.56 ± 0.08 [2.73]	72%	8.39 ± 0.09 [4.17]	8.79 ± 0.08 [1.61]	62%	8.89 ± 0.06 [1.30]
	Reported data	8.48 ± 0.05 [3.3]	110%		7.79 ± 0.11 [16]	96%	
23b (MDMB-PINACA)[81]	Experimental data	8.59 ± 0.07 [2.60]	66%	8.68 ± 0.09 [2.10]	9.89 ± 0.09 [0.13]	68%	9.70 ± 0.04 [0.26]
	Reported data	8.84 ± 0.06 [1.4]	112%		7.56 ± 0.06 [28]	91%	
23c (5F-AMB)[81]	Experimental data	8.90 ± 0.04 [1.27]	90%	8.77 ± 0.06 [1.74]	9.24 ± 0.06 [0.58]	81%	9.30 ± 0.07 [0.52]
	Reported data	8.71 ± 0.04 [1.9]	109%	7.63 ± 0.08 [23.3]	7.99 ± 0.13 [10]	103%	8.22 ± 0.04 [5.97]
23d (5FMDMBPINACA)[81]	Experimental data	9.24 ± 0.06 [0.58]	75%	9.10 ± 0.09 [0.80]	10.0 ± 0.09 [0.10]	88%	10.0 ± 0.08 [0.10]
	Reported data	9.23 ± 0.11 [0.59]	108%	7.6 ± 0.07 [23.3]	8.12 ± 0.06 [7.5]	94%	8.22 ± 0.07 [6.03]
23e (AMB-CHMINACA)[81]	Experimental data	8.69 ± 0.07 [2.02]	104%	8.72 ± 0.05 [1.90]	8.05 ± 0.05 [8.82]	83%	9.30 ± 0.07 [0.51]
	Reported data	8.29 ± 0.07 [5.1]	109%	9.46 ± 0.09 [0.34]	7.54 ± 0.13 [29]	92%	9.52 ± 0.09 [0.30]
23f (MDMB-CHMINACA)[81]	Experimental data	9.12 ± 0.05 [0.76]	84%	9.00 ± 0.07 [1.08]	8.72 ± 0.06 [1.92]	76%	9.52 ± 0.08 [0.33]
	Reported data	7.99 ± 0.04 [10]	111%	9.88 ± 0.09 [0.13]	6.89 ± 0.04 [128]	96%	9.65 ± 0.04 [0.22]
23g (AMB-FUBINACA)[81]	Experimental data	8.64 ± 0.09 [2.29]	115%	8.14 ± 0.03 [3.90]	9.92 ± 0.08 [0.12]	80%	9.22 ± 0.05 [0.62]
	Reported data	8.71 ± 0.10 [2.0]	103%	9.42 ± 0.06 [0.38]	7.75 ± 0.05 [18]	92%	9.26 ± 0.07 [0.54]
23h (MDMBFUBINACA)[81]	Experimental data	9.04 ± 0.07 [0.92]	81%	9.10 ± 0.02 [0.83]	9.77 ± 0.06 [0.17]	82%	9.52 ± 0.07 [0.30]
	Reported data	8.41 ± 0.04 [3.9]	108%	10.1 ± 0.07 [0.09]	7.26 ± 0.14 [55]	101%	9.88 ± 0.08 [0.13]

USC UNIVERSIDADE DE SANTIAGO DE COMPOSTELA

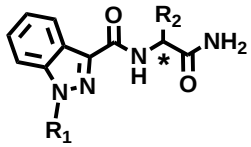
Table S3. Comparison table between the experimental and the reported data for the indole amides **24a-p.**



Compound	Experimental data vs reported data	CB_1R			CB_2R		
		pEC_{50}±SEM[a) [EC_{50} nM)]	E_{max} ±SEM[b)	pK_i±SEM[c) [K_i nM)]	pEC_{50}±SEM[a) [EC_{50} nM)]	E_{max} ±SEM[b)	pK_i±SEM[d) [K_i nM)]
24a (AB-PICA)[83]	Experimental data	6.92 ± 0.02 [120]	85%	7.76 ± 0.03 [17.5]	8.36 ± 0.07 [4.32]	120%	7.95 ± 0.04 [11.2]
	Reported data	7.92 ± 0.07 [12]	99%		7.92 ± 0.21 [12]	94%	
24b (AD-BICA)[83]	Experimental data	8.79 ± 0.07 [1.64]	76%	9.10 ± 0.08 [0.80]	9.00 ± 0.09 [1.00]	105%	9.30 ± 0.09 [0.52]
	Reported data	9.16 ± 0.16 [0.69]	98%		8.75 ± 0.18 [1.8]	94%	
24c (5F-AB-PICA)[83]	Experimental data	8.31 ± 0.07 [4.95]	109%	7.83 ± 0.07 [14.8]	8.67 ± 0.09 [2.15]	123%	8.07 ± 0.05 [8.60]
	Reported data	8.28 ± 0.21 [5.2]	123%	7.45 ± 0.06 [35]	8.05 ± 0.53 [8.9]	121%	7.05 ± 0.05 [89]
24d (5F-AD-BICA)[83]	Experimental data	7.88 ± 0.03 [13.1]	109%	9.05 ± 0.09 [0.91]	9.62 ± 0.05 [0.24]	122%	9.15 ± 0.09 [0.74]
	Reported data	9.12 ± 0.14 [0.77]	110%	8.56 ± 0.05 [2.72]	8.91 ± 14 [1.2]	92%	8.7 ± 0.04 [1.83]
24e (AB-CHMICA)[3]	Experimental data	9.60 ± 0.07 [0.25]	95%	8.62 ± 0.09 [2.43]	8.70 ± 0.07 [1.98]	86%	7.45 ± 0.04 [35.3]
	Reported data						
24f (ADB-CHMICA)[3]	Experimental data	6.66 ± 0.05 [221]	70%	8.96 ± 0.07 [1.10]	8.09 ± 0.03 [8.20]	73%	9.12 ± 0.06 [0.76]
	Reported data			8.90 ± 0.08 [1.24]			9.02± 0.07 [0.62]
24g (AB-FUBICA)[83]	Experimental data	7.94 ± 0.04 [11.5]	89%	7.45 ± 0.04 [35.2]	8.04 ± 0.07 [9.15]	86%	6.22 ± 0.06 [83.2]
	Reported data	7.67 ± 0.14 [21]			7.84 ± 0.27 [15]	99%	
24h (ADB-FUBICA)[83]	Experimental data	7.19 ± 0.06 [64.1]	69%	7.27 ± 0.04 [53.8]	8.95 ± 0.09 [1.11]	77%	8.29 ± 0.07 [5.15]
	Reported data	8.58 ± 0.15 [2.6]	113%		8.52 ± 0.16 [3.0]	96%	

USC UNIVERSIDADE DE SANTIAGO DE COMPOSTELA

Table S4. Comparison table between the experimental and the reported data for the indazole amides **25a-p**.



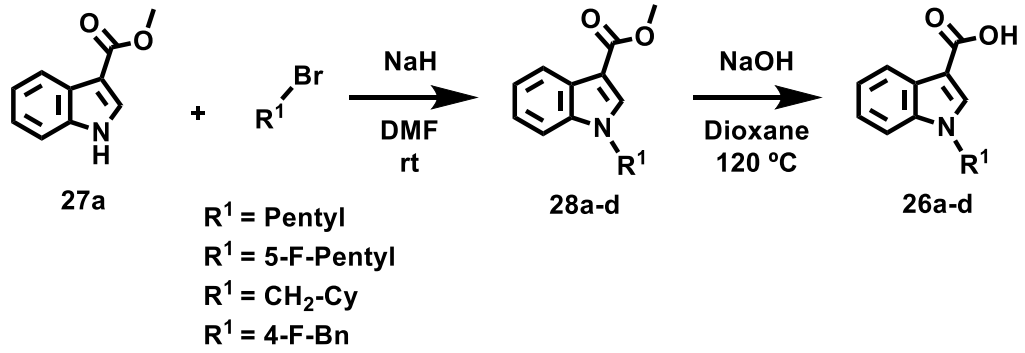
Compound	Experimental data vs Reported data	CB_1R			CB_2R		
		pEC_{50}±SEM[a) [EC_{50} nM)]	E_{max} ±SEM[b)	pK_i±SEM[c) [K_i nM)]	pEC_{50}±SEM[a) [EC_{50} nM)]	E_{max} ±SEM[b)	pK_i±SEM[d) [K_i nM)]
25a (AB-PINACA)[83]	Experimental data	8.83 ± 0.07 [1.49]	94%	8.96 ± 0.08 [1.16]	9.68 ± 0.09 [0.21]	128%	9.05 ± 0.08 [0.94]
	Reported data	8.91 ± 0.09 [1.2]			8.60 ± 0.16 [2.5]	104%	
25b (ADB-PINACA)[83]	Experimental data	11.0 ± 0.09 [0.01]	138%	9.40 ± 0.08 [0.40]	9.89 ± 0.08 [0.13]	129%	9.52 ± 0.08 [0.30]
	Reported data	9.28 ± 0.08 [0.52]	117%		9.06 ± 0.31 [0.88]	107%	
25c (5F-AB-PINACA)[83]	Experimental data	8.87 ± 0.09 [1.36]	164%	7.75 ± 0.07 [17.9]	9.17 ± 0.06 [0.67]	127%	7.84 ± 0.05 [14.3]
	Reported data	9.32 ± 0.10 [0.48]	94%	8.32 ± 0.02 [4.96]	8.59 ± 0.25 [2.6]	110%	8.42 ± 0.06 [3.8]
25d (5F-ADB-PINACA)[83]	Experimental data	8.91 ± 0.08 [1.22]	98%	8.57 ± 0.05 [2.73]	9.44 ± 0.07 [0.36]	107%	9.52 ± 0.03 [0.31]
	Reported data	9.61 ± 0.19 [0.24]	91%	8.84 ± 0.02 [1.43]	8.68 ± 0.11 [2.1]	94%	9.15 ± 0.05 [0.71]
25e (AB-CHMINACA)[3]	Experimental data	8.89 ± 0.06 [1.04]	78%	9.05 ± 0.09 [0.90]	8.12 ± 0.08 [7.67]	63%	8.96 ± 0.06 [1.10]
	Reported data			8.76 ± 0.09 [1.72]			8.71 ± 0.09 [1.91]
25f (ABD-CHMINACA)[3]	Experimental data	7.34 ± 0.04 [46.2]	80%	9.05 ± 0.09 [0.98]	8.46 ± 0.04 [3.49]	53%	9.22 ± 0.09 [0.60]
	Reported data			9.48 ± 0.06 [0.33]			9.51 ± 0.05 [0.31]
25g (AB-FUBINACA)[83]	Experimental data	8.41 ± 0.08 [3.86]	95%	8.64 ± 0.06 [2.31]	8.24 ± 0.06 [5.77]	86%	8.96 ± 0.08 [1.17]
	Reported data	8.76 ± 0.10 [1.8]	108%		8.50 ± 0.20 [3.2]	95%	
25h (ADB-FUBINACA)[83]	Experimental data	7.67 ± 0.03 [21.3]	104%	9.10 ± 0.04 [0.83]	8.40 ± 0.08 [3.96]	84%	10.0 ± 0.07 [0.14]
	Reported data	8.92 ± 0.16 [1.2]	152%	9.44 ± 0.09 [0.36]	8.46 ± 0.13 [3.5]	104%	9.46 ± 0.05 [0.34]

USC UNIVERSIDADE DE SANTIAGO DE COMPOSTELA

4.5 GENERAL PROCEDURES OF SYNTHESIS AND SPECTROSCOPIC DATA

4.5.1 General pathways for the synthesis of *N*-alkyl-1*H*-indole-3-carboxylic acid (26a-d)

To a solution of methyl 1H-indole-3-carboxylate (1 equiv.) in DMF (40 mL), NaH (1,2 equiv.) as 60% dispersion in mineral oil was added at 0 ºC. After 30 minutes, alkyl bromide (1,2 equiv.) was added, and the reaction was stirred a room temperature for 24 h. The reaction was quenched with water and extracted with CH_2Cl_2. The organic phase was dried over $MgSO_4$, filtered, and concentrated. The resulting product was purified by column chromatography on silica gel using $MeOH/CH_2Cl_2$. To a solution methyl 1-alkyl-1H-indole-3-carboxylate (**28a-d**) in dioxane (100 mL), 2N NaOH aq. (5 equiv.) was added, and the reaction was stirred a 120 ºC for 12 h. After completion of the reaction, the solvent was removed under reduced pressure and the pH was adjusted to 2 by addition of a solution of 2N HCl aq. The formation of a suspension is observed and was filtered and washed with water. The white solid was purified by column chromatography on silica gel using $MeOH/CH_2Cl_2$.



Scheme S1: General procedure for the synthesis of *N*-alkyl-1*H*-indole-3-carboxylic acid (**26a-d**).

4.5.1.1 Spectroscopic and analytical data of *N*-alkyl-1*H*-indole-3-carboxylic acid

1-pentyl-1*H*-indole-3-carboxylic acid (26a) Yield: 85%. Mp: 125-126. ^{1}H NMR (300 MHz, DMSO-d_6) δ (ppm): 11.92 (s, 1H, OH), 8.08 – 7.94 (m, 2H, Ar-H), 7.59 – 7.49 (m, 1H, Ar-H), 7.34 – 7.04 (m, 2H, Ar-H), 4.21 (t, J = 7.0 Hz, 2H, $NCH_2CH_2(CH_2)_2CH_3$), 1.84 – 1.66 (m, 2H, $NCH_2CH_2(CH_2)_2CH_3$), 1.36 – 1.10 (m, 4H, $NCH_2CH_2(CH_2)_2CH_3$), 0.85 – 0.78 (m, 3H, $NCH_2CH_2(CH_2)_2CH_3$). LRMS (CI) m/z calcd. For $C_{14}H_{18}NO_2$ $[M+H]^+$: 232.1; found: 232.1.

USC UNIVERSIDADE DE SANTIAGO DE COMPOSTELA

1-(5-fluoropentyl)-1*H*-indole-3-carboxylic acid (26b) Yield: 87%. Mp: 126-127 ºC. ^{1}H NMR (300 MHz, DMSO-d_6) δ (ppm): 11.94 (s, 1H, OH), 8.18 – 7.90 (m, 2H, Ar-H), 7.64 – 7.42 (m, 1H, Ar-H), 7.31 – 6.99 (m, 2H, Ar-H), 4.49 – 4.42 (m, 1H, $NCH_2CH_2CH_2CH_2CH_2F$), 4.33 – 4.27 (m, 1H, $NCH_2CH_2CH_2CH_2CH_2F$), 4.23 (t, *J* = 7.0 Hz, 2H, NC*H2*CH2CH2 CH2CH2F), 1.87 – 1.73 (m, 2H, $NCH_2CH_2CH_2CH_2CH_2F$), 1.73 – 1.53 (m, 2H, $NCH_2CH_2CH_2$ CH_2CH_2F), 1.37 – 1.22 (m, 2H, $NCH_2CH_2CH_2CH_2CH_2F$). LRMS (CI) m/z calcd. For $C_{14}H_{17}FNO_2$ $[M+H]^+$: 250.1; found: 250.1.

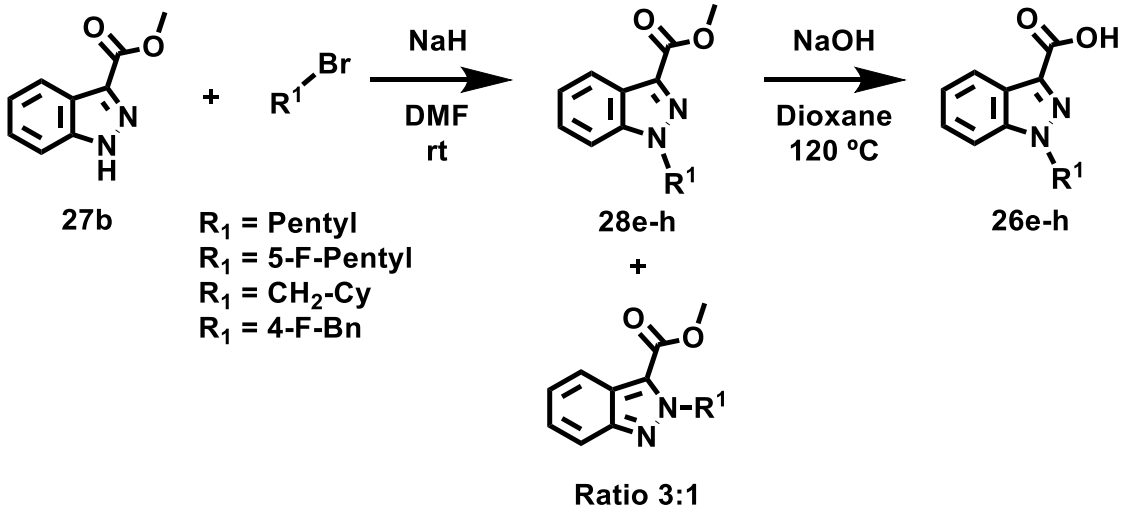
1-(cyclohexylmethyl)-1*H*-indole-3-carboxylic acid (26c) Yield: 92%. Mp: 187-188 ºC. ^{1}H NMR (300 MHz, DMSO-d_6) δ (ppm): 11.94 (s, 1H, OH), 8.10 – 7.87 (m, 2H, Ar-H), 7.64 – 7.42 (m, 1H, Ar-H), 7.32 – 7.06 (m, 2H, Ar-H), 4.07 (d, *J* = 7.2 Hz, 2H, CH_2-Cy), 1.90 – 1.71 (m, 1H, *CH*-Cy), 1.70 – 1.37 (m, 5H, CH_2-*Cy*), 1.37 – 0.74 (m, 5H, *Cy*). LRMS (CI) m/z calcd. For $C_{16}H_{20}NO_2$ $[M+H]^+$: 258.1; found: 258.1.

1-(4-fluorobenzyl)-1*H*-indole-3-carboxylic acid (26d) Yield: 86%. Mp: 209-210 ºC. ^{1}H NMR (300 MHz, DMSO-d_6) δ (ppm): 12.01 (s, 1H, OH), 8.21 (s, 1H, Ar-H), 8.09 – 7.89 (m, 1H, Ar-H), 7.61 – 7.45 (m, 1H, Ar-H), 7.40 – 7.25 (m, 2H, Ar-H), 7.25 – 7.02 (m, 4H, Ar-H), 5.46 (s, 2H, CH_2-Ph). LRMS (CI) m/z calcd. For $C_{16}H_{13}FNO_2$ $[M+H]^+$: 270.1; found: 270.1.

USC UNIVERSIDADE DE SANTIAGO DE COMPOSTELA

4.5.2 General procedure for the synthesis of 1-alkyl-1*H*-indazole-3-carboxylic acid (26e-h)

To a solution of methyl 1*H*-indazole-3-carboxylate (1 equiv.) in DMF (40 mL), NaH (1,2 equiv.) as 60% dispersion in mineral oil was added at 0 ºC. After 30 minutes, alkyl bromide (1,2 equiv.) was added, and the reaction was stirred a room temperature for 24 h. The reaction was quenched with water and extracted with CH_2Cl_2. The organic phase was dried over $MgSO_4$, filtered, and concentrated. The resulting product was purified by column chromatography on silica gel using MeOH/CH_2Cl_2. To a solution methyl 1-alkyl-1*H*-indazole-3-carboxylate (28e-h) in dioxane (100 mL), 2N NaOH aq. (5 equiv.) was added, and the reaction was stirred a 120 ºC for 12 h. After completion of the reaction, the solvent was removed under reduced pressure and the pH was adjusted to 2 by addition of a solution of 2N HCl aq. The formation of a suspension is observed and was filtered and washed with water. The white solid was purified by column chromatography on silica gel using MeOH/CH_2Cl_2. The two alkylated isomers were isolated, with a ratio of 3:1 between the *N*1 - alkylated (the desired product) and *N*2 - alkylated.



Scheme S2: General procedure for the synthesis of 1-alkyl-1*H*-indazole-3-carboxylic acid (**26e-h**).

4.5.2.1 Spectroscopic and analytical data of 1-alkyl-1*H*-indazole-3-carboxylic acid

1-pentyl-1*H*-indazole-3-carboxylic acid (26e) Yield: 81%. Mp: 123-124 ºC. ^{1}H NMR (300 MHz, DMSO-d_6) δ (ppm): 12.96 (s, 1H, OH), 8.06 (d, *J* = 8.1 Hz, 1H, Ar-H), 7.78 (d, *J* = 8.5 Hz, 1H, Ar-H), 7.51 – 7.39 (m, 1H, Ar-H), 7.34 – 7.23 (m, 1H, Ar-H), 4.47 (t, *J* = 7.0 Hz, 2H, NC*H*$_2$CH$_2$ (CH$_2$)$_2$CH$_3$), 1.92 – 1.76 (m, 2H, NCH$_2$*CH*$_2$

$(CH_2)_2CH_3$), 1.34 – 1.12 (m, 4H, NCH_2CH_2 $(CH_2)_2CH_3$), 0.80 (t, *J* = 7.0 Hz, 3H, NCH_2CH_2 $(CH_2)_2CH_3$). LRMS (CI) m/z calcd. for $C_{13}H_{17}N_2O_2$ $[M+H]^+$: 233.1; found: 233.1.

1-(5-fluoropentyl)-1*H*-indazole-3-carboxylic acid (26f) Yield: 86%. Mp: 122-123 ºC. ^{1}H NMR (300 MHz, DMSO-d_6) δ (ppm): 12.97 (s, 1H, OH), 8.09 (d, *J* = 8.1 Hz, 1H, Ar-H), 7.82 (d, *J* = 8.5 Hz, 1H, Ar-H), 7.48 (t, *J* = 7.4 Hz, 1H, Ar-H), 7.32 (t, *J* = 7.4 Hz, 1H, Ar-H), 4.60 – 4.44 (m, 3H, $NCH_2CH_2CH_2CH_2CH_2F$, $NCH_2CH_2CH_2CH_2CH_2F$), 4.37-4.28 (m, 1H, $NCH_2CH_2CH_2CH_2CH_2F$), 2.01 – 1.84 (m, 2H, $NCH_2CH_2CH_2CH_2CH_2F$), 1.78 – 1.55 (m, 2H, $NCH_2CH_2CH_2CH_2CH_2F$), 1.44 – 1.21 (m, 2H, $NCH_2CH_2CH_2CH_2CH_2F$). LRMS (CI) m/z calcd. for $C_{13}H_{16}FN_2O_2$ $[M+H]^+$: 251.1; found: 251.1.

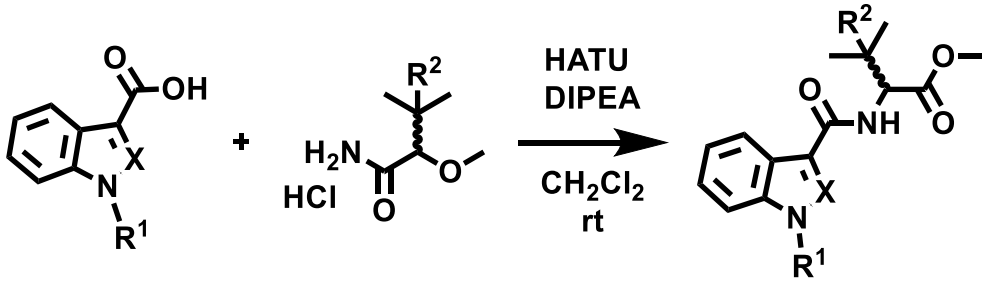
1-(cyclohexylmethyl)-1*H*-indazole-3-carboxylic acid (26g) Yield: 91%. Mp: 145-146 ºC. ^{1}H NMR (300 MHz, DMSO-d_6) δ (ppm): 12.96 (s, 1H, OH), 8.06 (d, *J* = 8.1 Hz, 1H, Ar-H), 7.79 (d, *J* = 8.5 Hz, 1H, Ar-H), 7.44 (t, *J* = 7.6 Hz, 1H, Ar-H), 7.28 (t, *J* = 7.6 Hz, 1H, Ar-H), 4.33 (d, *J* = 7.1 Hz, 2H, CH_2-Cy), 1.91 (s, 1H, *CH*-Cy), 1.76 – 1.35 (m, 5H, Cy), 1.30 – 0.92 (m, 5H, Cy). LRMS (CI) m/z calcd. for $C_{15}H_{19}N_2O_2$ $[M+H]^+$: 259.1; found: 259.1.

1-(4-fluorobenzyl)-1*H*-indazole-3-carboxylic acid (26h) Yield: 88%. Mp: 199-200 ºC. ^{1}H NMR (300 MHz, DMSO-d_6) δ (ppm): 13.07 (s, 1H, OH), 8.27 – 7.97 (m, 1H, Ar-H), 7.97 – 7.73 (m, 1H, Ar-H), 7.55 – 7.45 (m, 1H, Ar-H), 7.40 – 7.30 (m, 3H), 7.23 – 7.13 (m, 2H, Ar-H), 5.79 (s, 2H, CH_2-(Ph). LRMS (CI) m/z calcd. for $C_{15}H_{12}FN_2O_2$ $[M+H]^+$: 271.1; found: 271.1.

USC UNIVERSIDADE DE SANTIAGO DE COMPOSTELA

4.5.3 General pathways for the synthesis methyl (1*H*-indole (or indazole)-3-carbonyl)glycinate polysubstituted (22a-p and 23a-p)

A mixture of the 1-alkyl-1*H*-indole (or indazole)-3-carboxylic acid (1 equiv.), DIPEA (4 equiv.) and HATU (1,5 equiv.) in CH_2Cl_2 (2 mL) and stirred with orbital stirring at room temperature for 30 minutes and then the corresponding amino acid methyl esters (1,5 equiv.) was added. The reaction mixture was stirred overnight at room temperature. After completion of the reaction, water was added, and the mixture was extracted with CH_2Cl_2. The organic phase was dried over $MgSO_4$, filtered, and concentrated. The resulting product was purified by column chromatography on silica gel using MeOH/CH_2Cl_2.



26a-h
X = CH
X = N

30a-d
R^2 = H
R^2 = CH_3

22a-p, 23a-p

R^1 = Pentyl
R^1 = 5-F-Pentyl
R^1 = CH_2-Cy
R^1 = 4-F-Bn

Scheme S3: General procedure for the synthesis of methyl (1H-indole (or indazole)-3-carbonyl)glycinate polysubstituted (**22a-p**, **23a-p**).

4.5.3.1 Spectroscopic and analytical data of methyl (1*H*-indole (or indazole)-3-carbonyl)glycinate polysubstituted

Methyl (*S*)-(1-pentyl-1*H*-indole-3-carbonyl)valinate (22a). Yield: 67%. Mp: 133-134 ºC. ^{1}H NMR (300 MHz, $CDCl_3$) d (ppm): 7.99 (m, 1H, Ar-H), 7.74 (s, 1H, Ar-H), 7.39 (m, 1H, Ar-H), 7.28 (m, 2H, Ar-H), 6.46 (d, *J* = 8.7 Hz, 1H, NH), 4.87 (dd, *J* = 8.7, 4.8 Hz, 1H, *CH*CH$(CH_3)_2$), 4.14 (t, *J* = 7.2 Hz, 2H, N*CH*$_2$CH$_2(CH_2)_2CH_3$), 3.79 (s, 3H, OCH_3), 2.31 (m, 1H, CHC*H*$(CH_3)_2$), 1.87 (quin. *J* = 7.4 Hz, 2H, NCH$_2$C*H*$_2(CH_2)_2CH_3$), 1.33 (m, 4H, NCH$_2$CH$_2$*(CH$_2$)$_2$*CH$_3$), 1.04 (t, *J* = 6.9 Hz, 6H,

CHCH*(CH$_3$)$_2$*), 0.89 (t, *J* = 6.7 Hz, 3H, NCH$_2$CH$_2$(CH$_2$)*CH$_3$*). LRMS (CI) *m/z* calcd. for $C_{20}H_{29}N_2O_3$ $[M+H]^+$: 345.2; found: 345.2.

Methyl (*S*)-3,3-dimethyl-2-(1-pentyl-1*H*-indole-3-carboxamido)butanoate (22b) Yield: 75%. Mp: 135-136 ºC. ^{1}H NMR (300 MHz, $CDCl_3$) d (ppm): 7.98 (m, 1H, Ar-H), 7.76 (s, 1H, Ar-H), 7.40 (m, 1H, Ar-H), 7.28 (m, 2H, Ar-H), 6.53 (d, *J* = 9.3 Hz, 1H, NH), 4.79 (d, *J* = 9.3 Hz, 1H, *CH*C(CH$_3$)$_3$), 4.14 (t, *J* = 7.2 Hz, 2H, N*CH$_2$*CH$_2$(CH$_2$)$_2$CH$_3$), 3.76 (s, 3H, OCH$_3$), 1.87 (m, 2H, NCH$_2$*CH$_2$*(CH$_2$)$_2$CH$_3$), 1.33 (m, 4H, N*CH$_2$*CH$_2$*(CH$_2$)$_2$*CH$_3$), 1.09 (s, 9H, C(C*H$_3$*)$_3$), 0.89 (t, *J* = 6.5 Hz, 3H, NCH$_2$CH$_2$(CH$_2$)$_2$*CH$_3$*). LRMS (CI) m/z calcd. for $C_{21}H_{31}N_2O_3$ $[M+H]^+$: 359.2; found: 359.2.

Methyl (*S*)-(1-(5-fluoropentyl)-1*H*-indole-3-carbonyl)valinate (22c). Yield: 64%. Mp: 139-140 ºC. ^{1}H NMR (300 MHz, $CDCl_3$) δ (ppm): 8.00 (m, 1H, Ar-H), 7.76 (s, 1H, Ar-H), 7.38 (m, 1H, Ar-H), 7.28 (m, 2H, Ar-H), 6.50 (d, *J* = 8.7 Hz, 1H, NH), 4.87 (dd, *J* = 8.6, 4.8 Hz, 1H, *CH*CH(CH$_3$)$_2$), 4.50 (t, *J* = 5.9 Hz, 1H, NCH$_2$CH$_2$CH$_2$CH$_2$*CH$_2$*F), 4.34 (t, *J* = 5.9 Hz, 1H, NCH$_2$CH$_2$CH$_2$CH$_2$*CH$_2$*F), 4.16 (t, *J* = 7.1 Hz, 2H, N*CH$_2$*CH$_2$CH$_2$CH$_2$CH$_2$F), 3.79 (s, 3H, OCH$_3$), 2.31 (m, 1H, CHC*H*(CH$_3$)$_2$), 1.92 (quin, *J* = 7.2 Hz, 2H, NCH$_2$*CH$_2$*CH$_2$CH$_2$CH$_2$F), 1.81–1.62 (m, 2H, NCH$_2$CH$_2$CH$_2$*CH$_2$*CH$_2$F), 1.52–1.40 (m, 2H, NCH$_2$CH$_2$C*H$_2$*CH$_2$CH$_2$F), 1.04 (t, *J* = 7.0 Hz, 6H, CHCH*(CH$_3$)$_2$*). ^{13}C NMR (75 MHz, $CDCl_3$) δ (ppm): 173.3, 165.0, 136.7, 131.7, 125.6, 122.6, 121.7, 120.3, 110.7, 110.3, 83.7 (d, $J_{C\text{-}F}$ = 165.0 Hz), 57.0, 52.2, 46.8, 31.7, 30.0 (d, $J_{C\text{-}F}$ = 19.8 Hz), 29.7, 22.9 (d, $J_{C\text{-}F}$ = 5.0 Hz), 19.2, 18.2. LRMS (CI) m/z calcd. for $C_{20}H_{28}FN_2O_3$ $[M+H]^+$: 363.2; found: 363.2.

Methyl (*S*)-2-(1-(5-fluoropentyl)-1*H*-indole-3-carboxamido)-3,3-dimethyl-butanoate (22d). Yield: 71%. Mp: 134-135 ºC. ^{1}H NMR (300 MHz, $CDCl_3$) δ (ppm): 7.98 (m, 1H, Ar-H), 7.75 (s, 1H, Ar-H), 7.38 (m, 1H, Ar-H), 7.29 (m, 2H, Ar-H), 6.53 (d, *J* = 9.4 Hz, 1H, NH), 4.78 (d, *J* = 9.3 Hz, 1H, *CH*C(CH$_3$)$_3$), 4.50 (t, *J* = 5.9 Hz, 1H, NCH$_2$CH$_2$CH$_2$CH$_2$*CH$_2$*F), 4.34 (t, *J* = 5.9 Hz, 1H, NCH$_2$CH$_2$CH$_2$CH$_2$*CH$_2$*F), 4.17 (t, *J* = 7.1 Hz, 2H, N*CH$_2$*CH$_2$CH$_2$CH$_2$CH$_2$F), 3.77 (s, 3H, OCH$_3$), 1.93 (quin, *J* = 7.3 Hz, 2H, NCH$_2$*CH$_2$*CH$_2$CH$_2$CH$_2$F), 1.82–1.63 (m, 2H, NCH$_2$CH$_2$CH$_2$*CH$_2$*CH$_2$F), 1.47 (m, 2H,

USC UNIVERSIDADE DE SANTIAGO DE COMPOSTELA

$NCH_2CH_2\mathit{CH_2}CH_2CH_2F$), 1.09 (s, 9H, $C(CH_3)_3$). LRMS (CI) m/z calcd for $C_{21}H_{30}FN_2O_3$ $[M+H]^+$: 377.2; found: 377.2.

Methyl (*S*)-(1-(cyclohexylmethyl)-1*H*-indole-3-carbonyl)valinate (22e) (MMB-CHMICA). Yield: 61%. Mp: 132-133 ºC. ^{1}H NMR (300 MHz, $CDCl_3$) δ (ppm): 8.01 (m, 1H, Ar-H), 7.73 (s, 1H, Ar-H), 7.38 (m, 1H, Ar-H), 7.28 (m, 2H, Ar-H), 6.57 (d, *J* = 8.7 Hz, 1H, NH), 4.88 (dd, *J* = 8.7, 4.9 Hz, 1H, $\mathit{CH}CH(CH_3)_2$), 3.93 (d, *J* = 7.1 Hz, 2H, $C\mathit{H_2}$-Cy), 3.79 (s, 3H, OCH_3), 2.31 (m, 1H, $CHC\mathit{H}(CH_3)_2$), 1.85 (m, 1H, *CH*-Cy), 1.77–1.53 (m, 5H, Cy, 1.30–0.90 (m, 11 H, Cy, $CHCH\mathit{(CH_3)_2}$). LRMS (CI) m/z calcd. for $C_{22}H_{31}N_2O_3$ $[M+H]^+$: 371.2; found: 371.2.

Methyl (*S*)-2-(1-(cyclohexylmethyl)-1*H*-indole-3-carboxamido)-3,3-dimethylbutanoate (22f) (MDBM-CHMICA). Yield: 63%. Mp: 137-138 ºC. ^{1}H NMR (300 MHz, $CDCl_3$) δ (ppm): 7.98 (m, 1H, Ar-H), 7.71 (s, 1H, Ar-H), 7.39 (m, 1H, Ar-H), 7.28 (m, 2H, Ar-H), 6.53 (d, *J* = 9.4 Hz, 1H, NH), 4.79 (d, *J* = 9.3 Hz, 1H, $\mathit{CH}C(CH_3)_3$), 3.96 (d, *J* = 7.2 Hz, 2H, $NC\mathit{H_2}$-Cy), 3.77 (s, 3H, OCH_3), 1.87 (m, 1H, *CH*-Cy), 1.77–1.58 (m, 5H, Cy), 1.32–0.93 (m, 14H, Cy, $C(C\mathit{H_3})_3$). ^{13}C NMR (75 MHz, $CDCl_3$) δ (ppm): 172.8, 164.9, 137.1, 132.8, 125.3, 122.5, 121.6, 120.0, 110.8, 110.5, 59.9, 53.5, 51.9, 38.7, 35.2, 31.1, 26.9, 26.3, 25.7. LRMS (CI) m/z calcd. for $C_{23}H_{33}N_2O_3$ $[M+H]^+$: 385.2; found: 385.2.

Methyl (*S*)-(1-(4-fluorobenzyl)-1*H*-indole-3-carbonyl)valinate (22g) (MMB-FUBICA). Yield: 72%. Mp: 147-148 ºC. ^{1}H NMR (300 MHz, $CDCl_3$) δ (ppm): 8.03 (m, 1H, Ar-H), 7.75 (s, 1H, Ar-H), 7.27 (m, 3H, Ar-H), 7.12 (m, 2H, Ar-H), 7.00 (m, 2H, Ar-H), 6.52 (d, *J* = 8.7 Hz, 1H, NH), 5.28 (s, 2H, $C\mathit{H_2}$-Ph), 4.87 (dd, *J* = 8.7, 4.9 Hz, 1H, $\mathit{CH}CH(CH_3)_2$), 3.79 (s, 3H, OCH_3), 2.31 (quind, *J* = 6.9, 4.9 Hz, 1H, $CHC\mathit{H}(CH_3)_2$) 1.04 (t, *J* = 7.2 Hz, 6H, $CHCH\mathit{(CH_3)_2}$). LRMS (CI) m/z calcd. for $C_{22}H_{24}FN_2O_3$ $[M+H]^+$: 383.2; found: 383.2.

Methyl (*S*)-2-(1-(4-fluorobenzyl)-1*H*-indole-3-carboxamido)-3,3-dimethylbutanoate (22h). Yield: 83%. Mp: 132-133 ºC. ^{1}H NMR (300 MHz, $CDCl_3$) δ (ppm): 8.01 (m, 1H, Ar-H), 7.76 (s, 1H, Ar-H), 7.28 (m, 3H, Ar-H), 7.11 (m, 2H, Ar-H), 7.00 (m, 2H, Ar-H), 6.57 (d, *J* = 9.3 Hz, 1H, NH), 5.27 (s, 2H $C\mathit{H_2}$-Ph), 4.78 (d, *J* = 9.3 Hz,

1H, *CH*C(CH$_3$)$_3$), 3.75 (s, 3H, OCH$_3$), 1.09 (s, 9H, C(C*H$_3$*)$_3$). LRMS (CI) m/z calcd. for $C_{23}H_{26}FN_2O_3$ $[M+H]^+$: 397.2; found: 397.2.

Methyl (*R*)-1-pentyl-1*H*-indole-3-carbonyl)valinate (22i). Yield: 52%. Mp: 137-138 ºC. ^{1}H NMR (300 MHz, $CDCl_3$) δ (ppm): 7.99 (m, 1H, Ar-H), 7.74 (s, 1H, Ar-H), 7.39 (m, 1H, Ar-H), 7.28 (m, 2H, Ar-H), 6.47 (d, *J* = 8.7 Hz, 1H, NH), 4.87 (dd, *J* = 8.7, 4.8, 1H, *CH*CH(CH$_3$)$_2$), 4.13 (t, *J* = 7.2 Hz, 2H, N*CH$_2$*CH$_2$(CH$_2$)$_2$CH$_3$), 3.79 (s, 3H, OCH$_3$), 2.31 (m, 1H, CHC*H*(CH$_3$)$_2$), 1.87 (quin. *J* = 7.3 Hz, 2H, NCH$_2$*CH$_2$*(CH$_2$)$_2$CH$_3$), 1.33 (m, 4H, NCH$_2$CH$_2$*(CH$_2$)$_2$*CH$_3$), 1.04 (t, *J* = 6.9 Hz, 6H, CHCH*(CH$_3$)$_2$*), 0.89 (t, *J* = 6.7 Hz, 3H, NCH$_2$CH$_2$(CH$_2$)$_2$*CH$_3$*). ^{13}C NMR (75 MHz, $CDCl_3$) δ (ppm): 173.3, 165.1, 136.8, 131.9, 125.5, 122.5, 121.7, 120.2, 110.6, 110.4, 57.1, 52.2, 47.0, 31.8, 29.8, 29.1, 22.4, 19.2, 18.2, 14.0. LRMS (CI) m/z calcd. for $C_{20}H_{29}N_2O_3$ $[M+H]^+$: 345.2; found: 345.2.

Methyl (*R*)-3,3-dimethyl-2-(1-pentyl-1*H*-indole-3-carboxamido)butanoate (22j). Yield: 62%. Mp: 135-136 ºC. ^{1}H NMR (300 MHz, $CDCl_3$) δ (ppm): 7.98 (m, 1H, Ar-H), 7.76 (s, 1H, Ar-H), 7.40 (m, 1H, Ar-H), 7.28 (m, 2H, Ar-H), 6.53 (d, *J* = 9.6 Hz, 1H, NH), 4.79 (d, *J* = 9.3 Hz, 1H, *CH*C(CH$_3$)$_3$), 4.14 (t, *J* = 7.2 Hz, 2H, N*CH$_2$*CH$_2$(CH$_2$)$_2$CH$_3$), 3.77 (s, 3H, OCH$_3$), 1.87 (m, 2H, NCH$_2$*CH$_2$*(CH$_2$)$_2$CH$_3$), 1.33 (m, 4H, NCH$_2$CH$_2$*(CH$_2$)$_2$*CH$_3$), 1.09 (s, 9H, C(CH$_3$)$_3$), 0.89 (t, *J* = 6.5 Hz, 3H, NCH$_2$CH$_2$(CH$_2$)$_2$*CH$_3$*). LRMS (CI) m/z calcd for $C_{21}H_{31}N_2O_3$ $[M+H]^+$: 359.2; found: 359.2.

Methyl (*R*)-(1-(5-fluoropentyl)-1*H*-indole-3-carbonyl)valinate (22k). Yield: 58%. Mp: 142-143 ºC.^{1}H NMR (300 MHz, $CDCl_3$) δ (ppm): 8.00 (m, 1H, Ar-H), 7.75 (s, 1H, Ar-H), 7.39 (m, 1H, Ar-H), 7.28 (m, 2H, Ar-H), 6.48 (d, *J* = 8.7 Hz, 1H, NH), 4.87 (dd, *J* = 8.8, 4.8 Hz, 1H, *CH*CH(CH$_3$)$_2$), 4.50 (t, *J* = 6.0 Hz, 1H, NCH$_2$CH$_2$CH$_2$CH$_2$*CH$_2$*F), 4.34 (t, *J* = 5.9 Hz, 1H, NCH$_2$CH$_2$CH$_2$CH$_2$*CH$_2$*F), 4.17 (t, *J* = 7.1 Hz, 2H, N*CH$_2$*CH$_2$CH$_2$CH$_2$CH$_2$F), 3.79 (s, 3H, OCH$_3$), 2.31 (m, 1H, CHC*H*(CH$_3$)$_2$), 1.92 (quin, *J* = 7.2 Hz, 2H, NCH$_2$*CH$_2$*CH$_2$CH$_2$CH$_2$F), 1.82–1.62 (m, 2H, NCH$_2$CH$_2$CH$_2$C*H$_2$*CH$_2$F), 1.53–1.40 (m, 2H, NCH$_2$CH$_2$C*H$_2$*CH$_2$CH$_2$F), 1.04 (t, *J* = 6.9 Hz, 6H, CHCH*(CH$_3$)$_2$*). LRMS (CI) m/z calcd. for $C_{20}H_{28}FN_2O_3$ $[M+H]^+$: 363.2; found: 363.2.

UdC UNIVERSIDADE

Methyl (*R*)-2-(1-(5-fluoropentyl)-1*H*-indole-3-carboxamido)-3,3-dimethylbutanoate (22l). Yield: 57%. Mp: 120-121 ºC. ^{1}H NMR (300 MHz, $CDCl_3$) δ (ppm): 7.98 (m, 1H, Ar-H), 7.75 (s, 1H, Ar-H), 7.38 (m, 1H, Ar-H), 7.29 (m, 2H, Ar-H), 6.53 (d, *J* = 9.4 Hz, 1H, NH), 4.78 (d, *J* = 9.3 Hz, 1H, $CHC(CH_3)_3$), 4.50 (t, *J* = 5.9 Hz, 1H, $NCH_2CH_2CH_2CH_2\mathit{CH_2}F$), 4.34 (t, *J* = 5.9 Hz, 1H, $NCH_2CH_2CH_2CH_2\mathit{CH_2}F$), 4.17 (t, *J* = 7.1 Hz, 2H, $N\mathit{CH_2}CH_2CH_2CH_2CH_2F$), 3.77 (s, 3H, OCH_3), 1.93 (quin, *J* = 7.3 Hz, 2H, $NCH_2\mathit{CH_2}CH_2CH_2CH_2F$), 1.82–1.63 (m, 2H, $NCH_2CH_2CH_2\mathit{CH_2}CH_2F$), 1.47 (m, 2H, $NCH_2CH_2C\mathit{H_2}CH_2CH_2F$), 1.09 (s, 9H, $C(CH_3)_3$). LRMS (CI) m/z calcd. for $C_{21}H_{30}FN_2O_3$ $[M+H]^+$: 377.2; found: 377.2.

Methyl (*R*)-(1-(cyclohexylmethyl)-1*H*-indole-3-carbonyl)valinate (22m). Yield: 62%. Mp: 132-133 ºC. ^{1}H NMR (300 MHz, $CDCl_3$) δ (ppm): 7.98 (m, 1H, Ar-H), 7.72 (s, 1H, Ar-H), 7.38 (m, 1H, Ar-H), 7.28 (m, 2H, Ar-H), 6.50 (d, *J* = 8.7 Hz, 1H, NH), 4.87 (dd, *J* = 8.6, 4.8 Hz, 1H, $\mathit{CH}CH(CH_3)_2$), 3.96 (d, *J* = 7.2 Hz, 2H, $C\mathit{H_2}$-Cy), 3.79 (s, 3H, OCH_3), 2.31 (m, 1H, $CHC\mathit{H}(CH_3)_2$), 1.86 (m, 1H, *CH*-Cy), 1.77–1.55 (m, 5H, Cy), 1.31–0.91 (m, 11 H, Cy, $CHCH\mathit{(CH_3)_2}$). LRMS (CI) m/z calcd. for $C_{22}H_{31}N_2O_3$ $[M+H]^+$: 371.2; found: 371.2.

Methyl (*R*)-2-(1-(cyclohexylmethyl)-1*H*-indole-3-carboxamido)-3,3-dimethylbutanoate (22n). Yield: 52%. Mp: 133-134 ºC. ^{1}H NMR (300 MHz, $CDCl_3$) δ (ppm): 7.98 (m, 1H, Ar-H), 7.72 (s, 1H, Ar-H), 7.39 (m, 1H, Ar-H), 7.28 (m, 2H Ar-H), 6.54 (d, *J* = 9.4 Hz, 1H, NH), 4.80 (d, *J* = 9.4 Hz, 1H, $\mathit{CH}C(CH_3)_3$), 3.96 (d, *J* = 7.2 Hz, 2H, $C\mathit{H_2}$-Cy), 3.77 (s, 3H, OCH_3), 1.87 (m, 1H, *CH*-Cy), 1.77–1.58 (m, 5H, Cy), 1.32–0.93 (m, 14 H,Cy, $C(CH_3)_3$). LRMS (CI) m/z calcd. for $C_{23}H_{33}N_2O_3$ $[M+H]^+$: 385.2; found: 385.2.

Methyl (*R*)-(1-(4-fluorobenzyl)-1*H*-indole-3-carbonyl)valinate (22o). Yield: 71%. Mp: 148-149 ºC. ^{1}H NMR (300 MHz, $CDCl_3$) δ (ppm): 8.02 (m, 1H, Ar-H), 7.76 (s, 1H, Ar-H), 7.27 (m, 3H, Ar-H), 7.12 (m, 2H, Ar-H), 7.00 (m, 2H, Ar-H), 6.51 (d, *J* = 8.7 Hz, 1H, NH), 5.30 (s, 2H, $C\mathit{H_2}$-Ph), 4.87 (dd, *J* = 8.7, 4.9 Hz, 1H, $\mathit{CH}CH(CH_3)_2$), 3.79 (s, 3H, OCH_3), 2.31 (quind, *J* = 6.9, 5.0 Hz, 1H, $CHC\mathit{H}(CH_3)_2$), 1.04 (t, *J* = 7.1 Hz, 6H, $CHCH\mathit{(CH_3)_2}$). ^{13}C NMR (75 MHz, $CDCl_3$) δ (ppm): 173.3, 164.9, 162.5 (d, $J_{C\text{-}F}$ = 247.1 Hz), 136.8, 132.0 (d, $J_{C\text{-}F}$ = 3.3 Hz), 131.9, 128.9 (d, $J_{C\text{-}F}$ = 8.1 Hz), 125.8, 123.0,

122.0, 120.4, 116,0 (d, J_{C-F} = 21.8 Hz), 111.4, 110.6, 57.1, 52.2, 50.0, 31.7, 19.2, 18.2. LRMS (CI) m/z calcd. for $C_{22}H_{24}FN_2O_3$ $[M+H]^+$: 383.2; found: 383.2.

Methyl (*R*)-2-(1-(4-fluorobenzyl)-1*H*-indole-3-carboxamido)-3,3-dimethyl-butanoate (22p). Yield: 48%. Mp: 128-129 ºC. ^{1}H NMR (300 MHz, $CDCl_3$) δ (ppm): 8.00 (m, 1H, Ar-H), 7.76 (s, 1H, Ar-H), 7.28 (m, 3H, Ar-H), 7.12 (m, 2H, Ar-H), 7.00 (m, 2H, Ar-H), 6.53 (d, *J* = 9.3 Hz, 1H, NH), 5.31 (s, 2H, CH_2-Ph), 4.78 (d, *J* = 9.3 Hz, 1H, *CH*C$(CH_3)_3$), 3.77 (s, 3H, OCH_3), 1.09 (s, 9H, C$(CH_3)_3$). ^{13}C NMR (75 MHz, $CDCl_3$) δ (ppm): 172.8, 164.7, 162.6 (d, J_{C-F} = 246.8 Hz), 136.9, 132.2, 131.9 (d, J_{C-F} = 3.2 Hz), 128.9 (d, J_{C-F} = 8.2 Hz), 125.6, 123.0, 122.1, 120.2, 116.0 (d, J_{C-F} = 21.8 Hz), 111.5, 110.8, 59.9, 51.9, 50.1, 35.2, 26.9. LRMS (CI) m/z calcd. for $C_{23}H_{26}FN_2O_3$ $[M+H]^+$: 397.2; found: 397.2.

Methyl (*S*)-(1-pentyl-1*H*-indazole-3-carbonyl)valinate (23a). Yield: 64%. Mp: 138-139 ºC. ^{1}H NMR (300 MHz, $CDCl_3$) δ (ppm): 8.35 (dt, *J* = 8.2, 1.0 Hz, 1H, Ar-H), 7.47 (d, *J* = 9.1 Hz, 1H, NH), 7.41 (m, 2H, Ar-H), 7.27 (m, 1H, Ar-H), 4.80 (dd, *J* = 9.1, 5.2 Hz, 1H, *CH*CH$(CH_3)_2$), 4.39 (t, *J* = 7.2 Hz, 2H, N*CH*$_2$CH$_2$$(CH_2)_2CH_3$), 3.78 (s, 3H, OCH_3), 2.31 (m, 1H, CHC*H*$(CH_3)_2$), 1.96 (m, 2H, NCH$_2$*CH*$_2$$(CH_2)_2CH_3$), 1.35 (m, 4H, NCH$_2CH_2$*(CH$_2$)$_2$*CH$_3$), 1.05 (dd, *J* = 6.9, 4.1 Hz, 6H, CHCH*(CH$_3$)$_2$*), 0.90 (t, *J* = 6.9 Hz, 3H, NCH$_2$CH$_2$$(CH_2)_2$*CH$_3$*). LRMS (CI) m/z calcd. for $C_{19}H_{28}N_3O_3$ $[M+H]^+$: 346.2; found: 346.2.

Methyl (*S*)-3,3-dimethyl-2-(1-pentyl-1*H*-indazole-3-carboxamido)butanoate (23b). Yield: 55%. Mp: 145-146 ºC. ^{1}H NMR (300 MHz, $CDCl_3$) δ (ppm): 8.34 (dt, *J* = 8.2, 1.0 Hz, 1H, Ar-H), 7.55 (d, *J* = 9.7 Hz, 1H, NH), 7.40 (m, 2H, Ar-H), 7.26 (m, 1H, Ar-H), 4.73 (d, *J* = 9.8 Hz, 1H, *CH*C$(CH_3)_3$), 4.39 (t, *J* = 7.2 Hz, 2H, N*CH*$_2$CH$_2$$(CH_2)_2CH_3$), 3.76 (s, 3H, OCH_3), 1.96 (quin, *J* = 7.4 Hz, 2H, NCH$_2$*CH*$_2$$(CH_2)_2CH_3$), 1.35 (m, 4H, NCH$_2CH_2$*(CH$_2$)$_2$*CH$_3$), 1.09 (s, 9H, C$(CH_3)_3$), 0.90 (t, *J* = 6.8 Hz, 3H, NCH$_2$CH$_2$$(CH_2)_2$*CH$_3$*). ^{13}C NMR (75 MHz, $CDCl_3$) δ (ppm): 172.3, 162.5, 141.0, 136.7, 126.7, 123.0, 122.9, 122.6, 109.3, 59.6, 51.9, 49.6, 35.1, 29.5, 29.0, 26.8, 22.3, 14.0. LRMS (CI) m/z calcd. for $C_{20}H_{30}N_3O_3$ $[M+H]^+$: 360.2; found: 360.2.

USC UNIVERSIDADE DE SANTIAGO DE COMPOSTELA

Methyl (*S*)-(1-(5-fluoropentyl)-1*H*-indazole-3-carbonyl)valinate (23c). Yield: 61%. Mp: 138-139 ºC. ^{1}H NMR (300 MHz, $CDCl_3$) δ (ppm): 8.35 (d, *J* = 8.2 Hz, 1H, Ar-H), 7.44 (m, 3H, Ar-H, NH), 7.27 (m, 1H, Ar-H), 4.80 (dd, *J* = 9.1, 5.2 Hz, 1H, *CH*CH$(CH_3)_2$), 4.51 (t, *J* = 6.0 Hz, 1H, $NCH_2CH_2CH_2CH_2CH_2F$), 4.42 (t, *J* = 7.1 Hz, 2H, $NCH_2CH_2CH_2CH_2CH_2F$), 4.36 (t, *J* = 5.9 Hz, 1H, $NCH_2CH_2CH_2CH_2CH_2F$), 3.78 (s, 3H, OCH_3), 2.31 (m, 1H, CHC*H*$(CH_3)_2$), 2.02 (quin, *J* = 7.3 Hz, 2H, $NCH_2CH_2CH_2CH_2CH_2F$), 1.85–1.64 (m, 2H, $NCH_2CH_2CH_2CH_2CH_2F$), 1.49 (m, 2H, $NCH_2CH_2CH_2CH_2CH_2F$), 1.05 (dd, *J* = 6.9, 4.4 Hz, 6H, CHCH$(CH_3)_2$). LRMS (CI) m/z calcd. for $C_{19}H_{27}FN_3O_3$ $[M+H]^+$: 364.2; found: 364.2.

Methyl (*S*)-2-(1-(5-fluoropentyl)-1*H*-indazole-3-carboxamido)-3,3-dimethylbutanoate (23d). Yield: 67%. Mp: 143-144 ºC. ^{1}H NMR (300 MHz, $CDCl_3$) δ (ppm): 8.35 (dt, *J* = 8.2, 1.0 Hz, 1H, Ar-H), 7.54 (d, *J* = 9.7 Hz, 1H, NH), 7.40 (m, 2H, Ar-H), 7.27 (m, 1H, Ar-H), 4.73 (d, *J* = 9.7 Hz, 1H, *CH*C$(CH_3)_3$), 4.51 (t, *J* = 6.0 Hz, 1H, $NCH_2CH_2CH_2CH_2CH_2F$), 4.42 (t, *J* = 7.1 Hz, 2H, $NCH_2CH_2CH_2CH_2CH_2F$), 4.36 (t, *J* = 5.9 Hz, 1H, $NCH_2CH_2CH_2CH_2CH_2F$), 3.76 (s, 3H, OCH_3), 2.02 (quin, *J* = 7.3 Hz, 2H, $NCH_2CH_2CH_2CH_2CH_2F$), 1.85–1.65 (m, 2H, $NCH_2CH_2CH_2CH_2CH_2F$), 1.49 (m, 2H, $NCH_2CH_2CH_2CH_2CH_2F$), 1.09 (s, 9H, C$(CH_3)_3$). LRMS (CI) m/z calcd. for $C_{20}H_{29}FN_3O_3$ $[M+H]^+$: 378.2; found: 378.2.

Methyl (*S*)-(1-(cyclohexylmethyl)-1*H*-indazole-3-carbonyl)valinate (23e). Yield: 69%. Mp: 141-142 ºC. ^{1}H NMR (300 MHz, $CDCl_3$) δ (ppm): 8.35 (d, *J* = 8.2 Hz, 1H, Ar-H), 7.48 (d, *J* = 9.0 Hz, 1H, NH), 7.41 (m, 2H, Ar-H), 7.26 (ddd, *J* = 8.0, 4.8, 2.2 Hz, 1H, Ar-H), 4.81 (dd, *J* = 9.0, 5.3 Hz, 1H, *CH*CH$(CH_3)_2$), 4.22 (d, *J* = 7.1 Hz, 2H, C*H*$_2$-Cy), 3.79 (s, 3H, OCH_3), 2.31 (m, 1H, CHC*H*$(CH_3)_2$), 2.04 (m, 1H, *CH*-Cy), 1.78–1.57 (m, 5H, Cy), 1.31–0.97 (m, 11H, Cy, CH$(CH_3)_2$). LRMS (CI) m/z calcd for $C_{21}H_{30}N_3O_3$ $[M+H]^+$: 372.2; found: 372.2.

Methyl (*S*)-2-(1-(cyclohexylmethyl)-1*H*-indazole-3-carboxamido)-3,3-dimethylbutanoate (23f). Yield: 58%. Mp: 135-136 ºC. ^{1}H NMR (300 MHz, $CDCl_3$) δ (ppm): 8.34 (dd, *J* = 8.2, 1.2 Hz, 1H, Ar-H), 7.55 (d, *J* = 9.7 Hz, 1H, NH), 7.39 (m, 2H, Ar-H), 7.25 (m, 1H, Ar-H), 4.73 (d, *J* = 9.7 Hz, 1H, *CH*C$(CH_3)_3$), 4.22 (d, *J* = 7.2 Hz, 2H, N*CH*$_2$Cy), 3.76 (s, 3H, OCH_3), 2.03 (m, 1H, *CH*-Cy), 1.79–1.53 (m, 5H, Cy), 1.32–

0.96 (m, 14H, Cy, C(CH_3)$_3$). LRMS (CI) m/z calcd. for $C_{22}H_{32}N_3O_3$ $[M+H]^+$: 386.2; found: 386.2.

Methyl (*S*)-(1-(4-fluorobenzyl)-1*H*-indazole-3-carbonyl)valinate (23g). Yield: 62%. Mp: 130-131 ºC.^{1}H NMR (300 MHz, $CDCl_3$) δ (ppm): 8.37 (dt, *J* = 8.1, 1.0 Hz, 1H, Ar-H), 7.48 (d, *J* = 9.0 Hz, 1H, NH), 7.41–7.16 (m, 5H, Ar-H), 7.01 (m, 2H, Ar-H), 5.60 (s, 2H, C*H*$_2$-Ph), 4.81 (dd, *J* = 9.0, 5.2 Hz, 1H, *CH*CH(CH_3)$_2$), 3.79 (s, 3H, OCH_3), 2.32 (m, 1H, CHC*H*(CH_3)$_2$), 1.05 (dd, *J* = 6.8, 4.7 Hz, 6H, CHCH*(CH$_3$)$_2$*). LRMS (CI) m/z calcd. for $C_{21}H_{23}FN_3O_3$ $[M+H]^+$: 384.2; found: 384.2.

Methyl (*S*)-2-(1-(4-fluorobenzyl)-1*H*-indazole-3-carboxamido)-3,3-dimethylbutanoate (23h). Yield: 72%. Mp: 127-128 ºC. ^{1}H NMR (300 MHz, $CDCl_3$) δ (ppm): 8.36 (dd, *J* = 8.1, 1.2 Hz, 1H, Ar-H), 7.57 (d, *J* = 9.7 Hz, 1H, NH), 7.39–7.13 (m, 5H, Ar-H), 6.99 (t, *J* = 8.6 Hz, 2H, Ar-H), 5.58 (s, 2H, C*H*$_2$-Ph), 4.74 (d, *J* = 9.7 Hz, 1H, *CH*C(CH_3)$_3$), 3.76 (s, 3H, OCH_3), 1.09 (s, 9H, C(CH_3)$_3$). LRMS (CI) m/z calcd. for $C_{22}H_{25}FN_3O_3$ $[M+H]^+$: 398.2; found: 398.2.

Methyl (*R*)-(1-pentyl-1*H*-indazole-3-carbonyl)valinate (23i). Yield: 41%. Mp: 127-128 ºC. ^{1}H NMR (300 MHz, $CDCl_3$) δ (ppm): 8.35 (dt, *J* = 8.2, 1.0 Hz, 1H, Ar-H), 7.48 (d, *J* = 9.1 Hz, 1H, NH), 7.41 (m, 2H, Ar-H), 7.26 (m, 1H, Ar-H), 4.81 (dd, *J* = 9.1, 5.3 Hz, 1H, *CH*CH(CH_3)$_2$), 4.39 (t, *J* = 7.2 Hz, 2H, N*CH*$_2$CH$_2$(CH_2)$_2$$CH_3$), 3.78 (s, 3H, OCH_3), 2.32 (m, 1H, CHC*H*(CH_3)$_2$), 1.96 (m, 2H, NCH$_2$*CH*$_2$(CH_2)$_2$$CH_3$), 1.35 (m, 4H, NCH$_2CH_2$*(CH$_2$)$_2$*$CH_3$), 1.05 (dd, *J* = 6.9, 4.1 Hz, 6H, CHCH*(CH$_3$)$_2$*), 0.90 (t, *J* = 6.9 Hz, 3H, NCH$_2$CH$_2$(CH_2)$_2$*CH*$_3$). LRMS (CI) m/z calcd. for $C_{19}H_{28}N_3O_3$ $[M+H]^+$: 346.2; found: 346.2.

Methyl (*R*)-3,3-dimethyl-2-(1-pentyl-1*H*-indazole-3-carboxamido)butanoate (23j). Yield: 64%. Mp: 134-135 ºC. ^{1}H NMR (300 MHz, $CDCl_3$) δ (ppm): 8.34 (dt, *J* = 8.2, 1.0 Hz, 1H, Ar-H), 7.55 (d, *J* = 9.7 Hz, 1H, NH), 7.40 (m, 2H, Ar-H), 7.26 (m, 1H, Ar-H), 4.73 (d, *J* = 9.7 Hz, 1H, *CH*C(CH_3)$_3$), 4.39 (t, *J* = 7.2 Hz, 2H, N*CH*$_2$CH$_2$(CH_2)$_2$$CH_3$), 3.76 (s, 3H, OCH_3), 1.96 (quin, *J* = 7.4 Hz, 2H, NCH$_2$*CH*$_2$(CH_2)$_2$$CH_3$), 1.35 (m, 4H, NCH$_2CH_2$*(CH$_2$)$_2$*$CH_3$), 1.09 (s, 9H, C($CH_3$)$_3$), 0.90

USC UNIVERSIDADE DE SANTIAGO DE COMPOSTELA

(t, *J* = 6.8 Hz, 3H, $NCH_2CH_2(CH_2)_2CH_3$). LRMS (CI) m/z calcd. for $C_{20}H_{30}N_3O_3$ $[M+H]^+$: 360.2; found: 360.2.

Methyl (*R*)-(1-(5-fluoropentyl)-1*H*-indazole-3-carbonyl)valinate (23k). Yield: 72%. Mp: 126-127 ºC. ^{1}H NMR (300 MHz, $CDCl_3$) δ (ppm): 8.35 (d, *J* = 8.2 Hz, 1H, Ar-H), 7.43 (m, 3H, Ar-H, NH), 7.27 (m, 1H, Ar-H), 4.80 (dd, *J* = 9.1, 5.2 Hz, 1H, $CHCH(CH_3)_2$), 4.51 (t, *J* = 6.0 Hz, 1H, $NCH_2CH_2CH_2CH_2CH_2F$), 4.42 (t, *J* = 7.1 Hz, 2H, $NCH_2CH_2CH_2CH_2CH_2F$), 4.35 (t, *J* = 5.9 Hz, 1H, $NCH_2CH_2CH_2CH_2CH_2F$), 3.78 (s, 3H, OCH_3), 2.31 (m, 1H, $CHCH(CH_3)_2$), 2.02 (quin, *J* = 7.3 Hz, 2H, $NCH_2CH_2CH_2CH_2CH_2F$), 1.85–1.64 (m, 2H, $NCH_2CH_2CH_2CH_2CH_2F$), 1.49 (m, 2H, $NCH_2CH_2CH_2CH_2CH_2F$), 1.05 (dd, *J* = 6.9, 4.4 Hz, 6H, $CHCH(CH_3)_2$). LRMS (CI) m/z calcd. for $C_{19}H_{27}FN_3O_3$ $[M+H]^+$: 364.2; found: 364.2.

Methyl (*R*)-2-(1-(5-fluoropentyl)-1*H*-indazole-3-carboxamido)-3,3-dimethyl-butanoate (23l). Yield: 61%. Mp: 132-133 ºC. ^{1}H NMR (300 MHz, $CDCl_3$) δ (ppm): 8.35 (dt, *J* = 8.2, 1.0 Hz, 1H, Ar-H), 7.54 (d, *J* = 9.7 Hz, 1H, NH), 7.40 (m, 2H, Ar-H), 7.26 (m, 1H, Ar-H), 4.74 (d, *J* = 9.7 Hz, 1H, $CHC(CH_3)_3$), 4.51 (t, *J* = 6.0 Hz, 1H, $NCH_2CH_2CH_2CH_2CH_2F$), 4.42 (t, *J* = 7.1 Hz, 2H, $NCH_2CH_2CH_2CH_2CH_2F$), 4.36 (t, *J* = 6.0 Hz, 1H, $NCH_2CH_2CH_2CH_2CH_2F$), 3.76 (s, 3H, OCH_3), 2.02 (quin, *J* = 7.3 Hz, 2H, $NCH_2CH_2CH_2CH_2CH_2F$), 1.85–1.63 (m, 2H, $NCH_2CH_2CH_2CH_2CH_2F$), 1.49 (m, 2H, $NCH_2CH_2CH_2CH_2CH_2F$), 1.10 (s, 9H, $C(CH_3)_3$). ^{13}C NMR (75 MHz, $CDCl_3$) δ (ppm): 172.3, 162.4, 141.0, 136.9, 126.8, 123.0, 122.9, 122.7, 109.2, 83.8 (d, $J_{C\text{-}F}$ = 164.9 Hz), 59.6, 51.9, 49.3, 35.1, 30.0 (d, $J_{C\text{-}F}$ = 19.9 Hz), 29.4, 26.8, 22.8 (d, $J_{C\text{-}F}$ = 5.3 Hz). LRMS (CI) m/z calcd for $C_{20}H_{29}FN_3O_3$ $[M+H]^+$: 378.2; found: 378.2.

Methyl (*R*)-(1-(cyclohexylmethyl)-1*H*-indazole-3-carbonyl)valinate (23m). Yield: 62%. Mp: 125-126 ºC. ^{1}H NMR (500 MHz, $CDCl_3$) δ (ppm): 8.35 (d, *J* = 8.2 Hz, 1H, Ar-H), 7.49 (d, *J* = 9.1 Hz, 1H, NH), 7.41 (m, 2H, Ar-H), 7.26 (ddd, *J* = 8.0, 6.1, 1.8 Hz, 1H, Ar-H), 4.81 (dd, *J* = 9.0, 5.3 Hz, 1H, $CHCH(CH_3)_2$), 4.23 (d, *J* = 7.2 Hz, 2H, CH_2-Cy), 3.79 (s, 3H, OCH_3), 2.32 (quind, *J* = 6.9, 5.3 Hz, 1H, $CHCH(CH_3)_2$), 2.04 (m, 1H, *CH*-Cy), 1.76–1.57 (m, 5H, Cy), 1.28–1.12 (m, 3H, Cy), 1.11–0.99 (m, 8H, Cy, $CHCH(CH_3)_2$). ^{13}C NMR (75 MHz, $CDCl_3$) δ (ppm): 172.8, 162.7, 141.5, 136.8, 126.7,

UNIVERSIDADE DE SANTIAGO DE COMPOSTELA

122.9, 122.8, 122.6, 109.6, 56.9, 55.8, 52.2, 38.9, 31.8, 31.1, 26.4, 25.8, 19.3, 18.3. LRMS (CI) m/z calcd for $C_{21}H_{30}N_3O_3$ $[M+H]^+$: 372.2; found: 372.2.

Methyl (*R*)-2-(1-(cyclohexylmethyl)-1*H*-indazole-3-carboxamido)-3,3-dimethylbutanoate (23n). Yield: 69%. Mp: 133-134 ºC. ^{1}H NMR (300 MHz, $CDCl_3$) δ (ppm): 8.34 (dd, *J* = 8.2, 0.9 Hz, 1H, Ar-H), 7.55 (d, *J* = 9.7 Hz, 1H, NH), 7.39 (m, 2H, Ar-H), 7.25 (m, 1H, Ar-H), 4.74 (d, *J* = 9.7 Hz, 1H, *CH*C$(CH_3)_3$), 4.22 (d, *J* = 7.2 Hz, 2H, *CH*$_2$-Cy), 3.76 (s, 3H, OCH_3), 2.03 (m, 1H, *CH*-Cy), 1.79–1.53 (m, 5H,Cy), 1.32–0.96 (m, 14H, Cy, C$(CH_3)_3$). LRMS (CI) m/z calcd. for $C_{22}H_{32}N_3O3$ $[M+H]^+$: 386.2; found: 386.2.

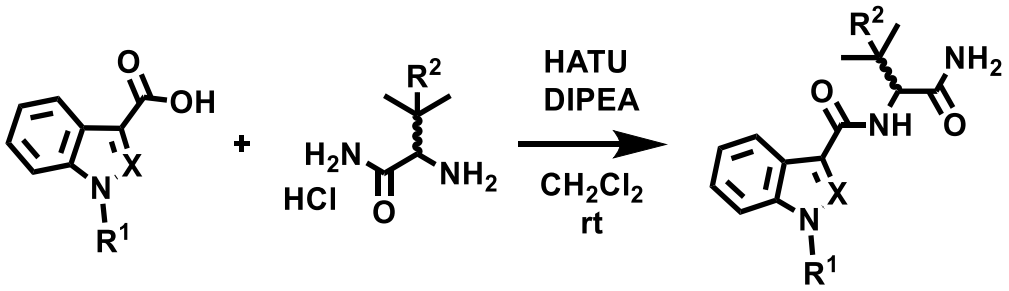
Methyl (*R*)-(1-(4-fluorobenzyl)-1*H*-indazole-3-carbonyl)valinate (23o). Yield: 69%. Mp: 141-142 ºC. ^{1}H NMR (300 MHz, $CDCl_3$) δ (ppm): 8.37 (dt, *J* = 8.1, 1.1 Hz, 1H, Ar-H), 7.51 (d, *J* = 9.0 Hz, 1H, NH), 7.41–7.16 (m, 5H, Ar-H), 7.01 (m, 2H, Ar-H), 5.60 (s, 2H, C*H*$_2$-Ph), 4.81 (dd, *J* = 9.0, 5.2 Hz, 1H, *CH*CH$(CH_3)_2$), 3.79 (s, 3H, OCH_3), 2.33 (m, 1H, CHC*H*$(CH_3)_2$), 1.06 (dd, *J* = 6.9, 4.5 Hz, 6H, CHCH(C*H*$_3)_2$). ^{13}C NMR (75 MHz, $CDCl_3$) δ (ppm): 172.7, 162.6 (d, $J_{C\text{-}F}$ = 247.0 Hz), 162.5, 140.9, 137.5, 131.9 (d, $J_{C\text{-}F}$ = 3.2 Hz), 129.1 (d, $J_{C\text{-}F}$ = 8.2 Hz), 127.2, 123.5, 123.1, 123.0, 115.9 (d, $J_{C\text{-}F}$ = 21.7 Hz), 109.6, 56.9, 53.0, 52.3, 31.7, 19.2, 18.2. LRMS (CI) m/z calcd for $C_{21}H_{23}FN_3O_3$ $[M+H]^+$: 384.2; found: 384.2.

Methyl (*R*)-2-(1-(4-fluorobenzyl)-1*H*-indazole-3-carboxamido)-3,3-dimethylbutanoate (23p). Yield: 89%. Mp: 136-137 ºC. ^{1}H NMR (300 MHz, $CDCl_3$) δ (ppm): 8.36 (dd, *J* = 8.2, 1.3 Hz, 1H, Ar-H), 7.56 (d, *J* = 9.7 Hz, 1H, NH), 7.39–7.13 (m, 5H, Ar-H), 6.99 (m, 2H, Ar-H), 5.58 (s, 2H, C*H*$_2$-Ph), 4.74 (d, *J* = 9.7 Hz, 1H, *CH*C$(CH_3)_3$), 3.76 (s, 3H, OCH_3), 1.09 (s, 9H, C$(CH_3)_3$). LRMS (CI) m/z calcd. for $C_{22}H_{25}FN_3O_3$ $[M+H]^+$: 398.2; found: 398.2.

USC UNIVERSIDADE DE SANTIAGO DE COMPOSTELA

4.5.5 General pathways for the synthesis of *N*-(1-amino-3-methyl-1-oxobutan-2yl)-1*H*-indole (indazole)-3-carboxamide polysubstituted (24a-p and 25a-p)

A mixture of the 1-alkyl-1H-indole (or indazole)-3-carboxylic acid (1 equiv.), DIPEA (4 equiv.) and HATU (1,5 equiv.) in CH_2Cl_2 (2 mL) and stirred with orbital stirring at room temperature for 30 minutes and then the corresponding amino acid amide (1,5 equiv.) was added. The reaction mixture was stirred overnight at room temperature. After completion of the reaction, water was added, and the mixture was extracted with CH_2Cl_2. The organic phase was dried over $MgSO_4$, filtered, and concentrated. The resulting product was purified by column chromatography on silica gel using MeOH/CH_2Cl_2.



26a-h
X= CH
X= N

31 a-d
R2 = H
R2 = CH_3

24a-p, 25a-p

R1 = Pentyl
R1 = 5-F-Pentyl
R1 = CH_2-Cy
R1 = 4-F-Bn

Scheme S4: General procedure for the synthesis of *N*-(1-amino-3-methyl-1-oxobutan-2yl)-1*H*-indole (indazole)-3-carboxamide polysubstituted (**24a-p**, **25a-p**).

4.5.5.1 Spectroscopic and analytical data of *N*-(1-amino-3-methyl-1-oxobutan-2yl)-1*H*-indole (indazole)-3-carboxamide polysubstituted

(*S*)-*N*-(1-Amino-3-methyl-1-oxobutan-2-yl)-1-pentyl-1*H*-indole-3-carboxamide (24a). Yield: 75%. Mp: 198-199 ºC. ^{1}H NMR (300 MHz, DMSO-d_6) δ (ppm): 8.24 (s, 1H, Ar-H), 8.10 (d, *J* = 7.7 Hz, 1H, Ar-H), 7.49 (m, 3H, Ar-H, NH, NH_2), 7.25–7.09 (m, 2H, ArH), 7.04 (br s, 1H, NH_2), 4.35 (dd, *J* = 8.8, 7.0 Hz, 1H, *CH*CH$(CH_3)_2$), 4.20 (m, 2H, N*CH*$_2$CH$_2$$(CH_2)_2CH_3$), 2.09 (m, 1H, CHC*H*$(CH_3)_2$), 1.81

(quin, *J* = 7.1 Hz, 2H, $NCH_2CH_2(CH_2)_2CH_3$), 1.38–1.19 (m, 4H, $NCH_2CH_2(CH_2)_2CH_3$), 0.94 (dd, *J* = 6.8, 2.5 Hz, 6H, $CHCH(CH_3)_2$), 0.85 (t, *J* = 6.9 Hz, 3H, $NCH_2CH_2(CH_2)_2CH_3$). ^{13}C NMR (75 MHz, $CDCl_3$) δ (ppm): 174.0, 165.4, 136.8, 131.7, 125.6, 122.7, 121.8, 120.4, 110.5, 110.4, 58.0, 47.1, 31.1, 29.8, 29.2, 22.4, 19.6, 18.5, 14.0. LRMS (CI) m/z calcd. for $C_{19}H_{28}N_3O_2$ $[M+H]^+$: 330.2; found: 330.2.

(*S*)-*N*-(1-Amino-3,3-dimethyl-1-oxobutan-2-yl)-1-pentyl-1*H*-indole-3-carboxamide (24b). Yield: 67%. Mp: 124-125 ºC. ^1H NMR (300 MHz,$CDCl_3$) δ (ppm): 8.02 (m, 1H, Ar-H), 7.72 (s, 1H, Ar-H), 7.37 (m, 1H, Ar-H), 7.27 (m, 2H, Ar-H), 6.81 (br s, 1H, NH_2), 6.77 (d, *J* = 9.3 Hz, 1H, NH), 5.81 (br s, 1H, NH_2), 4.77 (d, *J* = 9.2 Hz, 1H, $CHC(CH_3)_3$), 4.11 (t, *J* = 7.2 Hz, 2H, $NCH_2CH_2(CH_2)_2CH_3$), 1.85 (quin, *J* = 7.5 Hz, 2H, $NCH_2CH_2(CH_2)_2CH_3$), 1.40–1.25 (m, 4H, $NCH_2CH_2(CH_2)_2CH_3$), 1.16 (s, 9H, $C(CH_3)_3$), 0.89 (t, *J* = 6.8 Hz, 3H, NCH2-CH2$(CH_2)_2CH_3$). LRMS (CI) m/z calcd. for $C_{20}H_{30}N_3O2$ $[M+H]^+$: 344.2; found: 344.2.

(*S*)-*N*-(1-Amino-3-methyl-1-oxobutan-2-yl)-1-(5-fluoropentyl)-1*H*-indole-3-carboxa-mide (24c). Yield: 63%. Mp: 199-200 ºC. ^1H NMR (300 MHz, DMSO-d_6) δ (ppm): 8.25 (s, 1H, Ar-H), 8.10 (dt, *J* = 7.8, 1.1 Hz, 1H, ArH), 7.54 (d, *J* = 7.7 Hz, 1H, NH), 7.45 (m, 2H, Ar-H, NH), 7.25–7.09 (m, 2H, ArH), 7.04 (br s, 1H, NH_2), 4.49 (t, *J* = 6.0 Hz, 1H, $NCH_2CH_2CH_2CH_2CH_2F$), 4.34 (m, 2H, $CHCH(CH_3)_2$, $NCH_2CH_2CH_2CH_2CH_2F$), 4.22 (t, *J* = 7.1 Hz, 2H, $NCH_2CH_2CH_2CH_2CH_2F$), 2.09 (m, 1H, $CHCH(CH_3)_2$), 1.85 (quin, *J* = 7.2 Hz, 2H, $NCH_2CH_2CH_2CH_2CH_2F$), 1.78–1.56 (m, 2H, $NCH_2CH_2CH_2CH_2CH_2F$), 1.37 (m, 2H, $NCH_2CH_2CH_2CH_2CH_2F$), 0.94 (dd, *J* = 6.8, 2.5 Hz, 6H, $CHCH(CH_3)_2$). LRMS (CI) m/z calcd. for $C_{19}H_{27}FN_3O_2$ $[M+H]^+$: 348.2; found: 348.2.

(*S*)-*N*-(1-Amino-3,3-dimethyl-1-oxobutan-2-yl)-1-(5-fluoropentyl)-1*H*-indole-3-car-boxamide (24d). Yield: 76%. Mp: 132-133 ºC. ^1H NMR (300 MHz, $CDCl_3$) δ (ppm): 8.01 (m, 1H, Ar-H), 7.72 (s, 1H, Ar-H), 7.37 (m, 1H, Ar-H), 7.32–7.23 (m, 2H, Ar-H), 6.72 (d, *J* = 9.1 Hz, 1H, NH), 6.34 (br s, 1H, NH_2), 5.61 (br s, 1H, NH_2), 4.67 (d, *J* = 9.2 Hz, 1H, $CHC(CH_3)_3$), 4.50 (t, *J* = 5.9 Hz, 1H, $NCH_2CH_2CH_2CH_2CH_2F$), 4.34 (t, *J* = 5.9 Hz, 1H, $NCH_2CH_2CH_2CH_2CH_2F$), 4.15 (t, *J* = 7.1 Hz, 2H, $NCH_2CH_2CH_2CH_2CH_2F$), 1.91 (quin, *J* = 7.3 Hz, 2H, $NCH_2CH_2CH_2CH_2CH_2F$), 1.83–

1.60 (m, 2H, $NCH_2CH_2CH_2\mathit{CH_2}CH_2F$), 1.45 (m, 2H, $NCH_2CH_2\mathit{CH_2}CH_2CH_2F$), 1.15 (s, 9H, $C(CH_3)_3$). ^{13}C NMR (75 MHz, $CDCl_3$) δ (ppm): 173.5, 165.2, 136.7, 131.6, 125.7, 122.7, 121.8, 120.5, 110.7, 110.3, 83.8 (d, $J_{C\text{-}F}$ = 165.0 Hz), 59.9, 46.9, 34.9, 30.1 (d, $J_{C\text{-}F}$ = 19.9 Hz), 29.8, 27.0, 23.0 (d, $J_{C\text{-}F}$ = 4.9 Hz). LRMS (CI) m/z calcd. for $C_{20}H_{29}FN_3O_2$ $[M+H]^+$: 362.2; found: 362.2.

(*S*)-*N*-(1-Amino-3-methyl-1-oxobutan-2-yl)-1-(cyclohexylmethyl)-1*H*-indole-3-carbo-xamide (24e). Yield: 68%. Mp: 210-211 ºC. ^1H NMR (300 MHz, $CDCl_3$) δ (ppm): 8.00 (m, 1H, Ar-H), 7.68 (s, 1H, Ar-H), 7.37 (m, 1H, Ar-H), 7.31–7.22 (m, 2H, Ar-H), 6.57 (d, *J* = 8.5 Hz, 1H, NH), 6.25 (br s, 1H, NH_2), 5.50 (br s, 1H, NH_2), 4.61 (dd, *J* = 8.5, 6.6 Hz 1H, $\mathit{CH}CH(CH_3)_2$), 3.94 (d, *J* = 7.2 Hz, 2H, $C\mathit{H_2}$-Cy), 2.31 (m, 1H, $CHC\mathit{H}(CH_3)_2$), 1.86 (m, 1H, *CH*-Cy), 1.77–1.55 (m, 5H, Cy), 1.27–0.91 (m, 11 H, Cy, $CHCH\mathit{(CH_3)_2}$). LRMS (CI) m/z calcd. for $C_{21}H_{30}N_3O_2$ $[M+H]^+$: 356.2; found: 356.2.

(*S*)-*N*-(1-Amino-3,3-dimethyl-1-oxobutan-2-yl)-1-(cyclohexylmethyl)-1*H*-indole-3-carboxamide (24f). Yield: 83%. Mp: 210-211 ºC. ^1H NMR (300 MHz, $CDCl_3$) δ (ppm): 8.02 (m, 1H, Ar-H), 7.68 (s, 1H, Ar-H), 7.36 (m, 1H, Ar-H), 7.26 (m, 2H, Ar-H), 7.13 (br s, 1H, NH_2), 6.82 (d, *J* = 9.5 Hz, 1H, NH), 5.96 (br s, 1H, NH_2), 4.82 (d, *J* = 9.2 Hz, 1H, $\mathit{CH}C(CH_3)_3$), 3.91 (d, *J* = 7.1 Hz, 2H, $C\mathit{H_2}$-Cy), 1.83 (m, 1H, *CH*-Cy), 1.76–1.54 (m, 5H, Cy), 1.27–0.89 (m, 14 H, Cy, $C(CH_3)_3$). LRMS (CI) m/z calcd. for $C_{22}H_{32}N_3O_2$ $[M+H]^+$: 370.2; found: 370.2.

(*S*)-*N*-(1-Amino-3-methyl-1-oxobutan-2-yl)-1-(4-fluorobenzyl)-1*H*-indole-3-carboxa-mide (24g). Yield: 65%. Mp: 136-137 ºC. ^1H NMR (300 MHz, $CDCl_3$) δ (ppm): 8.03 (dt, *J* = 7.2, 1.2 Hz, 1H, Ar-H), 7.73 (s, 1H, Ar-H), 7.27 (m, 3H, Ar-H), 7.12 (m, 2H, Ar-H), 7.00 (t, *J* = 8.6 Hz, 2H, Ar-H), 6.59 (d, *J* = 8.5 Hz, 1H, NH), 6.14 (br s, 1H, NH_2), 5.49 (br s, 1H, NH_2), 5.28 (s, 2H, $C\mathit{H_2}$-Ph), 4.59 (dd, *J* = 8.6, 6.5 Hz, 1H, $\mathit{CH}CH(CH_3)_2$), 2.29 (m, 1H, $CHC\mathit{H}(CH_3)_2$), 1.09 (d, *J* = 6.8 Hz, 6H, $CHCH\mathit{(CH_3)_2}$). LRMS (CI) m/z calcd. for $C_{21}H_{23}FN_3O_2$ $[M+H]^+$: 368.2; found: 368.2.

(*S*)-*N*-(1-Amino-3,3-dimethyl-1-oxobutan-2-yl)-1-(4-fluorobenzyl)-1*H*-indole-3-car-boxamide (24h). Yield: 61%. Mp: 150-151 ºC. ^1H NMR (300 MHz, $CDCl_3$) δ (ppm): 8.03 (m, 1H, Ar-H), 7.74 (s, 1H, Ar-H), 7.27 (m, 3H, Ar-H), 7.09 (m,

2H, Ar-H), 6.98 (m, 2H, Ar-H), 6.81 (d, J = 9.3 Hz, 1H, NH), 6.75 (br s, 1H, NH_2), 5.81 (br s, 1H, NH_2), 5.26 (s, 2H, CH_2-Ph), 4.75 (d, J = 9.1 Hz, 1H, CHC$(CH_3)_3$),1.14 (s, 9H, C$(CH_3)_3$). ^{13}C NMR (75 MHz, $CDCl_3$) δ (ppm): 173.6, 165.1, 162.6 (d, $J_{C\text{-}F}$ = 247.0 Hz), 136.8, 132.0 (d, $J_{C\text{-}F}$ = 3.2 Hz), 131.8, 128.8 (d, $J_{C\text{-}F}$ = 8.3 Hz), 125.9, 123.1, 122.1, 120.5, 116.0 (d, $J_{C\text{-}F}$ = 21.8 Hz), 111.4, 110.7, 60.0, 50.0, 34.9, 27.0. LRMS (CI) m/z calcd. for $C_{22}H_{25}FN_3O_2$ $[M+H]^+$: 382.2; found: 382.2.

(*R*)-*N*-(1-Amino-3-methyl-1-oxobutan-2-yl)-1-pentyl-1*H*-indole-3-carboxamide (24i). Yield: 78%. Mp: 211-212 ºC. ^{1}H NMR (300 MHz, $CDCl_3$) δ (ppm): 8.03 (m, 1H, Ar-H), 7.73 (s, 1H, Ar-H), 7.37 (m, 1H, Ar-H), 7.27 (m, 2H, Ar-H), 6.71 (d, J = 8.8 Hz, 1H, NH), 6.61 (br s, 1H, NH_2), 5.69 (br s, 1H, NH_2), 4.66 (dd, J = 8.6, 6.7 Hz, 1H, CHCH$(CH_3)_2$), 4.09 (t, J = 7.2 Hz, 2H, N$CH_2$$CH_2(CH_2)_2CH_3$), 2.29 (hept, J = 6.8 Hz, 1H, CH$CH(CH_3)_2$), 1.84 (quin, J = 7.3 Hz, 2H, $NCH_2CH_2(CH_2)_2CH_3$), 1.30 (m, 4H, $NCH_2CH_2(CH_2)_2CH_3$), 1.10 (d, J = 6.8 Hz, 6H, $CHCH(CH_3)_2$), 0.88 (t, J = 6.9 Hz, 3H, $NCH_2CH_2(CH_2)_2CH_3$). ^{13}C NMR (75 MHz, $CDCl_3$) δ (ppm): 174.1, 165.5, 136.8, 131.7, 125.7, 122.7, 121.8, 120.5, 110.4, 110.4, 58.0, 47.1, 31.2, 29.8, 29.2, 22.4, 19.6, 18.5, 14.0. LRMS (CI) m/z calcd. for $C_{19}H_{28}N_3O_2$ $[M+H]^+$: 330.2; found: 330.2.

(*R*)-*N*-(1-Amino-3,3-dimethyl-1-oxobutan-2-yl)-1-pentyl-1*H*-indole-3-carboxamide (24j). Yield: 77%. Mp: 139-140 ºC. ^{1}H NMR (300 MHz,$CDCl_3$) δ (ppm): 8.01 (m, 1H, Ar-H), 7.72 (s, 1H, Ar-H), 7.37 (m, 1H, Ar-H), 7.27 (m, 2H, Ar-H), 6.74 (d, J = 9.2 Hz, 1H, NH), 6.61 (br s, 1H, NH_2), 5.72 (br s, 1H, NH_2), 4.73 (d, J = 9.2 Hz, 1H, CHC$(CH_3)_3$), 4.11 (t, J = 7.2 Hz, 2H, N$CH_2$$CH_2(CH_2)_2CH_3$), 1.85 (quin, J = 7.3 Hz, 2H, $NCH_2CH_2(CH_2)_2CH_3$), 1.40–1.25 (m, 4H, $NCH_2CH_2(CH_2)_2CH_3$), 1.15 (s, 9H, C$(CH_3)_3$), 0.89 (t, J = 6.7 Hz, 3H, NCH_2CH_2-$(CH_2)_2CH_3$). LRMS (CI) m/z calcd. for $C_{20}H_{30}N_3O_2$ $[M+H]^+$: 344.2; found: 344.2.

(*R*)-*N*-(1-Amino-3-methyl-1-oxobutan-2-yl)-1-(5-fluoropentyl)-1*H*-indole-3-carboxa-mide (24k). Yield: 67%. Mp: 200-201 ºC. ^{1}H NMR (300 MHz, $CDCl_3$) δ (ppm): 8.03 (m, 1H, Ar-H), 7.73 (s, 1H, Ar-H), 7.36 (m, 1H, Ar-H), 7.32–7.22 (m, 2H, Ar-H), 6.69 (d, J = 8.5 Hz, 1H, NH), 6.50 (br s, 1H, NH_2), 5.66 (br s, 1H, NH_2), 4.64 (dd, J = 8.5, 6.7 Hz, 1H, CHCH$(CH_3)_2$), 4.48 (t, J = 5.9 Hz, 1H,

$NCH_2CH_2CH_2CH_2CH_2F$), 4.33 (t, *J* = 5.9 Hz, 1H, $NCH_2CH_2CH_2CH_2CH_2F$), 4.12 (t, *J* = 7.1 Hz, 2H, $NCH_2CH_2CH_2CH_2CH_2F$), 2.29 (m, 1H, $CHCH(CH_3)_2$), 1.89 (quin, *J* = 7.3 Hz, 2H, $NCH_2CH_2CH_2CH_2CH_2F$), 1.81–1.59 (m, 2H, $NCH_2CH_2CH_2CH_2CH_2F$), 1.43 (m, 2H, $NCH_2CH_2CH_2CH_2CH_2F$), 1.09 (d, *J* = 6.7 Hz, 6H, $CHCH(CH_3)_2$). ^{13}C NMR (75 MHz, $CDCl_3$) δ (ppm): 174.2, 165.4, 136.7, 131.5, 125.8, 122.8, 121.9, 120.6, 110.6, 110.3, 83.8 (d, $J_{C\text{-}F}$ = 165.0 Hz), 58.1, 46.9, 31.2, 30.1 (d, $J_{C\text{-}F}$ = 19.8 Hz), 29.8, 23.0 (d, $J_{C\text{-}F}$ = 5.0 Hz), 19.6, 18.5. LRMS (CI) m/z calcd. for $C_{19}H_{27}FN_3O_2$ $[M+H]^+$: 348.2; found: 348.2.

(*R*)-*N*-(1-Amino-3,3-dimethyl-1-oxobutan-2-yl)-1-(5-fluoropentyl)-1*H*-indole-3-car-boxamide (24l). ^{1}H NMR (300 MHz, $CDCl_3$) δ (ppm): 8.01 (m, 1H, Ar-H), 7.72 (s, 1H, Ar-H), 7.37 (m, 1H, Ar-H), 7.32–7.23 (m, 2H, Ar-H), 6.74 (d, *J* = 9.2 Hz, 1H, NH), 6.55 (br s, 1H, NH_2), 5.70 (br s, 1H, NH_2), 4.72 (d, *J* = 9.2 Hz, 1H, $CHC(CH_3)_3$), 4.49 (t, *J* = 5.9 Hz, 1H, $NCH_2CH_2CH_2CH_2CH_2F$), 4.33 (t, *J* = 5.9 Hz, 1H, $NCH_2CH_2CH_2CH_2CH_2F$), 4.14 (t, *J* = 7.1 Hz, 2H, $NCH_2CH_2CH_2CH_2CH_2F$), 1.91 (quin, *J* = 7.3 Hz, 2H, $NCH_2CH_2CH_2CH_2CH_2F$), 1.82–1.61 (m, 2H, $NCH_2CH_2CH_2CH_2CH_2F$), 1.45 (m, 2H, $NCH_2CH_2CH_2CH_2CH_2F$), 1.15 (s, 9H, $C(CH_3)_3$). LRMS (CI) m/z calcd. for $C_{20}H_{29}FN_3O_2$ $[M+H]^+$: 362.2; found: 362.2.

(*R*)-*N*-(1-Amino-3-methyl-1-oxobutan-2-yl)-1-(cyclohexylmethyl)-1*H*-indole-3-car-boxamide (24m). Yield: 65%. Mp: 209-210 ºC. ^{1}H NMR (300 MHz, $CDCl_3$) δ (ppm): 8.03 (m, 1H, Ar-H), 7.71 (s, 1H, Ar-H), 7.36 (m, 1H, Ar-H), 7.31–7.21 (m, 2H, Ar-H), 6.75 (m, 2H, NH + NH_2), 5.76 (br s, 1H, NH_2), 4.66 (dd, *J* = 8.5, 6.8 Hz 1H, $CHCH(CH_3)_2$), 3.91 (d, *J* = 7.2 Hz, 2H, CH_2-Cy), 2.30 (m, 1H, $CHCH(CH_3)_2$), 1.83 (m, 1H, *CH*-Cy), 1.76–1.54 (m, 5H, Cy, 1.25–0.90 (m, 11 H, Cy, $CHCH(CH_3)_2$). ^{13}C NMR (75 MHz, $CDCl_3$) δ (ppm): 174.2, 165.5, 137.1, 132.3, 125.6, 122.6, 121.7, 120.4, 110.7, 110.2, 58.1, 53.5, 38.7, 31.2, 31.1, 31.1, 26.3, 25.8, 19.6, 18.6. LRMS (CI) m/z calcd. for $C_{21}H_{30}N_3O_2$ $[M+H]^+$: 356.2; found: 356.2.

(*R*)-*N*-(1-Amino-3,3-dimethyl-1-oxobutan-2-yl)-1-(cyclohexylmethyl)-1*H*-indole-3-carboxamide (24n). Yield: 67%. Mp: 200-201 ºC. ^{1}H NMR (300 MHz, $CDCl_3$) δ (ppm): 8.01 (m, 1H, Ar-H), 7.68 (s, 1H, Ar-H), 7.37 (m, 1H, Ar-H), 7.26 (m, 2H, Ar-H), 6.70 (d, *J* = 9.1 Hz, 1H, NH), 6.19 (br s, 1H, NH_2), 5.57 (br s, 1H, NH_2),

4.65 (d, *J* = 9.1 Hz 1H, *CH*C(CH_3)$_3$), 3.95 (d, *J* = 7.1 Hz, 2H, C*H*$_2$-Cy), 1.86 (m, 1H, *CH*-Cy), 1.76 – 1.55 (m, 5H, Cy)1.29-0.90 (m, 14 H, Cy, C(CH_3)$_3$). LRMS (CI) m/z calcd. For $C_{22}H_{32}N_3O_2$ $[M+H]^+$: 370.2; found: 370.2.

(*R*)-*N*-(1-Amino-3-methyl-1-oxobutan-2-yl)-1-(4-fluorobenzyl)-1*H*-indole-3-carboxamide (24o). Yield: 59%. Mp: 188-189 ºC. ^{1}H NMR (300 MHz, $CDCl_3$) δ (ppm): 8.03 (d, *J* = 7.4 Hz, 1H, Ar-H), 7.73 (s, 1H, Ar-H), 7.27 (m, 3H, Ar-H), 7.12 (m, 2H, Ar-H), 7.01 (t, *J* = 8.5 Hz, 2H, Ar-H), 6.57 (d, *J* = 8.5 Hz, 1H, NH), 6.07 (br s, 1H, NH_2), 5.47 (br s, 1H, NH_2), 5.30 (s, 2H, C*H*$_2$Ph), 4.58 (dd, *J* = 8.5, 6.5 Hz, 1H, *CH*CH(C*H*$_3$)$_2$), 2.29 (m, 1H, CHC*H*(CH_3)$_2$), 1.09 (d, *J* = 6.8 Hz, 6H, CHCH*(CH*$_3$*)*$_2$). LRMS (CI) m/z calcd. for $C_{21}H_{23}FN_3O_2$ $[M+H]^+$: 368.2; found: 368.2.

(*R*)-*N*-(1-Amino-3,3-dimethyl-1-oxobutan-2-yl)-1-(4-fluorobenzyl)-1*H*-indole-3-carboxamide (24p). Yield: 71%. Mp: 175-176 ºC. ^{1}H NMR (300 MHz, $CDCl_3$) δ (ppm): 8.03 (m, 1H, Ar-H), 7.74 (s, 1H, Ar-H), 7.27 (m, 3H, Ar-H), 7.09 (m, 2H, Ar-H), 6.98 (m, 2H, Ar-H), 6.75 (d, *J* = 9.2 Hz, 1H, NH), 6.37 (br s, 1H, NH_2), 5.65 (br s, 1H, NH_2), 5.28 (s, 2H, C*H*$_2$-Ph), 4.68 (dd, *J* = 9.2, 1.4 Hz, 1H, *CH*C(CH_3)$_3$),1.14 (s, 9H, C(CH_3)$_3$). LRMS (CI) m/z calcd. for $C_{22}H_{25}FN_3O_2$ $[M+H]^+$: 382.2; found: 382.2.

(*S*)-*N*-(1-amino-3-methyl-1-oxobutan-2-yl)-1-pentyl-1*H*-indazole-3-carboxamide (**25a**). Yield: 73%. Mp: 125-126 ºC. ^{1}H NMR (300 MHz, $CDCl_3$) δ (ppm): 8.30 (dt, *J* = 8.2, 1.1 Hz, 1H, Ar-H), 7.53 (d, *J* = 9.0 Hz, 1H, NH), 7.40 (m, 2H, Ar-H), 7.26 (m, 1H, Ar-H), 6.64 (br s, 1H, NH_2), 5.87 (br s, 1H, NH_2), 4.62 (dd, *J* = 9.0, 6.7 Hz, 1H, *CH*CH(C*H*$_3$)$_2$), 4.37 (t, *J* = 7.2 Hz, 2H, N*CH*$_2$CH$_2$(CH$_2$)$_2$CH$_3$), 2.34 (m, 1H, CHC*H*(CH_3)$_2$), 1.94 (quin, *J* = 7.3 Hz, 2H, NCH$_2$*CH*$_2$(CH$_2$)$_2$CH$_3$), 1.45–1.23 (m, 4H, NCH$_2$CH$_2$*(CH*$_2$*)*$_2$CH$_3$), 1.09 (dd, *J* = 6.8, 3.4 Hz, 6H, CHCH*(CH*$_3$*)*$_2$), 0.89 (t, *J* = 6.8 Hz, 3H, NCH$_2$CH$_2$(CH$_2$)$_2$*CH*$_3$). ^{13}C NMR (75 MHz, $CDCl_3$) δ (ppm): 173.9, 163.1, 141.0, 136.5, 126.8, 123.0, 122.8, 122.6, 109.5, 57.9, 49.6, 30.8, 29.5, 29.0, 22.3, 19.6, 18.3, 14.0. LRMS (CI) m/z calcd. for $C_{18}H_{27}N_4O_2$ $[M+H]^+$: 331.2; found: 331.2.

(*S*)-*N*-(1-amino-3,3-dimethyl-1-oxobutan-2-yl)-1-pentyl-1*H*-indazole-3-carboxamide (25b). Yield: 67%. Mp: 140-141 ºC. ^{1}H NMR (300 MHz, $CDCl_3$) δ (ppm): 8.28 (dt, *J* = 8.2, 1.1 Hz, 1H, Ar-H), 7.73 (d, *J* = 9.5 Hz, 1H, NH), 7.41 (m, 2H, Ar-H), 7.26 (m, 1H, Ar-H), 6.79 (br s, 1H, NH_2), 5.86 (br s, 1H, NH_2), 4.73 (d, *J* = 9.6 Hz, 1H,

USC UNIVERSIDADE DE SANTIAGO DE COMPOSTELA

*CH*C(CH$_3$)$_3$), 4.39 (t, *J* = 7.2 Hz, 2H, N*CH$_2$*CH$_2$(CH$_2$)$_2$CH$_3$), 1.95 (quin, *J* = 7.3 Hz, 2H, NCH$_2$*CH$_2$*(CH$_2$)$_2$CH$_3$), 1.45–1.27 (m, 4H, NCH$_2$CH$_2$*(CH$_2$)$_2$*CH$_3$), 1.17 (s, 9H, C(CH$_3$)$_3$), 0.90 (t, *J* = 6.8 Hz, 3H, NCH$_2$CH$_2$-(CH$_2$)$_2$*CH$_3$*). LRMS (CI) m/z calcd. for $C_{19}H_{29}N_4O_2$ $[M+H]^+$: 345.2; found: 345.2.

(*S*)-*N*-(1-amino-3-methyl-1-oxobutan-2-yl)-1-(5-fluoropentyl)-1*H*-indazole-3-carboxamide (25c). Yield: 59%. Mp: 126-127 ºC. ^{1}H NMR (300 MHz, CDCl$_3$) δ (ppm): 8.31 (dt, *J* = 8.1, 1.1 Hz, 1H, Ar-H), 7.53 (d, *J* = 9.0 Hz, 1H, NH), 7.41 (m, 2H, Ar-H), 7.27 (m, 1H, Ar-H), 6.61 (br s, 1H, NH$_2$), 5.85 (br s, 1H, NH$_2$), 4.61 (dd, *J* = 9.0, 6.7 Hz, 1H, *CH*CH(CH$_3$)$_2$), 4.51 (t, *J* = 5.9 Hz, 1H, NCH$_2$CH$_2$CH$_2$CH$_2$*CH$_2$*F), 4.41 (t, *J* = 7.1 Hz, 2H, N*CH2*CH2CH2-CH2CH2F), 4.35 (t, *J* = 5.9 Hz, 1H, NCH$_2$CH$_2$CH$_2$CH$_2$*CH$_2$*F), 2.35 (m, 1H, CHC*H*(CH$_3$)$_2$), 2.01 (quin, *J* = 7.3 Hz, 2H, NCH$_2$*CH$_2$*CH$_2$CH$_2$CH$_2$F), 1.83–1.64 (m, 2H, NCH2CH2CH2-*CH2*CH2F), 1.47 (m, 2H, NCH$_2$CH$_2$*CH$_2$*CH$_2$CH$_2$F), 1.09 (dd, *J* = 6.8, 3.5 Hz, 6H, CHCH*(CH$_3$)$_2$*). LRMS (CI) m/z calcd. for $C_{18}H_{26}FN_4O_2$ $[M+H]^+$: 349.2; found: 349.2.

(*S*)-*N*-(1-amino-3,3-dimethyl-1-oxobutan-2-yl)-1-(5-fluoropentyl)-1*H*-indazole-3-carboxamide (25d). Yield: 66%. Mp: 120-121 ºC. ^{1}H NMR (300 MHz, CDCl$_3$) δ (ppm): 8.29 (dt, *J* = 8.2, 1.0 Hz, 1H, Ar-H), 7.69 (d, *J* = 9.4 Hz, 1H, NH), 7.42 (m, 2H, Ar-H), 7.26 (m, 1H, Ar-H), 6.39 (br s, 1H, NH$_2$), 5.66 (br s, 1H, NH$_2$), 4.64 (d, *J* = 9.5 Hz, 1H, *CH*C(CH$_3$)$_3$), 4.51 (t, *J* = 6.0 Hz, 1H, NCH$_2$CH$_2$CH$_2$CH$_2$*CH$_2$*F), 4.41 (t, *J* = 7.1 Hz, 2H, N*CH$_2$*CH$_2$CH$_2$CH$_2$CH$_2$F), 4.35 (t, *J* = 5.9 Hz, 1H, NCH$_2$CH$_2$CH$_2$CH$_2$*CH$_2$*F), 2.01 (quin, *J* = 7.3 Hz, 2H, NCH2*CH2*CH2-CH2CH2F), 1.85–1.65 (m, 2H, NCH$_2$CH$_2$CH$_2$*CH$_2$*CH$_2$F), 1.47 (m, 2H, NCH2CH2*CH2*-CH2CH2F), 1.16 (s, 9H, C(CH$_3$)$_3$). LRMS (CI) m/z calcd. for $C_{19}H_{28}FN_4O_2$ $[M+H]^+$: 363.2; found: 363.2.

(*S*)-*N*-(1-amino-3-methyl-1-oxobutan-2-yl)-1-(cyclohexylmethyl)-1*H*-indazole-3-carboxamide (25e). Yield: 64%. Mp: 123-124 ºC. ^{1}H NMR (300 MHz, CDCl$_3$) δ (ppm): 8.30 (dt, *J* = 8.2, 1.0 Hz, 1H, Ar-H), 7.53 (d, *J* = 8.9 Hz, 1H, NH), 7.45-7.35 (m, 2H, Ar-H), 7.26 (m, 1H, Ar-H), 6.62 (br s, 1H, NH$_2$), 5.82 (br s, 1H, NH$_2$), 4.60 (dd, *J* = 8.9, 6.8 Hz, 1H, *CH*CH(CH$_3$)$_2$), 4.21 (d, *J* = 7.2 Hz, 2H, C*H$_2$*-Cy), 2.36 (m, 1H, CHC*H*(CH$_3$)$_2$), 2.02 (m, 1H, *CH*-Cy), 1.78–1.51 (m, 5H, Cy), 1.30–0.95 (m, 11H, Cy,

CHCH*(CH₃)₂*). ^{13}C NMR (75 MHz, $CDCl_3$) δ (ppm): 173.9, 163.1, 141.6, 136.6, 126.7, 122.8, 122.7, 122.6, 109.7, 58.0, 55.9, 38.8, 31.1, 31.0, 30.8, 26.3, 25.8, 25.7, 19.6, 18.4. LRMS (CI) m/z calcd. for $C_{20}H_{29}N_4O_2$ $[M+H]^+$: 357.2; found: 357.2.

(*S*)-*N*-(1-amino-3,3-dimethyl-1-oxobutan-2-yl)-1-(cyclohexylmethyl)-1*H*-indazole-3-carboxamide (25f). Yield: 71%. Mp: 115-116 ºC. ^{1}H NMR (300 MHz, $CDCl_3$) δ (ppm): 8.27 (dt, *J* = 8.1, 1.1 Hz, 1H, Ar-H), 7.72 (d, *J* = 9.5 Hz, 1H, NH), 7.45 – 7.35 (m, 2H, Ar-H), 7.25 (m, 1H, Ar-H), 6.73 (br s, 1H, NH_2), 5.80 (br s, 1H, NH_2), 4.71 (d, *J* = 9.5 Hz, 1H, *CH*C$(CH_3)_3$), 4.21 (d, *J* = 7.2 Hz, 2H, C*H₂*-Cy), 2.03 (m, 1H, *CH*-Cy), 1.78–1.51 (m, 5H, Cy), 1.31–0.95 (m, 14H, Cy, C$(CH_3)_3$). LRMS (CI) m/z calcd. for $C_{21}H_{31}N_4O_2$ $[M+H]^+$: 371.2; found: 371.2.

(*S*)-*N*-(1-amino-3-methyl-1-oxobutan-2-yl)-1-(4-fluorobenzyl)-1*H*-indazole-3-carboxamide (25g). Yield: 67%. Mp: 123-124 ºC. ^{1}H NMR (300 MHz, $CDCl_3$) δ (ppm): 8.33 (dt, *J* = 8.2, 1.1 Hz, 1H, Ar-H), 7.56 (d, *J* = 8.9 Hz, 1H, NH), 7.41–7.14 (m, 5H, Ar-H), 7.00 (m, 2H, Ar-H), 6.49 (br s, 1H, NH_2), 5.77 (br s, 1H, NH_2), 5.57 (s, 2H, C*H₂*-Ph), 4.60 (dd, *J* = 8.9, 6.8 Hz, 1H, *CH*CH$(CH_3)_2$), 2.34 (m, 1H, CHC*H*$(CH_3)_2$), 1.09 (dd, *J* = 6.8, 3.3 Hz, 6H, CHCH*(CH₃)₂*). LRMS (CI) m/z calcd. for $C_{20}H_{22}FN_4O_2$ $[M+H]^+$: 369.2; found: 369.2.

(*S*)-*N*-(1-amino-3,3-dimethyl-1-oxobutan-2-yl)-1-(4-fluorobenzyl)-1*H*-indazole-3-carboxamide (25h). Yield: 60%. Mp: 132-133 ºC. ^{1}H NMR (300 MHz, $CDCl_3$) δ (ppm): 8.30 (dt, *J* = 8.2, 1.1 Hz, 1H, Ar-H), 7.73 (d, *J* = 9.5 Hz, 1H, NH), 7.41–7.16 (m, 5H, Ar-H), 7.00 (t, *J* = 8.6 Hz, 2H, Ar-H), 6.58 (br s, 1H, NH_2), 5.79 (br s, 1H, NH_2), 5.58 (s, 2H, C*H₂*-Ph), 4.69 (d, *J* = 9.5 Hz, 1H, *CH*C$(CH_3)_3$), 1.17 (s, 9H, C$(CH_3)_3$). ^{13}C NMR (75 MHz, $CDCl_3$) δ (ppm): 172.9, 162.7, 162.6 (d, $J_{C\text{-}F}$ = 246.8 Hz), 140.9, 137.4, 131.8 (d, $J_{C\text{-}F}$ = 3.2 Hz), 129.2 (d, $J_{C\text{-}F}$ = 8.3 Hz), 127.2, 123.4, 123.0, 122.8, 116.0 (d, $J_{C\text{-}F}$ = 21.5 Hz), 109.7, 59.9, 53.1, 34.8, 26.9. LRMS (CI) m/z calcd. for $C_{21}H_{24}FN_4O_2$ $[M+H]^+$: 383.2; found: 383.2.

(*R*)-*N*-(1-amino-3-methyl-1-oxobutan-2-yl)-1-pentyl-1*H*-indazole-3-carboxamide (25i). Yield: 71%. Mp: 145-146 ºC. ^{1}H NMR (300 MHz, $CDCl_3$) δ (ppm): 8.30 (dt, *J* = 8.2, 1.1 Hz, 1H, Ar-H), 7.51 (d, *J* = 8.9 Hz, 1H, NH), 7.41 (m, 2H, Ar-H), 7.26

(m, 1H, Ar-H), 6.50 (br s, 1H, NH_2), 5.75 (br s, 1H, NH_2), 4.58 (dd, *J* = 9.0, 6.7 Hz, 1H, *CH*CH(CH_3)$_2$), 4.38 (t, *J* = 7.2 Hz, 2H, N*CH*$_2$$CH_2$($CH_2$)$_2$$CH_3$), 2.35 (m, 1H, CHC*H*($CH_3$)$_2$), 1.94 (quin, *J* = 7.3 Hz, 2H, NCH$_2$*CH*$_2$(CH_2)$_2$$CH_3$), 1.45–1.23 (m, 4H, NCH$_2CH_2$*(CH*$_2$*)*$_2$$CH_3$), 1.08 (dd, *J* = 6.8, 3.0 Hz, 6H, CHCH*(CH*$_3$*)*$_2$), 0.89 (t, *J* = 6.8 Hz, 3H, NCH$_2$CH$_2$(CH_2)$_2$*CH*$_3$). LRMS (CI) m/z calcd. for $C_{18}H_{27}N_4O_2$ $[M+H]^+$: 331.2; found: 331.2.

(*R*)-*N*-(1-amino-3,3-dimethyl-1-oxobutan-2-yl)-1-pentyl-1*H*-indazole-3-carboxamide (25j). Yield: 79%. Mp: 134-135 ºC. ^{1}H NMR (300 MHz, $CDCl_3$) δ (ppm): 8.30 (dt, *J* = 8.2, 1.1 Hz, 1H, Ar-H), 7.68 (d, *J* = 9.4 Hz, 1H, NH), 7.41 (m, 2H, Ar-H), 7.26 (m, 1H, Ar-H), 6.25 (br s, 1H, NH_2), 5.57 (br s, 1H, NH_2), 4.60 (d, *J* = 9.5 Hz, 1H, *CH*C(CH_3)$_3$), 4.39 (t, *J* = 7.2 Hz, 2H, N*CH*$_2$$CH_2$($CH_2$)$_2$$CH_3$), 1.95 (quin, *J* =7.3 Hz, 2H, NCH$_2$*CH*$_2$(CH_2)$_2$$CH_3$), 1.45–1.27 (m, 4H, NCH$_2CH_2$*(CH*$_2$*)*$_2$$CH_3$), 1.16 (s, 9H, C($CH_3$)$_3$), 0.90 (t, *J* = 6.9 Hz, 3H, NCH$_2$CH$_2$-(CH_2)$_2$*CH*$_3$). LRMS (CI) m/z calcd. for $C_{19}H_{29}N_4O_2$ $[M+H]^+$: 345.2; found: 345.2.

(*R*)-*N*-(1-amino-3-methyl-1-oxobutan-2-yl)-1-(5-fluoropentyl)-1*H*-indazole-3-carboxamide (25k). Yield: 61%. Mp: 125-126 ºC. ^{1}H NMR (300 MHz, $CDCl_3$) δ (ppm): 8.31 (dd, *J* = 8.2, 1.0 Hz, 1H, Ar-H), 7.52 (d, *J* = 8.9 Hz, 1H, NH), 7.41 (m, 2H, Ar-H), 7.27 (m, 1H, Ar-H), 6.51 (br s, 1H, NH_2), 5.76 (br s, 1H, NH_2), 4.59 (dd, *J* = 8.9, 6.7 Hz, 1H, *CH*CH(CH_3)$_2$), 4.51 (t, *J* = 5.9 Hz, 1H, NCH$_2$CH$_2$CH$_2$CH$_2$*CH*$_2$F), 4.41 (t, *J* = 7.1 Hz, 2H, N*CH*$_2$CH$_2$CH$_2$CH$_2$CH$_2$F), 4.35 (t, *J* = 5.9 Hz, 1H, NCH$_2$CH$_2$CH$_2$CH$_2$*CH*$_2$F), 2.35 (m, 1H, CHC*H*(CH_3)$_2$), 2.01 (quin, *J* = 7.2 Hz, 2H, NCH$_2$*CH*$_2$CH$_2$CH$_2$CH$_2$F), 1.84–1.64 (m, 2H, NCH$_2$CH$_2$CH$_2$*CH*$_2$CH$_2$F), 1.47 (m, 2H, NH$_2$CH$_2$C*H*$_2$CH$_2$CH$_2$F), 1.09 (dd, *J* = 6.8, 3.2 Hz, 6H, CHCH*(CH*$_3$*)*$_2$). ^{13}C NMR (75 MHz, $CDCl_3$) δ (ppm): 173.7, 163.1, 141.0, 136.7, 127.0, 123.0, 122.9, 122.8, 109.4, 83.8 (d, $J_{C\text{-}F}$ = 165.0 Hz), 58.0, 49.4, 30.7, 30.0 (d, $J_{C\text{-}F}$ = 19.8 Hz), 29.4, 22.8 (d, $J_{C\text{-}F}$ = 4.7 Hz), 19.6, 18.3. LRMS (CI) m/z calcd. for $C_{18}H_{26}FN_4O_2$ $[M+H]^+$: 349.2; found: 349.2.

(*R*)-*N*-(1-amino-3,3-dimethyl-1-oxobutan-2-yl)-1-(5-fluoropentyl)-1*H*-indazole-3-carboxamide (25l). Yield: 58%. Mp: 135-136 ºC. ^{1}H NMR (300 MHz, $CDCl_3$) δ (ppm): 8.30 (dt, *J* = 8.2, 1.0 Hz, 1H, Ar-H), 7.68 (d, *J* = 9.4 Hz, 1H, NH), 7.41 (m, 2H,

Ar-H), 7.26 (m, 1H, Ar-H), 6.28 (br s, 1H, NH_2), 5.60 (br s, 1H, NH_2), 4.62 (d, *J* = 9.5 Hz, 1H, $CHC(CH_3)_3$), 4.51 (t, *J* = 6.0 Hz, 1H, $NCH_2CH_2CH_2CH_2CH_2F$), 4.41 (t, *J* = 7.1 Hz, 2H, $NCH_2CH_2CH_2CH_2CH_2F$), 4.35 (t, *J* = 5.9 Hz, 1H, $NCH_2CH_2CH_2CH_2CH_2F$), 2.01 (quin, *J*= 7.3 Hz, 2H, $NCH_2CH_2CH_2CH_2CH_2F$), 1.85–1.65 (m, 2H, $NCH_2CH_2CH_2CH_2CH_2F$), 1.47 (m, 2H, $NCH_2CH_2CH_2CH_2CH_2F$), 1.16 (s, 9H, $C(CH_3)_3$). LRMS (CI) m/z calcd. for $C_{19}H_{28}FN_4O_2$ $[M+H]^+$: 363.2; found: 363.2.

(*R*)-*N*-(1-amino-3-methyl-1-oxobutan-2-yl)-1-(cyclohexylmethyl)-1*H*-indazole-3-carboxamide (25m). Yield: 68%. Mp: 123-124 ºC. ^{1}H NMR (300 MHz, $CDCl_3$) d (ppm): 8.30 (dt, *J* = 8.2, 1.0 Hz, 1H, Ar-H), 7.54 (d, *J* = 8.9 Hz, 1H, NH), 7.45–7.35 (m, 2H, Ar-H), 7.26 (m, 1H, Ar-H), 6.66 (br s, 1H, NH_2), 5.86 (br s, 1H, NH_2), 4.61 (dd, *J* = 9.0, 6.8 Hz, 1H, $CHCH(CH_3)_2$), 4.21 (d, *J* = 7.2 Hz, 2H, CH_2-Cy), 2.36 (m, 1H, $CHCH(CH_3)_2$), 2.02 (m, 1H, *CH*-Cy), 1.78–1.51 (m, 5H, Cy), 1.30–0.95 (m, 11H, Cy, $CHCH(CH_3)_2$). ^{13}C NMR (75 MHz, $CDCl_3$) d (ppm): 173.9, 163.1, 141.6, 136.6, 126.7, 122.8, 122.7, 122.6, 109.7, 58.0, 55.9, 38.8, 31.1, 31.0, 30.8, 26.3, 25.8, 25.7, 19.6, 18.4. LRMS (CI) m/z calcd. for $C_{20}H_{29}N_4O_2$ $[M+H]^+$: 357.2; found: 357.2.

(*R*)-*N*-(1-amino-3,3-dimethyl-1-oxobutan-2-yl)-1-(cyclohexylmethyl)-1*H*-indazole-3-carboxamide (25n). Yield: 67%. Mp: 142-143 ºC. ^{1}H NMR (300 MHz, $CDCl_3$) d (ppm): 8.30 (dt, *J* = 8.2, 1.0 Hz, 1H, Ar-H), 7.67 (d, *J* = 9.4 Hz, 1H, NH), 7.45–7.35 (m, 2H, Ar-H), 7.25 (m, 1H, Ar-H), 6.18 (br s, 1H, NH_2), 5.54 (br s, 1H, NH_2), 4.59 (d, *J* = 9.4 Hz, 1H, $CHC(CH_3)_3$), 4.21 (d, *J* = 7.2 Hz, 2H, CH_2-Cy), 2.03 (m, 1H, *CH*-Cy), 1.79–1.51 (m, 5H, Cy), 1.31–0.95 (m, 14H, Cy, $C(CH_3)_3$). LRMS (CI) m/z calcd. for $C_{21}H_{31}N_4O_2$ $[M+H]^+$: 371.2; found: 371.2.

(*R*)-*N*-(1-amino-3-methyl-1-oxobutan-2-yl)-1-(4-fluorobenzyl)-1*H*-indazole-3-carboxamide (25o). Yield: 65%. Mp: 149-150 ºC. ^{1}H NMR (300 MHz, $CDCl_3$) d (ppm): 8.33 (dt, *J* = 8.1, 1.1 Hz, 1H, Ar-H), 7.56 (d, *J* = 8.9 Hz, 1H, NH), 7.41–7.14 (m, 5H, Ar-H), 7.00 (m, 2H, Ar-H), 6.48 (br s, 1H, NH_2), 5.76 (br s, 1H, NH_2), 5.57 (s, 2H, CH_2-Ph), 4.60 (dd, *J* = 8.9, 6.7 Hz, 1H, $CHCH(CH_3)_2$), 2.35 (m, 1H, $CHCH(CH_3)_2$), 1.09 (dd, *J* = 6.8, 3.2 Hz, 6H, $CHCH(CH_3)_2$). LRMS (CI) m/z calcd. for $C_{20}H_{22}FN_4O_2$ $[M+H]^+$: 369.2; found: 369.2.

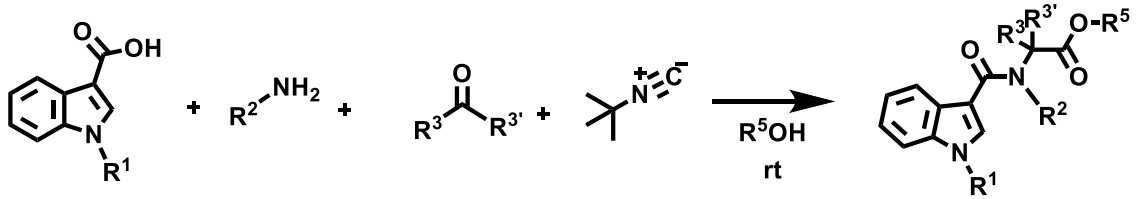
USC UNIVERSIDADE DE SANTIAGO DE COMPOSTELA

(*R*)-*N*-(1-amino-3,3-dimethyl-1-oxobutan-2-yl)-1-(4-fluorobenzyl)-1*H*-indazole-3-carboxamide (25p). Yield: 58%. Mp: 145-146 ºC. ^{1}H NMR (300 MHz, $CDCl_3$) δ (ppm): 8.32 (d, *J* = 8.1 Hz, 1H, Ar-H), 7.70 (d, *J* = 9.5 Hz, 1H, NH), 7.41 –7.16 (m, 5H, Ar-H), 7.00 (t, *J* = 8.5 Hz, 2H, Ar-H), 6.20 (br s, 1H, NH_2), 5.59 (s, 3H, C*H*$_2$-Ph, NH_2), 4.61 (d, *J* = 9.4 Hz, 1H, *CH*C$(CH_3)_3$), 1.16 (s, 9H, C$(CH_3)_3$). LRMS (CI) m/z calcd. for $C_{21}H_{24}FN_4O_2$ $[M+H]^+$: 383.2; found: 383.2.

USC UNIVERSIDADE DE SANTIAGO DE COMPOSTELA

4.5.7 General pathways for the synthesis of alkyl (1*H*-indole-3-carbonyl)glycinate polysubstituted (35a-r and 36a-r)

A mixture of the *N*-alkyl-1*H*-indole-3-carboxylic acid (1 equiv.), the corresponding aldehyde (or ketone) (1 equiv.), the appropriate amine (1 equiv.) and the tert-Butyl isocyanide (1 equiv.) in MeOH or EtOH or iPA (2 mL) was stirred with orbital stirring at room temperature for 24 h. After completion of the reaction, PS-p-TsOH (2.0 mmol) and CH_2Cl_2 (3 mL) were added. The reaction mixture was submitted to orbital stirring at room temperature until complete consumption of the unreacted isocyanide (30-60 min). The polystyrene-supported salt was filtered off and successively washed with MeOH (EtOH or iPA) (3 × 5 mL) and CH_2Cl_2 (3 × 5 mL). The resulting product was purified by column chromatography on silica gel using MeOH/CH_2Cl_2.



26d,c
R1 = CH_2-Cy
R1 = 4-F-Bn

32a,b
R2 = H
R2 = CH_3

34a,g
R3, R3' = H, H
R3, R3' = *i*-Pr, H
R3, R3' = *t*-Bu, H
R3, R3' = Ph, H
R3, R3' = Ad, H
R3, R3' = Me, Me
R3, R3' = Et, Et

33a

R5 = Me
R5 = Et
R5 = i-Pr

35a-r, 36a-r

Scheme S5: General procedure for the synthesis of alkyl (1*H*-indole-3-carbonyl)glycinate polysubstituted (**35a-r**, **36a-r**).

4.5.7.1 Spectroscopic and analytical data of alkyl (1*H*-indole-3-carbonyl)glycinate polysubstituted

Methyl (1-(4-fluorobenzyl)-1*H*-indole-3-carbonyl)glycinate (35a). Yield: 47%. Mp: 166-167 ºC. ^{1}H NMR (300 MHz, $CDCl_3$) δ (ppm): 8.15 – 8.00 (m, 1H, Ar-H), 7.75 (s, 1H, Ar-H), 7.28 (d, *J* = 6.3 Hz, 2H, Ar-H), 7.19 – 6.92 (m, 4H, Ar-H), 6.56 (s, 1H, NH), 5.27 (s, 2H, C*H*$_2$-Ph), 4.31 (s, 2H, CH_2), 3.83 (s, 3H, OCH_3). ^{13}C NMR (75 MHz, $CDCl_3$) δ (ppm): 131.7, 128.9, 128.8, 125.7, 122.9, 121.9, 120.5, 116.1, 115.8, 110.5, 52.4, 49.9, 41.3. LRMS (CI) m/z calcd for $C_{19}H_{18}FN_2O_3$ $[M+H]^+$: 341.1; found: 341.1.

Methyl (1-(4-fluorobenzyl)-1*H*-indole-3-carbonyl)valinate (35b). Yield: 50%. Mp: 125-126 ºC. ^{1}H NMR (300 MHz, $CDCl_3$) δ (ppm): 8.03 (m, 1H, Ar-H), 7.75 (s, 1H, Ar-H), 7.27 (m, 3H, Ar-H), 7.12 (m, 2H, Ar-H), 7.00 (m, 2H, Ar-H), 6.52 (d, *J* = 8.7 Hz, 1H, NH), 5.28 (s, 2H, C*H*$_2$-Ph), 4.87 (dd, *J* = 8.7, 4.9 Hz, 1H, *CH*CH$(CH_3)_2$), 3.79 (s, 3H, OCH_3), 2.31 (quind, *J* = 6.9, 4.9 Hz, 1H, CHC*H*$(CH_3)_2$) 1.04 (t, *J* = 7.2 Hz, 6H, CHCH*(CH$_3$)$_2$*). LRMS (CI) m/z calcd for $C_{22}H_{24}FN_2O_3$ $[M+H]^+$: 383.2; found: 383.2.

Methyl 2-(1-(4-fluorobenzyl)-1*H*-indole-3-carboxamido)-3,3-dimethylbutanoate (35c). Yield: 43%. Mp: 142-143 ºC. ^{1}H NMR (300 MHz, $CDCl_3$) δ (ppm):8.03 (d, *J* = 7.0 Hz, 1H, Ar-H), 7.78 (s, 1H, Ar-H), 7.40 – 7.21 (m, 3H, Ar-H), 7.21 – 6.92 (m, 4H, Ar-H), 6.56 (d, *J* = 9.3 Hz, 1H, NH), 5.32 (s, 2H, C*H*$_2$-Ph), 4.80 (d, *J* = 9.4 Hz, 1H, CH), 3.78 (s, 3H, OCH_3), 1.11 (s, Hz, 9H, $C(CH_3)_3$). ^{13}C NMR (75 MHz, $CDCl_3$) δ (ppm): 172.7, 164.6, 136.7, 132.1, 131.8, 128.8, 128.7, 125.5, 122.9, 122.0, 120.1, 116.1, 115.8, 111.4, 110.6, 59.8, 51.8, 50.0, 35.1, 26.8.LRMS (CI) m/z calcd for $C_{23}H_{26}FN_2O_3$ $[M+H]^+$: 397.2; found: 397.2.

Methyl 2-(1-(4-fluorobenzyl)-1*H*-indole-3-carboxamido)-2-phenylacetate (35d) Yield: 41%. Mp: 195-197 ºC. ^{1}H NMR (300 MHz, $CDCl_3$) δ (ppm): 8.13 – 8.01 (m, 1H, Ar-H), 7.75 (s, 1H, Ar-H), 7.55 – 7.45 (m, 2H, Ar-H), 7.45 – 7.20 (m, 6H, Ar-H), 7.19 – 7.06 (m, 2H, Ar-H), 7.07 – 6.94 (m, 2H, Ar-H), 5.89 (d, *J* = 7.0 Hz, 1H, CH), 5.30 (s, 2H, C*H*$_2$-Ph), 3.80 (s, 3H, OCH_3). ^{13}C NMR (75 MHz, $CDCl_3$) δ (ppm): 171.9, 164.0, 137.1, 131.9, 128.9, 128.8, 128.7, 128.4, 127.3, 125.7, 122.9, 121.9, 120.4, 116.1, 115.8, 110.5, 56.4, 52.8, 49.9. LRMS (CI) m/z calcd for $C_{25}H_{22}FN_2O_3$ $[M+H]^+$: 417.2; found: 417.2.

Methyl 2-(adamantan-1-yl)-2-(1-(4-fluorobenzyl)-1*H*-indole-3-carboxamido) acetate (35e). Yield: 45%. Mp: 135-136 ºC. ^{1}H NMR (300 MHz, $CDCl_3$) δ (ppm): 8.06 – 7.98 (m, 1H, Ar-H), 7.79 (s, 1H, Ar-H), 7.39 – 7.24 (m, 3H, Ar-H), 7.21 – 7.09 (m, 2H, Ar-H), 7.08 – 6.96 (m, 2H, Ar-H), 6.56 (d, *J* = 9.4 Hz, 1H, NH), 5.32 (s, 2H, C*H*$_2$-Ph), 4.68 (d, *J* = 9.4 Hz, 1H, CH), 3.79 (s, 3H, OCH_3), 2.15 – 1.93 (m, 2H, Ad), 1.83 – 1.48 (m, 13H, Ad). LRMS (CI) m/z calcd for $C_{29}H_{32}FN_2O_3$ $[M+H]^+$: 475.2; found: 475.2.

USC UNIVERSIDADE DE SANTIAGO DE COMPOSTELA

Methyl 2-(1-(4-fluorobenzyl)-1*H*-indole-3-carboxamido)-2-methylpropanoate (35f). Yield: 45%. Mp: 169-170 ºC. ^{1}H NMR (300 MHz, $CDCl_3$) δ (ppm): 8.03 (d, *J* = 6.5 Hz, 1H, Ar-H), 7.74 (s, 1H, Ar-H), 7.41 – 7.20 (m, 3H, Ar-H), 7.20 – 6.90 (m, 4H), 6.72 (s, 1H, NH), 5.28 (d, *J* = 4.6 Hz, 2H, C*H*$_2$-Ph), 3.81 (s, 3H, OCH_3), 1.74 (s, 6H, CH_3, CH_3). ^{13}C NMR (75 MHz, $CDCl_3$) δ (ppm): 175.5, 164.3, 136.7, 131.9, 128.8, 128.7, 125.5, 122.8, 121.8, 120.3, 116.0, 115.7, 111.8, 110.5, 56.8, 52.7, 49.9, 25.1.LRMS (CI) m/z calcd for $C_{21}H_{22}FN_2O_3$ $[M+H]^+$: 369.2; found: 369.2.

Methyl 2-ethyl-2-(1-(4-fluorobenzyl)-1*H*-indole-3-carboxamido)butanoate (35g). Yield: 47%. Mp: 155-157 ºC. ^{1}H NMR (300 MHz, $CDCl_3$) δ (ppm): 8.16 – 7.98 (m, 1H, Ar-H), 7.80 (s, 1H, Ar-H), 7.37 – 7.23 (m, 3H, Ar-H), 7.20 – 7.09 (m, 3H. Ar-H), 7.07 – 6.97 (m, 2H, Ar-H, NH), 5.32 (s, 2H, C*H*$_2$-Ph), 3.87 (s, 3H, OCH_3), 2.74 (dq, *J* = 13.8, 7.5 Hz, 2H, C*H*$_2$-CH_3), 1.93 (dq, *J* = 14.5, 7.3 Hz, 2H, C*H*$_2$-CH_3), 0.85 (t, *J* = 7.4 Hz, 6H, CH_2CH_3, CH_2CH_3). ^{13}C NMR (75 MHz, $CDCl_3$) δ (ppm): 175.4, 163.6, 136.8, 132.2, 131.9, 128.9, 128.8, 125.4, 122.7, 121.9, 120.0, 116.1, 115.8, 112.3, 110.6, 66.9, 52.8, 50.0, 28.6, 8.7. LRMS (CI) m/z calcd for $C_{23}H_{26}FN_2O_3$ $[M+H]^+$: 397.2; found: 397.2.

Ethyl 2-(1-(4-fluorobenzyl)-1*H*-indole-3-carboxamido)-3,3-dimethylbutanoate (35h). Yield: 37%. Mp: 133-134 ºC. ^{1}H NMR (300 MHz, $CDCl_3$) δ (ppm): 8.01 (d, *J* =8.2 Hz, 1H, Ar-H), 7.77 (s, 1H, Ar-H), 7.35 – 7.20 (m, 3H, Ar-H), 7.20 – 7.06 (m, 2H, Ar-H), 7.06 – 6.92 (m, 2H, Ar-H), 6.57 (d, *J* = 9.3 Hz, 1H, NH), 5.30 (s, 2H, C*H*$_2$-Ph), 4.76 (dd, *J* = 9.4, 1.2 Hz, 1H, CH), 4.33 – 4.10 (m, 2H, OC*H*$_2$$CH_3$), 1.32 (t, *J* = 7.1 Hz, 3H, OCH_2CH_3), 1.10 (s, 9H, $CH(CH_3)_3$). LRMS (CI) m/z calcd for $C_{24}H_{28}FN_2O_3$ $[M+H]^+$: 411.2; found: 411.2.

Isopropyl 2-(1-(4-fluorobenzyl)-1*H*-indole-3-carboxamido)-3,3-dimethylbutanoate 35i). Yield: 33%. Mp: 126-127 ºC. ^{1}H NMR (300 MHz, $CDCl_3$) δ (ppm): δ 8.00 (d, *J* = 7.7 Hz, 1H, Ar-H), 7.76 (s, 1H, Ar-H), 7.34 – 7.19 (m, 3H, Ar-H), 7.18 – 7.04 (m, 2H, Ar-H), 7.04 – 6.93 (m, 2H, Ar-H), 6.58 (d, *J* = 9.4 Hz, 1H, NH), 5.30 (s, 2H, C*H*$_2$-Ph), 5.08 (dt, *J* = 12.5, 6.1 Hz, 1H, OC*H*$(CH_3)_2$), 4.72 (d, *J* = 9.4 Hz, 1H, CH), 1.34 – 1.19 (m, 6H, $OCH(CH_3)_2$), 1.08 (s, 9H, $C(CH_3)_3$). LRMS (CI) m/z calcd for $C_{25}H_{30}FN_2O_3$ $[M+H]^+$: 425.2; found: 425.2.

USC UNIVERSIDADE DE SANTIAGO

Methyl *N*-(1-(4-fluorobenzyl)-1*H*-indole-3-carbonyl)-*N*-methylglycinate (35j). Yield: 55%. Mp: 126-127 ºC. ^{1}H NMR (300 MHz, $CDCl_3$) δ (ppm): 7.92 – 7.77 (m, 1H, Ar-H), 7.45 (s, 1H, Ar-H), 7.33 – 7.19 (m, 3H, Ar-H), 7.19 – 7.06 (m, 2H, Ar-H), 7.07 – 6.91 (m, 2H, Ar-H), 5.29 (s, 2H, C*H*$_2$-Ph), 4.30 (s, 2H, CH_2), 3.77 (s, 3H, OCH_3), 3.22 (s, 3H, NCH_3). LRMS (CI) m/z calcd for $C_{20}H_{20}FN_2O_3$ $[M+H]^+$: 355.1; found: 355.1.

Methyl *N*-(1-(4-fluorobenzyl)-1*H*-indole-3-carbonyl)-*N*-methylvalinate (35k). Yield: 42%. Oil at room temperature. ^{1}H NMR (300 MHz, $CDCl_3$) δ (ppm): 7.91 – 7.77 (m, 1H, Ar-H), 7.46 (s, 1H, Ar-H), 7.32 – 7.17 (m, 3H, Ar-H), 7.17 – 7.06 (m, 2H, Ar-H), 7.05 – 6.90 (m, 2H, Ar-H), 5.28 (s, 2H, C*H*$_2$-Ph), 4.81 (s, 1H, CH), 3.75 (s, 3H, OCH_3), 3.15 (s, 3H, NCH_3), 2.43 – 2.22 (m, 1H, C*H*$(CH_3)_2$), 1.07 – 0.85 (m, 6H, CH(C*H*$_3)_2$). LRMS (CI) m/z calcd for $C_{23}H_{26}FN_2O_3$ $[M+H]^+$: 397.2; found: 397.2.

Methyl 2-(1-(4-fluorobenzyl)-*N*-methyl-1*H*-indole-3-carboxamido)-3,3-dimethylbutanoate (35l). Yield: 45%. Mp: 120-121 ºC. ^{1}H NMR (300 MHz, $CDCl_3$) δ (ppm): 7.97 – 7.73 (m, 1H, Ar-H), 7.43 (s, 1H, Ar-H), 7.32-7.19 (m, 3H, Ar-H), 7.18-7.09 (m, 2H, Ar-H), 7.07-6.95 (m, 2H, Ar-H), 5.39 – 5.22 (m, 3H, C*H*$_2$-Ph, CH), 3.76 (s, 3H, OCH_3), 3.28 (s, 3H, NCH_3), 1.17 (s, 9H, C(C*H*$_3)_3$). ^{13}C NMR (75 MHz, $CDCl_3$) δ (ppm): 171.1, 168.5, 164.1, 160.8, 136.0, 132.2, 128.7, 128.6, 127.1, 122.8, 121.4, 121.3, 116.0, 115.7, 111.1, 110.0, 51.6, 49.7, 35.6, 28.2. LRMS (CI) m/z calcd for $C_{24}H_{28}FN_2O_3$ $[M+H]^+$: 411.2; found: 411.2.

Methyl 2-(1-(4-fluorobenzyl)-*N*-methyl-1*H*-indole-3-carboxamido)-2-phenylacetate (35m). Yield: 51%. Mp: 123-124 ºC. ^{1}H NMR (300 MHz, $CDCl_3$) δ (ppm): 7.92 – 7.80 (m, 1H, Ar-H), 7.53 – 7.19 (m, 9H, Ar-H), 7.19 – 6.92 (m, 4H, Ar-H), 6.47 (s, 1H, CH), 5.30 (s, 2H, C*H*$_2$-Ph), 3.85 (s, 3H, OCH_3), 3.01 (s, 3H, NCH_3). HRMS (APCI) m/z calcd for $C_{26}H_{24}FN_2O_3$ $[M+H]^+$: 431.1693; found: 431.1775.

Methyl 2-(adamantan-1-yl)-2-(1-(4-fluorobenzyl)-*N*-methyl-1*H*-indole-3-carboxamido)acetate (35n). Yield: 42%. Mp: 125-126 ºC. ^{1}H NMR (300 MHz, $CDCl_3$) δ (ppm): 7.95 – 7.76 (m, 1H, Ar-H), 7.45 (s, 1H, Ar-H), 7.33 – 7.16 (m, 3H, Ar-H), 7.16 – 7.04 (m, 2H, Ar-H), 7.03 – 6.92 (m, 2H, Ar-H), 6.89 (m, 4H, Ar-H), 5.28 (m,

USC DE COMPOSTELA

3H, C*H*$_2$-Ph, CH), 3.73 (s, 3H, OCH$_3$), 3.32 (s, 3H, NCH$_3$), 2.13 – 1.52 (m, 15H, Ad). LRMS (CI) m/z calcd for $C_{30}H_{34}FN_2O_3$ $[M+H]^+$: 489.2; found: 489.2.

Methyl 2-(1-(4-fluorobenzyl)-*N*-methyl-1*H*-indole-3-carboxamido)-2-methylpropanoate (35o). Yield: 47%. Mp: 154-156 ºC. ^{1}H NMR (300 MHz, $CDCl_3$) δ (ppm): 7.92 – 7.70 (m, 1H, Ar-H), 7.47 (s, 1H, Ar-H), 7.33 – 7.19 (m, 3H, Ar-H), 7.18 – 7.09 (m, 2H, Ar-H), 7.09 – 6.93 (m, 2H, Ar-H), 5.28 (s, 2H, C*H*$_2$-Ph), 3.73 (s, 3H, OCH$_3$), 3.17 (s, 3H, NCH$_3$), 1.59 (s, 6H, CH$_3$, CH$_3$). ^{13}C NMR (75 MHz, $CDCl_3$) δ (ppm): 175.0, 167.7, 164.1, 136.0, 132.1, 130.6, 128.9, 128.8, 126.6, 122.7, 121.3, 121.2, 116.0, 115.7, 112.0, 110.1, 60.7, 52.3, 49.8, 33.5, 23.2. LRMS (CI) m/z calcd for $C_{22}H_{24}FN_2O_3$ $[M+H]^+$: 383.2; found: 383.2.

Methyl 2-ethyl-2-(1-(4-fluorobenzyl)-*N*-methyl-1*H*-indole-3-carboxamido)-butanoate (35p). Yield: 51%. Mp: 172-173 ºC. ^{1}H NMR (300 MHz, $CDCl_3$) δ (ppm): 7.84 – 7.64 (m, 1H, Ar-H), 7.45 (s, 1H, Ar-H), 7.35 – 7.08 (m, 5H, Ar-H), 7.08 – 6.92 (m, 2H, Ar-H), 5.29 (s, 2H, C*H*$_2$-Ph), 3.72 (s, 3H, OCH$_3$), 3.22 (s, 3H, NCH$_3$), 2.27 (dq, *J* = 13.9, 7.5 Hz, 2H, C*H*$_2$CH$_3$), 1.97 (dq, *J* = 14.7, 7.4 Hz, 2H, C*H*$_2$CH$_3$), 0.95 (t, *J* = 7.5 Hz, 6H, CH$_2$C*H*$_3$, CH$_2$C*H*$_3$). LRMS (CI) m/z calcd for $C_{24}H_{28}FN_2O_3$ $[M+H]^+$: 411.2; found: 411.2.

Ethyl 2-(1-(4-fluorobenzyl)-*N*-methyl-1*H*-indole-3-carboxamido)-3,3-dimethylbutanoate (35q). Yield: 35%. Mp: 125-126 ºC. ^{1}H NMR (300 MHz, $CDCl_3$) δ (ppm): 7.95 – 7.74 (m, 1H, Ar-H), 7.41 (s, 1H, Ar-H), 7.32 – 7.17 (m, 3H, Ar-H), 7.17 – 7.05 (m, 2H, Ar-H), 7.05 – 6.91 (m, 2H, Ar-H), 5.28 (s, 2H, C*H*$_2$-Ph), 4.23 (q, *J* = 7.2 Hz, 2H, OCH$_2$CH$_3$), 3.27 (s, 3H, NCH$_3$), 1.29 (t, *J* = 7.1 Hz, 3H, OCH$_2$C*H*$_3$), 1.15 (s, 9H, C(CH$_3$)$_3$). LRMS (CI) m/z calcd for $C_{25}H_{30}FN_2O_3$ $[M+H]^+$: 425.2; found: 425.2.

Isopropyl 2-(1-(4-fluorobenzyl)-*N*-methyl-1*H*-indole-3-carboxamido)-3,3-dimethylbutanoate (35r). Yield: 34%. Mp: 125-126 ºC. ^{1}H NMR (300 MHz, $CDCl_3$) δ (ppm): 7.84 (d, *J* = 7.4 Hz, 1H, Ar-H), 7.42 (s, 1H, Ar-H), 7.32 – 7.18 (m, 3H, Ar-H), 7.17 – 7.09 (m, 2H, Ar-H), 7-06 – 6.96 (m, 2H, Ar-H), 5.31 (s, 3H, C*H*$_2$-Ph, CH), 5.13 (dt, *J* = 12.6, 6.2 Hz, 1H, OC*H*(CH$_3$)$_2$), 3.27 (s, 3H, NCH$_3$), 1.31 (d, *J* = 2.6 Hz, 3H, OCH(C*H*$_3$)$_2$), 1.29 (d, *J* = 2.7 Hz, 3H, OCH(C*H*$_3$)$_2$), 1.15 (s, 9H, C(CH$_3$)$_3$). LRMS (CI) m/z calcd for $C_{26}H_{32}FN_2O_3$ $[M+H]^+$: 439.2; found: 439.2.

USC DE COMPOSTELA

Methyl (1-(cyclohexylmethyl)-1*H*-indole-3-carbonyl)glycinate (36a). Yield: 59%. Mp: 125-126 ºC. ^{1}H NMR (300 MHz, $CDCl_3$) δ (ppm): 8.19 – 7.85 (m, 1H, Ar-H), 7.70 (s, 1H, Ar-H), 7.46 – 7.12 (m, 3H, Ar-H), 6.54 (s, 1H, NH), 4.30 (s, 2H, CH_2), 3.92 (d, *J* = 7.2 Hz, 2H, C*H*$_2$-Cy), 3.80 (s, 3H, OCH_3), 1.95 – 1.75 (m, 1H, C*H*-Cy), 1.76 – 1.49 (m, 4H, Cy), 1.29 – 0.70 (m, 6H, Cy). LRMS (CI) m/z calcd for $C_{19}H_{25}N_2O_3$ $[M+H]^+$: 329.2; found: 329.2.

Methyl (1-(cyclohexylmethyl)-1*H*-indole-3-carbonyl)valinate (36b). Yield: 47%. Mp: 125-126 ºC. ^{1}H NMR (300 MHz, $CDCl_3$) δ (ppm): 8.01 (m, 1H, Ar-H), 7.73 (s, 1H, Ar-H), 7.38 (m, 1H, Ar-H), 7.28 (m, 2H, Ar-H), 6.57 (d, *J* = 8.7 Hz, 1H, NH), 4.88 (dd, *J* = 8.7, 4.9 Hz, 1H, *CH*CH$(CH_3)_2$), 3.93 (d, *J* = 7.1 Hz, 2H, C*H*$_2$-Cy), 3.79 (s, 3H, OCH_3), 2.31 (m, 1H, CHC*H*$(CH_3)_2$), 1.85 (m, 1H, *CH*-Cy), 1.77–1.53 (m, 5H, Cy), 1.30–0.90 (m, 11 H, Cy, CHCH*(CH$_3$)$_2$*). LRMS (CI) m/z calcd. for $C_{22}H_{31}N_2O_3$ $[M+H]^+$: 371.2; found: 371.2.

Methyl 2-(1-(cyclohexylmethyl)-1*H*-indole-3-carboxamido)-3,3-dimethylbutanoate (36c). Yield: 53%. Mp: 123-124 ºC.^{1}H NMR (300 MHz, $CDCl_3$) δ (ppm): 8.09 – 7.85 (m, 1H, Ar-H), 7.73 (s, 1H, Ar-H), 7.56 – 7.15 (m, 3H, Ar-H), 6.55 (d, *J* = 9.2 Hz, 1H, NH), 4.85 – 4.74 (m, 1H, CH), 3.98 (d, *J* = 6.8 Hz, 2H, CH_2-Cy), 3.78 (s, 3H, OCH_3), 2.01 – 1.78 (m, 1H, C*H*-Cy), 1.81 – 1.52 (m, 6H, Cy), 1.36 – 0.89 (m, 13H, C(C*H*$_3$)$_3$, Cy). ^{13}C NMR (75 MHz, $CDCl_3$) δ (ppm): 127.7, 164.8, 137.0, 132.7, 122.4, 121.5, 119.8, 110.7, 59.8, 53.4, 51.8, 38.5, 35.1, 31.0, 26.8, 26.2, 25.6. LRMS (CI) m/z calcd for $C_{23}H_{33}N_2O_3$ $[M+H]^+$: 385.2; found: 385.2.

Methyl 2-(1-(cyclohexylmethyl)-1*H*-indole-3-carboxamido)-2-phenylacetate (36d). Yield: 46%. Mp: 167-168 ºC. ^{1}H NMR (300 MHz, $CDCl_3$) δ (ppm): 8.09 – 7.99 (m, 1H, Ar-H), 7.71 (s, 1H, Ar-H), 7.57 – 7.47 (m, 2H, Ar-H), 7.45 – 7.23 (m, 6H, Ar-H), 7.00 (d, *J* = 7.0 Hz, 1H, NH), 5.90 (d, *J* = 6.9 Hz, 1H, CH), 3.97 (d, *J* = 7.2 Hz, 2H, C*H*$_2$-Cy), 3.81 (s, 3H, OCH_3), 1.96 – 1.80 (m, 1H, C*H*-Cy), 1.79 – 1.48 (m, 5H, Cy), 1.38 – 0.78 (m, 5H, Cy). LRMS (CI) m/z calcd for $C_{25}H_{29}N_2O_3$ $[M+H]^+$: 405.2; found: 405.2.

USC UNIVERSIDADE DE SANTIAGO DE COMPOSTELA

Methyl 2-(adamantan-1-yl)-2-(1-(cyclohexylmethyl)-1*H*-indole-3-carboxamido)acetate (36e). Yield: 41%. Mp: 190-192 ºC. ^{1}H NMR (300 MHz, $CDCl_3$) δ

(ppm): 8.02 – 7.95 (m, 1H, Ar-H), 7.72 (s, 1H, Ar-H), 7.38 (s, 1H, Ar-H), 7.34 – 7.22 (m, 2H, Ar-H), 6.54 (d, *J* = 8.4 Hz, 1H, NH), 4.67 (d, *J* = 9.6 Hz, 1H, CH), 3.96 (d, *J* = 7.0 Hz, 2H, C*H*$_2$-Cy), 3.77 (s, 3H, OCH_3), 2.10 – 1.97 (m, 3H, Cy, Ad), 1.94 – 1.56 (m, 18H, Cy, Ad), 1.37 – 1.11 (m, 3H, Cy, Ad), 1.11 – 0.81 (m, 2H, Cy). LRMS (CI) m/z calcd for $C_{29}H_{39}N_2O_3$ $[M+H]^+$: 463.3; found: 463.3.

Methyl 2-(1-(cyclohexylmethyl)-1*H*-indole-3-carboxamido)-2-methylpropanoate (36f). Yield: 43%. Mp: 158-160 ºC. ^{1}H NMR (300 MHz, $CDCl_3$) δ (ppm): 8.10 – 7.85 (m, 1H, Ar-H), 7.67 (s, 1H, Ar-H), 7.47 – 7.07 (m, 3H, Ar-H), 6.66 (s, 1H, NH), 3.93 (d, *J* = 7.2 Hz, 2H, C*H*$_2$-Cy), 3.79 (s, 3H, OCH_3), 1.93 – 1.77 (m, 1H, C*H*-Cy), 1.77 –1.55 (m, 11H, CH_3, CH_3, Cy), 1.36 – 0.85 (m, 5H, Cy). LRMS (CI) m/z calcd for $C_{21}H_{29}N_2O_3$ $[M+H]^+$: 357.2; found: 357.2.

Methyl 2-(1-(cyclohexylmethyl)-1*H*-indole-3-carboxamido)-2-ethylbutanoate (36g). Yield: 42%. Mp: 162-163 ºC. ^{1}H NMR (300 MHz, $CDCl_3$) δ (ppm): 8.18 – 7.92 (m, 1H, Ar-H), 7.74 (s, 1H, Ar-H), 7.44 – 7.36 (m, 1H, Ar-H), 7.35 – 7.25 (m, 2H, Ar-H), 7.10 (s, 1H, NH), 3.97 (d, *J* = 7.2 Hz, 2H, C*H*$_2$-Cy), 3.87 (s, 3H, OCH_3), 2.74 (dq, *J* = 13.9, 7.5 Hz, 2H, C*H*$_2$$CH_3$), 2.05 – 1.80 (m, 3H, C*H*$_2$$CH_3$, C*H*-Cy), 1.80 – 1.57 (m, 5H, Cy), 1.32 – 0.93 (m, 5H, Cy), 0.85 (t, *J* = 7.4 Hz, 6H, CH_2CH_3, CH_2CH_3). LRMS (CI) m/z calcd for $C_{23}H_{33}N_2O_3$ $[M+H]^+$: 385.2; found: 385.2.

Ethyl 2-(1-(cyclohexylmethyl)-1*H*-indole-3-carboxamido)-3,3-dimethylbutanoate (36h). Yield: 38%. Mp: 127-128 ºC. ^{1}H NMR (300 MHz, $CDCl_3$) δ (ppm): 8.05 – 7.90 (m, 1H, Ar-H), 7.73 (s, 1H, Ar-H), 7.44 – 7.34 (m, 1H, Ar-H), 7.33 – 7.24 (m, 2H, Ar-H), 6.57 (d, *J* = 9.4 Hz, 1H, NH), 4.78 (d, *J* = 9.4 Hz, 1H, CH), 4.35 – 4.10 (m, 2H, OC*H*$_2$$CH_3$), 3.97 (d, *J* = 7.2 Hz, 2H, C*H*$_2$-Cy), 1.98 – 1.81 (m, 1H, C*H*-Cy), 1.80 – 1.51 (m, 6H, Cy), 1.42 – 0.94 (m, 16H, C(C*H*$_3$)$_3$, OCH_2CH_3, Cy). LRMS (CI) m/z calcd for $C_{24}H_{35}N_2O_3$ $[M+H]^+$: 399.3; found: 399.3.

Isopropyl 2-(1-(cyclohexylmethyl)-1*H*-indole-3-carboxamido)-3,3-dimethylbutanoate (36i). Yield: 36%. Mp: 126-127 ºC. ^{1}H NMR (300 MHz, $CDCl_3$) δ (ppm): 8.08 – 7.93 (m, 1H, Ar-H), 7.74 (s, 1H, Ar-H), 7.45 – 7.37 (m, 1H, Ar-H), 7.35 – 7.26 (m, 2H, Ar-H), 6.61 (d, *J* = 9.3 Hz, 1H, Ar-H), 5.12 (hept, *J* = 6.3 Hz, 1H, OC*H*$(CH_3)_2$), 4.76 (d, *J* = 9.4 Hz, 1H, CH), 3.98 (d, *J* = 7.2 Hz, 2H, C*H*$_2$-Cy), 1.99 –

1.81 (m, 1H, C*H*-Cy), 1.81 – 1.57 (m, 6H, Cy), 1.38 – 1.27 (m, 6H, OCH(C*H*$_3$)$_2$), 1.27 – 0.93 (m, 13H, C(C*H*$_3$)$_3$, Cy). LRMS (CI) m/z calcd for $C_{25}H_{37}N_2O_3$ $[M+H]^+$: 413.3; found: 413.3.

Methyl *N*-(1-(cyclohexylmethyl)-1*H*-indole-3-carbonyl)-*N*-methylglycinate (36j). Yield: 55%. Oil at room temperature. ^{1}H NMR (300 MHz, $CDCl_3$) δ (ppm): 7.84 (d, *J* = 6.9 Hz, 1H, Ar-H), 7.42 (s, 1H, Ar-H), 7.38 – 7.31 (m, 1H, Ar-H), 7.29 – 7.16 (m, 2H, Ar-H), 4.31 (s, 2H, CH_2), 3.95 (d, *J* = 7.1 Hz, 2H, CH_2-Cy), 3.78 (s, 3H, OCH_3), 3.24 (s, 3H, NCH_3), 2.02 – 1.76 (m, 1H, C*H*-Cy), 1.76 – 1.50 (m, 5H, Cy), 1.36 – 0.83 (m, 5H, Cy). LRMS (CI) m/z calcd for $C_{20}H_{27}N_2O_3$ $[M+H]^+$: 343.2; found: 343.2.

Methyl *N*-(1-(cyclohexylmethyl)-1*H*-indole-3-carbonyl)-*N*-methylvalinate (36k). Yield: 55%. Mp: 124-125 ºC. ^{1}H NMR (300 MHz, $CDCl_3$) δ (ppm): 7.87 – 7.80 (m, 1H, Ar-H), 7.44 (s, 1H, Ar-H), 7.38 – 7.33 (m, 1H, Ar-H), 7.29 – 7.15 (m, 2H, Ar-H), 4.94 – 4.69 (m, 1H, Ar-H), 3.97 (d, *J* = 7.2 Hz, 2H, C*H*$_2$-Cy), 3.80 (s, 3H, OCH_3), 3.17 (s, 3H, NCH_3), 2.42 – 2.23 (m, 1H, C*H*(CH$_3$)$_2$), 1.98 – 1.79 (m, 1H, C*H*-Cy), 1.78 – 1.58 (m, 5H, Cy), 1.45 – 0.71 (m, 11H, CH(C*H*$_3$)$_2$, Cy). LRMS (CI) m/z calcd for $C_{23}H_{33}N_2O_3$ $[M+H]^+$: 385.2; found: 385.2.

Methyl 2-(1-(cyclohexylmethyl)-*N*-methyl-1*H*-indole-3-carboxamido)-3,3-dimethylbutanoate (36l). Yield: 56%. Mp: 125-126 ºC. ^{1}H NMR (300 MHz, $CDCl_3$) δ (ppm): 7.82 (d, *J* = 7.7 Hz, 1H, Ar-H), 7.43 – 7.30 (m, 2H, Ar-H), 7.30 – 7.13 (m, 2H, Ar-H), 5.28 (s, 1H, CH), 3.95 (d, *J* = 7.1 Hz, 2H, C*H*$_2$-Cy), 3.76 (s, 3H, OCH_3), 3.27 (s, 3H, NCH_3), 1.93 – 1.78 (m, 1H, C*H*-Cy), 1.77 – 1.53 (m, 6H, Cy), 1.34 – 0.88 (m, 13H, C(C*H*$_3$)$_3$, Cy). LRMS (CI) m/z calcd for $C_{24}H_{35}N_2O_3$ $[M+H]^+$: 399.3; found: 399.3.

Methyl 2-(1-(cyclohexylmethyl)-*N*-methyl-1*H*-indole-3-carboxamido)-2-phenylacetate (36m). Yield: 52%. Mp: 124-125 ºC^{1}H NMR (300 MHz, $CDCl_3$) δ (ppm): 7.83 (d, *J* = 7.6 Hz, 1H, Ar-H), 7.50 – 7.32 (m, 6H, Ar-H), 7.32 – 7.13 (m, 3H, Ar-H), 6.46 (s, 1H, CH), 3.96 (d, *J* = 7.1 Hz, 2H, C*H*$_2$-Cy), 3.85 (s, 3H, OCH_3), 3.01 (s, 3H, NCH_3), 1.98 – 1.78 (m, 1H, C*H*-Cy), 1.78 – 1.54 (m, 6H, Cy), 1.33 – 0.87 (m, 4H, Cy). LRMS (CI) m/z calcd for $C_{26}H_{31}N_2O_3$ $[M+H]^+$: 419.2; found: 419.2.

USC DE COMPOSTELA

Methyl 2-(adamantan-1-yl)-2-(1-(cyclohexylmethyl)-*N*-methyl-1*H*-indole-3-carboxamido)acetate (36n). Yield: 48%. Mp: 149-150 ºC. ^{1}H NMR (300 MHz, $CDCl_3$) δ (ppm): 7.84 (d, *J* = 8.2 Hz, 1H, Ar-H), 7.45 – 7.30 (m, 2H, Ar-H), 7.29 – 7.13 (m, 2H, Ar-H) 5.12 (s, 1H, CH), 3.95 (d, *J* = 7.1 Hz, 2H, C*H*$_2$-Cy), 3.76 (s, 3H, OCH_3), 3.30 (s, 3H, NCH_3), 2.05 – 1.52 (m, 19H, Cy, Ad), 1.42 – 0.88 (m, 7H, Cy, Ad). LRMS (CI) m/z calcd for $C_{30}H_{41}N_2O_3$ $[M+H]^+$: 477.3; found: 477.3.

Methyl 2-(1-(cyclohexylmethyl)-*N*-methyl-1*H*-indole-3-carboxamido)-2-methylpropanoate (36o). Yield: 54%. Mp: 153-155 ºC. ^{1}H NMR (300 MHz, $CDCl_3$) δ (ppm): 7.79 (d, *J* = 8.1 Hz, 1H, Ar-H), 7.42 (s, 1H, Ar-H), 7.37 – 7.30 (m, 1H, Ar-H), 7.28 – 7.15 (m, 2H, Ar-H), 3.93 (d, *J* = 7.1 Hz, 2H, C*H*$_2$-Cy), 3.71 (s, 3H, OCH_3), 3.16 (s, 3H, NCH_3), 1.95 – 1.76 (m, 1H, C*H*-Cy), 1.76 – 1.61 (m, 5H, Cy), 1.58 (s, 6H, CH_3, CH_3), 1.25 – 1.10 (m, 3H, Cy), 1.09 – 0.91 (m, 2H, Cy). LRMS (CI) m/z calcd for $C_{22}H_{31}N_2O_3$ $[M+H]^+$: 371.2; found: 371.2.

Methyl 2-(1-(cyclohexylmethyl)-*N*-methyl-1*H*-indole-3-carboxamido)-2-ethylbutanoate (36p). Yield: 55%. Mp: 145-146 ºC. ^{1}H NMR (300 MHz, $CDCl_3$) δ (ppm): 7.76 (d, *J* = 7.4 Hz, 1H, Ar-H), 7.41 (s, 1H, Ar-H), 7.38 – 7.29 (m, 1H, Ar-H), 7.29 – 7.12 (m, 2H, Ar-H), 3.93 (d, *J* = 7.1 Hz, 2H, C*H*$_2$-Cy), 3.72 (s, 3H, OCH_3), 3.23 (s, 3H, NCH_3), 2.28 (dq, *J* = 14.9, 7.5 Hz, 2H, C*H*$_2$$CH_3$), 1.97 (dq, *J* = 14.8, 7.5 Hz, 2H, C*H*$_2$$CH_3$), 1.89 – 1.78 (m, 1H, C*H*-Cy), 1.78 – 1.54 (m, 5H, Cy), 1.29 – 1.09 (m, 5H, Cy), 0.95 (t, *J* = 7.5 Hz, 6H, CH_2C*H*$_3$, CH_2C*H*$_3$). LRMS (CI) m/z calcd for $C_{24}H_{35}N_2O_3$ $[M+H]^+$: 399.3; found: 399.3.

Ethyl 2-(1-(cyclohexylmethyl)-*N*-methyl-1*H*-indole-3-carboxamido)-3,3-dimethylbutanoate (36q). Yield: 35%. Mp: 124-125 ºC. ^{1}H NMR (300 MHz, $CDCl_3$) δ (ppm): 7.82 (d, *J* = 7.7 Hz, 1H, Ar-H), 7.41 – 7.29 (m, 2H, Ar-H), 7.28 – 7.12 (m, 2H, Ar-H), 5.28 (s, 1H, CH), 4.31 – 4.17 (m, 2H, OC*H*$_2$$CH_3$), 3.94 (d, *J* = 7.1 Hz, 2H, C*H*$_2$-Cy), 3.27 (s, 3H, NCH_3), 1.97 – 1.77 (m, 1H, C*H*-Cy), 1.77 – 1.52 (m, 5H, Cy), 1.44 – 0.73 (m, 17H, $C(CH_3)_3$, OCH_2C*H*$_3$, Cy). LRMS (CI) m/z calcd for $C_{25}H_{37}N_2O_3$ $[M+H]^+$: 413.3; found: 413.3.

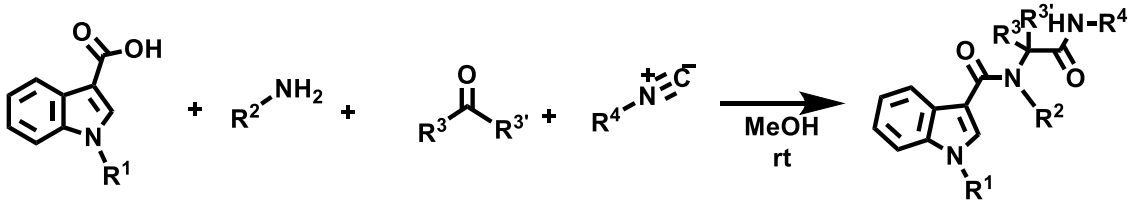
USC UNIVERSIDADE DE SANTIAGO DE COMPOSTELA

Isopropyl 2-(1-(cyclohexylmethyl)-*N*-methyl-1*H*-indole-3-carboxamido)-3,3-dimethylbutanoate (36r). Yield: 35%. Mp: 120-121 ºC. ^{1}H NMR (300 MHz, $CDCl_3$) δ (ppm): 7.83 (d, *J* = 7.4 Hz, 1H, Ar-H), 7.40 – 7.32 (m, 2H, Ar-H), 7.30 – 7.12 (m, 2H, Ar-H), 5.31 (s, 1H, CH), 5.25 – 4.98 (m, 1H, OC*H*$(CH_3)_2$), 4.41 (d, *J* = 7.2 Hz, 2H, C*H*$_2$-Cy), 3.28 (s, 3H, NCH_3), 2.01 – 1.80 (m, 1H, C*H*-Cy), 1.78 – 1.60 (m, 5H, Cy), 1.36 – 1.29 (m, 6H, OCH(C*H*$_3$)$_2$), 1.29 – 0.95 (m, 14H, C(C*H*$_3$)$_3$, Cy). HRMS (APCI) m/z calcd for $C_{26}H_{39}N_2O_3$ $[M+H]^+$: 427.2882; found: 427.2969.

USC UNIVERSIDADE DE SANTIAGO DE COMPOSTELA

4.5.8 General pathways for the synthesis of *N*-(2-amino-2-oxoethyl)-1*H*-indole-3-carboxamide polysubstituted (37a-v, 38a-v)

A mixture of the *N*-alkyl-1*H*-indole-3-carboxylic acid (1 equiv.), the corresponding aldehyde (or ketone) (1 equiv.), amine (1 equiv.) and isocyanide (1 equiv.) in MeOH (2 mL) was stirred with orbital stirring at room temperature for 24 h. After completion of the reaction, PS-p-TsOH (2.0 mmol) and CH_2Cl_2 (3 mL) were added. The reaction mixture was submitted to orbital stirring at room temperature until complete consumption of the unreacted isocyanide (30-60 min). The polystyrene-supported salt was filtered off and successively washed with MeOH (3 × 5 mL) and CH_2Cl_2 (3 × 5 mL). The resulting product was purified by column chromatography on silica gel using MeOH/CH_2Cl_2.



26d,c
R¹ = CH_2-Cy
R¹ = 4-F-Bn

32a,b
R² = H
R² = CH_3

34a,g
R³, R³' = H, H
R³, R³' = *i*-Pr, H
R³, R³' = *t*-Bu, H
R³, R³' = Ph, H
R³, R³' = Ad, H
R³, R³' = Me, Me
R³, R³' = Et, Et

33a-c
R⁴ = *t*-Bu
R⁴ = Bn
R⁴ = 6-Br-pyridine

37a-v, 38a-v

Scheme S6: General procedure for the synthesis of *N*-(2-amino-2-oxoethyl)-1*H*-indole-3-carboxamide polysubstituted (**37a-v**, **38a-v**).

4.5.8.1 Spectroscopic and analytic data of *N*-(2-amino-2-oxoethyl)-1*H*-indole-3-carboxamide polysubstituted

***N*-(2-(*tert*-butylamino)-2-oxoethyl)-1-(4-fluorobenzyl)-1*H*-indole-3-carboxamide (37a).** Yield: 49%. Mp: 175-176 ºC. ^{1}H NMR (300 MHz, $CDCl_3$) δ (ppm): 8.12 (d, *J* = 7.0 Hz, 1H, Ar-H), 7.79 (s, 1H, Ar-H), 7.33 – 7.17 (m, 3H, Ar-H), 7.15 – 7.03 (m, 3H, Ar-H, NH), 7.02 – 6.91 (m, 2H, Ar-H), 6.31 (s, 1H, NH), 5.23 (s, 2H, C*H*$_2$-Ph), 4.10 (d, *J* = 4.2 Hz, 2H, CH_2), 1.39 (s, 9H, $C(CH_3)_3$). ^{13}C NMR (75 MHz, $CDCl_3$) δ (ppm): 168.8, 165.4, 164.0, 160.8, 136.6, 131.8, 131.5, 128.8, 128.6, 126.1, 122.9, 121.9, 121.0, 116.0, 115.7, 110.9, 110.3, 51.5, 49.8, 44.2, 28.8. LRMS (CI) m/z calcd for $C_{22}H_{25}FN_3O_2$ $[M+H]^+$: 382.2; found: 382.2.

***N*-(1-amino-3-methyl-1-oxobutan-2-yl)-1-(4-fluorobenzyl)-1*H*-indole-3-carboxa-mide (37b).** Yield: 21%. Mp: 132-133 ºC. ^{1}H NMR (300 MHz, $CDCl_3$) δ (ppm): 8.03 (dt, *J* = 7.2, 1.2 Hz, 1H, Ar-H), 7.73 (s, 1H, Ar-H), 7.27 (m, 3H, Ar-H), 7.12 (m, 2H, Ar-H), 7.00 (t, *J* = 8.6 Hz, 2H, Ar-H), 6.59 (d, *J* = 8.5 Hz, 1H, NH), 6.14 (brs, 1H, NH_2), 5.49 (br s, 1H, NH_2), 5.28 (s, 2H, C*H*$_2$-Ph), 4.59 (dd, *J* = 8.6, 6.5 Hz, 1H, *CH*CH$(CH_3)_2$), 2.29 (m, 1H, CHC*H*$(CH_3)_2$), 1.09 (d, *J* = 6.8 Hz, 6H, CHCH*(CH$_3$)$_2$*). LRMS (CI) m/z calcd. for $C_{21}H_{23}FN_3O_2$ $[M+H]^+$: 368.2; found: 368.2.

***N*-(1-(*tert*-butylamino)-3-methyl-1-oxobutan-2-yl)-1-(4-fluorobenzyl)-1*H*-indole-3-carboxamide (37c).** Yield: 45%. Mp: 232-233 ºC. ^{1}H NMR (300 MHz, $CDCl_3$) δ (ppm): 8.08 (d, *J* = 7.3 Hz, 1H, Ar-H), 7.78 (s, 1H, Ar-H), 7.35 – 7.18 (m, 3H, Ar-H), 7.17 – 7.05 (m, 2H, Ar-H), 7.05 – 6.93 (m, 2H, Ar-H), 6.82 (brs, 1H, NH), 5.94 (brs, 1H, NH), 5.27 (s, 2H, C*H*$_2$-Ph), 4.48 – 4.35 (m, 1H, CH), 2.29 – 2.08 (m, 1H, C*H*$(CH_3)_2$), 1.37 (s, 9H, C$(CH_3)_3$), 1.04 (d, *J* = 6.6 Hz, 6H, CH(C*H*$_3$)$_2$). ^{13}C NMR (75 MHz, $CDCl_3$) δ (ppm): 170.8, 164.8, 164.1, 160.8, 136.7, 131.5, 128.8, 128.7, 125.9, 122.9, 121.9, 120.7, 116.0, 115.8, 110.4, 58.8, 49.9, 31.8, 28.8, 19.3, 18.6. LRMS (CI) m/z calcd for $C_{25}H_{31}FN_3O_2$ $[M+H]^+$: 424.2; found: 424.2.

***N*-(1-(benzylamino)-3-methyl-1-oxobutan-2-yl)-1-(4-fluorobenzyl)-1*H*-indole-3-carboxamide (37d).** Yield: 42%. Mp: 216-217 ºC. ^{1}H NMR (300 MHz, DMSO-d_6) δ (ppm): 8.55 (brs, 1H, NH), 8.33 (s, 1H, Ar-H), 8.11 (d, *J* = 7.9 Hz, 1H, Ar-H), 7.71 (d, *J* = 8.4 Hz, 1H, NH), 7.52 (d, *J* = 8.6 Hz, 1H, Ar-H), 7.36 – 7.23 (m, 7H, Ar-H), 7.21 – 7.09 (m, 4H, Ar-H), 5.44 (s, 2H, C*H*$_2$-Ph), 4.44 –4.33 (m, 1H, CH), 4.30 (d, *J* = 5.9 Hz, 2H, C*H*$_2$-Ph), 2.16 –2.03 (m, 1H, C*H*$(CH_3)_2$), 0.91 (t, *J* = 6.3 Hz, 6H, CH(C*H*$_3$)$_2$). LRMS (CI) m/z calcd for $C_{28}H_{29}FN_3O_2$ $[M+H]^+$: 458.2; found: 458.2.

***N*-(1-Amino-3,3-dimethyl-1-oxobutan-2-yl)-1-(4-fluorobenzyl)-1*H*-indole-3-carboxamide (37e).** Yield: 18%. Mp: 150-151 ºC. ^{1}H NMR (300 MHz, $CDCl_3$) δ (ppm): 8.03 (m, 1H, Ar-H), 7.74 (s, 1H, Ar-H), 7.27 (m, 3H, Ar-H), 7.09 (m, 2H, Ar-H), 6.98 (m, 2H, Ar-H), 6.81 (d, *J* = 9.3 Hz, 1H, NH), 6.75 (br s, 1H, NH_2), 5.81 (br s, 1H, NH_2), 5.26 (s, 2H, C*H*$_2$-Ph), 4.75 (d, *J* = 9.1 Hz, 1H, *CH*C$(CH_3)_3$),1.14 (s, 9H, C$(CH_3)_3$). LRMS (CI) m/z calcd. for $C_{22}H_{25}FN_3O_2$ $[M+H]^+$: 382.2; found: 382.2.

USC UNIVERSIDADE DE SANTIAGO DE COMPOSTELA

***N*-(1-(*tert*-butylamino)-3,3-dimethyl-1-oxobutan-2-yl)-1-(4-fluorobenzyl)-1*H*-indole-3-carboxamide (37f).** Yield: 58%. Mp: 210-211 ºC. ^{1}H NMR (300 MHz, $CDCl_3$) δ (ppm): 8.07 (d, *J* = 7.7 Hz, 1H, Ar-H), 7.77 (s, 1H, Ar-H), 7.34 – 7.21 (m, 3H, Ar-H), 7.17 – 7.07 (m, 2H, Ar-H), 7.05 – 6.94 (m, 2H, Ar-H), 6.87 (d, *J* = 8.2 Hz, 1H, NH), 5.85 (brs, 1H, NH), 5.30 (s, 2H, C*H*$_2$-Ph), 4.46 (d, *J* = 9.0 Hz, 1H, CH), 1.34 (s, 9H, C(CH_3)$_3$), 1.10 (s, 9H, C(CH_3)$_3$). ^{13}C NMR (75 MHz, $CDCl_3$) δ (ppm): 170.2, 164.5, 160.8, 136.7, 131.9, 131.7, 128.8, 128.7, 125.7, 122.8, 121.9, 120.6, 116.0, 115.8, 111.6, 110.4, 60.4, 51.5, 49.9, 35.4, 28.7, 26.9. HRMS (APCI) m/z calcd for $C_{26}H_{33}FN_3O_2$ $[M+H]^+$: 438.2479; found: 438.2556.

***N*-(1-(benzylamino)-3,3-dimethyl-1-oxobutan-2-yl)-1-(4-fluorobenzyl)-1*H*-indole-3-carboxamide (37g).** Yield: 45%. Mp: 196-197 ºC. ^{1}H NMR (300 MHz, $CDCl_3$) δ (ppm): 8.07 – 7.99 (m, 1H, Ar-H), 7.64 (s, 1H, Ar-H), 7.38 – 7.12 (m, 9H, Ar-H, NH), 7.12 – 6.84 (m, 5H, Ar-H, NH), 5.24 (s, 2H, C*H*$_2$-Ph), 4.74 (d, *J* = 9.2 Hz, 1H, CH), 4.61 – 4.41 (m, 1H, NH-C*H*$_2$-Ph), 4.38 – 4.23 (m, 1H, NH-C*H*$_2$-Ph), 1.09 (s, 9H, C(CH_3)$_3$). ^{13}C NMR (75 MHz, $CDCl_3$) δ (ppm): 171.1, 164.7, 164.0, 160.8, 138.2, 136.7, 131.8, 128.6, 128.5, 127.8, 127.2, 122.9, 122.0, 120.5, 116.0, 115.7, 111.3, 110.5, 60.2, 49.9, 43.5, 35.3, 26.9. LRMS (CI) m/z calcd for $C_{29}H_{31}FN_3O_2$ $[M+H]^+$: 472.2; found: 472.2.

***N*-(2-(*tert*-butylamino)-2-oxo-1-phenylethyl)-1-(4-fluorobenzyl)-1*H*-indole-3-carboxamide (37h).** Yield: 49%. Mp: 188-189 ºC. ^{1}H NMR (300 MHz, $CDCl_3$) δ (ppm): 8.18 – 8.09 (m, 1H, Ar-H), 7.88 – 7.79 (m, 1H, NH), 7.72 (s, 1H, Ar-H), 7.56 – 7.19 (m, 8H, Ar-H), 7.12 – 7.03 (m, 2H, Ar-H), 7.03 – 6.92 (m, 2H, Ar-H), 5.90 (s, 1H, NH), 5.71 (d, *J* = 6.4 Hz, 1H, CH), 5.24 (s, 2H, C*H*$_2$-Ph), 1.29 (s, 9H, C(CH_3)$_3$). LRMS (CI) m/z calcd for $C_{28}H_{29}FN_3O_2$ $[M+H]^+$: 458.2; found: 458.2.

***N*-(1-(adamantan-1-yl)-2-(*tert*-butylamino)-2-oxoethyl)-1-(4-fluorobenzyl)-1*H*-indole-3-carboxamide (37i).** Yield: 42%. Mp: 315-316 ºC. ^{1}H NMR (300 MHz, $CDCl_3$) δ (ppm): 8.10 (d, *J* = 8.6 Hz, 1H, Ar-H), 7.80 (s, 1H, Ar-H), 7.36 – 7.21 (m, 3H, Ar-H), 7.20 – 7.09 (m, 2H, Ar-H), 7.08 – 6.97 (m, 2H, Ar-H), 6.87 (d, *J* = 8.7 Hz, 1H, NH), 5.61 (s, 1H, NH), 5.32 (s, 2H, C*H*$_2$-Ph), 4.28 (d, *J* = 9.0 Hz, 1H, CH), 2.10 – 1.97 (m, 4H, Ad), 1.84 – 1.59 (m, 11H, Ad), 1.39 (s, 9H, C(CH_3)$_3$). LRMS (CI) m/z calcd for $C_{32}H_{39}FN_3O_2$ $[M+H]^+$: 516.3; found: 516.3.

USC

***N*-(1-(*tert*-butylamino)-2-methyl-1-oxopropan-2-yl)-1-(4-fluorobenzyl)-1*H*-indole-3-carboxamide (37j).** Yield: 54%. Mp: 158-159 ºC. ^{1}H NMR (300 MHz, $CDCl_3$) δ (ppm): 8.05 (d, *J* = 8.4 Hz, 1H, Ar-H), 7.72 (s, 1H, Ar-H), 7.33 – 7.18 (m, 3H, Ar-H), 7.15 – 7.04 (m, 2H, Ar-H), 7.01 – 6.92 (m, 2H, Ar-H), 6.88 (s, 1H, NH), 6.51 (s, 1H, NH), 5.26 (s, 2H, C*H*$_2$-Ph), 1.69 (s, 6H, CH_3, CH_3), 1.37 (s, 9H, $C(CH_3)_3$). LRMS (CI) m/z calcd for $C_{24}H_{29}FN_3O_2$ $[M+H]^+$: 410.2; found: 410.2.

***N*-(3-(*tert*-butylcarbamoyl)pentan-3-yl)-1-(4-fluorobenzyl)-1*H*-indole-3-carboxamide (37k).** Yield: 51%. Mp: 197-199 ºC. ^{1}H NMR (300 MHz, $CDCl_3$) δ (ppm): 8.20 (d, *J* = 8.0 Hz, 1H, Ar-H), 7.78 (s, 1H, Ar-H), 7.62 (s, 1H, NH), 7.37 – 7.19 (m, 3H, Ar-H), 7.17 – 7.08 (m, 2H, Ar-H), 7.06 – 6.92 (m, 2H, Ar-H), 5.54 (s, 1H, NH) 5.30 (s, 2H, C*H*$_2$-Ph), 2.90 (dq, *J* = 15.0, 7.3 Hz, 2H, C*H*$_2$$CH_3$), 1.51 (dq, *J* = 14.4, 7.4 Hz, 2H, C*H*$_2$$CH_3$), 1.42 (s, 9H, $C(CH_3)_3$), 0.85 (t, *J* = 7.3 Hz, 6H, CH_2C*H*$_3$, CH_2C*H*$_3$). LRMS (CI) m/z calcd for $C_{26}H_{33}FN_3O_2$ $[M+H]^+$: 438.2; found: 438.2.

***N*-(2-(*tert*-butylamino)-2-oxoethyl)-1-(4-fluorobenzyl)-*N*-methyl-1*H*-indole-3-carboxamide (37l).** Yield: 56%. Mp: 142-143 ºC. ^{1}H NMR (300 MHz, $CDCl_3$) δ (ppm): 7.94 – 7.83 (m, 1H, Ar-H), 7.46 (s, 1H, Ar-H), 7.32 – 7.21 (m, 3H, Ar-H), 7.20 – 7.08 (m, 2H, Ar-H), 7.06 – 6.90 (m, 2H, Ar-H), 6.51 (s, 1H, NH), 5.28 (s, 2H, C*H*$_2$-Ph), 4.09 (s, 2H, CH_2), 3.24 (s, 3H, NCH_3), 1.36 (s, 6H, $C(CH_3)_3$), 1.26 (s, 3H, $C(CH_3)_3$). LRMS (CI) m/z calcd for $C_{23}H_{27}FN_3O_2$ $[M+H]^+$: 396.2; found: 396.2.

***N*-(1-amino-3-methyl-1-oxobutan-2-yl)-1-(4-fluorobenzyl)-*N*-methyl-1*H*-indole-3-carboxamide (37m).** Yield: 18%. Mp: 176-178 ºC. ^{1}H NMR (300 MHz, $CDCl_3$) δ (ppm): 7.84 – 7.64 (m, 1H, Ar-H), 7.48 (s, 1H, Ar-H), 7.35 – 7.21 (m, 3H, Ar-H), 7.18 – 7.08 (m, 2H, Ar-H), 7.07 – 6.96 (m, 2H, Ar-H), 6.85 (s, 2H, NH_2), 5.31 (s, 2H, C*H*$_2$-Ph), 4.60 (d, *J* = 11.3 Hz, 1H, CH), 3.13 (s, 3H, NCH_3), 2.55 – 2.30 (m, 1H, C*H*$(CH_3)_2$), 1.06 (t, *J* = 6.2 Hz, 6H, CH(C*H*$_3$)$_2$). LRMS (CI) m/z calcd for $C_{22}H_{25}FN_3O_2$ $[M+H]^+$: 381.2; found: 381.2.

***N*-(1-(*tert*-butylamino)-3-methyl-1-oxobutan-2-yl)-1-(4-fluorobenzyl)-*N*-methyl-1*H*-indole-3-carboxamide (37n).** Yield: 54%. Mp: 199-200 ºC. ^{1}H NMR (300 MHz, $CDCl_3$) δ (ppm): 7.89 – 7.72 (m, 1H, Ar-H), 7.45 (s, 1H, Ar-H), 7.32 – 7.17 (m,

USC UNIVERSIDADE DE SANTIAGO DE COMPOSTELA

3H, Ar-H), 7.17 – 7.06 (m, 2H, Ar-H), 7.05 – 6.92 (m, 2H, Ar-H), 6.68 (s, 1H, NH), 5.30 (s, 2H, C*H*$_2$-Ph), 4.48 (d, *J* = 10.5 Hz, 1H, CH), 3.13 (s, 3H, NCH$_3$), 2.50 – 2.30 (m, 1H, C*H*(CH$_3$)$_2$), 1.35 (s, 9H, C(CH$_3$)$_3$), 1.08 – 0.96 (m, 6H, CH(C*H*$_3$)$_2$). LRMS (CI) m/z calcd for $C_{26}H_{33}FN_3O_2$ $[M+H]^+$: 438.2; found: 438.2.

***N*-(1-(benzylamino)-3-methyl-1-oxobutan-2-yl)-1-(4-fluorobenzyl)-*N*-methyl-1*H*-indole-3-carboxamide (37o).** Yield: 48%. Mp: 132-133 ºC. ^{1}H NMR (300 MHz, $CDCl_3$) δ (ppm): 7.77 – 7.65 (m, 1H, Ar-H), 7.39 (s, 1H, Ar-H), 7.37 – 7.18 (m, 9H, Ar-H, NH), 7.17 – 7.08 (m, 2H, Ar-H), 7.07 – 6.95 (m, 2H, Ar-H), 5.29 (s, 2H, C*H*$_2$-Ph), 4.62 (d, *J* = 11.2 Hz, 1H, CH), 4.53 (dd, *J* = 15.0, 6.5 Hz, 1H, NH-C*H*$_2$-Ph), 4.39 (dd, *J* = 15.1, 5.4 Hz, 1H, NH-C*H*$_2$-Ph), 3.11 (s, 3H, NCH$_3$), 2.57 – 2.38 (m, 1H, C*H*(CH$_3$)$_2$), 1.14 – 0.99 (m, 6H, CH(C*H*$_3$)$_2$). HRMS (APCI) m/z calcd for $C_{29}H_{31}FN_3O_2$ $[M+H]^+$: 472.2322; found: 472.2396.

***N*-(1-amino-3,3-dimethyl-1-oxobutan-2-yl)-1-(4-fluorobenzyl)-*N*-methyl-1*H*-indole-3-carboxamide (37p).** Yield: 18%. Mp: 176-178 ºC. ^{1}H NMR (300 MHz, $CDCl_3$) δ (ppm): 7.91 – 7.79 (m, 1H, Ar-H), 7.48 (s, 1H, Ar-H), 7.32 – 7.20 (m, 3H, Ar-H), 7.16 – 7.07 (m, 2H, Ar-H), 7.01 (t, *J* = 8.8 Hz, 2H, Ar-H), 6.44 (s, 2H, NH$_2$), 5.35 – 5.26 (m, 3H, C*H*$_2$-Ph, CH), 3.28 (s, 3H, NCH$_3$), 1.22 (s, 9H, C(CH$_3$)$_3$). LRMS (CI) m/z calcd for $C_{23}H_{27}FN_3O_2$ $[M+H]^+$: 396.2; found: 396.2.

***N*-(1-(*tert*-butylamino)-3,3-dimethyl-1-oxobutan-2-yl)-1-(4-fluorobenzyl)-*N*-methyl-1*H*-indole-3-carboxamide (37q).** Yield: 53%. Mp: 141-143 ºC. ^{1}H NMR (300 MHz, $CDCl_3$) δ (ppm): 7.94 – 7.79 (m, 1H, Ar-H), 7.48 (s, 1H, Ar-H), 7.32 – 7.20 (m, 3H, Ar-H), 7.20 – 7.07 (m, 2H, Ar-H), 7.07 – 6.93 (m, 2H, Ar-H), 6.13 (s, 1H, NH), 5.32 (s, 2H, C*H*$_2$-Ph), 4.95 (s, 1H, CH), 3.30 (s, 3H, NCH$_3$), 1.35 (s, 9H, C(CH$_3$)$_3$), 1.20 (s, 9H, C(CH$_3$)$_3$). LRMS (CI) m/z calcd for $C_{27}H_{35}FN_3O_2$ $[M+H]^+$: 452.3; found: 452.3.

***N*-(1-(benzylamino)-3,3-dimethyl-1-oxobutan-2-yl)-1-(4-fluorobenzyl)-*N*-methyl-1*H*-indole-3-carboxamide (37r).** Yield: 51%. Mp: 140-141 ºC. ^{1}H NMR (300 MHz, $CDCl_3$) δ (ppm): 7.78 (d, *J* = 8.6 Hz ,1H, Ar-H), 7.40 (s, 1H, Ar-H), 7.33 – 7.17 (m, 8H, Ar-H), 7.16 – 7.06 (m, 2H, Ar-H), 7.05 – 6.94 (m, 3H, Ar-H, NH), 5.28 (s, 2H, C*H*$_2$-Ph), 5.11 (s, 1H, CH), 4.49 – 4.33 (m, 2H, NH-C*H*$_2$-Ph), 3.26 (s, 3H, NCH$_3$), 1.22

USC UNIVERSIDADE DE COMPOSTELA

(s, 9H, C(CH_3)$_3$). HRMS (APCI) m/z calcd for $C_{30}H_{33}FN_3O_2$ $[M+H]^+$: 486.2479; found: 486.2552.

***N*-(2-(*tert*-butylamino)-2-oxo-1-phenylethyl)-1-(4-fluorobenzyl)-*N*-methyl-1*H*-indole-3-carboxamide (37s).** Yield: 45%. Mp: 140-141 ºC. ^{1}H NMR (300 MHz, $CDCl_3$) δ (ppm): 7.90 – 7.79 (m, 1H, Ar-H), 7.54 – 7.31 (m, 7H, Ar-H), 7.31 – 7.17 (m, 2H, Ar-H), 7.17 – 7.05 (m, 2H, Ar-H), 7.05 – 6.93 (m, 2H, Ar-H), 6.23 (s, 1H, CH), 5.95 (s, 1H, NH), 5.27 (s, 2H, C*H*$_2$-Ph), 3.04 (s, 3H, NCH_3), 1.39 (s, 9H, C(CH_3)$_3$). LRMS (CI) m/z calcd for $C_{29}H_{31}FN_3O_2$ $[M+H]^+$: 472.2; found: 472.2.

***N*-(1-(adamantan-1-yl)-2-(*tert*-butylamino)-2-oxoethyl)-1-(4-fluorobenzyl)-*N*-methyl-1*H*-indole-3-carboxamide (37t).** Yield: 48%. Mp: 176-177 ºC. ^{1}H NMR (300 MHz, $CDCl_3$) δ (ppm): 7.90 (d, *J* = 6.4 Hz, 1H, Ar-H), 7.48 (s, 1H, Ar-H), 7.32 – 7.19 (m, 3H, Ar-H), 7.16 – 7.05 (m, 2H, Ar-H), 7.05 – 6.94 (m, 2H, Ar-H), 6.12 (s, 1H, NH), 5.30 (s, 2H, C*H*$_2$-Ph), 4.79 (s, 1H, CH), 3.34 (s, 3H, NCH_3), 2.06 – 1.91 (m, 6H, Ad), 1.89 – 1.62 (m, 9H, Ad), 1.35 (s, 9H, C(CH_3)$_3$). LRMS (CI) m/z calcd for $C_{33}H_{41}FN_3O_2$ $[M+H]^+$: 530.3; found: 530.3.

***N*-(1-(*tert*-butylamino)-2-methyl-1-oxopropan-2-yl)-1-(4-fluorobenzyl)-*N*-methyl-1*H*-indole-3-carboxamide (37u).** Yield: 53%. Mp: 172-173 ºC. ^{1}H NMR (300 MHz, $CDCl_3$) δ (ppm): 7.83 – 7.69 (m, 1H, Ar-H), 7.54 (s, 1H, Ar-H), 7.34 – 7.20 (m, 3H, Ar-H), 7.18 – 7.08 (m, 2H, Ar-H), 7.05 – 6.93 (m, 2H, Ar-H), 6.33 (s, 1H, NH), 5.28 (s, 2H, C*H*$_2$-Ph), 3.12 (s, 3H, NCH_3), 1.62 (s, 6H, CH_3, CH_3), 1.35 (s, 9H, C(CH_3)$_3$). LRMS (CI) m/z calcd for $C_{25}H_{31}FN_3O_2$ $[M+H]^+$: 424.2; found: 424.2.

***N*-(3-(*tert*-butylcarbamoyl)pentan-3-yl)-1-(4-fluorobenzyl)-*N*-methyl-1*H*-indole-3-carboxamide (37v).** Yield: 52%. Mp: 185-186 ºC. ^{1}H NMR (300 MHz, $CDCl_3$) δ (ppm): 7.83 – 7.71 (m, 1H, Ar-H), 7.49 (s, 1H, Ar-H), 7.31 – 7.18 (m, 3H, Ar-H), 7.17 – 7.08 (m, 2H, Ar-H), 7.07 – 6.91 (m, 2H, Ar-H), 6.55 (s, 1H, NH), 5.28 (s, 2H, C*H*$_2$-Ph), 3.16 (s, 3H, NCH_3), 2.31 – 1.96 (m, 4H, C*H*$_2$$CH_3$, C*H*$_2$$CH_3$), 1.36 (s, 9H, C($CH_3$)$_3$), 0.96 (t, *J* = 7.3 Hz, 6H, CH_2C*H*$_3$, CH_2C*H*$_3$). LRMS (CI) m/z calcd for $C_{27}H_{35}FN_3O_2$ $[M+H]^+$: 452.3; found: 452.3.

USC UNIVERSIDADE DE SANTIAGO DE COMPOSTELA

***N*-(2-(*tert*-butylamino)-2-oxoethyl)-1-(cyclohexylmethyl)-1*H*-indole-3-carboxamide (38a).** Yield: 49%. Mp: 220-221 ºC. ^{1}H NMR (300 MHz, $CDCl_3$) δ (ppm): 8.17 – 8.02 (m, 1H, Ar-H), 7.73 (s, 1H, Ar-H), 7.42 – 7.32 (m, 1H, Ar-H), 7.32 – 7.21 (m, 2H, Ar-H), 6.96 (t, *J* = 5.1 Hz, 1H, NH), 6.28 (s, 1H, NH), 4.11 (d, *J* = 5.1 Hz, 2H, CH_2), 3.93 (d, *J* = 7.2 Hz, 2H, C*H*$_2$-Cy), 1.95 – 1.54 (m, 6H, Cy), 1.40 (s, 9H, $C(CH_3)_3$), 1.27 – 1.09 (m, 3H, Cy), 1.09 – 0.84 (m, 2H, Cy). LRMS (CI) m/z calcd for $C_{22}H_{32}N_3O_2$ $[M+H]^+$: 370.2; found: 370.2.

***N*-(1-Amino-3-methyl-1-oxobutan-2-yl)-1-(cyclohexylmethyl)-1*H*-indole-3-carboxamide (38b).** Yield: 18%. Mp: 198-200 ºC. ^{1}H NMR (300 MHz, $CDCl_3$) δ (ppm): 8.00 (m, 1H, Ar-H), 7.68 (s, 1H, Ar-H), 7.37 (m, 1H, Ar-H), 7.31 – 7.22 (m, 2H, Ar-H), 6.57 (d, *J* = 8.5 Hz, 1H, NH), 6.25 (br s, 1H, NH_2), 5.50 (br s, 1H, NH_2), 4.61 (dd, *J* = 8.5, 6.6 Hz 1H, *CH*CH$(CH_3)_2$), 3.94 (d, *J* = 7.2 Hz, 2H, C*H*$_2$-Cy), 2.31 (m, 1H, CHC*H*$(CH_3)_2$), 1.86 (m, 1H, CH-Cy), 1.77–1.55 (m, 5H, Cy), 1.27–0.91 (m, 11 H, Cy, CHCH*(CH$_3$)$_2$*). LRMS (CI) m/z calcd. for $C_{21}H_{30}N_3O_2$ $[M+H]^+$: 356.2; found: 356.2.

***N*-(1-(*tert*-butylamino)-3-methyl-1-oxobutan-2-yl)-1-(cyclohexylmethyl)-1*H*-indole-3-carboxamide (38c).** Yield: 54%. Mp: 192-194 ºC. ^{1}H NMR (300 MHz, $CDCl_3$) δ (ppm): 8.20 – 8.11 (m, 1H, Ar-H), 7.84 (s, 1H, Ar-H) 7.44 – 7.23 (m, 3H, Ar-H), 7.16 (d, *J* = 8.7 Hz, 1H, NH), 6.38 (s, 1H, NH), 4.51 (t, *J* = 8.7 Hz, 1H, CH), 3.91 (d, *J* = 7.2 Hz, 2H, C*H*$_2$-Cy), 2.24 (h, *J* = 6.6 Hz, 1H, C*H*$(CH_3)_2$), 1.98 – 1.53 (m, 6H, C*H*$(CH_3)_2$, Cy), 1.39 (s, 9H, $C(CH_3)_3$), 1.32 – 0.83 (m, 11H, CH(C*H*$_3$)$_2$, Cy). ^{13}C NMR (75 MHz, $CDCl_3$) δ (ppm): 171.4, 168.6, 136.9, 135.7, 132.1, 122.3, 121.8, 121.4, 120.8, 110.3, 58.9, 53.6, 53.4, 51.6, 38.5, 38.4, 31.5, 30.9, 28.7, 26.2, 25.6, 19.4, 18.7. HRMS (APCI) m/z calcd for $C_{25}H_{38}N_3O_2$ $[M+H]^+$: 412.2886; found: 412.2962.

***N*-(1-(benzylamino)-3-methyl-1-oxobutan-2-yl)-1-(cyclohexylmethyl)-1*H*-indole-3-carboxamide (38d).** Yield: 45%. Mp: 155-156 ºC. ^{1}H NMR (300 MHz, $CDCl_3$) δ (ppm): 8.07 (d, *J* = 6.9 Hz, 1H, Ar-H), 7.65 (s, 1H, Ar-H), 7.60 (brs, 1H, NH), 7.38 – 7.14 (m, 8H, Ar-H), 7.02 (d, *J* = 8.4 Hz, 1H, NH), 4.70 (t, *J* = 8.0 Hz, 1H, CH), 4.50 (dd, *J* = 14.9, 6.0 Hz, 1H, C*H*$_2$-Ph), 4.31 (dd, *J* = 15.0, 5.4 Hz, 1H, C*H*$_2$-Ph), 3.81 (d, *J* = 7.0 Hz, 2H, CH_2-Cy), 2.30 – 2.13 (m, 1H, C*H*$(CH_3)_2$), 2.09 – 1.94 (m, 1H, C*H*-Cy), 1.83 –1.45 (m, 5H, Cy), 1.20 – 0.82 (m, 11H, Cy, CH(C*H*$_3$)$_2$). HRMS (APCI) m/z calcd for $C_{28}H_{36}N_3O_2$ $[M+H]^+$: 446.2729; found: 446.2792.

***N*-(1-Amino-3,3-dimethyl-1-oxobutan-2-yl)-1-(cyclohexylmethyl)-1*H*-indole-3-carboxamide (38e).** Yield: 16%. Mp: 201-202 ºC. ^{1}H NMR (300 MHz, $CDCl_3$) δ (ppm): 8.02 (m, 1H, Ar-H), 7.68 (s, 1H, Ar-H), 7.36 (m, 1H, Ar-H), 7.26 (m, 2H, Ar-H), 7.13 (br s, 1H, NH_2), 6.82 (d, *J* = 9.5 Hz, 1H, NH), 5.96 (br s, 1H, NH_2), 4.82 (d, *J* = 9.2 Hz, 1H, *CH*C$(CH_3)_3$), 3.91 (d, *J* = 7.1 Hz, 2H, C*H*$_2$-Cy), 1.83 (m, 1H, *CH*-Cy), 1.76–1.54 (m, 5H, Cy), 1.27–0.89 (m, 14 H, Cy, C$(CH_3)_3$). LRMS (CI) m/z calcd. for $C_{22}H_{32}N_3O_2$ $[M+H]^+$: 370.2; found: 370.2.

***N*-(1-(*tert*-butylamino)-3,3-dimethyl-1-oxobutan-2-yl)-1-(cyclohexylmethyl)-1*H*-indole-3-carboxamide (38f).** Yield: 55%. Mp:246-248 ºC. ^{1}H NMR (300 MHz, $CDCl_3$) δ (ppm): 8.13 – 8.01 (m, 1H, Ar-H), 7.72 (s, 1H, Ar-H), 7.44 – 7.33 (m, 1H, Ar-H), 7.32 – 7.22 (m, 2H, Ar-H), 6.88 (d, *J* = 9.1 Hz, 1H, NH), 6.27 (s, 1H, NH), 4.57 (d, *J* = 9.0 Hz, 1H, CH), 3.95 (d, *J* = 7.1 Hz, 2H, C*H*$_2$-Cy), 1.95 – 1.80 (m, 1H, Cy), 1.78 – 1.56 (m, 5H, Cy), 1.37 (s, 9H, C$(CH_3)_3$), 1.27 – 0.88 (m, 14H, C$(CH_3)_3$, Cy). ^{13}C NMR (75 MHz, $CDCl_3$) δ (ppm): 170.3, 164.7, 137.0, 132.3, 125.4, 122.3, 121.5, 120.4, 110.5, 110.4, 60.3, 53.3, 51.5, 45.8, 38.5, 35.3, 31.0, 31.0, 28.7, 26.9, 26.2, 25.6. HRMS (APCI) m/z calcd for $C_{26}H_{40}N_3O_2$ $[M+H]^+$: 426.3042; found: 426.3122.

***N*-(1-(benzylamino)-3,3-dimethyl-1-oxobutan-2-yl)-1-(cyclohexylmethyl)-1*H*-indole-3-carboxamide (38g).** Yield: 48%. Mp: 188-189 ºC. ^{1}H NMR (300 MHz, $CDCl_3$) δ (ppm): 8.06 – 7.98 (m, 1H, Ar-H), 7.57 (s, 1H, Ar-H), 7.36 (d, *J* = 7.5 Hz, 1H, Ar-H), 7.32 – 7.13 (m, 8H, Ar-H, NH), 6.88 (d, *J* = 9.2 Hz, 1H, NH), 4.86 – 4.70 (m, 1H, CH), 4.56 (dd, *J* = 14.7, 6.2 Hz, 1H, C*H*$_2$-Ph), 4.32 (dd, *J* = 15.1, 3.5 Hz, 1H, C*H*$_2$-Ph), 3.89 (d, *J* = 7.2 Hz, 2H, C*H*$_2$-Cy), 1.99 – 1.46 (m, 6H, Cy), 1.29 – 0.81 (m, 14H, C$(CH_3)_3$, Cy). LRMS (CI) m/z calcd for $C_{29}H_{38}N_3O_2$ $[M+H]^+$: 460.3; found: 460.3.

***N*-(2-(*tert*-butylamino)-2-oxo-1-phenylethyl)-1-(cyclohexylmethyl)-1*H*-indole-3-carboxamide (38h).** Yield: 47%. Mp: 215-217 ºC. ^{1}H NMR (300 MHz, $CDCl_3$) δ (ppm): 8.20 – 8.07 (m, 1H, Ar-H), 7.70 (s, 1H, Ar-H), 7.61 – 7.47 (m, 3H, Ar-H), 7.44 – 7.20 (m, 6H, Ar-H, NH), 6.03 (s, 1H, NH), 5.76 (d, *J* = 6.7 Hz, 1H, CH), 3.92 (d, *J* = 7.0 Hz, 2H, C*H*$_2$-Cy), 1.96 – 1.78 (m, 1H, C*H*-Cy), 1.78 – 1.55 (m, 5H, Cy), 1.32 (s, 9H, C$(CH_3)_3$), 1.26 – 1.08 (m, 3H, Cy), 1.07 – 0.87 (m, 2H, Cy). LRMS (CI) m/z calcd for $C_{28}H_{36}N_3O_2$ $[M+H]^+$: 446.3; found: 446.3.

***N*-(1-(adamantan-1-yl)-2-(*tert*-butylamino)-2-oxoethyl)-1-(cyclohexylmethyl)-1*H*-indole-3-carboxamide (38i).** Yield: 44%. Mp: 269-270 ºC. ^{1}H NMR (300 MHz, $CDCl_3$) δ (ppm): 8.16 – 8.06 (m, 1H, Ar-H), 7.73 (s, 1H, Ar-H), 7.41 – 7.33 (m, 1H, Ar-H), 7.33 – 7.23 (m, 2H, Ar-H), 6.90 (d, *J* = 9.0 Hz, 1H, NH), 6.23 (s, 1H, NH), 4.43 (d, *J* = 9.1 Hz, 1H, CH), 3.95 (d, *J* = 7.1 Hz, 2H, C*H*$_2$-Cy), 2.06 – 1.94 (m, 3H, Ad, Cy), 1.94 – 1.57 (m, 18H, Ad, Cy), 1.38 (s, 9H, $C(CH_3)_3$), 1.28 – 1.09 (m, 3H, Cy), 1.11 – 0.89 (m, 2H, Cy). LRMS (CI) m/z calcd for $C_{32}H_{46}N_3O_2$ $[M+H]^+$: 504.4; found: 504.4.

***N*-(1-(*tert*-butylamino)-2-methyl-1-oxopropan-2-yl)-1-(cyclohexylmethyl)-1*H*-indole-3-carboxamide (38j).** Yield: 44%. Mp: 222-223 ºC. ^{1}H NMR (300 MHz, $CDCl_3$) δ (ppm): 8.07 – 7.97 (m, 1H, Ar-H), 7.68 (s, 1H, Ar-H), 7.42 – 7.33 (m, 1H, Ar-H), 7.33 – 7.22 (m, 2H, Ar-H), 6.77 (s, 1H, NH), 6.65 (s, 1H, NH), 3.94 (d, *J* = 7.2 Hz, 2H, C*H*$_2$-Cy), 1.96 – 1.79 (m, 1H, C*H*-Cy), 1.79 – 1.57 (m, 11H, CH_3, CH_3, Cy), 1.40 (s, 9H, $C(CH_3)_3$), 1.27 – 1.10 (m, 3H, Cy), 1.10 – 0.91 (m, 2H, Cy). LRMS (CI) m/z calcd for $C_{24}H_{36}N_3O_2$ $[M+H]^+$: 398.3; found: 398.3.

***N*-(3-(*tert*-butylcarbamoyl)pentan-3-yl)-1-(cyclohexylmethyl)-1*H*-indole-3-carboxamide (38k).** Yield: 48%. Mp: 224-225 ºC. ^{1}H NMR (300 MHz, $CDCl_3$) δ (ppm): 8.23 – 8.14 (m, 1H, Ar-H), 7.70 (s, 1H, Ar-H), 7.55 (s, 1H, NH), 7.41 – 7.22 (m, 3H, Ar-H), 5.61 (s, 1H, NH), 3.95 (d, *J* = 7.2 Hz, 2H, C*H*$_2$-Cy), 2.90 (dq, *J* = 14.9, 7.5 Hz, 2H, C*H*$_2$$CH_3$), 1.96 – 1.80 (m, 1H, C*H*-Cy), 1.79 – 1.59 (m, 5H, Cy), 1.53 (dq, *J* = 13.8, 6.9 Hz, 2H, C*H*$_2$$CH_3$), 1.43 (s, 9H, $C(CH_3)_3$), 1.30 – 1.12 (m, 3H, Cy), 1.11 – 0.93 (m, 2H, Cy), 0.87 (t, *J* = 7.3 Hz, 6H, CH_2C*H*$_3$, CH_2C*H*$_3$). LRMS (CI) m/z calcd for $C_{26}H_{40}N_3O_2$ $[M+H]^+$: 426.3; found: 426.3.

***N*-(2-(*tert*-butylamino)-2-oxoethyl)-1-(cyclohexylmethyl)-*N*-methyl-1*H*-indole-3-carboxamide (38l).** Yield: 46%. Mp: 152-153 ºC. ^{1}H NMR (300 MHz, $CDCl_3$) δ (ppm): 7.88 (d, *J* = 7.6 Hz, 1H, Ar-H), 7.40 (s, 1H, Ar-H), 7.38 – 7.30 (m, 1H, Ar-H), 7.31 – 7.16 (m, 2H, Ar-H), 6.60 (s, 1H, NH), 4.09 (s, 2H, CH_2), 3.94 (d, *J* = 7.0 Hz, 2H, C*H*$_2$-Cy), 3.24 (s, 3H, NCH_3), 1.95 – 1.55 (m, 6H, Cy), 1.37 (s, 9H, $C(CH_3)_3$), 1.30 – 1.09 (m, 3H, Cy), 1.09 – 0.90 (m, 2H, Cy). LRMS (CI) m/z calcd for $C_{23}H_{34}N_3O_2$ $[M+H]^+$: 384.3; found: 384.3.

USC UNIVERSIDADE DE SANTIAGO DE COMPOSTELA

***N*-(1-amino-3-methyl-1-oxobutan-2-yl)-1-(cyclohexylmethyl)-*N*-methyl-1*H*-indole-3-carboxamide (38m).** Yield: 17%. Mp: 174-175 ºC. ^{1}H NMR (300 MHz, $CDCl_3$) δ (ppm): 7.79 (d, *J* = 7.6 Hz, 1H, Ar-H), 7.43 (s, 1H, Ar-H), 7.42 – 7.33 (m, 1H, Ar-H), 7.31 – 7.17 (m, 2H, Ar-H), 6.91 (brs, 1H, NH_2), 5.31 (brs, 1H NH_2), 4.60 (d, *J* = 11.2 Hz, 1H, CH), 3.96 (d, *J* = 7.1 Hz, 2H, C*H*$_2$-Cy), 3.14 (s, 3H, NCH_3), 2.57 – 2.29 (m, 1H, C*H*$(CH_3)_2$), 1.95 – 1.80 (m, 1H, C*H*-Cy), 1.79 – 1.49 (m, 5H, Cy), 1.30 – 0.91 (m, 11H, Cy, CH(C*H*$_3$)$_2$). LRMS (CI) m/z calcd for $C_{22}H_{32}N_3O_2$ $[M+H]^+$: 367.2; found: 367.2.

***N*-(1-(*tert*-butylamino)-3-methyl-1-oxobutan-2-yl)-1-(cyclohexylmethyl)-*N*-methyl-1*H*-indole-3-carboxamide (38n).** Yield: 57%. Mp: 149-150 ºC. ^{1}H NMR (300 MHz, $CDCl_3$) δ (ppm): 7.80 (d, *J* = 6.9 Hz, 1H, Ar-H), 7.42 – 7.32 (m, 2H, Ar-H), 7.30 – 7.14 (m, 2H, Ar-H), 6.73 (s, 1H, NH), 4.47 (d, *J* = 11.4 Hz, 1H, CH), 4.40 (d, *J* = 7.2 Hz, 2H, C*H*$_2$-Cy), 3.13 (s, 3H, NCH_3), 2.50 – 2.30 (m, 1H, C*H*$(CH_3)_2$), 1.94 – 1.80 (m, 1H, Cy), 1.78 –1.60 (m, 5H, Cy), 1.35 (s, 9H, $C(CH_3)_3$), 1.25 – 0.90 (m, 11H, CH(C*H*$_3$)$_2$, Cy). ^{13}C NMR (75 MHz, $CDCl_3$) δ (ppm): 169.6, 168.9, 136.2, 131.1, 126.7, 122.4, 121.2, 121.0, 110.2, 110.1, 53.3, 51.0, 38.6, 31.1, 31.0, 28.8, 26.2, 25.6, 20.0, 19.0. HRMS (APCI) m/z calcd for $C_{26}H_{40}N_3O_2$ $[M+H]^+$: 426.3042; found: 426.3121.

***N*-(1-(benzylamino)-3-methyl-1-oxobutan-2-yl)-1-(cyclohexylmethyl)-*N*-methyl-1*H*-indole-3-carboxamide (38o).** Yield: 46%. Oil at room temperature. ^{1}H NMR (300 MHz, $CDCl_3$) δ (ppm): 7.72 (d, *J* = 7.7 Hz, 1H, Ar-H), 7.47 – 7.32 (m, 3H, Ar-H), 7.32 – 7.15 (m, 7H, Ar-H, NH), 4.63 (d, *J* = 11.4 Hz, 1H, CH), 4.54 (dd, *J* = 15.1, 6.4 Hz, 1H, C*H*$_2$-Ph), 4.40 (dd, *J* = 15.1, 5.7 Hz, 1H, C*H*$_2$-Ph), 3.95 (d, *J* = 7.2 Hz, 2H, C*H*$_2$-Cy), 3.13 (s, 3H, NCH_3), 2.58 – 2.40 (m, 1H, C*H*$(CH_3)_2$), 1.93 – 1.80 (m, 1H, Cy), 1.78 – 1.55 (m, 5H, Cy), 1.31 – 0.92 (m, 11H, CH(C*H*$_3$)$_2$, Cy). LRMS (CI) m/z calcd for $C_{29}H_{38}N_3O_2$ $[M+H]^+$: 460.3; found: 460.3.

***N*-(1-amino-3,3-dimethyl-1-oxobutan-2-yl)-1-(cyclohexylmethyl)-*N*-methyl-1*H*-indole-3-carboxamide (38p).** Yield: 16%. Mp: 180-181 ºC. ^{1}H NMR (300 MHz, $CDCl_3$) δ (ppm): 7.86 (d, *J* = 7.5 Hz, 1H, Ar-H), 7.44 (s, 1H, Ar-H), 7.36 (d, *J* = 7.7 Hz, 1H, Ar-H), 7.31 – 7.15 (m, 2H, Ar-H), 6.39 (brs, 1H, NH_2), 5.29 (brs, 1H, NH_2), 5.11 (s, 1H, CH), 3.97 (d, *J* = 7.2 Hz, 2H, C*H*$_2$-Cy), 3.28 (s, 3H, NCH_3), 1.95 – 1.78 (m, 1H,

USC

C*H*-Cy), 1.77 – 1.49 (m, 5H, Cy), 1.31 – 1.13 (m, 12H, C(CH_3)$_3$), 1.10 – 0.90 (m, 2H, Cy). LRMS (CI) m/z calcd for $C_{23}H_{34}N_3O_2$ $[M+H]^+$: 384.3; found: 384.3.

***N*-(1-(*tert*-butylamino)-3,3-dimethyl-1-oxobutan-2-yl)-1-(cyclohexylmethyl)-*N*-methyl-1*H*-indole-3-carboxamide (38q).** Yield: 53%. Mp: 160-161 ºC. ^{1}H NMR (300 MHz, $CDCl_3$) δ (ppm): 7.88 (d, *J* = 8.3 Hz, 1H, Ar-H), 7.43 (s, 1H, Ar-H), 7.40 – 7.34 (m, 1H, Ar-H), 7.33 – 7.19 (m, 2H, Ar-H), 6.20 (brs, 1H, NH), 4.96 (s, 1H, CH), 3.98 (d, *J* = 7.1 Hz, 2H, C*H*$_2$-Cy), 3.31 (s, 3H, NCH_3), 1.96 – 1.81 (m, 1H, Cy), 1.80 – 1.60 (m, 5H, Cy), 1.37 (s, 9H, C(CH_3)$_3$), 1.31 – 1.13 (m, 12H, C(CH_3)$_3$, Cy), 1.13 – 0.94 (m, 2H, Cy). HRMS (APCI) m/z calcd for $C_{27}H_{42}N_3O_2$ $[M+H]^+$: 440.3199; found: 440.3278.

***N*-(1-(benzylamino)-3,3-dimethyl-1-oxobutan-2-yl)-1-(cyclohexylmethyl)-*N*-methyl-1*H*-indole-3-carboxamide (38r).** Yield: 52%. Mp: 130-132 ºC. ^{1}H NMR (300 MHz, $CDCl_3$) δ (ppm): 7.77 (d, *J* = 7.8 Hz, 1H, Ar-H), 7.38 – 7.30 (m, 2H, Ar-H), 7.30 – 7.10 (m, 8H, Ar-H, NH), 5.11 (s, 1H, CH), 4.39 (d, *J* = 5.9 Hz, 2H, C*H*$_2$-Ph), 3.90 (d, *J* = 7.1 Hz, 2H, C*H*$_2$-Cy), 3.26 (s, 3H, NCH_3), 1.94 – 1.50 (m, 6H, Cy), 1.31 – 1.07 (m, 12H, C(CH_3)$_3$, Cy), 1.06 – 0.85 (m, 2H, Cy). HRMS (APCI) m/z calcd for $C_{30}H_{40}N_3O_2$ $[M+H]^+$: 474.3042; found: 474.3118.

***N*-(2-(*tert*-butylamino)-2-oxo-1-phenylethyl)-1-(cyclohexylmethyl)-*N*-methyl-1*H*-indole-3-carboxamide (38s).** Yield: 51%. Mp: 156-157 ºC. ^{1}H NMR (300 MHz, $CDCl_3$) δ (ppm): 7.86 (d, *J* = 8.4 Hz, 1H, Ar-H), 7.54 – 7.31 (m, 7H, Ar-H), 7.30 – 7.15 (m, 2H, Ar-H), 6.25 (s, 1H, NH), 5.98 (s, 1H, CH), 3.96 (d, *J* = 7.1 Hz, 2H, C*H*$_2$-Cy), 3.07 (s, 3H, NCH_3), 1.97 – 1.80 (m, 1H, C*H*-Cy), 1.79 – 1.57 (m, 5H, Cy), 1.42 (s, 9H, C(CH_3)$_3$), 1.26 – 1.10 (m, 3H, Cy), 1.10 – 0.92 (m, 2H, Cy). LRMS (CI) m/z calcd for $C_{29}H_{38}N_3O_2$ $[M+H]^+$: 460.3; found: 460.3.

***N*-(1-(adamantan-1-yl)-2-(*tert*-butylamino)-2-oxoethyl)-1-(cyclohexylmethyl)-*N*-methyl-1*H*-indole-3-carboxamide (38t).** Yield: 43%. Mp: 193-194 ºC. ^{1}H NMR (300 MHz, $CDCl_3$) δ (ppm): 7.90 (d, *J* = 8.0 Hz, 1H, Ar-H), 7.43 (s, 1H, Ar-H), 7.40 – 7.34 (m, 1H, Ar-H), 7.32 – 7.19 (m, 2H, Ar-H), 6.13 (s, 1H, NH), 4.78 (s, 1H, CH), 3.97 (d, *J* = 7.1 Hz, 2H, C*H*$_2$-Cy), 3.35 (s, 3H, NCH_3), 2.12 – 1.60 (m,

USC DE COMPOSTELA

21H, Ad, Cy), 1.36 (s, 9H, C(CH_3)$_3$), 1.30 – 1.12 (m, 3H, Cy), 1.10 – 0.93 (m, 2H, Cy). LRMS (CI) m/z calcd for $C_{33}H_{48}N_3O_2$ $[M+H]^+$: 518.4; found: 518.4.

***N*-(1-(*tert*-butylamino)-2-methyl-1-oxopropan-2-yl)-1-(cyclohexylmethyl)-*N*-methyl-1*H*-indole-3-carboxamide (38u).** Yield: 48%. Mp: 186-188 ºC. ^{1}H NMR (300 MHz, $CDCl_3$) δ (ppm): 7.79 – 7.69 (m, 1H, Ar-H), 7.51 (s, 1H, Ar-H), 7.42 – 7.33 (m, 1H, Ar-H), 7.32 – 7.18 (m, 2H, Ar-H), 6.48 (s, 1H, NH), 3.95 (d, *J* = 7.1 Hz, 2H, C*H*$_2$-Cy), 3.13 (s, 3H, NCH_3), 1.97 – 1.80 (m, 1H, C*H*-Cy), 1.63 (s, 11H, CH_3, CH_3, Cy), 1.35 (s, 9H, C(CH_3)$_3$), 1.30 – 1.11 (m, 3H, Cy), 1.11 – 0.93 (m, 2H, Cy). LRMS (CI) m/z calcd for $C_{25}H_{38}N_3O_2$ $[M+H]^+$: 412.3; found: 412.3.

***N*-(3-(*tert*-butylcarbamoyl)pentan-3-yl)-1-(cyclohexylmethyl)-*N*-methyl-1*H*-indole-3-carboxamide (38v).** Yield: 48%. Mp: 165-167 ºC. ^{1}H NMR (300 MHz, $CDCl_3$) δ (ppm): 7.81 – 7.73 (m, 1H, Ar-H), 7.46 (s, 1H, Ar-H), 7.40 – 7.33 (m, 1H, Ar-H), 7.31 – 7.17 (m, 2H, Ar-H), 6.76 (s, 1H, NH), 3.96 (d, *J* = 7.2 Hz, 2H, C*H*$_2$-Cy), 3.17 (s, 3H, NCH_3), 2.19 (dq, *J* = 7.5, 4.0 Hz, 4H, C*H*$_2$$CH_3$), 1.96 – 1.79 (m, 1H, C*H*-Cy), 1.80 – 1.54 (m, 7H, C*H*$_2$$CH_3$, Cy), 1.38 (s, 9H, C($CH_3$)$_3$), 1.26 – 1.13 (m, 3H, Cy), 1.10 – 0.92 (m, 8H, CH_2C*H*$_3$, CH_2C*H*$_3$, Cy). LRMS (CI) m/z calcd for $C_{27}H_{42}N_3O_2$ $[M+H]^+$: 440.3; found: 440.3.

Methyl *(S)*-2-(1-(4-fluorobenzyl)-*N*-methyl-1*H*-indole-3-carboxamido)-2-phenylacetate [(*S*)-35m]. Chiral separation with a 250 mm x 20 mm Chiralpak® 5µm IE-3 (DAICEL) (isocratic mobile phase DCM) to give an enantiomeric excess of 99%. ^{1}H NMR (300 MHz, $CDCl_3$) δ (ppm): 7.92 – 7.80 (m, 1H, Ar-H), 7.53 – 7.19 (m, 9H, Ar-H), 7.19 – 6.92 (m, 4H, Ar-H), 6.47 (s, 1H, CH), 5.30 (s, 2H, C*H*$_2$-Ph), 3.85 (s, 3H, OCH_3), 3.18 (s, 3H, NCH_3). LRMS (CI) m/z calcd for $C_{26}H_{24}FN_2O_3$ $[M+H]^+$: 431.1693; found: 431.1775.

Methyl *(R)*-2-(1-(4-fluorobenzyl)-*N*-methyl-1*H*-indole-3-carboxamido)-2-phenylacetate [(*R*)-35m)]. Chiral separation with a 250 mm x 20 mm Chiralpak® 5µm IE-3 (DAICEL) (isocratic mobile phase DCM) to give an enantiomeric excess of 99%. ^{1}H NMR (300 MHz, $CDCl_3$) δ (ppm): 7.92 – 7.80 (m, 1H, Ar-H), 7.53 – 7.19 (m, 9H, Ar-H), 7.19 – 6.92 (m, 4H, Ar-H), 6.47 (s, 1H, CH), 5.30 (s, 2H, C*H*$_2$-Ph), 3.85 (s, 3H,

USC DE COMPOSTELA

OCH_3), 3.18 (s, 3H, NCH_3). LRMS (CI) m/z calcd for $C_{26}H_{24}FN_2O_3$ $[M+H]^+$: 431.1693; found: 431.1775.

***(S)*-*N*-(1-(*tert*-butylamino)-3,3-dimethyl-1-oxobutan-2-yl)-1-(4-fluorobenzyl)-1*H*-indole-3-carboxamide [*(S)*-37f].** Chiral separation with a 250 mm x 20 mm Chiralpak® 5µm IE-3 (DAICEL) (isocratic mobile phase Hex-IPA 9:1) to give an enantiomeric excess of 99%. ^{1}H NMR (300 MHz, $CDCl_3$) δ (ppm): 8.07 (d, *J* = 7.7 Hz, 1H, Ar-H), 7.77 (s, 1H, Ar-H), 7.34 – 7.21 (m, 3H, Ar-H), 7.17 – 7.07 (m, 2H, Ar-H), 7.05 – 6.94 (m, 2H, Ar-H), 6.87 (d, *J* = 8.2 Hz, 1H, NH), 5.85 (brs, 1H, NH), 5.30 (s, 2H, C*H*$_2$-Ph), 4.46 (d, *J* = 9.0 Hz, 1H, CH), 1.34 (s, 9H, $C(CH_3)_3$), 1.10 (s, 9H, $C(CH_3)_3$). LRMS (CI) m/z calcd for $C_{26}H_{33}FN_3O_2$ $[M+H]^+$: 438.2479; found: 438.2556.

***(R)*-*N*-(1-(*tert*-butylamino)-3,3-dimethyl-1-oxobutan-2-yl)-1-(4-fluorobenzyl)-1*H*-indole-3-carboxamide [*(R)*-37f].** Chiral separation with a 250 mm x 20 mm Chiralpak® 5µm IE-3 (DAICEL) (isocratic mobile phase Hex-IPA 9:1) to give an enantiomeric excess of 98%. ^{1}H NMR (300 MHz, $CDCl_3$) δ (ppm): 8.07 (d, *J* = 7.7 Hz, 1H, Ar-H), 7.77 (s, 1H, Ar-H), 7.34 – 7.21 (m, 3H, Ar-H), 7.17 – 7.07 (m, 2H, Ar-H), 7.05 – 6.94 (m, 2H, Ar-H), 6.87 (d, *J* = 8.2 Hz, 1H, NH), 5.85 (brs, 1H, NH), 5.30 (s, 2H, C*H*$_2$-Ph), 4.46 (d, *J* = 9.0 Hz, 1H, CH), 1.34 (s, 9H, $C(CH_3)_3$), 1.10 (s, 9H, $C(CH_3)_3$). LRMS (CI) m/z calcd for $C_{26}H_{33}FN_3O_2$ $[M+H]^+$: 438.2479; found: 438.2556.

***(S)*-*N*-(1-(benzylamino)-3,3-dimethyl-1-oxobutan-2-yl)-1-(4-fluorobenzyl)-*N*-methyl-1*H*-indole-3-carboxamide [*(S)*-37r].** Chiral separation with a 250 mm x 20 mm Chiralpak® 5µm IE-3 (DAICEL) (isocratic mobile phase Hex-IPA 7:3) to give an enantiomeric excess of 99%. ^{1}H NMR (300 MHz, $CDCl_3$) δ (ppm): 7.78 (d, *J* = 8.6 Hz ,1H, Ar-H), 7.40 (s, 1H, Ar-H), 7.33 – 7.17 (m, 8H, Ar-H), 7.16 – 7.06 (m, 2H, Ar-H), 7.05 – 6.94 (m, 3H, Ar-H, NH), 5.28 (s, 2H, C*H*$_2$-Ph), 5.11 (s, 1H, CH), 4.49 – 4.33 (m, 2H, NH-C*H*$_2$-Ph), 3.26 (s, 3H, NCH_3), 1.22 (s, 9H, $C(CH_3)_3$). LRMS (CI) m/z calcd for $C_{30}H_{33}FN_3O_2$ $[M+H]^+$: 486.2; found: 486.2.

***(R)*-*N*-(1-(benzylamino)-3,3-dimethyl-1-oxobutan-2-yl)-1-(4-fluorobenzyl)-*N*-me-thyl-1*H*-indole-3-carboxamide [*(R)*-37r].** Chiral separation with a 250 mm x 20 mm Chiralpak® 5µm IE-3 (DAICEL) (isocratic mobile phase Hex-IPA 7:3) to give an enantiomeric excess of 99%. ^{1}H NMR (300 MHz, $CDCl_3$) δ (ppm): 7.78 (d, *J* = 8.6 Hz

USC DE COMPOSTELA

,1H, Ar-H), 7.40 (s, 1H, Ar-H), 7.33 – 7.17 (m, 8H, Ar-H), 7.16 – 7.06 (m, 2H, Ar-H), 7.05 – 6.94 (m, 3H, Ar-H, NH), 5.28 (s, 2H, C*H*$_2$-Ph), 5.11 (s, 1H, CH), 4.49 – 4.33 (m, 2H, NH-C*H*$_2$-Ph), 3.26 (s, 3H, NCH_3), 1.22 (s, 9H, $C(CH_3)_3$). LRMS (CI) m/z calcd for $C_{30}H_{33}FN_3O_2$ $[M+H]^+$: 486.2; found: 486.2.

Isopropyl *(S)*-2-(1-(cyclohexylmethyl)-*N*-methyl-1*H*-indole-3-carboxamido)-3,3-dimethylbutanoate [*(S)*-36r] Chiral separation with a 250 mm x 20 mm Chiralpak® 5µm IE-3 (DAICEL) (isocratic mobile phase Hex-IPA 7:3) to give an enantiomeric excess of 93%. ^{1}H NMR (300 MHz, $CDCl_3$) δ (ppm): 7.83 (d, *J* = 7.4 Hz, 1H, Ar-H), 7.40 – 7.32 (m, 2H, Ar-H), 7.30 – 7.12 (m, 2H, Ar-H), 5.31 (s, 1H, CH), 5.25 – 4.98 (m, 1H, OC*H*$(CH_3)_2$), 4.41 (d, *J* = 7.2 Hz, 2H, C*H*$_2$-Cy), 3.28 (s, 3H, NCH_3), 2.01 – 1.80 (m, 1H, C*H*-Cy), 1.78 – 1.60 (m, 5H, Cy), 1.36 – 1.29 (m, 6H, OCH(C*H*$_3$)$_2$), 1.29 – 0.95 (m, 14H, C(C*H*$_3$)$_3$, Cy). LRMS (CI) m/z calcd for $C_{26}H_{39}N_2O_3$ $[M+H]^+$: 427.2; found: 427.2.

Isopropyl *(R)*-2-(1-(cyclohexylmethyl)-*N*-methyl-1*H*-indole-3-carboxamido)-3,3-dimethylbutanoate [*(R)*-36r] Chiral separation with a 250 mm x 20 mm Chiralpak® 5µm IE-3 (DAICEL) (isocratic mobile phase Hex-IPA 7:3) to give an enantiomeric excess of 94%. ^{1}H NMR (300 MHz, $CDCl_3$) δ (ppm): 7.83 (d, *J* = 7.4 Hz, 1H, Ar-H), 7.40 – 7.32 (m, 2H, Ar-H), 7.30 – 7.12 (m, 2H, Ar-H), 5.31 (s, 1H, CH), 5.25 – 4.98 (m, 1H, OC*H*$(CH_3)_2$), 4.41 (d, *J* = 7.2 Hz, 2H, C*H*$_2$-Cy), 3.28 (s, 3H, NCH_3), 2.01 – 1.80 (m, 1H, C*H*-Cy), 1.78 – 1.60 (m, 5H, Cy), 1.36 – 1.29 (m, 6H, OCH(C*H*$_3$)$_2$), 1.29 – 0.95 (m, 14H, C(C*H*$_3$)$_3$, Cy). LRMS (CI) m/z calcd for $C_{26}H_{39}N_2O_3$ $[M+H]^+$: 427.2; found: 427.2.

***(S)*-*N*-(1-(*tert*-butylamino)-3-methyl-1-oxobutan-2-yl)-1-(cyclohexylmethyl)-*N*-methyl-1*H*-indole-3-carboxamide [*(S)*-38n].** Chiral separation with a 250 mm x 20 mm Chiralpak® 5µm IE-3 (DAICEL) (isocratic mobile phase Hex-IPA 9:1) to give an enantiomeric excess of 98%. ^{1}H NMR (300 MHz, $CDCl_3$) δ (ppm): 7.80 (d, *J* = 6.9 Hz, 1H, Ar-H), 7.42 – 7.32 (m, 2H, Ar-H), 7.30 – 7.14 (m, 2H, Ar-H), 6.73 (s, 1H, NH), 4.47 (d, *J* = 11.4 Hz, 1H, CH), 4.40 (d, *J* = 7.2 Hz, 2H, C*H*$_2$-Cy), 3.13 (s, 3H, NCH_3), 2.50 – 2.30 (m, 1H, C*H*$(CH_3)_2$), 1.94 – 1.80 (m, 1H, Cy), 1.78 –1.60 (m, 5H, Cy), 1.35 (s, 9H, $C(CH_3)_3$), 1.25 – 0.90 (m, 11H, CH(C*H*$_3$)$_2$, Cy). LRMS (CI) m/z calcd for $C_{26}H_{40}N_3O_2$ $[M+H]^+$: 426.3; found: 426.3.

USC

***(R)*-*N*-(1-(*tert*-butylamino)-3-methyl-1-oxobutan-2-yl)-1-(cyclohexylmethyl)-*N*-methyl-1*H*-indole-3-carboxamide [*(R)*-38n].** Chiral separation with a 250 mm x 20 mm Chiralpak® 5µm IE-3 (DAICEL) (isocratic mobile phase Hex-IPA 9:1) to give an enantiomeric excess of 99%. ^{1}H NMR (300 MHz, $CDCl_3$) δ (ppm): 7.80 (d, *J* = 6.9 Hz, 1H, Ar-H), 7.42 – 7.32 (m, 2H, Ar-H), 7.30 – 7.14 (m, 2H, Ar-H), 6.73 (s, 1H, NH), 4.47 (d, *J* = 11.4 Hz, 1H, CH), 4.40 (d, *J* = 7.2 Hz, 2H, C*H*$_2$-Cy), 3.13 (s, 3H, NCH_3), 2.50 – 2.30 (m, 1H, C*H*$(CH_3)_2$), 1.94 – 1.80 (m, 1H, Cy), 1.78 –1.60 (m, 5H, Cy), 1.35 (s, 9H, $C(CH_3)_3$), 1.25 – 0.90 (m, 11H, CH(C*H*$_3$)$_2$, Cy). LRMS (CI) m/z calcd for $C_{26}H_{40}N_3O_2$ $[M+H]^+$: 426.3; found: 426.3.

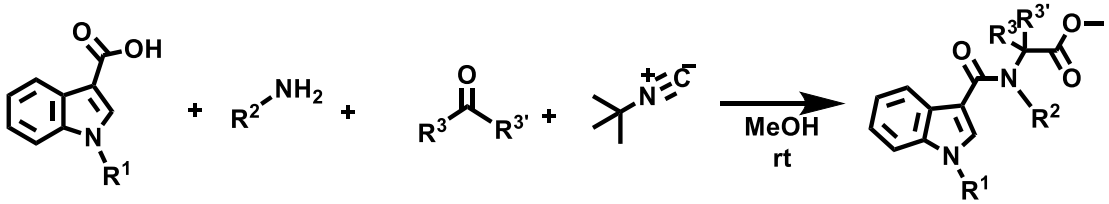
***(S)*-*N*-(1-(benzylamino)-3,3-dimethyl-1-oxobutan-2-yl)-1-(cyclohexylmethyl)-*N*-methyl-1*H*-indole-3-carboxamide [*(S)*-38r].** Chiral separation with a 250 mm x 20 mm Chiralpak® 5µm IE-3 (DAICEL) (isocratic mobile phase Hex-IPA 7:3) to give an enantiomeric excess of 99%. ^{1}H NMR (300 MHz, $CDCl_3$) δ (ppm): 7.77 (d, *J* = 7.8 Hz, 1H, Ar-H), 7.38 – 7.30 (m, 2H, Ar-H), 7.30 – 7.10 (m, 8H, Ar-H, NH), 5.11 (s, 1H, CH), 4.39 (d, *J* = 5.9 Hz, 2H, C*H*$_2$-Ph), 3.90 (d, *J* = 7.1 Hz, 2H, C*H*$_2$-Cy), 3.26 (s, 3H, NCH_3), 1.94 – 1.50 (m, 6H, Cy), 1.31 – 1.07 (m, 12H, $C(CH_3)_3$, Cy), 1.06 – 0.85 (m, 2H, Cy). LRMS (CI) m/z calcd for $C_{30}H_{40}N_3O_2$ $[M+H]^+$: 474.3; found: 474.3.

***(R)*-*N*-(1-(benzylamino)-3,3-dimethyl-1-oxobutan-2-yl)-1-(cyclohexylmethyl)-*N*-methyl-1*H*-indole-3-carboxamide [*(R)*-38r].** Chiral separation with a 250 mm x 20 mm Chiralpak® 5µm IE-3 (DAICEL) (isocratic mobile phase Hex-IPA 7:3) to give an enantiomeric excess of 99%. ^{1}H NMR (300 MHz, $CDCl_3$) δ (ppm): 7.77 (d, *J* = 7.8 Hz, 1H, Ar-H), 7.38 – 7.30 (m, 2H, Ar-H), 7.30 – 7.10 (m, 8H, Ar-H, NH), 5.11 (s, 1H, CH), 4.39 (d, *J* = 5.9 Hz, 2H, C*H*$_2$-Ph), 3.90 (d, *J* = 7.1 Hz, 2H, C*H*$_2$-Cy), 3.26 (s, 3H, NCH_3), 1.94 – 1.50 (m, 6H, Cy), 1.31 – 1.07 (m, 12H, $C(CH_3)_3$, Cy), 1.06 – 0.85 (m, 2H, Cy). LRMS (CI) m/z calcd for $C_{30}H_{40}N_3O_2$ $[M+H]^+$: 474.3; found: 474.3.

USC UNIVERSIDADE DE SANTIAGO DE COMPOSTELA

4.5.9 General pathway for the synthesis of alkyl (1*H*-indole-3-carbonyl)glycinate polysubstituted (39a-x and 40a-x)

A mixture of the *N*-alkyl-1*H*-indole-3-carboxylic acid (1 equiv.), the corresponding aldehyde (or ketone) (1 equiv.), the appropriate amine (1 equiv.) and *tert*-Butyl isocyanide (1 equiv.) in MeOH (2 mL) was stirred with orbital stirring at room temperature for 24 h. After completion of the reaction, PS-p-TsOH (2.0 mmol) and CH_2Cl_2 (3 mL) were added. The reaction mixture was submitted to orbital stirring at room temperature until complete consumption of the unreacted isocyanide (30-60 min). The polystyrene-supported salt was filtered off and successively washed with MeOH (3 × 5 mL) and CH_2Cl_2 (3 × 5 mL). The resulting product was purified by column chromatography on silica gel using MeOH/CH_2Cl_2.



26d,c
R^1 = CH_2-Cy
R^1 = 4-F-Bn

32a,b
R^2 = H
R^2 = CH_3

34a,g
R^3, $R^{3'}$ = H, H
R^3, $R^{3'}$ = *i*-Pr, H
R^3, $R^{3'}$ = *i*-Bu, H
R^3, $R^{3'}$ = *t*-Bu, H
R^3, $R^{3'}$ = 4,4-DMPN, H
R^3, $R^{3'}$ = Ph, H
R^3, $R^{3'}$ = Ad, H
R^3, $R^{3'}$ = Me, Me
R^3, $R^{3'}$ = Et, Et
R^3, $R^{3'}$ = Cyp

33a

39a-x, 40a-x

Scheme S7: General procedure for the synthesis of alkyl (1*H*-indole-3-carbonyl)glycinate polysubstituted (**39a-x**, **40a-x**).

4.5.9.1 Spectroscopic and analytic data of alkyl (1*H*-indole-3-carbonyl)glycinate polysubstituted

Methyl (1-(4-fluorobenzyl)-1*H*-indole-3-carbonyl)leucinate (39d). Yield: 41%. Mp: 150-152 ºC. ^{1}H NMR (300 MHz, $CDCl_3$) δ (ppm): 8.10 – 8.02 (m, 1H, Ar-H), 7.74 (s, 1H, Ar-H), 7.34 – 7.18 (m, 3H, Ar-H), 7.16 – 7.08 (m, 2H, Ar-H), 7.05 – 6.94 (m, 2H, Ar-H), 6.48 (d, *J* = 8.3 Hz, 1H, NH), 5.25 (s, 2H, C*H*$_2$-Ph), 5.01 – 4.89 (m, 1H, CH), 3.79 (s, 3H, OCH_3), 1.91 – 1.63 (m, 3H, C*H*$_2$C*H*$(CH_3)_2$), 1.02 (t, *J* = 6.5 Hz, 6H, $CH_2CH(CH_3)_2$). ^{13}C NMR (75 MHz, $CDCl_3$) δ (ppm): 174.3, 164.6, 160.8, 136.7,

131.7, 128.9, 128.8, 125.7, 122.9, 121.8, 120.4, 116.0, 115.8, 111.1, 110.5, 52.3, 50.7, 49.9, 42.1, 25.0, 22.9, 22.1. LRMS (CI) m/z calcd for $C_{23}H_{26}FN_2O_3$ $[M+H]^+$: 397.2; found: 397.2.

Methyl 5-cyano-2-(1-(4-fluorobenzyl)-1*H*-indole-3-carboxamido)-3,3-dimethylpentanoate (39e). Yield: 46%. Mp: 126-127 ºC ^{1}H NMR (300 MHz, $CDCl_3$) δ (ppm): 8.00 (d, *J* = 7.2 Hz, 1H, Ar-H), 7.77 (s, 1H, Ar-H), 7.38 – 7.22 (m, 3H, Ar-H), 7.19 – 7.09 (m, 2H, Ar-H), 7.09 – 6.95 (m, 2H, Ar-H), 6.55 (d, *J* = 9.3 Hz, 1H, NH), 5.32 (s, 2H, C*H*$_2$-Ph), 4.85 (d, *J* = 9.4 Hz, 1H, CH), 3.81 (s, 3H, OCH_3), 2.69 – 2.40 (m, 2H, $C(CH_3)_2CH_2CH_2CN$), 1.98 – 1.68 (m, 2H, $C(CH_3)_2CH_2CH_2CN$), 1.10 (s, 6H, $C(CH_3)_2CH_2CH_2CN$). LRMS (CI) m/z calcd for $C_{25}H_{27}FN_3O_3$ $[M+H]^+$: 436.2; found: 436.2.

Methyl 2-cyclopropyl-2-(1-(4-fluorobenzyl)-1*H*-indole-3-carboxamido) acetate (39f). Yield: 48%. Mp: 175-176 ºC. ^{1}H NMR (300 MHz, $CDCl_3$) δ (ppm): 8.11 – 8.02 (m, 1H, Ar-H), 7.75 (s, 1H, Ar-H), 7.39 – 7.20 (m, 3H, Ar-H), 7.19 – 7.09 (m, 2H, Ar-H), 7.08 – 6.95 (m, 2H, Ar-H), 6.54 (d, *J* = 7.6 Hz, 1H, NH), 5.30 (s, 2H, C*H*$_2$-Ph), 4.41 (t, *J* = 7.9 Hz, 1H, CH), 3.83 (s, 3H, OCH_3), 1.32 – 1.16 (m, 1H, CH-*c*-Pr), 0.74 – 0.48 (m, 4H, *c*-Pr). LRMS (CI) m/z calcd for $C_{22}H_{22}FN_2O_3$ $[M+H]^+$: 381.2; found: 381.2.

Methyl 2-cyclobutyl-2-(1-(4-fluorobenzyl)-1*H*-indole-3-carboxamido)acetate (39g). Yield: 45%. Mp: 127-128 ºC ^{1}H NMR (300 MHz, $CDCl_3$) δ (ppm): 8.05 (d, *J* = 7.3 Hz, 1H, Ar-H), 7.78 (s, 1H, Ar-H), 7.37 – 7.23 (m, 3H, Ar-H), 7.20 – 7.10 (m, 2H, Ar-H), 7.08 – 6.94 (m, 2H, Ar-H), 6.48 (d, *J* = 8.4 Hz, 1H, NH), 5.30 (s, 2H, C*H*$_2$-Ph), 4.90 (t, *J* = 8.0 Hz, 1H, CH), 3.79 (s, 3H, OCH_3), 2.91– 2.71 (m, 1H, C*H*-*c*-Bu), 2.18 – 1.74 (m, 6H, *c*-Bu). LRMS (CI) m/z calcd for $C_{23}H_{24}FN_2O_3$ $[M+H]^+$: 395.2; found: 395.2.

Methyl 1-(1-(4-fluorobenzyl)-1*H*-indole-3-carboxamido)cyclopentane-1-carboxylate (39l). Yield: 43%. Oil at room temperature. ^{1}H NMR (300 MHz, $CDCl_3$) δ (ppm): 8.03 – 7.93 (m, 1H, Ar-H), 7.74 (s, 1H, Ar-H), 7.33 – 7.20 (m, 3H, Ar-H), 7.16 – 7.07 (m, 2H, Ar-H), 7.03 – 6.92 (m, 2H, Ar-H), 6.50 (s, 1H, NH), 5.27 (s, 2H, C*H*$_2$-Ph), 3.77 (s, 3H, OCH_3), 2.47 – 2.28 (m, 2H, *c*-Pent), 2.27 – 2.10 (m, 2H, *c*-Pent), 2.02 –

USC DE COMPOSTELA

1.80 (m, 4H, *c*-Pent). ^{13}C NMR (75 MHz, $CDCl_3$) δ (ppm): 175.4, 164.7, 164.1, 136.7, 131.9, 128.8, 128.7, 125.6, 122.8, 121.8, 120.3, 116.0, 115.7, 111.5, 110.5, 66.1, 52.6, 49.9, 37.6, 25.0. LRMS (CI) m/z calcd for $C_{23}H_{24}FN_2O_3$ $[M+H]^+$: 395.2; found: 395.2.

Methyl *N*-(1-(4-fluorobenzyl)-1*H*-indole-3-carbonyl)-*N*-methylleucinate (39p). Yield: 53%. Oil at room temperature. ^{1}H NMR (300 MHz, $CDCl_3$) δ (ppm): 7.83 – 7.74 (m, 1H, Ar-H), 7.45 (s, 1H, Ar-H), 7.31 – 7.18 (m, 3H, Ar-H), 7.16 – 7.08 (m, 2H, Ar-H), 7.06 – 6.94 (m, 2H, Ar-H), 5.36 – 5.22 (m, 3H, CH, C*H*$_2$-Ph), 3.75 (s, 3H, OCH_3), 3.10 (s, 3H, NCH_3), 1.95 – 1.64 (m, 3H, C*H*$_2$C*H*$(CH_3)_2$), 0.98 (t, *J* = 6.5 Hz, 6H, $CH_2CH(CH_3)_2$). LRMS (CI) m/z calcd for $C_{24}H_{28}FN_2O_3$ $[M+H]^+$: 411.2; found: 411.2.

Methyl 5-cyano-2-(1-(4-fluorobenzyl)-*N*-methyl-1*H*-indole-3-carboxamido)-3,3-dimethylpentanoate (39q). Yield: 49%. Oil at room temperature. ^{1}H NMR (300 MHz, $CDCl_3$) δ (ppm): 7.91 – 7.82 (m, 1H, Ar-H), 7.47 (s, 1H, Ar-H), 7.35 – 7.21 (m, 3H, Ar-H), 7.20 – 7.10 (m, 2H, Ar-H), 7.07 – 6.96 (m, 2H, Ar-H), 5.36 (s, 1H, CH), 5.31 (s, 2H, C*H*$_2$-Ph), 3.78 (s, 3H, OCH_3), 3.29 (s, 3H, NCH_3), 2.53 – 2.27 (m, 2H, $C(CH_3)_2CH_2CH_2CN$), 2.12 – 1.77 (m, 2H, $C(CH_3)_2CH_2CH_2CN$), 1.20 (s, 6H, $C(CH_3)_2CH_2CH_2CN$). HRMS (APCI) m/z calcd for $C_{26}H_{29}FN_3O_3$ $[M+H]^+$: 450.2115; found: 450.2192.

Methyl 2-cyclopropyl-2-(1-(4-fluorobenzyl)-*N*-methyl-1*H*-indole-3-carboxamido)acetate (39r). Yield: 48%. Oil at room temperature. ^{1}H NMR (300 MHz, $CDCl_3$) δ (ppm): 7.86 – 7.77 (m, 1H, Ar-H), 7.48 (s, 1H, Ar-H), 7.33 – 7.20 (m, 3H, Ar-H), 7.19 – 7.10 (m, 2H, Ar-H), 7.07 – 6.97 (m, 2H, Ar-H), 5.31 (s, 2H, CH_2-Ph), 4.33 (d, *J* = 10.1 Hz, 1H, CH), 3.80 (s, 3H, OCH_3), 3.30 (s, 3H, NCH_3), 1.42 – 1.23 (m, 1H, C*H*-*c*-Pr), 0.90 –0.76 (m, 2H, *c*-Pr), 0.75 – 0.57 (m, 2H, *c*-Pr). ^{13}C NMR (75 MHz, $CDCl_3$) δ (ppm): 172.0, 167.8, 157.9, 135.9, 128.8, 128.7, 122.8, 121.3, 121.2, 116.0, 115.7, 111.0, 110.0, 52.1, 49.8, 11.4, 6.1, 3.4. LRMS (CI) m/z calcd for $C_{23}H_{24}FN_2O_3$ $[M+H]^+$: 395.2; found: 395.2.

USC DE COMPOSTELA

Methyl 2-cyclobutyl-2-(1-(4-fluorobenzyl)-*N*-methyl-1*H*-indole-3-carboxamido)acetate (39s). Yield: 49%. Oil at room temperature. ^{1}H NMR (300 MHz, $CDCl_3$) δ (ppm): 7.81 – 7.72 (m, 1H, Ar-H), 7.45 (s, 1H, Ar-H), 7.31 – 7.19 (m, 3H, Ar-H), 7.17

– 7.08 (m, 2H, Ar-H), 7.05 – 6.95 (m, 2H, Ar-H), 5.30 (s, 2H, C*H*$_2$-Ph), 5.16 – 5.02 (m, 1H, CH), 3.74 (s, 3H, OCH_3), 3.06 (s, 3H, NCH_3), 2.98 – 2.80 (m, 1H, C*H*-*c*-Bu), 2.30 – 2.16 (m, 2H, *c*-Bu), 2.14 – 1.80 (m, 4H, *c*-Bu). LRMS (CI) m/z calcd for $C_{24}H_{26}FN_2O_3$ $[M+H]^+$: 409.2; found: 409.2.

Methyl 1-(1-(4-fluorobenzyl)-*N*-methyl-1*H*-indole-3-carboxamido)cyclopentane-1-carboxylate (39x). Yield: 48%. Mp: 164-165 ºC. ^{1}H NMR (300 MHz, $CDCl_3$) δ (ppm): 7.80 – 7.72 (m, 1H Ar-H), 7.52 (s, 1H, Ar-H), 7.32 – 7.20 (m, 3H, Ar-H), 7.19 – 7.10 (m, 2H, Ar-H), 7.06 – 6.93 (m, 2H, Ar-H), 5.29 (s, 2H, C*H*$_2$-Ph), 3.75 (s, 3H, OCH_3), 3.27 (s, 3H, NCH_3), 2.56 – 2.40 (m, 2H, *c*-Pent), 2.20 – 2.01 (m, 2H, *c*-Pent), 1.95 – 1.72 (m, 4H, *c*-Pent). ^{13}C NMR (75 MHz, $CDCl_3$) δ (ppm): 175.3, 169.0, 160.8, 136.0, 132.0, 131.3, 128.9, 128.8, 126.4, 122.6, 121.2, 121.2, 116.0, 115.7, 112.5, 110.1, 71.2, 52.1, 49.8, 35.9, 35.8, 24.5.LRMS (CI) m/z calcd for $C_{24}H_{26}FN_2O_3$ $[M+H]^+$: 409.2; found: 409.2.

Methyl (1-(cyclohexylmethyl)-1*H*-indole-3-carbonyl)leucinate (40d). Yield: 46%. Mp: 150-151 ºC. ^{1}H NMR (300 MHz, $CDCl_3$) δ (ppm): 8.05 – 7.96 (m, 1H, Ar-H), 7.71 (s, 1H, Ar-H), 7.42 – 7.33 (m, 1H, Ar-H), 7.32 – 7.23 (m, 2H, Ar-H), 6.40 (d, *J* = 8.5 Hz, 1H, NH), 5.04 – 4.89 (m, 1H, CH), 3.95 (d, *J* = 7.2 Hz, 2H, C*H*$_2$-Cy), 3.79 (s, 3H, OCH_3), 2.00 – 1.53 (m, 8H, C*H*$_2$CH$(CH_3)_2$, CH_2C*H*$(CH_3)_2$, Cy), 1.23 –1.12 (m, 2H, Cy), 1.11 – 0.90 (m, 9H, CH_2CH(C*H*$_3$)$_2$, Cy). ^{13}C NMR (75 MHz, $CDCl_3$) δ (ppm): 174.2, 164.8, 137.0, 132.4, 125.3, 122.4, 121.4, 120.1, 110.5, 110.2, 53.4, 52.3, 50.7, 42.2, 38.5, 31.0, 26.2, 25.6, 25.0, 22.9, 22.2. LRMS (CI) m/z calcd for $C_{23}H_{33}N_2O_3$ $[M+H]^+$: 385.2; found: 385.2.

Methyl 5-cyano-2-(1-(cyclohexylmethyl)-1*H*-indole-3-carboxamido)-3,3-dimethylpentanoate (40e). Yield: 45%. Mp: 126-127 ºC. ^{1}H NMR (300 MHz, $CDCl_3$) δ (ppm): 8.01 – 7.92 (m, 1H, Ar-H), 7.72 (s, 1H, Ar-H), 7.47 – 7.35 (m, 1H, Ar-H), 7.35 – 7.23 (m, 2H, Ar-H), 6.55 (d, *J* = 9.4 Hz, 1H, NH), 4.86 (d, *J* = 9.3 Hz, 1H, CH), 3.98 (d, *J* = 7.2 Hz, 2H, C*H*$_2$-Cy), 3.80 (s, 3H, OCH_3), 2.70 – 2.41 (m, 2H, C$(CH_3)_2$$CH_2$C*H*$_2$CN), 1.98 – 1.56 (m, 8H, C$(CH_3)_2$C*H*$_2$$CH_2$CN, Cy), 1.34 – 0.90 (m, 11H, C(C*H*$_3$)$_2$$CH_2$$CH_2$CN, Cy). LRMS (CI) m/z calcd for $C_{25}H_{34}N_3O_3$ $[M+H]^+$: 424.3; found: 424.3.

USC DE COMPOSTELA

Methyl 2-(1-(cyclohexylmethyl)-1*H*-indole-3-carboxamido)-2-cyclopropyl-acetate (40f). Yield: 52%. Mp: 145-146 ºC. ^{1}H NMR (300 MHz, $CDCl_3$) δ (ppm): 8.08 – 7.97 (m, 1H, Ar-H), 7.72 (s, 1H, Ar-H), 7.43 – 7.34 (m, 1H, Ar-H), 7.32 – 7.20 (m, 2H, Ar-H), 6.60 – 6.47 (m, 1H, NH), 4.44 (d, *J* = 8.1 Hz, 1H, CH), 3.95 (d, *J* = 7.1 Hz, 2H, C*H*$_2$-Cy), 3.83 (s, 3H, OCH_3), 2.95 – 1.80 (m, 1H, C*H*-Cy), 1.79 – 1.55 (m, 6H, C*H*-*c*-Pr, Cy), 1.35 – 0.90 (m, 5H, Cy), 0.77 – 0.44 (m, 4H, *c*-Pr). ^{13}C NMR (75 MHz, $CDCl_3$) δ (ppm): 173.1, 164.8, 137.0, 132.4, 125.4, 122.4, 121.5, 120.2, 110.5, 110.0, 55.1, 53.4, 52.3, 38.5, 31.0, 26.2, 25.6, 14.1, 3.1, 3.0. LRMS (CI) m/z calcd for $C_{22}H_{29}N_2O_3$ $[M+H]^+$: 369.2; found: 369.2.

Methyl 2-cyclobutyl-2-(1-(cyclohexylmethyl)-1*H*-indole-3-carboxamido)ace-tate (40g). Yield: 49%. Mp: 129-130 ºC. ^{1}H NMR (300 MHz, $CDCl_3$) δ (ppm): 8.10 – 7.89 (m, 1H, Ar-H), 7.72 (s, 1H, Ar-H), 7.44 – 7.35 (m, 1H, Ar-H), 7.34 – 7.24 (m, 2H, Ar-H), 6.44 (d, *J* = 7.9 Hz, 1H, NH), 4.91 (t, *J* = 7.9 Hz, 1H, CH), 3.97 (d, *J* = 7.2 Hz, 2H, C*H*$_2$-Cy), 3.79 (s, 3H, OCH_3), 2.92 – 2.73 (m, 1H, C*H*-*c*-Bu), 2.19 – 1.58 (m, 12H, *c*-Bu, Cy), 1.30 – 0.90 (m, 5H, Cy). LRMS (CI) m/z calcd for $C_{23}H_{31}N_2O_3$ $[M+H]^+$: 383.2; found: 383.2.

Methyl 1-(1-(cyclohexylmethyl)-1*H*-indole-3-carboxamido)cyclopentane-1-carboxylate (40l). Yield: 48%. Mp: 190-191 ºC. ^{1}H NMR (300 MHz, $CDCl_3$) δ (ppm): 8.00 – 7.91 (m, 1H, Ar-H), 7.70 (s, 1H, Ar-H), 7.42 – 7.33 (m, 1H, Ar-H), 7.30 –7.19 (m, 2H, Ar-H), 6.49 (s, 1H, NH), 3.94 (d, *J* = 7.0 Hz, 2H, C*H*$_2$-Cy), 3.78 (s, 3H, OCH_3), 2.46 – 2.30 (m, 2H, *c*-Pent), 2.27 – 2.13 (m, 2H, *c*-Pent), 2.03 – 1.82 (m, 3H, *c*-Pent, C*H*-Cy), 1.77 – 1.56 (m, 7H, *c*-Pent, Cy), 1.24 – 1.12 (m, 2H, Cy), 1.08 – 0.90 (m, 3H, Cy). LRMS (CI) m/z calcd for $C_{23}H_{31}N_2O_3$ $[M+H]^+$: 383.2; found: 383.2.

Methyl *N*-(1-(cyclohexylmethyl)-1*H*-indole-3-carbonyl)-*N*-methylleucinate (40p). Yield: 48%. Mp: 122-123 ºC. ^{1}H NMR (300 MHz, $CDCl_3$) δ (ppm): 7.82 – 7.75 (m, 1H, Ar-H), 7.42 (s, 1H, Ar-H), 7.38 – 7.32 (m, 1H, Ar-H), 7.29 – 7.15 (m, 2H, Ar-H), 5.34 – 5.19 (m, 1H, CH), 3.96 (d, *J* = 7.1 Hz, 2H, C*H*$_2$-Cy), 3.78 (s, 3H, OCH_3), 3.13 (s, 3H, NCH_3), 1.97 – 1.49 (m, 9H, C*H*$_2$CH$(CH_3)_3$, CH_2C*H*$(CH_3)_3$, Cy), 1.33 – 0.74 (m, 11H, CH_2CH(C*H*$_3$)$_3$, Cy). ^{13}C NMR (75 MHz, $CDCl_3$) δ (ppm): 172.8, 168.4, 136.2, 130.8, 126.7, 122.3, 121.2, 120.8, 110.0, 53.2, 52.1, 38.6, 37.8, 31.0, 26.2, 25.6,

USC DE COMPOSTELA

25.0, 23.3, 21.5. HRMS (APCI) m/z calcd for $C_{24}H_{35}N_2O_3$ $[M+H]^+$: 399.2569; found: 399.2649.

Methyl 5-cyano-2-(1-(cyclohexylmethyl)-*N*-methyl-1*H*-indole-3-carboxamido)-3,3 -dimethylpentanoate (40q). Yield: 56%. Oil at room temperature. ^{1}H NMR (300 MHz, $CDCl_3$) δ (ppm): 7.90 – 7.78 (m, 1H, Ar-H), 7.41 (s, 1H, Ar-H), 7.40 – 7.34 (m, 1H, Ar-H), 7.32 – 7.18 (m, 2H, Ar-H), 5.36 (s, 1H, CH), 3.98 (d, *J* = 7.2 Hz, 2H, C*H*$_2$-Cy), 3.79 (s, 3H, OCH_3), 3.30 (s, 3H, NCH_3), 2.51 –2.31 (m, 2H, $C(CH_3)_2CH_2CH_2CN$), 2.10 – 1.58 (m, 8H, $C(CH_3)_2CH_2CH_2CN$, Cy), 1.35 – 0.90 (m, 11H, $C(CH_3)_2CH_2CH_2CN$, Cy). HRMS (APCI) m/z calcd for $C_{26}H_{36}N_3O_3$ $[M+H]^+$: 438.2678; found: 438.2754.

Methyl 2-(1-(cyclohexylmethyl)-*N*-methyl-1*H*-indole-3-carboxamido)-2-cyclopropylacetate (40r). Yield: 51%. Mp: 123-124 ºC. ^{1}H NMR (300 MHz, $CDCl_3$) δ (ppm): 7.80 (d, *J* = 7.2 Hz, 1H, Ar-H), 7.42 (s, 1H, Ar-H), 7.35 (d, *J* = 7.3 Hz, 1H, Ar-H), 7.30 – 7.15 (m, 2H, Ar-H), 4.33 (d, *J* = 10.0 Hz, 1H, CH), 3.96 (d, *J* = 7.2 Hz, 2H, C*H*$_2$-Cy), 3.81 (s, 3H, OCH_3), 3.31 (s, 3H, NCH_3), 1.95 – 1.80 (m, 1H, C*H*-Cy), 1.79 – 1.60 (m, 6H, C*H*-*c*-Pr, Cy), 1.25 – 1.12 (m, 3H, Cy), 1.11 – 0.95 (m, 2H, Cy), 0.89 – 0.76 (m, 2H, *c*-Pr), 0.72 – 0.58 (m, 2H, *c*-Pr). LRMS (CI) m/z calcd for $C_{23}H_{31}N_2O_3$ $[M+H]^+$: 383.2; found: 383.2.

Methyl 2-cyclobutyl-2-(1-(cyclohexylmethyl)-*N*-methyl-1*H*-indole-3-carboxamido)acetate (40s). Yield: 49%. Mp: 125-126 ºC. ^{1}H NMR (300 MHz, $CDCl_3$) δ (ppm): 7.75 (d, *J* = 7.8 Hz, 1H, Ar-H), 7.42 (s, 1H, Ar-H), 7.35 (d, *J* = 8.2 Hz, 1H, Ar-H), 7.28 – 7.14 (m, 2H, Ar-H), 5. 15 – 5.00 (m, 1H, CH), 3.95 (d, *J* = 7.8 Hz, 2H, C*H*$_2$-Cy), 3.76 (s, 3H, OCH_3), 3.07 (s, 3H, NCH_3), 2.34 – 1.50 (m, 13H, *c*-Pr, Cy), 1.41 – 0.78 (m, 5H, *c*-Pr, Cy). LRMS (CI) m/z calcd for $C_{24}H_{33}N_2O_3$ $[M+H]^+$: 397.2; found: 397.2.

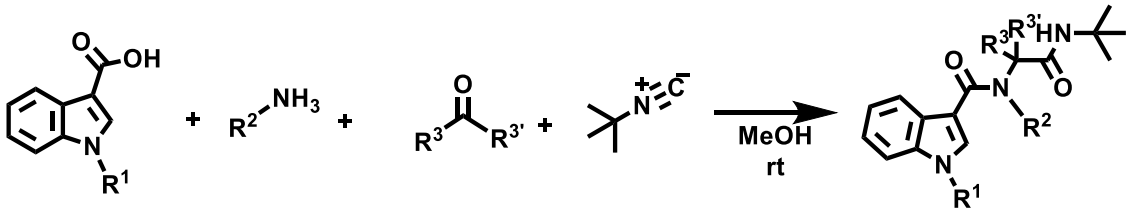
Methyl 1-(1-(cyclohexylmethyl)-*N*-methyl-1*H*-indole-3-carboxamido) cyclopentane-1-carboxylate (40x). Yield: 51%. Mp: 157-158 ºC. ^{1}H NMR (300 MHz, $CDCl_3$) δ (ppm): 7.78 – 7.71 (m, 1H, Ar-H), 7.49 (s, 1H, Ar-H), 7.39 – 7.31 (m, 1H, Ar-H), 7.29 – 7.15 (m, 2H, Ar-H), 3.95 (d, *J* = 7.1 Hz, 2H, C*H*$_2$-Cy), 3.76 (s, 3H, OCH_3), 3.28 (s, 3H, NCH_3), 2.57 – 2.40 (m, 2H, *c*-Pent), 2.20 – 2.02 (m, 2H, *c*-Pent), 1.97 –

USC UNIVERSIDADE DE SANTIAGO DE COMPOSTELA

1.56 (m, 10H, *c*-Pent, Cy), 1.31 – 0.90 (m, 5H, Cy). LRMS (CI) m/z calcd for $C_{24}H_{33}N_2O_3$ $[M+H]^+$: 397.2; found: 397.2.

4.5.1 General pathway for the synthesis of *N*-(2-amino-2-oxoethyl)-1*H*-indole-3-carboxamide polysubstituted (41a-x, 42a-x, 43a-h)

A mixture of the *N*-alkyl-1*H*-indole-3-carboxylic acid (1 equiv.), the corresponding aldehyde (or ketone) (1 equiv.), the appropriate amine (1 equiv.) and *tert*-Butyl isocyanide (1 equiv.) in MeOH (2 mL) was stirred with orbital stirring at room temperature for 24 h. After completion of the reaction, PS-p-TsOH (2.0 mmol) and CH_2Cl_2 (3 mL) were added. The reaction mixture was submitted to orbital stirring at room temperature until complete consumption of the unreacted isocyanide (30-60 min). The polystyrene-supported salt was filtered off and successively washed with MeOH (3 × 5 mL) and CH_2Cl_2 (3 × 5 mL). The resulting product was purified by column chromatography on silica gel using MeOH/CH_2Cl_2.



26a-d
R1 = 5-F-Pentyl
R1 = Pentyl
R1 = CH_2-Cy
R1 = 4-F-Bn

32a,b
R2 = H
R2 = CH_3

34a,g
R3, R3' = H, H
R3, R3' = *i*-Pr, H
R3, R3' = *i*-Bu, H
R3, R3' = *t*-Bu, H
R3, R3' = 4,4-DMPN, H
R3, R3' = Ph, H
R3, R3' = Ad, H
R3, R3' = Me, Me
R3, R3' = Et, Et
R3, R3' = Cyp

33a

41a-x, 42a-x, 43a-h

Scheme S8: General procedure for the synthesis of *N*-(2-amino-2-oxoethyl)-1*H*-indole-3-carboxamide polysubstituted (**41a-x**, **42a-x**, **43a-h**).

USC UNIVERSIDADE DE SANTIAGO DE COMPOSTELA

4.5.1.1 Spectroscopic and analytic data of *N*-(2-amino-2-oxoethyl)-1*H*-indole-3-carboxamide polysubstituted

***N*-(1-(*tert*-butylamino)-4-methyl-1-oxopentan-2-yl)-1-(4-fluorobenzyl)-1*H*-indole-3-carboxamide (41d).** Yield: 46%. Mp: 220-221 ºC**.** ^{1}H NMR (300 MHz, DMSO-d_6) δ (ppm): 8.26 (s, 1H, Ar-H), 8.11 (d, *J* = 7.4 Hz, 1H, Ar-H), 7.72 (d, *J* = 8.6 Hz, 1H, NH), 7.57 – 7.48 (m, 2H, Ar-H), 7.35 – 7.25 (m, 2H, Ar-H), 7.22 – 7.05 (m, 3H, Ar-H), 6.01 (s, 1H, NH), 5.44 (s, 2H, CH_2-Ph), 4.58 – 4.40 (m, 1H, CH), 1.72 – 1.39 (m, 3H, CHCH_2(CH_3)$_2$), 1.24 (s, 9H, C(CH_3)$_3$), 0.89 (t, *J* = 6.5 Hz, 6H, CHCH_2(CH_3)$_2$). LRMS (CI) m/z calcd for $C_{26}H_{33}FN_3O_2$ $[M+H]^+$: 438.2; found: 438.2.

***N*-(1-(*tert*-butylamino)-5-cyano-3,3-dimethyl-1-oxopentan-2-yl)-1-(4-fluorobenzyl)-1*H*-indole-3-carboxamide (41e).** Yield: 47%. Mp: 257-258 ºC**.** ^{1}H NMR (300 MHz, $CDCl_3$) δ (ppm): 8.03 (d, *J* = 7.6 Hz, 1H, Ar-H), 7.76 (s, 1H, Ar-H), 7.37 – 7.22 (m, 3H, Ar-H), 7.20 – 7.09 (m, 2H, Ar-H), 7.07 – 6.96 (m, 2H, Ar-H), 6.82 (d, *J* = 9.1 Hz, 1H, NH), 6.04 (s, 1H, NH), 5.31 (s, 2H, CH_2-Ph), 4.54 (d, *J* = 9.2 Hz, 1H, CH), 2.69 – 2.30 (m, 2H, C(CH_3)$_2$CH_2CH_2CN), 1.95 – 1.50 (m, 2H, C(CH_3)$_2$CH_2CH_2CN), 1.35 (s, 9H, C(CH_3)$_3$), 1.12 (d, *J* = 8.8 Hz, 6H, C(CH_3)$_2$CH_2CH_2CN). HRMS (APCI) m/z calcd for $C_{28}H_{34}FN_4O_2$ $[M+H]^+$: 477.2588; found: 477.2670.

***N*-(2-(*tert*-butylamino)-1-cyclopropyl-2-oxoethyl)-1-(4-fluorobenzyl)-1*H*-indole-3-carboxamide (41f).** Yield: 45%. Mp: 237-238 ºC. ^{1}H NMR (300 MHz, DMSO-d_6) δ (ppm): 8.31 (s, 1H, Ar-H), 8.09 (d, *J* = 7.3 Hz, 1H, Ar-H), 7.76 (d, *J* = 8.0 Hz, 1H, NH), 7.56 – 7.48 (m, 2H, Ar-H), 7.37 – 7.25 (m, 2H, Ar-H), 7.21 – 7.07 (m, 4H, Ar-H, NH), 5.44 (s, 2H, CH_2-Ph), 4.04 – 3.92 (m, 1H, CH), 1.26 (s, 9H, C(CH_3)$_3$), 1.20 – 1.07 (m, 1H, CH-*c*-Pr), 0.58 – 0.26 (m, 4H, *c*-Pr). LRMS (CI) m/z calcd for $C_{25}H_{29}FN_3O_2$ $[M+H]^+$: 422.2; found: 422.2.

***N*-(2-(*tert*-butylamino)-1-cyclobutyl-2-oxoethyl)-1-(4-fluorobenzyl)-1*H*-indole-3-carboxamide (41g).** Yield: 51%. Mp: 182-183 ºC. ^{1}H NMR (300 MHz, DMSO-d_6) δ (ppm): 8.28 (s, 1H, Ar-H), 8.09 (d, *J* = 7.0 Hz, 1H, Ar-H), 7.58 – 7.45 (m, 3H, Ar-H, NH), 7.37 – 7.26 (m, 2H, Ar-H), 7.20 – 7.08 (m, 3H, Ar-H), 6.02 (s, 1H, NH), 5.44 (s, 2H, CH_2-Ph), 4.57 – 4.41 (m, 1H, CH), 2.69 – 2.56 (m, 1H, CH-*c*-Bu), 2.05 – 1.64 (m,

USC UNIVERSIDADE DE SANTIAGO DE COMPOSTELA

6H, *c*-Bu), 1.24 (s, 9H, C(CH_3)$_3$). LRMS (CI) m/z calcd for $C_{26}H_{31}FN_3O_2$ $[M+H]^+$: 436.2; found: 436.2.

***N*-(1-(*tert*-butylcarbamoyl)cyclopentyl)-1-(4-fluorobenzyl)-1*H*-indole-3-carboxamide (41l).** Yield: 49%. Mp: 165-167 ºC. ^{1}H NMR (300 MHz, $CDCl_3$) δ (ppm): 7.97 – 7.88 (m, 1H, Ar-H), 7.73 (s, 1H, Ar-H), 7.41 – 7.22 (m, 4H, Ar-H, NH), 7.20 – 7.08 (m, 2H, Ar-H), 7.06 – 6.94 (m, 2H, Ar-H), 6.24 (s, 1H, NH), 5.30 (s, 2H, CH_2-Ph), 2.47 – 2.28 (m, 2H, *c*-Pent), 2.25 – 2.10 (m, 2H, *c*-Pent), 1.89 – 1.72 (m, 4H, *c*-Pent), 1.35 (s, 9H, C(CH_3)$_3$). LRMS (CI) m/z calcd for $C_{26}H_{31}FN_3O_2$ $[M+H]^+$: 436.2; found: 436.2.

***N*-(1-(*tert*-butylamino)-4-methyl-1-oxopentan-2-yl)-1-(4-fluorobenzyl)-*N*-methyl-1*H*-indole-3-carboxamide (41p).** Yield: 47%. Mp: 155-156 ºC. ^{1}H NMR (300 MHz, $CDCl_3$) δ (ppm): 7.86 – 7.71 (m, 1H, Ar-H), 7.45 (s, 1H, Ar-H), 7.32 – 7.21 (m, 3H, Ar-H), 7.17 – 7.08 (m, 2H, Ar-H), 7.04 – 6.95 (m, 2H, Ar-H), 6.77 (s, 1H, NH), 5.31 (s, 2H, CH_2-Ph), 5.12 – 4.97 (m, 1H, CH), 3.06 (s, 3H, NCH_3), 1.82 – 1.60 (m, 3H, CHCH_2(CH_3)$_2$), 1.35 (s, 9H, C(CH_3)$_3$), 1.07 – 0.84 (m, 6H, CHCH_2(CH_3)$_2$). LRMS (CI) m/z calcd for $C_{27}H_{35}FN_3O_2$ $[M+H]^+$: 452.3; found: 452.3.

***N*-(1-(*tert*-butylamino)-5-cyano-3,3-dimethyl-1-oxopentan-2-yl)-1-(4-fluorobenzyl)-*N*-methyl-1*H*-indole-3-carboxamide (41q).** Yield: 51%. Mp: 142-143 ºC. ^{1}H NMR (300 MHz, $CDCl_3$) δ (ppm): 7.95 – 7.84 (m, 1H, Ar-H), 7.52 (s, 1H, Ar-H), 7.36 – 7.22 (m, 3H, Ar-H), 7.19 – 7.10 (m, 2H, Ar-H), 7.07 – 6.92 (m, 2H, Ar-H), 6.34 (s, 1H, NH), 5.33 (s, 2H, CH_2-Ph), 5.04 (s, 1H, CH), 3.30 (s, 3H, NCH_3), 2.45 – 2.25 (m, 2H, C(CH_3)$_2$CH_2CH_2CN), 2.09 – 1.94 (m, 1H, C(CH_3)$_2$CH_2CH_2CN), 1.93 – 1.78 (m, 1H, C(CH_3)$_2$CH_2CH_2CN), 1.35 (s, 9H, C(CH_3)$_3$), 1.25 (s, 3H, C(CH_3)$_2$CH_2CH_2CN), 1.20 (s, 3H, C(CH_3)$_2$CH_2CH_2CN). LRMS (CI) m/z calcd for $C_{29}H_{36}FN_4O_2$ $[M+H]^+$: 491.3; found: 491.3.

***N*-(2-(*tert*-butylamino)-1-cyclopropyl-2-oxoethyl)-1-(4-fluorobenzyl)-*N*-methyl-1*H*-indole-3-carboxamide (41r).** Yield: 51%. Mp: 134-135 ºC. ^{1}H NMR (300 MHz, $CDCl_3$) δ (ppm): 7.85 – 7.76 (m, 1H, Ar-H), 7.49 (s, 1H, Ar-H), 7.31 – 7.18 (m, 3H, Ar-H), 7.17 – 7.05 (m, 2H, Ar-H), 7.04 – 6.92 (m, 2H, Ar-H), 6.73 (s, 1H, NH), 5.29 (s, 2H, CH_2-Ph), 4.17 – 4.07 (m, 1H, CH), 3.22 (s, 3H, NCH_3), 1.61 – 1.45 (m, 1H,

USC UNIVERSIDADE DE SANTIAGO DE COMPOSTELA

C*H*-*c*-Pr), 1.36 (s, 9H, C(CH_3)$_3$), 0.90 – 0.75 (m, 1H, *c*-Pr), 0.72 – 0.57 (m, 1H, *c*-Pr), 0.53 – 0.41 (m, 1H, *c*-Pr), 0.40 – 0.30 (m, 1H, *c*-Pr). LRMS (CI) m/z calcd for $C_{26}H_{31}FN_3O_2$ $[M+H]^+$: 436.2; found: 436.2.

***N*-(2-(*tert*-butylamino)-1-cyclobutyl-2-oxoethyl)-1-(4-fluorobenzyl)-*N*-methyl-1*H*-indole-3-carboxamide (41s).** Yield: 85%. Mp: 144-145 ºC. ^{1}H NMR (300 MHz, $CDCl_3$) δ (ppm): 7.79 – 7.68 (m, 1H, Ar-H), 7.47 (s, 1H, Ar-H), 7.33 – 7.19 (m, 3H, Ar-H), 7.17 – 7.08 (m, 2H, Ar-H), 7.06 – 6.96 (m, 2H, Ar-H), 6.76 (s, 1H, NH), 5.31 (s, 2H, CH_2-Ph), 4.89 (d, *J* = 11.3 Hz, 1H, CH), 3.16 – 3.03 (m, 1H, *c*-Bu), 3.01 (s, 3H, NCH_3), 2.38 – 2.22 (m, 1H, *c*-Bu), 2.20 – 2.08 (m, 1H, *c*-Bu), 2.03 – 1.74 (m, 4H, *c*-Bu) 1.34 (s, 9H, C(CH_3)$_3$). LRMS (CI) m/z calcd for $C_{27}H_{33}FN_3O_2$ $[M+H]^+$: 450.2; found: 450.2.

***N*-(1-(*tert*-butylcarbamoyl)cyclopentyl)-1-(4-fluorobenzyl)-*N*-methyl-1*H*-indole-3-carboxamide (41x).** Yield: 54%. Mp: 198-200 ºC. ^{1}H NMR (300 MHz, $CDCl_3$) δ (ppm): 8.15 (s, 1H, NH), 7.84 –7.74 (m, 1H, Ar-H), 7.57 (s, 1H, Ar-H), 7.35 – 7.22 (m, 3H, Ar-H), 7.20 – 7.11 (m, 2H, Ar-H), 7.08 – 6.98 (m, 2H, Ar-H), 5.33 (s, 2H, CH_2-Ph),3.11 (s, 3H, NCH_3), 2.82 – 2.70 (m, 2H, *c*-Pent), 2.06 –1.91 (m, 2H, *c*-Pent), 1.83 – 1.72 (m, 9H, *c*-Pent), 1.38 (s, 9H, C(CH_3)$_3$). LRMS (CI) m/z calcd for $C_{27}H_{33}FN_3O_2$ $[M+H]^+$: 450.2; found: 450.2.

***N*-(1-(*tert*-butylamino)-4-methyl-1-oxopentan-2-yl)-1-(cyclohexylmethyl)-1*H*-indole-3-carboxamide (42d).** Yield: 46%. Mp: 244-246 ºC. ^{1}H NMR (300 MHz, $CDCl_3$) δ (ppm): 8.16 – 8.05 (m, 1H, Ar-H), 7.76 (s, 1H, Ar-H), 7.44 – 7.14 (m, 3H, Ar-H), 6.85 (d, *J* = 8.6 Hz, 1H, NH), 6.51 (s, 1H, NH), 4.77 – 4.61 (m, 1H, CH), 3.96 (d, *J* = 7.5 Hz, 2H, CH_2-Cy), 2.28 – 2.14 (m, 1H, C*H*-Cy), 2.13 – 1.96 (m, 2H, CH_2CH(CH_3)$_2$), 1.94 – 1.54 (m, 6H, CH_2C*H*(CH_3)$_2$, Cy), 1.43 (s, 9H, C(CH_3)$_3$), 1.28 – 1.10 (m, 3H, Cy), 1.08 – 0.94 (m, 2H, Cy), 0.91 (d, *J* = 6.7 Hz, 3H, CH_2CHCH_3)$_2$), 0.82 (d, *J* = 6.6 Hz, 3H, CH_2CHCH_3)$_2$). LRMS (CI) m/z calcd for $C_{26}H_{40}N_3O_2$ $[M+H]^+$: 426.3; found: 426.3.

***N*-(1-(*tert*-butylamino)-5-cyano-3,3-dimethyl-1-oxopentan-2-yl)-1-(cyclohexylmethyl)-1*H*-indole-3-carboxamide (42e).** Yield: 47%. Mp: 242-244 ºC. ^{1}H NMR (300 MHz, $CDCl_3$) δ (ppm): 8.06 – 7.97 (m, 1H, Ar-H), 7.72 (s, 1H, Ar-H), 7.46 – 7.35

(m, 1H, Ar-H), 7.35 – 7.23 (m, 2H, Ar-H), 6.79 (d, *J* = 9.0 Hz, 1H, NH), 5.99 (s, 1H, NH), 4.54 (d, *J* = 9.0 Hz, 1H, CH), 3.98 (d, *J* = 7.2 Hz, 2H, C*H*$_2$-Cy), 2.66 – 2.36 (m, 2H, C(CH$_3$)$_2$CH$_2$C*H*$_2$CN), 1.97 – 1.53 (m, 8H, C(CH$_3$)$_2$C*H*$_2$CH$_2$CN, Cy), 1.38 (s, 9H, C(CH$_3$)$_3$), 1.30 – 0.93 (m, 11H, C(C*H*$_3$)$_2$CH$_2$CH$_2$CN, Cy). HRMS (APCI) m/z calcd for $C_{28}H_{41}N_4O_2$ $[M+H]^+$: 465.3151; found: 465.3241.

***N*-(2-(*tert*-butylamino)-1-cyclopropyl-2-oxoethyl)-1-(cyclohexylmethyl)-1*H*-indole -3-carboxamide (42f).** Yield: 45%. Oil at room temperature. ^{1}H NMR (300 MHz, $CDCl_3$) δ (ppm): 8.11 – 8.04 (m, 1H, Ar-H), 7.76 (s, 1H, Ar-H), 7.42 – 7.34 (m, 1H, Ar-H), 7.32 – 7.19 (m, 2H, Ar-H), 6.74 (d, *J* = 8.7 Hz, 1H, NH), 5.96 (s, 1H, NH), 4.61 – 4.52 (m, 1H, CH), 3.97 (d, *J* = 7.1 Hz, 2H, C*H*$_2$-Cy), 2.01 – 1.95 (m, 1H, C*H*-Cy), 1.94 – 1.58 (m, 5H, Cy), 1.41 – 1.32 (m, 1H, C*H*-*c*-Pr), 1.30 (s, 9H, C(CH$_3$)$_3$), 1.29 – 0.95 (m, 5H, Cy), 0.91 – 0.78 (m, 2H, *c*-Pr). LRMS (CI) m/z calcd for $C_{25}H_{36}N_3O_2$ $[M+H]^+$: 410.3; found: 410.3.

***N*-(2-(*tert*-butylamino)-1-cyclobutyl-2-oxoethyl)-1-(cyclohexylmethyl)-1*H*-indole-3-carboxamide (42g).** Yield: 48%. Mp: 225-226 ºC. ^{1}H NMR (300 MHz, $CDCl_3$) δ (ppm): 8.10 – 8.00 (m, 1H, Ar-H), 7.72 (s, 1H, Ar-H), 7.41 – 7.32 (m, 1H, Ar-H), 7.30 – 7.20 (m, 2H, Ar-H), 6.71 (d, *J* = 7.3 Hz ,1H, NH), 6.07 (s, 1H, NH), 4.65 – 4.51 (m, 1H, CH), 3.92 (d, *J* = 7.3 Hz, 2H, C*H*$_2$-Cy), 2.87 – 2.50 (m, 1H, C*H*-Cy), 2.15 – 1.53 (m, 12H, *c*-Bu, Cy), 1.35 (s, 9H, C(CH$_3$)$_3$), 1.25 – 0.86 (m, 5H, *c*-Bu, Cy). LRMS (CI) m/z calcd for $C_{26}H_{38}N_3O_2$ $[M+H]^+$: 424.3; found: 424.3.

***N*-(1-(*tert*-butylcarbamoyl)cyclopentyl)-1-(cyclohexylmethyl)-1*H*-indole-3-carboxamide (42l).** Yield: 51%. Mp: 226-227 ºC. ^{1}H NMR (300 MHz, $CDCl_3$) δ (ppm): 8.00 – 7.91 (m, 1H, Ar-H), 7.73 (s, 1H, Ar-H), 7.50 (s, 1H, NH), 7.43 – 7.34 (m, 1H, Ar-H), 7.33 – 7.22 (m, 2H, Ar-H), 6.34 (s, 1H, NH), 3.95 (d, *J* = 7.1 Hz, 2H, C*H*$_2$-Cy), 2.48 – 2.31 (m, 2H, *c*-Pent), 2.26 – 2.11 (m, 2H, *c*-Pent), 1.95 – 1.54 (m, 10H, *c*-Pent, Cy), 1.38 (s, 9H, C(CH$_3$)$_3$), 1.30 – 1.12 (m, 2H, Cy), 1.10 – 0.89 (m, 3H, Cy). LRMS (CI) m/z calcd for $C_{26}H_{38}N_3O_2$ $[M+H]^+$: 424.3; found: 424.3.

USC DE COMPOSTELA

***N*-(1-(*tert*-butylamino)-4-methyl-1-oxopentan-2-yl)-1-(cyclohexylmethyl)-*N*-methyl-1*H*-indole-3-carboxamide (42p).** Yield: 47%. Mp: 152-153 ºC. ^{1}H NMR (300 MHz, $CDCl_3$) δ (ppm): 7.84 (d, *J* = 7.9 Hz, 1H, Ar-H), 7.45 – 7.34 (m, 2H, Ar-H), 7.33

– 7.20 (m, 2H, Ar-H), 6.84 (s, 1H, NH), 5.08 (t, *J* = 7.6 Hz, 1H, CH), 3.98 (d, *J* = 7.0 Hz, 2H, C*H*$_2$-Cy), 3.09 (s, 3H, NCH$_3$), 1.97 – 1.60 (m, 9H, C*H*C*H*$_2$(CH$_3$)$_2$, Cy), 1.37 (s, 9H, C(CH$_3$)$_3$), 1.28 – 1.14 (m, 2H, Cy), 1.13 – 0.89 (m, 9H, CHCH$_2$(C*H*$_3$)$_2$, Cy). LRMS (CI) m/z calcd for $C_{27}H_{42}N_3O_2$ $[M+H]^+$: 440.3; found: 440.3.

***N*-(1-(*tert*-butylamino)-5-cyano-3,3-dimethyl-1-oxopentan-2-yl)-1-(cyclohexylmethyl)-*N*-methyl-1*H*-indole-3-carboxamide (42q).** Yield: 51%. Mp: 156-157 ºC. ^{1}H NMR (300 MHz, $CDCl_3$) δ (ppm): 7.91 – 7.82 (m, 1H, Ar-H), 7.44 (s, 1H, Ar-H), 7.41 – 7.34 (m, 1H, Ar-H), 7.32 – 7.20 (m, 2H, Ar-H), 6.33 (s, 1H, NH), 5.01 (s, 1H, CH), 3.98 (d, *J* = 7.6 Hz, 2H, C*H*$_2$-Cy), 3.30 (s, 3H, NCH$_3$), 2.46 – 2.32 (m, 2H, C(CH$_3$)$_2$CH$_2$C*H*$_2$CN), 2.10 – 1.59 (m, 8H, C(CH$_3$)$_2$C*H*$_2$CH$_2$CN, Cy), 1.35 (s, 9H, C(CH$_3$)$_3$), 1.30 – 0.92 (m, 11H, C(C*H*$_3$)$_2$CH$_2$CH$_2$CN, Cy). LRMS (CI) m/z calcd for $C_{29}H_{43}N_4O_2$ $[M+H]^+$: 479.3; found: 479.3.

***N*-(2-(*tert*-butylamino)-1-cyclopropyl-2-oxoethyl)-1-(cyclohexylmethyl)-*N*-methyl-1*H*-indole-3-carboxamide (42r).** Yield: 49%. Mp: 125-127 ºC. ^{1}H NMR (300 MHz, $CDCl_3$) δ (ppm): 7.79 (d, *J* = 7.5 Hz, 1H, Ar-H), 7.43 (s, 1H, Ar-H), 7.40 – 7.32 (m, 2H, Ar-H), 7.31 – 7.16 (m, 2H, Ar-H), 6.79 (s, 1H, NH), 4.12 (d, *J* = 9.1 Hz, 1H, CH), 3.96 (d, *J* = 7.3 Hz, 2H, C*H*$_2$-Cy), 3.23 (s, 3H, NCH$_3$), 1.96 – 1.80 (m, 1H, C*H*-Cy), 1.78 – 1.49 (m, 5H, Cy), 1.38 (s, 9H, C(CH$_3$)$_3$), 1.28 – 1.10 (m, 2H, Cy), 1.10 – 0.92 (m, 3H, Cy), 0.90 – 0.76 (m, 1H, *c*-Pr), 0.73 – 0.58 (m, 1H, *c*-Pr), 0.56 – 0.30 (m, 2H, *c*-Pr). LRMS (CI) m/z calcd for $C_{26}H_{38}N_3O_2$ $[M+H]^+$: 424.3; found: 424.3.

***N*-(2-(*tert*-butylamino)-1-cyclobutyl-2-oxoethyl)-1-(cyclohexylmethyl)-*N*-methyl-1*H*-indole-3-carboxamide (42s).** Yield: 46%. Mp: 132-133 ºC. ^{1}H NMR (300 MHz, $CDCl_3$) δ (ppm): 7.73 (d, *J* = 7.7 Hz, 1H, Ar-H), 7.41 (s, 1H, Ar-H), 7.39 – 7.32 (m, 1H, Ar-H), 7.30 – 7.16 (m, 2H, Ar-H), 6.82 (s, 1H, NH) 4.90 (d, *J* = 11.4 Hz, 1H, CH), 3.96 (d, *J* = 7.2 Hz, 2H, C*H*$_2$-Cy), 3.17 – 2.94 (m, 4H, NCH$_3$, CH-*c*-Bu), 2.38 – 2.23 (m, 1H, *c*-Bu), 2.20 – 2.07 (m, 1H, *c*-Bu), 2.06 – 1.56 (m, 10H, *c*-Bu, Cy), 1.35 (s, 9H, C(CH$_3$)$_3$), 1.28 – 1.10 (m, 2H, Cy, *c*-Bu), 1.10 – 0.91 (m, 3H, Cy). LRMS (CI) m/z calcd for $C_{27}H_{40}N_3O_2$ $[M+H]^+$: 438.3; found: 438.3.

USC UNIVERSIDADE DE SANTIAGO DE COMPOSTELA

***N*-(1-(*tert*-butylcarbamoyl)cyclopentyl)-1-(cyclohexylmethyl)-*N*-methyl-1*H*-indole-3-carboxamide (42x).** Yield: 47%. Mp: 150-151 ºC. ^{1}H NMR (300 MHz, $CDCl_3$) δ (ppm): 8.24 (s, 1H, NH), 7.78 (d, *J* = 6.8 Hz, 1H, Ar-H), 7.52 (s, 1H, Ar-H), 7.43 – 7.35 (m, 1H, Ar-H), 7.33 –7.21 (m, 2H, Ar-H), 3.98 (d, *J* = 7.1 Hz, 2H, C*H*$_2$-Cy), 3.12 (s, 3H, NCH_3), 2.84 – 2.68 (m, 2H, *c*-Pent), 2.11 – 1.60 (m, 12H, *c*-Pent, Cy), 1.39 (s, 9H, $C(CH_3)_3$), 1.31 – 0.97 (m, 5H, Cy). LRMS (CI) m/z calcd for $C_{27}H_{40}N_3O_2$ $[M+H]^+$: 438.3; found: 438.3.

***N*-(1-(*tert*-butylamino)-3-methyl-1-oxobutan-2-yl)-1-(5-fluoropentyl)-1*H*-indole-3-carboxamide (43a).** Yield: 51%. Mp: 196-197 ºC. ^{1}H NMR (300 MHz, $CDCl_3$) δ (ppm): 8.05 (d, *J* = 6.0 Hz, 1H, Ar-H), 7.74 (s, 1H, Ar-H), 7.43 – 7.33 (m, 1H, Ar-H), 7.33 – 7.21 (m, 2H, Ar-H), 6.69 (d, *J* = 8.3 Hz, 1H, NH), 5.80 (s, 1H, NH), 4.49 (t, *J* = 6.0 Hz, 1H, CH), 4.44 – 4.29 (m, 2H, $CH_2CH_2CH_2CH_2CH_2F$), 4.15 (t, *J* = 7.0 Hz, 2H, $CH_2CH_2CH_2CH_2CH_2F$), 2.29 – 2.09 (m, 1H, $CH(CH_3)_2$), 2.00 – 1.82 (m, 2H, $CH_2CH_2CH_2CH_2CH_2F$), 1.82 – 1.60 (m, 2H, $CH_2CH_2CH_2CH_2CH_2F$), 1.53 – 1.40 (m, 2H, $CH_2CH_2CH_2CH_2CH_2F$) 1.39 (s, 9H, $C(CH_3)_3$), 1.04 (d, *J* = 6.8 Hz, 6H, $CH(CH_3)_2$). HRMS (APCI) m/z calcd for $C_{23}H_{35}FN_3O_2$ $[M+H]^+$: 404.2635; found: 404.2716.

***N*-(1-(*tert*-butylamino)-3,3-dimethyl-1-oxobutan-2-yl)-1-(5-fluoropentyl)-1*H*-in-dole-3-carboxamide (43b).** Yield: 47%. Mp: 206-207 ºC. ^{1}H NMR (300 MHz, $CDCl_3$) δ (ppm): 8.10 – 8.02 (m, 1H, Ar-H), 7.79 (s, 1H, Ar-H), 7.44 – 7.36 (m, 1H, Ar-H), 7.34 – 7.28 (m, 2H, Ar-H), 6.84 (d, *J* = 7.2 Hz, 1H, NH), 5.54 (s, 1H, NH), 4.53 (t, *J* = 5.7 Hz, 1H, $CH_2CH_2CH_2CH_2CH_2F$), 4.45 – 4.32 (m, 2H, $CH_2CH_2CH_2CH_2CH_2F$, CH), 4.19 (t, *J* = 6.9 Hz, 2H, $CH_2CH_2CH_2CH_2CH_2F$), 2.08 – 1.87 (m, 2H, $CH_2CH_2CH_2CH_2CH_2F$), 1.84 – 1.73 (m, 2H, $CH_2CH_2CH_2CH_2CH_2F$), 1.55 – 1.44 (m, 2H, $CH_2CH_2CH_2CH_2CH_2F$), 1.39 (s, 9H, $C(CH_3)_3$), 1.12 (s, 9H, $C(CH_3)_3$). HRMS (APCI) m/z calcd for $C_{24}H_{37}FN_3O_2$ $[M+H]^+$: 418.27792.; found: 418.2877.

***N*-(1-(*tert*-butylamino)-4-methyl-1-oxopentan-2-yl)-1-(5-fluoropentyl)-1*H*-indole-3-carboxamide (43c).** Yield: 51%. Mp: 195-196 ºC. ^{1}H NMR (300 MHz, $CDCl_3$) δ (ppm): 8.09 – 7.97 (m, 1H, Ar-H), 7.71 (s, 1H, Ar-H), 7.40 – 7.32 (m, 1H, Ar-H), 7.30 – 7.24 (m, 2H, Ar-H), 6.43 (d, *J* = 7.6 Hz, 1H, NH), 6.04 (s, 1H, NH), 4.68 – 4.55 (m, 1H, CH), 4.50 (t, *J* = 5.9 Hz, 1H, $CH_2CH_2CH_2CH_2CH_2F$), 4.34 (t, *J* = 5.8 Hz, 1H, $CH_2CH_2CH_2CH_2CH_2F$), 4.15 (t, *J* = 7.1 Hz, 2H, $CH_2CH_2CH_2CH_2CH_2F$), 2.00 –

USC DE COMPOSTELA

1.83 (m, 2H, CHC*H*$_2$(CH$_3$)$_2$), 1.82 – 60 (m, 5H, C*H*CH$_2$(CH$_3$)$_2$, CH$_2$C*H*$_2$CH$_2$C*H*$_2$CH$_2$F), 1.54 – 1.40 (m, 2H, CH$_2$CH$_2$C*H*$_2$CH$_2$CH$_2$F), 1.36 (s, 9H, C(CH$_3$)$_3$), 1.03 – 0.94 (m, 6H, CH$_2$CH(C*H*$_3$)$_2$). LRMS (CI) m/z calcd for $C_{24}H_{37}FN_3O_2$ $[M+H]^+$: 418.3; found: 418.3.

***N*-(1-(*tert*-butylamino)-5-cyano-3,3-dimethyl-1-oxopentan-2-yl)-1-(5-fluoropentyl)-1*H*-indole-3-carboxamide (43d).** Yield: 55%. Mp: 198-200 ºC. ^{1}H NMR (300 MHz, CDCl$_3$) δ (ppm): 8.07 – 7.97 (m, 1H, Ar-H), 7.75 (s, 1H, Ar-H), 7.44 – 7.35 (m, 1H, Ar-H), 7.34 – 7.27 (m, 2H, Ar-H), 6.82 (d, *J* = 8.6 Hz, 1H, NH), 6.27 (s, 1H, NH), 4.60 (d, *J* = 9.1 Hz, 1H, CH), 4.51 (t, *J* = 5.7 Hz, 1H, CH$_2$CH$_2$CH$_2$CH$_2$C*H*$_2$F), 4.35 (t, *J* = 5.8 Hz, 1H, CH$_2$CH$_2$CH$_2$CH$_2$C*H*$_2$F), 4.18 (t, *J* = 7.3 Hz, 2H, C*H*$_2$CH$_2$CH$_2$CH$_2$CH$_2$F), 2.64 – 2.32 (m, 2H, C(CH$_3$)$_2$CH$_2$C*H*$_2$CN), 2.02 – 1.55 (m, 6H, C(CH$_3$)$_2$C*H*$_2$CH$_2$CN), CH$_2$C*H*$_2$CH$_2$C*H*$_2$CH$_2$F, 1.55 – 1.40 (m, 2H, CH$_2$CH$_2$C*H*$_2$CH$_2$CH$_2$F), 1.36 (s, 9H, C(CH$_3$)$_3$), 1.14 (s, 3H, C(C*H*$_3$)$_2$CH$_2$CH$_2$CN), 1.11 (s, 3H, C(C*H*$_3$)$_2$CH$_2$CH$_2$CN). HRMS (APCI) m/z calcd for $C_{26}H_{38}FN_4O_2$ $[M+H]^+$: 457.2901; found: 457.2964.

***N*-(1-(*tert*-butylamino)-3-methyl-1-oxobutan-2-yl)-1-pentyl-1*H*-indole-3-carboxamide (43e).** Yield: 45%. Mp: 205-206 ºC. ^{1}H NMR (300 MHz, CDCl$_3$) δ (ppm): 8.13 – 7.96 (m, 1H, Ar-H), 7.74 (s, 1H, Ar-H), 7.42 – 7.33 (m, 1H, Ar-H), 7.31 – 7.16 (m, 2H, Ar-H), 6.69 (d, *J* = 8.3 Hz, 1H, NH), 5.85 (s, 1H, NH), 4.40 (t, *J* = 7.7 Hz, 1H, CH), 4.11 (t, *J* = 7.2 Hz, 2H, C*H*$_2$CH$_2$CH$_2$CH$_2$CH$_3$), 2.28 – 2.08 (m, 1H, C*H*(CH$_3$)$_2$), 1.93 – 1.77 (m, 2H, CH$_2$C*H*$_2$CH$_2$CH$_2$CH$_3$), 1.53 – 1.21 (m, 13H, CH$_2$CH$_2$C*H*$_2$C*H*$_2$CH$_3$, C(CH$_3$)$_3$), 1.10 – 0.97 (m, 6H, CH(C*H*$_3$)$_2$), 0.88 (t, *J* = 6.8 Hz, 3H, CH$_2$CH$_2$CH$_2$CH$_2$C*H*$_3$). LRMS (CI) m/z calcd for $C_{23}H_{36}N_3O_2$ $[M+H]^+$: 386.3; found: 386.3.

***N*-(1-(*tert*-butylamino)-3,3-dimethyl-1-oxobutan-2-yl)-1-pentyl-1*H*-indole-3-carboxamide (43f).** Yield: 45%. Mp: 215-216 ºC. ^{1}H NMR (300 MHz, CDCl$_3$) δ (ppm): 8.12 – 8.03 (m, 1H, Ar-H), 7.77 (s, 1H, Ar-H), 7.44 – 7.35 (m, 1H, Ar-H), 7.34 – 7.23 (m, 2H, Ar-H), 6.86 (d, *J* = 9.0 Hz, 1H, NH), 5.93 (s, 1H, NH), 4.49 (d, *J* = 9.1 Hz, 1H, CH), 4.14 (t, *J* = 7.2 Hz, 2H, C*H*$_2$CH$_2$CH$_2$CH$_2$CH$_3$), 1.96 – 1.80 (m, 2H, CH$_2$C*H*$_2$CH$_2$CH$_2$CH$_3$), 1.48 – 1.21 (m, 13H, CH$_2$CH$_2$C*H*$_2$C*H*$_2$CH$_3$, C(CH$_3$)$_3$), 1.12 (s, 9H, C(CH$_3$)$_3$), 0.91 (t, *J* = 6.7 Hz, 3H, CH$_2$CH$_2$CH$_2$CH$_2$C*H*$_3$). HRMS (APCI) m/z calcd for $C_{24}H_{38}N_3O_2$ $[M+H]^+$: 400.2886; found: 400.2961.

USC DE COMPOSTELA

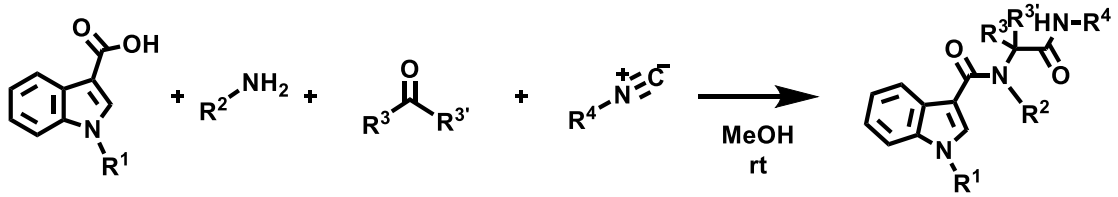
***N*-(1-(*tert*-butylamino)-4-methyl-1-oxopentan-2-yl)-1-pentyl-1*H*-indole-3-carboxamide (43g).** Yield: 51%. Mp: 185-187 ºC. ^{1}H NMR (300 MHz, $CDCl_3$) δ (ppm): 8.06 – 7.96 (m, 1H, Ar-H), 7.73 (s, 1H, Ar-H), 7.41 – 7.33 (m, 1H, Ar-H), 7.31 – 7.21 (m, 2H, Ar-H), 6.45 (s, 1H, NH), 6.12 (s, 1H, NH), 4.62 (d, *J* = 6.1 Hz, 1H, CH), 4.12 (t, *J* = 7.2 Hz, 2H, C*H*$_2$CH$_2$CH$_2$CH$_2$CH$_3$), 1.93 – 1.80 (m, 2H, C*H*$_2$CH(CH$_3$)$_2$), 1.79 – 1.68 (m, 3H, CH$_2$C*H*(CH$_3$)$_2$, CH$_2$C*H*$_2$CH$_2$CH$_2$CH$_3$), 1.43 – 1.25 (m, 13H, CH$_2$CH$_2$C*H*$_2$C*H*$_2$CH$_3$, CH(CH$_3$)$_3$), 1.04 – 0.94 (m, 6H, CH$_2$CH(C*H*$_3$)$_2$), 0.89 (t, *J* = 6.8 Hz, 3H, CH$_2$CH$_2$CH$_2$CH$_2$C*H*$_3$). LRMS (CI) m/z calcd for $C_{24}H_{38}N_3O_2$ $[M+H]^+$: 400.3; found: 400.3.

***N*-(1-(*tert*-butylamino)-5-cyano-3,3-dimethyl-1-oxopentan-2-yl)-1-pentyl-1*H*-indole-3-carboxamide (43h).** Yield: 48%. Mp: 215-216 ºC. ^{1}H NMR (300 MHz, $CDCl_3$) δ (ppm): 8.08 – 7.98 (m, 1H, Ar-H), 7.75 (s, 1H, Ar-H), 7.45 – 7.35 (m, 1H, Ar-H), 7.33 – 7.22 (m, 2H, Ar-H), 6.84 (d, *J* = 9.1 Hz, 1H, NH), 6.49 (s, 1H, NH), 4.66 (d, *J* = 9.1 Hz, 1H, CH), 4.14 (t, *J* = 7.2 Hz, 2H, C*H*$_2$CH$_2$CH$_2$CH$_2$CH$_3$), 2.64 – 2.30 (m, 2H, C(CH$_3$)$_2$CH$_2$C*H*$_2$CN), 1.98 – 1.68 (m, 4H, C(CH$_3$)$_2$C*H*$_2$CH$_2$CN, CH$_2$C*H*$_2$CH$_2$CH$_2$CH$_3$), 1.49 – 1.25 (m, 13H, CH$_2$CH$_2$C*H*$_2$C*H*$_2$CH$_3$, C(CH$_3$)$_3$), 1.14 (s, 3H, C(C*H*$_3$)$_2$CH$_2$CH$_2$CN), 1.11 (s, 3H, C(C*H*$_3$)$_2$CH$_2$CH$_2$CN), 0.89 (t, *J* = 6.7 Hz, 3H, CH$_2$CH$_2$CH$_2$CH$_2$C*H*$_3$). HRMS (APCI) m/z calcd for $C_{26}H_{39}N_4O_2$ $[M+H]^+$: 439.2995; found: 439.3073.

USC UNIVERSIDADE DE SANTIAGO DE COMPOSTELA

4.5.2 General pathways for the synthesis of *N*-(2-amino-2-oxoethyl)-1*H*-indole-3-carboxamide polysubstituted (44a-r, 45a-r, 46a-l, 47a-r)

A mixture of the *N*-alkyl-1*H*-indole-3-carboxylic acid (1 equiv.), the corresponding aldehyde (or ketone) (1 equiv.), amine (1 equiv.) and isonitrile (1 equiv.) in MeOH (2 mL) was stirred with orbital stirring at room temperature for 24 h. After completion of the reaction, PS-p-TsOH (2.0 mmol) and CH_2Cl_2 (3 mL) were added. The reaction mixture was submitted to orbital stirring at room temperature until complete consumption of the unreacted isocyanide (30-60 min). The polystyrene-supported salt was filtered off and successively washed with MeOH (3 × 5 mL) and CH_2Cl_2 (3 × 5 mL). The resulting product was purified by column chromatography on silica gel using MeOH/CH_2Cl_2.



26a-d
R1 = 5-F-Pentyl
R1 = Pentyl
R1 = CH_2-Cy
R1 = 4-F-Bn

32a,b
R2 = H
R2 = CH_3

34b,c,h
R3, R3' = *i*-Pr, H
R3, R3' = *t*-Bu, H
R3, R3' = *i*-Bu, H

33a,b,d-k
R4 = *t*-Bu
R4 = Bn
R4 = Cy
R4 = *c*-Pr
R4 = Ad
R4 = Pentyl
R4 = Et-Morpholine
R4 = CH_2-P(O)-$(OEt)_2$
R4 = CH_2COOCH_3
R4 = Piperidine derivative

44a-r, 45a-r, 46a-l, 47a-r

Scheme S9: General procedure for the synthesis of *N*-(2-amino-2-oxoethyl)-1*H*-indole-3-carboxamide polysubstituted (**44a-r**, **45a-r**, **46a-l**, **47a-r**).

4.5.2.1 Spectroscopic and analytic data of *N*-(2-amino-2-oxoethyl)-1*H*-indole-3-carboxamide polysubstituted

***N*-(1-(cyclohexylamino)-3-methyl-1-oxobutan-2-yl)-1-(4-fluorobenzyl)-1*H*-indole-3-carboxamide (44c).** Yield: 47%. Mp: 227-228 ºC. ^{1}H NMR (300 MHz, $CDCl_3$) δ (ppm): 8.11 (d, *J* = 8.7 Hz, 1H, Ar-H), 7.77 (s, 1H, Ar-H), 7.33 – 7.19 (m, 3H, Ar-H), 7.14 – 7.03 (m, 2H, Ar-H), 7.02 – 6.89 (m, 3H, Ar-H, NH), 6.45 (brs, 1H, NH), 5.21 (s, 2H, C*H*$_2$-Ph), 4.52 (t, *J* = 8.0 Hz, 1H, CH), 3.86 – 3.69 (m, 1H, C*H*-Cy), 2.28 – 2.11 (m, 1H, C*H*$(CH_3)_2$), 2.00 – 1.79 (m, 2H, Cy), 1.76 – 1.51 (m, 3H, Cy), 1.45 – 1.07

(m, 5H, Cy), 1.07 – 0.99 (m, 6H, CH(C*H*$_3$)$_2$). LRMS (CI) m/z calcd for $C_{27}H_{33}FN_3O_2$ $[M+H]^+$: 450.2; found: 450.2.

***N*-(1-(cyclohexylamino)-3,3-dimethyl-1-oxobutan-2-yl)-1-(4-fluorobenzyl)-1*H*-indole-3-carboxamide (44f).** Yield: 44%. Mp: 248-249 ºC. ^{1}H NMR (300 MHz, $CDCl_3$) δ (ppm): 8.06 (d, *J* = 8.3 Hz, 1H, Ar-H), 7.75 (s, 1H, Ar-H), 7.37 – 7.19 (m, 3H, Ar-H), 7.18 – 7.07 (m, 2H, Ar-H), 7.06 – 6.92 (m, 2H, Ar-H), 6.82 (d, *J* = 9.3 Hz, 1H, NH), 5.74 – 5.59 (m, 1H, NH), 5.30 (s, 2H, C*H*$_2$-Ph), 4.45 (d, *J* = 9.3 Hz, 1H, CH), 3.87 – 3.70 (m, 1H, C*H*-Cy), 2.08 – 1.79 (m, 2H, Cy), 1.77 – 1.50 (m, 3H, Cy), 1.43 – 1.27 (m, 2H, Cy), 1.26 – 1.01 (m, 12H, C(CH$_3$)$_3$, Cy). LRMS (CI) m/z calcd for $C_{28}H_{35}FN_3O_2$ $[M+H]^+$: 464.3; found: 464.3.

***N*-(1-(benzylamino)-4-methyl-1-oxopentan-2-yl)-1-(4-fluorobenzyl)-1*H*-indole-3-carboxamide (44h).** Yield: 47%. Mp: 182-184 ºC. ^{1}H NMR (300 MHz, DMSO-*d*$_6$) δ (ppm): 8.47 (t, *J* = 5.8 Hz, 1H, Ar-H), 8.26 (s, 1H, Ar-H), 8.14 (d, *J* = 7.2 Hz, 1H, NH), 7.91 (d, *J* = 8.3 Hz, 1H, NH), 7.53 (d, *J* = 8.1 Hz, 1H, Ar-H), 7.36 – 7.06 (m, 11H, Ar-H), 5.44 (s, 2H, C*H*$_2$-Ph), 4.63 – 4.49 (m, 1H, CH), 4.27 (d, *J* = 5.9 Hz, 2H, NH-C*H*$_2$-Ph), 1.72 – 1.60 (m, 2H, CHC*H*$_2$(CH$_3$)$_2$), 1.60 – 1.48 (m, 1H, C*H*CH$_2$(CH$_3$)$_2$), 0.91 (d, *J* = 6.2 Hz, 3H, CHCH$_2$(C*H*$_3$)$_2$), 0.87 (d, *J* = 6.4 Hz, 3H, CHCH$_2$(C*H*$_3$)$_2$). LRMS (CI) m/z calcd for $C_{29}H_{31}FN_3O_2$ $[M+H]^+$: 472.2; found: 472.2.

***N*-(1-(cyclohexylamino)-4-methyl-1-oxopentan-2-yl)-1-(4-fluorobenzyl)-1*H*-indole-3-carboxamide (44i).** Yield: 51%. Mp: 144-145 ºC. ^{1}H NMR (300 MHz, DMSO-*d*$_6$) δ (ppm): 8.25 (s, 1H, Ar-H), 8.11 (d, *J* = 7.2 Hz, 1H, Ar-H), 7.80 (t, *J* = 9.6 Hz, 2H, Ar-H), 7.52 (d, *J* = 7.1 Hz, 1H, Ar-H), 7.36 – 7.25 (m, 2H, Ar-H), 7.21 – 7.09 (m, 4H, Ar-H, NH, NH), 5.43 (s, 2H, C*H*$_2$-Ph), 4.58 – 4.42 (m, 1H, CH), 3.58 – 3.42 (m, 1H, C*H*-Cy), 1.78 – 1.39 (m, 8H, CHC*H*$_2$(CH$_3$)$_2$, Cy), 1.32 – 1.03 (m, 5H, C*H*CH$_2$(CH$_3$)$_2$, Cy), 0.95 – 0.81 (m, 6H, CHCH$_2$(C*H*$_3$)$_2$). LRMS (CI) m/z calcd for $C_{28}H_{35}FN_3O_2$ $[M+H]^+$: 464.3; found: 464.3.

***N*-(1-(cyclohexylamino)-3-methyl-1-oxobutan-2-yl)-1-(4-fluorobenzyl)-*N*-methyl-1*H*-indole-3-carboxamide (44l).** Yield: 46%. Mp: 130-131 ºC. ^{1}H NMR (300 MHz, $CDCl_3$) δ (ppm): 7.85 – 7.74 (m, 1H, Ar-H), 7.44 (s, 1H, Ar-H), 7.32 – 7.19 (m, 3H, Ar-H), 7.16 – 7.07 (m, 2H, Ar-H), 7.05 – 6.94 (m, 2H, Ar-H), 6.78 (s, 1H, NH),

USC DE COMPOSTELA

5.30 (s, 2H, C*H*$_2$-Ph), 4.53 (d, *J* = 11.2 Hz, 1H, CH), 3.85 – 3.67 (m, 1H, C*H*-Cy), 3.12 (s, 3H, NCH$_3$), 2.53 – 2.35 (m, 1H, C*H*(CH$_3$)$_2$ CH(CH$_3$)$_2$), 2.20 – 1.50 (m, 5H, Cy), 1.46 – 1.09 (m, 5H, Cy), 1.10 – 0.97 (m, 6H, CH(C*H*$_3$)$_2$). LRMS (CI) m/z calcd for $C_{28}H_{35}FN_3O_2$ $[M+H]^+$: 464.3; found: 464.3.

***N*-(1-(cyclohexylamino)-3,3-dimethyl-1-oxobutan-2-yl)-1-(4-fluorobenzyl)-*N*-methyl-1*H*-indole-3-carboxamide (44o).** Yield: 45%. Mp: 133-135 ºC. ^{1}H NMR (300 MHz, $CDCl_3$) δ (ppm): 7.91 – 7.79 (m, 1H, Ar-H), 7.46 (s, 1H, Ar-H), 7.31 – 7.18 (m, 3H, Ar-H), 7.16 – 7.06 (m, 2H, Ar-H), 7.04 – 6.90 (m, 2H, Ar-H), 6.30 (s, 1H, NH), 5.30 (s, 2H, C*H*$_2$-Ph), 5.03 (s, 1H, CH), 3.87 – 3.65 (m, 1H, C*H*-Cy), 3.28 (s, 3H, NCH$_3$), 1.98 – 1.48 (m, 5H, Cy), 1.45 – 1.01 (m, 14H, C(CH$_3$)$_3$, Cy). LRMS (CI) m/z calcd for $C_{29}H_{37}FN_3O_2$ $[M+H]^+$: 478.3; found: 478.3.

***N*-(1-(benzylamino)-4-methyl-1-oxopentan-2-yl)-1-(4-fluorobenzyl)-*N*-methyl-1*H*-indole-3-carboxamide (44q).** Yield: 54%. Oil at room temperature. ^{1}H NMR (300 MHz, $CDCl_3$) δ (ppm): 7.75 – 7.68 (m, 1H, Ar-H), 7.40 (s, 1H, Ar-H), 7.32 – 7.18 (m, 9H, Ar-H, NH), 7.16 – 7.08 (m, 2H, Ar-H), 7.07 – 6.97 (m, 2H, Ar-H), 5.29 (s, 2H, C*H*$_2$-Ph), 5.18 (t, *J* = 6.3 Hz, 1H, CH), 4.53 (dd, *J* = 15.0, 6.6 Hz, 1H, NH-C*H*$_2$-Ph), 4.40 (dd, *J* = 14.7, 5.4 Hz, NH-C*H*$_2$-Ph), 3.07 (s, 3H, NCH$_3$), 1.85 (t, *J* = 7.4 Hz, 2H, CH$_2$CH(CH$_3$)$_2$), 1.77 – 1.61 (m, 1H, CH$_2$CH(CH$_3$)$_2$), 1.02 (t, *J* = 6.6 Hz, 3H, CH$_2$CH(C*H*$_3$)$_2$), 0.94 (t, *J* = 5.8 Hz, 3H, CH$_2$CH(C*H*$_3$)$_2$). LRMS (CI) m/z calcd for $C_{30}H_{33}FN_3O_2$ $[M+H]^+$: 486.2; found: 486.2.

***N*-(1-(cyclohexylamino)-4-methyl-1-oxopentan-2-yl)-1-(4-fluorobenzyl)-*N*-methyl-1*H*-indole-3-carboxamide (44r).** Yield: 51%. Oil at room temperature. ^{1}H NMR (300 MHz, $CDCl_3$) δ (ppm): 7.85 – 7.76 (m, 1H, Ar-H), 7.44 (s, 1H, Ar-H), 7.32 – 7.20 (m, 3H, Ar-H), 7.17 – 7.07 (m, 2H, Ar-H), 7.07 – 6.95 (m, 2H, Ar-H), 6.94 – 6.70 (m, 1H, NH), 5.31 (s, 2H, C*H*$_2$-Ph), 5.16 – 5.03 (m, 1H, CH), 3.84 – 3.68 (m, 1H, C*H*-Cy), 3.06 (s, 3H, NCH$_3$), 1.98 – 1.48 (m, 8H, C*H*C*H*$_2$(CH$_3$)$_2$, Cy), 1.48 – 1.07 (m, 5H, Cy), 1.06 – 0.84 (m, 6H, CHCH$_2$(C*H*$_3$)$_2$). LRMS (CI) m/z calcd for $C_{29}H_{37}FN_3O_2$ $[M+H]^+$: 478.3; found: 478.3.

USC UNIVERSIDADE DE SANTIAGO DE COMPOSTELA

***N*-(1-(cyclohexylamino)-3-methyl-1-oxobutan-2-yl)-1-(cyclohexylmethyl)-1*H*-indole-3-carboxamide (45c).** Yield: 47%. Mp: 199-200 ºC. ^{1}H NMR (300 MHz, $CDCl_3$) δ (ppm): 8.15 – 8.06 (m, 1H, Ar-H), 7.73 (s, 1H, Ar-H), 7.40 – 7.17 (m, 3H, Ar-H), 6.96 (d, *J* = 8.7 Hz, 1H, NH), 6.73 (d, *J* = 8.0 Hz, 1H, NH), 4.58 (t, *J* = 7.9 Hz, 1H, CH), 3.95 – 3.68 (m, 3H, C*H*$_2$-Cy, NH-C*H*-Cy), 2.31 – 1.47 (m, 12H, C*H*$(CH_3)_2$, NH-Cy, Cy), 1.45 – 0.75 (m, 16H, CH(C*H*$_3)_2$, NH-Cy, Cy). LRMS (CI) m/z calcd for $C_{27}H_{40}N_3O_2$ $[M+H]^+$: 438.3; found: 438.3.

***N*-(1-(cyclohexylamino)-3,3-dimethyl-1-oxobutan-2-yl)-1-(cyclohexylmethyl)-1*H*-indole-3-carboxamide (45f).** Yield: 46%. Mp: 260-261 ºC. ^{1}H NMR (300 MHz, $CDCl_3$) δ (ppm): 8.16 – 8.05 (m, 1H, Ar-H), 7.71 (s, 1H, Ar-H), 7.41 – 7.33 (m, 1H, Ar-H), 7.31 – 7.21 (m, 2H, Ar-H), 6.91 (d, *J* = 9.0 Hz, 1H, NH), 4.78 – 4.63 (m, 1H, CH), 3.93 (d, *J* = 7.2 Hz, 2H, C*H*$_2$-Cy), 3.85 – 3.70 (m, 1H, NH-C*H*-Cy), 2.06 – 1.92 (m, 1H, C*H*-Cy), 1.92 – 1.47 (m, 10H, NH-Cy, Cy), 1.44 – 0.87 (m, 19H, C$(CH_3)_3$, NH-Cy, Cy). LRMS (CI) m/z calcd for $C_{28}H_{42}N_3O_2$ $[M+H]^+$: 452.3; found: 452.3.

***N*-(1-(benzylamino)-4-methyl-1-oxopentan-2-yl)-1-(cyclohexylmethyl)-1*H*-indole-3-carboxamide (45h).** Yield: 45%. Mp: 149-151 ºC. ^{1}H NMR (300 MHz, $CDCl_3$) δ (ppm): 8.08 – 7.97 (m, 1H, Ar-H), 7.68 (s, 1H, Ar-H), 7.41 – 7.19 (m, 8H, Ar-H), 7.18 –7.08 (m, 1H, NH), 6.62 (d, *J* = 8.7 Hz, 1H, NH), 4.88 – 4.77 (m, 1H, CH), 4.44 (dq, *J* = 15.1, 6.0 Hz, 2H, C*H*$_2$-Ph), 3.89 (d, *J* = 7.1 Hz, 2H, C*H*$_2$-Cy), 2.04 – 1.39 (m, 9H, C*H*C*H*$_2(CH_3)_2$, Cy), 1.23 – 1.07 (m, 2H, Cy), 1.06 – 0.72 (m, 9H, CHCH$_2$(C*H*$_3)_2$, Cy). HRMS (APCI) m/z calcd for $C_{29}H_{38}N_3O_2$ $[M+H]^+$: 460.2826; found: 460.2956.

***N*-(1-(cyclohexylamino)-4-methyl-1-oxopentan-2-yl)-1-(cyclohexylmethyl)-1*H*-indole-3-carboxamide (45i).** Yield: 47%. Mp: 154-155 ºC. ^{1}H NMR (300 MHz, $CDCl_3$) δ (ppm): 8.08 – 7.95 (m, 1H, Ar-H), 7.68 (s, 1H, Ar-H), 7.40 – 7.31 (m, 1H, Ar-H), 7.30 – 7.18 (m, 2H, Ar-H), 6.54 (d, *J* = 5.3 Hz, 1H, NH), 6.32 (d, *J* = 5.6 Hz, 1H, NH), 4.72 – 4.62 (m, 1H, CH), 3.92 (d, *J* = 7.1 Hz, 2H, C*H*$_2$-Cy), 3.82 – 3.68 (m, 1H, NH-C*H*-Cy), 1.98 – 1.49 (m, 13H, C*H*C*H*$_2(CH_3)_2$, NH-Cy, Cy), 1.48 – 1.06 (m, 10H, NH-Cy, Cy), 0.96 (d, *J* = 5.6 Hz, 6H, CHCH$_2$(C*H*$_3)_2$). LRMS (CI) m/z calcd for $C_{28}H_{42}N_3O_2$ $[M+H]^+$: 452.3; found: 452.3.

USC UNIVERSIDADE DE SANTIAGO

***N*-(1-(cyclohexylamino)-3-methyl-1-oxobutan-2-yl)-1-(cyclohexylmethyl)-*N*-methyl-1*H*-indole-3-carboxamide (45l).** Yield: 48%. Oil at room temperature. ^{1}H NMR (300 MHz, $CDCl_3$) δ (ppm): 7.78 (d, *J* = 7.8 Hz, 1H, Ar-H), 7.43 – 7.31 (m, 2H, Ar-H), 7.29 – 7.14 (m, 2H, Ar-H), 6.86 (s, 1H, NH), 4.52 (d, *J* = 11.7 Hz, 1H, CH), 3.94 (d, *J* = 7.2 Hz, 2H, C*H*$_2$-Cy), 3.83 – 3.67 (m, 1H, NH-C*H*-Cy), 3.12 (s, 3H, NCH_3), 2.53 – 2.35 (m, 1H, C*H*$(CH_3)_2$), 1.95 – 1.48 (m, 11H, NH-Cy, Cy), 1.46 – 0.87 (m, 16H, CH(C*H*$_3$)$_2$,NH-Cy, Cy). LRMS (CI) m/z calcd for $C_{28}H_{42}N_3O_2$ $[M+H]^+$: 452.3; found: 452.3.

***N*-(1-(cyclohexylamino)-3,3-dimethyl-1-oxobutan-2-yl)-1-(cyclohexylmethyl)-*N*-methyl-1*H*-indole-3-carboxamide (45o).** Yield: 46%. Mp: 136-137 ºC. ^{1}H NMR (300 MHz, $CDCl_3$) δ (ppm): 7.84 (d, *J* = 7.2 Hz, 1H, Ar-H), 7.40 (s, 1H, Ar-H), 7.38 – 7.31 (m, 1H, Ar-H), 7.30 – 7.15 (m, 2H, Ar-H), 6.50 (brs, 1H, NH), 5.00 (s, 1H, CH), 3.95 (d, *J* = 7.1 Hz, 2H, C*H*$_2$-Cy), 3.83 – 3.66 (m, 1H, NH-C*H*-Cy), 3.29 (s, 3H, NCH_3), 2.28 – 2.11 (M, 1H, C*H*-Cy), 1.96 – 1.50 (m, 10H, NH-Cy, Cy), 1.45 – 0.88 (m, 19H, C$(CH_3)_3$,NH-Cy, Cy). LRMS (CI) m/z calcd for $C_{29}H_{44}N_3O_2$ $[M+H]^+$: 466.3; found: 466.3.

***N*-(1-(benzylamino)-4-methyl-1-oxopentan-2-yl)-1-(cyclohexylmethyl)-*N*-methyl-1*H*-indole-3-carboxamide (45q).** Yield: 43%. Oil at room temperature. ^{1}H NMR (300 MHz, $CDCl_3$) δ (ppm): 7.74 (d, *J* = 7.2 Hz, 1H, Ar-H), 7.46 (brs, 1H, NH), 7.40 – 7.17 (m, 9H, Ar-H), 5.21 (t, *J* = 7.8 Hz, 1H, CH), 4.55 (dd, *J* = 15.0, 6.4 Hz, 1H, C*H*$_2$-Ph), 4.42 (dd, *J* = 15.0, 5.7 Hz, 1H, C*H*$_2$-Ph), 3.95 (d, *J* = 7.2 Hz, 2H, C*H*$_2$-Cy), 3.09 (s, 3H, NCH_3), 1.98 – 1.54 (m, 9H, C*H*C*H*$_2$$(CH_3)_2$, Cy), 1.28 – 1.13 (m, 3H, Cy), 1.12 – 0.89 (m, 8H, $CHCH_2$(C*H*$_3$)$_2$, Cy). HRMS (APCI) m/z calcd for C30H40N3O2 $[M+H]^+$: 474.3042; found: 474.3116.

***N*-(1-(cyclohexylamino)-4-methyl-1-oxopentan-2-yl)-1-(cyclohexylmethyl)-*N*-methyl-1*H*-indole-3-carboxamide (45r).** Yield: 41%. Oil at room temperature. ^{1}H NMR (300 MHz, $CDCl_3$) δ (ppm): 7.82 (d, *J* = 7.0 Hz, 1H, Ar-H), 7.40 (s, 1H, Ar-H), 7.38 – 7.32 (m, 1H, Ar-H), 7.30 – 7.17 (m, 2H, Ar-H), 6.90 (s, 1H, NH), 5.12 (t, *J* = 7.6 Hz, 1H, CH), 3.96 (d, *J* = 7.2 Hz, 2H, C*H*$_2$-Cy), 3.88 – 3.70 (m, 1H, NH-C*H*-Cy), 3.08 (s, 3H, NCH_3), 2.00 – 1.50 (m, 14H, C*H*C*H*$_2$$(CH_3)_2$, NH-Cy, Cy), 1.48 – 1.09 (m, 6H,

USC

NH-Cy, Cy), 1.09 – 0.87 (m, 10H, $CHCH_2(CH_3)_2$, NH-Cy, Cy). LRMS (CI) m/z calcd for $C_{29}H_{44}N_3O_2$ $[M+H]^+$: 466.3; found: 466.3.

***N*-(1-(cyclopropylamino)-3,3-dimethyl-1-oxobutan-2-yl)-1-(4-fluorobenzyl)-1*H*-indole-3-carboxamide (46a).** Yield: 46%. Mp: 189-191 ºC. ^{1}H NMR (300 MHz, $CDCl_3$) δ (ppm): 8.06 (d, *J* = 9.1 Hz, 1H, Ar-H), 7.80 (s, 1H, Ar-H), 7.35 – 7.23 (m, 3H, Ar-H), 7.18 – 7.09 (m, 2H, Ar-H), 7.05 – 6.97 (m, 2H, Ar-H), 6.81 (d, *J* = 9.2 Hz, 1H, NH), 6.19 (s, 1H, NH), 5.31 (s, 2H, CH_2-Ph), 4.49 (d, *J* = 9.2 Hz, 1H, CH), 2.83 – 2.65 (m, 1H, CH-*c*-Pr), 1.10 (s, 9H, $C(CH_3)_3$), 0.83 – 0.72 (m, 2H, *c*-Pr), 0.57 – 0.48 (m, 2H, *c*-Pr). LRMS (CI) m/z calcd for $C_{25}H_{29}FN_3O_2$ $[M+H]^+$: 422.2; found: 422.2.

***N*-(1-(adamantan-1-ylamino)-3,3-dimethyl-1-oxobutan-2-yl)-1-(4-fluorobenzyl)-1*H*-indole-3-carboxamide (46b).** Yield: 41%. Mp: 305-306 ºC. ^{1}H NMR (300 MHz, $CDCl_3$) δ (ppm): 8.05 (d, *J* = 7.4 Hz ,1H, Ar-H), 7.77 (s, 1H, Ar-H), 7.35 – 7.20 (m, 3H, Ar-H), 7.18 – 7.07 (m, 2H, Ar-H), 7.05 – 6.95 (m, 2H, Ar-H), 6.84 (d, *J* = 8.9 Hz, 1H, NH), 5.44 (s, 1H, NH), 5.30 (s, 2H, CH_2-Ph), 4.39 (d, *J* = 9.0 Hz, 1H, CH), 2.12 – 1.95 (m, 8H, Ad), 1.80 – 1.62 (m, 7H, Ad), 1.10 (s, 9H, $C(CH_3)_3$). LRMS (CI) m/z calcd for $C_{32}H_{39}FN_3O_2$ $[M+H]^+$: 516.3; found: 516.3.

***N*-(3,3-dimethyl-1-oxo-1-(pentylamino)butan-2-yl)-1-(4-fluorobenzyl)-1*H*-indole-3-carboxamide (46c).** Yield: 48%. Mp: 172-173 ºC. ^{1}H NMR (300 MHz, $CDCl_3$) δ (ppm): 8.10 (d, *J* = 8.6 Hz, 1H, Ar-H), 7.76 (s, 1H, Ar-H), 7.33 – 7.19 (m, 3H, Ar-H, NH), 7.15 – 7.03 (m, 2H, Ar-H), 7.02 – 6.86 (m, 4H, Ar-H, NH), 5.25 (s, 2H), 4.70 (d, *J* = 9.3 Hz, 1H, CH), 3.39 – 3.22 (m, 1H, $CH_2CH_2CH_2CH_3$), 3.21 – 3.05 (m, 1H, $CH_2CH_2CH_2CH_3$), 1.55 – 1.41 (m, 2H, $CH_2CH_2CH_2CH_3$), 1.33 – 1.18 (m, 2H, $CH_2CH_2CH_2CH_3$), 1.11 (s, 9H, $C(CH_3)_3$), 0.89 – 0.74 (m, 3H, $CH_2CH_2CH_2CH_3$). LRMS (CI) m/z calcd for $C_{27}H_{35}FN_3O_2$ $[M+H]^+$: 451.2635; found: 451.2712.

***N*-(3,3-dimethyl-1-((2-morpholinoethyl)amino)-1-oxobutan-2-yl)-1-(4-fluorobenzyl)-1*H*-indole-3-carboxamide (46d).** Yield: 44%. Mp: 165-166 ºC. ^{1}H NMR (300 MHz, $CDCl_3$) δ (ppm): 8.07 (d, *J* = 8.6 Hz, 1H, Ar-H), 7.75 (s, 1H, Ar-H), 7.35 – 7.17 (m, 3H, Ar-H), 7.14 – 7.04 (m, 2H, Ar-H), 7.03 – 6.91 (m, 2H, Ar-H), 6.86 (d, *J* = 8.9 Hz, 1H, NH), 6.70 – 6.64 (m, 1H, NH), 5.27 (s, 2H, CH_2-Ph), 4.59 (d, *J* = 9.1 Hz, 1H, CH), 3.74 – 3.58 (m, 4H, NCH_2CH_2O, NCH_2CH_2O), 3.52 – 3.37 (m, 1H,

USC DE COMPOSTELA

NC*H*$_2$CH$_2$), 3.33 – 3.20 (m, 1H, NC*H*$_2$CH$_2$), 2.55 – 2.30 (m, 6H, NCH$_2$C*H*$_2$, NC*H*$_2$CH$_2$O, NC*H*$_2$CH$_2$O), 1.10 (s, 9H, C(CH$_3$)$_3$). HRMS (APCI) m/z calcd for $C_{28}H_{36}FN_4O_3$ $[M+H]^+$: 495.2693; found: 495.2778.

Diethyl ((2-(1-(4-fluorobenzyl)-1*H*-indole-3-carboxamido)-3,3-dimethyl butanamido)methyl)phosphonate (46e). Yield: 41%. Mp: 168-169 ºC. ^{1}H NMR (300 MHz, $CDCl_3$) δ (ppm): 8.11 – 7.95 (m, 3H, Ar-H, NH), 7.33 – 7.16 (m, 3H, Ar-H), 7.16 – 7.05 (m, 2H, Ar-H), 7.00 – 6.85 (m, 3H, Ar-H, NH), 5.29 (s, 2H, C*H*$_2$-Ph), 4.94 (d, *J* = 9.3 Hz, 1H, CH), 4.21 – 3.96 (m, 5H, C*H*$_2$PO(OC*H*$_2$CH$_3$)$_2$), 3.52 – 3.35 (m, 1H, C*H*$_2$PO(OC*H*$_2$CH$_3$)$_2$), 1.28 (t, *J* = 7.0 Hz, 6H, CH$_2$PO(OCH$_2$C*H*$_3$)$_2$), 1.10 (s, 9H, C(CH$_3$)$_3$). HRMS (APCI) m/z calcd for $C_{27}H_{36}FN_3O_5P$ $[M+H]^+$: 532.2298; found: 532.2380.

Methyl (2-(1-(4-fluorobenzyl)-1*H*-indole-3-carboxamido)-3,3-dimethylbutanoyl) glycinate (46f). Yield: 45%. Mp: 164-165 ºC. ^{1}H NMR (300 MHz, $CDCl_3$) δ (ppm): 8.12 – 8.01 (m, 1H, Ar-H), 7.90 – 7.77 (m, 2H, Ar-H, NH), 7.30 – 7.15 (m, 3H, Ar-H), 7.12 – 7.02 (m, 2H, Ar-H), 7.01 – 6.86 (m, 3H, Ar-H, NH), 5.22 (s, 2H, C*H*$_2$-Ph), 4.89 (d, *J* = 9.3 Hz, 1H, CH), 4.20 (dd, *J* = 17.8, 6.3 Hz ,1H, C*H*$_2$COOCH$_3$), 3.77 (dd, *J* = 17.9, 4.9 Hz, 1H, C*H*$_2$COOCH$_3$), 3.66 (s, 3H, CH$_2$COOC*H*$_3$), 1.14 (s, 9H, C(CH$_3$)$_3$). LRMS (CI) m/z calcd for $C_{25}H_{29}FN_3O_4$ $[M+H]^+$: 454.2; found: 454.2.

Ethyl 2-(1-((2-(1-(4-fluorobenzyl)-1*H*-indole-3-carboxamido)-3,3-dimethylbutanoyl)glycyl)piperidin-4-yl)acetate (46g). Yield: 45%. Oil at room temperature. ^{1}H NMR (300 MHz, $CDCl_3$) δ (ppm): 8.06 (d, *J* = 8.2 Hz, 1H, Ar-H), 7.78 (s, 1H, Ar-H), 7.35 – 7.20 (m, 3H, Ar-H), 7.18 – 7.08 (m, 2H, Ar-H), 7.06 – 6.89 (m, 3H, Ar-H, NH), 6.79 (d, *J* = 8.7 Hz, 1H, NH), 5.31 (s, 2H, C*H*$_2$-Ph), 4.65 (d, *J* = 9.0 Hz, 1H, CH), 4.21 – 4.07 (m, 2H, COOC*H*$_2$CH$_3$), 3.83 – 3.66 (m, 2H, CH$_2$), 3.15 – 2.93 (m, 2H, C_5H_9N), 2.77 – 2.54 (m, 2H, C_5H_9N), 2.32 – 2.22 (m, 2H, C*H*$_2$COOCH$_2$CH$_3$), 2.11 – 1.99 (m, 1H, C_5H_9N), 1.90 – 1.66 (m, 4H, C_5H_9N), 1.27 (t, *J* = 7.2 Hz, 3H, CH$_2$COOCH$_2$C*H*$_3$), 1.13 (s, 9H, C(CH$_3$)$_3$). LRMS (CI) m/z calcd for $C_{33}H_{42}FN_4O_5$ $[M+H]^+$: 593.3; found: 593.3.

USC UNIVERSIDADE DE SANTIAGO DE COMPOSTELA

***N*-(1-(cyclopropylamino)-3,3-dimethyl-1-oxobutan-2-yl)-1-(4-fluorobenzyl)-*N*-methyl-1*H*-indole-3-carboxamide (46h).** Yield: 47%. Mp: 187-189 ºC. ^{1}H NMR (300 MHz, $CDCl_3$) δ (ppm): 8.08 (d, *J* = 9.1 Hz, 1H, Ar-H), 7.83 (s, 1H, Ar-H), 7.33 – 7.24 (m, 3H, Ar-H), 7.17 – 7.10 (m, 2H, Ar-H), 7.07 – 7.01 (m, 2H, Ar-H), 6.20 (s, 1H, NH), 5.31 (s, 2H, C*H*$_2$-Ph), 4.30 (s, 1H, CH), 3.02 (s, 3H, NCH_3), 2.81 – 2.68 (m, 1H, CH-*c*-Pr), 1.08 (s, 9H, $C(CH_3)_3$), 0.83 – 0.73 (m, 2H, *c*-Pr), 0.72 – 0.62 (m, 2H, *c*-Pr). LRMS (CI) m/z calcd for $C_{26}H_{31}FN_3O_2$ $[M+H]^+$: 436.2; found: 436.2.

***N*-(3,3-dimethyl-1-oxo-1-(pentylamino)butan-2-yl)-1-(4-fluorobenzyl)-*N*-methyl-1*H*-indole-3-carboxamide (46i).** Yield: 45%. Mp: 178-180 ºC. ^{1}H NMR (300 MHz, $CDCl_3$) δ (ppm): 8.27 – 8.21 (m, 1H, Ar-H), 7.75 (s, 1H, Ar-H), 7.31 – 7.21 (m, 3H, Ar-H), 7.16 – 7.02 (m, 2H, Ar-H), 6.99 – 6.88 (m, 3H, Ar-H, NH), 5.25 (s, 2H, C*H*$_2$-Ph), 4.28 (s, 1H, CH), 3.37 – 3.21 (m, 2H, C*H*$_2$CH$_2$CH$_2$CH$_2$CH$_3$), 3.03 (s, 3H, NCH_3), 1.96 – 1.75 (m, 2H, CH$_2$C*H*$_2$CH$_2$CH$_2$CH$_3$), 1.53 – 1.43 (m, 2H, CH$_2$CH$_2$C*H*$_2$CH$_2$CH$_3$), 1.37 – 1.24 (m, 2H, CH$_2$CH$_2$CH$_2$C*H*$_2$CH$_3$), 1.06 (s, 9H, $C(CH_3)_3$), 0.92 – 0.82 (m, 3H, CH$_2$CH$_2$CH$_2$CH$_2$C*H*$_3$). LRMS (CI) m/z calcd for $C_{28}H_{37}FN_3O_2$ $[M+H]^+$: 466.2; found: 466.2.

***N*-(3,3-dimethyl-1-((2-morpholinoethyl)amino)-1-oxobutan-2-yl)-1-(4-fluorobenzyl)-*N*-methyl-1*H*-indole-3-carboxamide (46j).** Yield: 48%. Mp: 176-178 ºC. ^{1}H NMR (300 MHz, $CDCl_3$) δ (ppm): 8.10 (d, *J* = 8.6 Hz, 1H, Ar-H), 7.76 (s, 1H, Ar-H), 7.37 – 7.15 (m, 3H, Ar-H), 7.12 – 7.05 (m, 2H, Ar-H), 7.02 – 6.93 (m, 2H, Ar-H), 6.72 – 6.66 (m, 1H, NH), 5.25 (s, 2H, C*H*$_2$-Ph), 4.29 (s, 1H, CH), 3.73 – 3.56 (m, 4H, NCH$_2$C*H*$_2$O, NCH$_2$C*H*$_2$O), 3.51 – 3.36 (m, 1H, NC*H*$_2$CH$_2$), 3.31 – 3.22 (m, 1H, NC*H*$_2$CH$_2$), 3.10 (s, 3H, NCH_3), 2.54 – 2.32 (m, 6H, NCH$_2$C*H*$_2$, NC*H*$_2$CH$_2$O, NC*H*$_2$CH$_2$O), 1.03 (s, 9H, $C(CH_3)_3$). LRMS (CI) m/z calcd for $C_{29}H_{38}FN_4O_3$ $[M+H]^+$: 509.2; found: 509.2.

Methyl (2-(1-(4-fluorobenzyl)-*N*-methyl-1*H*-indole-3-carboxamido)-3,3-dimethylbutanoyl)glycinate (46k). Yield: 46%. Mp: 185-186 ºC. ^{1}H NMR (300 MHz, $CDCl_3$) δ (ppm): 8.10 – 8.02 (m, 1H, Ar-H), 7.79 (s, 1H, Ar-H), 7.31 – 7.16 (m, 3H, Ar-H), 7.11 – 7.03 (m, 2H, Ar-H), 6.99 – 6.88 (m, 3H, Ar-H, NH), 5.21 (s, 2H, C*H*$_2$-Ph), 4.30 (s, 1H, CH), 4.19 (dd, *J* = 17.8, 6.3 Hz ,1H, C*H*$_2$COOCH$_3$), 3.76 (dd, *J* = 17.9, 4.9

USC DE COMPOSTELA

Hz, 1H, C*H*$_2$COOCH$_3$), 3.65 (s, 3H, CH$_2$COOC*H*$_3$), 3.18 (s, 3H, NCH$_3$) 1.08 (s, 9H, C(CH$_3$)$_3$). LRMS (CI) m/z calcd for $C_{26}H_{31}FN_3O_4$ $[M+H]^+$: 468.2; found: 468.2.

Ethyl 2-(1-((2-(1-(4-fluorobenzyl)-*N*-methyl-1*H*-indole-3-carboxamido)-3,3-dimethylbutanoyl)glycyl)piperidin-4-yl)acetate (46l). Yield: 45%. Oil at room temperature. ^{1}H NMR (300 MHz, $CDCl_3$) δ (ppm): 8.07 (d, *J* = 7.7 Hz, 1H, Ar-H), 7.77 (s, 1H, Ar-H), 7.35 – 7.19 (m, 4H, Ar-H), 7.18 – 7.06 (m, 1H, Ar-H), 7.05 – 6.85 (m, 2H, Ar-H), 5.29 (s, 2H, C*H*$_2$-Ph), 4.68 – 4.47 (m, 2H, CH, CH$_2$), 4.24 – 3.56 (m, 7H, CH$_2$, C$_5$*H*$_9$N, C*H*$_2$COOCH$_2$CH$_3$), 3.14 – 2.97 (m, 2H, CH$_2$COOC*H*$_2$CH$_3$), 2.95 (s, 3H, NCH$_3$) 2.77 – 2.50 (m, 1H, C$_5$*H*$_9$N), 2.31 – 1.53 (m, 4H, C$_5$*H*$_9$N), 1.24 – 1.21 (m, 3H, CH$_2$COOCH$_2$C*H*$_3$), 1.10 (s, 9H, C(CH$_3$)$_3$). LRMS (CI) m/z calcd for $C_{34}H_{44}FN_4O_5$ $[M+H]^+$: 607.3; found: 607.3.

1-(cyclohexylmethyl)-*N*-(3,3-dimethyl-1-((2-morpholinoethyl)amino)-1-oxobutan-2-yl)-1*H*-indole-3-carboxamide (47c). Yield: 41%. Mp: 150-151 ºC. ^{1}H NMR (300 MHz, $CDCl_3$) δ (ppm): 8.09 – 7.98 (m, 1H, Ar-H), 7.68 (s, 1H, Ar-H), 7.41 – 7.33 (m, 1H, Ar-H), 7.31 – 7.20 (m, 2H, Ar-H), 6.79 (d, *J* = 9.1 Hz, 1H, NH), 6.53 (t, *J* = 5.0 Hz, 1H, NH), 4.57 (d, *J* = 9.1 Hz, 1H, CH), 3.94 (d, *J* = 7.2 Hz, 2H, C*H*$_2$-Cy), 3.73 – 3.59 (m, 4H, C*H*$_2$CH$_2$, NC*H*$_2$CH$_2$O), 3.52 – 3.37 (m, 1H, NCH$_2$C*H*$_2$O), 3.35 – 3.18 (m, 1H, NCH$_2$C*H*$_2$O), 2.53 – 2.35 (m, 6H, NC*H*$_2$CH$_2$O, NCH$_2$C*H*$_2$O, CH$_2$*CH*$_2$), 1.95 – 1.77 (m, 1H, C*H*-Cy), 1.74 – 1.54 (m, 5H, Cy), 1.27 – 0.83 (m, 14H, C(CH$_3$)$_3$, Cy). LRMS (CI) m/z calcd for $C_{28}H_{43}N_4O_3$ $[M+H]^+$: 483.3; found: 483.3.

***N*-(1-(benzylamino)-3,3-dimethyl-1-oxobutan-2-yl)-1-(5-fluoropentyl)-1*H*-indole-3-carboxamide (47e).** Yield: 85%. Mp: 158-160 ºC. ^{1}H NMR (300 MHz, $CDCl_3$) δ (ppm): 8.15 – 7.90 (m, 1H, Ar-H), 7.72 (s, 1H, Ar-H), 7.44 – 7.36 (m, 1H, Ar-H), 7.37 – 7.21 (m, 7H, Ar-H), 6.83 (d, *J* = 9.1 Hz, 1H, NH), 6.57 (s, 1H, NH), 4.66 – 4.47 (m, 3H, CH, CH$_2$CH$_2$CH$_2$CH$_2$C*H*$_2$F), 4.45 – 4.31 (m, 2H, C*H*$_2$-Ph), 4.17 (t, *J* = 7.0 Hz, 2H, C*H*$_2$CH$_2$CH$_2$CH$_2$CH$_2$F), 1.92 (q, *J* = 7.4 Hz, 2H, CH$_2$CH$_2$CH$_2$C*H*$_2$CH$_2$F), 1.84 – 1.62 (m, 2H, CH$_2$C*H*$_2$CH$_2$CH$_2$CH$_2$F), 1.56 – 1.39 (m, 2H, CH$_2$CH$_2$C*H*$_2$CH$_2$CH$_2$F), 1.13 (s, 9H, C(CH$_3$)$_3$). LRMS (CI) m/z calcd for $C_{27}H_{35}FN_3O_2$ $[M+H]^+$: 452.3; found: 452.3.

USC UNIVERSIDADE DE SANTIAGO DE COMPOSTELA

***N*-(3,3-dimethyl-1-((2-morpholinoethyl)amino)-1-oxobutan-2-yl)-1-(5-fluoropentyl)-1*H*-indole-3-carboxamide (47f).** Yield: 45%. Mp: 161-162 ºC. ^{1}H NMR (300 MHz, $CDCl_3$) δ (ppm): 8.10 – 8.00 (m, 1H, Ar-H), 7.75 (s, 1H, Ar-H), 7.42 – 7.33 (m, 1H, Ar-H), 7.32 – 7.20 (m, 2H, Ar-H), 6.81 (d, *J* = 9.0 Hz, 1H, NH), 6.51 (s, 1H, NH), 4.55 (d, *J* = 9.1 Hz, 1H, CH), 4.49 (t, *J* = 5.7 Hz, 1H, $CH_2CH_2CH_2CH_2CH_2F$), 4.33 (t, *J* = 5.8 Hz, 1H, $CH_2CH_2CH_2CH_2CH_2F$), 4.15 (t, *J* = 7.1 Hz, 2H, $CH_2CH_2CH_2CH_2CH_2F$), 3.77 – 3.59 (m, 4H, $N(CH_2CH_2)_2O$), 3.54 – 3.39 (m, 1H, NCH_2CH_2), 3.38 – 3.24 (m, 1H, NCH_2CH_2), 2.59 – 2.37 (m, 6H, NCH_2CH_2, $N(CH_2CH_2)_2O$), 1.99 – 1.84 (m, 2H, $CH_2CH_2CH_2CH_2CH_2CH_2F$), 1.81 – 1.59 (m, 2H, $CH_2CH_2CH_2CH_2CH_2F$), 1.53 – 1.37 (m, 2H, $CH_2CH_2CH_2CH_2CH_2F$), 1.10 (s, 9H, $C(CH_3)_3$). LRMS (CI) m/z calcd for $C_{26}H_{40}FN_4O_3$ $[M+H]^+$: 475.3; found: 475.3.

***N*-(1-(benzylamino)-3,3-dimethyl-1-oxobutan-2-yl)-1-pentyl-1*H*-indole-3-carboxamide (47h).** Yield: 46%. Mp: 182-184 ºC. ^{1}H NMR (300 MHz, $CDCl_3$) δ (ppm): 8.04 (d, *J* = 7.2 Hz, 1H, Ar-H), 7.66 (s, 1H, Ar-H), 7.43 – 7.35 (m, 1H, Ar-H), 7.35 – 7.20 (m, 7H, Ar-H), 7.08 (t, *J* = 6.0 Hz, 1H, NH), 6.87 (d, *J* = 9.2 Hz, 1H, NH), 4.72 (d, *J* = 9.2 Hz, 1H, CH), 4.57 (dd, *J* = 14.8, 6.0 Hz, 1H, CH_2-Ph), 4.37 (dd, *J* = 14.8, 5.3 Hz, 1H, CH_2-Ph), 4.11 (t, *J* = 7.2 Hz, 2H, $CH_2CH_2CH_2CH_2CH_3$), 1.86 (p, *J* = 7.6 Hz, 2H, $CH_2CH_2CH_2CH_2CH_3$), 1.45 – 1.24 (m, 4H, $CH_2CH_2CH_2CH_2CH_3$), 1.13 (s, 9H, $C(CH_3)_3$), 0.91 (t, *J* = 6.7 Hz, 3H, $CH_2CH_2CH_2CH_2CH_3$). LRMS (CI) m/z calcd for $C_{27}H_{36}N_3O_2$ $[M+H]^+$: 434.3; found: 434.3.

***N*-(3,3-dimethyl-1-((2-morpholinoethyl)amino)-1-oxobutan-2-yl)-1-pentyl-1*H*-indole-3-carboxamide (47i).** Yield: 53%. Oil at room temperature. ^{1}H NMR (300 MHz, $CDCl_3$) δ (ppm): 8.08 – 7.99 (m, 1H, Ar-H), 7.79 (s, 1H, Ar-H), 7.42 – 7.33 (m, 1H, Ar-H), 7.32 – 7.20 (m, 1H, Ar-H), 6.83 (d, *J* = 9.0 Hz, 1H, NH), 6.71 (s, 1H, NH), 4.56 (d, *J* = 8.9 Hz, 1H, CH), 4.11 (t, *J* = 7.2 Hz, 2H, $CH_2CH_2CH_2CH_2CH_3$), 3.80 – 3.60 (m, 4H, $N(CH_2CH_2)_2O$), 3.56 – 3.30 (m, 2H, NCH_2CH_2), 2.68 – 2.43 (m, 6H, NCH_2CH_2, $N(CH_2CH_2)_2O$), 1.93 – 1.77 (m, 2H, $CH_2CH_2CH_2CH_2CH_3$), 1.42 – 1.22 (m, 4H, $CH_2CH_2CH_2CH_2CH_3$), 1.11 (s, 9H, $C(CH_3)_3$), 0.88 (t, *J* = 6.5 Hz, 3H, $CH_2CH_2CH_2CH_2CH_3$). HRMS (APCI) m/z calcd for $C_{26}H_{41}N_4O_3$ $[M+H]^+$: 457.3100; found: 457.3165.

USC UNIVERSIDADE DE SANTIAGO DE COMPOSTELA

***N*-(1-(tert-butylamino)-3,3-dimethyl-1-oxobutan-2-yl)-1-(5-fluoropentyl)-*N*-methyl-1*H*-indole-3-carboxamide (47m).** Yield: 45%. Oil at room temperature. ^{1}H NMR (300 MHz, $CDCl_3$) δ (ppm): 7.87 (d, *J* = 7.9 Hz, 1H, Ar-H), 7.48 (s, 1H, Ar-H), 7.41 – 7.35 (m, 1H, Ar-H), 7.33 – 7.20 (m, 2H, Ar-H), 6.23 (s, 1H, NH), 4.97 (s, 1H, CH), 4.52 (t, *J* = 5.9 Hz, 1H, $CH_2CH_2CH_2CH_2CH_2F$), 4.36 (t, *J* = 5.8 Hz, 1H, $CH_2CH_2CH_2CH_2CH_2F$), 4.19 (t, *J* = 7.1 Hz, 2H, $CH_2CH_2CH_2CH_2CH_2F$), 3.31 (s, 3H, NCH_3), 1.94 (p, *J* = 7.2 Hz, 2H, $CH_2CH_2CH_2CH_2CH_2F$), 1.85 – 1.63 (m, 2H, $CH_2CH_2CH_2CH_2CH_2F$), 1.57 – 1.42 (m, 2H, $CH_2CH_2CH_2CH_2CH_2F$), 1.37 (s, 9H, $C(CH_3)_3$), 1.21 (s, 9H, $C(CH_3)_3$). LRMS (CI) m/z calcd for $C_{25}H_{39}FN_3O_2$ $[M+H]^+$: 432.3; found: 432.3.

***N*-(1-(benzylamino)-3,3-dimethyl-1-oxobutan-2-yl)-1-(5-fluoropentyl)-*N*-methyl-1*H*-indole-3-carboxamide (47n).** Yield: 47%. Oil at room temperature. ^{1}H NMR (300 MHz, $CDCl_3$) δ (ppm): 7.80 (d, *J* = 7.8 Hz, 1H, Ar-H), 7.47 – 7.34 (m, 2H, Ar-H), 7.34 – 7.19 (m, 7H, Ar-H) 7.16 (t, *J* = 6.0 Hz, NH), 5.14 (s, 1H, CH), 4.52 (t, *J* = 5.8 Hz, 1H, $CH_2CH_2CH_2CH_2CH_2F$), 4.44 (dd, *J* = 6.0, 2.0 Hz, 2H, CH_2-Ph), 4.36 (t, *J* = 5.8 Hz, 1H, $CH_2CH_2CH_2CH_2CH_2F$), 4.15 (t, *J* = 7.1 Hz, 2H, $CH_2CH_2CH_2CH_2CH_2F$), 3.29 (s, 3H, NCH_3), 1.91 (p, *J* = 7.2 Hz, 2H, $CH_2CH_2CH_2CH_2CH_2F$), 1.84 – 1.63 (m, 2H, $CH_2CH_2CH_2CH_2CH_2F$), 1.56 – 1.40 (m, 2H, $CH_2CH_2CH_2CH_2CH_2F$), 1.24 (s, 9H, $C(CH_3)_3$). LRMS (CI) m/z calcd for $C_{28}H_{37}FN_3O_2$ $[M+H]^+$: 466.3; found: 466.3.

***N*-(3,3-dimethyl-1-((2-morpholinoethyl)amino)-1-oxobutan-2-yl)-1-(5-fluoropentyl)-*N*-methyl-1*H*-indole-3-carboxamide (47o).** Yield: 48%. Mp: 171-172 ºC. ^{1}H NMR (300 MHz, $CDCl_3$) δ (ppm): 8.08 – 8.00 (m, 1H, Ar-H), 7.74 (s, 1H, Ar-H), 7.42 – 7.33 (m, 1H, Ar-H), 7.31 – 7.22 (m, 2H, Ar-H), 6.54 (s, 1H, NH), 4.29 (s, 1H, CH), 4.50 (t, *J* = 5.7 Hz, 1H, $CH_2CH_2CH_2CH_2CH_2F$), 4.31 (t, *J* = 5.8 Hz, 1H, $CH_2CH_2CH_2CH_2CH_2F$), 4.14 (t, *J* = 7.1 Hz, 2H, $CH_2CH_2CH_2CH_2CH_2F$), 3.77 – 3.59 (m, 4H, $N(CH_2CH_2)_2O$), 3.56 – 3.41 (m, 1H, NCH_2CH_2), 3.37 – 3.21 (m, 1H, NCH_2CH_2), 3.17 (s, 3H, NCH_3), 2.57 – 2.35 (m, 6H, NCH_2CH_2, $N(CH_2CH_2)_2O$), 1.96 – 1.82 (m, 2H, $CH_2CH_2CH_2CH_2CH_2F$), 1.80 – 1.57 (m, 2H, $CH_2CH_2CH_2CH_2CH_2F$), 1.52 – 1.35 (m, 2H, $CH_2CH_2CH_2CH_2CH_2F$), 1.08 (s, 9H, $C(CH_3)_3$). LRMS (CI) m/z calcd for $C_{27}H_{42}FN_4O_3$ $[M+H]^+$: 489.3; found: 489.3.

USC UNIVERSIDADE DE SANTIAGO DE COMPOSTELA

***N*-(1-(tert-butylamino)-3,3-dimethyl-1-oxobutan-2-yl)-*N*-methyl-1-pentyl-1*H*-indole-3-carboxamide (47p).** Yield: 48%. Oil at room temperature. ^{1}H NMR (300 MHz, $CDCl_3$) δ (ppm): 7.88 (d, *J* = 7.5 Hz, 1H, Ar-H), 7.49 (s, 1H, Ar-H), 7.43 – 7.35 (m, 1H, Ar-H), 7.34 – 7.20 (m, 2H, Ar-H), 6.21 (s, 1H, NH), 4.97 (s, 1H, CH), 4.16 (t, *J* = 7.2 Hz, 2H, $CH_2CH_2CH_2CH_2CH_3$), 3.31 (s, 3H, NCH_3), 1.86 (p, *J* = 7.4 Hz, 2H, $CH_2CH_2CH_2CH_2CH_3$), 1.46 – 1.30 (m, 13H, $CH_2CH_2CH_2CH_2CH_3$, $C(CH_3)_3$), 1.22 (s, 9H, $C(CH_3)_3$), 0.91 (t, *J* = 7.1 Hz, 3H, $CH_2CH_2CH_2CH_2CH_3$). LRMS (CI) m/z calcd for $C_{25}H_{40}N_3O_2$ $[M+H]^+$: 414.3; found: 414.3.

***N*-(1-(benzylamino)-3,3-dimethyl-1-oxobutan-2-yl)-*N*-methyl-1-pentyl-1*H*-indole-3-carboxamide (47q).** Yield: 43%. Oil at room temperature. ^{1}H NMR (300 MHz, $CDCl_3$) δ (ppm): 7.80 (d, *J* = 7.2 Hz, 1H, Ar-H), 7.48 – 7.35 (m, 2H, Ar-H), 7.34 – 7.18 (m, 7H, Ar-H), 7.07 (t, *J* = 6.0 Hz, 1H, NH), 5.13 (s, 1H, CH), 4.45 (dd, *J* = 5.9, 2.6 Hz, 2H, CH_2-Ph), 4.13 (t, *J* = 7.2 Hz, 2H, $CH_2CH_2CH_2CH_2CH_3$), 3.29 (s, 3H, NCH_3), 1.97 – 1.78 (m, 2H, $CH_2CH_2CH_2CH_2CH_3$), 1.47 – 1.29 (m, 4H, $CH_2CH_2CH_2CH_2CH_3$), 1.25 (s, 9H, $C(CH_3)_3$), 0.91 (t, *J* = 6.8 Hz, 3H, $CH_2CH_2CH_2CH_2CH_3$). LRMS (CI) m/z calcd for $C_{28}H_{38}N_3O_2$ $[M+H]^+$: 448.3; found: 448.3.

***N*-(3,3-dimethyl-1-((2-morpholinoethyl)amino)-1-oxobutan-2-yl)-*N*-methyl-1-pentyl-1*H*-indole-3-carboxamide (47r).** Yield: 48%. Mp: 168-169 ºC. ^{1}H NMR (300 MHz, $CDCl_3$) δ (ppm): 8.10 – 8.02 (m, 1H, Ar-H), 7.80 (s, 1H, Ar-H), 7.41 – 7.34 (m, 1H, Ar-H), 7.30 – 7.18 (m, 2H, Ar-H), 6.67 (s, 1H, NH), 4.56 (s, 1H, CH), 4.10 (t, *J* = 7.2 Hz, 2H, $CH_2CH_2CH_2CH_2CH_3$), 3.70 – 3.62 (m, 4H, $N(CH_2CH_2)_2O$), 3.54 – 3.28 (m, 2H, NCH_2CH_2), 3.19 (s, 3H, NCH_3), 2.66 – 2.42 (m, 6H, NCH_2CH_2, $N(CH_2CH_2)_2O$), 1.91 – 1.79 (m, 2H, $CH_2CH_2CH_2CH_2CH_3$), 1.41 – 1.24 (m, 4H, $CH_2CH_2CH_2CH_2CH_3$), 1.09 (s, 9H, $C(CH_3)_3$), 0.88 (t, *J* = 6.5 Hz, 3H, $CH_2CH_2CH_2CH_2CH_3$). LRMS (CI) m/z calcd for $C_{26}H_{43}N_4O_3$ $[M+H]^+$: 471.3; found: 471.3.

USC UNIVERSIDADE DE SANTIAGO DE COMPOSTELA

4.6 HPLC TRACES OF COMPOUNDS 22, 23, 24, 25, 35, 36, 37, 38

All the information about HPLC is available in the following link or scanning the QR code below: https://www.dropbox.com/s/n7zybs62053augq/HPLC.pdf?dl=0

4.7 HIGH-RESOLUTION MASS SPECTROMETRY (HRMS)

All the information about HRMS is available in the following link or scanning the QR code below: https://www.dropbox.com/s/dxsmqbdd1hj9plu/HMRS.pdf?dl=0

USC UNIVERSIDADE DE SANTIAGO DE COMPOSTELA

5 CONCLUSIONS

USC
UNIVERSIDADE
DE SANTIAGO
DE COMPOSTELA

USC
UNIVERSIDADE
DE SANTIAGO
DE COMPOSTELA

- A collection of 64 indole and indazole derivatives, which are Synthetic Cannabinoid Receptor Agonists (SCRAs), has been prepared and pharmacologically characterized (binding and functional). 32 of the 64 SCRAs herein documented had not been previously reported (derivatives featuring the *(R)* configuration within the pendant amino acid residue).
- The identification of the main salient features emerging from the structural-activity relationship (SAR) and the identification of some CB_2R selective ligands are documented.
- The *(S)* stereoisomers are more potent than the corresponding *(R)* stereoisomers at both receptor subtypes. Furthermore, binding data analysis evidence that the *(R)* stereoisomers are generally less affine (at both cannabinoid receptors) and slightly more affine towards CB_2R.
- Preliminary neurotoxicity results suggest that all tested SCRAs significantly reduced the cell viability, showing a high neurotoxicity in primary mouse neuronal cells. It has been observed that the reduction in cell viability seems to be functional and scaffold dependent, with amides derived from the indazole core eliciting superior neurotoxicity.
- A pharmacomodulation process allows us to transform the promiscuous profile (CB_1R and CB_2R) of the SCRAs into selective CB_2R drugs. Herein a previously unexplored, efficient, and versatile Ugi-based approach that enables the rapid generation of novel CB_2R selective ligands is documented. The optimized strategy exemplifies the importance of discovering diverse and previously unexplored moieties in the pharmacophoric models, thus enabling to dissociate completely the binding profile of these receptors (CB_1R and CB_2R).
- The herein proposed MCR-based synthetic method permits the rapid assembly of ester and amide libraries. 168 new derivatives bearing several explored substitution patterns in SCRA-like series have been synthetized.
- For this Doctoral Thesis, the *N*-alkyl-1*H*-indole-3-carboxylic acid has been maintained as central core with different substitutions at R^1, while at R^2 we decided to examine not only the classical substituents (H), but also the effect of a methyl group at this position. The availability of an efficient method, based on the Ugi reaction, allowed us to expand the SAR study of these series in Chapters 2, 3 and 4. Specifically, we aimed at extensively exploring the effect of groups at R^3 and R^4 and their roles in

USC UNIVERSIDADE DE SANTIAGO

achieving potent and selective CB_2R ligands. At R^3, the maximum affinity is reached when R^3 = *t*-Bu or 4,4-DMPN in both series (4-F-Bn and CH_2-Cy). Furthermore, it has been observed that R^4 plays an important role in dissociating the affinity of CB_1R and CB_2R, leading to potent and CB_2R selective ligands. At R^4, *t*-Bu and Bn are well tolerated, while Et-Morpholine group leads to highly potent and CB_2R selective compounds.

- Several new ligands combining remarkable affinity (K_i < 100 nM) and exquisite selectivity (> 100-fold over CB_1R) were identified.
- A combination of chiral HPLC and circular dichroism analysis provided experimental support to the stereospecific interaction between the stereoisomers of the most attractive compounds obtained and the CB_2R.
- Preliminary docking assays allowed a comprehensive understanding of the binding mode and SARs within the series. Accordingly, further studies are now in progress to establish the role of stereochemistry in the interaction with the CB_2R.
- The agonist behavior of representative compounds was corroborated through functional cAMP experiments.
- A detailed study of the signaling pathways these compounds affect (biased or unbiased) has been conducted. The pharmacological characterization of the new series of compounds enabled the identification of several agonist that elicit excellent CB_2R selectivity and remarkable functional selectivity by either the cAMP or β-arrestin signaling pathways.
- Since the role of CB_2R agonists in the context of cancer therapy, four of our best agonists have been tested in a model tumor cell line to study their proliferative activity. It has been observed that our agonists significantly reduced cell proliferation of glioblastoma (U87) cell line in a dose-dependent manner.
- Preliminary investigation of the potential of four representative CB_2R agonists for treating inflammatory-based pathologies has been conducted. It has been observed that our agonists exhibited a significant decrease in the production of pro-inflammatory cytokines and a notable increase in the production of anti-inflammatory cytokines, in both resting and activated monocytes and macrophages.
- Jointly, the herein documented results highlight the synthetic potential of multicomponent reactions to accelerate the discovery, optimization, and profiling of new prototypes in Medicinal Chemistry.

USC UNIVERSIDADE DE SANTIAGO

6 REFERENCES

USC
UNIVERSIDADE
DE SANTIAGO
DE COMPOSTELA

USC
UNIVERSIDADE
DE SANTIAGO
DE COMPOSTELA

(1) Mackie, K. Cannabinoid Receptors as Therapeutic Targets. *Annu. Rev. Pharmacol. Toxicol.* **2006**, *46*, 101–122.

(2) Spinelli, F.; Capparelli, E.; Abate, C.; Colabufo, N. A.; Contino, M. Perspectives of Cannabinoid Type 2 Receptor (CB2R) Ligands in Neurodegenerative Disorders: Structure-Affinity Relationship (SAfiR) and Structure-Activity Relationship (SAR) Studies. *J. Med. Chem.* **2017**, *60* (24), 9913–9931.

(3) Schoeder, C. T.; Hess, C.; Madea, B.; Meiler, J.; Müller, C. E. Pharmacological Evaluation of New Constituents of "Spice": Synthetic Cannabinoids Based on Indole, Indazole, Benzimidazole and Carbazole Scaffolds. *Forensic Toxicol.* **2018**, *36* (2), 385–403.

(4) Lu, H. C.; Mackie, K. Review of the Endocannabinoid System. *Biol. Psychiatry Cogn. Neurosci. Neuroimaging* **2021**, *6* (6), 607–615.

(5) Navarrete, F.; García-Gutiérrez, M. S.; Jurado-Barba, R.; Rubio, G.; Gasparyan, A.; Austrich-Olivares, A.; Manzanares, J. Endocannabinoid System Components as Potential Biomarkers in Psychiatry. *Front. Psychiatry* **2020**, *11* (April), 1–30.

(6) Reyes-Resina, I.; Navarro, G.; Aguinaga, D.; Canela, E. I.; Schoeder, C. T.; Załuski, M.; Kieć-Kononowicz, K.; Saura, C. A.; Müller, C. E.; Franco, R. Molecular and Functional Interaction between GPR18 and Cannabinoid CB2 G-Protein-Coupled Receptors. Relevance in Neurodegenerative Diseases. *Biochem. Pharmacol.* **2018**, *157* (June), 169–179.

(7) Chemical, C. Cannabinoid Signaling: Insights to Future Pharmacotherapeutic Development https://www.caymanchem.com/news/cannabinoid-signaling-insights-to-future-pharmacotherapeutic-development.

(8) Abbate, V.; Schwenk, M.; Presley, B. C.; Uchiyama, N. The Ongoing Challenge of Novel Psychoactive Drugs of Abuse. Part I. Synthetic Cannabinoids (IUPAC Technical Report). *Pure Appl. Chem.* **2018**, *90* (8), 1255–1282.

(9) Chiurchiù, V.; van der Stelt, M.; Centonze, D.; Maccarrone, M. The Endocannabinoid System and Its Therapeutic Exploitation in Multiple Sclerosis: Clues for Other Neuroinflammatory Diseases. *Prog. Neurobiol.* **2018**, *160*, 82–100.

(10) Wouters, E.; Walraed, J.; Robertson, M. J.; Meyrath, M.; Szpakowska, M.; Chevigné, A.; Skiniotis, G.; Stove, C. Assessment of Biased Agonism among Distinct Synthetic Cannabinoid Receptor Agonist Scaffolds. *ACS Pharmacol. Transl. Sci.* **2020**, *3* (2), 285–295.

USC UNIVERSIDADE DE SANTIAGO DE COMPOSTELA

(11) Cabrera-Vera, T. M.; Vanhauwe, J.; Thomas, T. O.; Medkova, M.; Preininger, A.; Mazzoni, M. R.; Hamm, H. E. Insights into G Protein Structure, Function, and Regulation. *Endocr. Rev.* **2003**, *24* (6), 765–781.

(12) Howlett, A. C.; Abood, M. E. *CB1 and CB2 Receptor Pharmacology*, 1st ed.; Elsevier Inc., 2017; Vol. 80.

(13) Dhopeshwarkar, A.; Mackie, K. Functional Selectivity of CB2 Cannabinoid Receptor Ligands at a Canonical and Noncanonical Pathways. *J. Pharmacol. Exp. Ther.* **2016**, *358* (2), 342–351.

(14) Blume, L. C.; Leone-Kabler, S.; Luessen, D. J.; Marrs, G. S.; Lyons, E.; Bass, C. E.; Chen, R.; Selley, D. E.; Howlett, A. C. Cannabinoid Receptor Interacting Protein Suppresses Agonist-Driven CB1 Receptor Internalization and Regulates Receptor Replenishment in an Agonist-Biased Manner. *J. Neurochem.* **2016**, *139* (3), 396–407.

(15) Shao, Z.; Yin, J.; Chapman, K.; Grzemska, M.; Clark, L.; Rosenbaum, D. M. High-Resolution Crystal Structure of the Human CB1 Cannabinoid Receptor. *Nature* **2017**, 1–24.

(16) Krishna Kumar, K.; Shalev-Benami, M.; Robertson, M. J.; Hu, H.; Banister, S. D.; Hollingsworth, S. A.; Latorraca, N. R.; Kato, H. E.; Hilger, D.; Maeda, S.; Weis, W. I.; Farrens, D. L.; Dror, R. O.; Malhotra, S. V.; Kobilka, B. K.; Skiniotis, G. Structure of a Signaling Cannabinoid Receptor 1-G Protein Complex. *Cell* **2019**, *176* (3), 448-458.e12.

(17) Munro, S.; Thomas, K. L.; Abu-Shaar, M. Molecular Characterization of a Peripheral Receptor for Cannabinoids. *Nature* **1993**, *365* (6441), 61–65.

(18) Li, X.; Hua, T.; Vemuri, K.; Ho, J. H.; Wu, Y.; Wu, L.; Popov, P.; Benchama, O.; Zvonok, N.; Locke, K.; Qu, L.; Han, G. W.; Iyer, M. R.; Cinar, R.; Coffey, N. J.; Wang, J.; Wu, M.; Katritch, V.; Zhao, S.; Kunos, G.; Bohn, L. M.; Makriyannis, A.; Stevens, R. C.; Liu, Z. J. Crystal Structure of the Human Cannabinoid Receptor CB2. *Cell* **2019**, *176* (3), 459-467.e13.

(19) Ross, R. A. The Enigmatic Pharmacology of GPR55. *Trends Pharmacol. Sci.* **2009**, *30* (3), 156–163.

(20) Morales, P.; Lago-Fernandez, A.; Hurst, D. P.; Sotudeh, N.; Brailoiu, E.; Reggio, P. H.; Abood, M. E.; Jagerovic, N. Therapeutic Exploitation of GPR18: Beyond the Cannabinoids? *J. Med. Chem.* **2020**, *63* (23), 14216–14227.

(21) Overton, H. A.; Fyfe, M. C. T.; Reynet, C. GPR119, a Novel G Protein-Coupled

USC UNIVERSIDADE DE SANTIAGO DE COMPOSTELA

Receptor Target for the Treatment of Type 2 Diabetes and Obesity. *Br. J. Pharmacol.* **2008**, *153* (SUPPL. 1), 76–81.

(22) Miller, S.; Kulkarni, S.; Ciesielski, A.; Nikas, S. P.; Mackie, K.; Makriyannis, A.; Straiker, A. Controlled-Deactivation CB1 Receptor Ligands as a Novel Strategy to Lower Intraocular Pressure. *Pharmaceuticals* **2018**, *11* (2), 3–10.

(23) Moreira, F. A.; Grieb, M.; Lutz, B. Central Side-Effects of Therapies Based on CB1 Cannabinoid Receptor Agonists and Antagonists: Focus on Anxiety and Depression. *Best Pract. Res. Clin. Endocrinol. Metab.* **2009**, *23* (1), 133–144.

(24) Khan, N.; Laudermilk, L.; Ware, J.; Rosa, T.; Mathews, K.; Gay, E.; Amato, G.; Maitra, R. Peripherally Selective CB1 Receptor Antagonist Improves Symptoms of Metabolic Syndrome in Mice. *ACS Pharmacol. Transl. Sci.* **2021**, *4* (2), 757–764.

(25) Aghazadeh Tabrizi, M.; Baraldi, P. G.; Borea, P. A.; Varani, K. Medicinal Chemistry, Pharmacology, and Potential Therapeutic Benefits of Cannabinoid CB2Receptor Agonists. *Chem. Rev.* **2016**, *116* (2), 519–560.

(26) Shang, Y.; Tang, Y. The Central Cannabinoid Receptor Type-2 (CB2) and Chronic Pain. *Int. J. Neurosci.* **2017**, *127* (9), 812–823.

(27) Bu, W.; Ren, H.; Deng, Y.; Mar, N. Del; Guley, N. M.; Moore, B. M.; Honig, M. G.; Reiner, A. Mild Traumatic Brain Injury Produces Neuron Loss That Can Be Rescued by Modulating Microglial Activation Using a CB2 Receptor Inverse Agonist. *Front. Neurosci.* **2016**, *10* (OCT).

(28) Montanari, S.; Mahmoud, A. M.; Pruccoli, L.; Rabbito, A.; Naldi, M.; Petralla, S.; Moraleda, I.; Bartolini, M.; Monti, B.; Iriepa, I.; Belluti, F.; Gobbi, S.; Di Marzo, V.; Bisi, A.; Tarozzi, A.; Ligresti, A.; Rampa, A. Discovery of Novel Benzofuran-Based Compounds with Neuroprotective and Immunomodulatory Properties for Alzheimer's Disease Treatment. *Eur. J. Med. Chem.* **2019**, *178*, 243–258.

(29) Lastres-Becker, I.; Molina-Holgado, F.; Ramos, J. A.; Mechoulam, R.; Fernández-Ruiz, J. Cannabinoids Provide Neuroprotection against 6-Hydroxydopamine Toxicity in Vivo and in Vitro: Relevance to Parkinson's Disease. *Neurobiol. Dis.* **2005**, *19* (1–2), 96–107.

(30) Swinnen, B.; Robberecht, W. The Phenotypic Variability of Amyotrophic Lateral Sclerosis. *Nat. Rev. Neurol.* **2014**, *10* (11), 661–670.

(31) Baker, D.; Pryce, G.; Ludovic Croxford, J.; Brown, P.; Pertwee, R. G.; Huffman,

USC UNIVERSIDADE DE SANTIAGO DE COMPOSTELA

J. W.; Layward, L. Cannabinoids Control Spasticity and Tremor in a Multiple Sclerosis Model. *Nature* **2000**, *404* (6773), 84–87.

(32) Glogauer, J.; Blay, J. Cannabinoids, Their Cellular Receptors, and Effects on the Invasive Phenotype of Carcinoma and Metastasis. *Cancer Rep.* **2021**, No. January, 1–10.

(33) Martínez-Martínez, E.; Gómez, I.; Martín, P.; Sánchez, A.; Román, L.; Tejerina, E.; Bonilla, F.; Merino, A. G.; de Herreros, A. G.; Provencio, M.; García, J. M. Cannabinoids Receptor Type 2, CB2, Expression Correlates with Human Colon Cancer Progression and Predicts Patient Survival. *Oncoscience* **2015**, *2* (2), 131–141.

(34) Zhang, Y.; Zheng, W.; Shen, K.; Shen, W. Δ9-Tetrahydrocannabinol Inhibits Epithelial-Mesenchymal Transition and Metastasis By Targeting Matrix Metalloproteinase-9 in Endometrial Cancer. *Oncol. Lett.* **2018**, *15* (6), 8527–8535.

(35) Gholizadeh, F.; Ghahremani, M. H.; Aliebrahimi, S.; Shadboorestan, A.; Ostad, S. N. Assessment of Cannabinoids Agonist and Antagonist in Invasion Potential of K562 Cancer Cells. *Iran. Biomed. J.* **2019**, *23* (2), 153–158.

(36) Xian, X. S.; Park, H.; Cho, Y. K.; Lee, I. S.; Kim, S. W.; Choi, M. G.; Chung, I. S.; Han, K. H.; Park, J. M. Effect of a Synthetic Cannabinoid Agonist on the Proliferation and Invasion of Gastric Cancer Cells. *J. Cell. Biochem.* **2010**, *110* (2), 321–332.

(37) Nithipatikom, K.; Endsley, M. P.; Isbell, M. A.; Falck, J. R.; Iwamoto, Y.; Hillard, C. J.; Campbell, W. B. 2-Arachidonoylglycerol: A Novel Inhibitor of Androgen-Independent Prostate Cancer Cell Invasion. *Cancer Res.* **2004**, *64* (24), 8826–8830.

(38) Pourkhalili, N.; Ghahremani, M. H.; Farsandaj, N.; Tavajohi, S.; Majdzadeh, M.; Parsa, M.; Lavasani, N. J.; Ostad, S. N. Evaluation of Anti-Invasion Effect of Cannabinoids on Human Hepatocarcinoma Cells. *Toxicol. Mech. Methods* **2013**, *23* (2), 120–126.

(39) Elbaz, M.; Ahirwar, D.; Ravi, J.; Nasser, M. W.; Ganju, R. K. Novel Role of Cannabinoid Receptor 2 in Inhibiting EGF/EGFR and IGF-I/IGF-IR Pathways in Breast Cancer. *Oncotarget* **2017**, *8* (18), 29668–29678.

(40) Xu, S.; Ma, H.; Bo, Y.; Shao, M. The Oncogenic Role of CB2 in the Progression of Non-Small-Cell Lung Cancer. *Biomed. Pharmacother.* **2019**, *117* (June),

109080.

(41) Gülck, T.; Møller, B. L. Phytocannabinoids: Origins and Biosynthesis. *Trends Plant Sci.* **2020**, *25* (10), 985–1004.

(42) Sharma, P.; Murthy, P.; Bharath, M. M. S. Chemistry, Metabolism, and Toxicology of Cannabis: Clinical Implications. *Iran. J. Psychiatry* **2012**, *7* (4), 149–156.

(43) Farokhnia, M.; McDiarmid, G. R.; Newmeyer, M. N.; Munjal, V.; Abulseoud, O. A.; Huestis, M. A.; Leggio, L. Effects of Oral, Smoked, and Vaporized Cannabis on Endocrine Pathways Related to Appetite and Metabolism: A Randomized, Double-Blind, Placebo-Controlled, Human Laboratory Study. *Transl. Psychiatry* **2020**, *10* (1).

(44) Englund, A.; Morrison, P. D.; Nottage, J.; Hague, D.; Kane, F.; Bonaccorso, S.; Stone, J. M.; Reichenberg, A.; Brenneisen, R.; Holt, D.; Feilding, A.; Walker, L.; Murray, R. M.; Kapur, S. Cannabidiol Inhibits THC-Elicited Paranoid Symptoms and Hippocampal-Dependent Memory Impairment. *J. Psychopharmacol.* **2013**, *27* (1), 19–27.

(45) Izzo, A. A.; Capasso, R.; Aviello, G.; Borrelli, F.; Romano, B.; Piscitelli, F.; Gallo, L.; Capasso, F.; Orlando, P.; Di Marzo, V. Inhibitory Effect of Cannabichromene, a Major Non-Psychotropic Cannabinoid Extracted from Cannabis Sativa, on Inflammation-Induced Hypermotility in Mice. *Br. J. Pharmacol.* **2012**, *166* (4), 1444–1460.

(46) Hippalgaonkar, K.; Gul, W.; ElSohly, M. A.; Repka, M. A.; Majumdar, S. Enhanced Solubility, Stability, and Transcorneal Permeability of δ-8-Tetrahydrocannabinol in the Presence of Cyclodextrins. *AAPS PharmSciTech* **2011**, *12* (2), 723–731.

(47) Hall, W. *Uso Médico Del Cannabis y Los Cannabinoides*; 2018.

(48) Adams, A. J.; Banister, S. D.; Irizarry, L.; Trecki, J.; Schwartz, M.; Gerona, R. "Zombie" Outbreak Caused by the Synthetic Cannabinoid AMB-FUBINACA in New York. *N. Engl. J. Med.* **2017**, *376* (3), 235–242.

(49) Toxicomanías, O. E. de las D. y las. Cannabinoides Sintéticos En Europa. 2017.

(50) Yu, X. H.; Cao, C. Q.; Martino, G.; Puma, C.; Morinville, A.; St-Onge, S.; Lessard, É.; Perkins, M. N.; Laird, J. M. A. A Peripherally Restricted Cannabinoid Receptor Agonist Produces Robust Anti-Nociceptive Effects in Rodent Models of Inflammatory and Neuropathic Pain. *Pain* **2010**, *151* (2), 337–

USC UNIVERSIDADE DE SANTIAGO DE COMPOSTELA

344.

(51) Kale, V. P.; Gibbs, S.; Taylor, J. A.; Zmarowski, A.; Novak, J.; Patton, K.; Sparrow, B.; Gorospe, J.; Anand, S.; Cinar, R.; Kunos, G.; Chorvat, R. J.; Terse, P. S. Preclinical Toxicity Evaluation of JD5037, a Peripherally Restricted CB1 Receptor Inverse Agonist, in Rats and Dogs for Treatment of Nonalcoholic Steatohepatitis. *Regul. Toxicol. Pharmacol.* **2019**, *109*, 104483.

(52) Cluny, N. L.; Vemuri, V. K.; Chambers, A. P.; Limebeer, C. L.; Bedard, H.; Wood, J. T.; Lutz, B.; Zimmer, A.; Parker, L. A.; Makriyannis, A.; Sharkey, K. A. A Novel Peripherally Restricted Cannabinoid Receptor Antagonist, AM6545, Reduces Food Intake and Body Weight, but Does Not Cause Malaise, in Rodents. *Br. J. Pharmacol.* **2010**, *161* (3), 629–642.

(53) Polini, B.; Cervetto, C.; Carpi, S.; Pelassa, S.; Gado, F.; Ferrisi, R.; Bertini, S.; Nieri, P.; Marcoli, M.; Manera, C. Positive Allosteric Modulation of CB1 and CB2 Cannabinoid Receptors Enhances the Neuroprotective Activity of a Dual CB1R/CB2R Orthosteric Agonist. *Life* **2020**, *10* (12), 1–14.

(54) Graziano, G.; Delre, P.; Carofiglio, F.; Kostrzewa, M.; Riganti, C.; Gio, C.; Majellaro, M.; Nicolotti, O.; Antonio, N.; Abate, C.; Isabel, M.; Sotelo, E.; Felice, G.; Contino, M.; Stefanachi, A.; Leonetti, F. European Journal of Medicinal Chemistry N- Adamantyl-Anthranil Amide Derivatives : New Selective Ligands for the Cannabinoid Receptor Subtype 2 (CB2R). **2023**, *248* (December 2022).

(55) Intranuovo, F.; Brunetti, L.; Delre, P.; Mangiatordi, G. F.; Stefanachi, A.; Laghezza, A.; Niso, M.; Leonetti, F.; Loiodice, F.; Ligresti, A.; Kostrzewa, M.; Brea, J.; Loza, M. I.; Sotelo, E.; Saviano, M.; Colabufo, N. A.; Riganti, C.; Abate, C.; Contino, M. Development of N-(1-Adamantyl)Benzamides as Novel Anti-Inflammatory Multitarget Agents Acting as Dual Modulators of the Cannabinoid CB2 Receptor and Fatty Acid Amide Hydrolase. *J. Med. Chem.* **2023**, *66* (1), 235–250.

(56) Tabrizi, M. A.; Baraldi, P. G. *Chemistry of Cannabinoid Receptor Agonists*; Elsevier Inc., 2017.

(57) Horváth, B.; Magid, L.; Mukhopadhyay, P.; Bátkai, S.; Rajesh, M.; Park, O.; Tanchian, G.; Gao, R. Y.; Goodfellow, C. E.; Glass, M.; Mechoulam, R.; Pacher, P. A New Cannabinoid CB 2receptor Agonist HU-910 Attenuates Oxidative Stress, Inflammation and Cell Death Associated with Hepatic

USC UNIVERSIDADE DE SANTIAGO DE COMPOSTELA

Ischaemia/Reperfusion Injury. *Br. J. Pharmacol.* **2012**, *165* (8), 2462–2478.

(58) Tiberi, M.; Evron, T.; Saracini, S.; Boffa, L.; Mercuri, N. B.; Chintalacharuvu, S. R.; Atamas, S. P.; Chiurchiù, V. Potent T Cell-Mediated Anti-Inflammatory Role of the Selective CB2 Agonist Lenabasum in Multiple Sclerosis. *Neuropathol. Appl. Neurobiol.* **2022**, *48* (2), 1–11.

(59) ClinicalTrialsGov. No Title https://clinicaltrials.gov/.

(60) Ibrahim, M. M.; Deng, H.; Zvonok, A.; Cockayne, D. A.; Kwan, J.; Mata, H. P.; Vanderah, T. W.; Lai, J.; Porreca, F.; Makriyannis, A.; Malan, T. P. Activation of CB2 Cannabinoid Receptors by AM1241 Inhibits Experimental Neuropathic Pain: Pain Inhibition by Receptors Not Present in the CNS. *Proc. Natl. Acad. Sci. U. S. A.* **2003**, *100* (18), 10529–10533.

(61) Yao, B. B.; Hsieh, G. C.; Frost, J. M.; Fan, Y.; Garrison, T. R.; Daza, A. V.; Grayson, G. K.; Zhu, C. Z.; Pai, M.; Chandran, P.; Salyers, A. K.; Wensink, E. J.; Honore, P.; Sullivan, J. P.; Dart, M. J.; Meyer, M. D. In Vitro and in Vivo Characterization of A-796260: A Selective Cannabinoid CB 2 Receptor Agonist Exhibiting Analgesic Activity in Rodent Pain Models. *Br. J. Pharmacol.* **2008**, *153* (2), 390–401.

(62) Yrjölä, S.; Sarparanta, M.; Airaksinen, A. J.; Hytti, M.; Kauppinen, A.; Pasonen-Seppänen, S.; Adinolfi, B.; Nieri, P.; Manera, C.; Keinänen, O.; Poso, A.; Nevalainen, T. J.; Parkkari, T. Synthesis, in Vitro and in Vivo Evaluation of 1,3,5-Triazines as Cannabinoid CB2 Receptor Agonists. *Eur. J. Pharm. Sci.* **2015**, *67*, 85–96.

(63) Ferrisi, R.; Ceni, C.; Bertini, S.; Macchia, M.; Manera, C.; Gado, F. Medicinal Chemistry Approach, Pharmacology and Neuroprotective Benefits of CB2R Modulators in Neurodegenerative Diseases. *Pharmacol. Res.* **2021**, *170* (March), 105607.

(64) Deveaux, V.; Cadoudal, T.; Ichigotani, Y.; Teixeira-Clerc, F.; Louvet, A.; Manin, S.; Nhieu, J. T. Van; Belot, M. P.; Zimmer, A.; Even, P.; Cani, P. D.; Knauf, C.; Burcelin, R.; Bertola, A.; Le Marchand-Brustel, Y.; Gual, P.; Mallat, A.; Lotersztajn, S. Cannabinoid CB2 Receptor Potentiates Obesity-Associated Inflammation, Insulin Resistance and Hepatic Steatosis. *PLoS One* **2009**, *4* (6).

(65) Rinaldi-Carmona, M.; Barth, F.; Millan, J.; Derocq, J. M.; Casellas, P.; Congy, C.; Oustric, D.; Sarran, M.; Bouaboula, M.; Calandra, B.; Portier, M.; Shire, D.; Brelière, J. C.; Le Fur, G. SR 144528, the First Potent and Selective Antagonist

USC UNIVERSIDADE DE SANTIAGO DE COMPOSTELA

of the CB2 Cannabinoid Receptor. *J. Pharmacol. Exp. Ther.* **1998**, *284* (2), 644–650.

(66) Alghamdi, S. S.; Mustafa, S. M.; Moore, B. M. Synthesis and Biological Evaluation of a Ring Analogs of the Selective CB2 Inverse Agonist SMM-189. *Bioorganic Med. Chem.* **2021**, *33* (January), 116035.

(67) Lunn, C. A.; Fine, J. S.; Rojas-Triana, A.; Jackson, J. V.; Fan, X.; Kung, T. T.; Gonsiorek, W.; Schwarz, M. A.; Lavey, B.; Kozlowski, J. A.; Narula, S. K.; Lundell, D. J.; Hipkin, R. W.; Bober, L. A. A Novel Cannabinoid Peripheral Cannabinoid Receptor-Selective Inverse Agonist Blocks Leukocyte Recruitment in Vivo. *J. Pharmacol. Exp. Ther.* **2006**, *316* (2), 780–788.

(68) Gado, F.; Di Cesare Mannelli, L.; Lucarini, E.; Bertini, S.; Cappelli, E.; Digiacomo, M.; Stevenson, L. A.; Macchia, M.; Tuccinardi, T.; Ghelardini, C.; Pertwee, R. G.; Manera, C. Identification of the First Synthetic Allosteric Modulator of the CB 2 Receptors and Evidence of Its Efficacy for Neuropathic Pain Relief. *J. Med. Chem.* **2019**, *62* (1), 276–287.

(69) Delgado-Peraza, F.; Ahn, K. H.; Nogueras-Ortiz, C.; Mungrue, I. N.; Mackie, K.; Kendall, D. A.; Yudowski, G. A. Mechanisms of Biased β-Arrestin-Mediated Signaling Downstream from the Cannabinoid 1 Receptor. *Mol. Pharmacol.* **2016**, *89* (6), 618–629.

(70) Wouters, E.; Walraed, J.; Banister, S. D.; Stove, C. P. Insights into Biased Signaling at Cannabinoid Receptors: Synthetic Cannabinoid Receptor Agonists. *Biochem. Pharmacol.* **2019**, *169* (August), 113623.

(71) Laprairie, R. B.; Bagher, A. M.; Denovan-Wright, E. M. Cannabinoid Receptor Ligand Bias: Implications in the Central Nervous System. *Curr. Opin. Pharmacol.* **2017**, *32*, 32–43.

(72) UNODC. Early warning advisory on new psychoactive substances https://www.unodc.org/LSS/Page/NPS.

(73) Shafi, A.; Berry, A. J.; Sumnall, H.; Wood, D. M.; Tracy, D. K. New Psychoactive Substances: A Review and Updates. *Ther. Adv. Psychopharmacol.* **2020**, *10*, 204512532096719.

(74) Zapata, F.; Matey, J. M.; Montalvo, G.; García-Ruiz, C. Chemical Classification of New Psychoactive Substances (NPS). *Microchem. J.* **2021**, *163* (December 2020).

(75) Santos-Toscano, R.; Guirguis, A.; Davidson, C. How Preclinical Studies Have

USC UNIVERSIDADE DE SANTIAGO DE COMPOSTELA

Influenced Novel Psychoactive Substance Legislation in the UK and Europe. *Br. J. Clin. Pharmacol.* **2020**, *86* (3), 452–481.

(76) Ruck, C. A. P.; Bigwood, J.; Staples, D.; Ott, J.; Wasson, G. Entheogens. *J. Psychoactive Drugs* **1979**, *11* (1–2), 145–146.

(77) da Cunha, K. F.; Oliveira, K. D.; Huestis, M. A.; Costa, J. L. Screening of 104 New Psychoactive Substances (NPS) and Other Drugs of Abuse in Oral Fluid by LC–MS-MS. *J. Anal. Toxicol.* **2020**, *44* (7), 697–707.

(78) Moosmann, B.; Auwärter, V. Designer Benzodiazepines: Another Class of New Psychoactive Substances. *Handb. Exp. Pharmacol.* **2018**, *252*, 383–410.

(79) Greenblatt, H. K.; Greenblatt, D. J. Designer Benzodiazepines: A Review of Published Data and Public Health Significance. *Clin. Pharmacol. Drug Dev.* **2019**, *8* (3), 266–269.

(80) Gaoni, Y.; Mechoulam, R. Isolation, Structure, and Partial Synthesis of an Active Constituent of Hashish. *J. Am. Chem. Soc.* **1964**, *86* (8), 1646–1647.

(81) Banister, S. D.; Longworth, M.; Kevin, R.; Sachdev, S.; Santiago, M.; Stuart, J.; Mack, J. B. C.; Glass, M.; McGregor, I. S.; Connor, M.; Kassiou, M. Pharmacology of Valinate and Tert-Leucinate Synthetic Cannabinoids 5F-AMBICA, 5F-AMB, 5F-ADB, AMB-FUBINACA, MDMB-FUBINACA, MDMB-CHMICA, and Their Analogues. *ACS Chem. Neurosci.* **2016**, *7* (9), 1241–1254.

(82) Hess, C.; Schoeder, C. T.; Pillaiyar, T.; Madea, B.; Müller, C. E. Pharmacological Evaluation of Synthetic Cannabinoids Identified as Constituents of Spice. *Forensic Toxicol.* **2016**, *34* (2), 329–343.

(83) Banister, S. D.; Moir, M.; Stuart, J.; Kevin, R. C.; Wood, K. E.; Longworth, M.; Wilkinson, S. M.; Beinat, C.; Buchanan, A. S.; Glass, M.; Connor, M.; McGregor, I. S.; Kassiou, M. Pharmacology of Indole and Indazole Synthetic Cannabinoid Designer Drugs AB-FUBINACA, ADB-FUBINACA, AB-PINACA, ADB-PINACA, 5F-AB-PINACA, 5F-ADB-PINACA, ADBICA, and 5F-ADBICA. *ACS Chem. Neurosci.* **2015**, *6* (9), 1546–1559.

(84) Cannaert, A.; Sparkes, E.; Pike, E.; Luo, J. L.; Fang, A.; Kevin, R. C.; Ellison, R.; Gerona, R.; Banister, S. D.; Stove, C. P. Synthesis and in Vitro Cannabinoid Receptor 1 Activity of Recently Detected Synthetic Cannabinoids 4F-MDMB-BICA, 5F-MPP-PICA, MMB-4en-PICA, CUMYL-CBMICA, ADB-BINACA, APP-BINACA, 4F-MDMB-BINACA, MDMB-4en-PINACA, A-CHMINACA,

USC UNIVERSIDADE DE SANTIAGO DE COMPOSTELA

5F-AB-P7AICA, 5F-MDMB-P7AICA, An. *ACS Chem. Neurosci.* **2020**, *11* (24), 4434–4446.

(85) Deventer, M. H.; Van Uytfanghe, K.; Vinckier, I. M. J.; Reniero, F.; Guillou, C.; Stove, C. P. Cannabinoid Receptor Activation Potential of the next Generation, Generic Ban Evading OXIZID Synthetic Cannabinoid Receptor Agonists. *Drug Test. Anal.* **2022**, *14* (9), 1565–1575.

(86) Robert Schelkun. Synthetic Cannabinoid News from 2021. In *CaymanChem*; 2022.

(87) Banister, S. D.; Olson, A.; Winchester, M.; Stuart, J.; Edington, A. R.; Kevin, R. C.; Longworth, M.; Herrera, M.; Connor, M.; McGregor, I. S.; Gerona, R. R.; Kassiou, M. The Chemistry and Pharmacology of Synthetic Cannabinoid SDB-006 and Its Regioisomeric Fluorinated and Methoxylated Analogs. *Drug Test. Anal.* **2018**, *10* (7), 1099–1109.

(88) Patel, M.; Manning, J. J.; Finlay, D. B.; Javitch, J. A.; Banister, S. D.; Grimsey, N. L.; Glass, M. Signalling Profiles of a Structurally Diverse Panel of Synthetic Cannabinoid Receptor Agonists. *Biochem. Pharmacol.* **2020**, *175* (December 2019), 113871.

(89) Banister, S. D.; Connor, M. The Chemistry and Pharmacology of Synthetic Cannabinoid Receptor Agonists as New Psychoactive Substances: Origins. *Handb. Exp. Pharmacol.* **2018**, *252*, 165–190.

(90) Morales, P.; Jagerovic, N. Novel Approaches and Current Challenges with Targeting the Endocannabinoid System. *Expert Opin. Drug Discov.* **2020**, *15* (8), 917–930.

(91) Le Boisselier, R.; Alexandre, J.; Lelong-Boulouard, V.; Debruyne, D. Focus on Cannabinoids and Synthetic Cannabinoids. *Clin. Pharmacol. Ther.* **2017**, *101* (2), 220–229.

(92) Yano, H.; Adhikari, P.; Naing, S.; Hoffman, A. F.; Baumann, M. H.; Lupica, C. R.; Shi, L. Positive Allosteric Modulation of the 5-HT1A Receptor by Indole-Based Synthetic Cannabinoids Abused by Humans. *ACS Chem. Neurosci.* **2020**, *11* (10), 1400–1405.

(93) Fantegrossi, W. E.; Wilson, C. D.; Berquist, M. D. Pro-Psychotic Effects of Synthetic Cannabinoids: Interactions with Central Dopamine, Serotonin, and Glutamate Systems. *Drug Metab. Rev.* **2018**, *50* (1), 65–73.

(94) Abdulrahim, D.; Bowden-Jones, O. Harms of Synthetic Cannabinoid Receptor

USC UNIVERSIDADE DE SANTIAGO DE COMPOSTELA

Agonists (SCRAs) and Their Management. *Nov. Psychoact. Treat. UK Netw.* **2016**, *2015* (1), 25.

(95) Hourani, W.; Alexander, S. P. H. Cannabinoid Ligands, Receptors and Enzymes: Pharmacological Tools and Therapeutic Potential. *Brain Neurosci. Adv.* **2018**, *2*, 239821281878390.

(96) Cohen, K.; Weinstein, A. M. Synthetic and Non-Synthetic Cannabinoid Drugs and Their Adverse Effects-A Review From Public Health Prospective. *Front. Public Heal.* **2018**, *6* (June), 13–16.

(97) Deventer, M. H.; Van Uytfanghe, K.; Vinckier, I. M. J.; Reniero, F.; Guillou, C.; Stove, C. P. A New Cannabinoid Receptor 1 Selective Agonist Evading the 2021 "China Ban": ADB-FUBIATA. *Drug Test. Anal.* **2022**, *14* (9), 1639–1644.

(98) Fredriksson, R.; Lagerström, M. C.; Lundin, L. G.; Schiöth, H. B. The G-Protein-Coupled Receptors in the Human Genome Form Five Main Families. Phylogenetic Analysis, Paralogon Groups, and Fingerprints. *Mol. Pharmacol.* **2003**, *63* (6), 1256–1272.

(99) Howlett, A. C.; Barth, F.; Bonner, T. I.; Cabral, G.; Casellas, P.; Devane, W. A.; Felder, C. C.; Herkenham, M.; Mackie, K.; Martin, B. R.; Mechoulam, R.; Pertwee, R. G. International Union of Pharmacology. XXVII. Classification of Cannabinoid Receptors. *Pharmacol. Rev.* **2002**, *54* (2), 161–202.

(100) Ashton, C. H. Pharmacology and Effects of Cannabis: A Brief Review. *Br. J. Psychiatry* **2001**, *178* (FEB.), 101–106.

(101) Cabral, G. A.; Raborn, E. S.; Griffin, L.; Dennis, J.; Marciano-Cabral, F. CB 2 Receptors in the Brain: Role in Central Immune Function. *Br. J. Pharmacol.* **2008**, *153* (2), 240–251.

(102) Miller, A. M.; Stella, N. CB 2 Receptor-Mediated Migration of Immune Cells: It Can Go Either Way. *Br. J. Pharmacol.* **2008**, *153* (2), 299–308.

(103) Turcotte, C.; Blanchet, M. R.; Laviolette, M.; Flamand, N. The CB2 Receptor and Its Role as a Regulator of Inflammation. *Cell. Mol. Life Sci.* **2016**, *73* (23), 4449–4470.

(104) Liu, C.; Jia, W.; Hua, Z.; Qian, Z. Identification and Analytical Characterization of Six Synthetic Cannabinoids NNL-3, 5F–NPB-22-7N, 5F–AKB-48-7N, 5F–EDMB-PINACA, EMB-FUBINACA, and EG-018. *Drug Test. Anal.* **2017**, *9* (8), 1251–1261.

(105) Longworth, M.; Banister, S. D.; Boyd, R.; Kevin, R. C.; Connor, M.; McGregor,

USC UNIVERSIDADE DE SANTIAGO DE COMPOSTELA

I. S.; Kassiou, M. Pharmacology of Cumyl-Carboxamide Synthetic Cannabinoid New Psychoactive Substances (NPS) CUMYL-BICA, CUMYL-PICA, CUMYL-5F-PICA, CUMYL-5F-PINACA, and Their Analogues. *ACS Chem. Neurosci.* **2017**, *8* (10), 2159–2167.

(106) Buchler, I.P., Hayes, M. LJ., Hegde, S. G., Hockerman, S. L., Jones, D. E., Kortum, S. W., Rico, J. G., Tenbrink, R. E., Wu, K. K. Indazole Derivatives. WO 2009106980 A2, 2009.

(107) Doi, T.; Asada, A.; Takeda, A.; Tagami, T.; Katagi, M.; Kamata, H.; Sawabe, Y. Enantioseparation of the Carboxamide-Type Synthetic Cannabinoids N-(1-Amino-3-Methyl-1-Oxobutan-2-Yl)-1-(5-Fluoropentyl)-1H-Indazole-3-Carboxamide and Methyl [1-(5-Fluoropentyl)-1H-Indazole-3-Carbonyl]-Valinate in Illicit Herbal Products. *J. Chromatogr. A* **2016**, *1473*, 83–89.

(108) Antonides, L. H.; Cannaert, A.; Norman, C.; Vives, L.; Harrison, A.; Costello, A.; Daeid, N. N.; Stove, C. P.; Sutcliffe, O. B.; McKenzie, C. Enantiospecific Synthesis, Chiral Separation, and Biological Activity of Four Indazole-3-Carboxamide-Type Synthetic Cannabinoid Receptor Agonists and Their Detection in Seized Drug Samples. *Front. Chem.* **2019**, *7* (MAY), 1–20.

(109) Williams, R.; Sellors, T. H. Particularly For. **1977**, *788* (12), 1977.

(110) Caputo, F.; Corbetta, S.; Piccolo, O.; Vigo, D. Seeking for Selectivity and Efficiency: New Approaches in the Synthesis of Raltegravir. *Org. Process Res. Dev.* **2020**, *24* (6), 1149–1156.

(111) Lakowicz, J. R. *Principles of Fluorescence Spectroscopy, 3rd Principles of Fluorescence Spectroscopy, Springer, New York, USA, 3rd Edn, 2006.*; 2006.

(112) Berova, N., Nakanishi, K. & Woody, R. W. *Circular Dichroism - Principles and Applications*; John Wiley & Sons, 2000.

(113) Eto, S.; Yamaguchi, M.; Bounoshita, M.; Mizukoshi, T.; Miyano, H. High-Throughput Comprehensive Analysis of d- and l-Amino Acids Using Ultra-High Performance Liquid Chromatography with a Circular Dichroism (CD) Detector and Its Application to Food Samples. *J. Chromatogr. B Anal. Technol. Biomed. Life Sci.* **2011**, *879* (29), 3317–3325.

(114) Jenkins, A. L.; Hedgepeth, W. A. Analysis of Chiral Pharmaceuticals Using HPLC with CD Detection. *Chirality* **2005**, *17* (SUPPL.), 24–29.

(115) Fujioka, M.; Omori, N. Subtleties in GPCR Drug Discovery: A Medicinal Chemistry Perspective. *Drug Discov. Today* **2012**, *17* (19–20), 1133–1138.

USC DE COMPOSTELA

(116) Markham, J.; Sparkes, E.; Boyd, R.; Chen, S.; Manning, J. J.; Finlay, D.; Lai, F.; McGregor, E.; Maloney, C. J.; Gerona, R. R.; Connor, M.; McGregor, I. S.; Hibbs, D. E.; Glass, M.; Kevin, R. C.; Banister, S. D. Defining Steric Requirements at CB1and CB2Cannabinoid Receptors Using Synthetic Cannabinoid Receptor Agonists 5F-AB-PINACA, 5F-ADB-PINACA, PX-1, PX-2, NNL-1, and Their Analogues. *ACS Chem. Neurosci.* **2022**, *13* (8), 1281–1295.

(117) Tait, R. J.; Caldicott, D.; Mountain, D.; Hill, S. L.; Lenton, S. A Systematic Review of Adverse Events Arising from the Use of Synthetic Cannabinoids and Their Associated Treatment. *Clin. Toxicol.* **2016**, *54* (1), 1–13.

(118) Jordan Trecki, Ph.D., Roy R. Gerona, Ph.D., and Michael D. Schwartz, M.D., M. P. H. Synthetic Cannabinoid–Related Illnesses and Deaths. *N. Engl. J. Med.* **2015**, *373* (2), 103–107.

(119) Hussain, N.; Hussain, F.; Haque, D.; Saeed, S.; Jesudas, R. An Outbreak of Brodifacoum Coagulopathy Due to Synthetic Marijuana in Central Illinois. *Mayo Clin. Proc.* **2018**, *93* (7), 957–958.

(120) Alipour, A.; Patel, P. B.; Shabbir, Z.; Gabrielson, S. Review of the Many Faces of Synthetic Cannabinoid Toxicities. *Ment. Heal. Clin.* **2019**, *9* (2), 93–99.

(121) Alexandre, J.; Malheiro, R.; Silva, D. D. da; Carmo, H.; Carvalho, F.; Silva, J. P. The Synthetic Cannabinoids Thj-2201 and 5f-Pb22 Enhance in Vitro Cb1 Receptor-Mediated Neuronal Differentiation at Biologically Relevant Concentrations. *Int. J. Mol. Sci.* **2020**, *21* (17), 1–22.

(122) Sezer, Y.; Jannuzzi, A. T.; Huestis, M. A.; Alpertunga, B. In Vitro Assessment of the Cytotoxic, Genotoxic and Oxidative Stress Effects of the Synthetic Cannabinoid JWH-018 in Human SH-SY5Y Neuronal Cells. *Toxicol. Res. (Camb).* **2020**, *9* (6), 734–740.

(123) Finlay, D. B.; Manning, J. J.; Ibsen, M. S.; Macdonald, C. E.; Patel, M.; Javitch, J. A.; Banister, S. D.; Glass, M. Do Toxic Synthetic Cannabinoid Receptor Agonists Have Signature in Vitro Activity Profiles? A Case Study of AMB-FUBINACA. *ACS Chem. Neurosci.* **2019**, *10* (10), 4350–4360.

(124) Murray, R. M.; Quigley, H.; Quattrone, D.; Englund, A.; Di Forti, M. Traditional Marijuana, High-Potency Cannabis and Synthetic Cannabinoids: Increasing Risk for Psychosis. *World Psychiatry* **2016**, *15* (3), 195–204.

(125) Tomiyama, K.; Funada, M. Cytotoxicity of Synthetic Cannabinoids on Primary Neuronal Cells of the Forebrain: The Involvement of Cannabinoid CB1

USC

Receptors and Apoptotic Cell Death. *Toxicol. Appl. Pharmacol.* **2013**.

(126) El-Faham, A.; Albericio, F. Peptide Coupling Reagents, More than a Letter Soup. *Chem. Rev.* **2011**, *111* (11), 6557–6602.

(127) Zhu, J. Bienaymè, J. *Multicomponent Reactions*; Wiley, 2005.

(128) Mallo-Abreu, A.; Reyes-Resina, I.; Azuaje, J.; Franco, R.; García-Rey, A.; Majellaro, M.; Miranda-Pastoriza, D.; García-Mera, X.; Jespers, W.; Gutiérrez-De-Terán, H.; Navarro, G.; Sotelo, E. Potent and Subtype-Selective Dopamine D2Receptor Biased Partial Agonists Discovered via an Ugi-Based Approach. *J. Med. Chem.* **2021**, *64* (12), 8710–8726.

(129) Azuaje, J.; El Maatougui, A.; García-Mera, X.; Sotelo, E. Ugi-Based Approaches to Quinoxaline Libraries. *ACS Comb. Sci.* **2014**, *16* (8), 403–411.

(130) Azuaje, J.; Pérez-Rubio, J. M.; Yaziji, V.; El Maatougui, A.; González-Gomez, J. C.; Sánchez-Pedregal, V. M.; Navarro-Vázquez, A.; Masaguer, C. F.; Teijeira, M.; Sotelo, E. Integrated Ugi-Based Assembly of Functionally, Skeletally, and Stereochemically Diverse 1,4-Benzodiazepin-2-Ones. *J. Org. Chem.* **2015**, *80* (3), 1533–1549.

(131) Dömling, A.; Ugi, I. Multicomponent Reactions with Isocyanides. *Angew. Chemie - Int. Ed.* **2000**, *39* (18), 3168–3210.

(132) Ugi, I., Meyr, R., Fetzer, U., Steinbrucker, C. No Title. *Angew. Chem*, **1985**, No. 71, 386.

(133) Giovenzana, G. B.; Tron, G. C.; Di Paola, S.; Menegotto, I. G.; Pirali, T. A Mimicry of Primary Amines by Bis-Secondary Diamines as Components in the Ugi Four-Component Reaction. *Angew. Chemie - Int. Ed.* **2006**, *45* (7), 1099–1102.

(134) Woodlands, T.; Woodlands, T. (12) United States Patent. **2002**, *1* (12).

(135) Azuaje, J.; El Maatougui, A.; Pérez-Rubio, J. M.; Coelho, A.; Fernández, F.; Sotelo, E. Multicomponent Assembly of Diverse Pyrazin-2(1 H)-One Chemotypes. *J. Org. Chem.* **2013**, *78* (9), 4402–4409.

(136) Hulme, C.; Dietrich, J. Emerging Molecular Diversity from the Intra-Molecular Ugi Reaction: Iterative Efficiency in Medicinal Chemistry. *Mol. Divers.* **2009**, *13* (2), 195–207.

(137) Fouad, M. A.; Abdel-Hamid, H.; Ayoup, M. S. Two Decades of Recent Advances of Ugi Reactions: Synthetic and Pharmaceutical Applications. *RSC Adv.* **2020**, *10* (70), 42644–42681.

USC UNIVERSIDADE DE SANTIAGO DE COMPOSTELA

(138) Azuaje, J. Nuevas Aplicaciones de La Reacción de Ugi En El Descubrimiento de Fármacos, 2012.

(139) Van Der Heijden, G.; Jong, J. A. W.; Ruijter, E.; Orru, R. V. A. 2-Bromo-6-Isocyanopyridine as a Universal Convertible Isocyanide for Multicomponent Chemistry. *Org. Lett.* **2016**, *18* (5), 984–987.

(140) Kelly, S. M.; Jess, T. J.; Price, N. C. How to Study Proteins by Circular Dichroism. *Biochim. Biophys. Acta - Proteins Proteomics* **2005**, *1751* (2), 119–139.

(141) Raïch, I.; Rivas-Santisteban, R.; Lillo, A.; Lillo, J.; Reyes-Resina, I.; Nadal, X.; Ferreiro-Vera, C.; de Medina, V. S.; Majellaro, M.; Sotelo, E.; Navarro, G.; Franco, R. Similarities and Differences upon Binding of Naturally Occurring Δ9-Tetrahydrocannabinol-Derivatives to Cannabinoid CB1 and CB2 Receptors. *Pharmacol. Res.* **2021**, *174*.

(142) Kenakin, T. Biased Receptor Signaling in Drug Discovery. *Pharmacol. Rev.* **2019**, *71* (2), 267–315.

(143) Shchepinova, M. M.; Hanyaloglu, A. C.; Frost, G. S.; Tate, E. W. Chemical Biology of Noncanonical G Protein–Coupled Receptor Signaling: Toward Advanced Therapeutics. *Curr. Opin. Chem. Biol.* **2020**, *56*, 98–110.

(144) Alexander, S. P. H.; Christopoulos, A.; Davenport, A. P.; Kelly, E.; Mathie, A.; Peters, J. A.; Veale, E. L.; Armstrong, J. F.; Faccenda, E.; Harding, S. D.; Pawson, A. J.; Southan, C.; Davies, J. A.; Abbracchio, M. P.; Alexander, W.; Al-hosaini, K.; Bäck, M.; Barnes, N. M.; Bathgate, R.; Beaulieu, J. M.; Bernstein, K. E.; Bettler, B.; Birdsall, N. J. M.; Blaho, V.; Boulay, F.; Bousquet, C.; Bräuner-Osborne, H.; Burnstock, G.; Caló, G.; Castaño, J. P.; Catt, K. J.; Ceruti, S.; Chazot, P.; Chiang, N.; Chini, B.; Chun, J.; Cianciulli, A.; Civelli, O.; Clapp, L. H.; Couture, R.; Csaba, Z.; Dahlgren, C.; Dent, G.; Singh, K. D.; Douglas, S. D.; Dournaud, P.; Eguchi, S.; Escher, E.; Filardo, E. J.; Fong, T.; Fumagalli, M.; Gainetdinov, R. R.; Gasparo, M. de; Gerard, C.; Gershengorn, M.; Gobeil, F.; Goodfriend, T. L.; Goudet, C.; Gregory, K. J.; Gundlach, A. L.; Hamann, J.; Hanson, J.; Hauger, R. L.; Hay, D. L.; Heinemann, A.; Hollenberg, M. D.; Holliday, N. D.; Horiuchi, M.; Hoyer, D.; Hunyady, L.; Husain, A.; IJzerman, A. P.; Inagami, T.; Jacobson, K. A.; Jensen, R. T.; Jockers, R.; Jonnalagadda, D.; Karnik, S.; Kaupmann, K.; Kemp, J.; Kennedy, C.; Kihara, Y.; Kitazawa, T.; Kozielewicz, P.; Kreienkamp, H. J.; Kukkonen, J. P.; Langenhan, T.; Leach, K.;

USC UNIVERSIDADE DE SANTIAGO DE COMPOSTELA

Lecca, D.; Lee, J. D.; Leeman, S. E.; Leprince, J.; Li, X. X.; Williams, T. L.; Lolait, S. J.; Lupp, A.; Macrae, R.; Maguire, J.; Mazella, J.; McArdle, C. A.; Melmed, S.; Michel, M. C.; Miller, L. J.; Mitolo, V.; Mouillac, B.; Müller, C. E.; Murphy, P.; Nahon, J. L.; Ngo, T.; Norel, X.; Nyimanu, D.; O'Carroll, A. M.; Offermanns, S.; Panaro, M. A.; Parmentier, M.; Pertwee, R. G.; Pin, J. P.; Prossnitz, E. R.; Quinn, M.; Ramachandran, R.; Ray, M.; Reinscheid, R. K.; Rondard, P.; Rovati, G. E.; Ruzza, C.; Sanger, G. J.; Schöneberg, T.; Schulte, G.; Schulz, S.; Segaloff, D. L.; Serhan, C. N.; Stoddart, L. A.; Sugimoto, Y.; Summers, R.; Tan, V. P.; Thal, D.; Thomas, W.; Timmermans, P. B. M. W. M.; Tirupula, K.; Tulipano, G.; Unal, H.; Unger, T.; Valant, C.; Vanderheyden, P.; Vaudry, D.; Vaudry, H.; Vilardaga, J. P.; Walker, C. S.; Wang, J. M.; Ward, D. T.; Wester, H. J.; Willars, G. B.; Woodruff, T. M.; Yao, C.; Ye, R. D. THE CONCISE GUIDE TO PHARMACOLOGY 2021/22: G Protein-Coupled Receptors. *Br. J. Pharmacol.* **2021**, *178* (S1), S27–S156.

(145) Kolb, P.; Kenakin, T.; Alexander, S. P. H.; Bermudez, M.; Bohn, L. M.; Breinholt, C. S.; Bouvier, M.; Hill, S. J.; Kostenis, E.; Martemyanov, K. A.; Neubig, R. R.; Onaran, H. O.; Rajagopal, S.; Roth, B. L.; Selent, J.; Shukla, A. K.; Sommer, M. E.; Gloriam, D. E. Community Guidelines for GPCR Ligand Bias: IUPHAR Review 32. *Br. J. Pharmacol.* **2022**, *179* (14), 3651–3674.

(146) Navarro, G.; Reyes-Resina, I.; Rivas-Santisteban, R.; Sánchez de Medina, V.; Morales, P.; Casano, S.; Ferreiro-Vera, C.; Lillo, A.; Aguinaga, D.; Jagerovic, N.; Nadal, X.; Franco, R. *Cannabidiol Skews Biased Agonism at Cannabinoid CB1 and CB2 Receptors with Smaller Effect in CB1-CB2 Heteroreceptor Complexes*; 2018; Vol. 157.

(147) Chen, L.; Chen, H.; Li, Y.; Li, L.; Qiu, Y.; Ren, J. Endocannabinoid and Ceramide Levels Are Altered in Patients with Colorectal Cancer. **2015**, 447–454.

(148) Sun, Y.; Liu, W. Z.; Liu, T.; Feng, X.; Yang, N.; Zhou, H. F. Signaling Pathway of MAPK/ERK in Cell Proliferation, Differentiation, Migration, Senescence and Apoptosis. *J. Recept. Signal Transduct.* **2015**, *35* (6), 600–604.

(149) Colabufo, N. A.; Berardi, F.; Contino, M.; Niso, M.; Abate, C.; Perrone, R.; Tortorella, V. Antiproliferative and Cytotoxic Effects of Some Σ2 Agonists and Σ1 Antagonists in Tumour Cell Lines. *Naunyn. Schmiedebergs. Arch. Pharmacol.* **2004**, *370* (2), 106–113.

(150) Phillips, H. S.; Kharbanda, S.; Chen, R.; Forrest, W. F.; Soriano, R. H.; Wu, T.

USC UNIVERSIDADE DE SANTIAGO DE COMPOSTELA

D.; Misra, A.; Nigro, J. M.; Colman, H.; Soroceanu, L.; Williams, P. M.; Modrusan, Z.; Feuerstein, B. G.; Aldape, K. Molecular Subclasses of High-Grade Glioma Predict Prognosis , Delineate a Pattern of Disease Progression , and Resemble Stages in Neurogenesis. **2006**, No. March, 157–173.

(151) Solinas, M.; Massi, P.; Cinquina, V.; Valenti, M.; Bolognini, D.; Gariboldi, M.; Monti, E.; Rubino, T.; Parolaro, D. Cannabidiol , a Non-Psychoactive Cannabinoid Compound , Inhibits Proliferation and Invasion in U87- MG and T98G Glioma Cells through a Multitarget Effect. **2013**, *8* (10).

(152) Singer, E.; Judkins, J.; Salomonis, N.; Matlaf, L.; Soteropoulos, P.; Mcallister, S.; Soroceanu, L. Reactive Oxygen Species-Mediated Therapeutic Response and Resistance in Glioblastoma. **2015**, *7*, 1–11.

(153) Velasco, G.; Salazar, M.; García-taboada, E.; Barcia, J.; Guzm, M. A Combined Preclinical Therapy of Cannabinoids and Temozolomide against Glioma. **2011**, *10* (January), 90–103.

(154) Minniti, G.; De Sanctis, V.; Muni, R.; Filippone, F.; Bozzao, A.; Valeriani, M.; Osti, M. F.; De Paula, U.; Lanzetta, G.; Tombolini, V.; Maurizi Enrici, R. Radiotherapy plus Concomitant and Adjuvant Temozolomide for Glioblastoma in Elderly Patients. *J. Neurooncol.* **2008**, *88* (1), 97–103.

(155) Arora, A.; Somasundaram, K. Glioblastoma vs Temozolomide: Can the Red Queen Race Be Won? *Cancer Biol. Ther.* **2019**, *20* (8), 1083–1090.

(156) Navarro, G.; Cordomí, A.; Brugarolas, M.; Moreno, E.; Aguinaga, D.; Pérez-Benito, L.; Ferre, S.; Cortés, A.; Casadó, V.; Mallol, J.; Canela, E. I.; Lluís, C.; Pardo, L.; McCormick, P. J.; Franco, R. Cross-Communication between Gi and Gs in a G-Protein-Coupled Receptor Heterotetramer Guided by a Receptor C-Terminal Domain. *BMC Biol.* **2018**, *16* (1), 1–15.

(157) Navarro, G.; Ferré, S.; Cordomi, A.; Moreno, E.; Mallol, J.; Casadó, V.; Cortés, A.; Hoffmann, H.; Ortiz, J.; Canela, E. I.; Lluís, C.; Pardo, L.; Franco, R.; Woods, A. S. Interactions between Intracellular Domains as Key Determinants of the Quaternary Structure and Function of Receptor Heteromers. *J. Biol. Chem.* **2010**, *285* (35), 27346–27359.

(158) Medrano, M.; Aguinaga, D.; Reyes-Resina, I.; Canela, E. I.; Mallol, J.; Navarro, G.; Franco, R. Orexin A/Hypocretin Modulates Leptin Receptor-Mediated Signaling by Allosteric Modulations Mediated by the Ghrelin GHS-R1A Receptor in Hypothalamic Neurons. *Mol. Neurobiol.* **2018**, *55* (6), 4718–4730.

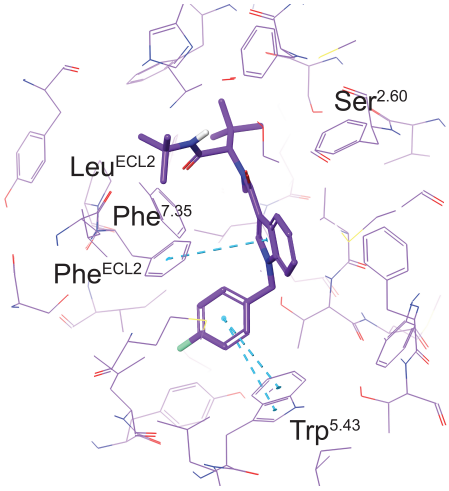
USC UNIVERSIDADE DE SANTIAGO DE COMPOSTELA

(159) Hradsky, J.; Raghuram, V.; Reddy, P. P.; Navarro, G.; Hupe, M.; Casado, V.; McCormick, P. J.; Sharma, Y.; Kreutz, M. R.; Mikhaylova, M. Post-Translational Membrane Insertion of Tail-Anchored Transmembrane EF-Hand Ca2+sensor Calneurons Requires the TRC40/Asna1 Protein Chaperone. *J. Biol. Chem.* **2011**, *286* (42), 36762–36776.

(160) Hua, T.; Vemuri, K.; Pu, M.; Qu, L.; Han, G. W.; Wu, Y.; Zhao, S.; Shui, W.; Li, S.; Korde, A.; Laprairie, R. B.; Stahl, E. L.; Ho, J. H.; Zvonok, N.; Zhou, H.; Kufareva, I.; Wu, B.; Zhao, Q.; Hanson, M. A.; Bohn, L. M.; Makriyannis, A.; Stevens, R. C.; Liu, Z. J. Crystal Structure of the Human Cannabinoid Receptor CB1. *Cell* **2016**, *167* (3), 750-762.e14.

USC
UNIVERSIDADE DE SANTIAGO DE COMPOSTELA

USC
UNIVERSIDADE
DE SANTIAGO
DE COMPOSTELA



This PhD Thesis describes the design, synthesis and characterization of new CB_2R selective agonists, thus enabling the discovery of new therapeutic agents for the treatment of inflammatory-based pathologies and cancer. Taking designer drugs as a model, a collection of dual agonists was synthesized and pharmacologically evaluated. Based on the study of new SAR trends identified, we developed an MCR-assisted pharmacomodulation process that enabled us to explore the structural features governing ligand binding and to discover new series of selective CB_2R agonists. Several of these ligands show excellent affinity and selectivity for the CB_2R, modulating it in an enantiospecific manner and exhibiting biased signaling. Finally, we demonstrated the anti-inflammatory and anti-cancer activity of herein discovered CB_2R ligands.